EXPLORING THE POTENTIAL OF NANOPHARMACEUTICALS: EXTENDING OUR FOCUS BEYOND CONVENTIONAL DRUGS

EDITED BY: Saeed Ahmad Khan, Amirali Popat, Alam Zeb, Hussain Ali and Faisal Raza

PUBLISHED IN: Frontiers in Pharmacology

frontiers Research Topics

ISSN 1664-8714
ISBN 978-2-83250-811-4
DOI 10.3389/978-2-83250-811-4

About Frontiers

Frontiers is more than just an open-access publisher of scholarly articles: it is a pioneering approach to the world of academia, radically improving the way scholarly research is managed. The grand vision of Frontiers is a world where all people have an equal opportunity to seek, share and generate knowledge. Frontiers provides immediate and permanent online open access to all its publications, but this alone is not enough to realize our grand goals.

Frontiers Journal Series

The Frontiers Journal Series is a multi-tier and interdisciplinary set of open-access, online journals, promising a paradigm shift from the current review, selection and dissemination processes in academic publishing. All Frontiers journals are driven by researchers for researchers; therefore, they constitute a service to the scholarly community. At the same time, the Frontiers Journal Series operates on a revolutionary invention, the tiered publishing system, initially addressing specific communities of scholars, and gradually climbing up to broader public understanding, thus serving the interests of the lay society, too.

Dedication to Quality

Each Frontiers article is a landmark of the highest quality, thanks to genuinely collaborative interactions between authors and review editors, who include some of the world's best academicians. Research must be certified by peers before entering a stream of knowledge that may eventually reach the public - and shape society; therefore, Frontiers only applies the most rigorous and unbiased reviews.
Frontiers revolutionizes research publishing by freely delivering the most outstanding research, evaluated with no bias from both the academic and social point of view. By applying the most advanced information technologies, Frontiers is catapulting scholarly publishing into a new generation.

What are Frontiers Research Topics?

Frontiers Research Topics are very popular trademarks of the Frontiers Journals Series: they are collections of at least ten articles, all centered on a particular subject. With their unique mix of varied contributions from Original Research to Review Articles, Frontiers Research Topics unify the most influential researchers, the latest key findings and historical advances in a hot research area! Find out more on how to host your own Frontiers Research Topic or contribute to one as an author by contacting the Frontiers Editorial Office: frontiersin.org/about/contact

EXPLORING THE POTENTIAL OF NANOPHARMACEUTICALS: EXTENDING OUR FOCUS BEYOND CONVENTIONAL DRUGS

Topic Editors:
Saeed Ahmad Khan, Kohat University of Science and Technology, Pakistan
Amirali Popat, The University of Queensland, Australia
Alam Zeb, Riphah International University, Pakistan
Hussain Ali, Quaid-i-Azam University, Pakistan
Faisal Raza, Shanghai Jiao Tong University, China

Citation: Khan, S. A., Popat, A., Zeb, A., Ali, H., Raza, F., eds. (2022). Exploring the Potential of Nanopharmaceuticals: Extending our Focus Beyond Conventional Drugs. Lausanne: Frontiers Media SA. doi: 10.3389/978-2-83250-811-4

Table of Contents

frontiers in Pharmacology

ORIGINAL RESEARCH
published: 04 February 2022
doi: 10.3389/fphar.2022.838168

Tacrolimus Loaded Cationic Liposomes for Dry Eye Treatment

Xiang Chen[1], *Jicheng Wu*[2,3], *Xueqi Lin*[1], *Xingdi Wu*[1], *Xuewen Yu*[1], *Ben Wang*[2,3]*† and *Wen Xu*[1]*†

[1]Eye Center, The Second Affiliated Hospital of Zhejiang University School of Medicine, Hangzhou, China, [2]Cancer Institute (Key Laboratory of Cancer Prevention and Intervention, China National Ministry of Education), The Second Affiliated Hospital, Zhejiang University School of Medicine, Hangzhou, China, [3]Institute of Translational Medicine, Zhejiang University, Hangzhou, China

Eye drops are ophthalmic formulations routinely used to treat dry eye. However, the low ocular bioavailability is an obvious drawback of eye drops owing to short ocular retention time and weak permeability of the cornea. Herein, to improve the ocular bioavailability of eye drops, a cationic liposome eye drop was constructed and used to treat dry eye. Tacrolimus liposomes exhibit a diameter of around 300 nm and a surface charge of +30 mV. Cationic liposomes could interact with the anionic ocular surface, extending the ocular retention time and improving tacrolimus amount into the cornea. The cationic liposomes notably prolonged the ocular retention time of eye drops, leading to an increased tacrolimus concentration in the ocular surface. The tacrolimus liposomes were also demonstrated to reduce reactive oxygen species and dry eye–related inflammation factors. The use of drug-loaded cationic liposomes is a good formulation in the treatment of ocular disease; the improved ocular retention time and biocompatibility give tremendous scope for application in the treatment of ocular disease, with further work in the area recommended.

Keywords: cationic liposome, drug delivery system, tacrolimus, dry eye, ocular bioavailability

OPEN ACCESS

Edited by:
Amirali Popat,
The University of Queensland, Australia

Reviewed by:
Tejal Mehta,
Nirma University, India
Marta Vicario-de-la-Torre,
Complutense University of Madrid, Spain

***Correspondence:**
Ben Wang
benwang@zju.edu.cn
Wen Xu
xuwen2003@zju.edu.cn

†These authors have contributed equally to this work and share last authorship

Specialty section:
This article was submitted to Experimental Pharmacology and Drug Discovery, a section of the journal Frontiers in Pharmacology

Received: *17 December 2021*
Accepted: *13 January 2022*
Published: *04 February 2022*

Citation:
Chen X, Wu J, Lin X, Wu X, Yu X, Wang B and Xu W (2022) Tacrolimus Loaded Cationic Liposomes for Dry Eye Treatment. Front. Pharmacol. 13:838168. doi: 10.3389/fphar.2022.838168

1 INTRODUCTION

Eye drops are pretty restricted by low ocular bioavailability. Despite this, many clinicians prefer topical ophthalmic solutions to other treatment options as eye drops are accessible and noninvasive, and this formulation accounts for nearly 90% of ophthalmic drugs (Weng et al., 2018; Jain et al., 2019). Prolonging ocular retention time and prompting the ability to permeate into the cornea are two primary approaches to increase ocular bioavailability. The structure of the ocular surface comprises the adnexa, tear film, lacrimal gland, meibomian glands, cornea, conjunctiva, and eyelids (Craig et al., 2017). It protects the eyes from bacteria and chemicals, also becoming an obstacle to drug permeability. The blink reflex and tear turnover rate are the main contributing factors to a short ocular retention time (Chhonker et al., 2015). To remedy this problem, eye drops need to be frequently used to improve the therapeutic effect. This frequent administration leads to excess eye drops draining into the lacrimal duct and absorbed into the nasal mucosa, which may cause serious side effects (Yuan et al., 2012; Lin et al., 2019). Besides, the requirement of multiple administrations, in turn, may cause patients to become noncompliant.

Therefore, there have been many researchers devoted to investigating various ophthalmic drug delivery systems (DDSs) to optimize the delivery mechanism of the drug (Dave et al., 2021; Tsao et al., 2021). An ideal ophthalmic DDS is expected to have properties including stimuli responsiveness, ocular biocompatibility, and ocular biodegradability (Nguyen and Lai, 2020).

Likewise, there are many diseases in ophthalmology which require long-period administration, such as severe dry eye and glaucoma. Ocular DDSs are promising in this field according to recent research studies. Hollow mesoporous ceria nanoparticles loading Y-27632 were synthesized to control high intraocular pressure owing to its ability of sustained release (Luo et al., 2021). The DDS of ophthalmology has also been used to improve bioavailability. Kumari et al. (2021) developed a lipophile carrier using cholesterol-Labrafac^{TM} to deliver dexamethasone. It is found that this formulation had high internalization capacity for corneal epithelial cell and showed superior ability to reduce inflammatory factor expression, such as TNF-α, MMP-9, and IL-6, suggesting that it could be a viable choice to treat dry eye. Han et al. (2022) constructed a temperature-sensitive tacrolimus (FK506) gel to treat dry eye. It was made of monofunctional, polyhedral, oligomeric silsesquioxane and exhibited outstanding mucoadhesive ability. Besides, it could more effectively treat dry eye than other FK506 formulations in a murine model. Carbonized nano-gels showed superior antibacterial and antioxidant effects on keratitis caused by *S. aureus*, attributing to its ability of corneal penetration *via* opening epithelial tight junction (Lin et al., 2021). Axitinib nano-wafer contained arrays of nano-reservoirs loading drugs. It was proven that this ocular DDS could realize slow release to increase pre-ocular retention time and effective inhibition of corneal neovascularization in a lower dosing frequency (Yuan et al., 2015).

Dry eye is a prevalent and multifactor-induced autoimmune disease of the ocular surface. The characteristic symptoms are as follows: discomfort, visual disturbance, and tear film instability; the disease can damage the ocular surface (Workshop, 2007; Chen et al., 2020). Immunoregulation includes two parts, and they are in homeostasis in the normal state. One is immunosuppression including $CD4^+$ regulatory T cells (Treg) that restrict and suppress excessive inflammation-like autoimmunity. The other is pro-inflammatory, including Th1, Th2, and Th17. However, in dry eye, the regulatory function of Treg is compromised (Chen et al., 2013). More and more evidences from experiments and clinics show that Th17-mediated pathogenesis plays a primary role in persistent ocular surface inflammation (Chen and Dana, 2021). Continued inflammation is the primary pathogenesis of dry eye (Wei and Asbell, 2014). Dry eye has a global prevalence of 5%–50%, making it a widespread problem (Stapleton et al., 2017). Using tear substitutes to relieve ocular discomfort is the primary treatment of the condition. Immune modulators such as cyclosporine A and FK506 are also medications to treat dry eye (Valim et al., 2015). FK506 is a potent macrolide immunosuppressant. As a hydrophobic drug, it would penetrate the cell membrane and then interact with FK506-binding protein-12 to regulate the activity of the calmodulin-dependent protein phosphatase. Calcineurin inhibition could inhibit the release of cytokines by the blockage of T cell activation and differentiation (Rusnak and Mertz, 2000). Compared with cyclosporine A, it is more effective and causes more minor irritation to the surrounding tissue, so FK506 is increasingly used in the clinical setting (Siegl et al., 2019). However, the narrow therapeutic window for FK506 raises concerns for its use clinically.

Lipids are the composition of the tear film and can slow evaporation of the liquid layer, so a supplement of lipids also can relieve the clinical manifestations of dry eye. Due to this, nanoscale DDSs, such as liposomes, have become increasingly of interest to ophthalmologists. Liposomes, primarily constituting phospholipids, are a good choice of the delivery system owing to their outstanding biocompatibility, feasibility, and tenability. They are spherical vesicles with a hydrophilic core and lipidic bilayers; they have also been proven to increase the solubility of both hydrophilic and hydrophobic drugs (Kayser et al., 2005; Lopez-Cano et al., 2021). A substantial body of studies shows that lipid constitution, particle size, and zeta potential affect delivery efficiency (Inokuchi et al., 2010; Schäfer et al., 2010). Positively charged or larger liposomes exhibit extended ocular residence times in and around the injection site during subconjunctival administration, while neutral, negatively charged, or small liposomes are rich in the limbus (Chaw et al., 2020).

Cationic liposomes can conjunct with negatively charged sulfated proteoglycans in the cell membrane, preventing rapid clearance and encouraging integration (Steffes et al., 2017; Han et al., 2020b). Many studies have demonstrated that positively charged nanoparticles can modulate cell membrane potential. The depolarization of the cell membrane could prompt cell drug uptake, but it is detrimental to cell proliferation. The extent of membrane potential change is concentration-dependent (Arvizo et al., 2010; Kim et al., 2013). The eye is a suitable organ for cationic liposome eye drops. First, the cornea is regarded as a relatively immuno-privileged site; this is attributed to the absence of both blood and lymphatic vessels (Kumar and Kumar, 2014). Second, the conjunctival sac is a small lacuna that would not contain many liposomes. In addition, blinking helps form a tear film on the cornea, and this efficiently redistributes free cationic liposomes across the ocular surface. Furthermore, the ocular surface is an anionic environment derived from a mucin layer, and this predisposes the surface to attract cationic liposomes electrostatically (Lin et al., 2019; Han et al., 2020a), which increases the pre-ocular time of liposomes. There are two main approaches to generate liposomes with positive zeta potential (Lin et al., 2019). One is to utilize cationic phospholipids to prepare the liposomes, such as (2,3-dioleoyloxy-propyl)-trimethylammonium (DOTAP). The other is to modify the liposomes with positive substances, such as poly-L-lysine (PLL), chitosan, and polyethyleneimine (PEI) (Schäfer et al., 2010; Chaiyasan et al., 2013; Sasaki et al., 2013). Due to its adjuvanticity, cationic lipids are used to carry therapeutic molecules, such as antigens, in the form of liposomes (Farhadi et al., 2021). DOTAP is a synthetic lipid widely used *in vitro* and *in vivo* (Firouzmand et al., 2013). It was reported that liposomes containing DOTAP and 1,2-dioleoyl-sn-glycero-3-phosphoethanolamine (DOPE) could activate the immune responses of Th1 and Th2 cells in mice (Nikpoor et al., 2019).

Herein, this study aimed to develop a cationic FK506 liposome with DOTAP, so that it would have increased interactions with the ocular surface, improving ocular retention time. This treatment may not only alleviate the ocular inflammatory response to dry eyes but also prompt the bioavailability of eye drops. It would reduce the administration time of the treatment, reduce the risk of adverse events, and improve patient compliance. The chemical and physical characteristics of the

FK506 liposomes, including particle size, zeta potential, and entrapment efficiency, were assessed. The efficacy of the cationic liposomes for dry eye treatment was evaluated both *in vitro* and *in vivo*.

2 MATERIALS AND METHODS

2.1 Materials

DOTAP, DOPE, cholesterol, 2,7-dichlorodi -hydrofluorescein diacetate (DCFH-DA), fluorescein isothiocyanate (FITC), 4',6-diamidino-2-phenylindole (DAPI), and benzalkonium chloride were purchased from Sigma. 1,2-distearoyl-sn-glycero-3-phosphoethanolamine-N-[amino(poly(ethylene glycol))2000] (DSPE-PEG2000) and FITC- DSPE-PEG2000 were purchased from Yuan Ye Biological Company. FK506 was purchased from MedChemExpress. Sodium dodecyl sulfate was purchased from Sangon Biotech. 1X phosphate buffer solution (PBS) was purchased from Biosharp. Commercial FK506 eye drops were purchased from SENJU (FK506 concentration: .1%), and it was a white turbid liquid. Hylo-COMOD was a commercial artificial tear whose first ingredient listed .1% sodium hyaluronate, and it was purchased from URSA PHARM Arzneimittel DmbH. The chemicals and solvents used for mass spectrum–high-performance liquid chromatography (MS-HPLC) and HPLC were of HPLC grade, while the others were of analytical grade.

2.2 Synthesis of FK506 Liposome and FITC-Labeled FK506 Liposome

The FK506 liposomes were prepared using the thin film hydrated dispersion method. Five mg DOTAP, 5.3 mg DOPE (DOTAP: DOPE = 1:1 in molar rate), 5 mg DSPE-PEG2000, 2.77 mg cholesterol, and 2 mg FK506 were dissolved in 6 ml of trichloromethane in a round-bottom flask. A rotary evaporator was used to remove the organic solvent in a 40°C water bath under a .06–.08 MPa vacuum; the rotation speed was kept at a rate of 100 rpm. Then, solvent traces were removed by keeping the solution in a 0.1-MPa vacuum for 1 h at 100 rpm. The resultant dried lipid film was hydrated with 10 ml 1X PBS at 40°C for 20 min until it formed a homogenous emulsion. Last, the final product was obtained by squeezing the liposomes through a 0.4-μm pore-size polycarbonate film (Whatman, Life Science) to decrease the particle size at room temperature. The liposomes were stored at 4°C until use.

The FITC-labeled FK506 liposome was synthesized following the abovementioned steps, except using FITC-labeled DSPE-PEG2000 to replace DSPE-PEG2000.

2.3 Particle Size and Zeta Potential of the FK506 Liposome

Particle size, zeta potential, and polydispersity index (PDI) of the liposomes were measured by dynamic light scattering (DLS) conducted on a particle size analyzer (Zetasizer nano-ZSE, Malvern). The liposomes were diluted with ultrapure water at a ratio of 1:100 in advance. Every sample was tested three times.

2.4 Transmission Electron Microscopy

The morphology of the liposomes was analyzed using negative staining TEM (Tecnai G2 spirit, Thermo FEI). Ten μl of FK506 liposomes was dropped onto a 300-mesh carbon-coated copper grid. Excess liposome solution was stained before 1 μl 2% uranium acetate was added for 60s. The uranium acetate was then blotted, and another 1 μl drop of 2% uranium acetate was added; this process was repeated three times. The samples were then dried and examined at 120 kV.

2.5 Entrapment Efficiency and Loading Level

The entrapment efficiency was determined by ultrafiltration. Freshly prepared FK506 liposomes were added to the ultrafiltration centrifugal tube (Merck Millipore, 10,000 NMWL) and centrifuged at 3,000 g at 4°C for 60 min. The filtered liquid, which contained free FK506, was collected, then lyophilized for 24 h, and redissolved with .6 ml methyl alcohol. The concentration of FK506 in the filtered liquid was determined by HPLC. Entrapment efficiency was calculated by the following formula:

$$\text{Entrapment efficiency}(\%) = \frac{\textbf{total mass of added FK506} - \textbf{the mass of free FK506}}{\textbf{total mass of added FK506}} \times \mathbf{100\%}. \quad (1)$$

Product loss was not considered in the preparation process, where the mass of free FK506 stands for the amount of FK506 in the filtered liquid, and the total mass of added FK506 is the initial mass of FK506 added into trichloromethane.

The FK506 loading level was calculated by the following formula:

$$\text{FK506 loading level}(\%) = \frac{\textbf{total mass of FK506 encapsulated in liposomes}}{\textbf{total mass of FK506 liposomes}} \times \mathbf{100\%}. \quad (2)$$

Total mass of FK506 encapsulated in liposomes equals total mass of added FK506 minus the mass of free FK506, and the total mass of the FK506 liposome equals 20.07 mg minus the mass of free FK506.

2.6 *In Vitro* Release Profile of FK506 Liposome

The release profile of the FK506 liposome was confirmed by dynamic dialysis. First, FK506 liposomes were freshly synthesized in accordance with the procedures mentioned above; following this, PBS containing .1% sodium dodecyl sulfate (SDS) was prepared to serve as a release medium under sink condition (Dai et al., 2013). Ten ml of the FK506 liposomes was pipetted into a preprocessed dialysis bag (Biosharp, 3,500 MW); this was placed in 30 ml of the release medium and stirred at 200 rpm at 37°C. At the pre-established time points (.5, 1, 2, 4, 6, 9, 12, 24, 48, 72, 120, and 168 h), 1 ml of the release medium was taken out before 1 ml of the new release medium was added to maintain the

volume of the release medium. All the samples were collected in centrifuge tubes and lyophilized for 24 h. The resulting powders were dissolved in .4 ml of methyl alcohol and centrifuged at 10,000 g for 10 min. The supernatant was then collected, and the final concentration of FK506 was measured by HPLC.

2.7 HPLC of FK506 Determination

The quantitative analysis of FK506 in entrapment efficiency was determined by HPLC (Shimadzu, Japan), while the corneal concentration was determined using MS-HPLC (Agilent Technologies, USA). The experimental conditions of HPLC were as follows: The mobile phase comprised acetonitrile/10 mM ammonium formate solution (72/28, v/v). The flow rate was kept at 1.2 ml/min, and 20 μl of the samples was injected; the absorption was monitored at 210 nm. Chromatographic separation was carried out on an InfinityLab Poroshell 120 SB-C18 column (50 × 4.6 mm, 2.7 μm), and the column temperature was maintained at 60°C. The retention time of FK506 on this column was approximately 1.6 min; the peak area was calculated using the least square method, and the standard curve of the FK506 concentration peak was pictured. The regression equation was used to calculate the corresponding FK506 concentrations when the areas were known.

2.8 Human Corneal Epithelial Cell Cultivation

HCECs were purchased from ATCC and cultivated at an atmosphere of 95% air/5% CO_2 at 37°C. The culture medium used was Dulbecco's modified Eagle medium (DMEM) (Solarbio); this was supplemented with 10% fetal bovine serum (Life Technologies, Grand Island, NY), 4.5 mg/ml glucose, 100 U/ml penicillin, and 100 ug/ml streptomycin.

2.9 Cytotoxicity

Cytotoxicity was measured using a cell counting kit-8 (CCK-8) assay (Dojindo, Japan) according to the manufacturer's protocol. HCECs were seeded into 96-well plates at a ratio of 5,000 cells per well with 100 μl culture medium. The plates were placed into a cell incubator to allow them to adhere for 24 h. The cell culture medium was removed, and the cells were washed three times. The cells were incubated with 100 μl DMEM, blank liposomes, FK506 liposomes, and commercial FK506 eye drops for 2, 4, and 6 h. FK506 concentration of FK506 liposomes was .2 mg/ml, as well as that of commercial FK506 eye drops. Subsequently, 10 μl of the CCK-8 solution was added into each well, and then the cells were re-incubated for 2 h. The optical density values were measured at 450 nm using a microplate reader (SpectraMax M5, Molecular Device), and cell viability was calculated. The optimum concentration of FK506 liposomes was also determined using CCK-8 assay. FK506 liposomes with a series of drug concentration gradients (.0025 mg/ml, .005 mg/ml, .01 mg/ml, .02 mg/ml, .05 mg/ml, .1 mg/ml, and .02 mg/ml) were tested, and cell viability was calculated.

2.10 Cell Uptake

$1*10^5$ HCECs were seeded into confocal dishes and adhered to for 24 h, the culture medium was then removed, and the cells were washed three times. Hundred μl of FK506 liposome labeled with FITC was co-incubated with cells for 2 h with 100 μl DMEM in the cell incubator. The excess liposomes and DMEM were removed, and the cells were washed three times. The nuclei of the HCECs were stained by DAPI. Confocal microscopy (A1 Ti, Nikon) was used to show the position of FK506 liposomes in cells.

2.11 Dry Eye Cell Model

The cell models of dry eye were established as follows: HCECs were seeded into 12-well plates at a density of 10^5 per well and cultivated in the conditions mentioned above. After 24 h, the culture medium was removed, and 200 μM of hydrogen peroxide (H_2O_2) was added, and the cells were incubated for 1 h (Li et al., 2019).

2.12 The Efficiency of Reactive Oxygen Species Inhibition *In Vitro*

The HCECs were seeded at a density of 1.0×10^5 cells per well with 100 μl culture medium. After 200 μM H_2O_2 treatment was carried out for 1 h, FK506 liposomes and commercial FK506 were added into each well. After co-incubation for 2 h, the cells were washed three times with PBS and stained with DCFH-DA for 30 min. The fluorescence intensity of intracellular ROS was measured by flow cytometry at 484 nm (excitation) and 520 nm (emission).

2.13 Dry Eye–Related Inflammatory Factor Determination

The processed HCECs were treated with 1 ml of TRIzol and collected. MRNA was collected, quantified, and reverse-transcribed in turn. Reverse transcription was performed using the PrimeScript™ RT-PCR Kit, followed by quantitative real-time polymerase chain reaction (qRT-PCR) using the SYBR® Premix Ex Taq™ Kit. All the experimental procedures were in accordance with the manufacturer's protocols. The primer pairs were as follows: human GAPDH, 5′-ACAACTTTGGTATCGTGGAAG G-3′ (forward) and 5′-GCCATCACGCCACAGTTTC-3′ (reverse); human interleukin-1β (IL-1β), 5′-AGCTACGAA TCTCCGACCAC -3′ (forward) and 5′-CGTTATCCCATG TGTCGAAGAA -3′ (reverse); and human interleukin-6 (IL-6), 5′- ACTCACCTCTTCAGAACGAATTG -3′ (forward) and 5′-CCATCTTTGGAAGGTTCAGGTTG -3′ (reverse).

2.14 Animal Model

Animal experiments were carried out after ethical approval (No. 2021057) and conformed to the ethical standards of The Second Affiliated Hospital of Zhejiang University. The animal models of dry eye were established as follows: New Zealand rabbits (2–2.5 kg, male) were obtained from the Zhejiang province medical science institute. They were housed in their own cages individually in an environment where the temperature was 20–26°C and the humidity was around 40%–70%. The rabbits were treated with 25 μl of .2% benzalkonium chloride twice a day in the interval of 12 h for 7 days according to a previously reported study (Tan et al., 2019). C57BL/6 mice (20–25 g,

male) were purchased from Shanghai SLAC Animal Co., Ltd. The mice were housed in pathogen-free conditions as stipulated.

2.15 *In Vivo* Biocompatibility

The biocompatibility of FK506 liposomes was evaluated in the aspect of central corneal thickness (TOMEY anterior segment optical coherence tomography, Japan), endothelial cell density (TOMEY specular microscope EM-3000, Japan), corneal edema and conjunctival edema, and hyperemia (slit lamp microscope). Eighteen normal New Zealand rabbits were randomly put into three groups: the PBS group, the FK506 liposome group, and the artificial tear group. Each group had six rabbits. The rabbits in the PBS group were given PBS, those in the FK506 liposome group were treated with fresh FK506 liposome, and those in the artificial tear group were given Hylo-COMOD eye drops. All of them were administered twice a day (8 a.m. and 8 p.m.) at 50 μl. The abovementioned indicators were rigorously observed at day 0, day 7, and day 28. The anatomical structure of the cornea and conjunctiva was observed by H and E staining.

2.16 Ocular Irritation Test

The ocular irritation of FK506 liposomes was evaluated *via* the modified Draize test (Bhatta et al., 2012). The normal rabbits were treated with 20 μl of FK506 liposomes directly on the cornea in the right eye and 20 μl of PBS in the left eye. All of them were installed at 30-min interval for 6 h. Then, ophthalmological tests were performed to observe the level of irritation, including secretions, redness of conjunctiva, and corneal opacity and swelling. The observations were conducted at a 12-hour interval for 72 h.

2.17 Amount of FK506 Permeating Into the Cornea

The dry eye rabbits were treated with 50 μl of FK506 liposomes in the right eye and 50 μl of the commercial FK506 eye drops in the left eye. After 5, 30 min, 1, and 2 h, the rabbits were euthanized. The cornea was excised wholly and washed gently three times with normal saline. All samples were stored at −20°C. In addition, the amount of FK506 in the cornea was determined by MS-HPLC.

2.18 MS-HPLC of FK506 Determination

The experimental conditions of MS-HPLC were as follows: The cornea was cut into pieces and placed in centrifuge tubes. One ml of methyl alcohol was added along with 2 mm ceramic beads to prepare the cornea homogenate. All the samples were centrifuged at 10,000 g for 10 min, and the liquid supernatant was removed. The FK506 concentrations were measured utilizing MS-HPLC. The mobile phase comprised 0.1% formic acid/5 mM ammonium acetate in water (Solvent A) and acetonitrile (Solvent B), the flow rate was kept at 0.3 ml/min, and 20 μl of the samples was injected. Chromatographic separation was carried out on a Zorbax SB C18 column (150 × 2.1 mm, 3.5 μm). The gradient program was as follows: 80% of B for .5 min; kept at 95% of B for 4.5 min and finally, remained at 100% of B. MS was performed under 5 L/min gas flow at 325°C and 11 L/min sheath gas flow at 350°C. The ion spray voltages were 3,000 V and −3,500 V in the positive and negative ionization modes, respectively. The integral peak area of m/z 821.5>786.4 was used for quantitative analysis.

2.19 Retention Time in the Ocular Surface *In Vivo*

The pre-ocular retention time was assessed by *in vivo* fluorescence imaging. The C57BL/6 mice were anesthetized, and a drop of FITC-labeled FK506 liposomes and commercial FK506 eye drops mixed with FITC and FITC solutions (nearly 5 μl) was added to their eyes according to the group. The excitation wavelength was set at 488 nm, and the emission wavelength was 520 nm. After 5, 10, and 30 min, the fluorescence signal was collected and analyzed.

2.20 Effect of Alleviating Dry Eye Clinical Signs *In Vivo*

The 16 dry eye rabbits were assigned into four groups using a random number table, and they were as follows: the negative control group, positive control group, commercial FK506 eye drop group, and FK506 liposome group. Each group had four rabbits. The rabbits in the negative control group had no treatment or intervention. The rabbits in the positive group were given PBS after modeling of dry eye, commercial FK506 eye drop in the commercial FK506 eye drop group, whereas FK506 liposome in the FK506 liposome group. All of them were administrated twice a day (8 a.m. and 8 p.m.) at 50 μl.

To evaluate the clinical signs of dry eye, two ophthalmological tests were carried out on day 0, day 7, and day 9, including corneal fluorescein staining and TFBUT. Corneal fluorescein staining was carried out as follows: sodium fluorescein strips were wetted with a drop of normal saline and used to dye the conjunctiva of the lower eyelid; the rabbits blinked, and then corneal staining was observed and graded according to the SICCA OSS Group Scale. TFBUT was measured as follows: the rabbits were helped to blink several times to form a tear film in the ocular surface, and it started to time until the first dark point or crack appeared, and the abovementioned steps were repeated three times, and the average value was counted (Valim et al., 2015).

2.21 Corneal Epithelial Layer Thickness Measurement

The corneal epithelial layer thickness was measured using ImageJ software. The H and E–stained slides were photographed using a fluorescence microscope (Nikon DM4000) at 400 times magnification, and ten points were randomly chosen to measure the thickness. The mean value was calculated, and the difference was analyzed.

2.22 Enzyme-Linked Immunosorbent Assay and Hematoxylin–Eosin Staining

The cornea and conjunctiva of rabbits were collected following euthanasia on day 9. Part of these was fixed by 4% paraformaldehyde, embedded, and sectioned to observe corneal epithelial regeneration, conjunctival goblet cell density, and

TABLE 1 | Characterization of the FK506 liposome.

Sample	Particle size (nm)	Polydispersity index	Zeta potential (mV)	Entrapment efficiency (%)	FK506 loading (%)
FK506 liposomes	292 ± 7	0.27 ± 0.02	31.13 ± 0.83	90.11 ± 2.87	9.07 ± 0.03

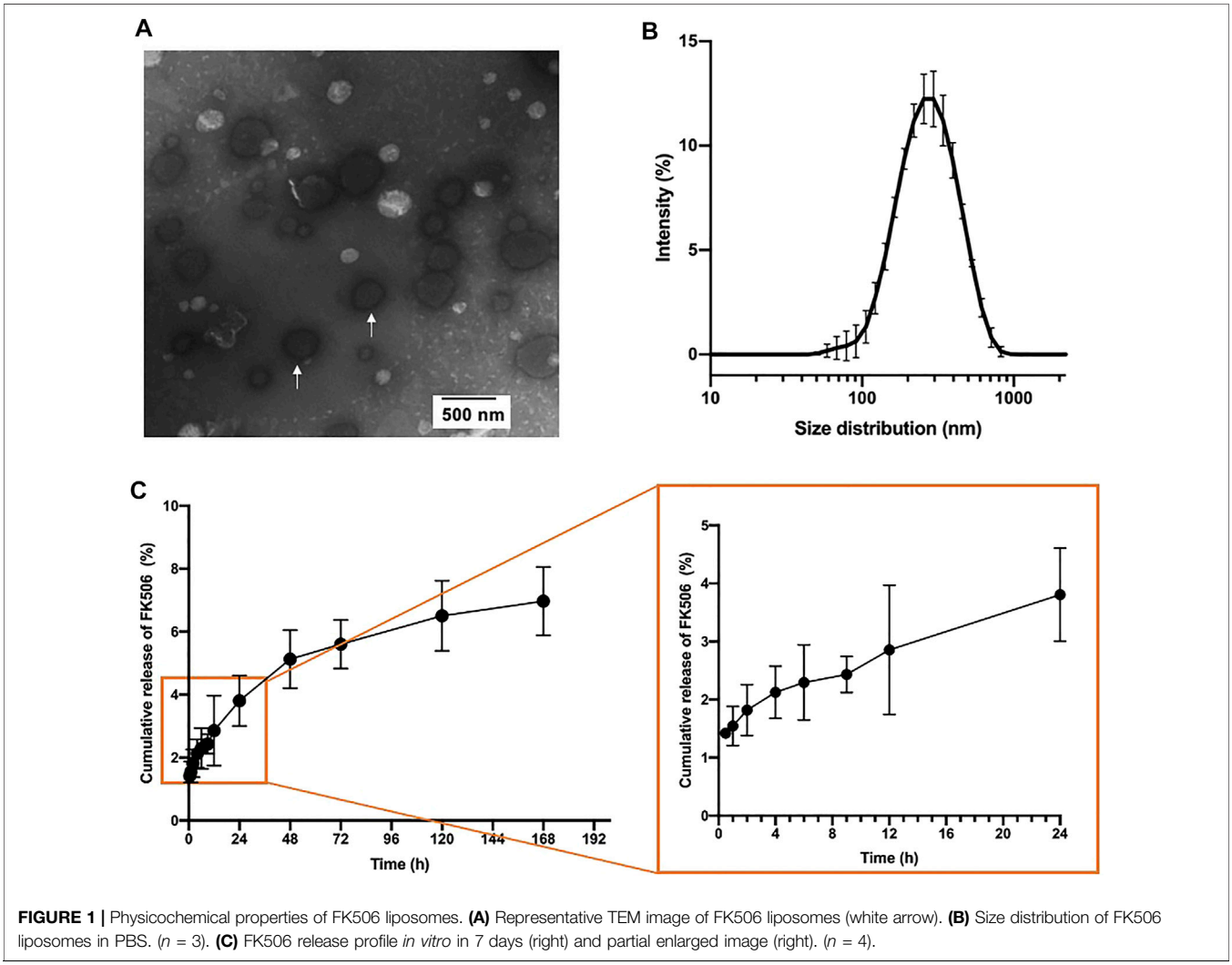

FIGURE 1 | Physicochemical properties of FK506 liposomes. **(A)** Representative TEM image of FK506 liposomes (white arrow). **(B)** Size distribution of FK506 liposomes in PBS. (n = 3). **(C)** FK506 release profile *in vitro* in 7 days (right) and partial enlarged image (right). (n = 4).

inflammation cell infiltration *via* H and E staining. The remaining tissue was kept in liquid nitrogen before being used to determine the level of inflammatory cytokines by ELISA. Inflammatory cytokines in the cornea and conjunctiva were extracted. The tissue was cut into pieces and further broken up using ultrasonication at 0°C. The resulting homogenate was centrifuged at 2,000 rpm for 20 min to collect the protein. The ELISA procedures were conducted according to the manufacturer's protocol (Jiancheng Bioengineering institute, Nanjing, China).

2.23 Statistical Analysis

All the data in this article were reported as the mean ± standard deviation (SD). The statistical analyses performed were one-way ANOVA to calculate the significance of experimental data, except the analysis of FK506 concentration in the cornea and the comparison of relative corneal fluorescein score change between day 7 and day 9 using unpaired t-test ($p < .05$).

3 RESULTS

3.1 Characterization of FK506 Liposomes

The FK506 liposomes were synthesized using the classical thin-film hydration dispersion method (Wang et al., 2021; Wu et al., 2021; Zhong et al., 2021), as described in the *Materials and Methods*. The physical and chemical properties of the liposomes

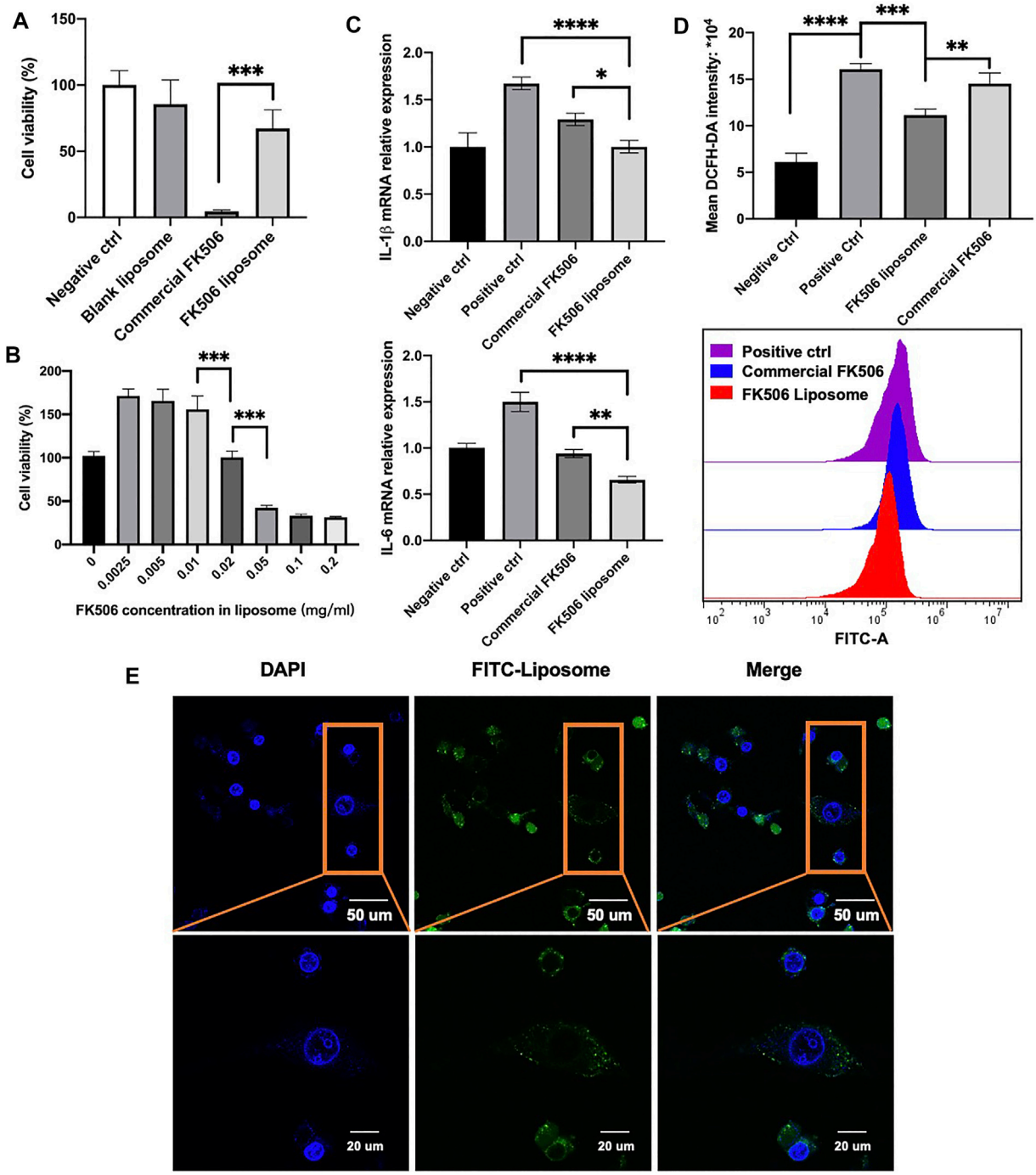

FIGURE 2 | *In vitro* cytotoxicity test and efficiency evaluation on HCECs. **(A)** Cell viability test *via* CCK-8. HCECs were treated in a 0.2-mg/ml concentration of FK506 for 2 h (n = 5). **(B)** Cell viability test of a gradient of FK506 concentration in liposomes. HCECs were treated for 24 h (n = 4). **(C)** mRNA expression level of inflammation-related factors in the cornea and conjunctiva tissues after receiving different treatment. IL-1β is shown in the upper image (n = 3), and IL-6 is shown in the lower image (n = 3). **(D)** Flow cytometry analysis of ROS level (n = 3). *p < .05, **p < .01, and ***p < .001. **(E)** Co-localization of FK506 liposomes and HCECs. The cell nucleus is stained blue, and the FK506 liposome is stained green.

were investigated. The particle size of the FK506 liposomes was around 292 ± 7 nm, while the surface zeta potential was 31.1 ± 0.83 mV (**Table 1**). TEM showed that the morphology of the FK506 liposomes was spherical (**Figure 1A**), and the size distribution of the FK506-loaded liposomes was a little smaller in TEM than DLS. It might be attributed to the fact that DLS

determined the hydrodynamic radius of nanoparticles. The entrapment efficiency of the FK506 liposomes was 90.11 ± 2.87%, and the FK506 loading level was around 9.07 ± 0.03%.

The *in vitro* release profile of the FK506 liposome showed that FK506 liposome released FK506 slowly overall (**Figure 1C**). This formulation released the drug slowly in the first 48 h, and nearly 5.13 ± 0.92% FK506 was released in this period. There was an accumulative concentration of 6.97 ± 1.08% of total FK506 released until day 7.

3.2 *In Vitro* Cytocompatibility

The positive charge of the liposome surface played a significant role in adhesion; however, it was also responsible for the cytotoxicity of cationic liposomes (Kim et al., 2013). Therefore, to evaluate the cytocompatibility of FK506 liposomes, the cell viability was measured using CCK-8. As shown in **Figure 2A**, the blank liposome group showed 85.54 ± 18.31% cell viability after 2-hour co-incubation with HCECs. In addition, there was no significant difference in viability between the blank liposome group and the negative control group. It suggested that the cationic liposomes did not exhibit apparent cytotoxicity. Furthermore, at the same FK506 concentration of 0.2 mg/ml, FK506-loaded liposomes were less detrimental to HCECs than commercial FK506 eye drops after 2 h. The cell viability was 67.17 ± 0.14% in the FK506-loaded liposome group and 4.38 ± 1.21% in the commercial FK506 eye drop group, and there was a statistically significant difference ($p < .001$). This result inferred that using liposomes as the drug delivery vehicle decreased drug toxicity.

To reduce the cytotoxicity further, a gradient of concentration test was then performed to determine the safe concentrations of the formulation *in vitro*. After 24-hour co-incubation, FK506 liposomes with a drug concentration below 0.02 mg/ml showed good cell viability (**Figure 2B**). Based on this result, .02 mg/ml FK506 concentration was chosen in the subsequent experiments *in vitro*.

3.3 FK506 Liposome Cellular Intake and Co-Localization *In Vitro*

The ability to enter cells was a prominent characteristic of cationic liposomes. It was important to deliver drugs (Takikawa et al., 2020). To investigate whether FK506 liposomes could enter cells, confocal microscopy was used. The nucleus was stained blue using DAPI, while FK506-loaded liposomes were stained green using FITC-labeled DSPE-PEG2000 (**Figure 2E**). After a 2-hour co-incubation with HCECs, FITC-labeled FK506 liposomes were shown to adhere to HCECs and were observed in the cytoplasm. This result implied that HCECs will uptake FK506 liposomes, facilitating the transfer of FK506 into cells.

3.4 The FK506 Liposome–Mediated Effect on Inflammatory Factor Expression and Reactive Oxygen Species Production *In Vitro*

Oxidative stress was pathogenesis of dry eye and was associated with its progression (Perez-Garmendia et al., 2020). ROS levels were evaluated using flow cytometry *via* the measurement of the mean intracellular fluorescence intensity. In **Figure 2D**, the mean ROS fluorescence intensity of the FK506 liposome group was $11.14 \pm .65*10^4$; this result was significantly lower than that of the positive control group, which scored $16.07 \pm .94*10^4$. It indicated that FK506 liposomes might reduce ROS generation following H_2O_2 stimulation. In addition, the FK506 liposome group had significantly lower ROS levels than the commercial FK506 eye drops group, which scored $14.52 \pm 1.16*10^4$ ($p < .001$).

In terms of the dry eye–related expression of inflammatory factors, the levels of IL-1β and IL-6 were assessed using qRT-PCR. Compared to the positive control group, FK506 liposomes and commercial FK506 eye drops both downregulated the expression of IL-1β and IL-6. FK506 liposomes exhibited a more significant inhibitory effect on IL-1β ($p < .05$) and IL-6 ($p < .01$) expression than commercial eye drops. It was attributed to the fact that the liposomal FK506 dosing method allowed the drug to enter the cell easily, making it more efficient to decrease the expression of inflammatory factors, which was in accordance with previous studies (Nattika et al., 2014).

3.5 *In Vivo* Biocompatibility

The cornea is an extremely sensitive tissue due to dense coverage of nerve endings within the corneal epithelium, which protects the eyes from harmful substances and foreign objects (Lum et al., 2019). Once stimulated, tearing, blinking, and foreign body sensation in the eye occur; this progresses into pain, edema, optical congestion, and increased secretions. To assess the biocompatibility of FK506 liposomes, central corneal thickness and endothelial cell density were observed *in vivo*. The FK506 concentration in the FK506 liposome was 0.2 mg/ml. Both of the central corneal thickness and endothelial cell density remained stable after 28-day administration; there was no significant difference among the PBS group, commercial eye drop group, and FK506 liposome eye drops group. In addition to this, none of the groups presented obvious clinical signs of irritation. The cornea remained transparent throughout; there was no evidence of conjunctival congestion, edema, or a change to eye secretions during the observation period (**Figure 3A**). Moreover, H and E staining of the cornea and conjunctiva showed that there were no corneal epithelial defects, no corneal stromal edema, and no evidence of inflammatory cell infiltration (**Figure 3B**). Overall, it was concluded that FK506 liposome eye drops (FK506 concentration was 0.2 mg/ml) were compatible with the ocular surface and were safe for ophthalmic use.

3.6 Ocular Irritation Test

It was necessary to evaluate the ocular irritation *in vivo* because the surfactant is one of the materials to prepare FK506 liposomes. To study the ocular irritation of FK506 liposomes, the ocular irritation test was carried out. During the 72-hour observation, there were no signs of irritation after installing FK506 liposomes and PBS (**Figure 3C**). Specifically, there was no conjunctival redness, no secretions, and no corneal swelling. Thus, it was concluded that FK506 liposomes have no ocular irritation.

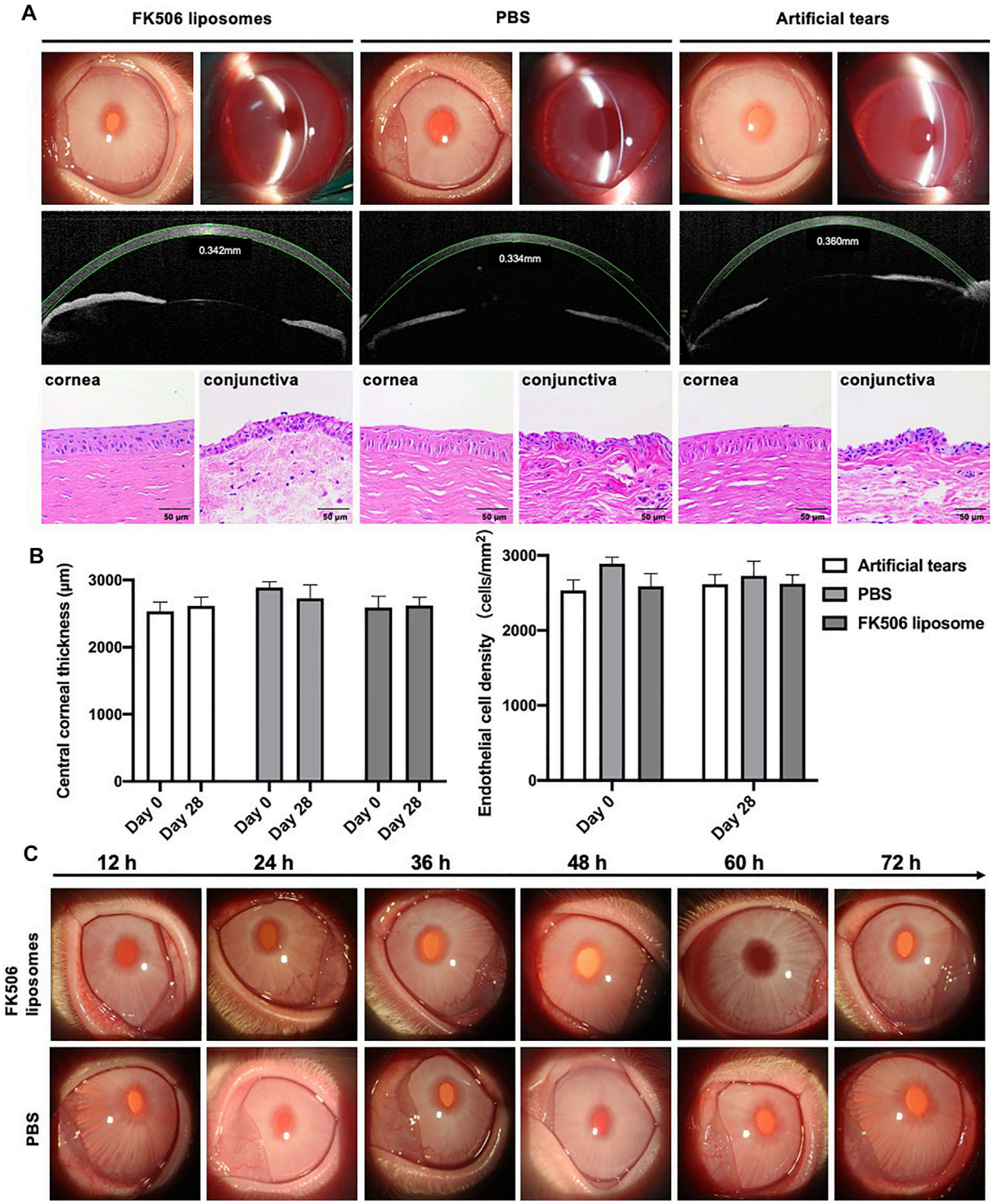

FIGURE 3 | *In vivo* biocompatibility and ocular irritation evaluation of FK506 liposomes in New Zealand rabbits. **(A)** Upper image: anterior segment images observed by a slit-lamp microscope after the four-week administration of different eye drops. Middle image: corneal thickness measured by anterior segment optical coherence tomography after the 4-week administration of different eye drops. Lower image: H and E of the cornea (left) and conjunctiva (right) after the four-week administration of different eye drops. **(B)** Quantitative analysis of central corneal thickness (left) and endothelial cell density (right). **(C)** 72-hour observations of the ocular irritation test. The above-described images belonged to the FK506 liposome group, and the below images belonged to the PBS group.

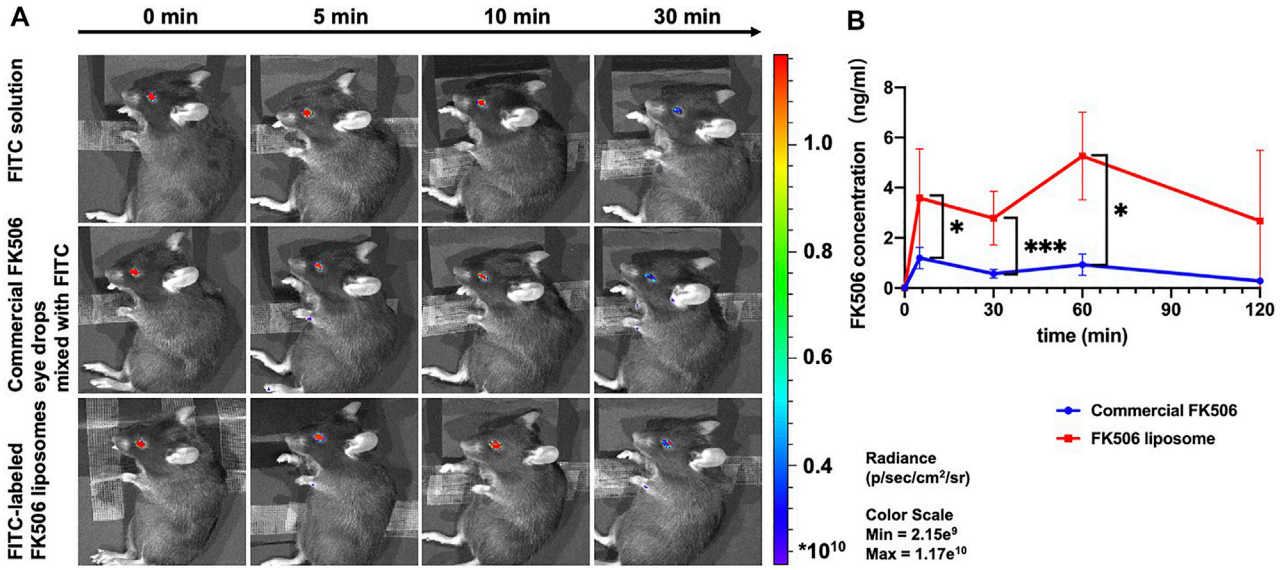

FIGURE 4 | *In vivo* ocular retention evaluation of FK506 liposomes in C57BL/6 mice and trans-corneal FK506 amount change in New Zealand rabbits. **(A)** *In vivo* fluorescence images of FITC solution, commercial FK506 eye drops mixed with FITC, and FITC-labeled FK506 liposomes at 0, 5, 10, and 30 min. **(B)** *In vivo* trans-corneal FK506 amount changes of commercial FK506 eye drops (blue) and FK506 liposomes (red) after administration. Quantitative analysis of FK506 concentration in the cornea at 5, 30 min, 1 h, and 2 h. *$P < .05$ and **$p < .01$.

3.7 Ocular Retention Time and Amount of FK506 Permeating Into the Cornea

To investigate whether the use of FK506 liposomes would prolong retention time in the ocular surface, the fluorescence intensity following eye drop treatment was compared. Ten minutes after administration, there were similar fluorescence intensity levels among the three following groups, which are the FITC solution group, commercial FK506 eye drops mixed with FITC group, and FITC-labeled FK506 liposomes group (**Figure 4A**). However, only the group treated with FITC-labeled FK506 liposomes showed an intense signal after 30 min. Following this experiment, it can be concluded that FK506 liposomes can extend the ocular retention time.

In addition, the group treated with FK506 liposomes had a significantly higher FK506 concentration in the corneal tissue 1 h after administration than the group treated with commercial FK506 eye drops (**Figure 4B** ($p < .01$)). The FK506 concentration of the cornea in the FK506 liposome group was 3.59 ± 1.96 ng/ml, 2.79 ± 1.07 ng/ml, and 5.26 ± 1.75 ng/ml after 5, 30 min, and 1 h, respectively, while it was 1.20 ± .43 ng/ml, .57 ± .17 ng/ml, and .93 ± .43 ng/ml at the corresponding time points in the commercial FK506 eye drop group. It was in accordance with the ocular retention time, suggesting that the liposome was a promising drug delivery vehicle to facilitate FK506 penetration into the cornea.

3.8 The Effect on Alleviating Signs of Dry Eye *In Vivo*

As well as being a kind of macrolide antibiotic, FK506 is more commonly used in the suppression of the immune system. In ophthalmology, the primary use for FK506 eye drops was conjunctivitis catarrhalis aestiva. In addition, clinicians also prescribe FK506 for patients with severe dry eye or following corneal transplantation surgery.

The scheme of the evaluation of the effect on alleviating signs of dry eye *in vivo* is shown in **Figure 5A**. As shown in **Figure 5D**, there was a sharp improvement to the tear film break up time (TFBUT) of the FK506 liposome group. Dry eye would interfere with the stability of the tear film and influence the health state of the ocular surface. TFBUT is an indicator of the stability of the tear film. The long TFBUT implies the stable tear film and mild dry eye. On the contrary, the short TFBUT hints at a brittle tear film and severe dry eye. Corneal fluorescein staining score could evaluate the health state of the ocular surface, especially the cornea. The appearance of fluorescein staining suggests that the integrity of the cell is compromised. The high corneal fluorescein score means corneal epithelial layer defect and severe dry eye (Workshop, 2007; Wolffsohn et al., 2017). Hence, TFBUT and corneal fluorescein staining score are indicators used to assess the severity of dry eye.

Compared with baseline (day 7), TFBUT increased by 3.57 ± 1.50 s when using FK506 liposomes; this was statistically significantly different to the 1.50 ± 1.29 s when using the commercial FK506 eye drops ($p < .05$). Notably, TFBUT was notably longer in the FK506 liposome group than in the positive control group at day 9 ($p < .01$). It showed that liposomes prepared as given above promote tear film stability. Similarly, corneal fluorescein staining levels were lower at day 9 in all groups than at day 7; the lowest levels were found in the FK506 liposome eye drop group. Statistical analysis showed a significant difference between day 7 and 9 ($p < .01$). By contrast, the

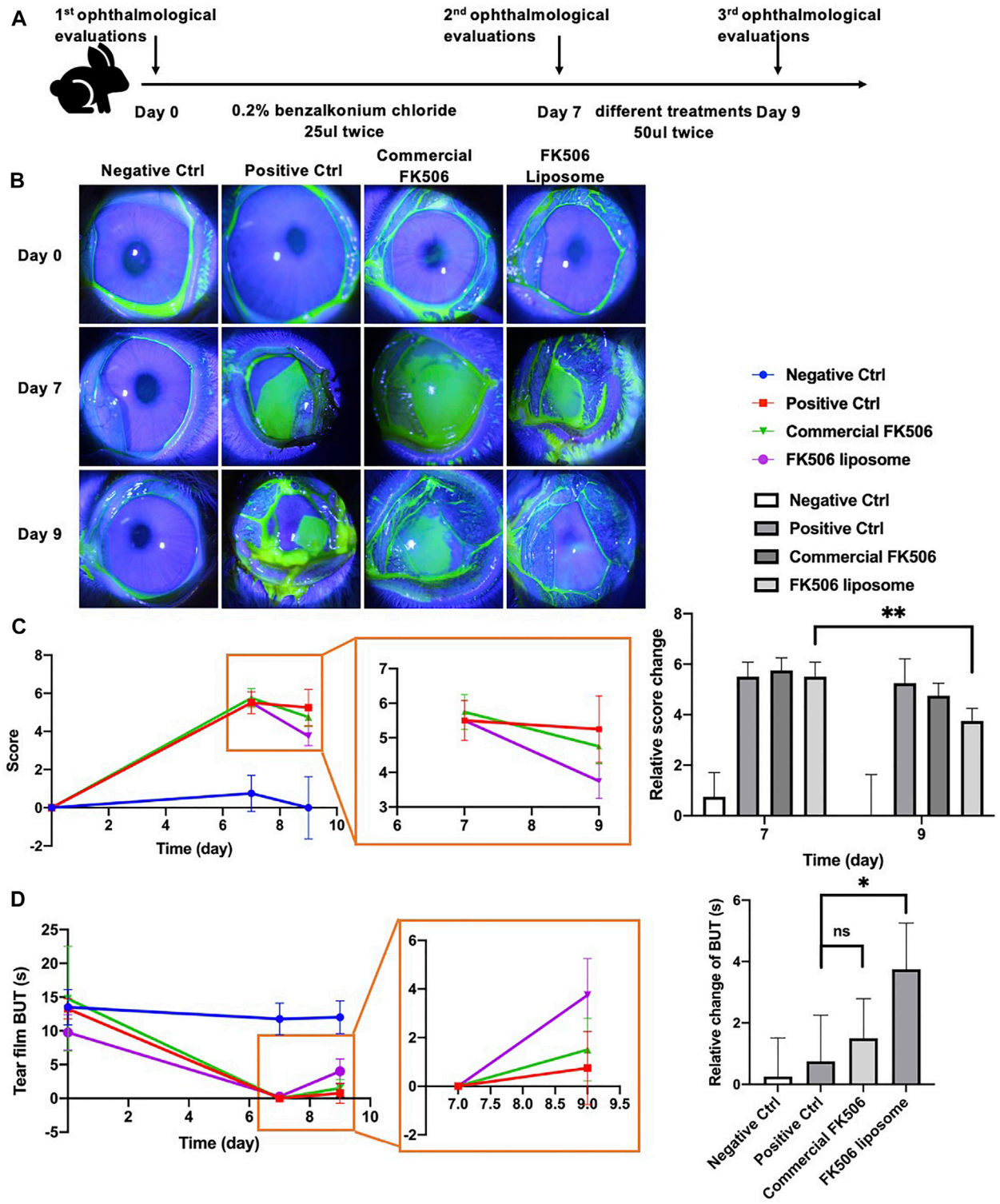

FIGURE 5 | *In vivo* ophthalmological evaluations of FK506 liposomes in New Zealand rabbits with dry eye. **(A)** Flow diagram of the dry eye model and treatment plan. **(B)** Representative slit-lamp images of corneal fluorescein sodium staining at day 0, day 7, and day 9. **(C)** Relative corneal fluorescein staining score change at day 0, day 7, and day 9 (left); partial enlarged image (middle) and quantitative analysis of relative changes of score compared with baseline (day 0) (right). **(D)** Absolute BUT change at day 0, day 7, and day 9 (left); partial enlarged image (middle) and quantitative analysis of relative changes of BUT compared with day 7 (right). *$p < .05$ and **$p < .01$.

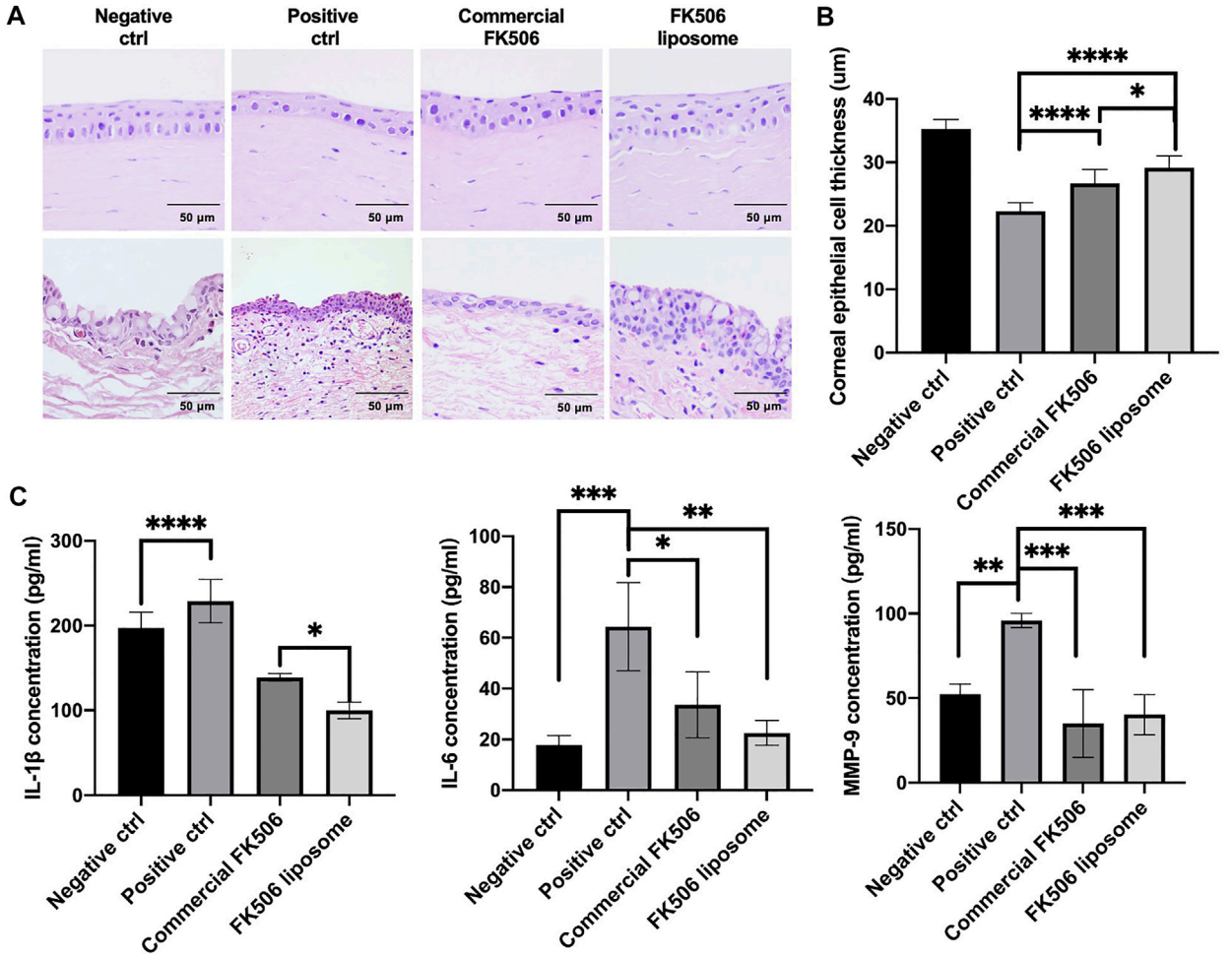

FIGURE 6 | *In vivo* therapeutic effect evaluations on New Zealand rabbits with dry eye. **(A)** Representative H and E images of the cornea (upper) and conjunctiva (below) at day 9. **(B)** Quantitative analysis of corneal thickness at day 9. **(C)** Concentrations of inflammatory factors, including IL-1β, IL-6, and MMP-9, in the cornea and conjunctiva tissue. *$p < .05$, **$p < .01$, and ***$p < .001$.

commercial FK506 eye drop group showed no statistical difference between day 7 and 9 (**Figures 5B,C**). It indicated that there was a more rapid recovery of the corneal epithelial cell layer in the FK506 liposome eye drop group. FK506 liposomes not only cure epithelial cell injury but also prompt clinical sign alleviation.

3.9 The Effect on Prompting Corneal Epithelial Cell Layer Reconstruction *In Vivo*

Severe dry eye always has severe punctate erosions on the cornea, and fluorescein staining could help evaluate the range of corneal damage (Workshop, 2007). To assess the depth of corneal injury, the thickness of the corneal epithelial layer was measured. As is shown in **Figure 6A**, the reconstruction of the corneal epithelial cell layer varied widely from group to group at day 9. The commercial FK506 eye drop group and the FK506 liposome group had a more significant increase in thickness than the positive control group; in addition, the FK506 liposome group had a more considerable increase than the commercial FK506 eye drop group. The mean thickness of the epithelial layer was 22.31 ± 1.35 μm in the positive control group, 26.69 ± 2.18 μm in the commercial FK506 group, 29.14 ± 1.89 μm in the FK506 liposome group, and 35.28 ± 1.51 μm in the negative control group (**Figure 6B**). There was a significant difference between the positive control group and the FK506 liposome group ($p < .0001$), as well as the commercial FK506 eye drop group ($p < .0001$). Moreover, the difference between the FK506 liposome group and the commercial FK506 eye drop group was significant ($p < .05$).

3.10 The Effect on Decreasing the Expressions of Dry Eye–Related Inflammatory Factors *In Vivo*

To determine the effect of FK506 liposome eye drops on dry eye, the expression levels of dry eye–related inflammatory factors were determined *via* ELISA. As shown in **Figure 6C**, after treatment

with .2% benzalkonium chloride, matrix metalloproteinase-9 (MMP-9), IL-1β, and IL-6 levels markedly increased in the cornea and conjunctiva. Following administration with FK506 liposomes, the concentration of IL-1β decreased to 99.91 ± 9.68 pg/ml, while the level in the commercial eye drops was 138.98 ± 4.32 pg/ml. This difference was statistically significant ($p < .05$). The level in the positive control group was 228.99 ± 25.59 pg/ml. Likewise, the expression levels of IL-6 and MMP-9 were downregulated in the FK506 liposome group at 22.58 ± 4.87 pg/ml and 40.26 ± 11.83 pg/ml, respectively. The concentration of IL-6 in the positive control group was 64.38 ± 17.35 pg/ml ($p < .01$) and the MMP-9 concentration was 95.95 ± 4.23 pg/ml ($p < .001$).

4 DISCUSSION

To improve the ocular bioavailability of eye drops, a more efficient ocular delivery method would be developed; due to this, nanoscale delivery systems, such as liposomes, have become increasingly of interest. Cationic liposomes have been demonstrated to adhere to the anionic surface of cells and can be internalized (Steffes et al., 2017); this property has become universally exploited as drug delivery. The ocular surface is an ideal environment for cationic liposomes to use due to its relative immune privilege and the ability to interact with cationic liposomes. Hence, cationic liposomes were chosen to encapsulate FK506 and treat dry eye. In this study, cationic FK506 liposomes were proven to prolong ocular retention time and increase FK506 amount in the cornea; at the same time, this treatment alleviated the signs of dry eye and reduced the expression of inflammatory factors *in vitro* and *in vivo*.

Landucci et al. (2021) developed a thymoquinone-loaded liposome and found that it could reduce the toxicity at high dose in HCEC-2 cells. Huang et al. (2017) constructed the liposome encapsulating montmorillonite and betaxolol hydrochloride to treat glaucoma and found that liposomal formulation could effectively reduce cytotoxicity of betaxolol hydrochloride. Likewise, our study showed that the FK506 liposome could improve the cytocompatibility of FK506 and decrease the expression of inflammatory factors *in vitro*. It is a limitation that a long-term systemic safety assessment is absent in this manuscript because FK506 is an immunosuppressor and could cause side effects.

In term of the release profile of FK506 liposomes, it released FK506 slowly overall, which was in accordance with previous studies and was attributed to its hydrophobic property (Dai et al., 2013). FK506 is hydrophobic and has little solubility in water. SDS could help increase the solubility of FK506 so that it was added into the release medium to achieve solubility. SDS is a tenso-active agent, which has surface activity and critical micelle concentrations of the surfactant (Onwosi and Odibo, 2012). It could interact with liposomes and has an influence on the release profile (Zhang et al., 2011).

In terms of ocular bioavailability, Lin et al. (2019) found that compared with anionic nanoparticles and a commercial formula, drug amount in the cornea was highest in the administration group of cationic nanoparticles. It was in accordance with our study. Cationic FK506 liposomes had relatively higher FK506 amount in the cornea than commercial FK506 eye drops. According to the medication guide, commercial FK506 eye drops mainly consist of FK506 hydrate and .01% benzalkonium chloride. Benzalkonium chloride is a common preservative in ophthalmic preparations. Meloni et al. (2010) and Meloni et al. (2019) found that acute exposure of .01% benzalkonium chloride could reduce transepithelial electrical resistance value and increase the release of lactate dehydrogenase after 24-hour treatment and 16-hour recovery *in vitro*, but it was nontoxic after 24-hour treatment. Transepithelial electrical resistance value is an indicator of corneal barrier property, reflecting the epithelial thickness and integrity of tight junction. The release of lactate dehydrogenase correlates to the damage of the cellular membrane (Meloni et al., 2019). The corneal barrier affects the ocular bioavailability of eye drops. In the part of FK506 permeability into the cornea in our studies, we administered 50 μl of the commercial FK506 eye drops once and observed for 2 h. Therefore, it was referred that .01% benzalkonium chloride might have a tiny effect on promoting FK506 penetration into the cornea in the commercial FK506 eye drops. Positive charge on the surface of FK506 liposomes significantly improved permeability into the cornea.

Benzalkonium chloride is detrimental to corneal epithelium cells and could decrease the tear film break up time, especially in the patients with long-period administration (Meloni et al., 2019). However, Okahara and Kawazu (2013) found that when installing eye drops with .005% and .01% benzalkonium chloride, there was no obvious change on the ocular surface after 52-week administration. In our study, the administration time of commercial FK506 eye drops is short. Therefore, it is inferred that the influence of 0.01% benzalkonium chloride on the ocular surface was small. Tong et al. (2019) studied the influence of benzalkonium chloride on ROS production on HCECs and found that it was concentration-dependent. Namely, higher concentration of benzalkonium chloride induced higher level of ROS. Benzalkonium chloride at .02% increased ROS production, while at .001% induced very little ROS production. In our studies, based on the result of cytotoxicity of FK506 liposomes, .02 mg/ml FK506 concentration was chosen in the subsequent experiments *in vitro*. To achieve this, commercial FK506 eye drops with 1 mg/ml FK506 concentration were diluted. Meanwhile, the concentration of the preservative contained in this product was diluted to .002%. Therefore, benzalkonium chloride might have slight influence on ROS production of HCECs.

It is also of note that FK506 liposomes work with lower concentrations of FK506. In practice, commercial FK506 eye drops have a .1% FK506 concentration. Patients need to use regular drops twice a day, and this means that approximately the patients receive a .05 mg dose of FK506 at each treatment. In this study using FK506 liposomes, 50 μL of liposomes contained .01 mg of FK506, a fourfold reduction compared to commercial FK506 eye drops. It means that FK506 liposomes could relieve the clinical signs of dry eye in a lower concentration of the drug. It was attributed to the cationic charge of the liposome and surface zeta potential. With the cationic charge on the liposomal surface, liposomes loaded with FK506 could

interact with HCECs and prolong ocular surface residence time. Nevertheless, when using regular eye drops, FK506 would be quickly cleared. To solve this problem, patients are required to install eye drops frequently to alleviate the clinical signs or use medications with high drug concentration. The FK506 concentration of commercial FK506 eye drops is higher than that of FK506 liposomes. Hence, commercial FK506 eye drops also alleviate the clinical signs of dry eye. In conclusion, both the commercial FK506 eye drops and FK506 liposomes boost epithelial cell regeneration and inhibit inflammatory reactions, while FK506 liposomes were significantly more effective. Using the liposome drops would increase ocular surface residence time, resulting in effective recovery of dry eye. Likewise, Gelfuso et al. (2020) found that liposomal formulations could enhance voriconazole penetration into the cornea, thus prompting recovery of fungal keratitis. Zhan et al. (2018) developed a tetrodotoxin-and-dexmedetomidine-loaded liposome to achieve long-acting ocular anesthesia. This liposome functionalized with Concanavalin A, which could be conjunct with corneal glycan moieties and prevent rapid clearance.

Above all, cationic FK506 liposomes could prolong precorneal time, prompt drug amount in the cornea, and relieve dry eye. The cationic liposome is a good choice of the ocular delivery system in ophthalmology.

5 CONCLUSION

This study reports that cationic liposomes encapsulating FK506 can prolong ocular retention time and increase FK506 amount in the cornea by interacting with the anionic ocular surface. Cationic FK506 liposomes could reduce ROS production in the cell model of dry eye following H_2O_2 treatment. In addition, it could decrease the expression of dry eye–related inflammatory factors *in vitro* and *in vivo*, as well as alleviate the signs of dry eye. Taken together, this study constructs a new delivery method for FK506 eye drops that have increased ocular bioavailability compared to standard treatments.

DATA AVAILABILITY STATEMENT

The original contributions presented in the study are included in the article/Supplementary Material; further inquiries can be directed to the corresponding authors.

ETHICS STATEMENT

The animal study was reviewed and approved by the Ethics Committee of the Second Affiliated Hospital of Zhejiang University.

AUTHOR CONTRIBUTIONS

BW and WX designed and supervised this study. XC, JW, and XL finished the animal experiments. XC, XW, and XY completed the experiments *in vitro* and characterization of the FK506 liposome. XC wrote the manuscript. BW and WX edited it.

FUNDING

The authors thank the financial support from Zhejiang Province Key Research and Development Program (2017C03046), the National Natural Science Foundation of China (Grant number 81800809), and the Natural Science Foundation of Zhejiang Province (Grant number Z21H160013).

ACKNOWLEDGMENTS

The authors thank core facilities, Zhejiang university school of medicine for the technical support on experiments, and thank the agriculture–biology–environment public instrument platform of Zhejiang University for the technical support of HPLC and MS-HPLC.

REFERENCES

Arvizo, R. R., Miranda, O. R., Thompson, M. A., Pabelick, C. M., Bhattacharya, R., Robertson, J. D., et al. (2010). Effect of Nanoparticle Surface Charge at the Plasma Membrane and beyond. *Nano. Lett.* 10 (7), 2543–2548. doi:10.1021/nl101140t

Bhatta, R. S., Chandasana, H., Chhonker, Y. S., Rathi, C., Kumar, D., Mitra, K., et al. (2012). Mucoadhesive Nanoparticles for Prolonged Ocular Delivery of Natamycin: *In Vitro* and Pharmacokinetics Studies. *Int. J. Pharm.* 432, 105–112. doi:10.1016/j.ijpharm.2012.04.060

Chaiyasan, W., Srinivas, S. P., and Tiyaboonchai, W. (2013). Mucoadhesive Chitosan-Dextran Sulfate Nanoparticles for Sustained Drug Delivery to the Ocular Surface. *J. Ocul. Pharmacol. Ther.* 29 (2), 200–207. doi:10.1089/jop.2012.0193

Chaw, S. Y., Novera, W., Chacko, A. M., Wong, T. T. L., and Venkatraman, S. (2020). *In Vivo* Fate of Liposomes after Subconjunctival Ocular Delivery. *J. Control. Release* 329, 162–174. doi:10.1016/j.jconrel.2020.11.053

Chen, H., Gan, X., Li, Y., Gu, J., Liu, Y., Deng, Y., et al. (2020). NLRP12- and NLRC4-Mediated Corneal Epithelial Pyroptosis Is Driven by GSDMD Cleavage Accompanied by IL-33 Processing in Dry Eye. *Ocul. Surf.* 18 (4), 783–794. doi:10.1016/j.jtos.2020.07.001

Chen, Y., Chauhan, S. K., Lee, H. S., Stevenson, W., Schaumburg, C. S., Sadrai, Z., et al. (2013). Effect of Desiccating Environmental Stress versus Systemic Muscarinic AChR Blockade on Dry Eye Immunopathogenesis. *Invest. Ophthalmol. Vis. Sci.* 54 (4), 2457–2464. doi:10.1167/iovs.12-11121

Chen, Y., and Dana, R. (2021). Autoimmunity in Dry Eye Disease - an Updated Review of Evidence on Effector and Memory Th17 Cells in Disease Pathogenicity. *Autoimmun. Rev.* 20, 102933. doi:10.1016/j.autrev.2021.102933

Chhonker, Y. S., Prasad, Y. D., Chandasana, H., Vishvkarma, A., Mitra, K., Shukla, P. K., et al. (2015). Amphotericin-B Entrapped Lecithin/Chitosan Nanoparticles for Prolonged Ocular Application. *Int. J. Biol. Macromol.* 72, 1451–1458. doi:10.1016/j.ijbiomac.2014.10.014

Craig, J. P., Nelson, J. D., Azar, D. T., Belmonte, C., Bron, A. J., Chauhan, S. K., et al. (2017). TFOS DEWS II Report Executive Summary. *Ocul. Surf.* 15 (4), 802–812. doi:10.1016/j.jtos.2017.08.003

Dai, Y., Zhou, R., Liu, L., Lu, Y., Qi, J., and Wu, W. (2013). Liposomes Containing Bile Salts as Novel Ocular Delivery Systems for Tacrolimus (FK506): *In Vitro* Characterization and Improved Corneal Permeation. *Int. J. Nanomedicine* 8, 1921–1933. doi:10.2147/IJN.S44487

Dave, R. S., Goostrey, T. C., Ziolkowska, M., Czerny-Holownia, S., Hoare, T., and Sheardown, H. (2021). Ocular Drug Delivery to the Anterior Segment Using Nanocarriers: A Mucoadhesive/mucopenetrative Perspective. *J. Controlled Release* 336, 71–88. doi:10.1016/j.jconrel.2021.06.011

Farhadi, F., Nayebzadeh, N., Badiee, A., Arabsalmani, M., Hatamipour, M., and Iranshahi, M. (2021). A Validated 1H-NMR Method for Quantitative Analysis of DOTAP Lipid in Nanoliposomes Containing Soluble Leishmania Antigen. *J. Pharm. Biomed. Anal.* 194, 113809. doi:10.1016/j.jpba.2020.113809

Firouzmand, H., Badiee, A., Khamesipour, A., Heravi Shargh, V., Alavizadeh, S. H., Abbasi, A., et al. (2013). Induction of Protection against Leishmaniasis in Susceptible BALB/c Mice Using Simple DOTAP Cationic Nanoliposomes Containing Soluble Leishmania Antigen (SLA). *Acta Trop.* 128 (3), 528–535. doi:10.1016/j.actatropica.2013.07.021

Gelfuso, G. M., Ferreira-Nunes, R., Dalmolin, L. F., Dos S Ré, A. C., Dos Santos, G. A., de Sá, F. A. P., et al. (2020). Iontophoresis Enhances Voriconazole Antifungal Potency and Corneal Penetration. *Int. J. Pharm.* 576, 118991. doi:10.1016/j.ijpharm.2019.118991

Han, H., Gao, Y., Chai, M., Zhang, X., Liu, S., Huang, Y., et al. (2020a). Biofilm Microenvironment Activated Supramolecular Nanoparticles for Enhanced Photodynamic Therapy of Bacterial Keratitis. *J. Control. Release* 327, 676–687. doi:10.1016/j.jconrel.2020.09.014

Han, H., Yin, Q., Tang, X., Yu, X., Gao, Q., Tang, Y., et al. (2020b). Development of Mucoadhesive Cationic Polypeptide Micelles for Sustained Cabozantinib Release and Inhibition of Corneal Neovascularization. *J. Mater. Chem. B* 8 (23), 5143–5154. doi:10.1039/d0tb00874e

Han, Y., Jiang, L., Shi, H., Xu, C., Liu, M., Li, Q., et al. (2022). Effectiveness of an Ocular Adhesive Polyhedral Oligomeric Silsesquioxane Hybrid Thermo-Responsive FK506 Hydrogel in a Murine Model of Dry Eye. *Bioact Mater.* 9, 77–91. doi:10.1016/j.bioactmat.2021.07.027

Huang, Y., Tao, Q., Hou, D., Hu, S., Tian, S., Chen, Y., et al. (2017). A Novel Ion-Exchange Carrier Based upon Liposome-Encapsulated Montmorillonite for Ophthalmic Delivery of Betaxolol Hydrochloride. *Int. J. Nanomedicine* 12, 1731–1745. doi:10.2147/ijn.S122747

Inokuchi, Y., Hironaka, K., Fujisawa, T., Tozuka, Y., Tsuruma, K., Shimazawa, M., et al. (2010). Physicochemical Properties Affecting Retinal Drug/Coumarin-6 Delivery from Nanocarrier Systems via Eyedrop Administration. *Invest. Ophthalmol. Vis. Sci.* 51 (6), 3162–3170. doi:10.1167/iovs.09-4697

Jain, P., Jaiswal, C. P., Mirza, M. A., Anwer, M. K., and Iqbal, Z. (2019). Preparation of Levofloxacin Loaded *In Situ* Gel for Sustained Ocular Delivery: *In Vitro* and *Ex Vivo* Evaluations. *Drug Dev. Ind. Pharm.* 46, 50–56. doi:10.1080/03639045.2019.1698598

Kayser, O., Lemke, A., and Hernández-Trejo, N. (2005). The Impact of Nanobiotechnology on the Development of New Drug Delivery Systems. *Curr. Pharm. Biotechnol.* 6 (1), 3–5. doi:10.2174/1389201053167158

Kim, S. T., Saha, K., Kim, C., and Rotello, V. M. (2013). The Role of Surface Functionality in Determining Nanoparticle Cytotoxicity. *Acc. Chem. Res.* 46 (3), 681–691. doi:10.1021/ar3000647

Kumar, V., and Kumar, A. (2014). Immunological Aspects of Corneal Transplant. *Immunol. Invest.* 43 (8), 888–901. doi:10.3109/08820139.2014.910024

Kumari, S., Dandamudi, M., Rani, S., Behaeghel, E., Behl, G., Kent, D., et al. (2021). Dexamethasone-Loaded Nanostructured Lipid Carriers for the Treatment of Dry Eye Disease. *Pharmaceutics* 13 (6), 905. doi:10.3390/pharmaceutics13060905

Landucci, E., Bonomolo, F., De Stefani, C., Mazzantini, C., Pellegrini-Giampietro, D. E., Bilia, A. R., et al. (2021). Preparation of Liposomal Formulations for Ocular Delivery of Thymoquinone: *In Vitro* Evaluation in HCEC-2 e HConEC Cells. *Pharmaceutics* 13 (12), 2093. doi:10.3390/pharmaceutics13122093

Li, Y. J., Luo, L. J., Harroun, S. G., Wei, S. C., Unnikrishnan, B., Chang, H. T., et al. (2019). Synergistically Dual-Functional Nano Eye-Drops for Simultaneous Anti-inflammatory and Anti-oxidative Treatment of Dry Eye Disease. *Nanoscale* 11 (12), 5580–5594. doi:10.1039/c9nr00376b

Lin, H.-Y., Wang, S.-W., Mao, J.-Y., Chang, H.-T., Harroun, S. G., Lin, H.-J., et al. (2021). Carbonized Nanogels for Simultaneous Antibacterial and Antioxidant Treatment of Bacterial Keratitis. *Chem. Eng. J.* 411, 128469. doi:10.1016/j.cej.2021.128469

Lin, S., Ge, C., Wang, D., Xie, Q., Wu, B., Wang, J., et al. (2019). Overcoming the Anatomical and Physiological Barriers in Topical Eye Surface Medication Using a Peptide-Decorated Polymeric Micelle. *ACS Appl. Mater. Inter.* 11 (43), 39603–39612. doi:10.1021/acsami.9b13851

López-Cano, J. J., González-Cela-Casamayor, M. A., Andrés-Guerrero, V., Herrero-Vanrell, R., and Molina-Martínez, I. T. (2021). Liposomes as Vehicles for Topical Ophthalmic Drug Delivery and Ocular Surface Protection. *Expert Opin. Drug Deliv.* 18 (7), 819–847. doi:10.1080/17425247.2021.1872542

Lum, E., Corbett, M. C., and Murphy, P. J. (2019). Corneal Sensitivity after Ocular Surgery. *Eye Contact Lens.* 45 (4), 226–237. doi:10.1097/ICL.0000000000000543

Luo, L. J., Nguyen, D. D., and Lai, J. Y. (2021). Harnessing the Tunable Cavity of Nanoceria for Enhancing Y-27632-Mediated Alleviation of Ocular Hypertension. *Theranostics* 11 (11), 5447–5463. doi:10.7150/thno.54525

Meloni, M., Balzaretti, S., and Ceriotti, L. (2019). Medical Devices Biocompatibility Assessment on HCE: Evidences of Delayed Cytotoxicity of Preserved Compared to Preservative Free Eye Drops. *Regul. Toxicol. Pharmacol.* 106, 81–89. doi:10.1016/j.yrtph.2019.04.022

Meloni, M., Pauly, A., Servi, B. D., Varlet, B. L., and Baudouin, C. (2010). Occludin Gene Expression as an Early *In Vitro* Sign for Mild Eye Irritation Assessment. *Toxicol. Vitro* 24 (1), 276–285. doi:10.1016/j.tiv.2009.08.016

Nguyen, D. D., and Lai, J.-Y. (2020). Advancing the Stimuli Response of Polymer-Based Drug Delivery Systems for Ocular Disease Treatment. *Polym. Chem.* 11 (44), 6988–7008. doi:10.1039/d0py00919a

Nikpoor, A. R., Jaafari, M. R., Zamani, P., Teymouri, M., Gouklani, H., Saburi, E., et al. (2019). Cell Cytotoxicity, Immunostimulatory and Antitumor Effects of Lipid Content of Liposomal Delivery Platforms in Cancer Immunotherapies. A Comprehensive *In-Vivo* and *In-Vitro* Study. *Int. J. Pharm.* 567, 118492. doi:10.1016/j.ijpharm.2019.118492

Okahara, A., and Kawazu, K. (2013). Local Toxicity of Benzalkonium Chloride in Ophthalmic Solutions Following Repeated Applications. *J. Toxicol. Sci.* 38 (4), 531–537. doi:10.2131/jts.38.531

Onwosi, C. O., and Odibo, F. J. (2012). Effects of Carbon and Nitrogen Sources on Rhamnolipid Biosurfactant Production by Pseudomonas Nitroreducens Isolated from Soil. *World J. Microbiol. Biotechnol.* 28 (3), 937–942. doi:10.1007/s11274-011-0891-3

Perez-Garmendia, R., Lopez de Eguileta Rodriguez, A., Ramos-Martinez, I., Zuñiga, N. M., Gonzalez-Salinas, R., Quiroz-Mercado, H., et al. (2020). Interplay between Oxidative Stress, Inflammation, and Amyloidosis in the Anterior Segment of the Eye; its Pathological Implications. *Oxid Med. Cel Longev* 2020, 6286105. doi:10.1155/2020/6286105

Rusnak, F., and Mertz, P. (2000). Calcineurin: Form and Function. *Physiol. Rev.* 80 (4), 1483–1521. doi:10.1152/physrev.2000.80.4.1483

Saengkrit, N., Saesoo, S., Srinuanchai, W., Phunpee, S., and Ruktanonchai, U. R. (2014). Influence of Curcumin-Loaded Cationic Liposome on Anticancer Activity for Cervical Cancer Therapy. *Colloids Surf. B: Biointerfaces* 114, 349–356. doi:10.1016/j.colsurfb.2013.10.005

Sasaki, H., Karasawa, K., Hironaka, K., Tahara, K., Tozuka, Y., and Takeuchi, H. (2013). Retinal Drug Delivery Using Eyedrop Preparations of Poly-L-Lysine-Modified Liposomes. *Eur. J. Pharm. Biopharm.* 83 (3), 364–369. doi:10.1016/j.ejpb.2012.10.014

Schäfer, J., Höbel, S., Bakowsky, U., and Aigner, A. (2010). Liposome-polyethylenimine Complexes for Enhanced DNA and siRNA Delivery. *Biomaterials* 31 (26), 6892–6900. doi:10.1016/j.biomaterials.2010.05.043

Siegl, C., König-Schuster, M., Nakowitsch, S., Koller, C., Graf, P., Unger-Manhart, N., et al. (2019). Pharmacokinetics of Topically Applied Tacrolimus Dissolved in Marinosolv, A Novel Aqueous Eye Drop Formulation. *Eur. J. Pharm. Biopharm.* 134, 88–95. doi:10.1016/j.ejpb.2018.11.015

Stapleton, F., Alves, M., Bunya, V. Y., Jalbert, I., Lekhanont, K., Malet, F., et al. (2017). TFOS DEWS II Epidemiology Report. *Ocul. Surf.* 15 (3), 334–365. doi:10.1016/j.jtos.2017.05.003

Steffes, V. M., Murali, M. M., Park, Y., Fletcher, B. J., Ewert, K. K., and Safinya, C. R. (2017). Distinct Solubility and Cytotoxicity Regimes of Paclitaxel-Loaded Cationic Liposomes at Low and High Drug Content Revealed by Kinetic Phase Behavior and Cancer Cell Viability Studies. *Biomaterials* 145, 242–255. doi:10.1016/j.biomaterials.2017.08.026

Takikawa, M., Fujisawa, M., Yoshino, K., and Takeoka, S. (2020). Intracellular Distribution of Lipids and Encapsulated Model Drugs from Cationic Liposomes

with Different Uptake Pathways. *Int. J. Nanomedicine* 15, 8401–8409. doi:10.2147/ijn.S267638

Tan, G., Li, J., Song, Y., Yu, Y., Liu, D., and Pan, W. (2019). Phenylboronic Acid-Tethered Chondroitin Sulfate-Based Mucoadhesive Nanostructured Lipid Carriers for the Treatment of Dry Eye Syndrome. *Acta Biomater.* 99, 350–362. doi:10.1016/j.actbio.2019.08.035

Tong, L., Matsuura, E., Takahashi, M., Nagano, T., and Kawazu, K. (2019). Effects of Anti-glaucoma Prostaglandin Ophthalmic Solutions on Cultured Human Corneal Epithelial Cells. *Curr. Eye Res.* 44 (8), 856–862. doi:10.1080/02713683.2019.1597127

Tsao, Y. T., Wu, W. C., Chen, K. J., Yeh, L. K., Hwang, Y. S., Hsueh, Y. J., et al. (2021). Analysis of Aqueous Humor Total Antioxidant Capacity and its Correlation with Corneal Endothelial Health. *Bioeng. Transl Med.* 6 (2), e10199. doi:10.1002/btm2.10199

Valim, V., Trevisani, V. F., de Sousa, J. M., Vilela, V. S., and Belfort, R. (2015). Current Approach to Dry Eye Disease. *Clin. Rev. Allergy Immunol.* 49 (3), 288–297. doi:10.1007/s12016-014-8438-7

Wang, K., Jiang, L., Zhong, Y., Zhang, Y., Yin, Q., Li, S., et al. (2021). Ferrostatin-1-loaded Liposome for Treatment of Corneal Alkali Burn via Targeting Ferroptosis. *Bioeng. Transl Med.*

Wei, Y., and Asbell, P. A. (2014). The Core Mechanism of Dry Eye Disease Is Inflammation. *Eye Contact Lens* 40 (4), 248–256. doi:10.1097/icl.0000000000000042

Weng, Y. H., Ma, X. W., Che, J., Li, C., Liu, J., Chen, S. Z., et al. (2018). Nanomicelle-Assisted Targeted Ocular Delivery with Enhanced Antiinflammatory Efficacy *In Vivo*. *Adv. Sci. (Weinh)* 5 (1), 1700455. doi:10.1002/advs.201700455

Wolffsohn, J. S., Arita, R., Chalmers, R., Djalilian, A., Dogru, M., Dumbleton, K., et al. (2017). TFOS DEWS II Diagnostic Methodology Report. *Ocul. Surf.* 15 (3), 539–574. doi:10.1016/j.jtos.2017.05.001

Workshop, S. o. t. I. D. E. (2007). The Definition and Classification of Dry Eye Disease: Report of the Definition and Classification Subcommittee of the International Dry Eye WorkShop (2007). *Ocul. Surf.* 5 (2), 75–92. doi:10.1016/s1542-0124(12)70081-2

Wu, D., Zhao, Z., Kim, J., Razmi, A., Wang, L. L. W., Kapate, N., et al. (2021). Gemcitabine and Doxorubicin in Immunostimulatory Monophosphoryl Lipid A Liposomes for Treating Breast Cancer. *Bioeng. Transl Med.* 6 (1), e10188. doi:10.1002/btm2.10188

Yuan, J., Zhai, J. J., Huang, X., Zhou, S. Y., and Chen, J. Q. (2012). Ocular Safety and Pharmacokinetics Study of FK506 Suspension Eye Drops after Corneal Transplantation. *J. Ocul. Pharmacol. Ther.* 28 (2), 153–158. doi:10.1089/jop.2011.0108

Yuan, X., Marcano, D. C., Shin, C. S., Hua, X., Isenhart, L. C., Pflugfelder, S. C., et al. (2015). Ocular Drug Delivery Nanowafer with Enhanced Therapeutic Efficacy. *ACS nano* 9 (2), 1749–1758. doi:10.1021/nn506599f

Zhan, C., Santamaria, C. M., Wang, W., McAlvin, J. B., and Kohane, D. S. (2018). Long-acting Liposomal Corneal Anesthetics. *Biomaterials* 181, 372–377. doi:10.1016/j.biomaterials.2018.07.054

Zhang, X. L., Taylor, D. J., Thomas, R. K., and Penfold, J. (2011). Adsorption of Polyelectrolyte/surfactant Mixtures at the Air-Water Interface: Modified Poly(ethyleneimine) and Sodium Dodecyl Sulfate. *Langmuir* 27 (6), 2601–2612. doi:10.1021/la104698w

Zhong, Y., Wang, K., Zhang, Y., Yin, Q., Li, S., Wang, J., et al. (2021). Ocular Wnt/β-Catenin Pathway Inhibitor XAV939-Loaded Liposomes for Treating Alkali-Burned Corneal Wound and Neovascularization. *Front. Bioeng. Biotechnol.* 9, 753879. doi:10.3389/fbioe.2021.753879

Conflict of Interest: The authors declare that the research was conducted in the absence of any commercial or financial relationships that could be construed as a potential conflict of interest.

Publisher's Note: All claims expressed in this article are solely those of the authors and do not necessarily represent those of their affiliated organizations, or those of the publisher, the editors, and the reviewers. Any product that may be evaluated in this article, or claim that may be made by its manufacturer, is not guaranteed or endorsed by the publisher.

frontiers in Pharmacology

ORIGINAL RESEARCH
published: 14 March 2022
doi: 10.3389/fphar.2022.855294

Design and Characterization of Paclitaxel-Loaded Polymeric Nanoparticles Decorated With Trastuzumab for the Effective Treatment of Breast Cancer

Mirina Sakhi[1], Abad Khan[1], Zafar Iqbal[2], Ismail Khan[1], Abida Raza[3], Asmat Ullah[1], Fazli Nasir[2] and Saeed Ahmad Khan[4]**

[1]Department of Pharmacy, University of Swabi, Swabi, Pakistan, [2]Department of Pharmacy, University of Peshawar, Peshawar, Pakistan, [3]National Institute of LASER and Optronics, Nilore, Pakistan, [4]Department of Pharmacy, Kohat University of Science and Technology, Kohat, Pakistan

OPEN ACCESS

Edited by:
Muhammad Afzal,
Jouf University, Saudi Arabia

Reviewed by:
Donatella Paolino,
University of Catanzaro, Italy
Emine Guven,
Düzce University, Turkey

***Correspondence:**
Abad Khan
drabadkhan@uoswabi.edu.pk
Saeed Ahmad Khan
saeedkhanphd@gmail.com

Specialty section:
This article was submitted to Experimental Pharmacology and Drug Discovery, a section of the journal Frontiers in Pharmacology

Received: *15 January 2022*
Accepted: *25 February 2022*
Published: *14 March 2022*

Citation:
Sakhi M, Khan A, Iqbal Z, Khan I, Raza A, Ullah A, Nasir F and Khan SA (2022) Design and Characterization of Paclitaxel-Loaded Polymeric Nanoparticles Decorated With Trastuzumab for the Effective Treatment of Breast Cancer. Front. Pharmacol. 13:855294. doi: 10.3389/fphar.2022.855294

The aim of the study was to design and formulate an antibody-mediated targeted, biodegradable polymeric drug delivery system releasing drug in a controlled manner to achieve a therapeutic goal for the effective treatment of breast cancer. Antibody-mediated paclitaxel-loaded PLGA polymeric nanoformulations were prepared by the solvent evaporation method using different experimental parameters and compatibility studies. The optimized formulations were selected for *in vitro* and *in vivo* evaluation and cytotoxicity studies. The *in vitro* drug release studies show a biphasic release pattern for the paclitaxel-loaded PLGA nanoparticles showing a burst release for 24 h followed by an extended release for 14 days; however, a more controlled and sustained release was observed for antibody-conjugated polymeric nanoparticles. The cytotoxicity of reference drug and paclitaxel-loaded PLGA nanoparticles with and without antibody was determined by performing MTT assay against MCF-7 cells. Rabbits were used as experimental animals for the assessment of various *in vivo* pharmacokinetic parameters of selected formulations. The pharmacokinetic parameters such as C_{max} (1.18–1.33 folds), $AUC_{0\text{-}t}$ (39.38–46.55 folds), MRT (10.04–12.79 folds), $t_{1/2}$ (3.06–4.6 folds), and V_d (6.96–8.38 folds) have been increased significantly while clearance (4.34–4.61 folds) has been decreased significantly for the selected nanoformulations as compared to commercially available paclitaxel formulation (Paclixil®). The surface conjugation of nanoparticles with trastuzumab resulted in an increase in *in vitro* cytotoxicity as compared to plain nanoformulations and commercially available conventional brand (Paclixil®). The developed PLGA-paclitaxel nanoformulations conjugated with trastuzumab have the desired physiochemical characteristics, surface morphology, sustained release kinetics, and enhanced targeting.

Keywords: biodegradable, polymeric, drug-delivery, breast cancer, paclitaxel, cytotoxicity, trastuzumab, PLGA

1 INTRODUCTION

Cancer is a disease in which genes regulating the functions of cells, i.e., cell growth, division, differentiation, and cell death losses are without any control (Liotta et al., 1991). Cancer is developing very rapidly in the whole world, especially in the developing countries. In women, among all the cancers diagnosed, breast cancer accounts for one-third (Miele et al., 2009), and 18.2% of deaths are caused by breast cancer worldwide. Breast cancer receptors are divided into two main types, i.e., estrogen receptor (ER) negative and human epidermal growth factor receptors (HER2) positive (Carey et al., 2006). Breast cancer is treated nowadays by different ways, i.e., hormone-blocking agents, chemotherapy, radiotherapy, monoclonal antibodies, and surgery (Waks & Winer, 2019).

Main problems with concventional drug delivery systems are fluctuations of drug concentrations in blood which in turn causes subtherapeutic concentration or toxic effects. Lack of specificity, multidrug resistance, toxicity of chemotherapeutic agents, side effects, limited aqueous solubility, and poor bioavailability are some of the limitations with available cancer therapy (Chidambaram et al., 2011). The major target of any drug delivery system and particularly controlled drug delivery system is to make the therapeutically effective amount of drug available at a desired site, at an optimum concentration, and for a desired period of time (Win, 2006).

Nanotechnology is gaining much popularity as mortality due to cancer continues to rise, and the advanced nanotechnology has provided an effective approach for targeting the drug to tumor tissues by overcoming the limitations that are associated with conventional chemotherapeutic agents (Ferlay et al., 2015). Nanotechnology has shown a new path for the development of various organic and inorganic drug carriers called as nanoparticles.

Biodegradable polymers are the first choice in nanoparticulate drug delivery because they not only release drugs in a controlled manner but are also compatible with tissues and cells (Fonseca et al., 2002). In the last 10–20 years, the polymeric biodegradable nanoparticle drug delivery has got a lot of importance in cancer treatments. Among these polymers, one of the biodegradable polymers used most successfully is poly lactic co glycolic acid (PLGA) which upon hydrolysis is metabolized to lactic and glycolic acid and excreted quickly (Kumari et al., 2010). PLGA has been approved by the Food and Drug Administration (FDA) for parenteral administrations due to its biodegradability and biocompatibility. It can be easily formulated with a variety of hydrophilic or hydrophobic molecules, and it imparts some extra properties to the drug molecules, i.e., protect drug from degradation effects, control the release, and can also modify the surface in order to interact with other biological materials and to achieve stealth or targeted delivery of nanoparticles (Danhier et al., 2012).

Poloxamer 407 is a cationic, tri-block copolymer containing polyethylene oxide (hydrophilic portion) and poly propylene oxide (hydrophobic portion). The hydrophobic end is anchored with the nanoparticle surface, while the water loving portion is toward the aqueous medium forming a hydrophilic layer (Redhead et al., 2001; Stolnik et al., 2001). It is amphiphilic in nature with bioadhesive properties and increases solubilization of hydrophobic drugs. Poloxamer 407 has been approved by the FDA as a bioactive ingredient for topical, ophthalmic, suspension, injectable, and other pharmaceutical preparations (Dumortier et al., 2006). Nanoparticles, whose surfaces have been modified with poloxamer 407 remain in blood circulation for a prolonged period of time, escapes the reticuloendothelial system (Stolnik et al., 2001). Poloxamer 407 increases drug accumulation inside tumor tissue by inhibiting the efflux transport protein system. This provides steric stabilization by inhibiting phagocytosis and prevention of protein adsorption (Moura et al., 2020). Poloxamer 407 enhances bioavailability by increasing drug residence time (Moghimi & Hunter, 2000). New therapeutic strategies can be developed using poloxamer because of its temperature-dependent self-assembly characteristic. It can be used for increasing the stability and solubility of drugs (Carvalho et al., 2021).

The HER family of receptors are of prime importance in the pathogenesis of several cancers by regulating the cell differentiation, growth, and survival through multiple pathways (Romond et al., 2005). This family of receptors is made up of four main members: HER (1, 2, 3, and 4) or Erb (B1, B2, B3, and B4). All four HERs consist of an intracellular and extracellular binding site (Sun et al., 2011b; Iqbal & Iqbal, 2014). Monoclonal antibodies are clones of a unique parent cell and recognize specific antigens that are located on the cancer cell surface, thereby causing an antigen–antibody-like effect through multiple mechanisms which include ligand–receptor binding interference or protein expression suppression (Steichen et al., 2013). Improved clinical efficacy and decreased toxicity associated with conventional anticancer drugs attributed to the significant use of monoclonal antibodies (Colzani et al., 2018). Trastuzumab, a humanized monoclonal antibody approved by the US-FDA for breast cancer, targets overexpressed HER2 receptors in breast cancer cells. Combination therapy of trastuzumab with conventional chemotherapeutics leads to increased response rates in comparison to trastuzumab alone (Piccart-Gebhart et al., 2005; P.; Yousefpour et al., 2011). The combination therapy of this antibody is of prime importance, especially with drugs of taxanes family since both the therapeutic response and survival rate are increased (Sun et al., 2008).

The study is designed for the formulation of paclitaxel-loaded PLGA nanoparticles conjugated with trastuzumab for the effective treatment of breast cancer. Physiochemical characterization, *in vitro* drug release, pharmacokinetic evaluation, and *in vitro* cytotoxicity studies were carried out. The proposed formulations were found safe and effective for the targeting of breast cancer. The developed nanoformulations have the advantage of using polymeric stabilizers which have the potential to improve solubility and enhance stability and bioavailability with no issue of hypersensitivity reactions and are also blocking the pgp efflux transport protein system. The drug delivery in nano-size and surface decoration with the antibody is a unique combination which will not only prevent

the particles from being entrapped by the reticuloendothelial systems but also help in accumulation of drug in tumor tissues through EPR (enhanced permeability and retention) effect. So, the therapeutic effectiveness of this drug delivery will be very much improved, and the toxic effects will be minimized. The use of PLGA grade (75:25) results in a more sustained release which has not been used previously with surface conjugation of antibody. Although surface functionalization of paclitaxel nanoparticles has been carried out previously by albumin, polyethylene glycol, and folate, the promising results were obtained in this work in terms of size, stability, drug release profile, *in vitro* cytotoxicity, and pharmacokinetic parameters.

2 MATERIALS AND METHODS

2.1 Materials

Paclitaxel (≥99.9% purity) was purchased from Qilu Antibiotic Pharmaceutical Co Ltd China. Poly lactic acid co-glycolic acid (75:25, Resomer® RG 756 H, MW 76000–115000 Da) from Evonik Germany, trastuzumab from Roche Pharmaceuticals United Kingdom, poloxamer 407 and sodium lauryl sulfate (SLS) from Sigma-Aldrich Germany, disodium hydrogen phosphate (Na_2HPO_4), dialysis tubing-Dia 27/32"-21.5 mm 30 M MWCO ~12,000–14,000 Da from Sigma-Aldrich Germany, acetonitrile (purity ≥ 99.9%), and other solvents used were of HPLC grade. The water used for solvent preparation was ultrapure.

2.2 Preformulation Studies

2.2.1 Preparation of the Sample

The physical mixtures of drug (paclitaxel) and polymer were prepared (1:1 w/w) with different excipients such as poloxamer (0.5, 1, 1.5, and 2%) and SLS (0.5%). The samples were prepared by simple mixing of drug, polymer, and excipients. The samples were stored for 1 month at 40° ± 2°C and 75 ± 5% RH (Peça et al., 2012). These physical samples were analyzed by FTIR for drug, polymer, and excipients preformulation compatibilities in comparison with nanoformulations.

2.2.2 Compatibility Studies

The interactions between drug (paclitaxel), polymer, and excipients were carried out by preparing binary mixtures. Drug content, physical consistency, and FTIR spectra were examined at each sampling point for any possible drug–excipient incompatibility. The physical interactions among the excipients, drug, and polymer were observed by noting changes in physical consistency.

2.2.3 Determination of the Drug Content Using a UV–Visible Spectrophotometer

The samples containing excipients, excipients and drug, and excipients and polymer were stored under stress conditions and analyzed for determination of the drug content. Samples and standard solutions were dissolved in acetonitrile (ACN) for analysis. The drug content was measured in triplicate.

2.2.4 Fourier Transform Infrared Spectroscopy

An FTIR spectrophotometer was used to analyze the samples for incompatibilities. The samples were prepared by the potassium bromide (KBr) pellet method. Dried potassium bromide was mixed with 1% w/w of the sample and grounded for 3–5 min. The sample was pulverized and converted to a compact mass by compression. The samples were analyzed in the region of 400–4,000 cm^{-1}.

2.3 Formulation of Plain and Antibody-Conjugated Nanoformulations

Paclitaxel-loaded polymeric nanoparticles were prepared using PLGA as a polymer, poloxamer 407, and sodium lauryl sulfate (SLS) as a stabilizer utilizing the solvent evaporation method (**Table 1**). PLGA concentration was kept constant (10 mg), while poloxamer 407, SLS, and drug were used in varying concentrations. The developed nanoformulations were characterized for their physicochemical properties [size, polydispersity index (PDI), and zeta potential], drug loading, % entrapment efficiency, and stability. The optimized nanoformulations were then decorated with trastuzumab.

A total of two (2 ml) reconstituted freeze-dried nanoparticles were incubated with trastuzumab at room temperature overnight for surface decoration of antibody on the nanoparticle surface. All the selected paclitaxel nanoformulations were negatively charged, whereas trastuzumab was positively charged (8.457 mV) which resulted in electrostatic attraction between oppositely charged species and trastuzumab. The antibody was easily coated on the surface of paclitaxel-loaded PLGA nanoformulations. The trastuzumab-modified paclitaxel-loaded PLGA nanoparticles were purified by centrifugation at 6,000 rpm at −4°C for 2 min, and 50 µl of trastuzumab (10 mg/ml) was reconstituted with PBS to make up the final volume up to 1 ml (500 µg/ml).

2.4 Physicochemical Characterization

2.4.1 Dynamic Light Scattering

The formulations were evaluated for size, polydispersity index (PDI), and zeta potential by dynamic light scattering (DLS, at 90° angle and 25°C) using a zetasizer (ZS-90, Malvern Instruments and Malvern, United Kingdom). The surface charge can be determined through zeta potential, i.e., the movements of charged particles in an electric field to predict the stability of colloids. The sample (0.5 ml) of nanoformulation and 1 ml of distilled water were taken, sonicated for 2 min, and placed in cuvettes. An average of three reported values was taken using Malvern software and analyzed statistically (Marsalek, 2014).

2.4.2 Drug Loading and Encapsulation Efficiency

Drug loading efficiency (%, w/w) and drug encapsulation efficiency (%, w/w) of paclitaxel in nanoformulations were determined by centrifugation (15,000 rpm at 25°C for 30 min), followed by UV spectroscopy at 235 nm. The absorbance of the samples was measured, and the % drug loading and %

TABLE 1 | Formulation of paclitaxel with PLGA, 0.05% SLS, and 0.5, 1, 1.5, and 2% poloxamer 407.

S.No	Code	Paclitaxel (mg)	PLGA (mg)	Poloxamer 407	SLS 0.05% (ml)	Time (min)	Temp	Sonication speed (%)
01	PTX 100	1 mg	10 mg	0.5% 5 ml	5 ml	4 min	25°C	99
02	PTX 101	2 mg	10 mg	0.5% 5 ml	5 ml	4 min	25°C	99
03	PTX 102	3 mg	10 mg	0.5% 5 ml	5 ml	4 min	25°C	99
04	PTX 103	4 mg	10 mg	0.5% 5 ml	5 ml	4 min	25°C	99
05	PTX 104	1 mg	10 mg	1% 5 ml	5 ml	4 min	25°C	99
06	PTX 105	2 mg	10 mg	1% 5 ml	5 ml	4 min	25°C	99
07	PTX 106	3 mg	10 mg	1% 5 ml	5 ml	4 min	25°C	99
08	PTX 107	4 mg	10 mg	1% 5 ml	5 ml	4 min	25°C	99
09	PTX 108	1 mg	10 mg	1.5% 5 ml	5 ml	4 min	25°C	99
10	PTX 109	2 mg	10 mg	1.5% 5 ml	5 ml	4 min	25°C	99
11	PTX 110	3 mg	10 mg	1.5% 5 ml	5 ml	4 min	25°C	99
12	PTX 111	4 mg	10 mg	1.5% 5 ml	5 ml	4 min	25°C	99
13	PTX 112	1 mg	10 mg	2% 5 ml	5 ml	4 min	25°C	99
14	PTX 113	2 mg	10 mg	2% 5 ml	5 ml	4 min	25°C	99
15	PTX 114	3 mg	10 mg	2% 5 ml	5 ml	4 min	25°C	99
16	PTX 115	4 mg	10 mg	2% 5 ml	5 ml	4 min	25°C	99

encapsulation were determined by the following formulae (Huang et al., 2007):

$$\% \text{ DL} = \frac{\text{Weight of Drug in Nanoparticles}}{\text{Weight of Nanoparticles}} \times 100; \quad (1)$$

$$\% \text{ EE} = \frac{\text{Weight of Drug in Nanoparticles}}{\text{Weight of Drug Feed}} \times 100. \quad (2)$$

2.4.3 Scanning Electron Microscopy

The morphology of the sample was determined by SEM. The sample was prepared for SEM as per standard protocol in order to make it conducive. The sample was then analyzed for its morphology.

2.4.4 X-Ray Diffraction Study

An X-Ray diffractometer (JDX-3532, Jeol, Japan) was used to carry out XRD patterns of paclitaxel, PLGA, Poloxamer 407, SLS, and paclitaxel nanoformulations. The XRD pattern was determined for its amorphous, semicrystalline, and crystalline nature. The pattern was taken at 3°–40° (2θ).

2.5 SDS-PAGE Analysis

After conjugation of antibody on the nanoparticle surface, the structural integrity of trastuzumab on the nanoparticle surface was compared with the native antibody by SDS-PAGE analysis. All the gels were run under reducing conditions using a Mini-PROTEAN® Electrophoresis system (BIO-RAD, United States). It is a technique based on specificity of binding between protein of interest and a probe to allow detection of protein of interest. The protein sample is separated and subjected to a SDS polyacrylamide gel. The sample is transferred electrophoretically from a gel to PVDF membrane. The remaining membrane is blocked by adding a 5% neutral protein (BSA or milk casein) overnight. The membrane is incubated with the primary antibody that is specific to the target protein for 2 h at room temperature. The band containing protein of interest will bind with the antibody. The membrane is then washed to remove the unbound antibody and incubated with the second radioactively labeled antibody for 1 h that binds specifically to the primary antibody–antigen complex which can be visualized on an autoradiograph. The bond will appear dark on the film (Pavlova et al., 2018).

TABLE 2 | Result of the drug–excipients compatibility study.

Time	Test	Sample 01	Sample 02	Sample 03	Sample 04	Sample 05	Sample 06	Sample 07	Sample 08	Sample 09
Day 01	FTIR spectra	Complies	Complies	Complies	Complies	Complies	Complies	Complies	Complies	Complies
	Physical consistency	〃	〃	〃	〃	〃	〃	〃	〃	〃
Day 30	FTIR spectra	〃	〃	〃	〃	〃	〃	〃	〃	〃
	Physical consistency	〃	〃	〃	〃	〃	〃	〃	〃	〃

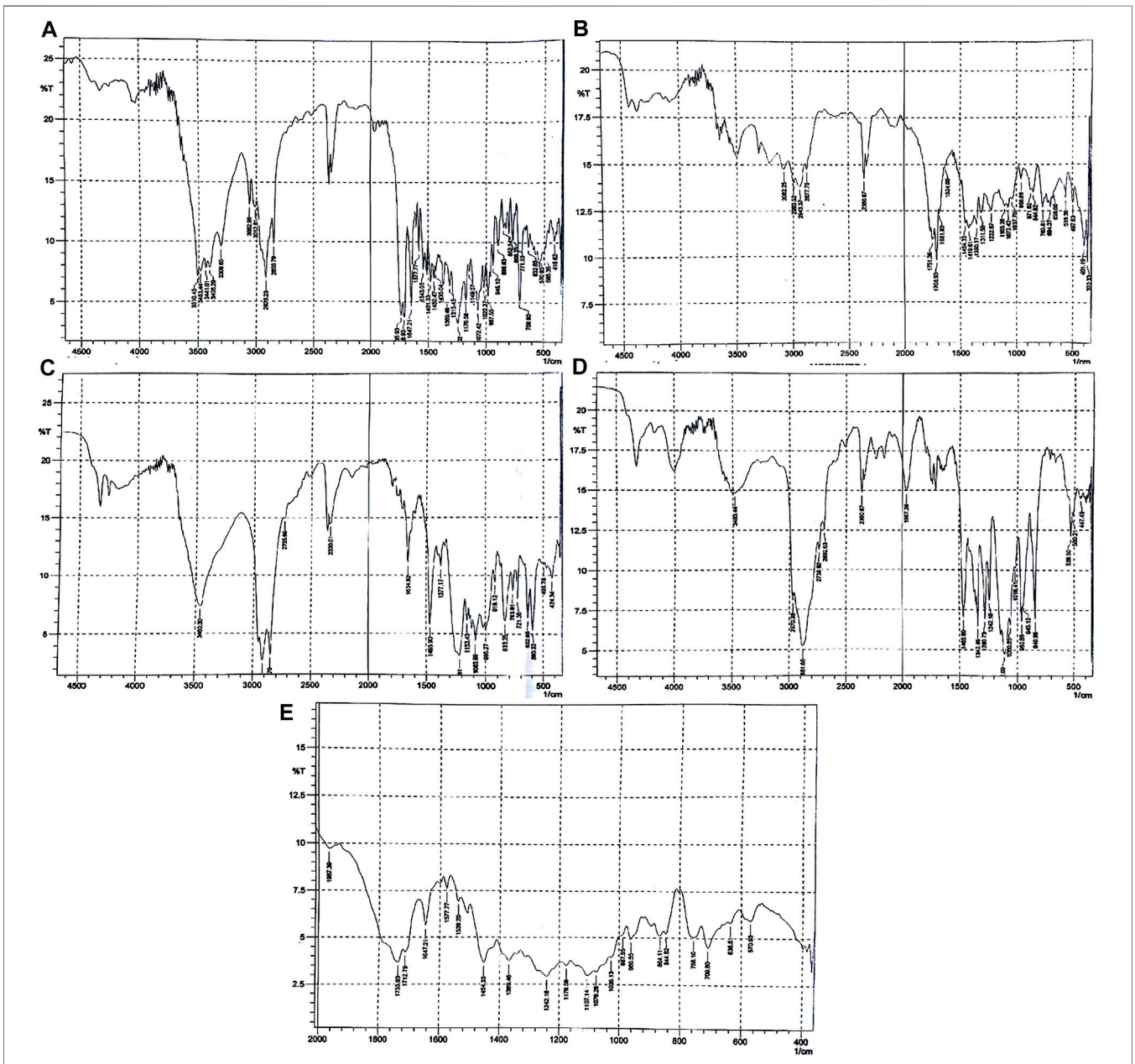

FIGURE 1 | FTIR spectra of **(A)** paclitaxel, **(B)** PLGA, **(C)** SLS, **(D)** poloxamer 407, and **(E)** nanoformulation.

TABLE 3 | Result of drug content determination.

Drug content (%)					
Time	**Standard drug**	**Sample 06**	**Sample 07**	**Sample 08**	**Sample 09**
Day 01	99.13	99.09	98.99	99.11	99.54
Day 15	99.27	99.03	99.19	99.63	98.17
Day 30	99.63	99.12	97.79	99.07	99.83

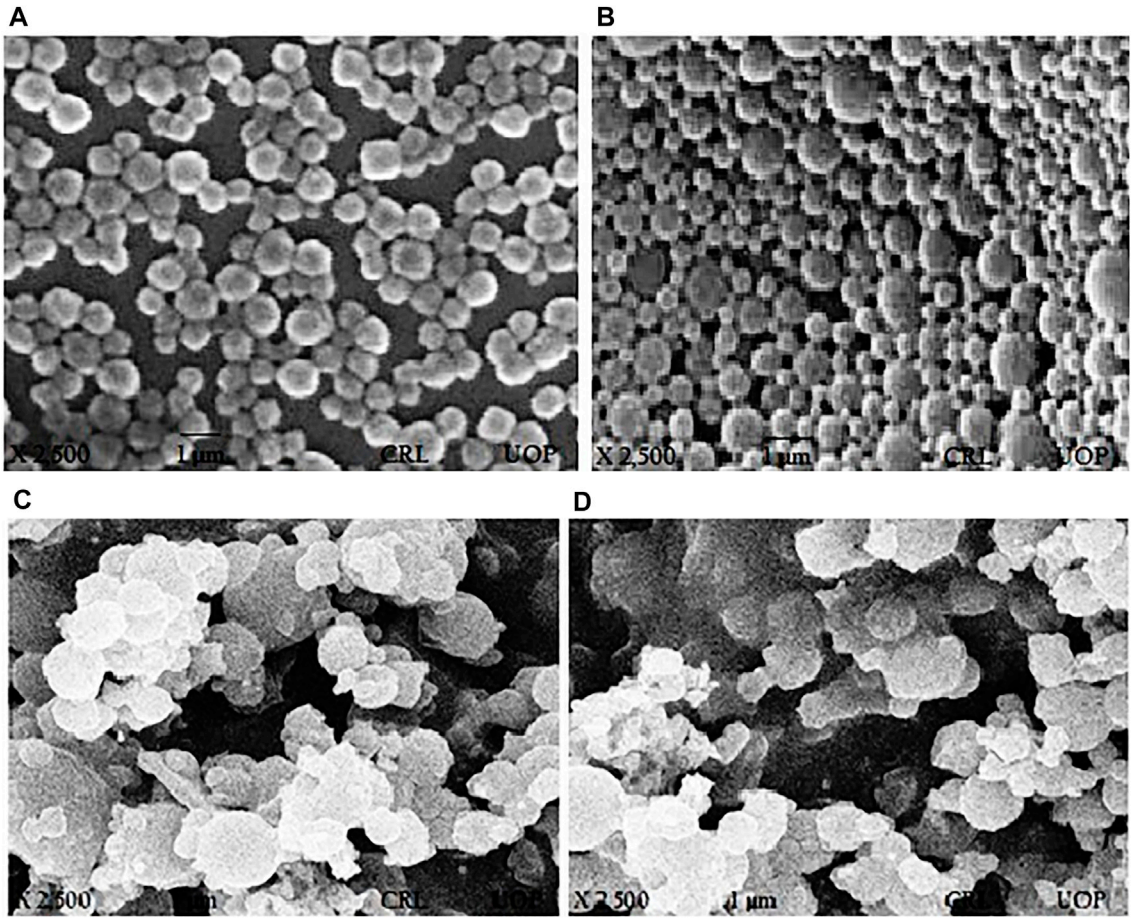

FIGURE 2 | SEM images of paclitaxel-loaded PLGA nanoformulations with poloxamer 407. **(A)** PTX 108, **(B)** PTX 112, **(C)** PTX 108ab, and **(D)** PTX 112ab.

2.6 *In Vitro* Evaluation

2.6.1 Drug Release Studies

The dialysis diffusion method was applied for release studies. The membrane having a molecular weight 12,000–14,000 Da was cut in such a way that it can accommodate 2 ml redispersed nanoformulations sealed at both ends. It was then dialyzed against 100 ml of PBS (pH 7.4) in a shaking water bath at 37°C and 60 rpm. At specified time intervals (0.5, 1, 1.5, 2, 3, 4, 5, 6, 7, 8, 10, 12, 24, 36, 48, 72, and 96 h), 2 ml sample was withdrawn and analyzed for drug release. An equal volume of dialyzing media was replaced for each sample. The drug content was determined by using a UV spectrophotometer at 235 nm in each sample. The analysis was conducted in triplicate (Bernkop-Schnürch & Jalil, 2018).

2.6.2 Drug Release Kinetics

The drug release mechanisms were evaluated by applying various release kinetic models (Paarakh et al., 2018).

2.6.3 *In Vitro* Cytotoxicity

In Vitro cytotoxicity assay of paclitaxel-loaded polymeric nanoparticles and paclitaxel-loaded polymeric nanoparticles conjugated with trastuzumab antibody and Taxol® was conducted by MTT [yellow tetrazolium salt, 3-(4, 5-dimethylthizol-2-yl)-2, 5, 5-diphenyl tetrazolium bromide] assay using MCF-7 breast cancer cell lines, a widely studied epithelial cancer cell line that has characteristics of differentiated mammary epithelium derived from breast adenocarcinoma (Lee et al., 2015). MCF-7 cell lines of breast

TABLE 4 | Formulation of paclitaxel with PLGA, 0.05% SLS, and poloxamer 407.

No.	Drug: PLGA (mg)	Poloxamer 407 (%)	Size (nm)	PDI	Zeta potential (mv)	(%) Encapsulation efficiency	(%)Drug loading
PTX 100	1:10	0.5	180 ± 1.22	0.11 ± 0.01	−22.1 ± 1.5	64	6.4
PTX 101	2:10	0.5	184.6 ± 1.03	0.13 ± 0.01	−20.1 ± 1.1	45	9.0
PTX 102	3:10	0.5	190 ± 3.48	0.13 ± 0.03	−20.7 ± 1.8	61	18.3
PTX 103	4:10	0.5	202 ± 36.17	0.3 ± 0.01	−19.1 ± 1.5	53	21.2
PTX 104	1:10	1	199 ± 21.80	0.4 ± 0.01	−26.85 ± 0.03	77	7.7
PTX 105	2:10	1	215 ± 18.72	0.6 ± 0.01	−24.1 ± 0.15	65	0.13
PTX 106	3:10	1	304 ± 12.99	0.6 ± 0.04	−26.8 ± 0.23	65	19.5
PTX 107	4:10	1	224 ± 26.98	0.8 ± 0.02	−23.08 ± 0.1	63	25.2
PTX 108	1:10	1.5	202.3 ± 14.5	0.17 ± 0.03	−35.2 ± 0.12	89	8.9
PTX 109	2:10	1.5	215 ± 28.3	0.2 ± 0.03	−34.5 ± 0.03	71	14.2
PTX 110	3:10	1.5	300 ± 17.1	0.19 ± 0.02	−30.25 ± 0.25	65	19.5
PTX 111	4:10	1.5	331 ± 22.5	0.3 ± 0.01	−29.75 ± 0.11	57	22.8
PTX 112	1:10	2	229 ± 13.24	0.2 ± 0.01	−40.4 ± 1.6	84	8.4
PTX 113	2:10	2	312 ± 12.41	0.3 ± 0.02	−39.08 ± 0.6	69	13.8
PTX 114	3:10	2	351 ± 10.49	0.3 ± 0.03	−34.21 ± 1.7	68	20.4
PTX 115	4:10	2	408 ± 11.27	0.7 ± 0.02	−28.11 ± 0.7	47	18.8

TABLE 5 | Particle size, PDI, and zeta potential of nanoformulations before and after surface modification.

Unconjugated nanoformulations					Conjugated nanoformulations				
No.	Size (nm)	PDI	ZP (mv)	EE (%)	No.	Size (nm)	PDI	ZP (mv)	EE (%)
PTX 108	202.3 ± 14.5	0.17 ± 0.03	−35.2 ± 0.12	89%	PTX 108ab	223 ± 11.08	0.42 ± 0.04	−25.7 ± 1.4	88%
PTX 112	229 ± 13.24	0.2 ± 0.01	−40.4 ± 1.6	84%	PTX 112 ab	256 ± 13.52	0.32 ± 0.01	−26.5 ± 0.1	84%

adenocarcinoma show moderate overexpression of HER^{+2} and serve as an excellent model for *in vitro* cytotoxic studies (Dhiman et al., 2004). Its hormone sensitivity through expression of estrogen receptor makes it an ideal model for *in vivo* and *in vitro* studies (Holliday & Speirs, 2011). The cells were seeded in a 96-well plate at a density of 1.0×10^4 cells/well and incubated for 24 h at 37°C in 5% CO_2 at an 85% humidity incubator (Model NU 5700; United States). The medium was replaced after 24 h by paclitaxel-loaded polymeric nanoparticles and paclitaxel-loaded polymeric nanoparticles conjugated with trastuzumab and Taxol® at concentrations ranging from 0.25 μg/ml to 50 μg/ml for 24, 48, and 72 h at 37°C. At specific intervals, the formulations were removed, and 5 mg/ml MTT was added before incubation for 4 h at 37°C. The culture solution was aspirated, and the resulting formazan crystals were dissolved in 100 μl of dimethyl sulfoxide, and the absorbance was measured at 570 nm using a microplate reader (Model FL ×800; Biotek, Winooski, VA, United States). Cytotoxicity was expressed as percentage of cell viability compared to untreated control cells.

$$\% \text{ Viability} = \frac{\text{Absorbance of sample}}{\text{Absorbance of control}} \times 100. \quad (3)$$

2.7 *In Vivo* Evaluation

2.7.1 Pharmacokinetic Studies

The New Zealand rabbits weighing 1.5–2.0 kg were purchased from the NIH (National Institute of Health), for *in vivo* pharmacokinetics. The design and study was approved by the Ethical Committee of Pharmacy Department, University of Swabi (Pharm/EC/002). The rabbits were given access to water and food. The animals were excluded by killing/using chloroform anesthesia during the study in case of any distress. The dose at the rate of 2 mg/kg body weight was injected into the marginal ear vein of rabbits, which were divided into two groups for the paclitaxel test and reference formulations. At designated time intervals (10 min, 30 min and 1, 2, 4, 6, 8, 12, 24, 96, and 120 h), blood samples were collected in EDTA tubes and centrifuged at 8,000 rpm for 10 min at 4°C. The Eppendorf tubes were used to collect and store samples at −20°C till analysis. HPLC-UV was used for the analysis of samples.

Various pharmacokinetic parameters such as peak plasma concentration (C_{max}), time of peak plasma concentration (T_{max}), elimination rate constant (K_{el}), elimination half-life ($t_{1/2}$), area under the plasma concentration-versus-time curve ($AUC_{0-\infty}$), clearance (Cl), steady state volume (V_{ss}), and mean residence time (MRT) were determined using PK-Summit® software.

2.7.2 Statistical Analysis

For the quantification of paclitaxel in samples, mean (X), SD, and %RSD were applied. Comparison between means of treatments was made at $p \leq 0.05$ using the Student *t* test.

3 RESULTS

3.1 Preformulation Studies

3.1.1 Drug–Excipients Compatibility Study

The samples were prepared using binary mixtures of the drug, polymer, and excipients (1:1), stored for 01 months under stress

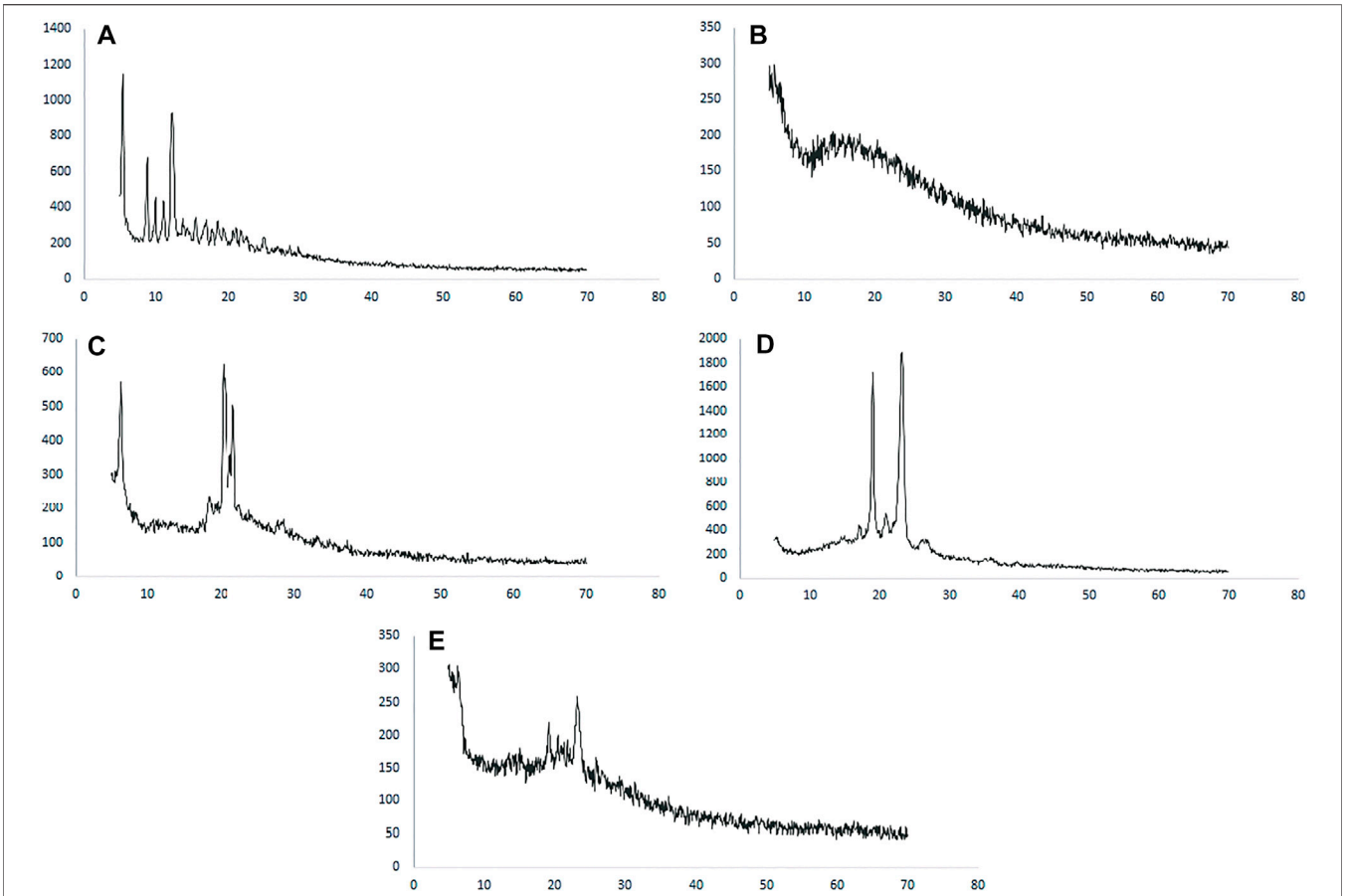

FIGURE 3 | XRD spectra of **(A)** paclitaxel, **(B)** PLGA, **(C)** SLS, **(D)** poloxamer 407, and **(E)** nanoformulation.

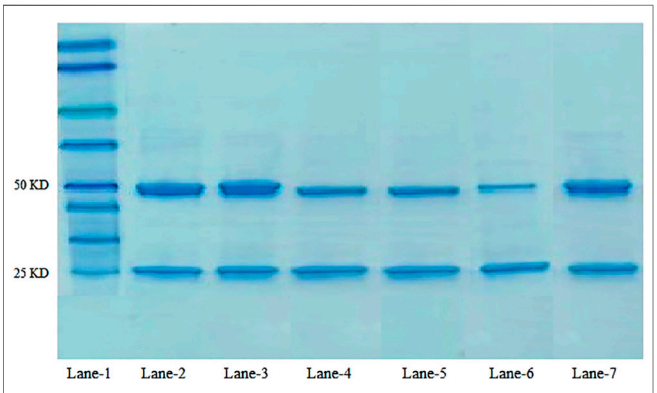

FIGURE 4 | SDS-PAGE of the antibody: lane-1: molecular weight marker; lane 2-3: native antibody trastuzumab; lane-6: PTX 108ab; and lane-7: PTX 112ab.

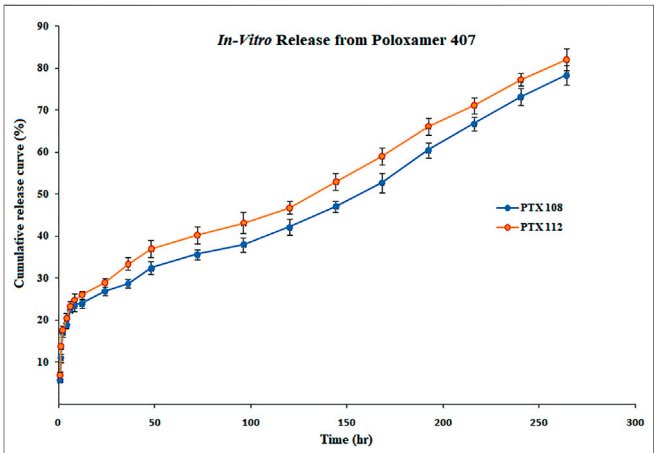

FIGURE 5 | *In vitro* release profile of paclitaxel from nanoformulations of poloxamer 407.

conditions, and inspected visually for any change in color and texture. The drug, polymer, and excipients compatibility study was performed by FTIR at day 1 and 30. The results of FTIR are shown in **Table 2** and **Figure 1**. The concentration of the standard drug and samples at day 1, 15, and 30 were evaluated as given in **Table 3**.

As shown in **Figure 1A**, the FTIR spectra of paclitaxel show characteristic peaks at 3,441 cm^{-1} (for O-H stretching), 3,309 cm^{-1} (for N-H stretching), aromatic C-H at 2,920–2,850 cm^{-1}, peaks at 1708 cm^{-1} for C = O stretching vibration of the ester group, peak at

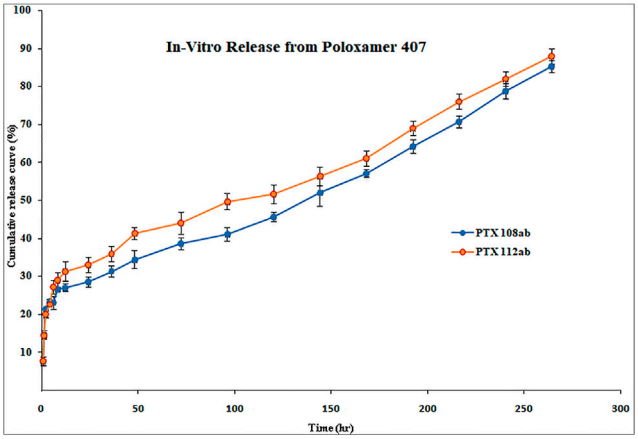

FIGURE 6 | *In vitro* release of Paclitaxel from surface-modified nanoformulations of poloxamer 407.

1,647 cm^{-1} for the amide bond, and peaks at 1,254 cm^{-1} for C-N stretching. The FTIR spectra of PLGA (75:25) showed distinct peaks at 3,200 cm^{-1} for -OH stretching, 2,943 cm^{-1} for -CH stretching, 1751 cm^{-1} for carbonyl –C = O stretching, and at 1,072 cm^{-1} for C-O stretching as given in **Figure 2B**. The FTIR spectra of poloxamer 407 showed characteristic peaks at 1,111 cm^{-1} and 1,060 cm^{-1} distinguishing of its PEO group and at 2,881 cm^{-1} for CH_2-CH_2 stretching as shown in **Figure 1C**. The FTIR spectra of SLS showed characteristic peaks at 1,219–1,153 cm^{-1} for S-O stretching and at 2,850 cm^{-1} for -CH stretching as shown in **Figure 1D**.

The characteristic peaks of paclitaxel was not present in the FTIR spectrum which means that the drug is completely encapsulated by the polymer, but the main peaks for PLGA, poloxamer 407, and SLS remain the same indicating the absence of any interaction between the drug, polymer, and stabilizers used as shown in **Figure 1E**.

3.2 Physicochemical Characterization

PTX 108 and PTX 112 were selected for conjugation of the antibody on the basis of particle size, polydispersity index, surface charge, zeta potential, and encapsulation efficiency. The physicochemical properties of the developed nanoformulations before and after antibody conjugation were determined.

TABLE 6 | *In vitro* drug release kinetics of the optimized nanoformulations. Bold values are drug release from nanoformulations best fits to Higuchi model.

Formulation	1st-order	Zero-order	Higuchi	Hixon–Crowell	Korsemeyer–Peppas	n*
	R^2	R^2	R^2	R^2	R^2	
PTX 108	0.181	0.8842	**0.9726**	0.8847	0.114	0.5
PTX 112	0.1935	0.8639	**0.9911**	0.8644	0.124	0.5
PTX 108ab	0.3741	0.8588	**0.9919**	0.9222	0.6226	0.5
PTX 112 ab	0.3701	0.8424	**0.9777**	0.9213	0.636	0.5

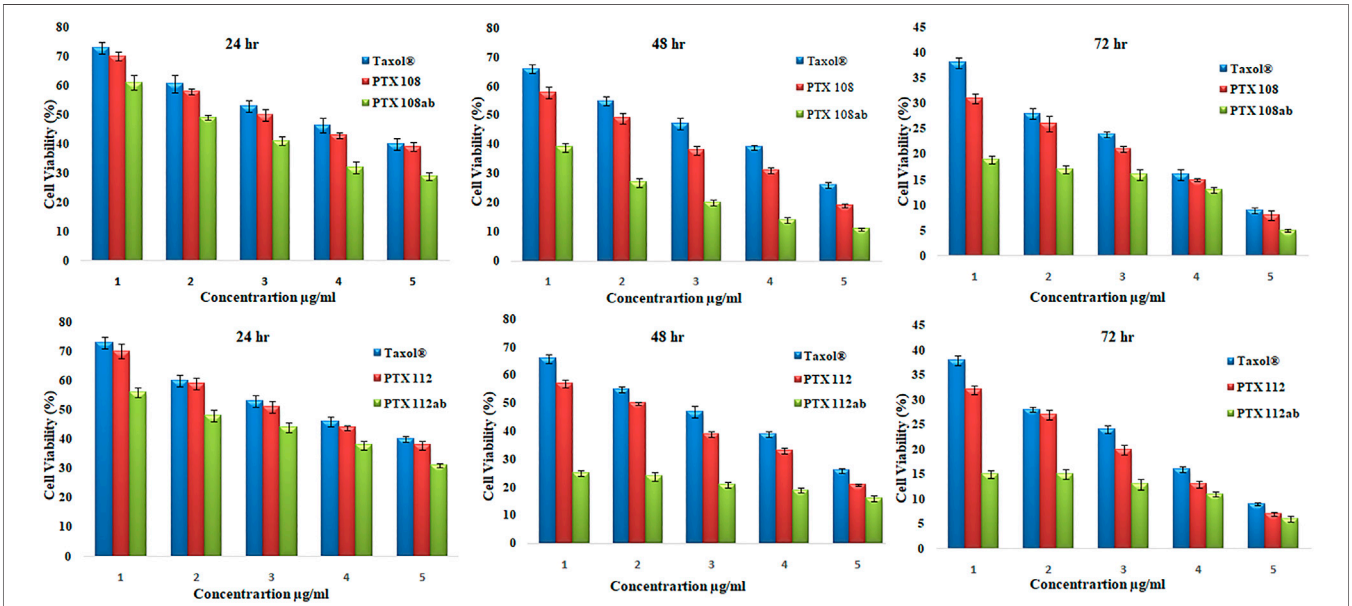

FIGURE 7 | Cell viability (%) of MCF-7 cell lines by Paclixil®, paclitaxel-loaded PLGA nanoformulations PTX 108 and PTX 112, and antibody-conjugated paclitaxel-loaded PLGA nanoformulations PTX 108ab and PTX 112ab at 0.25, 2.5, 10, 25, and 50 µg/ml concentration after 24, 42, and 72 h.

TABLE 7 | Pharmacokinetic parameters. The *p*-values are made bold as it shows the significance of results.

Parameter	C_{max}	AUC_{0-t}	$AUMC_{\infty}$	MRT	$t_{½}$	V_d	CL
	μgml^{-1}	$\mu ghrml^{-1}$	$mghr^2ml^{-1}$	Hr	Hr	ml	$mlh^{-1}kg^{-1}$
Paclixil®	3.05 ± 0.78	4.8 ± 0.035	27.2 ± 1.27	5.7 ± 0.14	7.9 ± 0.06	9.4 ± 1.14	7.37 ± 0.5
PTX 108	3.75 ± 0.09	194.9 ± 1.04	12433.1 ± 214.1	63.8 ± 1.61	31.2 ± 2.17	65.4 ± 1.98	1.7 ± 1.21
p-value	—	—	—	**0.001*****	**0.001*****	**0.003*****	**0.001*****
PTX 112	3.75 ± 0.87	189.4 ± 2.97	10840.2 ± 411.7	57.2 ± 1.16	24.2 ± 3.35	74.5 ± 1.74	1.7 ± 0.69
p-value	—	—	—	**0.001*****	**0.002*****	**0.001*****	**0.001*****

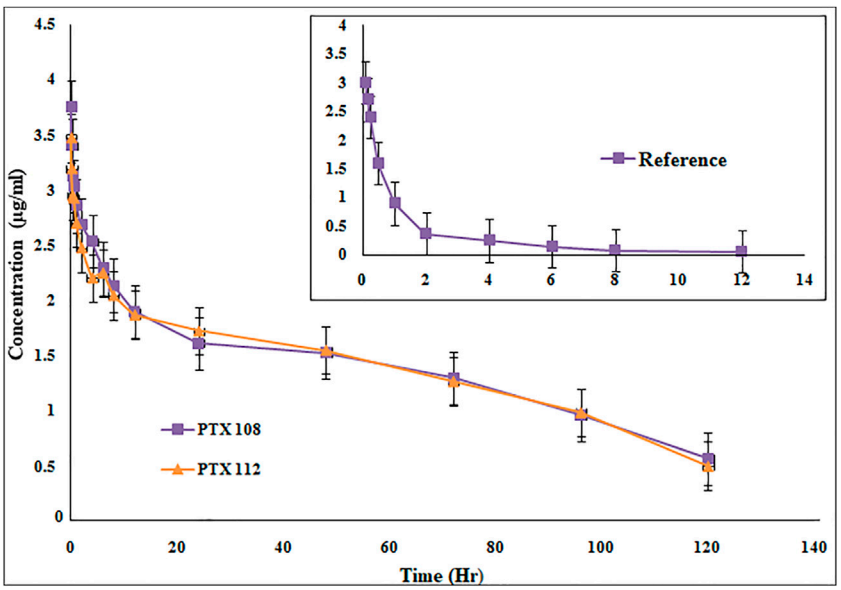

FIGURE 8 | Plasma concentration versus time profile of paclitaxel nanoformulations with poloxamer 407 and SLS.

3.2.1 Particle Size, PDI, Zeta Potential, and Encapsulation Efficiency

The particle size was within the range of 180 ± 1.22 to 202 ± 36.17 nm for 0.5%, 199 ± 21.80 to 224 ± 26.98 nm for 1%, 202.3 ± 14.5 to 224 ± 26.98 nm for 1.5%, and 229 ± 13.24 to 408 ± 11.27 nm for 2% poloxamer 407. The particle size, PDI, zeta potential, and drug loading and encapsulation efficiency of paclitaxel nanoparticles are given in **Table 4**. The physicochemical properties and encapsulation efficiency of paclitaxel nanoparticles with or without antibody conjugation are given in **Table 5**.

3.2.2 Surface Morphology

SEM was used for determining surface morphology of simple paclitaxel nanoparticles and conjugated paclitaxel nanoparticles as shown in **Figures 2A,B** and **Figures 2C,D**, respectively.

3.2.3 XRD Studies

The XRD patterns of paclitaxel, PLGA, Poloxamer 407, SLS, and paclitaxel nanoformulations are shown in **Figure 3A**, in which paclitaxel exhibits several peaks at 2θ value of 5.4°, 8.8°, and 12.25° which shows the crystalline nature of paclitaxel, while no peaks were observed for PLGA which depicts the amorphous nature of the polymer as shown in **Figure 3B**. The diffractogram of SLS shows two distinct peaks at 2θ value of 20.3° and 21.65° demonstrating the crystalline nature of SLS (**Figure 3C**), while poloxamer 407 exhibits peaks in the 2θ range at 19.05° and 23.2° as shown in **Figure 3D**). The XRD pattern of paclitaxel-loaded PLGA nanoformulations exhibits no discrete peaks at any position (**Figure 3E**).

3.3 SDS-PAGE Studies

The structural integrity of trastuzumab after conjugation of the antibody on the nanoparticle surface was confirmed. Under reducing conditions, trastuzumab is detected as two bands of molecular weight 50 KDa and 25 KDa representing heavy and light chains, respectively (Mohamed et al., 2018). An SDS-gel (10%) was ran under reducing conditions as follows: molecular weight marker in lane-1, native antibody in lane-2 and 3, and antibody-conjugated nanoformulations PTX 84ab, PTX 86ab, PTX 108ab, and PTX 112ab in lanes 4,5,6, and 7, respectively, as shown in **Figure 4**.

3.4 *In Vitro* Evaluation

3.4.1 Drug Release Studies

The *in vitro* release profile of paclitaxel nanoformulations and surface-modified nanoformulations was determined. At specified

time intervals (0.5, 1, 2, 4, 6, 8, 10, 12, 24, 36, 48, 72, 96, 120, 144, 168, 192, 216, 240, and 264 h), the samples were withdrawn and analyzed for drug release. All the paclitaxel-loaded PLGA nanoformulations and surface-modified nanoformulations exhibit a bi-phasic release pattern as shown in **Figures 5**, **6**, respectively, which is characterized by an initial burst release in first 24 h followed by a continuous slow release. The initial burst release of paclitaxel from nanoformulations at 24 h was 26 ± 0.23 and 28 ± 0.42% for PTX 108 and PTX 112, while at 264 h drug release was 79 ± 0.09 and 81 ± 0.43% for PTX 108 and PTX 112, respectively. Similarly the initial burst release of paclitaxel from modified nanoformulations at 24 h was 30 ± 0.28 and 33 ± 0.03% for PTX 108ab and PTX 112 ab, while at 264 h, the drug release was 85 ± 0.34 and 88 ± 0.14% for PTX 108 ab and PTX 112 ab, respectively.

3.4.2 *In Vitro* Drug Release Kinetics

Various kinetic models were employed for prediction of drug release mechanisms that include zero-order, first-order, Hixson–Crowell, Korsmeyer–Peppas, and Higuchi. The regression coefficient values (R^2) obtained and the drug release from PTX 108, PTX 112, PTX 108ab, and PTX 112 ab nanoformulations best fit to the Higuchi model on the basis of higher regression. coefficient (R^2) values as shown in **Table 6**.

3.4.3 *In Vitro* Cytotoxicity Studies

The cytotoxicity of the reference drug and paclitaxel-loaded PLGA nanoparticles with and without antibody surface modification was evaluated by performing MTT assay against MCF-7 cells. The MCF-7 cell lines were incubated with Paclixil®, paclitaxel-loaded PLGA nanoformulations PTX 112, and antibody-conjugated paclitaxel-loaded PLGA nanoformulations PTX 108ab and PTX 112 ab at 0.25, 2.5, 10, 25, and 50 μg/ml concentration. The cultured cells were analyzed for cell viability at 24, 48, and 72 h. Cytotoxicity as % of cell viability compared to untreated control cells is shown in **Figure 7**.

3.5 *In Vivo* Evaluation

3.5.1 Pharmacokinetic Studies

Rabbits weighing between 1.5 and 2 kg were used as an experimental model for the assessment of various *in vivo* pharmacokinetic parameters of the selected paclitaxel nanoformulations. Selected paclitaxel and its commercially available paclitaxel formulation Paclixil® (reference formulation) were administered (2 mg/kg body weight) *via* the marginal ear vein. For *in vivo* evaluation of selected and commercially available paclitaxel formulation Paclixil®, the developed RP-HPLC-UV method was successfully applied (Sakhi et al., 2021). The data were evaluated by non-compartmental analysis using PK-Summit®. The results are given in **Table 7** and **Figure 8**.

4 DISCUSSION

4.1 Preformulation Studies

4.1.1 Drug–Excipients Compatibility Study

The stabilizers used for preparing nanoformulations may interact with each other and other active pharmaceutical ingredients which may affect the stability of nanoparticles. Due to change in temperature and humidity, the physical and chemical changes in the dosage form are occurred which can affect stability, biocompatibility, and therapeutic properties of the drug (Chadha & Bhandari, 2014; Patel, et al., 2015). In order to avoid these possible interactions, the drug, polymer, and excipients compatibility study was performed, and the samples were evaluated for drug content, physical consistency, and FTIR spectra. Drug concentration in a dosage form may decrease due to degradation of the drug when stored under stress conditions. Physical and chemical incompatibilities may be triggered by humidity and temperature. The drug contents in the dosage form remained the same throughout the stored period. The IR spectra show no changes in samples at day 1 while showing chemical interaction between drug, polymer, and other drug excipients used in nanoformulations after 30 days (Martins et al., 2014). The FTIR spectrum of the paclitaxel-loaded PLGA nanoparticle showed no characteristic peaks of paclitaxel which means that the drug is completely encapsulated by the polymer, but the main peaks for PLGA, poloxamer 407, and SLS remain same, thus indicating the absence of any interaction between the drug, polymer, and stabilizers used. After visual inspection of samples, no changes in color or physical consistency were noted which indicates the compatibility of drugs and active ingredients with each other.

4.2 Physicochemical Characterization

PTX 108 and PTX 112 were selected for having small particle size, high negative zeta potential, and encapsulation efficiency greater than 80% and monodispersed particles. These formulations were further evaluated. The physicochemical properties of nanoformulations before and after antibody conjugation were compared.

4.2.1 Particle Size, PDI, Zeta Potential, and Encapsulation Efficiency

The particle size and PDI change with change in concentration of the stabilizer and amount of the drug in nanoparticle formulations, whereas polymer concentration is kept constant. The size of the nanoparticles increases as the concentration of poloxamer 407 is increased, and there is an increase in PDI with change in stabilizer concentration. Present studies show that the mean particle size increases as the concentration of the stabilizer is increased (Pradhan et al., 2013). This increase in the nanoparticle size is due to excessive adsorption of poloxamer 407 on the nanoparticle surface which results in formation of a thick layer (Redhead et al., 2001). As the stabilizer concentration is increased, viscosity of the aqueous phase increases which results in an increase in particle size by decreasing the net shear stress (Pradhan et al., 2013). As the drug concentration is increased from 1 to 4 mg, there is an increase in the nanoparticle size. This increase in particle size is due to the fact that only a specified amount of the drug can be encapsulated by a constant concentration of the polymer. Any further increase in drug concentration will result in an increase in particle size, thus increasing viscosity of the organic phase (Mu & Feng, 2003;

Pradhan et al., 2013). The results show that after the attachment of trastuzumab on the nanoparticle surface there is an increase in size and polydispersity of nanoparticles.

Paclitaxel-loaded polymeric nanoformulations prepared by using poloxamer 407 (0.5, 1, 1.5, and 2%) and SLS (0.05%) show a negative charge, and the zeta potential values decrease as the concentration of the drug is increased from 1 to 4 mg. This decrease in zeta potential is due to an increase in concentration of the drug-to-polymer ratio in the organic phase (Stolnik et al., 2001; Moura et al., 2020). The negative zeta potential was due to the ester and termination group of PLGA chains on the nanoparticle surface (Mu & Feng, 2003) and due to the presence of the anionic surfactant, SLS. As the concentration of poloxamer 407 is increased, there is an increase in zeta potential values. There is an increase in zeta potential values ranging from −19.1 ± 1.5 to −40.4 ± 1.6 mV as the poloxamer 407 concentration is increased from 0.5 to 2% (Redhead et al., 2001; Reddy & Murthy, 2005). High negative potential provides stability as there will be an increase in electrostatic repulsive forces among the nanoparticles which will prevent particle aggregation. The results indicated that the surface charge was shifted to less negative after conjugation of the antibody on the nanoparticle surface due to the positive charge of trastuzumab (Sun et al., 2011a; Sun et al., 2008; P.; Yousefpour et al., 2011).

There is an increase in encapsulation efficiency as the concentration of poloxamer 407 is increased from 0.5 to 2% while keeping PLGA and SLS concentrations constant (**Table 4**). There is an increase in encapsulation efficiency as the initial concentration of the drug is increased, as more drug molecules are available to interact with the polymer resulting in an increase in encapsulation efficiency. However any further increase in the drug amount will result in saturation of the polymer, leading to a decrease in encapsulation efficiency (Keum et al., 2011; Pradhan et al., 2013). In this work, nanoformulations having encapsulation efficiencies greater than 80% were selected for surface modification which resulted in an increase in size; however, no significant change in encapsulation efficiency was observed with conjugation of the antibody as shown in **Table 5**.

Surface morphology of nanoparticles determines the circulation time, biodistribution, targeted delivery, and enhanced tumor accumulation as well as cellular uptake of nanoparticles (Truong et al., 2015). The surface of nanoparticles using poloxamer 407 was spherical in shape. After the conjugation of the antibody, the surface of nanoparticles becomes blurry which is due to attachment of the antibody on the surface of nanoparticles and adhesion of nanoparticles (Yousefpour et al., 2011; Mehata et al., 2019).

The XRD pattern of paclitaxel-loaded PLGA nanoformulations exhibits no discrete peaks at any position, so it can be concluded that paclitaxel was completely encapsulated by the polymer and transformed to an amorphous state (Chowdhury et al., 2019; de Oliveira Fortes et al., 2012; Wei et al., 2009).

4.3 SDS-PAGE Analysis

The structural integrity of trastuzumab on the nanoparticle surface was compared with the native antibody by SDS-PAGE analysis. As trastuzumab is a protein, when subjected to any type of stress such as preparation process, packaging materials, heating, and agitation, the major response of the monoclonal antibody is aggregation which can result in immunogenic reactions, loss of significant therapeutic activity, denaturation, or inactivation (M Pabari et al., 2013; Mohamed et al., 2018). From the results, it can be observed that trastuzumab shows same behavior after conjugation on the nanoparticle surface as the native antibody which confirms that the integrity of trastuzumab remains the same, and there is no evidence of reduced protein as shown in bands. This validates the feasibility of antibody-decorated paclitaxel nanoparticles for targeting HER^{2+}-overexpressed cancer cells.

4.4 *In Vitro* Evaluation

All the paclitaxel-loaded PLGA nanoformulations with and without antibody conjugation exhibit a bi-phasic release pattern, which is characterized by an initial burst release in first 24 h followed by a continuous slow release. This slow release is due to the slow degradation of PLGA because the release of paclitaxel from nanoparticles mainly depends on drug diffusion and matrix erosion. The drug that is poorly entrapped/adsorbed on the polymeric matrix results in initial fast release, while the diffusion mechanism is responsible for the slow release of the drug that is localized in the polymeric core of nanoparticles (Fonseca et al., 2002; Pradhan et al., 2013).

It was observed that the drug release from PTX 108, PTX 112, PTX 108ab, and PTX 112 ab nanoformulations best fits to the Higuchi model on the basis of higher regression. coefficient (R^2) values. The "n" value primarily shows the mechanism of drug release from the polymeric matrix, and it was measured at 60% release concentration. The most common release mechanism followed by these formulations is diffusion followed by erosion. The n value also showed that Fickian diffusion has taken place in the optimized formulations (Costa & Lobo, 2001).

The cytotoxicity studies, as given in **Figure 7**, shows viability of MCF-7 cells after incubation with Paclixil®, paclitaxel-loaded PLGA nanoformulations, and antibody-decorated paclitaxel-loaded PLGA nanoformulations at various concentrations after 24, 48, and 72 h. There is a more effective decrease in cell viability after 72 h than that after 24 and 48 h, which signifies that as the incubation period increases the cellular inhibition increases. The second column in each group in **Figure 7** shows viability of MCF-7 cells after treatment with unconjugated paclitaxel nanoformulations, and there is an increase in *in vitro* cytotoxicity as compared to paclitaxel solution. As the concentration of the drug is increased from 0.25 to 50 μg/ml, % viability decreases. The third column in each group shows cellular toxicity of antibody-conjugated paclitaxel-loaded PLGA nanoformulations. There is a significant decrease in % cell viability which indicates that antibody-functionalized nanoformulations are more effective therapeutically than paclitaxel and nanoformulations without antibody conjugation.

It can be depicted from our results that as the concentration of the drug and incubation time increase, cell viability decreases. The surface conjugation of nanoparticles results in an increase in *in vitro* cytotoxicity as compared to

nanoformulations without antibody conjugation and Paclixil®. Our results are in line with previous data available (Yousefpour et al., 2011; Butt et al., 2012).

4.5 *In Vivo* Evaluation

The C_{max}, AUC, AUMC, MRT, $t_{1/2}$, and V_d have been significantly increased, while Cl has been decreased (**Table 7** and **Figure 8**). The selected formulations were compared statistically with conventional paclitaxel formulation. The plasma concentrations of polymeric nanoformulations were 1.23-fold greater than those commercially available formulation (Guo et al., 2012). The results show 39.38–40.41-fold increase in AUC of polymeric-loaded paclitaxel nanoparticles than that of commercially available paclitaxel. The reported AUC of paclitaxel after administration to rats at a dose of 30 mg/kg were 80.06 ± 5.74 μg-hr/ml for paclitaxel self-microemulsion and 14.61 ± 2.16 μg-hr/ml for paclitaxel solution (Guo et al., 2012). The data suggest that at same concentration, nanoformulations remain in blood for a prolonged period of time and, hence, increase the therapeutic efficacy of the drug. As in nanoformulations, the drug is encapsulated within the hydrophobic polymer which results in sustained release and increase in bioavailability which attributes to an increase in AUC. The other reason of enhanced bioavailability may be due to a decrease in plasma protein binding of polymeric-loaded paclitaxel nanoformulations (Stage et al., 2018). The $AUMC_{\infty}$ values of polymeric nanoformulations were significantly greater than those of commercially available formulation.

The MRT of polymeric-loaded paclitaxel nanoparticles is 10.04–11.2-fold than that of the commercially available paclitaxel formulations**.** The reported MRT values of paclitaxel nanoparticles were much higher than that of the pure drug which is in accordance with our results. Polymeric-loaded paclitaxel nanoparticles significantly increase the MRT value by controlling the release of the drug. Drugs formulated in nanoparticles remain in blood circulation for prolonged time due to reduced uptake by the reticuloendothelial system (RES) (Fu et al., 2016). The $t_{1/2}$ of polymeric paclitaxel nanoparticles is 3.06–3.95-fold than that of the commercially available paclitaxel formulations. The V_d of polymeric-loaded paclitaxel nanoparticles has increased 6.96–7.93-fold than that of commercially available paclitaxel formulations. The V_d of paclitaxel liposome was 0.926 ± 0.057 L and paclitaxel injection was 0.827 ± 0.052 L after IV administration of 3 mg/kg body weight to rabbits (Y. Wei et al., 2014). (Xu et al., 2005). The clearance values of the polymeric nanoformulations decreased than those of the commercially available formulations as reported in the previous literature. The clearance values of paclitaxel liposome was 0.397 ± 0.022 L/h/kg and paclitaxel injection was 0.539 ± 0.038 L/h/kg after IV administration of 3 mg/kg body weight to rabbits (Y. Wei et al., 2014).

The drug eliminates quickly from the systemic circulation after IV administration of paclitaxel injection whereas paclitaxel nanoparticles have shown to improve the pharmacokinetic parameters. The small size of nanoparticles, decreased protein binding, and use of suitable stabilizers result in increased bioavailability of the drug. There is a significant change in pharmacokinetic parameters after encapsulation of paclitaxel in nanoparticles. Paclitaxel-loaded polymeric nanoformulations exhibit an increase in MRT and AUC, while blood clearance is decreased. As the drug remains in blood for a prolonged period of time with nanoparticles, the uptake by the reticuloendothelial system is reduced and uptake of the drug at the target site is enhanced, so improved therapeutic efficacy is achieved with nanoformulations. The use of PLGA grade (75:25) results in a more sustained release which has not been used previously with surface conjugation of the antibody. Although surface functionalization of paclitaxel nanoparticles has been carried out previously by albumin, polyethylene glycol, and folate, however, we got promising results in terms of size, stability, drug release profile, *in vitro* cytotoxicity, and pharmacokinetic parameters in comparison with the reported work (Singla et al., 2002; Nehate et al., 2014).

5 CONCLUSION

Sustained release of paclitaxel-loaded polymeric nanoparticles decorated with trastuzumab was developed using PLGA, SLS, and poloxamer 407 by the solvent evaporation method. The formulations were evaluated for its *in vitro* cellular cytotoxicity against HER^{2+} breast cancer cell lines. The optimized nanoparticles were of particle size less than 300 nm, having a negative charge, and encapsulation efficiency ˃80%. The selected optimized nanoformulations were conjugated with trastuzumab having the desired particle size, PDI, zeta potential, and encapsulation efficiency. SDS-PAGE analyses have shown no evidence of reduced protein, and integrity of trastuzumab remains the same. Scanning electron microscopy (SEM) results have shown that the surface of nanoparticles before antibody conjugation were smooth and spherical, while after the conjugation of the antibody, the surface became blurred which is due to attachment of the antibody on the surface of nanoparticles. The drug release from antibody-conjugated nanoparticles was rapid as compared to unconjugated nanoparticles due to rough surfaces of nanoparticles.

The pharmacokinetic parameters of paclitaxel-loaded polymeric nanoformulations exhibit an increase in MRT, AUC, $t_{1/2}$, and V_d, while Cl was decreased as compared to those of commercially available paclitaxel nanoformulation. The results of cytotoxicity studies have shown a significant decrease in cell viability as the drug concentration and incubation time increase. The surface conjugation of nanoparticles resulted in greater *in vitro* cytotoxicity than nanoformulations without antibody conjugation and conventional paclitaxel formulations.

DATA AVAILABILITY STATEMENT

The original contributions presented in the study are included in the article/Supplementary Materials, further inquiries can be directed to the corresponding authors.

ETHICS STATEMENT

The animal study was reviewed and approved by the Ethical Committee of Pharmacy Department, University of Swabi (Pharm/EC/002).

AUTHOR CONTRIBUTIONS

MS: experimental work and manuscript writing. AK, ZI, IK, AR, AU, FN, and SK: critical revision of the manuscript. All authors approved the final version of the manuscript to be published and agreed to be accountable for all aspects of the work in ensuring that questions related to the accuracy or integrity of any part of the work are appropriately investigated and resolved.

FUNDING

This study was funded by the Higher Education Commission of Pakistan.

ACKNOWLEDGMENTS

We are thankful to the Department of Pharmacy, University of Peshawar, for their support.

REFERENCES

Bernkop-Schnürch, A., and Jalil, A. (2018). Do drug Release Studies from SEDDS Make Any Sense? *J. controlled release* 271, 55–59.

Butt, A. M., Amin, M. C. I. M., Katas, H., Sarisuta, N., Witoonsaridsilp, W., and Benjakul, R. (2012). *In Vitro* characterization of Pluronic F127 and D-Ttocopheryl Polyethylene Glycol 1000 Succinate Mixed Micelles as Nanocarriers for Targeted Anticancer-Drug Delivery. *J. Nanomater.* 2014, 11. doi:10.1155/2012/916573

Carey, L. A., Perou, C. M., Livasy, C. A., Dressler, L. G., Cowan, D., Conway, K., et al. (2006). Race, Breast Cancer Subtypes, and Survival in the Carolina Breast Cancer Study. *Jama* 295 (21), 2492–2502. doi:10.1001/jama.295.21.2492

Carvalho, G. C., Araujo, V. H. S., Fonseca-Santos, B., de Araújo, J. T. C., de Souza, M. P. C., Duarte, J. L., et al. (2021). Highlights in Poloxamer-Based Drug Delivery Systems as Strategy at Local Application for Vaginal Infections. *Int. J. Pharm.* 602, 120635. doi:10.1016/j.ijpharm.2021.120635

Chadha, R., and Bhandari, S. (2014). Drug-excipient Compatibility Screening-Rrole of Thermoanalytical and Spectroscopic Techniques. *J. Pharm. Biomed. Anal.* 87, 82–97. doi:10.1016/j.jpba.2013.06.016

Chidambaram, M., Manavalan, R., and Kathiresan, K. (2011). Nanotherapeutics to Overcome Conventional Cancer Chemotherapy Limitations. *J. Pharm. Pharm. Sci.* 14 (1), 67–77. doi:10.18433/j30c7d

Colzani, B., Pandolfi, L., Hoti, A., Iovene, P. A., Natalello, A., Avvakumova, S., et al. (2018). Investigation of Antitumor Activities of Trastuzumab Delivered by PLGA Nanoparticles. *Int. J. Nanomedicine* 13, 957–973. doi:10.2147/IJN.S152742

Costa, P., and Sousa Lobo, J. M. (2001). Modeling and Comparison of Dissolution Profiles. *Eur. J. Pharm. Sci.* 13 (2), 123–133. doi:10.1016/s0928-0987(01)00095-1

Danhier, F., Ansorena, E., Silva, J. M., Coco, R., Le Breton, A., and Préat, V. (2012). PLGA-based Nanoparticles: an Overview of Biomedical Applications. *J. Control. Release* 161 (2), 505–522. doi:10.1016/j.jconrel.2012.01.043

de Oliveira Fortes, V. D., Diniz, W. A., Araujo dos Santos, E., Resende, C. X., Almeida, L. E., and Teixeira, Z. (2012). "Nanostructures of Hydroxyapatite in Pluronic F 127: Preparation and Structural Characterization," in Paper presented at the Key Engineering Materials.

Dhiman, H. K., Ray, A. R., and Panda, A. K. (2004). Characterization and Evaluation of Chitosan Matrix for *In Vitro* Growth of MCF-7 Breast Cancer Cell Lines. *Biomaterials* 25 (21), 5147–5154. doi:10.1016/j.biomaterials.2003.12.025

Dumortier, G., Grossiord, J. L., Agnely, F., and Chaumeil, J. C. (2006). A Review of Poloxamer 407 Pharmaceutical and Pharmacological Characteristics. *Pharm. Res.* 23 (12), 2709–2728. doi:10.1007/s11095-006-9104-4

Ferlay, J., Soerjomataram, I., Dikshit, R., Eser, S., Mathers, C., Rebelo, M., et al. (2015). Cancer Incidence and Mortality Worldwide: Sources, Methods and Major Patterns in GLOBOCAN 2012. *Int. J. Cancer* 136 (5), E359–E386. doi:10.1002/ijc.29210

Fonseca, C., Simões, S., and Gaspar, R. (2002). Paclitaxel-loaded PLGA Nanoparticles: Preparation, Physicochemical Characterization and *In Vitro* Anti-tumoral Activity. *J. Control. Release* 83 (2), 273–286. doi:10.1016/s0168-3659(02)00212-2

Fu, Q., Hargrove, D., and Lu, X. (2016). Improving Paclitaxel Pharmacokinetics by Using Tumor-specific Mesoporous Silica Nanoparticles with Intraperitoneal Delivery. *Nanomedicine* 12 (7), 1951–1959. doi:10.1016/j.nano.2016.04.013

Guo, X., Han, J., Li, S., and Xiang, W. (2012). Pharmacokinetics and Tissue Distribution of a Paclitaxel Self-Microemulsion in Rats. *Asian J. Pharm. Sci.* 7 (1), 58–66.

Holliday, D. L., and Speirs, V. (2011). Choosing the Right Cell Line for Breast Cancer Research. *Breast Cancer Res.* 13 (4), 215–217. doi:10.1186/bcr2889

Huang, C. Y., Chen, C. M., and Lee, Y. D. (2007). Synthesis of High Loading and Encapsulation Efficient Paclitaxel-Loaded Poly(n-Butyl Cyanoacrylate) Nanoparticles via Miniemulsion. *Int. J. Pharm.* 338 (1-2), 267–275. doi:10.1016/j.ijpharm.2007.01.052

Iqbal, N., and Iqbal, N. (2014). Human Epidermal Growth Factor Receptor 2 (HER2) in Cancers: Overexpression and Therapeutic Implications. *Mol. Biol. Int.* 2014, 9. doi:10.1155/2014/852748

Keum, C. G., Noh, Y. W., Baek, J. S., Lim, J. H., Hwang, C. J., Na, Y. G., et al. (2011). Practical Preparation Procedures for Docetaxel-Loaded Nanoparticles Using Polylactic Acid-Co-Glycolic Acid. *Int. J. Nanomedicine* 6, 2225–2234. doi:10.2147/IJN.S24547

Kumar Mehata, A., Bharti, S., Singh, P., Viswanadh, M. K., Kumari, L., Agrawal, P., et al. (2019). Trastuzumab Decorated TPGS-G-Chitosan Nanoparticles for Targeted Breast Cancer Therapy. *Colloids Surf. B Biointerfaces* 173, 366–377. doi:10.1016/j.colsurfb.2018.10.007

Kumari, A., Yadav, S. K., and Yadav, S. C. (2010). Biodegradable Polymeric Nanoparticles Based Drug Delivery Systems. *Colloids Surf. B Biointerfaces* 75 (1), 1–18. doi:10.1016/j.colsurfb.2009.09.001

Lee, A. V., Oesterreich, S., and Davidson, N. E. (2015). MCF-7 Cells-Cchanging the Course of Breast Cancer Research and Care for 45 Years. *J. Natl. Cancer Inst.* 107 (7). doi:10.1093/jnci/djv073

Liotta, L. A., Steeg, P. S., and Stetler-Stevenson, W. G. (1991). Cancer Metastasis and Angiogenesis: an Imbalance of Positive and Negative Regulation. *Cell* 64 (2), 327–336. doi:10.1016/0092-8674(91)90642-c

Marsalek, R. (2014). Particle Size and Zeta Potential of ZnO. *APCBEE Proced.* 9, 13–17. doi:10.1016/j.apcbee.2014.01.003

Martins, K. F., Messias, A. D., Leite, F. L., and Duek, E. A. R. (2014). Preparation and Characterization of Paclitaxel-Loaded PLDLA Microspheres. *Mat. Res.* 17 (3), 650–656. doi:10.1590/s1516-14392014005000028

Miele, E., Spinelli, G. P., Miele, E., Tomao, F., and Tomao, S. (2009). Albumin-bound Formulation of Paclitaxel (Abraxane ABI-007) in the Treatment of Breast Cancer. *Int. J. Nanomedicine* 4 (1), 99–105. doi:10.2147/ijn.s3061

Moghimi, S. M., and Hunter, A. C. (2000). Poloxamers and Poloxamines in Nanoparticle Engineering and Experimental Medicine. *Trends Biotechnol.* 18 (10), 412–420. doi:10.1016/s0167-7799(00)01485-2

Mohamed, H. E., Mohamed, A. A., Al-Ghobashy, M. A., Fathalla, F. A., and Abbas, S. S. (2018). Stability Assessment of Antibody-Drug Conjugate Trastuzumab Emtansine in Comparison to Parent Monoclonal Antibody Using Orthogonal Testing Protocol. *J. Pharm. Biomed. Anal.* 150, 268–277. doi:10.1016/j.jpba.2017.12.022

Moura, S., Noro, J., Cerqueira, P., Silva, C., Cavaco-Paulo, A., and Loureiro, A. (2020). Poloxamer 407 Based-Nanoparticles for Controlled Release of Methotrexate. *Int. J. Pharm.* 575, 118924. doi:10.1016/j.ijpharm.2019.118924

Mu, L., and Feng, S. S. (2003). PLGA/TPGS Nanoparticles for Controlled Release of Paclitaxel: Effects of the Emulsifier and Drug Loading Ratio. *Pharm. Res.* 20 (11), 1864–1872. doi:10.1023/b:pham.0000003387.15428.42

Nehate, C., Jain, S., Saneja, A., Khare, V., Alam, N., Dubey, R. D., et al. (2014). Paclitaxel Formulations: Challenges and Novel Delivery Options. *Curr. Drug Deliv.* 11 (6), 666–686. doi:10.2174/1567201811666140609154949

Paarakh, M. P., Jose, P. A., Setty, C., and Christoper, G. P. (2018). Release Kinetics–Concepts and Applications. *Int. J. Pharm. Res. Technol.* 8 (1), 12–20.

Pabari, R. M., Ryan, B., Ahmad, W., and Ramtoola, Z. (2013). Physical and Structural Stability of the Monoclonal Antibody, Trastuzumab (Herceptin®), Intravenous Solutions. *Curr. Pharm. Biotechnol.* 14 (2), 220–225. doi:10.2174/138920113805219322

Patel, P., Ahir, K., Patel, V., Manani, L., and Patel, C. (2015). Drug-Excipient Compatibility Studies: First Step for Dosage Form Development. *The Pharma Innovation* 4 (5), 14.

Pavlova, A. S., Dyudeeva, E. S., Kupryushkin, M. S., Amirkhanov, N. V., Pyshnyi, D. V., and Pyshnaya, I. A. (2018). SDS-PAGE Procedure: Application for Characterization of New Entirely Uncharged Nucleic Acids Analogs. *Electrophoresis* 39 (4), 670–674. doi:10.1002/elps.201700415

Peça, I. N., Petrova, K. T., Cardoso, M. M., and Barros, M. T. (2012). Preparation and Characterization of Polymeric Nanoparticles Composed of Poly (Dl-lactide-co-glycolide) and Poly (Dl-lactide-co-glycolide)-co-poly (Ethylene Glycol)-10%-Triblock End-Capped with a Galactose Moiety. *Reactive Funct. Polym.* 72 (10), 729–735.

Piccart-Gebhart, M. J., Procter, M., Leyland-Jones, B., Goldhirsch, A., Untch, M., Smith, I., et al. (2005). Trastuzumab after Adjuvant Chemotherapy in HER2-Positive Breast Cancer. *N. Engl. J. Med.* 353 (16), 1659–1672. doi:10.1056/NEJMoa052306

Pradhan, R., Poudel, B. K., Ramasamy, T., Choi, H. G., Yong, C. S., and Kim, J. O. (2013). Docetaxel-loaded Polylactic Acid-Co-Glycolic Acid Nanoparticles: Formulation, Physicochemical Characterization and Cytotoxicity Studies. *J. Nanosci Nanotechnol* 13 (8), 5948–5956. doi:10.1166/jnn.2013.7735

Reddy, L. H., and Murthy, R. S. (2005). Etoposide-loaded Nanoparticles Made from Glyceride Lipids: Formulation, Characterization, *In Vitro* Drug Release, and Stability Evaluation. *AAPs PharmSciTech* 6 (2), E158–E166. doi:10.1208/pt060224

Redhead, H. M., Davis, S. S., and Illum, L. (2001). Drug Delivery in Poly(lactide-Co-Glycolide) Nanoparticles Surface Modified with Poloxamer 407 and Poloxamine 908: *In Vitro* Characterisation and *In Vivo* Evaluation. *J. Control. Release* 70 (3), 353–363. doi:10.1016/s0168-3659(00)00367-9

Romond, E. H., Perez, E. A., Bryant, J., Suman, V. J., Geyer, C. E., Jr, Davidson, N. E., et al. (2005). Trastuzumab Plus Adjuvant Chemotherapy for Operable HER2-Positive Breast Cancer. *N. Engl. J. Med.* 353 (16), 1673–1684. doi:10.1056/NEJMoa052122

Sakhi, M., Khan, A., Khan, I., Iqbal, Z., Khan, S. I., Khattak, M. A., et al. (2021). A New Sensitive HPLC/UV Method for Simultaneous Determination of Paclitaxel, Sorafenib and Omeprazole in Standard Solutions and Spiked Plasma: Application to *In-Vitro* and *In-Vivo* Evaluation of Paclitaxel Polymeric Nanoformulations. *Trop. J. Pharm. Res.* 20 (9), 1949–1959. doi:10.4314/tjpr.v20i9.23

Singla, A. K., Garg, A., and Aggarwal, D. (2002). Paclitaxel and its Formulations. *Int. J. Pharm.* 235 (1-2), 179–192. doi:10.1016/s0378-5173(01)00986-3

Stage, T. B., Bergmann, T. K., and Kroetz, D. L. (2018). Clinical Pharmacokinetics of Paclitaxel Monotherapy: an Updated Literature Review. *Clin. Pharmacokinet.* 57 (1), 7–19. doi:10.1007/s40262-017-0563-z

Steichen, S. D., Caldorera-Moore, M., and Peppas, N. A. (2013). A Review of Current Nanoparticle and Targeting Moieties for the Delivery of Cancer Therapeutics. *Eur. J. Pharm. Sci.* 48 (3), 416–427. doi:10.1016/j.ejps.2012.12.006

Stolnik, S., Daudali, B., Arien, A., Whetstone, J., Heald, C. R., Garnett, M. C., et al. (2001). The Effect of Surface Coverage and Conformation of Poly(ethylene Oxide) (PEO) Chains of Poloxamer 407 on the Biological Fate of Model Colloidal Drug Carriers. *Biochim. Biophys. Acta* 1514 (2), 261–279. doi:10.1016/s0005-2736(01)00376-5

Sun, B., Ranganathan, B., and Feng, S. S. (2008). Multifunctional poly(D,L-lactide-co-glycolide)/montmorillonite (PLGA/MMT) Nanoparticles Decorated by Trastuzumab for Targeted Chemotherapy of Breast Cancer. *Biomaterials* 29 (4), 475–486. doi:10.1016/j.biomaterials.2007.09.038

Sun, B., Rachmawati, H., Liu, Y., Zhao, J., and Feng, S.-S. (2011a). *Antibody-Conjugated Nanoparticles of Biodegradable Polymers for Targeted Drug Delivery* Bionanotechnology II. Singapore: CRC Press, 174–199.

Sun, B., Rachmawati, H., Liu, Y., Zhao, J., and Feng, S.-S. (2011b). *Antibody-conjugated Nanoparticles of Biodegradable Polymers for Targeted Drug Delivery: Bionanotechnology. II. Global Prospects*. Farmington, Connecticut: CRC Press.

Truong, N. P., Whittaker, M. R., Mak, C. W., and Davis, T. P. (2015). The Importance of Nanoparticle Shape in Cancer Drug Delivery. *Expert Opin. Drug Deliv.* 12 (1), 129–142. doi:10.1517/17425247.2014.950564

Waks, A. G., and Winer, E. P. (2019). Breast Cancer Treatment: a Review. *Jama* 321 (3), 288–300. doi:10.1001/jama.2018.19323

Wei, Y., Xue, Z., Ye, Y., Wang, P., Huang, Y., and Zhao, L. (2014). Pharmacokinetic and Tissue Distribution of Paclitaxel in Rabbits Assayed by LC-UV after Intravenous Administration of its Novel Liposomal Formulation. *Biomed. Chromatogr.* 28 (2), 204–212. doi:10.1002/bmc.3005

Wei, Z., Hao, J., Yuan, S., Li, Y., Juan, W., Sha, X., et al. (2009). Paclitaxel-loaded Pluronic P123/F127 Mixed Polymeric Micelles: Formulation, Optimization and *In Vitro* Characterization. *Int. J. Pharm.* 376 (1-2), 176–185. doi:10.1016/j.ijpharm.2009.04.030

Win, K. Y. (2006). *Paclitaxel Loaded Nanoparticles of Biodegradable Polymers for Cancer Chemotherapy*.

Xu, Z., Gu, W., Huang, J., Sui, H., Zhou, Z., Yang, Y., et al. (2005). *In Vitro* and *In Vivo* Evaluation of Actively Targetable Nanoparticles forPaclitaxel Delivery. *Int. J. Pharm.* 288 (2), 361–368. doi:10.1016/j.ijpharm.2004.10.009

Yousefpour, P., Atyabi, F., Vasheghani-Farahani, E., Movahedi, A. A., and Dinarvand, R. (2011). Targeted Delivery of Doxorubicin-Utilizing Chitosan Nanoparticles Surface-Functionalized with Anti-her2 Trastuzumab. *Int. J. Nanomedicine* 6, 1977–1990. doi:10.2147/IJN.S21523

Conflict of Interest: The authors declare that the research was conducted in the absence of any commercial or financial relationships that could be construed as a potential conflict of interest.

Publisher's Note: All claims expressed in this article are solely those of the authors and do not necessarily represent those of their affiliated organizations, or those of the publisher, the editors, and the reviewers. Any product that may be evaluated in this article, or claim that may be made by its manufacturer, is not guaranteed or endorsed by the publisher.

frontiers | Frontiers in Pharmacology

ORIGINAL RESEARCH
published: 08 April 2022
doi: 10.3389/fphar.2022.854859

Synthesis and Characterization of Poly (β-amino Ester) and Applied PEGylated and Non-PEGylated Poly (β-amino ester)/Plasmid DNA Nanoparticles for Efficient Gene Delivery

Sajid Iqbal[1], *Alessandro F. Martins*[2,3,4], *Muhammad Sohail*[5], *Jingjing Zhao*[1], *Qi Deng*[1], *Muhan Li*[1] *and Zhongxi Zhao*[1,6,7,8]*

[1]Department of Pharmaceutics, Key Laboratory of Chemical Biology of Ministry of Education, School of Pharmaceutical Sciences, Cheeloo College of Medicine, Shandong University, Jinan, China, [2]Laboratory of Materials, Macromolecules, and Composites (LaMMAC), Federal University of Technology - Paraná (UTFPR), Apucarana, Brazil, [3]Group of Polymers and Composite Materials (GMPC), Department of Chemistry, State University of Maringá (UEM), Maringá, Brazil, [4]Department of Chemical and Biological Engineering, Colorado State University (CSU), Fort Collins, CO, United States, [5]Key Laboratory of Molecular Pharmacology and Drug Evaluation, Yantai University, Yantai, China, [6]Key University Laboratory of Pharmaceutics and Drug Delivery Systems of Shandong Province, School of Pharmaceutical Sciences, Cheeloo College of Medicine, Shandong University, Jinan, China, [7]Pediatric Pharmaceutical Engineering Laboratory of Shandong Province, Shandong Dyne Marine Biopharmaceutical Company Limited, Rongcheng, China, [8]Chemical Immunopharmaceutical Engineering Laboratory of Shandong Province, Shandong Xili Pharmaceutical Company Limited, Heze, China

OPEN ACCESS

Edited by:
Faisal Raza,
Shanghai Jiao Tong University, China

Reviewed by:
Santosh Yadav,
Institute of Genomics and Integrative Biology (CSIR), India
Hajra Zafar,
Shanghai Jiao Tong University, China

***Correspondence:**
Zhongxi Zhao
zxzhao@sdu.edu.cn

Specialty section:
This article was submitted to Experimental Pharmacology and Drug Discovery, a section of the journal Frontiers in Pharmacology

Received: 14 January 2022
Accepted: 21 February 2022
Published: 08 April 2022

Citation:
Iqbal S, Martins AF, Sohail M, Zhao J, Deng Q, Li M and Zhao Z (2022) Synthesis and Characterization of Poly (β-amino Ester) and Applied PEGylated and Non-PEGylated Poly (β-amino ester)/Plasmid DNA Nanoparticles for Efficient Gene Delivery. Front. Pharmacol. 13:854859. doi: 10.3389/fphar.2022.854859

Polymer-based nanocarriers require extensive knowledge of their chemistries to learn functionalization strategies and understand the nature of interactions that they establish with biological entities. In this research, the poly (β-amino ester) (PβAE-447) was synthesized and characterized, aimed to identify the influence of some key parameters in the formulation process. Initially; PβAE-447 was characterized for aqueous solubility, swelling capacity, proton buffering ability, and cytotoxicity study before nanoparticles formulation. Interestingly, the polymer-supported higher cell viability than the Polyethylenimine (PEI) at 100 μg/ml. PβAE-447 complexed with GFP encoded plasmid DNA (pGFP) generated nanocarriers of 184 nm hydrodynamic radius (+7.42 mV Zeta potential) for cell transfection. Transfection assays performed with PEGylated and lyophilized PβAE-447/pDNA complexes on HEK-293, BEAS-2B, and A549 cell lines showed better transfection than PEI. The outcomes toward A549 cells (above 66%) showed the highest transfection efficiency compared to the other cell lines. Altogether, these results suggested that characterizing physicochemical properties pave the way to design a new generation of PβAE-447 for gene delivery.

Keywords: poly (β-amino ester), biodegradable polymer, stable polyplexes, gene delivery, transfection

INTRODUCTION

The rational designing of a vector is essential for the programmed transport of cargo to desired sites. In the academic field, various drug delivery systems (DDSs) have been abundantly introduced. Yet, these nanoplatforms have not achieved efficient *in vivo* gene expressions (Gonçalves and Paiva 2017). However, gene therapy is the only option to cure underlying genetic defects rather than managing

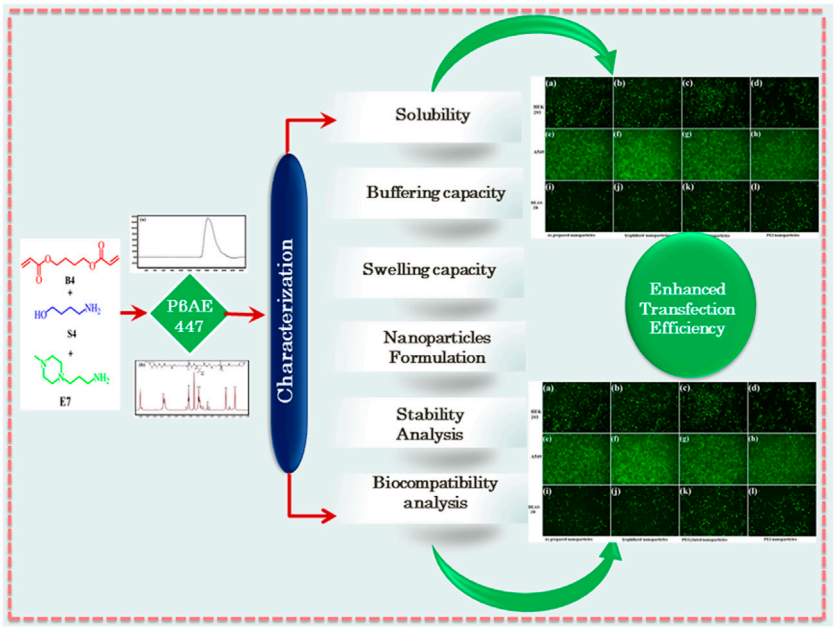

GRAPHICAL ABSTRACT |

symptoms. As of November 2020, 1,645 clinical trials out of 4,500 have been completed and 545 were in phase 3/4. This shows that gene therapy is developing rapidly and gradually translating into clinical practice. In all these trials, the lack of efficient and safe nanocarrier remains the most critical bottleneck (Yu et al., 2021). Although viral vectors are frequently used, non-viral vectors are also becoming more common.

In the domain of non-viral vectors, research on cationic polymers has been expanded since 2004. Substantial synthesis has developed advanced polymeric vectors with excellent cellular uptake toward cells and sustainable buffering capacities. Chemical modifications have improved the bioavailability of therapeutic materials at desired sites (Zeng et al., 2017). Besides, cationic polymers also receive attention because they stabilize negatively charged nucleic acids at physiological pH, forming polymer/gene nanocomplexes. This association protects plasmid DNA (pDNA) from enzymes, enhancing cargo-carrying capacities and promoting predefined unpacking payloads by supporting the controlled pDNA release (Chen et al., 2020). However, most of the cationic polymers are non-degradable, may accumulate in tissues particularly after continuous administration. Cytotoxicity of these polymers is another major issue generated from the loss of cytoplasmic proteins due to adverse interactions with membranes (Zou et al., 2009). Therefore, there is a persistent need to develop a biodegradable gene carrier, both in terms of payload capacity and capsid engineering.

Poly (β-amino ester)s (PβAEs) are the key family members of cationic synthetic and biodegradable polymers. They present tunable structures and potentialities for chemical functionalization (Iqbal and Zhao 2021). The structural modifications on PβAEs have resulted in stable and small size nanoparticles with pDNA, miRNA, and siRNA with target capacities toward tumor cells (Kim et al., 2020). The ester, amino, and disulfide moieties in their chemical structures resemble the chemical structures of glycosaminoglycans, proteoglycans, and proteins found on extracellular membrane matrices (Iqbal et al., 2020). PβAEs offer flexible design chemistries because they can be prepared from different monomers via Michael's addition, generating a vast combinatorial library with various kinetics profiles for different delivery purposes (Li et al., 2013; Rui et al., 2017). Until now, more than 2,350 PβAEs have been synthesized and evaluated for gene transfections in various cell lines (Wang et al., 2020). However, all of these PβAEs are not suitable gene carriers and much characterization is needed before use (Xia et al., 2011). A significant exception to this trend is the poly (β-amino ester)-447 (PβAE-447). It is more effective for gene delivery (Wilson et al., 2018) because the monomer 1,4-butanediol diacrylate ("B4") and the end-capping group 1-(3-aminopropyl)-4-methyl piperazine ("E7") have demonstrated high capacities for cell internalization (Shmueli et al., 2012; Kim et al., 2014). Although all these features make PβAE-447 an attractive pDNA delivery vector, it should be noticed that simple PβAE-447 nanoparticles are susceptible to aqueous degradation (Wilson et al., 2019). This limitation is more pronounced especially in the case when the final PβAE-447 and their nanoparticles are stored for long-term studies. Besides; the nanoparticle features; including size, charge density, and other physicochemical properties such as stability and particles aggregation have considerable influence on nanoparticles bioactivity (Zeb et al.,

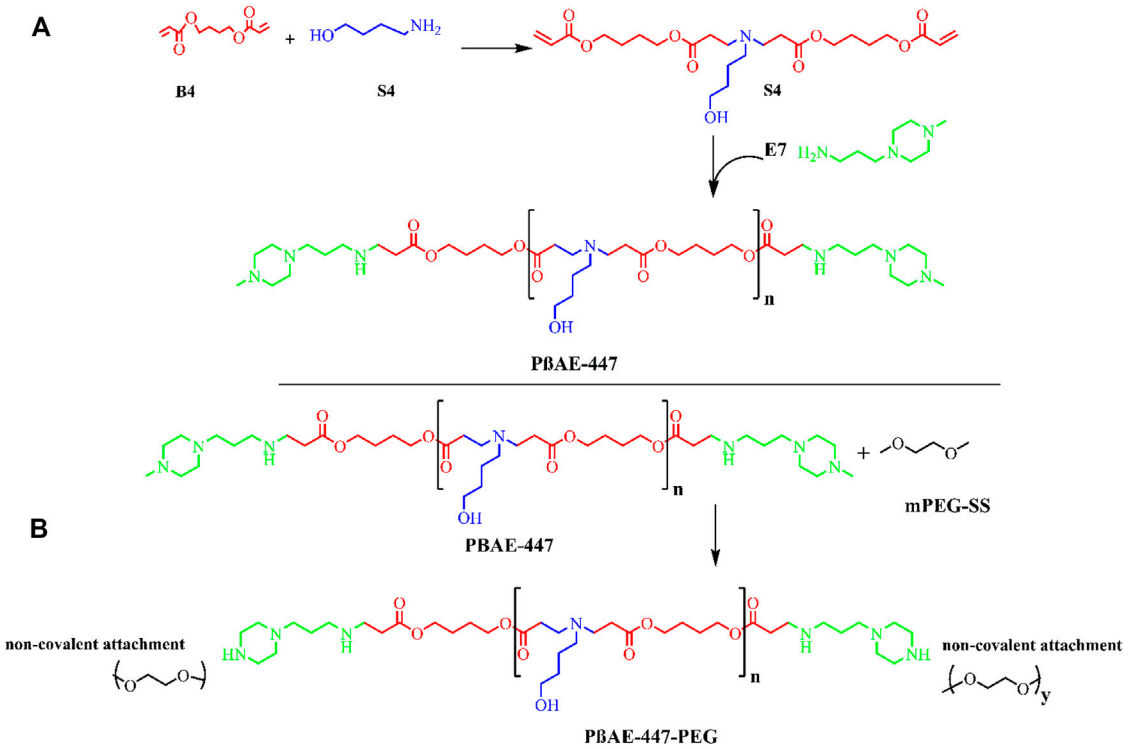

FIGURE 1 | Schematic synthesis reaction mechanism: **(A)** poly (β-amino ester)-447 (PβAE-447) synthesis **(B)** PβAE-447-PEG.

2020). Therefore, precise characterization of the polymer is necessary before its application (Zhang et al., 2016). Several studies have been conducted to optimize PβAEs architecture (Green et al., 2008) to formulate nanoparticles with desired characteristics for gene delivery (Perni and Prokopovich, 2020). However, reported studies have focused on a single variable such as slow-release (Helaly and Hashem, 2013). While in reality, PβAE-based nanocomplexes face a broad spectrum of bio-physicochemical challenges, including colloidal stability, swelling response, and incubation time.

For the first time, only PβAE-447 was characterized to improve its reproducibility and efficacy for enhanced cell transfection. In this regard, several different assays (solubility, stability, and buffering properties) were performed to analyze the critical formulation determinants that could affect the PβAE-447 mediated gene delivery. The surface was functionalized with polyethylene glycol (PEG) to improve colloidal stability. Besides, the incubation time for efficient cellular uptake was also explored. These approaches can be used to discover the parameter ranges that would produce optimized transfections and ensure robust reproducibility.

MATERIALS AND METHODS

Materials

The 1-(3-aminopropyl)-4-methyl piperazine (E7), 1,4-butanediol diacrylate (B4), 4-amino-1-butanol (S4), and Polyethylenimine (PEI) were obtained from Alfa Aesar (Beijing, China). Dimethyl sulfoxide (DMSO), N-hexane, dimethylformamide (DMF), Ethyl acetate (EtOAc), Dichloromethane (DCM), tetrahydrofuran (THF), and diethyl ether were purchased from Sigma-Aldrich (Beijing, China). Methoxy Polyethylene glycol-succinimidyl succinate (mPEG-SS) commonly referred to as PEG of 5 kDa was acquired from Shanghai Titan Technology Co., Ltd (Shanghai, China).

The cell culture media and all other reagents were used as received. Aqueous solutions of sodium acetate (NaAc, pH 5.1 ± 0.1 at 0.025 M), sodium chloride (NaCl, 150 mM), and sodium hydroxide (NaOH, 0.1 N) were prepared and sterilized. Plasmid DNA (pDNA) expressing green fluorescent protein (GFP) was prepared accordingly, while growth media and Hoechst dye were stored according to the manufacturer's instructions.

Poly (β-amino ester)-447 Synthesis

Poly (β-amino ester)-447 (PβAE-447) was synthesized following a previously published procedure (Smith et al., 2017), with alterations as outlined in (**Figure 1**). In the first step, the monomers B4 and S4 were mixed at a 1:1 M ratio and stirred (1,000 rpm) overnight at 90°C to yield the polymer B4-S4 (**Figure 1**).

In the second step, the polymer B4-S4 was dissolved in THF at 100 mg/ml and then combined with E7 (polymer end-capping group) in THF (0.2 M) at 500 rpm for 2 hours at room

temperature. The PβAE-447 was precipitated in cold diethyl ether and washed to remove the residual monomers. The polymer was dispersed again in diethyl ether to guarantee the removal of the remaining monomers. The polymer was vacuumed dried for 2 days to remove traces of solvents. The dry and clean polymer was dissolved in DMSO at 100 mg/ml and stored in small aliquots at −20 °C for further use.

The PβAE-447 was PEGylated. For this, PEG (2.05 M equivalent) and the prepared PβAE-447 solution were transferred into a glass vial, vacuumed, and then purged with nitrogen. The mixture was then reacted in anhydrous THF at room temperature overnight. The PEGylated PβAE was washed two times in cold diethyl ether, and then vacuumed dried. The PEGylated PβAE-447 was separately dissolved in DMSO at 100 mg/ml and stored at −20°C for further use.

Characterization

The polydispersity and molecular weight (M_w) of the PβAE-447 were determined by gel permeation chromatography (GPC). The polymer stock solution in DMSO was diluted in THF (100%) at 5.5 mg/ml. The prepared polymer solution was filtered in a 0.2 μm polytetrafluoroethylene syringe filter before flowing through a waters 515 liquid chromatograph equipped with three styragel columns and 2,414 refractive index detector at a flow rate of 1.0 ml/min at 40°C and then analyzed with Breeze two software. The number average molecular weight (M_n) and M_w were determined using the polystyrene standard.

The purified and dried PβAE-447 was dissolved in deuterated chloroform ($CDCl_3$) at 10 mg/ml and then analyzed by ^{1}H NMR spectroscopy, using a Bruker instrument 400 MHz, Topspin 2.0 (Toronto, Canada).

Polymer Solubility

Different aliquots of the PβAE-447 were mixed with NaAc buffer (25 mM), forming polymer suspensions ("milky" appearance). After sonication (15 min), the samples were kept in an orbital shaker at room temperature for 1 h. Exemplary, 1, 3, 5, 7, 10, and 20 mg of PβAE-447 were dissolved in NaAc (1 ml), and four wells of 96-well plate were used for each concentration. The absorbance of the systems (each well) was recorded with a plate reader at 620 nm. The polymer solubility was confirmed with the naked eye as well as by plotting the recorded absorbance at 620 nm. For this, the absorbance of the polymer systems was compared with the absorbance of references (NaAc and DMSO used to prepare the polymer systems) (Sunshine et al., 2011).

Acid-Base Titration

An acid-base titration was performed to evaluate the buffering capacity of PβAE-447. The polymer from its stock solution in DMSO (100 mg/ml) was diluted to 1 mg/ml in NaCl (2.0 ml, 150 mM), and then NaOH (0.1 M) was used to adjust the pH to 10. The pH of the solution (2.0 ml) was reduced to 3 with HCl (0.1 N). The pH alteration was continuously monitored (Gong et al., 2018). Distilled water was titrated in the same way to compare the pH changes as the polymer was titrated. The pH values of the polymer solution were recorded each time after the repeated addition of HCl. A pH meter (pH 211 microprocessor pH meter, HANA Instruments, Seoul, South Korea) was used to measure the pH constantly. The slope of the line in the plot for pH and the concentration of HCl used show the intrinsic buffering ability. The proton buffering capacity of the polymer was calculated through

$$\text{Buffering capacity} = \frac{\Delta V_{HCl} \times C_{HCl}}{m} \quad (1)$$

where ΔV_{HCl} is the HCl volume, C_{HCl} is the concentration of HCl, and m is the polymer mass (Hwang et al., 2014).

Swelling Capacity

The swelling property of the PβAE-447 was evaluated by immersing dried polymer disks (0.1 g) in DMSO, THF, DCM, and EtOAc at room temperature for a defined time. The dried mass for each polymer disk was called W_o, and the swollen polymer disk mass was labeled W_s. The polymer disks were taken out from the solvents at calculated times. The solvents in excess on the disks were gently removed with filter papers before measuring W_s (Biswal et al., 2011). The swelling degree (SD) was determined at different times after contact with the solvents. The SD (%) measurements were determined through .

$$SD = \frac{W_S - W_0}{W_0} \times 100 \quad (2)$$

Cytotoxicity Assay

The relative cytotoxicity of pure and PEGylated PβAE-447 was separately investigated by using the 3-(4,5-dimethylthiozol-2-yl)-2,5-diphenyl tetrazolium bromide (MTT) assay. Human embryonic kidney (HEK-293), bronchial epithelial (BEAS-2B), and lung adenocarcinoma epithelial (A549) cells were incubated in 96-well plates with DMEM (100 μL) for 24 h. When the cells achieved almost 70% confluence, the old media was removed. The new media containing various concentrations of pure and PEGylated PβAE-447 were added to each well. The 96 well plates were incubated for 24 h, and then 25 μL MTT solution (5.0 mg/ml) in PBS was added to each well. After 4 h of incubation, the MTT solution and DMEM were aspirated, and 150 μL DMSO was added to dissolve the formazan crystals. The plates were placed on a shaker for 10 min before recording the absorbance at 570 nm by an ELISA microplate reader (Bio-Rad, California, United States). The percentage of cell viability was calculated by using **Eq. (3)**

$$\text{Cell viability (\%)} = \left(\frac{A_{sample}}{A_{control}}\right) \times 100 \quad (3)$$

where A_{sample} is the absorbance from the treated cells and $A_{control}$ is the absorbance from untreated cells.

Moreover, the cell viability of PEI 25 KDa was also determined.

Nanoparticles Formulation and Characterization

The pDNA and PβAE-447 were diluted to 0.06 and 3.6 μg/ml in NaAc (25 mM, pH 5.0) at room temperature, respectively.

The polymer concentration was 60-fold higher than the pDNA concentration (PβAE-447/pDNA weight ratio equal to 60).

For preparing the PβAE-447/pDNA nanocomplexes, the diluted polymer (50 μL) was added to 50 μL pDNA and gently mixed by pipetting. The prepared suspension was kept for 10 min under rest to facilitate the self-assembling of the nanocomplexes. The as-prepared nanoparticle suspension was characterized by dynamic light scattering (DLS). Hydrodynamic radius and Zeta potential measurements were determined in a Malvern Zetasizer Nano (ZS) instrument (NanoSight Ltd, United Kingdom) at room temperature (Kamat et al., 2013).

An as-prepared nanoparticle suspension was mixed with sucrose (30 mg/ml in 25 mM NaAc), performing a 1:1 v/v nanoparticle/sucrose mixture to assess the nanoparticles' stability over time. The mixture was frozen for 2 h at −80°C, lyophilized for 2 days, and stored at 4°C. The lyophilized nanoparticles were re-dispersed in water (30 mg/ml) for further DLS analysis (Zeta potential and hydrodynamic radius). These nanoparticles were called lyophilized nanoparticles.

Nanoparticle Stability Analysis

The stability of the PβAE-447/pDNA and PEGylated PβAE-447/pDNA nanoparticles was evaluated in fetal bovine serum (FBS) and NaCl. The polyplexes were prepared the same way as mentioned above. Then FBS (10% w/v) and NaCl (300 mmol) were separately added to the nanoparticle's suspensions. The size and Zeta potential of the resulting suspensions were measured after 4 h of incubation at room temperature (Zeng et al., 2017).

Nanoparticles Hemagglutination Study

The agglutinating activity of PβAE-447/pDNA formulated at 60 wt/wt was examined in a 96-well plate. Briefly, fresh mice blood was centrifuged at 1000 rpm for 15 minutes. The supernatant containing plasma and buffy coat were removed. The erythrocytes were washed three times with PBS. After each cycle, the supernatant was carefully discarded. The red blood cells obtained in this method were found to be pure from cell debris and leucocytes. The erythrocytes were diluted in PBS to a final concentration of 2 % (v/v). 50 μL from this dilution was transferred to a 96-well microplate. The PβAE-447/pDNA complexes were added to the RBC suspension (1:1) and incubated for 30 minutes at room temperature. After incubation, hemagglutination was observed with the naked eye as well as under an optical microscope. The experiment was performed in triplicate.

Cell Transfection

HEK-293, BEAS-2B, and A549 cells) cell lines were grown at a density of 12,500 cells/well in 100 μL media in three separate 96-well plates for 24 h to allow cell adhesion. pDNA was dissolved in NaAc (25 mM, pH 5.0) to 0.06 μg/μL. Polymer (stock solution in DMSO) was diluted in NaAc (25 mM, pH 5.0) to 3.6 μg/μL (60 polymer/p-DNA weight ratio). The diluted pDNA (30 μL) and diluted polymer (30 μL) solutions were mixed for 5 seconds with a vortex mixer. The mixture was kept at rest for 10 minutes to promote the formation of the nanoparticles. Then, 20 μL nanoparticle suspension was added to 100 μL of the cell growth media.

Before adding the polymer/pDNA nanoparticles (as-prepared, lyophilized, and pegylated PβAE-447/pDNA nanoparticles) over the seeded cells, the media was aspirated, and new media containing mentioned nanoparticles were used for transfection. After 4 h of incubation, the media containing nanoparticles was poured out from each well, and an equal volume of fresh and prewarmed media was added. The 96-wells plates were kept in an incubator at 37°C under 5% CO_2 and examined for cell transfection after 48 h.

Control experiments with PEI (MW 25,000) were also performed as above. PEI/pDNA complexes were formulated at a 3:1 PEI to pDNA weight ratio in NaCl (25 mM, pH 5.0). PEI/pDNA suspension was shaken vigorously and then incubated for 15 min at room temperature. PEI/pDNA was added to cells for the final concentration of pDNA 600 ng/well.

A semi-quantitative analysis was performed on the images captured by fluorescent microscope (Carl Zeiss MicroImaging GmbH, Germany) to calculate the mean fluorescent intensity of GFP-expressed cells using the ImageJ (http://rsb.info.nih.gov/ij).

Confocal Microscopy

Four different experiments were performed to investigate the effect of the incubation period of the PEGYlated PβAE-447/pDNA nanoparticles on cellular uptake.

The different cell lines (HEK-293, BEAS-2B, and A549) were cultured in 96-wells for 24 h for cell adhesion. Nanocomplexes in culture media were added to the attached cells for different time periods. After the predefined incubation time intervals, the media containing the nanoparticles were replaced by new media, and the plates were incubated for 48 h. Afterward, the culture media was removed, and the cells were incubated for 10 min in the Hoechst dye 33,342 solutions. Immediately before confocal imaging, the media from the wells were aspirated, and the cells were rinsed twice with PBS(1X). Confocal microscopy images were recorded with a confocal laser scanning microscopy (GmbH Wetzlar, Germany).

Analysis

All the experiments were performed in triplicate ($n = 3$), and the results were expressed as the mean ± standard deviations.

RESULT

Synthesis and Characterization of the Poly (β-amino Ester)

In this study, PβAE-447 was synthesized following the Michael addition reaction mechanism by polymerizing 1,4-

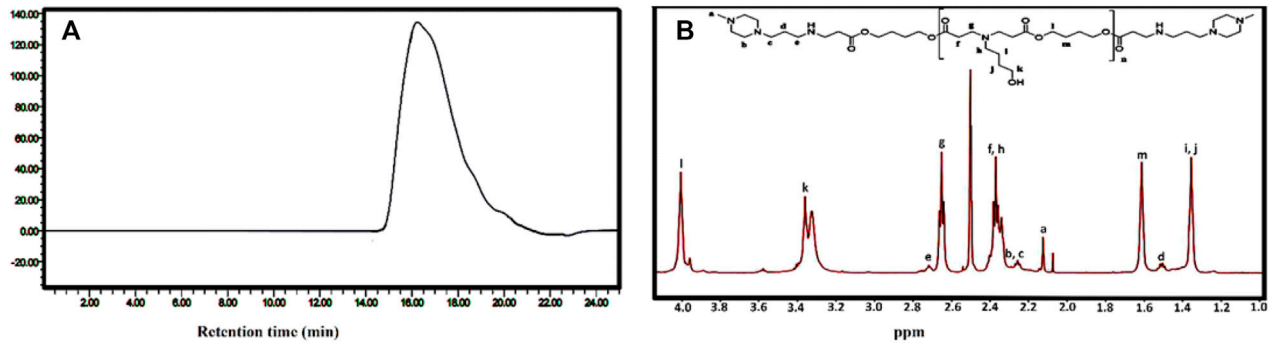

FIGURE 2 | Characterization of PβAE-447: **(A)** GPC chromatogram and **(B)** ^{1}H NMR spectrum in $CDCl_3$.

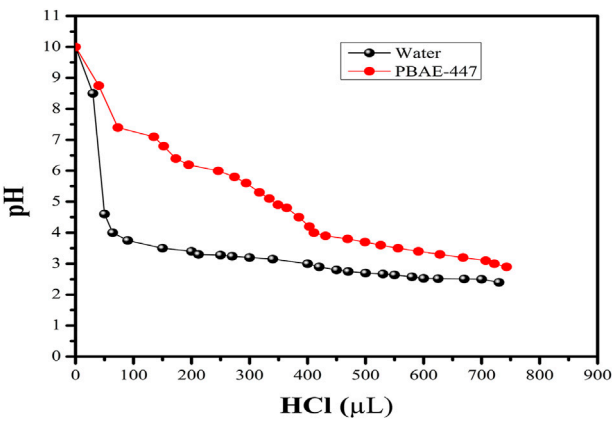

FIGURE 3 | Buffering capacity of the PβAE-447 is determined by titration.

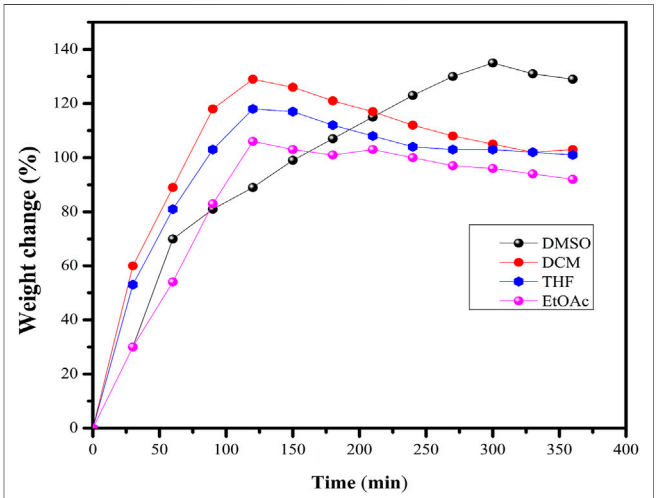

FIGURE 4 | The swelling degree (SD%) of the PβAE-447 in different solvents.

butanediol diacrylate "B4" and 4-amino-1-butanol "S4" stoichiometrically. The reaction formed a polymer base that was end-capped with 1-(3-aminopropyl)-4-methyl piperazine (E7). The yielded polymer obtained from the monomers "B4", "S4", and the end-capping reagent "E7" is named as 1-(3-aminopropyl)-4-methyl piperazine end-modified poly (1,4-butanediol diacrylate-*co*-4-amino-1- butanol) (PβAE-447). This nomenclature depends on four carbon atoms between the acrylate groups in "B4" and four carbon atoms across the amine and the alcohol groups in" S4" (Li et al., 2013). The polymerization of PβAEs can be carried out in a wide range of solvents. However, DMSO was preferred in the synthesis because it is a commonly used solvent in bio-assays including cellular-based assays.

The PβAE-447 was characterized by gel permeation chromatography (GPC) to determine the molecular weight and polydispersity index (PDI) (**Figure 2A**). The GPC chromatogram shows the presence of a single polymer with Mn of 5,354, Mw of 9,575, MP of 4,934, and PDI of 1.7.

The chemical structure of PβAE-447 was analyzed by ^{1}H NMR (**Figure 2B**), and the spectrum matches with previously published results (Chemical shift analysis **Supplementary Figure S2**). The PβAE-447 ^{1}H NMR spectrum shows peaks assigned to hydrogen atoms found on the monomers B4 and S4 and the disappearance of the acrylate peaks at the end of both sides of ppm shows completion of the end-capping reaction.

Solubility

The well-established method for investigating the carrier solubility is adding an extra quantity of carriers to a fixed buffer volume at a set pH. A 96-well plate absorbance assay was used to quantitatively evaluate the PβAE-447 solubility at 620 nm. The data (not shown) shows that PβAE-447 was completely soluble at 10 μg/μL in a NaAc buffer. The gene release depends on the PβAE-447 solubility inside the cells. The water-soluble and biodegradable cationic polymer has hydrolyzable ester bonds in its backbone (Agarwal et al., 2012). The polymer degradation should support the release of genetic materials in an active form, resulting in better gene expression. Other strategies can also be used to modify the hydrophilic PβAE nature, including its *N*-quaternization and

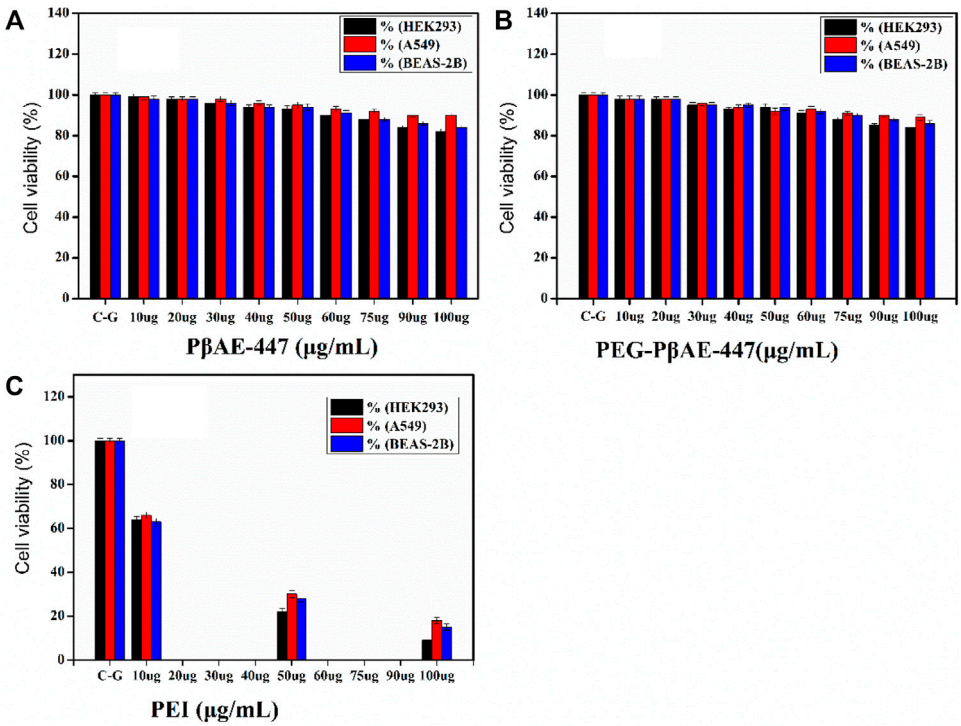

FIGURE 5 | Cell viability assay for pure and PEGYlated PβAE-447 at various concentrations towards HEK-293, BEAS-2B, and A549 cells. PEI (25 kDa) was used as a control (n = 3; and error bars represent standard deviation).

pegylation. These processes should increase the aqueous solubility and enhance pDNA release at physiological pH.

Proton-Buffering Capacity

For evaluating the buffering capacity of PβAE, direct polymer titration with HCl was performed. For comparison, the polymer titration was repeated with distilled water. It is pretty clear from (**Figure 3**) that approximately 0.013 mmol HCl is needed to change the pH from 7.4 to 5.1 (*i.e.*, endosomal pH range). PβAEs with the end-capping group E7 have high buffering capacities because the E7 comprises two tertiary amines. Similarly, PβAEs with the end-capping E6 would have high buffering capabilities than E4 and E6 groups. It has been hypothesized that the nanoparticles remain in the endosomes if the carriers have low buffering capacities (Sunshine et al., 2012). It suggests no relationship between cell uptake and buffering capacity. Still, there is a strong relationship between transfection efficiency and buffering capacity.

Additionally, the nanoparticles formulated at a 75 w/w PβAE-447/pDNA ratio would have a higher buffering capacity than at 60 w/w, because of the high polymer content at 75 w/w. The PβAE-447 can have different proton buffering capacities depending on its concentration. Moreover, the monomer ratio used to synthesize the PβAE-447 could also influence the proton buffering capacity because the amino group content in the polymer structure depends on the S4 concentration.

The titration curve for the water decreased promptly in the pH range between 4 and 10, and the PβAE-447 curve displayed a delayed pH reduction, suggesting that PβAE has a high buffering capability (**Figure 3**). Thus, the buffer capacity should accelerate endosomal escape and enhance the transfection toward treated cells that have already taken up the particles.

Swelling Studies

The PβAE-447 SD was investigated in conventional solvents such as DMSO, DCM, THF, and EtOAc at room temperature for 0, 100, 250, and 360 min (**Figure 4**). The PβAE-447 swelling increases as time rises, achieving the equilibrium condition. The maximum swelling is reached in approximately 2 h in DCM, THF, and EtOAc, whereas in DMSO, the maximum swelling occurs in around 5 h. The polymer SD reduces in the followed order DMSO > DCM > THF > EtOAc. The swelling is rationalized with the solvent-polymer interaction theory that predicts polymer solubility (Biswal et al., 2011). Solvent polymer interactions have a critical role in polymer synthesis. Maximized polymer-solvent interactions may lead to chain expansion, which is important to optimize material's processing; for example, resultant mechanical properties (Ferrell et al., 2017). PβAE-447 demonstrated an ability to absorb conventional solvents and increased in size, as revealed by the swelling behavior stated in **Figure 4**. The PβAE-447 could have a transition in the size through solvents absorption as a stimulus which shows that entrapped therapeutics would take

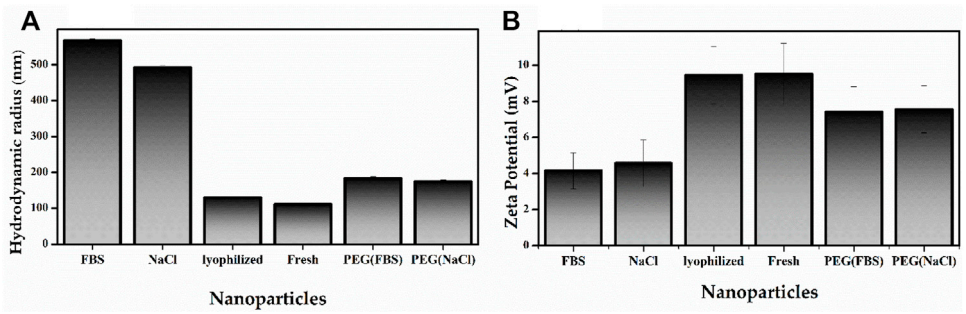

FIGURE 6 | Characterization studies of PβAE-447/pDNA nanoparticles; Nanoparticle Size **(A)** and Zeta potential **(B)** of the as-prepared PβAE-447/pDNA nanoparticles in FBS and NaCl after 4 hours at room temperature, Lypholized, as-prepared and PEGylated PβAE-447/pDNA nanoparticles in FBS and NaCl.

some time to diffuse out. Summarizing the above results, it can be observed that PβAE-447 showed significant swelling degree with respect to its dry discs.

Cytotoxic Activity

HEK-293 cell line is commonly used as a first-level screening host to evaluate new transfection vectors. The MTT assay is widely used as a first-level indicator of cytotoxicity. MTT assays help to determine the influence of the added substances on cell proliferation and metabolism. PβAE-447 cytotoxicity in different dosages (10, 20, 30, 40, 50, 60, 75, 90, and 100 μg/ml) was investigated against HEK-293, BEAS-2B, and A549 cells through MTT assay.

As shown in **Figure 5**, cells incubated with pure (**Figure 5A**) and PEGylated PβAE-447 (**Figure 5B**) show a cell viability sketch. For example, the cell viability of only PβAE-447 is higher than 80% for A549, 77% for BEAS-2B, and 76% for HEK-293 cells. The polymer is cytocompatible toward the investigated cell lines. We did not observe any significant difference in the cytotoxicity results by the conjugation of shielding polymer (PEG) to PβAE-447. PEG has been known as a safe, inert, and non-immunogenic synthetic polymer (Richter et al., 2021). The results are significantly better than the data obtained from the cells population treated with PEI (Mw ≈ 25 k) (**Figure 5C**), as a positive control as well as to facilitate the comparison. The PEI results revealed a dose-dependent decrease in cells viability. One of the remarkable decreases in cell viability was noted in the PEI treated group at a concentration of 100 μg/ml. Overall, PEI has a higher cytotoxic effect than PβAE-447. The cell viability percentage was (14 ± 5%) for PEI and (86 ± 4%) for PβAE-447 at 100 μg/ml concentration. High molecular weight PEI has a strong positive charge and is more cytotoxic than low molecular weight PEI (Valente et al., 2021).

On the other hand, PβAE-447 showed a dose-dependent decrease in cell viability. However, the cell viability was slightly reduced as the PβAE-447 concentration was raised; despite, the cell viability was higher than 75% for all 3 cell lines, confirming that the PβAE-447 is cytocompatible. Disulfide bonds in the PβAE support biodegradability, influencing vector cytotoxicity and pDNA release (Liu et al., 2019).

Nanoparticles Characterization

To study the particle size and zeta potential as potential variables, the nanoparticles were characterized as: 1) nanoparticles formed with 10% FBS; 2) nanoparticles formed with 300 mmol NaCl; 3) lyophilized nanoparticles; 4) PEGYlated nanoparticles in FBS, and 5) PEGYlated nanoparticles with 300 mmol NaCl. The obtained results were compared with the fresh nanoparticle properties (the as-prepared material). All these results were evaluated with the nanoparticles prepared at a 60:1 polymer: pDNA weight ratio.

The size of the as-prepared material was 111.1 nm while the lyophilized nanoparticle's size remained 129.9 nm after 4 months of storage (**Figure 6A** and **Supplementary Figure S3**). This size range is suitable for cellular uptake. It has been reported that nanoparticles between 20 and 200 nm can internalize in cells, acting as target nanocarriers. In this size range, the nanoparticles can prevent filtration and quickly penetrate the cells (Zhao et al., 2014).

The Zeta potential of the as-prepared material was 9.51 mV while the lyophilized nanoparticle's Zeta potential remained 9.45 mV nm after 4 months of storage. The Zeta potential is directly associated with the surface charge. So, it is critical for nanoparticle stability in physiological media and responsible for the initial nanoparticle adsorption on the cell membrane. After adsorption, the endocytic uptake rate is influenced by the particle's size (Green et al., 2008; Rasmussen et al., 2020). These statements indicate that nanoparticle sizes affect cellular internalization, transfection efficiency, and biodistribution *in vivo*.

The PβAE/pDNA nanoparticles incubated with FBS and NaCl were aggregated, leading to large-sized particles with low Zeta potentials (**Figure 6A,B** and **Supplementary Figure S3**).

The FBS accelerates the nanoparticle aggregation, indicating that the PβAE/pDNA nanoparticle zeta potential is quickly altered by the adsorption of serum proteins. The FBS adsorption increased the average nanoparticle size to 567 nm after 4 h (**Figure 6A**). For preventing or reducing nanoparticle aggregation, the PβAE-447 was PEGylated before nanoparticle formulation. PEGylated polymers have a lower affinity to blood proteins because PEG is not charged (Kim et al., 2015). Compared to PβAE/pDNA nanoparticles in FBS and

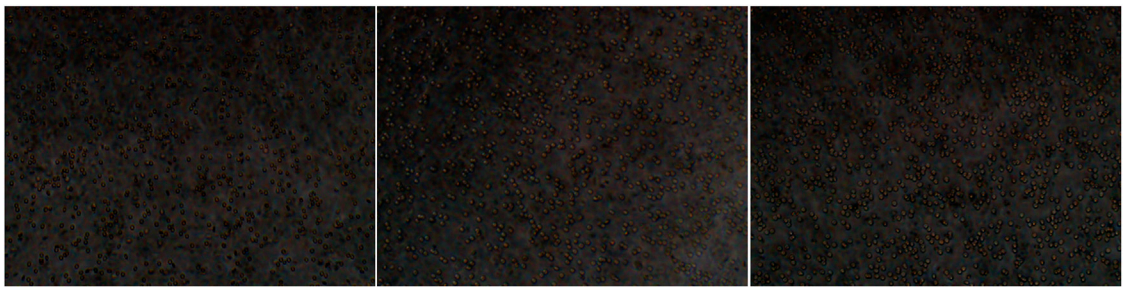

FIGURE 7 | Agglutination with erythrocytes **(**scale = 50 μm n = 3).

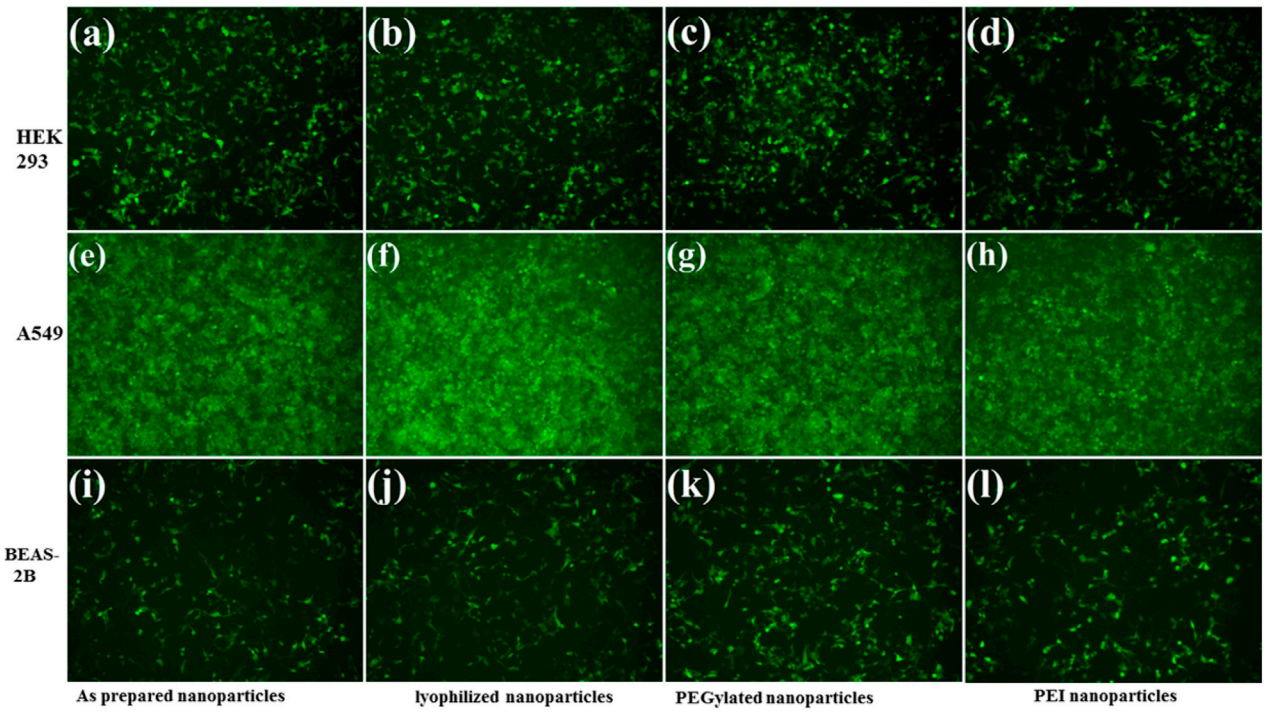

FIGURE 8 | Transfection efficiency of PβAE-447/pDNA nanoparticles in different cells after incubation for 4 hours with as-prepared PβAE-447/pDNA nanoparticles **(A,E,I)**, lyophilized PβAE-447/pDNA nanoparticles **(B,F,J)**, PEGylated PβAE-447/pDNA nanoparticles **(C,G,K)** and PEI **(D,H,L)**.

NaCl, the PEG adsorption reduced the PEGylated-PβAE/pDNA nanoparticles hydrodynamic radius to 184 nm in FBS and 175.1 nm in NaCl after 4 h (**Figure 6**). The size and Zeta potential of the PEGylated-PβAE-447/p-DNA nanoparticles in FBS and NaCl after 4 h were different compared to the as-prepared PβAE-447/p-DNA nanoparticles, confirming strong evidence of successful PEG coating. The PEGylated polymer reduced and prevented nonspecific interactions between the nanoparticles and FBS, avoided aggregation.

Non-PEGylated PβAE-based nanoparticle suspensions are unstable in NaAc solution, forming aggregates during long-term storage at room temperature (Wilson et al., 2019). For overcoming this disadvantage, the PβAE/pDNA nanoparticles were lyophilized and stored at 4 °C for 4 months. These nanoparticles were re-suspended in distilled water, and their average size and Zeta potential were measured and compared with the properties found for the fresh nanoparticles (as-prepared materials). The lyophilization and storage process at 4 °C for 4 months did not influence the nanoparticle features. The average sizes and Zeta potentials of the lyophilized and fresh nanoparticles are similar (**Figure 6**). These properties are desirable for gene delivery and cellular uptake. Therefore, the formulations that developed significant aggregations were eliminated for further considerations as candidates for gene delivery. The as-prepared PβAE-447/pDNA nanoparticles,

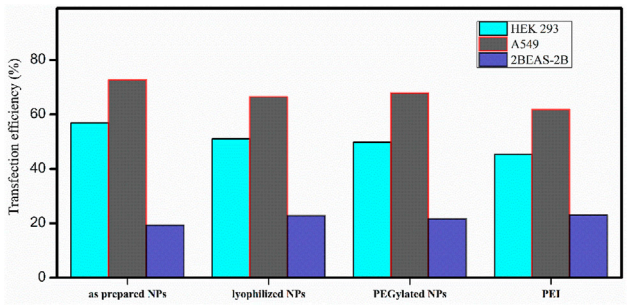

FIGURE 9 | Transfection efficiencies of PβAE-447 and PEI toward A-549, HEK 293, and BEAS-2B were calculated by ImageJ (n = 3).

lyophilized, and PEGylated nanoparticles were selected for further studies.

Various cationic non-viral gene vectors have shown agglutination activities (Kurosaki et al., 2009). Hemagglutination assay with mice erythrocytes was performed to investigate the agglutinating activity of PEGylated PβAE-447/pDNA complexes at a 60 wt/wt ratio. Subsequently, 2% erythrocytes suspension was selected because it supports best agglutination observation in the 96-well plate (Mrázková et al., 2019). Before using PEGylated PβAE-447/pDNA complexes for clinical applications, it is necessary to investigate its biocompatibility with blood components. The hemagglutination assay results ensure the PEGylated PβAE-447/pDNA complexes are cytocompatible with blood cells, as no RBC disruption was observed (**Figure 7**).

Cell Transfection

The transfection efficiency of the nanoparticles was investigated toward three different cell lines (HEK-293, BEAS-2B, and A549). HEK-293 cells are preferred as an easily transfectable cell line, while BEAS-2B and A549 cells are selected as relevant target cell lines for transfection. These cells were seeded in 96-well plates at 12,500 cells/well in 100 µL of media and were incubated overnight for adherence. The pDNA concentration (0.06 µg/µL) in each well was kept constant.

As a model system, the same protocols were followed in each transfection experiment by using pGFP as a reporter gene. The cells were incubated for 4 h with the nanoparticles (as prepared, lyophilized, and PEGlayted) and cellular uptake was investigated after 48 h. The transfection efficiency was calculated from the microscopic images by analyzing the fraction of stained cells (green color).

Fluorescence images demonstrate that transfection efficiency considerably depends on the cell line (**Figure 8**). The A549 and HEK-293 cells show more GFP expression than the BEAS-2B. The A549 cells have been well transfected by PβAE-447-based nanoparticles, followed by the HEK-293 cells. However, the BEAS-2B cells are less transfected. Overall, PEI was found to have slightly lower transfection efficiency than PβAE-447-based nanoparticles. These results are consistent with the sunshine et al., findings. Their optimal formulation of PβAE showed better transfection in retinal pigment epithelium cells than PEI (25 kDa) (Sunshine et al., 2012). In contrast to PEI, Poly (β-amino ester)s have demonstrated higher transfection efficacy *in vitro* and *in vivo* than many commercially available transfection reagents. PβAEs can deliver various pDNA to multiple tumor models with improved survival outcomes (Wilson et al., 2019). The transfection efficiency is not solely dependent on the PβAE nanoparticles. Additional parameters such as the number of cells, transfection method, and transfection reagents influence the transfection efficiency of a DDS.

No significant difference in the transfection efficiency is observed among the lyophilized PβAE-447/pDNA, PEGlated PβAE-447/pDNA, and as-prepared PβAE-447/pDNA nanoparticles (**Figure 9**). The highest transfection efficiency (72%) was shown by the as-prepared PβAE-447/pDNA nanoparticles toward A549 cells, followed by the HEK-293 cells (56%) at a 60 PβAE-447/pDNA weight ratio. Interestingly, we found that PEI has slightly high transfection in BEAS-2B cells. We assume that different levels of transfection of the same reagents may be due to variant specificity toward target cells.

Confocal Microscopy

This experiment explores the capability of PβAE-447 to deliver pDNA to the nucleus of the cells. HEK-293, BEAS-2B, and A549 cells were treated only with PEGYlated PβAE-447/pDNA nanoparticles at different times to evaluate the endocytosis and internalization. Endocytosis is the essential cellular process in which the extracellular materials and nanoparticles are internalized in cells (Rennick et al., 2021). The confocal images show that PEGYlated PβAE/pDNA nanoparticles are taken up by the evaluated cell lines.

The results demonstrate that the short incubation period (at least 2 h) did not show significant cellular uptake, while long incubation periods (6 and 8 h) led to high cytotoxic effects. This indicates that polymer has a harmful effect on cells if exposed for a longer time. This toxic effect may depend on the charge of the PβAE-447. Meantime, when PβAE-based nanoparticles were incubated with the cells for 4 h, the nanoparticles are found primarily distributed in the cytoplasm and nuclei region (**Figure 10**). It indicates that PβAE-based nanocomplexes can be used to target the nuclei effectively. However, long exposure times provide cytotoxic effects, because the strong influence of high charges may lyse the membranes. Long time disrupting the membrane cell walls fluidity due to the increased cell permeability and degeneration (Jeong et al., 2017).

DISCUSSION

Nanoparticles for therapeutic delivery have been a subject of research. However, many obstacles have to be addressed before clinical practice. The peculiar mechanism by which polymeric nanoparticles mediate specificity remains unclear. Primarily, it relies on the nature and structure of the polymer used to design the nanoparticles (Patra et al., 2018). The nanoparticle's properties depend on the polymer features, including the molecular mass, solubility, cytocompatibility, biodegradability, pH-responsiveness, etc. For promoting enhanced gene

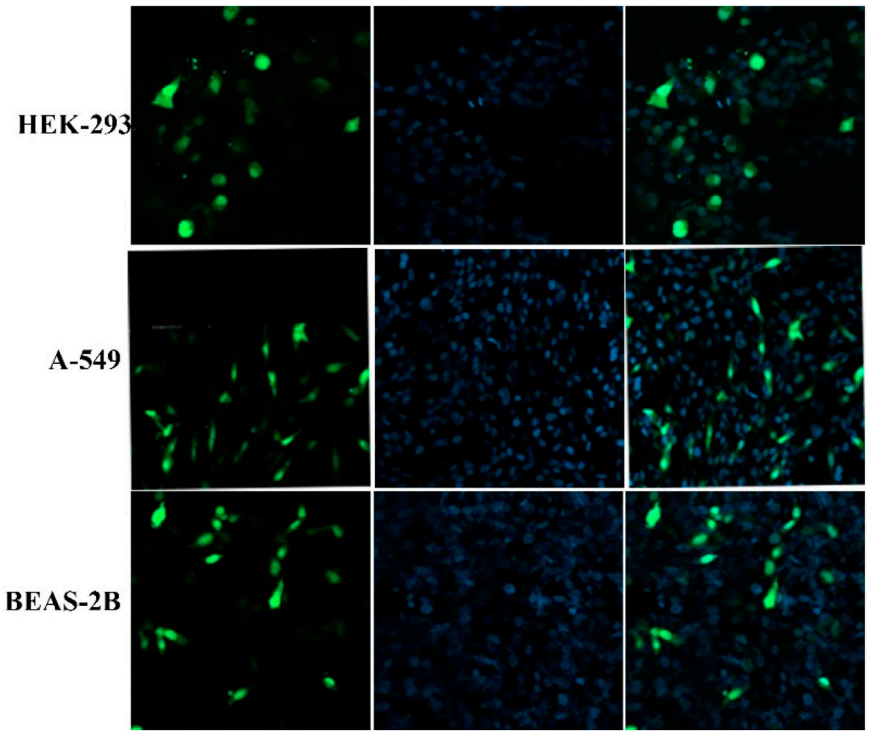

FIGURE 10 | Confocal microscopy images showed the cellular uptake of PEGylated nanoparticles after 4 h of incubation.

transfection, a biodegradable and linear PβAE-447 was synthesized and characterized. This polymer was used to design new DDSs with enhanced transfection efficiency toward different cell lines.

Poly (β-amino ester)s have been demonstrated as safe and efficient transfection vectors *in vitro* for various cell types. PβAEs can easily be formulated to selectively target desired tissues while avoiding nearby healthy tissues (Mangraviti et al., 2015). Various strategies can be applied for modulating the polymer properties to design DDSs for efficient transfection. The monomer concentration ratios result in significant changes in the polymerization kinetic rates (Safaei et al., 2021). The PβAE-447 synthesis proceeded through a conjugate addition reaction. The polymerization resulted in a broad molecular weight, indicating polymer lengths with chain end groups and molecular variant polymer dependent on the monomers' stoichiometric ratio during synthesis. An excess quantity of either monomer (diacrylate or amine) predominates acrylate or amine-terminated polymers, respectively. Theoretically, high molecular weight PβAEs are yielded in the stoichiometric equivalence of the monomers (Anderson et al., 2005). Therefore, monomers' molar ratio of 1: 1 is essential to promote a high degree of monomers conversion to prepare homogeneous polymers with high molecular weights.

PβAE-447 was selected for characterization studies because it is more conducive to efficient gene transfection than other PβAEs. More transfection occurs with B4S4 base polymer with end groups E6 and E7 (Sunshine et al., 2012; Sunshine et al., 2012; Tzeng and Green 2013). Polymers fabricated with E9 as an end group demonstrated significant cytotoxicity, while polymers formulated with E10 and E12 showed poor transfection performance (Sunshine et al., 2011). Besides varying monomers, the synthesis conditions and monomer ratios can also be altered to develop a vast library of polymers with diverse structures and applications (Rui et al., 2017). In addition, many different types of amines and diacrylates (**Supplementary Figure S1**) can be used at wide monomer ratios to synthesize PβAEs with various properties. However, the most significant factor for efficient transfection is the effect of end-capped groups on polymer performance (Iqbal et al., 2020).

The aqueous carrier solubility is an important requirement in the DDSs selection process. The solubility of polymer helps to determine the hydrophobic/hydrophilic nature of projected DDSs. The dissociation of the genetic materials from nanoparticles can be controlled by modulating the solubility of the carrier polymer concerning the external environment. Many publications recommended mixing equal volumes buffer system containing pDNA and transfection reagents, followed by an incubation period for complexation formation (Engelhardt et al., 2017). We hypothesize that partial PβAE-447 solubility in NaAc might influence the nanocomplex formation with pDNA before adding to the cells. Therefore, knowledge of polymer dissolution behavior is critical in understanding time-released applications.

The polymer buffering capacity is considered an essential parameter for polymeric vectors, regulating the pDNA release from the polymer matrix inside the cells after endocytosis. Amine moieties on the polymers can be protonated and deprotonated depending on the pH. Protonated amines increase the osmotic pressure inside endosomes, disrupting the endosomal membrane, leading the polymer matrix to escape (Bhise et al., 2010). The high buffering capacity of carriers contributes to the gene transfection, protecting the pDNA structure after endocytosis (Kim et al., 2013). Protonated polymers stabilize the negatively pDNA by electrostatic interactions. Therefore, understanding the proton buffering capacity of the PβAEs is essential not only because it is evolving non-viral vectors but also, because this knowledge may help to synthesize and design next-generation non-viral vectors.

The swelling property influences the drug diffusion and releases behavior from DDSs (Wang et al., 2010). Hydrophilic DDSs swell because of water diffusion and uptake. The adsorbed solvents interact with the drug, supporting the release of solid solutes from DDSs (Sienkiewicz et al., 2017). Cationic polymers have amino groups that can be protonated depending on the pH condition and pK_a of the protonated sites. Protonated amines interact better with solvent molecules than unprotonated amines. Ion-dipole interactions between solvent and cationic polymers increase swelling due to increased solvent solvation capacity toward the charged polymer structure (Deen and Loh 2018).

The PβAE-447 vector is cytocompatible, distinguishing it from other cationic vectors in terms of degradability in the physiological environment (Green et al., 2009). In contrast to non-degradable PEI-based polymers, PβAEs contain tertiary amines that facilitate rapid aqueous hydrolysis of the polymer backbone. This feature designates PβAE with generally low cytotoxicity and effectively no risk of accumulation following repeat administration *in vivo* (Wilson et al., 2019). All these findings ensure that PβAE-447 is biodegradable and that the degraded byproducts are also highly cytocompatible without causing any prominent cytotoxicity during the gene transfection experiment. Nonetheless, the excellent cell viability profile of PβAE-447 suggests that they are interested candidates for further study as pDNA condensing agents.

The size and zeta potential of DDS are the most critical parameters that regulate the therapeutic effects of nanoparticles. These features strongly affect the systemic circulation and stability of the DDS in the body and its cellular uptake by the cells. The binding affinity between pH-responsive PβAEs and p-DNA is critical for nanoparticle formation and p-DNA release due to pH alteration (Bishop et al., 2013). DDSs containing protonated amino groups interact better with negatively charged cells, supporting the DDS internalization. However, it is challenging to optimize the size and zeta potential of DDSs to improve carriers' efficacy.

Determination of cellular uptake or internalization is the most critical physicochemical parameter that must be evaluated before *in vivo* applications. The nanoparticle internalization should occur through endocytosis in many cells; however, only sub-micron-sized nanoparticles are effectively uptaken in the HepG2, Hepa one to six, and KLN205 cells (Nimesh 2012). The nanoparticle characterization under physiological conditions is critical and challenging. The surrounding environment such as the medium (solvent, body fluids, etc.), ionic strength, charged macromolecules (e.g., proteins) strongly influences the nanoparticle properties for example size, and charge density. The physiological fluids are composed of proteins that interact with charged nanoparticles, forming a "protein corona." This behavior affects the nanoparticle properties, altering its size, shape, and charge density (Van Hong Nguyen 2017). Besides, the polymer/pDNA nanocomplexes also naturally tend to aggregate in physiological fluids (Xia et al., 2011). In addition, the nanoparticles' aggregate as the Zeta potential is lower than +30 mV and higher than −30 mV because the attractive forces may exceed the repulsive forces provided by charged materials. Nanoparticles with Zeta potential higher than +30 mV can resist more against aggregation in solution, being electrically stable (Hwangbo et al., 2021). Therefore, the polyplexes' stability in the physiological environment containing FBS and NaCl was investigated by evaluating the size and Zeta potential of the nanoparticles over 4 h of incubation.

The lower Zeta potential is thought to be because of 10% FBS in the culture medium, which facilitates the attraction of negatively charged albumin that interacts with positively charged nanoparticles at neutral pH. Ions can adsorb on the nanoparticle surface, modify the magnitude of zeta potential. The decrease of zeta potential facilitates a closer approach of nanoparticles, and boost aggregations (Shrestha et al., 2020). In sum, the results show that the presence of FBS and NaCl are the leading factors to aggregate the PβAE/p-DNA nanoparticles, modifying their sizes. Besides, the non-specific interactions in physiological media may cause particle aggregation and opsonization, thereby reducing the systemic circulation time.

The lyophilized nanoparticles preserved their properties and efficacy after 4 months' storage. This result is remarkably important as it assures the stability, scalability, and robustness of the lyophilized particles over time. Corresponding to maintaining colloidal stability, the nanoparticles formulated with PEG-PβAE-447 displayed significantly better *in vitro* transfection efficiency. These findings revealed that PEGylated NPs retained *in vitro* transfection efficiency and stability compared to non-PEGylated NPs. These findings support that the PβAE-447/pDNA nanoparticles can be used as efficient gene delivery vectors, being exciting devices for further studies *in vivo*.

Successful transfection efficiency is also influenced by the cell type. Since different cells are likely to behave differently to the same transfection reagent, hence choosing an appropriate cell type is necessary to maximize results (Neuhaus et al., 2016). In summary, the positively charged PβAE/pDNA nanoparticles are effectively attached to the cell membrane (negatively charged) by electrostatic interactions, entering the cells by endocytosis. The protonated amines in the PβAE-447 raise the osmotic pressure inside the endosome, disrupting the endosomal membrane. Thus, the PβAE/pDNA nanoparticle internalizes, leading to gene expression in host cells (Iqbal et al., 2020).

Besides the incubation period, other factors such as nanoparticle properties (size, shape, zeta potential), cellular microenvironment, and experimental factors (temperature) significantly affect the intracellular fate of nanoparticles. Behzadi et al. mentioned that small-sized nanoparticles internalized in cells faster than large particles (Behzadi et al., 2017). Some nanocarriers cannot reach the cell nuclei of transfected cells, suppressing the transfection. PβAE-447 is a capable carrier to enter the cell, penetrate the nucleus and release some portion of the complexed pDNA, thus making it available for cell transfection.

To achieve the best possible formulation to display the highest stability, biocompatibility, and transfection efficiency, a series of PβAE/pDNA nanoparticles were synthesized and evaluated. PEG- PβAE/pDNA nanoparticles were found to be the best formulation which confirmed the optimal balance of all the parameters i.e. (size, zeta potential and colloidal stability). Hence, it exhibited the highest transfection efficacy with low toxicity. The outcomes of this work could be further used in multidisciplinary fields of cationic polymers, to design and fabricate a new generation of nanoparticle-based delivery systems for gene therapy and gene editing applications.

CONCLUSION

Characterizations studies open a gateway in improving vectors' design and architecture to increase cargo-carrying capacity, advance target specificity, and improve biodegradability, the basic requirements for successful gene therapy. In summary, PβAE-447 was successfully synthesized and various parameters were characterized to improve its robustness. The exhibition of the high buffering capacity of PβAE-447 at acidic pH would help early endosomal escape. Lyophilized nanoparticles maintained appropriate size, Zeta potential, and transfection activity after four 4 months of storage. First, it was revealed that PβAE-447/pDNA nanocomplexes tended to form aggregates in presence of serum and ions. As a result of PEG conjugation, the colloidal stability of nanocomplexes was improved. The transfection efficiency of PEGylated and lyophilized nanoparticles are better than PEI, particularly in A549 cells. These results reveal for the first time the importance of optimizations in the formulation process of PβAE-447. The results presented here can facilitate further investigation to fabricate and optimize DDSs for higher performance *in vivo*.

DATA AVAILABILITY STATEMENT

The original contributions presented in the study are included in the article/**Supplementary Material**, further inquiries can be directed to the corresponding author.

AUTHOR CONTRIBUTIONS

Conceptualization, methodology, formal analysis and investigation, original draft preparation, SI, Software, JZ and QD; validation, MS and ML; review and editing, Visualization, AM; Supervision, project administration, funding acquisition, ZZ. All authors have read and agreed to the published this version of the manuscript.

FUNDING

This research work was supported by the funds from the Major Project of Science and Technology of Shandong Province (Grant #2018CXGC1411 and 2021CXGC010514).

SUPPLEMENTARY MATERIAL

The Supplementary Material for this article can be found online at: https://www.frontiersin.org/articles/10.3389/fphar.2022.854859/full#supplementary-material

REFERENCES

Agarwal, S., Zhang, Y., Maji, S., and Greiner, A. (2012). PDMAEMA Based Gene Delivery Materials. *Mater. Today* 15, 388–393. doi:10.1016/s1369-7021(12)70165-7

Anderson, D. G., Akinc, A., Hossain, N., and Langer, R. (2005). Structure/property Studies of Polymeric Gene Delivery Using a Library of Poly(beta-Amino Esters). *Mol. Ther.* 11, 426–434. doi:10.1016/j.ymthe.2004.11.015

Behzadi, S., Serpooshan, V., Tao, W., Hamaly, M. A., Alkawareek, M. Y., Dreaden, E. C., et al. (2017). Cellular Uptake of Nanoparticles: Journey inside the Cell. *Chem. Soc. Rev.* 46, 4218–4244. doi:10.1039/c6cs00636a

Bhise, N. S., Gray, R. S., Sunshine, J. C., Htet, S., Ewald, A. J., and Green, J. J. (2010). The Relationship between Terminal Functionalization and Molecular Weight of a Gene Delivery Polymer and Transfection Efficacy in Mammary Epithelial 2-D Cultures and 3-D Organotypic Cultures. *Biomaterials* 31, 8088–8096. doi:10.1016/j.biomaterials.2010.07.023

Bishop, C. J., Ketola, T. M., Tzeng, S. Y., Sunshine, J. C., Urtti, A., Lemmetyinen, H., et al. (2013). The Effect and Role of Carbon Atoms in Poly(β-Amino Ester)s for DNA Binding and Gene Delivery. *J. Am. Chem. Soc.* 135, 6951–6957. doi:10.1021/ja4002376

Biswal, D., Wattamwar, P. P., Dziubla, T. D., and Hilt, J. Z. (2011). A Single-step Polymerization Method for Poly(β-Amino Ester) Biodegradable Hydrogels. *Polymer* 52, 5985–5992. doi:10.1016/j.polymer.2011.10.058

Chen, C. K., Huang, P. K., Law, W. C., Chu, C. H., Chen, N. T., and Lo, L. W. (2020). Biodegradable Polymers for Gene-Delivery Applications. *Int. J. Nanomedicine* 15, 2131–2150. doi:10.2147/IJN.S222419

Deen, G. R., and Loh, X. J. (2018). Stimuli-responsive Cationic Hydrogels in Drug Delivery Applications. *Gels* 4, 13. doi:10.3390/gels4010013

Engelhardt, K. H., Pinnapireddy, S. R., Baghdan, E., Jedelská, J., and Bakowsky, U. (2017). *Transfection Studies with Colloidal Systems Containing Highly Purified Bipolar Tetraether Lipids from Sulfolobus Acidocaldarius*. Archaea.2017.

Ferrell, W. H., Kushner, D. I., and Hickner, M. A. (2017). Investigation of Polymer-Solvent Interactions in Poly(styrene Sulfonate) Thin Films. *J. Polym. Sci. Part. B: Polym. Phys.* 55, 1365–1372. doi:10.1002/polb.24383

Gong, J. H., Wang, Y., Xing, L., Cui, P. F., Qiao, J. B., He, Y. J., et al. (2018). Biocompatible Fluorinated Poly(β-Amino Ester)s for Safe and Efficient Gene Therapy. *Int. J. Pharm.* 535, 180–193. doi:10.1016/j.ijpharm.2017.11.015

Gonçalves, G. A. R., and Paiva, R. M. A. (2017). Gene Therapy: Advances, Challenges and Perspectives. *Einstein (Sao Paulo).* 15, 369–375.

Green, J. J., Langer, R., and Anderson, D. G. (2008). A Combinatorial Polymer Library Approach Yields Insight into Nonviral Gene Delivery. *Acc. Chem. Res.* 41, 749–759. doi:10.1021/ar7002336

Green, J. J., Zugates, G. T., Langer, R., and Anderson, D. G. (2009). "Poly(β-amino Esters): Procedures for Synthesis and Gene Delivery," in *Macromolecular Drug Delivery* (Springer), 53–63. doi:10.1007/978-1-59745-429-2_4

Helaly, F. M., and Hashem, M. S. (2013). Preparation and Characterization of Poly (β-Amino Ester) Capsules for Slow Release of Bioactive Material. *J. Encapsulation Adsorption Sci.* 2013. doi:10.4236/jeas.2013.33008

Hwang, H. S., Hu, J., Na, K., and Bae, Y. H. (2014). Role of Polymeric Endosomolytic Agents in Gene Transfection: a Comparative Study of poly(L-Lysine) Grafted with Monomeric L-Histidine Analogue and poly(L-Histidine). *Biomacromolecules* 15, 3577–3586. doi:10.1021/bm500843r

Hwangbo, S. A., Kwak, M., Kim, J., and Lee, T. G. (2021). Novel Surfactant-free Water Dispersion Technique of TiO2 NPs Using Focused Ultrasound System. *Nanomaterials (Basel)* 11, 427. doi:10.3390/nano11020427

Iqbal, S., Qu, Y., Dong, Z., Zhao, J., Khan, A. R., Rehman, S., et al. (2020). Poly (β-Amino Esters) Based Potential Drug Delivery and Targeting Polymer; an Overview and Perspectives. *Eur. Polym. J.* 110097.

Iqbal, S., and Zhao, Z. (2022). Poly (β Amino Esters) Copolymers: Novel Potential Vectors for Delivery of Genes and Related Therapeutics. *Int. J. Pharm.* 611, 121289. doi:10.1016/j.ijpharm.2021.121289

Jeong, H., Hwang, J., Lee, H., Hammond, P. T., Choi, J., and Hong, J. (2017). *In Vitro* blood Cell Viability Profiling of Polymers Used in Molecular Assembly. *Sci. Rep.* 7, 9481–9513. doi:10.1038/s41598-017-10169-5

Kamat, C. D., Shmueli, R. B., Connis, N., Rudin, C. M., Green, J. J., and Hann, C. L. (2013). Poly(β-amino Ester) Nanoparticle Delivery of TP53 Has Activity against Small Cell Lung Cancer *In Vitro* and *In Vivo*. *Mol. Cancer Ther.* 12, 405–415. doi:10.1158/1535-7163.MCT-12-0956

Kim, J., Sunshine, J. C., and Green, J. J. (2014). Differential Polymer Structure Tunes Mechanism of Cellular Uptake and Transfection Routes of Poly(β-Amino Ester) Polyplexes in Human Breast Cancer Cells. *Bioconjug. Chem.* 25, 43–51. doi:10.1021/bc4002322

Kim, J., Wilson, D. R., Zamboni, C. G., and Green, J. J. (2015). Targeted Polymeric Nanoparticles for Cancer Gene Therapy. *J. Drug Target.* 23, 627–641. doi:10.3109/1061186X.2015.1048519

Kim, J., Mondal, S. K., Tzeng, S. Y., Rui, Y., Al-Kharboosh, R., Kozielski, K. K., et al. (2020). Poly(ethylene Glycol)-Poly(beta-Amino Ester)-Based Nanoparticles for Suicide Gene Therapy Enhance Brain Penetration and Extend Survival in a Preclinical Human Glioblastoma Orthotopic Xenograft Model. *ACS Biomater. Sci. Eng.* 6, 2943–2955. doi:10.1021/acsbiomaterials.0c00116

Kim, T.-H., Choi, H., Yu, G. S., Lee, J., and Choi, J. S. (2013). Novel Hyperbranched Polyethyleneimine Conjugate as an Efficient Non-viral Gene Delivery Vector. *Macromol. Res.* 21, 1097–1104. doi:10.1007/s13233-013-1154-y

Kurosaki, T., Kitahara, T., Kawakami, S., Nishida, K., Nakamura, J., Teshima, M., et al. (2009). The Development of a Gene Vector Electrostatically Assembled with a Polysaccharide Capsule. *Biomaterials* 30, 4427–4434. doi:10.1016/j.biomaterials.2009.04.041

Li, C., Tzeng, S. Y., Tellier, L. E., and Green, J. J. (2013). (3-aminopropyl)-4-methylpiperazine End-Capped Poly(1,4-Butanediol Diacrylate-Co-4-Amino-1-Butanol)-Based Multilayer Films for Gene Delivery. *ACS Appl. Mater. Inter.* 5, 5947–5953. doi:10.1021/am402115v

Liu, S., Gao, Y., Zhou, D., Zeng, M., Alshehri, F., Newland, B., et al. (2019). Highly Branched poly(β-Amino Ester) delivery of Minicircle DNA for Transfection of Neurodegenerative disease Related Cells. *Nat. Commun.* 10, 3307–3314. doi:10.1038/s41467-019-11190-0

Mangraviti, A., Tzeng, S. Y., Kozielski, K. L., Wang, Y., Jin, Y., Gullotti, D., et al. (2015). Polymeric Nanoparticles for Nonviral Gene Therapy Extend Brain Tumor Survival *In Vivo*. *ACS nano* 9, 1236–1249. doi:10.1021/nn504905q

Mrázková, J., Malinovská, L., and Wimmerová, M. (2019). Microscopy Examination of Red Blood and Yeast Cell Agglutination Induced by Bacterial Lectins. *PloS one* 14, e0220318.

Neuhaus, B., Tosun, B., Rotan, O., Frede, A., Westendorf, A. M., and Epple, M. (2016). Nanoparticles as Transfection Agents: a Comprehensive Study with Ten Different Cell Lines. *RSC Adv.* 6, 18102–18112. doi:10.1039/c5ra25333k

Nguyen, V. H., and Lee, B. J. (2017). Protein corona: a New Approach for Nanomedicine Design. *Int. J. Nanomedicine* 12, 3137–3151. doi:10.2147/IJN.S129300

Nimesh, S. (2012). Potential Implications of Nanoparticle Characterization on *In Vitro* and *In Vivo* Gene Delivery. *Ther. Deliv.* 3, 1347–1356. doi:10.4155/tde.12.110

Patra, J. K., Das, G., Fraceto, L. F., Campos, E. V. R., Rodriguez-Torres, M. D. P., Acosta-Torres, L. S., et al. (2018). Nano Based Drug Delivery Systems: Recent Developments and Future Prospects. *J. Nanobiotechnology* 16, 71–33. doi:10.1186/s12951-018-0392-8

Perni, S., and Prokopovich, P. (2020). Optimisation and Feature Selection of Poly-Beta-Amino-Ester as a Drug Delivery System for Cartilage. *J. Mater. Chem. B* 8, 5096–5108. doi:10.1039/c9tb02778e

Rasmussen, M. K., Pedersen, J. N., and Marie, R. (2020). Size and Surface Charge Characterization of Nanoparticles with a Salt Gradient. *Nat. Commun.* 11, 2337–2338. doi:10.1038/s41467-020-15889-3

Rennick, J. J., Johnston, A. P. R., and Parton, R. G. (2021). Key Principles and Methods for Studying the Endocytosis of Biological and Nanoparticle Therapeutics. *Nat. Nanotechnol* 16, 266–276. doi:10.1038/s41565-021-00858-8

Richter, F., Leer, K., Martin, L., Mapfumo, P., Solomun, J. I., Kuchenbrod, M. T., et al. (2021). The Impact of Anionic Polymers on Gene Delivery: How Composition and Assembly Help Evading the Toxicity-Efficiency Dilemma. *J. nanobiotechnology* 19, 1–15. doi:10.1186/s12951-021-00994-2

Rui, Y., Quiñones, G., and Green, J. J. (2017). Biodegradable and Bioreducible Poly(beta-Amino Ester) Nanoparticles for Intracellular Delivery to Treat Brain Cancer. *Aiche J.* 63, 1470–1482. doi:10.1002/aic.15698

Safaei, A., Terryn, S., Vanderborght, B., Van Assche, G., and Brancart, J. (2021). The Influence of the Furan and Maleimide Stoichiometry on the Thermoreversible Diels-Alder Network Polymerization. *Polymers (Basel)* 13, 2522. doi:10.3390/polym13152522

Shmueli, R. B., Sunshine, J. C., Xu, Z., Duh, E. J., and Green, J. J. (2012). Gene Delivery Nanoparticles Specific for Human Microvasculature and Macrovasculature. *Nanomedicine* 8, 1200–1207. doi:10.1016/j.nano.2012.01.006

Shrestha, S., Wang, B., and Dutta, P. (2020). Nanoparticle Processing: Understanding and Controlling Aggregation. *Adv. Colloid Interf. Sci* 279, 102162. doi:10.1016/j.cis.2020.102162

Sienkiewicz, A., Krasucka, P., Charmas, B., Stefaniak, W., and Goworek, J. (2017). Swelling Effects in Cross-Linked Polymers by Thermogravimetry. *J. Therm. Anal. Calorim.* 130, 85–93. doi:10.1007/s10973-017-6131-9

Smith, T. T., Stephan, S. B., Moffett, H. F., McKnight, L. E., Ji, W., Reiman, D., et al. (2017). *In Situ* programming of Leukaemia-specific T Cells Using Synthetic DNA Nanocarriers. *Nat. Nanotechnol* 12, 813–820. doi:10.1038/nnano.2017.57

Sunshine, J. C., Akanda, M. I., Li, D., Kozielski, K. L., and Green, J. J. (2011). Effects of Base Polymer Hydrophobicity and End-Group Modification on Polymeric Gene Delivery. *Biomacromolecules* 12, 3592–3600. doi:10.1021/bm200807s

Sunshine, J. C., Peng, D. Y., and Green, J. J. (2012). Uptake and Transfection with Polymeric Nanoparticles Are Dependent on Polymer End-Group Structure, but Largely Independent of Nanoparticle Physical and Chemical Properties. *Mol. Pharm.* 9, 3375–3383. doi:10.1021/mp3004176

Sunshine, J. C., Sunshine, S. B., Bhutto, I., Handa, J. T., and Green, J. J. (2012). Poly(β-amino Ester)-Nanoparticle Mediated Transfection of Retinal Pigment Epithelial Cells *In Vitro* and *In Vivo*. *PloS one* 7, e37543. doi:10.1371/journal.pone.0037543

Tzeng, S. Y., and Green, J. J. (2013). Subtle Changes to Polymer Structure and Degradation Mechanism Enable Highly Effective Nanoparticles for siRNA and DNA Delivery to Human Brain Cancer. *Adv. Healthc. Mater.* 2, 468–480. doi:10.1002/adhm.201200257

Valente, J. F. A., Pereira, P., Sousa, A., Queiroz, J. A., and Sousa, F. (2021). Effect of Plasmid DNA Size on Chitosan or Polyethyleneimine Polyplexes Formulation. *Polymers (Basel)* 13, 793. doi:10.3390/polym13050793

Wang, Q., Xie, X., Zhang, X., Zhang, J., and Wang, A. (2010). Preparation and Swelling Properties of pH-Sensitive Composite Hydrogel Beads Based on Chitosan-G-Poly (Acrylic Acid)/vermiculite and Sodium Alginate for Diclofenac Controlled Release. *Int. J. Biol. Macromol* 46, 356–362. doi:10.1016/j.ijbiomac.2010.01.009

Wang, Y., Wang, C.-F., Lie, M., Zhou, D.-Z., Huang, W., and Wang, W.-X. (2020). Effects of Branching Strategy on the Gene Transfection of Highly Branched Poly(β-Amino Ester)s. *Chin. J. Polym. Sci.* 38, 830–839. doi:10.1007/s10118-020-2393-y

Wilson, D. R., Sen, R., Sunshine, J. C., Pardoll, D. M., Green, J. J., and Kim, Y. J. (2018). Biodegradable STING Agonist Nanoparticles for Enhanced Cancer Immunotherapy. *Nanomedicine* 14, 237–246. doi:10.1016/j.nano.2017.10.013

Wilson, D. R., Suprenant, M. P., Michel, J. H., Wang, E. B., Tzeng, S. Y., and Green, J. J. (2019). The Role of Assembly Parameters on Polyplex Poly(beta-Amino Ester) Nanoparticle Transfections. *Biotechnol. Bioeng.* 116, 1220–1230. doi:10.1002/bit.26921

Xia, J., Tian, H., Chen, L., Lin, L., Guo, Z., Chen, J., et al. (2011). Oligoethylenimines Grafted to PEGylated Poly(β-Amino Ester)s for Gene Delivery. *Biomacromolecules* 12, 1024–1031. doi:10.1021/bm101361g

Yu, C., Li, L., Hu, P., Yang, Y., Wei, W., Deng, X., et al. (2021). Recent Advances in Stimulus-Responsive Nanocarriers for Gene Therapy. *Adv. Sci.*, 2100540. doi:10.1002/advs.202100540

Zeb, A., Rana, I., Choi, H. I., Lee, C. H., Baek, S. W., Lim, C. W., et al. (2020). Potential and Applications of Nanocarriers for Efficient Delivery of Biopharmaceuticals. *Pharmaceutics* 12, 1184. doi:10.3390/pharmaceutics12121184

Zeng, M., Zhou, D., Ng, S., Ahern, J. O. K., Alshehri, F., Gao, Y., et al. (2017). Highly Branched Poly(5-Amino-1-Pentanol-Co-1,4-Butanediol Diacrylate) for High Performance Gene Transfection. *Polymers (Basel)* 9, 161. doi:10.3390/polym9050161

Zhang, X. F., Liu, Z. G., Shen, W., and Gurunathan, S. (2016). Silver Nanoparticles: Synthesis, Characterization, Properties, Applications, and Therapeutic Approaches. *Int. J. Mol. Sci.* 17, 1534. doi:10.3390/ijms17091534

Zhao, X., Cui, H., Chen, W., Wang, Y., Cui, B., Sun, C., et al. (2014). Morphology, Structure and Function Characterization of PEI Modified Magnetic Nanoparticles Gene Delivery System. *PLoS One* 9, e98919. doi:10.1371/journal.pone.0098919

Zou, W., Liu, C., Chen, Z., and Zhang, N. (2009). Preparation and Characterization of Cationic PLA-PEG Nanoparticles for Delivery of Plasmid DNA. *Nanoscale Res. Lett.* 4, 982–992. doi:10.1007/s11671-009-9345-3

Conflict of Interest: Author ZZ Collaborated with Shandong Dyne Marine Biopharmaceutical Company Limited and Shandong Xili Pharmaceutical Company Limited.

The remaining authors declare that the research was conducted in the absence of any commercial or financial relationships that could be construed as a potential conflict of interest.

frontiers | Frontiers in Pharmacology

REVIEW
published: 02 June 2022
doi: 10.3389/fphar.2022.908713

Nanotechnology-Based Diagnostic and Therapeutic Strategies for Neuroblastoma

Hui Yan[1,2], *Bo Zhai*[1,2], *Fang Yang*[1,2], *Zhenliang Chen*[1,2], *Qiang Zhou*[1,3], *Ana Cláudia Paiva-Santos*[4], *Ziqiao Yuan*[5]* and *Yang Zhou*[1,2]*

[1]Children's Hospital Affiliated to Zhengzhou University, Henan Children's Hospital, Zhengzhou Children's Hospital, Zhengzhou University, Zhengzhou, China, [2]Department of Cardiothoracic Surgery, Children's Hospital Affiliated to Zhengzhou University, Henan Children's Hospital, Zhengzhou Children's Hospital, Zhengzhou, China, [3]Department of Pathology, Children's Hospital Affiliated to Zhengzhou University, Henan Children's Hospital, Zhengzhou Children's Hospital, Zhengzhou, China, [4]Group of Pharmaceutical Technology, Faculty of Pharmacy, University of Coimbra, Coimbra, Portugal, [5]School of Pharmaceutical Sciences, Zhengzhou University, Zhengzhou, China

Neuroblastoma (NB), as the most common extracranial solid tumor in childhood, is one of the critical culprits affecting children's health. Given the heterogeneity and invisibility of NB tumors, the existing diagnostic and therapeutic approaches are inadequate and ineffective in early screening and prognostic improvement. With the rapid innovation and development of nanotechnology, nanomedicines have attracted widespread attention in the field of oncology research for their excellent physiological and chemical properties. In this review, we first explored the current common obstacles in the diagnosis and treatment of NB. Then we comprehensively summarized the advancements in nanotechnology-based multimodal synergistic diagnosis and treatment of NB and elucidate the underlying mechanisms. In addition, a discussion of the pending challenges in biocompatibility and toxicity of nanomedicine was conducted. Finally, we described the development and application status of nanomaterials against some of the recognized targets in the field of NB research, and pointed out prospects for nanomedicine-based precision diagnosis and therapy of NB.

Keywords: neuroblastoma, nanotechnology, nanomedicines, diagnosis, therapy

OPEN ACCESS

Edited by:
Saeed Ahmad Khan, Kohat University of Science and Technology, Pakistan

Reviewed by:
Siavash Iravani, Isfahan University of Medical Sciences, Iran
Hao Wu, Chuzhou University, China
Zhongcheng Ke, Huangshan University, China

***Correspondence:**
Ziqiao Yuan
figaroyzq@163.com
Yang Zhou
zyangcpu@163.com

Specialty section:
This article was submitted to Experimental Pharmacology and Drug Discovery, a section of the journal Frontiers in Pharmacology

Received: *30 March 2022*
Accepted: *27 April 2022*
Published: *02 June 2022*

Citation:
Yan H, Zhai B, Yang F, Chen Z, Zhou Q, Paiva-Santos AC, Yuan Z and Zhou Y (2022) Nanotechnology-Based Diagnostic and Therapeutic Strategies for Neuroblastoma. Front. Pharmacol. 13:908713. doi: 10.3389/fphar.2022.908713

INTRODUCTION

Epidemic Burden of Neuroblastoma

Neuroblastoma (NB), composed of undifferentiated neuroblasts, is an immature embryonal tumor originating from the adrenal medulla and paravertebral sympathetic nervous system (Matthay et al., 2016). The most common origin of NB is the adrenal gland, which occurs in 40% of localized tumors and 60% of metastatic tumors (Nakagawara et al., 2018). In addition, NB is also found to occur in other parts of the sympathetic nervous system other than the adrenal gland (Pudela et al., 2020). As the most common cancer in infancy and the most common extracranial solid tumor in childhood, NB is the third most frequent childhood tumor, ranking after leukemia and brain tumors and accounting for 6–10% of pediatric tumors (Nicholas et al., 2016). Some high prevalence countries such as France, Israel, Switzerland and New Zealand have an annual incidence of 11/1 million (0–15 years), the United States has about 25/1 million, and China and India have less than 5/1 million (Moreno et al., 2016). The incidence of NB is age-dependent, with a mean age of 17.3 months at the time of clinical diagnosis (Matthay et al., 2016; Whittle et al., 2017). It has been estimated that NB accounts for 9–15% of all childhood cancer-related deaths and is a highly heterogeneous tumor, with

5-year survival rates of 90 and 50% for patients with NB in the non-high-risk and high-risk groups, respectively (Pudela et al., 2020).

Difficulty in Neuroblastoma Diagnosis

NB is diagnosed on the basis of histological confirmation combined with clinical manifestations, laboratory tests, imaging features and genetic examinations (Zhan et al., 2017; Swift et al., 2018a). Imaging analysis as visualization detection methods are irreplaceable in NB diagnosis and mainly include ultrasound imaging (US), magnetic resonance imaging (MRI), and optical imaging. However, the pathological characteristics of most tumors usually cannot be accurately estimated by imaging analysis alone. Ancillary detections of some specific tumor biomarkers such as neuron-specific enolase, S-100 protein and tryptophan were performed to improve the histological diagnostic accuracy of NB (Rajwanshi et al., 2009). In about 90% of NB cases, increased catecholamines and their metabolites includes dopamine, homovanillic acid and vanillylmandelic acid are found in the urine or blood (Weinstein et al., 2003). Also, the combination of tissue biopsy and pathological examination is an indicator of a definitive diagnosis of the disease. Actually, a synthetic assessment based on histological verification combined with chemical analysis and imaging features is necessary for the diagnosis of NB for a comprehensive assessment of disease progression (Swift et al., 2018b). Since biological methods have limited sensitivity and specificity and failure in precise tumor localization, invasiveness, and limited specimen acquisition, the development of imaging techniques will more likely to achieve early diagnosis of NB (Swift et al., 2018a). However, imaging methods are constrained by cost and risk, while it remains powerless for tumors smaller than 0.5 cm in diameter, thus it is urgent to develop advanced techniques for early diagnosis and monitoring of NB.

Current Challenges in Neuroblastoma Treatment

Although complete resection of the primary NB is expected to greatly improve overall survival and most children are inoperable due to metastases at the time of diagnosis, thus chemotherapy, radiotherapy, differentiation-inducing therapy, immunotherapy, and autologous hematopoietic stem cell transplantation remain the primary treatments in most cases (Perkins et al., 2014; Berlanga et al., 2017; Sait and Modak, 2017). The chemotherapeutics clinically used for NB include cisplatin, cyclophosphamide, vincristine, etoposide, teniposide, Adriamycin (DOX) (Berlanga et al., 2017). As a method of local treatment of tumors, nuclear medicine treatment is suitable for controlling localized tumors that cannot be completely removed or with unsatisfactory effect of chemotherapy (Perkins et al., 2014). Currently, the most promising immunotherapy is monoclonal antibody technology against the ganglioside 2 (GD2), and has achieved remarkable therapeutic results in the consolidation phase (Sait and Modak, 2017). Autologous stem cell transplantation is also applied greatly in clinical NB treatment with the advantages of low self-recurrence rate, early recovery from immune reconstitution, and rapid recovery from bone marrow transplantation (Weinstein et al., 2003). Conventional treatment has been shown to achieve good results in children with low-risk NB, but the outcome in children with high-risk NB remains unsatisfactory even with various combined treatments. Nevertheless, there are some insurmountable limitations of conventional therapies that require further improvement. Surgical intervention may result in incomplete tumor resection. Chemotherapy is highly prone to damage healthy tissues, leading to severe, dose-limiting side effects, including toxicity and bone marrow suppression, compromising efficacy and even leading to chemoresistance. In addition, emerging targeted drugs exhibit many drawbacks, such as high toxicities, low cure rates, and high off-target propensity (Hishiki et al., 2014).New treatment concepts are urgently needed to effectively treat children with NB, and nanomedicine as an emerging technology could provide better personalized treatment for tumor patients.

Prospects of Nanotheranostics for Precise Diagnosis and Treatment in Neuroblastoma

Nanomedicine refers to nanoparticles (NPs) whose size range is 1–1000 nm in pharmacy. Nanocarriers are various nanomaterials capable of dissolving or dispersing drugs, while nanodrugs are NPs processed directly from active pharmaceutical ingredients (Sosnik and Carcaboso, 2014; Raza et al., 2019). The main types of NPs include nanoliposomes, nanocapsules, nanospheres, solid lipid NPs, polymer micelles, and nanomedicines (Aleassa et al., 2015). The contrast agent encapsulated by nanomaterials facilitate the acquisition of detailed cellular and molecular images, real-time detection of targeted drugs within the tumor, and also provides more detailed data for maximum tumor removal, thus improving the diagnostic accuracy (Aleassa et al., 2015; Wang et al., 2022a). Nevertheless, the application of nanotechnology in NB therapy remains a challenging new strategic attempt. Nanodrug delivery systems possess superior advantages over conventional means in overcoming limitations associated with unfavorable drug properties, such as solubility, stability, permeability, toxicity, and increased drug accumulation in desired tumor-specific areas and thus eliminating unwanted side effects and toxicity (Rodríguez-Nogales et al., 2019; Raza et al., 2022). Nanodrug technology will be an emerging and more promising therapeutic strategy in the field of NB treatment, especially for high-risk NB patients who have suffered from failure in conventional treatment or relapsed. Here, we are summarizing the current literature on nanotechnology and providing insights into the applications of nanotechnology-based diagnosis and therapeutic strategy for NB, including US, MRI, optical imaging, chemotherapy, radiation therapy, phototherapy, immunotherapy, gene therapy, differentiation and tumor extracellular matrix (ECM) remodeling (**Figure 1**). Moreover, the opportunities and challenges of nanomedicine in the field of oncology research are described in detail, especially the biocompatibility and toxic effects of nanomaterials. Finally, some recognized targets for NB diagnosis or treatment are also

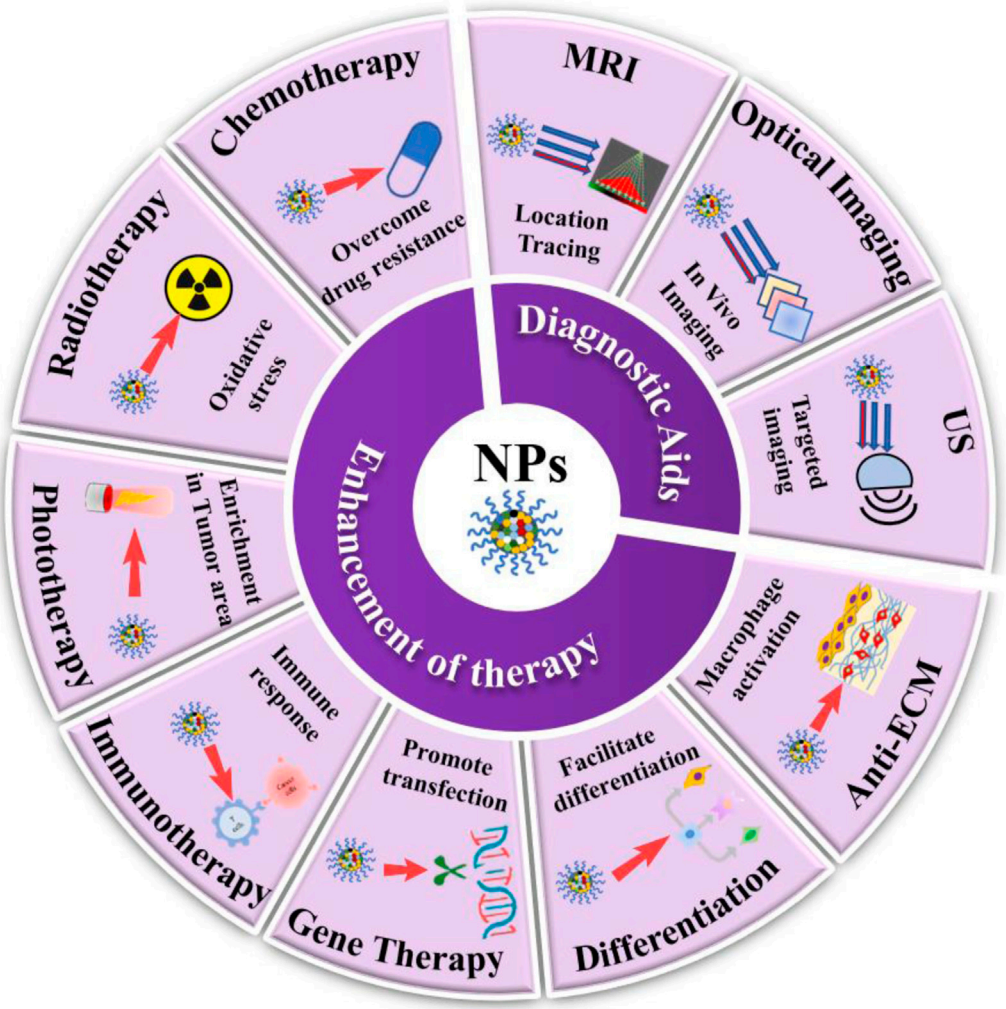

FIGURE 1 | Schematic illustration of emerging nanomedicines for NB diagnosis (MRI, optical. imaging and US) and therapies (chemotherapy, radiotherapy, phototherapy, immunotherapy, gene therapy, differentiation, and anti-ECM therapy).

highlighted, as well as a special focus on the current status of nanotechnology development and applications based on them.

NANOTECHNOLOGY ENABLES NEUROBLASTOMA DIAGNOSIS

Although image analysis is irreplaceable as a visualization detection method in NB diagnosis, it has the drawbacks of low detection capability and low accuracy rate. The development of nano-contrast agents or nanoprobes suitable for various types of imaging devices are currently available to visualize the physiological, pathological and metabolic conditions of the body with high accuracy and will present prospects for application in the diagnostic and prognostic evaluation of NB. This section focused on recently proposed approaches for the diagnosis of nanomedicines in patients with NB (**Table 1**).

Nanotechnology for US

US is unique in the field of medical imaging due to its safety and convenience and is usually performed for the first examination when an abdominal mass is suspected in a child (Swift et al., 2018b). In contrast to other types of diagnostic methods such as x-ray and computed tomography, US performs deeper tissue penetration and less invasiveness to the organism. Modification of contrast agents for US is one of the main directions regarding the improvement of ultrasound diagnostic performance. Through the integration with multiple nanosystems, ultrasound not only enables better high-resolution ultrasound imaging, but also facilitates the controlled release of drugs at specific tumor sites (Alphandéry, 2022). Although there have been numerous studies on the application of nanomaterial-based modified ultrasound technology for cancer diagnosis, i.e., nano-bubbles and inorganic NPs, there are still few reports on the diagnosis of NB (Devarakonda et al., 2017; Liu et al., 2019).

TABLE 1 | Summary of emerging nanomedicines for NB diagnostics.

Diagnostic type	Formulation	Type of NPs	Sizes (nm)	Model	Observed effects	Ref.
US	RVG-GNPs	Nanobubbles NPs	220	*In vitro* and *in vivo*	Enhanced US signals and reduced tumor growth in a tumor-bearing mouse model.	Lee et al. (2016a)
MRI	$DySiO_2$-$(Fe_3O_4)_n$	Inorganic NPs	30	*In vitro*	High-performance MRI and fluorescence imaging of NB	Lee et al. (2006b)
	Fe3O4-poly(acrylic acid) (PAA)	Magnetic polymer particles	20–200	*In vitro* and *in vivo*	Exhibited highly biocompatible and good contrast in T2-weighted imaging.	Chen et al. (2015)
	Fe3O4@GdPB	Iron oxide-gadolinium-containing Prussian blue	About 30	*In vitro* and *in vivo*	Increased the signal: noise ratio of the T1-weighted scan and reduced the growth rate of the tumor.	Kale et al. (2017)
	LPD	Composite of liposome, peptide and plasmid DNA	70–140	*In vitro* and *in vivo*	Targeted NB cell transfection and real-time monitoring of vector distribution in the tumor	Kenny et al. (2012)
Optical imaging	NDI-nip FONPs	Organic particles	50–70	*In vitro*	Targeted imaging and delivery of curcumin to NB cell	Ghosh et al. (2021)
	A&MMP@Ag2S-AF7P	Affinity peptide composites	160	*In vitro* and *in vivo*	Distinguish tumor tissue from non-cancerous tissue	Zhan et al. (2021)
	Anti-GD2/GQDs	Conjugates of graphene quantum dots and antibody	150–160	*In vitro* and *in vivo*	Tumor tracking and imaging	Lin et al. (2021)

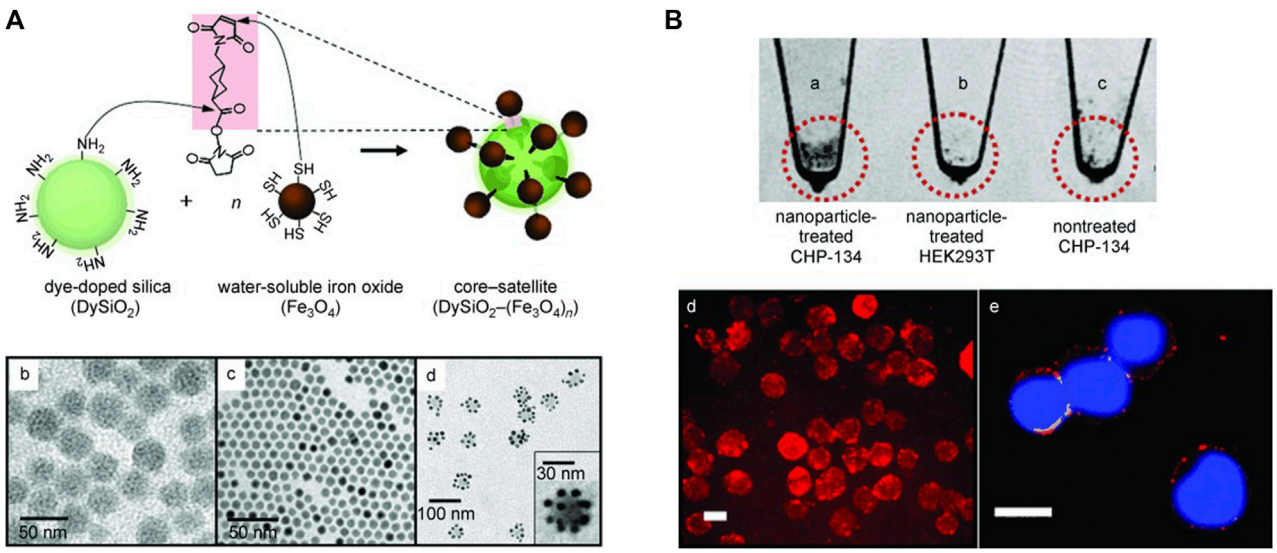

FIGURE 2 | Dual-Mode nanoparticle probes for high-performance magnetic resonance and fluorescence imaging of NB. **(A)** Schematic diagram for the synthesis of core–satellite DySiO2–(Fe3O4)n nanoparticles. **(B)** Dual-mode detection of PSAs. Reproduced with permission from (Lee et al., 2006a). Copyright 2006, Wiley-VCH Verlag GmbH & Co. KGaA, Weinheim.

Interestingly, Lee Jet al. have created cancer-targeting, gas-generating polymer NPs (GNPs) as a therapeutic tool for ultrasound imaging and treatment of NB (Lee et al., 2016a). In detail, the composite of GNPs modified with rabies virus glycoprotein (RVG) peptides that specifically target NB cells (RVG-GNPs) was used as the nanoimaging material. Importantly, it was found to greatly enhance the ultrasound signal in a tumor-bearing mouse model and to suppress tumor growth without conventional therapeutic agents. Since children are a vulnerable population to toxic contrast and therapeutic agents, adopting this approach promisingly enables both targeted therapy and highly accurate detection with guaranteed safety.

Nanotechnology Facilitates Magnetic Resonance Imaging

Magnetic NPs (MNPs) are extremely promising for NB imaging and targeted therapies. Modification of peptides or antibodies on the surface of MNPs allows direct targeting of tumor cells to disrupt the function of tumor cell-active signaling pathways (Chertok et al., 2008). MNPs show higher longitudinal relaxation, present an enhanced signal on T1-weighted images and shorten the transverse relaxation time in T1-and T2-weighted images, resulting in a significant decrease in signal intensity of the target organ on conventional T2-weighted images. Therefore, MNPs have been widely used as contrast agents and molecular imaging probes for

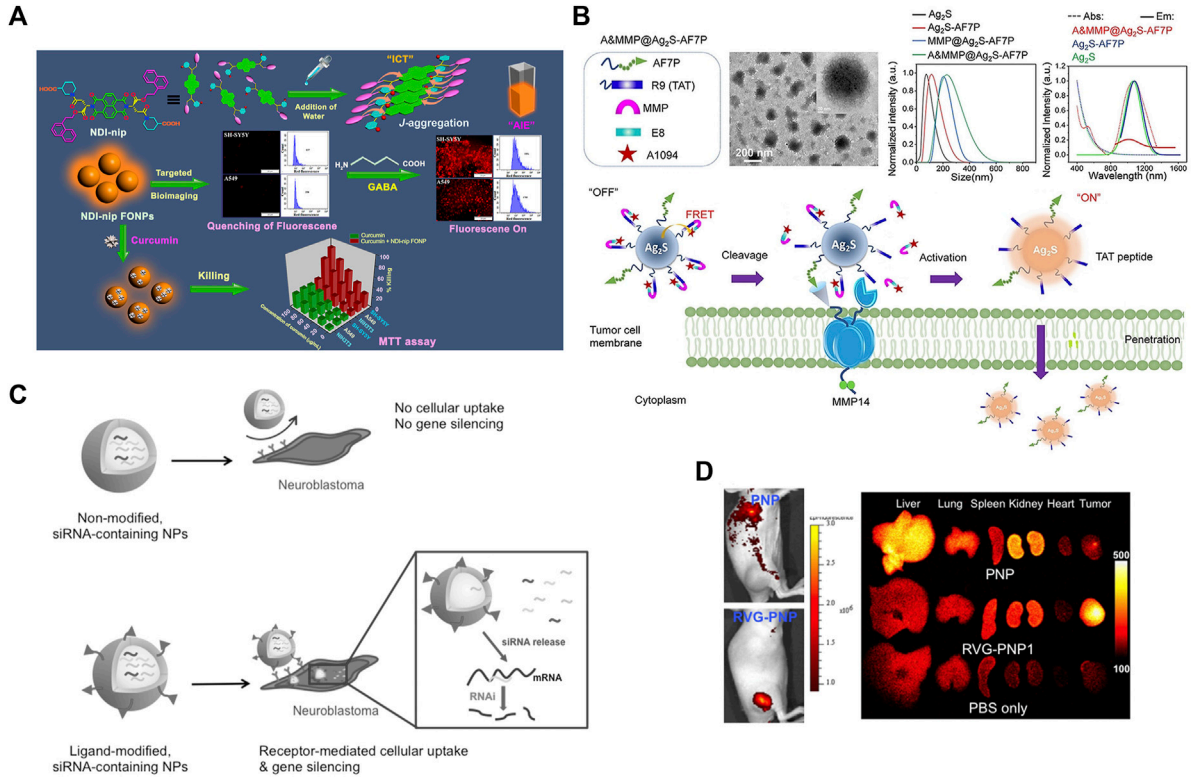

FIGURE 3 | Nanoparticle for optical imaging of NB. **(A)** Schematic diagram of targeted cell imaging of GABA (γ-aminobutyric acid)-rich SH-SY5Y cells by NDI-derived FONPs. Reproduced with permission from: Anup Kumar Ghosh, Monalisa Chowdhury, and Prasanta Kumar Das. Nanoparticles as Targeted Delivery Vehicle and Diagnostic Probe toward GABAA-Receptor-Enriched Cancer Cells. ACS applied bio materials, 2021, 4(10): 7563–7577 (Ghosh et al., 2021). Copyright 2021, American Chemical Society. **(B)** Schematic illustration of A&MMP@Ag2S-AF7P for NB detection. Reproduced with permission from (Zhan et al., 2021). Copyright 2020, Wiley-VCH Verlag GmbH & Co. KGaA, Weinheim. **(C–D)** Ligand-modified, gene-loaded NPs as a tumor-targeting theranostic agent. Reproduced with permission from (Lee et al., 2016b). Copyright 2015, Wiley-VCH Verlag GmbH & Co. KGaA, Weinheim.

MRI. Hybrid nanoparticle probes fabricated using rhodamine-dy-doped silica (DySiO2) NPs as the core material conjugated with high-quality water-soluble Fe3O4 (WSIO) NPs have been confirmed to have synergistic MRI enhancement and good fluorescence properties for polysialic acids (PSAs)-expressing NB cells (**Figure 2**) (Lee et al., 2006a). Superparamagnetic Fe3O4 NPs encapsulated in porous polyacrylic acid (PAA) nanogels to make hybrid nanodrugs with high drug loading capacity, good contrast in T2-weighted imaging, and high MRI sensitivity at NB cell-derived tumor sites (Chen et al., 2015). Composite iron oxide-gadolinium-containing Prussian blue NPs (Fe3O4@GdPB) perform a dual function as a novel therapeutic nanoparticle for diagnostic and therapeutic purposes, which is manifested in the availability for T1-weighted MRI and photothermal therapy (PTT) in NB cell-derived mouse tumor model (Kale et al., 2017). Notably, Fe3O4@GdPB NPs acted as effective MRI contrast agents and were able to effectively improve the signal-to-noise ratio of T1-weighted scans of tumor *in vivo*. Another study reported that a nanocomplex named as LPD, which composed of cationic DOTMA/DOPE liposomes (L), neurotensin-targeting peptide (P) and plasmid DNA (D) fulfilled the multiple functions of both targeted NB cell transfection and real-time monitoring of vector distribution in the tumor by MRI (Kenny et al., 2012).

Nanotechnology Adjunct to Optical Imaging

Although optical imaging is non-radioactive, non-invasive, high-resolution and controllable, its penetrating power is relatively inferior. Fluorescence imaging based on fluorescence signals generated by fluorescein compensates for this deficiency to some extent. Near-infrared fluorescence (NIRF) probes are widely adopted for their high transmission capability and safety, and have been implemented in the field of small animal bioimaging systems and translational medicine research on tumors. Nowadays, there are numerous nanomaterials such as liposomes, metallic as well as nonmetallic NPs are available to encapsulate NIRF for targeted tumor optical imaging (Setua et al., 2010). Fluorescent organic NPs (FONPs) derived from naphthalenediimine (NDI) can be used as targeted diagnostic probes for targeted cellular imaging and as drug delivery vehicles for the delivery of the anticancer drug curcumin to γ-aminobutyric acid receptor-rich cells such as the NB cell line SH-SY5Y (**Figure 3A**) (Ghosh et al., 2021). Such spherical organic particles are formed by self-assembly driven by piperidine-tethered l-aspartate attached NDI derivatives occurring through J-type aggregation, exhibiting aggregation-induced emission. It has been proposed that a matrix metalloproteinase 14 (MMP14)-activatable NIR-II nanoprobe

(A&MMP@Ag2S-AF7P) can be used to distinguish the NB tumor tissues from surrounding non-cancerous tissue (**Figure 3B**) (Zhan et al., 2021). This nanoprobe consists of three main functional components, an affinity peptide AF7P targeting the membrane-type ring structure of MMP14, an MMP14 activating peptide, and a fluorescence resonance energy transfer (FRET) system with NIR-II-emitting Ag2S QDs and a NIR absorber A1094. Cooperative interaction between its components selectively produces visible fluorescent signals in NB tissues with high expression of MMP14, which facilitates rapid and unperturbed tissue analysis for *ex vivo* NB diagnosis and greatly quickens intraoperative decisions. Another study reported that utilizing the nanomaterial graphene quantum dots (GQD) coupled with anti-GD2 antibodies enables tumor tracking and imaging in mice with minimal or no *in vitro* cytotoxicity (Lin et al., 2021). In addition, a biocompatible poly(d,l-lactide-co-glycolide) (PLG) nanoparticle containing imaging probes and therapeutic genes modified with RVG peptide can effectively target NB tumor sites for optical imaging both *in vitro* and *in vivo*, and can carry nanoparticles encapsulating therapeutic genes (siMyc, siBcl-2, and siVEGF) to significantly inhibit tumor growth in mouse models for targeted therapeutic effects (**Figures 3C,D**) (Lee et al., 2016b). Multimodal imaging technology based on nanoimaging agents integrates various types of imaging modalities to produce synergistic effects and provide more comprehensive and accurate imaging information for precise diagnosis and treatment of NB.

NANOTECHNOLOGY ENHANCES THERAPEUTIC TREATMENT FOR NEUROBLASTOMA

Nanotechnology and Chemotherapy

Chemotherapy, as a conventional therapeutic strategy for NB, has yielded great achievements in narrowing tumor area prior to surgery resection, preventing tumor metastatic spread, suppressing tumor proliferation, and prolonging patients' lifetime. Chemotherapeutics routinely administered for NB include several cytotoxic agents such as vincristine, DOX, cyclophosphamide, cisplatin, carboplatin, topotecan, irinotecan, and paclitaxel (PTX) (George et al., 2010). However, curative effects of these chemotherapeutic agents tended to be severely compromised due to their rapid clearance and non-specific distribution, which leads to unavoidable systemic toxicity. In addition, multidrug resistance is another major cause of chemotherapy failure (Wu et al., 2022). Currently, nanomaterial-based approaches have been proposed in combination with chemotherapy aim to enhance the efficacy of conventional chemotherapy regimens through multiple strategies. Nanomedicines enhance the effectiveness of chemotherapy for NB mainly through the following ways: 1) targeting chemotherapeutics through nanocarriers; 2) improving permeability to tumor tissues; 3) reversing multiple drug resistance; 4) collaborating with other therapeutic approaches for NB.

The abnormal vascular proliferation in tumor tissues is characterized by high vascular density and poor vessel wall integrity, wide gaps, permeability to macromolecular particles and comparatively slow lymphatic reflux, thus enabling NPs of a certain size to access and retain in tumor tissues, and achieving efficient and accurate enrichment in tumor tissues. Such effect is called the enhanced permeability and retention (EPR) effect, which belongs to the passive targeting effect (Matsumura and Maeda, 1986). Besides, various nanomaterial-based targeted drug delivery systems have been designed to enhance the aqueous solubility, stability and pharmacokinetics process of numerous hydrophobic drugs *in vivo*, enabling aggressive targeting of drug delivery to tumor sites, realizing targeted drug release and reducing drug toxicity while enhancing drug efficacy and overcoming drug resistance. NPs with diameter less than 200 nm exhibit stronger EPR efficacy which are widely utilized for tumor targeting therapy. Nanomaterials have a large specific surface area and are able to effectively load hydrophobic drugs, exhibit protective effect and increase their stability and bioavailability in the circulation, which allows for long circulation through modifications such as polyethylene glycol (PEG) (Wen et al., 2012). The small molecule chemotherapeutic agents mainly penetrate into the tumor cells through passive diffusion, which is less efficient and poorly targeted, susceptible to drug resistance through recognition and efflux by the transporter proteins on the membrane surface of tumor cells. Overcoming drug resistance by loading chemotherapeutics with nanomaterials to alter the drug delivery to tumor cells and improve drug uptake by tumor cells is considered to be a feasible and promising strategy (Khan et al., 2019; Amerigos Daddy J C et al., 2020). It was found that liposomal NPs overcame drug resistance by mediating the entrance of drugs into tumor cells through cytokinesis and further evading the efflux effect of transporter proteins and lysosomal phagocytosis (Li et al., 2013). Several cationic polymers such as Planic are characterized by their transportation to the nucleus (Batrakova and Kabanov, 2008), and such materials would be utilized for the loading of chemotherapeutics that specifically target the nucleus to allow them to deliver smoothly to the intended target.

Research reveals that NPs carriers may provide better anti-tumor efficacy of chemotherapeutics, especially topoisomerase inhibitors and PTX, in NB (**Table 2**). SN-38 as a novel topoisomerase I inhibitor exhibits an extensive anticancer activity in adult and pediatric tumors (Norris et al., 2014). However, this camptothecin (CPT) analogue is limited in clinical use due to its toxicity, metabolic instability and incompatibility with conventional drug delivery vehicles (Colletti et al., 2017). EZN-2208, a water-soluble polyethylene glycolized SN38 drug coupling, possesses strong cytotoxicity to NB cells, prolongs duration of drug activity, and is well tolerated *in vivo* without significant toxicity, acute or chronic hepatic and renal toxicity. The employment of hydroxypropyl-β-cyclodextrin (HP-β-CD) derivatives as a drug delivery system significantly enhanced the stability, bioactivity and antitumor activity of the alkaloids CPT and luotonin A in several cancer cell lines including breast, lung, liver, ovarian and NB (González-Ruiz et al., 2021). To improve the solubility and pharmacokinetic

TABLE 2 | Summary of emerging nanomedicines for NB chemotherapy.

Formulation	Type of NPs	Drug	Model	Observed effects	Ref.
CPT/HP-β-CD and CPT/β-CD	Cyclodextrin	CPT	*In vitro*	Enhanced the bioactivity and antitumor activity of the CPT	González-Ruiz et al. (2021)
LP-2- pyrazolo[3,4-d] pyrimidines	Liposome	Pyrazolo[3,4-d] pyrimidines	*In vitro*	Exhibited inhibitory activity against NB cell	Vignaroli et al. (2016)
ApoE3-C-PBCA-Curcumin	ApoE3-C-PBCA	Curcumin	*In vitro*	Enhanced anticancer activity of curcumin against NB cell	Mulik et al. (2012)
Nab-PTX	Nab	PTX	*In vitro* and *in vivo*	Inhibited NB cells growth and prolongs the survival of tumor-bearing mice	Zhang et al. (2013)
PLGA-PTX	PLGA	PTX	*In vitro*	Induced DNA damage in NB cells	Bacanlı et al. (2021)
Nab-PTX	Nab	PTX	phase I/II	Relatively safe for children with NB	(Moreno et al., 2018; Amoroso et al., 2020)

properties of chemotherapeutics such as cisplatin, and azithromycin, albumin NPs and liposomes were developed and exhibited strong inhibitory activity against NB cell line (Vignaroli et al., 2016). Mulik et al. produced apolipoprotein-E3-mediated curcumin-loaded poly(butyl) cyanoacrylate NPs using an anionic polymerization method (Mulik et al., 2012), and the formulation showed enhanced anticancer activity against SH-SY5Y cell compared to the natural curcumin solution and untargeted NPs. Albumin-bound PTX NPs (Nab-PTX) exhibited enhanced cellular transport capacity, better cytotoxic effect in NB cells-derived mouse model compared to non-encapsulated PTX (Zhang et al., 2013). Similarly, the nano-encapsulation formed by the biocompatible drug delivery vehicle Poly (lactic-co-glycolic acid) (PLGA) with PTX exhibited stronger cytotoxic effects on NB cells than that of free PTX (Bacanlı et al., 2021). Excitingly, the safety and efficacy of Nab-PTX has been assessed in Phase I/II clinical trials for refractory NB and other pediatric solid tumors (NCT01962103) (Moreno et al., 2018; Amoroso et al., 2020). Although limited activity was observed, the safety of Nab-PTX was confirmed in pediatric patients. Above all, incentivizing the effective delivery of drugs and improving their bioavailability and efficacy *in vivo* are the critical issues that should be addressed in a wide range of tumor treatments, including NB.

Nanotechnology and Radiotherapy

Although radiotherapy is one of the standard therapies applied for NB, its therapeutic efficacy is not satisfactory due to adverse effects, radioresistance and recurrence after radiotherapy. Upon radiation photon incidence, metal nanomaterials with higher atomic number (such as metal atoms of gold and silver) undergo energy level jumps and release oscillating electrons, simultaneously scattering Compton electrons (Bilynsky et al., 2022). The high density of ionization energy generated by these electrons on the surface of NPs leads to enhanced radiation energy and enrichment in tumor cells, which strengthens the radioactive DNA damage and further facilitates DNA double-strand breaks, suppresses DNA synthesis and repair (Nasir et al., 2021). Meanwhile, such ionization increases the production of free radicals in tumor cells and enhances the lethality of tumor cells (Calugaru et al., 2015). Furthermore, therapeutic effects of radiotherapy can be further improved with functional nanomaterials through modifying tumor hypoxia. Hemoglobin-based nanocarriers and perfluorocarbon-based NPs have been confirmed to facilitate the EPR effect of NPs via oxygen molecule loading on nanocarriers in preclinical animal experiments, thus efficiently enhancing the tumor oxygen levels, averting the hypoxic tumor microenvironment, and sensitizing tumor to radiotherapy (**Figures 4A,B**) (Murayama et al., 2012; Song et al., 2016). It has also been reported that MnO2 nanomaterials represent a promising nanomaterial for radiotherapy sensitization (Gong et al., 2018). William et al. has found that exposed m-iodobenzylguanidine (MIBG) and 3,4-dihydroxyphenylacetic acid (DOPAC) coated Fe3O4@TiO2 nanocomposites significantly increased the sensitivity of NB cells to radiotherapy (**Figures 4C,D**) (Liu et al., 2021). In addition, this nanocomposite also partially penetrates into the nucleus through mimicking the presence of epidermal growth factor peptides, thus enabling targeting of radiolabeled MIBG molecules into the nucleus with nucleus-targeting nanostructures in future. The nanocoupler can be used as a radiosensitizer for external irradiation therapy and also for delivery of internal emitters to near-genomic DNA regions.

Nanotechnology and Phototherapy

In recent years, phototherapy has received increasing attention in NB treatment in view of its great advantages in improving oncologic outcomes and diminishing side effects. Phototherapy mainly includes two types of therapies, photothermal therapy (PTT) and photodynamic therapy (PDT). Given the intrinsic characteristics of NB tumor tissues with tortuous blood vessels and low heat dissipation efficiency when undergoing heat, PTT is capable to selectively destroy tumor cells while preventing damage to normal cells. Although PTT is relatively safe and controllable, it is less permeable to deep tissues and has limited heat enrichment. Nanomaterials in PTT inherently possess therapeutic properties. Light absorbers typically include nanogold, graphene, and NIR dyes (Zakaria et al., 2016). Nanomaterials with photothermal effect that can effectively convert light energy into thermal energy specifically in tumor cells will undoubtedly beneficial in minimizing damage to surrounding tissue.

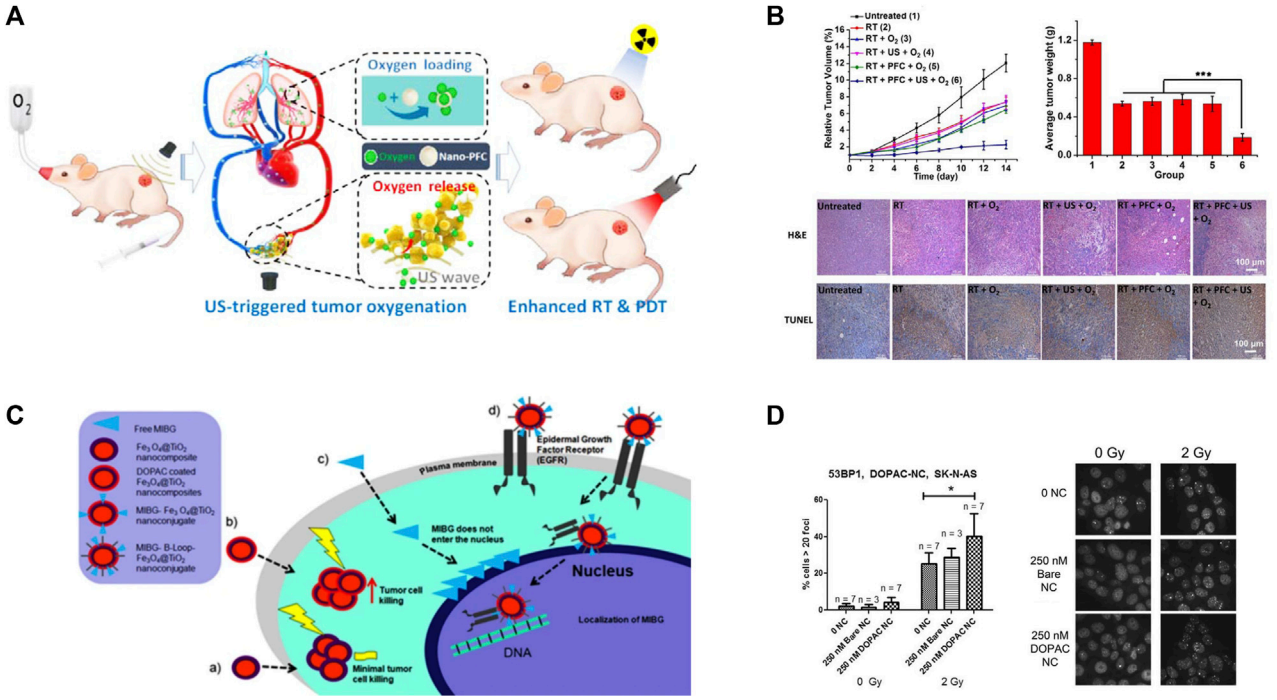

FIGURE 4 | Nanotechnology enhances radiotherapy in NB. **(A–B)** The tumor hypoxic microenvironment was modulated using perfluorocarbon nanoparticles as an oxygen shuttle, which significantly improved the therapeutic effect of PDT and RT on tumors. Reproduced with permission from: Xuejiao Song, Liangzhu Feng, Chao Liang, Kai Yang, and Zhuang Liu. Ultrasound triggered tumor oxygenation with oxygen-shuttle nanoperfluorocarbon to overcome hypoxia-associated resistance in cancer therapies. Nano letters, 2016, 16(10): 6145–6153 (Song et al., 2016). Copyright 2016, American Chemical Society. **(C–D)** Schematic diagram of MIBG and DOPAC-coated Fe3O4@TiO2 as potential radiosensitizers for NB. Reproduced with permission (Liu et al., 2021). Copyright 2021, Springer Nature.

The photosensitizers used for PDT-based tumor suppression mainly have two types: type I process in which the photosensitizer reacts directly with components of the cellular microenvironment to produce peroxides or superoxides that oxidatively disrupt tumor cells; and type II process in which a porphyrin-containing photosensitizer is utilized to produce highly reactive singlet oxygen and thus kill tumor cells upon light exposure at specific wavelengths (Tian et al., 2016). The ROS generated by the photosensitizer have short half-life and the cells adjacent to the photosensitizer undergo the PDT process following photosensitizer enrichment into the tumor area through nanomaterials, thus effectively reducing damage to surrounding normal tissues (Bechet et al., 2008). Photosensitizers themselves tend to be off-target, poorly water-soluble and bioavailable, and developing photosensitizers using nanomaterials will be a superior approach to overcome these flaws (Lim et al., 2013).

Complex iron oxide-gadolinium-containing Prussian blue NPs (Fe3O4 @GdPB) have become novel and effective PTT nanotherapeutic agents for reducing tumor growth rate and improving survival, owing to its cytotoxic effect on targeted tumor cells exposed to laser irradiation (Kale et al., 2017). NIR dyes and porphyrin analogs afford both multimodal imaging and PTT effects. For example, hyaluronic acid-anthocyanine-like dye-iron composite NPs are available for fluorescence imaging, magnetic resonance multimodality imaging and PTT (Della Sala et al., 2022; Wang et al., 2020; Hu et al., 2015). It is rapidly elevated to 28°C with approximately 5 min of irradiation at 1 W/cm2 under a 785 nm laser to facilitate tumor elimination in MCF-7 xenograft mice (Tian et al., 2016). Recently, the dual application of PDT and PTT for better therapeutic outcomes in cancer treatment has attracted a great deal of interest. Gold NPs (AuNP) are well suited as drug carriers due to their biocompatibility, ease of fabrication, and multiple physical properties, making them highly desirable for combining multiple therapeutic approaches in a variety of tumor treatments (**Figure 5A**) (Haimov et al., 2018). Based on this, a group has synthesized a functional complex based on AuNPs covalently linked to meso-tetrahydrobenzyl chloride (mTHPC) drug molecule (AuNP-mTHPC), which enhances the pro-cell death effect of PDT in NB (Haimov et al., 2018). Subsequently, they found that this highly biocompatible and soluble nanotherapeutic agent additionally exhibits a dual PDT/PTT phototoxic effect on NB cells (**Figure 5B**) (Varon et al., 2022).

In addition, the combination of mesoporous carbon NPs-based nanoformulations with chemotherapeutic agents has been found to trigger synergistic tumor suppressive effects with PDT or PTT therapy. For example, combining doxorubicin with mesoporous carbon NPs significantly improved the inhibitory effect of both PTT and PDT on tumor cells (Bechet et al., 2008). However, photothermal nanomaterials, especially inorganic nanomaterials, are not easily degradable in organisms and

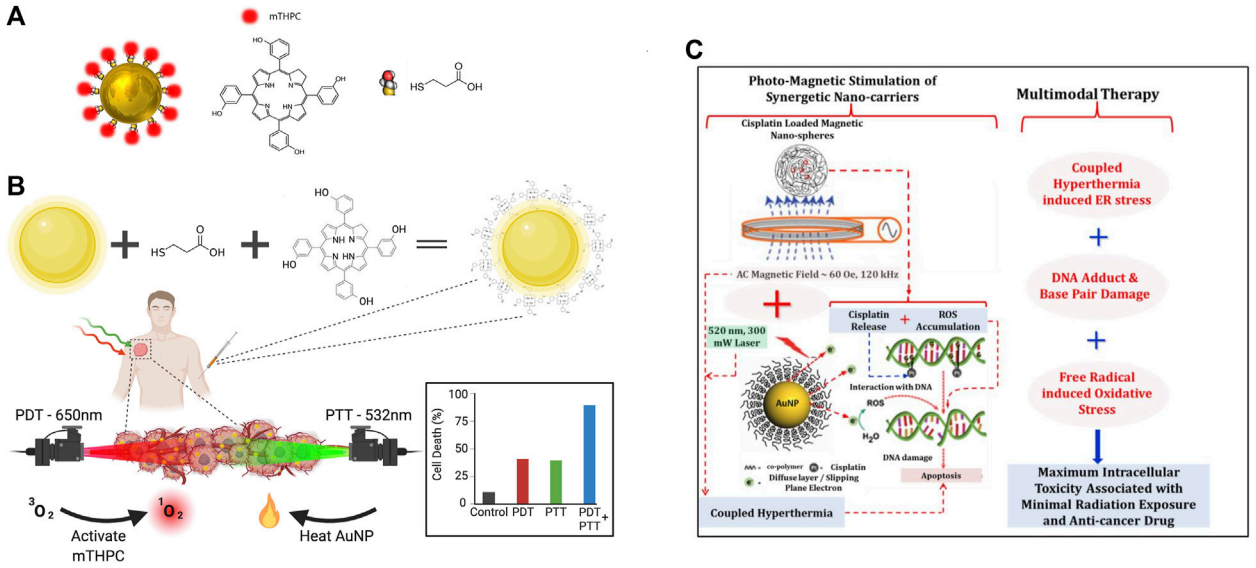

FIGURE 5 | Nanotechnology for phototherapy in NB. **(A)** The AuNP-mTHPC complex is illustrated with the chemical structure of mTHPC in the conjugate and the linker 3-mercaptopropionic acid. Reproduced with permission from: Elina Haimov, Hana Weitman, Shlomi Polani, Hadas Schori, David Zitoun, and Orit Shefi. meso-tetrahydroxyphenylchlorin-conjugated gold nanoparticles as a tool to Improve Photodynamic Therapy. ACS applied materials & interfaces, 2018, 10(3): 2319–2327 (Haimov et al., 2018). Copyright 2018, American Chemical Society. **(B)** AuNP-mTHPC complexes for PDT and PTT dual therapy. Reproduced from (Varon et al., 2022). **(C)** Photo-magnetic irradiation mediated multimodal therapeutic strategy of NB cells. Reproduced from (Atluri et al., 2018).

possess potential toxicity as well as the immune-related adverse effects. To reduce the intensity of photomagnetic irradiation and the required nanoparticle dose level, a hybrid photomagnetic irradiation method based on intelligent nanostructures were developed and exhibited high efficiency and low toxicity in killing NB cells (**Figure 5C**) (Atluri et al., 2018). Development of photothermal conversion materials with greater biocompatibility, degradability and lower toxicity will be a hot spot for future phototherapy.

Nanotechnology and Immune-Based Therapy

Immunotherapy as an emerging anti-cancer therapy refers to the comprehensive homeostatic regulation of tumor suppression through reactivation of the immune function or removal of immunosuppression in the organism (Raza et al., 2021). For the past few decades, immunotherapy has attracted tremendous research interest for its specificity, capacity to clear microscopic lesions and relapse reduction. Boosting immunity and eliminating tumors through the immune system has been the direction of all oncology researchers' efforts. Tumor-associated antigens (TAA) and tumor-specific antigens (TSA) are delivered to immune cells to trigger the specific immune response against tumor cells, thus providing a theoretical basis for tumor immunotherapy (Chen and Mellman, 2013). Currently, immunotherapies commonly employed in clinical practice include immune checkpoint inhibitors and adoptive cell therapy (ACT). Immune checkpoint inhibitors mainly include antibodies specifically targeting cytolytic T lymphocyte-associated antigen 4 (CTLA4), programmed death protein 1 (PD-1) and programmed death ligand 1 (PD-L1) (Krummel and Allison, 1995). ACT is a tumor-fighting method by introducing *ex vivo* modified immune cells into the patients. NB-associated immunotherapies mainly involved in cytokines, dendritic cell vaccines, anti-GD2 antibodies, and allogeneic hematopoietic stem cell transplantation (Sait and Modak, 2017).

Nanomaterials are known to stabilize antibodies and immune factors as well as increase the enrichment of immune factors at tumor regions, improve their targeting and effectiveness, and reduce the adverse effects associated with immunotherapy. While cancer vaccines are used to treat tumors by activating the body's immune response with TAA, TSA and immune factors, the assembly of nanomaterials protects immune components from the internal environment and automatically target tumor-specific T cells to activate a specific immune response (van der Burg et al., 2016). Recently, TSA-containing nanovaccines were designed to produce more tumor-specific cytotoxic T lymphocytes and stronger immune responses *in vivo* compared to vaccines without nanomaterials (Kuai et al., 2017). Moreover, the combination of this vaccine with immune checkpoint inhibitors exhibited a synergistic suppressive effect on tumor recurrence (Kuai et al., 2017). While conventional ACT requires isolation of immune cells from the organism, nanoscaffolds are able to recruit and enrich immune cells *in vivo*. Poelaert et al. developed an immune cell chemotactic agent CC motif chemokine ligand 21 (CCL21) from injectable, sustained-release and optimally loaded alginate nanoformulation, which significantly prolonged the survival, reduced tumor growth and improved immune and therapeutic efficacy compared with CCL21 alone (Poelaert et al., 2020).

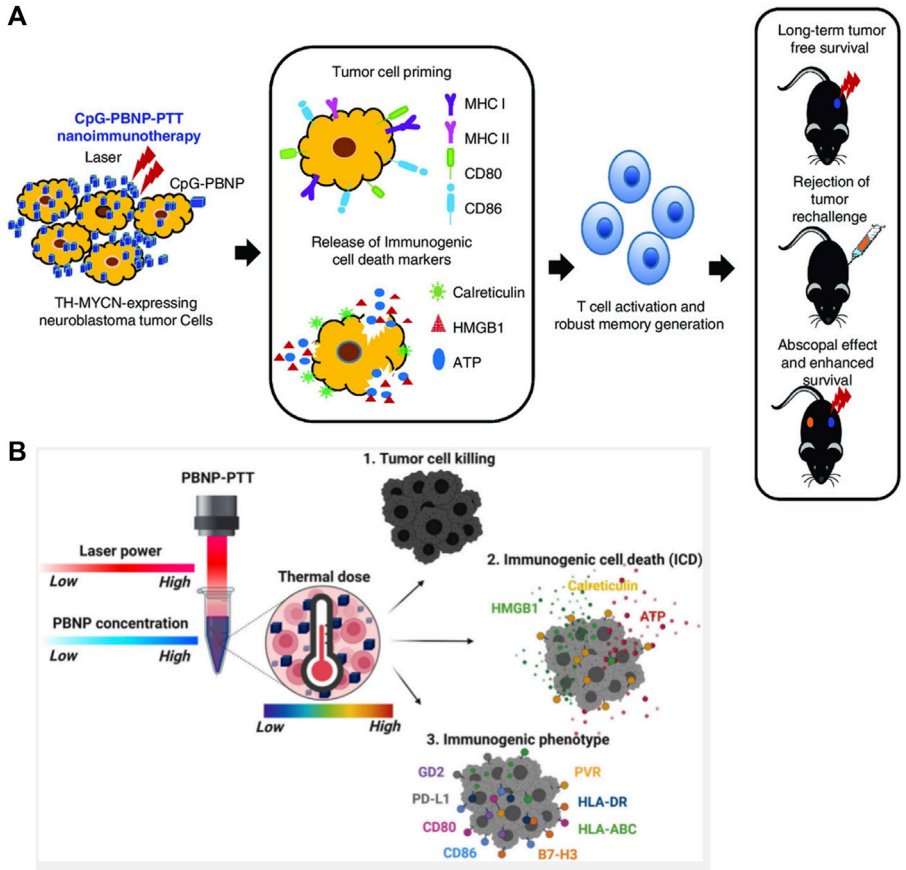

FIGURE 6 | Nanotechnology for immunotherapy in NB. **(A)** Schematic of the mechanism of action of the CpG-PBNP-PTT-based nanoimmunotherapy in the TH-MYCN model of NB. Reproduced with permission from (Shukla et al., 2021). Copyright 2021, Wiley-VCH Verlag GmbH & Co. KGaA, Weinheim. **(B)** Diagram of the induction of NB cell death and immunogenic cell death (ICD) by combined PBNP-PTT therapy. Reproduced from (Sekhri et al., 2022).

Scientifically advance studies have confirmed that individual immune status is inevitably affected by multiple therapeutic options while exerting therapeutic effects. For this reason, the combination of multimodal therapies with immunotherapy is emerging as a feasible treatment option for NB. Undoubtedly, the development of nano-agents enriches these therapeutic strategies. For example, radiotherapy-induced release of inflammatory factors and TAA from *in situ* tumors will trigger tumor-specific immune responses. Thus, radiotherapy and immunotherapy may synergistically exert systemic antitumor effect (Kwong et al., 2011). Nanoparticles capturing TSA have been reported to strengthen the effect of radiotherapy and their abscopal effect while combining with radiotherapy. Juliana et al. demonstrated that combination of PTT with nanomaterials containing immune adjuvant and CTLA-4 monoclonal antibody improved T-cell levels and inhibited tumor growth in NB mice, while exerting a memory effect to suppress tumor recurrence, with superior therapeutic efficacy than CTLA-4 monoclonal antibody or PTT therapy alone (Cano-Mejia et al., 2017). They showed in their mouse model of TH-MYCN gene-driven malignant NB that PTT therapy with PBNP coated with the immune adjuvant CpG oligonucleotide (CpG-PBNP-PTT) was effective in regressing mouse tumors, improving survival time and activating t cell-mediated systemic immune responses (**Figure 6A**) (Shukla et al., 2021). Similarly, combining CpG-PBNP with anti-CTLA-4 immunotherapy can not only cause ablative cell death, but also alter the surface levels of co-stimulatory, antigen-presenting, and co-inhibitory molecules on NB cells (Cano-Mejia et al., 2020). Mechanistically, they elucidated that a series of thermal doses administered to NB cells using Prussian blue PBNP-based PTT (PBNP-PT) upregulated immunogenicity-related markers and enhanced the toxic killing effect of T cells on NB cells (**Figure 6B**) (Sekhri et al., 2022). The organic combination of nanotechnology-based therapies with immunotherapy will fully engage the complementary advantages of multiple therapies.

Nanotechnology and Gene Therapy

Gene therapy as a novel oncology treatment has become a research hotspot in biomedicine. Currently, one of the serious challenges in gene therapy research is the issue of vehicle system (Whittle et al., 2017). Transfer vehicles applied for gene therapy include antisense nucleic acids, cationic polymers, plasmid DNA and recombinant viral vectors (Roy et al., 2005; Ullah et al., 2021).

However, antisense nucleic acids and plasmid DNA are inefficiently transferred and susceptible to degradation by nucleases, while viral vectors are defective in terms of safety and immunogenicity. Therefore, it seems crucial to develop new safe and efficient gene therapy vector systems. In addition, the target gene involved in the gene therapy should ideally be tumor cell-specific, otherwise some toxic effects or other concerns can be inducted. With the rapid development of nanobiotechnology, the emergence of a new non-viral vector system, the nanogene vector system, has brought new vitality to gene therapy in NB. It has the advantages of lower immunogenicity, larger capacity, better protection of DNA fragments, higher transfection rate and lower cytotoxicity compared to viral vectors (Roy et al., 2005).

Using nanotechnology not only improves transfection efficiency, but also confers properties that make the vector more suitable for transporting exogenous genes, such as resistance to lysosomal enzymes and DNAases. In addition, it features the advantages of being easy to produce and inexpensive. Integration of nanobiotechnology and gene therapy manifests favorable application prospects. Yoshida S et al. used antisense oligonucleotides (ASO) and superparamagnetic iron oxide (SPIO) NPs as the delivery vehicles for the transcriptional regulator MAX dimeric protein 3 (MXD3) (Yoshida et al., 2020). Under the treatment of MXD3 ASO-SPIO NP complex, MXD3 expression was down-regulated and apoptosis was significantly induced in NB cells. Miguel et al. identified D-lysine polymer as an effective gene delivery vehicle and could be used as a synthetic cell-penetrating peptide for gene therapy in the SH-SY5Y cell (Sanchez-Martos et al., 2021). Another study found that rabies virus glycoprotein peptide-modified poly D, L-lactide-co-glycolide NPs could specifically target NB *in vitro* and *in vivo* and significantly inhibited tumor growth in a mouse model (Lee et al., 2016b). In addition, a novel pH-sensitive liposomal nanocarrier quatsomes (QS) platform has been reported to deliver RNA *in vivo* and *in vitro* (Boloix et al., 2022). QS-miRNA complexes are well tolerated and enable subcutaneous NB xenografts and have a potential for the treatment of high-risk NB or other cancers.

Nanotechnology and Induction of Differentiation

Differentiation therapy aims to trigger an irreversible mature transformation of cancer cell phenotype with minimal cellular damage and to promote maturation of cancer cells, and is an alternative to conventional chemotherapy and radiotherapy as an important anti-cancer option (Yan and Liu, 2016; de Thé, 2018). Clinical observations have shown that spontaneous regression or differentiation occurs in a few cases of NB tissues (even with MYCN expression) without systemic treatment (Nakagawara et al., 2018). Therefore, it is believed that induction of mature differentiation and reversal of the malignant phenotype of tumor cells may have more favorable predispositions for NB than killing the tumor cells directly.

Studies have found that differentiation-induced substances for NB include 13-cis-retinoic acid (RA), γ-interferon, dibutyl cyclic adenosine monophosphate, sodium phenylacetate, insulin-like growth factor, nerve growth factor and glial cell-derived neurotrophic factor *in vitro*, among which RA is the most studied (Reynolds et al., 1991). The differentiation of tumor cells into normal tissue cells is modulated by genetic factors, nutritional conditions and chemical substances. However, regular administration of RA may produce toxic effects such as liver toxicity, skin chafing, and gastrointestinal damage (Cañón et al., 2004). With the in-depth research on nanomedicines, nanomaterials are able to increase the stability of tumor differentiation-inducing therapeutics, improve their targeting and ability to induce cell differentiation, and reduce the adverse effects associated with differentiation therapy.

The restoration of normal function or differentiated phenotype of tumor cells is associated with tumor suppressor function. It has been shown that silver NPs (AgNPs) induce neuronal differentiation by modulating reactive oxygen species, phosphatase and kinase signaling pathways in NB cell (Abdal Dayem et al., 2018). Furthermore, AgNPs-coated carriers serve as excellent drug targeting agents, and significantly promote neurite outgrowth (Abdal Dayem et al., 2018). Another study showed that graphene and graphene-associated nanomaterials exhibit biocompatibility with various cell lines and can be used as scaffolding agents to sustain cell attachment and induce proliferation and differentiation. Graphene oxide significantly promotes the differentiation efficiency of RA on NB cell by enhancing the expression of microtubule-associated protein 2 (Yeasmin et al., 2017). In a recent study, nanocomposite made of core-shelled topological insulator bismuth selenide NPs (Bi2Se3 NP) with silver (Ag@Bi2Se3) has been found to exhibit superior biocompatibility and plasmonic properties versus Ag NPs alone (**Figure 7**) (Mohammadniaei et al., 2019). Furthermore, they innovatively linked Ag@Bi2Se3 to cell-permeable RNA and fluoro-label with a newly developed RNA three-way junction (3WJ) structure to guide the gradual release of RA within the cell membrane. Remarkably, this designed nano-biohybrid material overcomes the long-plagued hydrophobic challenge of RA by conjugating RA to RNA strands (RA/R), while showing potent suppression of NB cell growth through differentiation induction. Together, these studies suggest that nanomaterial-based technologies may benefit the differentiation of NB cells through regulating intracellular oxidative homeostasis, activation of kinase signaling pathways, and solubility of differentiation inducers, thus potentially providing a new perspective for future NB therapy.

Nanotechnology and Tumor Extracellular Matrix Remodeling (ECM)

The tumor microenvironment (TME) represents the internal and external environment surrounding the tumor cells, which includes not only diverse functional cells but also some supportive noncellular components such as secreted signaling molecules and ECM (Ho et al., 2020; Ganguly et al., 2022; Saw et al., 2022). As an essential component of TME, the ECM is known to be a dense network with structural proteins, bridging proteins, proteoglycans and enzymes that mainly provide biochemical and structural support for tumorigenesis and

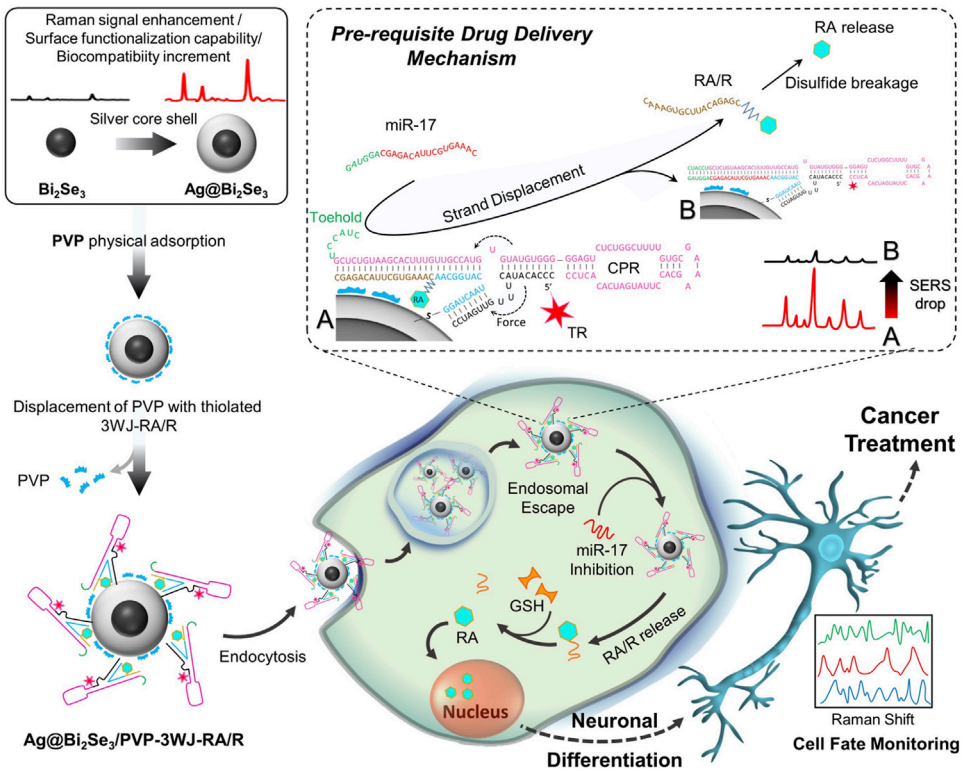

FIGURE 7 | Nanotechnology for induction of differentiation in NB. Schematic diagram of the Ag@Bi2Se3/PVP-3WJ-RA/R fabrication and its application in NB cell differentiation. Reproduced with permission from: Mohsen Mohammadniaei, Jinho Yoon, Hye Kyu Choi, Virginie Placide, Bapurao Gangaram Bharate, Taek Lee and Jeong-Woo Choi. Multifunctional Nanobiohybrid Material Composed of Ag@Bi(2)Se(3)/RNA Three-Way Junction/miRNA/Retinoic Acid for Neuroblastoma Differentiation. ACS applied materials & interfaces, 2019, 11(9): 8779–8788 (Mohammadniaei et al., 2019). Copyright 2019, American Chemical Society.

progression (Ho et al., 2020; Gonzalez-Molina et al., 2022; Jiang et al., 2022). Various chemokines, inflammatory factors, cytokines and growth factors secreted from TME-associated inflammatory cells or stromal cells collectively constitute a dynamic microhabitat possessing diverse functional states through crosstalk with the ECM (Wohlrab et al., 2014; Zhou et al., 2021). The aberrantly overexpressed ECM components in TME appear to be associated with stronger pro-invasive, pro-metastatic and pro-proliferative capacities of NB. Besides, an overly dense ECM tends to form a natural barrier that prevents cancer cells from accessing chemotherapeutics and immune cells, thus limiting the efficacy of endogenous and exogenous interference approaches against tumors to some extent (Burgos-Panadero et al., 2021). Given the oncogenic effect of abnormally high ECM expression, disturbing the interaction between ECM components and tumor cells becomes a powerful and reliable strategy for NB. However, most of the ECM-based drugs, including hyaluronidase, collagenase and proteolytic enzymes, are not applicable for oncology treatment, mainly due to their adverse effects such as short serum half-life, loss of function and insufficient accumulation in tumor area (Burgos-Panadero et al., 2021). The combination therapy of NPs with such drugs has emerged as one of the effective solutions to these problems. The matrix glycoprotein vitronectin contributes to the metastatic progression of tumors as an important mediator of crosstalk between ECM and tumor cells (Burgos-Panadero et al., 2019). Based on this, a high-affinity cyclic pentapeptide αv integrin antagonist, cilengitide, was employed to specifically target vitronectin for ECM disruption, and its combination with etoposide-loaded NPs more effectively enhanced the cytokilling effect on high-risk NB cell lines (Burgos-Panadero et al., 2021). Although nanomaterial-based ECM-targeting therapy has not been widely reported to be used for the diagnosis or treatment of NB, increasing research findings indicate that it will be one of the key directions for future research.

DEVELOPMENT AND APPLICATION OF NANOFORMULATIONS FOR SEVERAL PROMISING THERAPEUTIC TARGETS IN NEUROBLASTOMA

Tumor-targeted therapy refers to the means of selectively killing tumor cells through targeting specific sites or targets of tumors without harming normal tissues, and is classified into organ-targeted therapy and molecular-targeted therapy (Rössler et al., 2008). The former mainly involves the treatments for certain diseased organs, such as targeted aggregation radiotherapy. The latter refers to the development of therapeutic agents targeting

TABLE 3 | Summary of nanocomposite applications of potential targets available for NB diagnosis or therapy.

Target	Function	Formulations	Nanocarrier	Observed effects	Assays	Ref.
GD2	Promoted neural differentiation, repair, invasion and immunosuppression.	IGD-Targeted	DNA nanomedicine	Selective delivery of Dox to GD2-positive NB tumor cells	*In vitro* and *in vivo*	Zhang et al. (2021a)
		Self-assembly of aptamers DB99 and MYCN-siRNA and Dox	DNA nanomedicine	Specifically Knockdown of MYCN and release of Dox in GD2-positive NB cells	*In vitro* and *in vivo*	Zhang et al. (2021b)
		Gold NPs conjugated to anti-GD2 antibody HGNPs,	Gold NPs	Enhanced both CT imaging and NK cell-mediated cancer cell killing	*In vitro*	Jiao et al. (2016)
MYCN	Promoted tumorigenesis and malignant progression of NB	Folate-nanoliposome entrapped MYCN siRNA	Folate-nanoliposome	Pro-apoptotic effect	*In vitro*	Zhu et al. (2013)
ALK	Induced cellular overproliferation and the development of NB	TL-ALK-siRNA	Anti-GD2-targeted liposomes	Antitumor activity	*In vitro* and *in vivo*	Di Paolo et al. (2011)
VEGF	Angiogenesis and tumorigenesis of NB	SiO2@LDH-Bev-DOX	SiO2@LDH-Bev NPs	Antitumor and anti-angiogenesis efficiency	*In vitro* and *in vivo*	Zhu et al. (2017)
NCAM	Mediated tumor cell metastasis	PG-NTP-PTX-PEG	Dendritic polyglycerol	Inhibited the migration of proliferating endothelial cells	*In vitro* and *in vivo*	Vossen et al. (2018)
		PGA-PTX-NTP	Polyglutamic acid	Inhibited tumor growth	*In vitro* and *in vivo*	Markovsky et al. (2017)

some identified carcinogenic targets such as protein molecules or gene fragments in tumor cells, such as HER2, EGFR, and GD2 (Tian et al., 2015; Tian et al., 2017; Anderson et al., 2022). Carriers are essential components for achieving targeted therapy through improving the metabolic kinetic properties of drugs, increasing drug enrichment within tumor cells and tissues, enhancing therapeutic efficacy and minimizing unwanted side effects (Markovsky et al., 2017). Commonly utilized drug-assisted carrier systems include macromolecular delivery systems, particulate delivery systems, magnetically guided formulations and multi-targeting vectors (Jiao et al., 2011). Nanomedicine vectors allow to reduce or eliminate the effects of acids, bases, salts and other biochemical factors in body fluids on the drug encapsulated in the vector and prevent the drug from being completely metabolized before reaching the target site. In addition, nanomedicine carriers with large surface area and high interfacial activity avoid recognition and phagocytosis by the immune system, thus overcoming the "biological barrier" and enabling targeted drug delivery *in vivo* (Jiao et al., 2011). Notably, nanocarriers for drug delivery are required to be both readily absorbable and degradable in the biological environment and be biocompatible, non-cytotoxic and stable in the bloodstream (Aleassa et al., 2015). Since the research on NB targets-based nanodrug has been well reported, it is necessary to summarize them accordingly (**Table 3**).

GD2, a dialdehyde glycoside, is poorly expressed in tissues such as the cerebellum and peripheral nerves whereas abundantly expressed in neuroendocrine system-derived tumors, rendering monoclonal antibodies designed against GD2 an effective strategy for the diagnosis and treatment of multiple neurological tumors (Sait and Modak, 2017; Pastorino et al., 2019; Rodríguez-Nogales et al., 2019). Notably, GD2 is expressed on the cell surface of almost all types of primary NB, thus it seems to be one of the most desirable targets for NB-targeted therapy (Schulz et al., 1984; Matthay, 2018). Furthermore, unlike other tumor antigens, GD2 expression is maintained on the surface of NB cell even during treatment, which provides another strong evidence for its targetability (Mount et al., 2018). Nevertheless, GD2 is also found to be expressed in certain normal tissue cells such as peripheral neurons and CNS neurons, which causes some difficulties for anti-GD2 therapy (Yu et al., 2020). Currently, the GD2 monoclonal antibodies are unable to distinguish GD2-expressing normal cells from tumor cells, which would cause indiscriminate damage to both tumor and normal cells. Therefore, the exploration of new strategies for targeting GD2 exclusively in NB cells will be the primary issue to improve the safety and efficacy of anti-GD2 therapy. Zhang L et al. constructed IGD-Target, a PH-sensitive switchable drug delivery system based on GD2 inducers and i-motif elements, was able to specifically target and arrest the growth of GD2-expressing tumor cells without affecting surrounding normal cells. This formulation greatly enhanced the targetability for GD2 and reduced the adverse effects of anti-GD2 therapy (Zhang et al., 2021a). Moreover, they have developed a GD2 aptamer (DB99)-mediated multifunctional nanomedicine (ANM) with high efficiency, precision and biocompatibility for chemotherapy and gene therapy in NB (Zhang et al., 2021b). ANM is composed of synthetic aptamer DB99 and NB-specific MYCN-siRNA reloaded with the chemotherapeutic agent DOX for intracellular delivery and release of DOX (Zhang et al., 2021b). ANM was proven to selectively repress tumor cell growth with fewer side effects on normal tissues, greatly prolonging survival by specifically targeting GD2-positive tumor sites. Given the ubiquitously expression of GD2 in NB cells, nanodiagnostic enhancers based on GD2 have also been exploited for NB imaging. The gold NPs (GNPs) conjugated with tumor-targeting anti-GD2 antibodies, or HGNPs can specifically augment CT imaging while simultaneously stimulate NK cell-mediated killing of NB cells, which exerts a dual role of activating innate cytoimmune responses and potentiating imaging (Jiao et al., 2016). All of these suggest that GD2 aptamer-mediated targeted drug delivery systems will have promising applications in the precise treatment of NB.

MYCN gene amplification occurs in approximately 20–25% of NB patients and is typically associated with a poor prognosis for high-risk disease (Floros et al., 2021; Putra et al., 2021). Although MYCN performs critical role in the malignant phenotype of NB cells, it is extremely difficult to be targeted directly (Otto et al., 2009; Braoudaki et al., 2021). Current treatments for MYCN amplification are mainly indirect targeting strategies involve in manipulating its transcription, translation, protein stability and target gene transcription (Rickman et al., 2018; Ommer et al., 2020; Wang et al., 2022b). However, the development and application of nanomaterials for MYCN in NB therapy remains largely unknown. Based on the overexpression of folate receptors on the surface of neuroblastoma cells, folate nanoliposome delivery system, a low-toxic and high specificity nanomaterial, was utilized for encapsulating MYCN-siRNA to achieve MYCN-specific interference in tumor tissues and promotion of cell apoptosis (Zhu et al., 2013).

Vascular endothelial growth factor (VEGF), a heparin-binding growth factor specific for vascular endothelium, is an essential factor in angiogenesis *in vivo* (Rodríguez-Nogales et al., 2019). The application of nanoformulations targeted to VEGF for NB therapy is also not an inappropriate therapeutic option. Indeed, selective binding of bevacizumab to VEGF proteins coupled with SiO2-layered dihydroxane DOX-loaded nanocomposites for NB treatment significantly improved DOX cellular uptake and targeting delivery efficiency, inhibited tumor cell angiogenesis, reduced side effects of DOX, and inhibited VEGF-mediated angiogenesis and tumorigenesis (Zhu et al., 2017).

Neural cell adhesion molecule (NCAM) overexpressed in tumor initiating cells and tumor endothelial cells is also considered as a meaningful therapeutic target for NB (Wachowiak et al., 2008; Vossen et al., 2018). A new polyglutamic acid-PTX-NCAM Targeting Peptide (PGA-PTX-NTP) conjugate was developed and evaluated experimentally in neuroblastoma *in vivo*, and showed improvement in the NCAM-targeted tumor cell killing rate, prolonged drug action time and reduction of toxic effects (Kiselyov et al., 2009; Markovsky et al., 2017). Subsequently, a PG conjugate of polyethylene glycolated NCAM-targeted dendritic polyglycerol (PG) with PTX and NCAM-targeted peptide (NTP) (PG-NTP-PTX-PEG) was further developed to effectively suppress tumor angiogenesis (Vossen et al., 2018).

Anaplastic lymphoma kinase (ALK) has been identified as an oncogenic driver in several cancers especially in NB and is considered a critical contributor for tumorigenesis and a promising therapeutic target of NB (Frentzel et al., 2017; Li et al., 2021a). It has been reported that the novel ALK inhibitor X-396 in combination with an ALK-siRNA carrying targeted liposomes (TL-ALK-siRNA) exhibited superior drug bioavailability, moderate half-life, elevated plasma concentrations, and significantly prolonged lifespan in NB mice regardless of ALK gene mutation status (Di Paolo et al., 2011). More researches on new targets and corresponding potential nanocarriers are expected to further promote the advancement of NB targeted agents in the future.

BIOCOMPATIBILITY AND SAFETY OF NANOMATERIALS

Although numerous studies have confirmed that the emerging of nanomaterials has indeed facilitated the targeted diagnosis and treatment of various tumors, it is not easy to give a definite answer to the ambitious issue of biocompatibility and safety of nanomaterials. In this section, we will discuss the opportunities and challenges of nanomaterials, which are highly utilized and have achieved some breakthroughs in NB diagnosis and therapy, such as Gold NPs and AgNPs.

Noble metal NPs have attracted a lot of interest in cancer research owing to their unique optical properties and good biocompatibility (Zhao et al., 2022). Combining noble metal-based nanotechnology with diagnostic methods and therapies (from traditional radiotherapy to emerging immunotherapy) has improved the accuracy and efficiency of cancer diagnosis and treatment (Jiao et al., 2016; Mohammadniaei et al., 2019; Zhan et al., 2021). Gold NPs are the most frequently utilized noble metal NPs in tumor diagnosis and treatment due to their unique radiosensitizing properties, good biocompatibility, and relatively low toxicity (Boisselier and Astruc, 2009; Kovács et al., 2022; Li et al., 2022). Studies have also shown that GNPs may possess certain targeting properties, as demonstrated by the fact that GNPs selectively act on heparin-binding proteins, such as EGFR and VEGFR-2 (Mukherjee et al., 2005; Huang et al., 2021; Zhao et al., 2022). In addition, it improves the precise delivery and bioavailability of drugs by covalently and non-covalently binding and transporting drug molecules (Kim et al., 2012; Ren et al., 2021). Currently, numerous *in vitro* and *ex vivo* studies have almost demonstrated that the core components of AuNP do not possess significant biological toxicity, but their coating stabilizers, such as cetyltrimethylammonium bromide (CTAB), may present a risk of toxic effects on the organism (Li et al., 2014; Zhao et al., 2022). Moreover, the inherent physical properties of AuNPs also affect their safety, such as particle size and oxidation state (Li et al., 2014; Zhao et al., 2022). It is generally believed that the core of AuNPs larger than 5 nm behaves more inert, while the surface of AuNPs smaller than 2 nm shows an unusual chemical reactivity. For example, AuNPs with a diameter of 1.4 nm produced significant cytotoxicity by inducing oxidative stress and mitochondrial damage (Pan et al., 2009). Toxicity studies of citrate-capped AuNPs in mice by Chen et al. showed that small (3–5 nm) and large AuNPs (30 and 100 nm) were not toxic, while medium-sized AuNPs (8, 12, 17 and 37 nm) caused severe toxic effects (Chen et al., 2009). The high exposure of surface areas of anisotropic AuNPs poses a more serious toxicity risk due to oxidation than anisotropic AuNPs (Zhao et al., 2022). Therefore, it remains doubtful whether the results of *in vitro* cellular experiments could be translated equally to *in vivo* and clinical applications in the future. Initially silver NPs were used as antimicrobial agents due to their cytotoxicity (Panáček et al., 2018). It was subsequently proved to kill tumor cells through inducing cellular oxidative stress and affecting mitochondrial membrane stability in vivo and *in vitro* experiments (Cao et al., 2022; Ren et al., 2022; Skóra et al., 2022). As a result, silver nanomaterials have become a hot research topic in tumor

therapy. However, after all, silver ions are highly cytotoxic as heavy metals and are prone to undesired toxic effects (Choudhary et al., 2022). Moreover, similar to gold nanoparticles, the size and oxidation properties of silver nanoparticles also determine their cytotoxicity (Soenen et al., 2015).

Although, the application of NPs has effectively overcome the shortcomings of conventional oncology diagnosis and therapy, nanomaterial-based cancer treatment still faces many challenges. For example, when contrast agents in lipid therapeutic nanomedicines interact with biological materials due to their incompatibility or potential toxicity, adverse reactions such as inflammation, immune response or related diseases in the organism will occur (Dilnawaz et al., 2018; Bukhari et al., 2021). Superparamagnetic Fe3O4 NPs were once considered to be relatively inert carriers for therapeutic and diagnostic drugs. However, one study found that intravenous injection of Fe3O4 NPs induced inflammatory responses, cytotoxic damage and respiratory toxicity in mice (Hurbankova et al., 2017). Encouragingly, the biosafety of PBNPs has been evaluated in normal and cancer cell lines as well as in animal models (Busquets and Estelrich, 2020). It has been demonstrated that PBNPs do not cause significant organ damage or abnormalities in heart, liver, spleen, lungs and kidneys in mice (Fu et al., 2014; Zhao et al., 2018). Importantly, PBNPs exhibit good biocompatibility in humans, as demonstrated by their long-term presence in human serum without causing significant toxicity (Shokouhimehr et al., 2010; Montiel Schneider et al., 2018). Most current studies have focused only on the efficacy of nanomaterials *in vitro* and *in vivo*, while the observation of their resulting toxic effects is often neglected. In-depth study of their toxicological mechanisms is essential. The current NPs should be continuously improved accordingly based on the mechanism, so as to maximize their effectiveness and minimize the toxic effects.

CONCLUSION AND FUTURE DIRECTIONS

NB is a highly heterogeneous tumor with multiple non-specific clinical manifestations, and its prognosis is determined by multiple factors such as the patients' age and histological and biological characteristics of the tumor. Despite the growing maturity of the current NB diagnostic technology combined with various approaches, it still needs to be improved in terms of enhancing the diagnostic accuracy and simplifying the diagnostic method. Therapies available for NB have been developed, ranging from traditional chemoradiotherapy to the latest advances such as immunotherapy and gene therapy. While optimization of these treatments has improved the prognosis and outcome for the majority of patients, it remains incurable in approximately half of cases with high-risk NB.

In this review, we summarized the development and application of nanoformulations based on the existing potential therapeutic or diagnostic targets of NB. As most of the results are obtained from the preclinical study, there is still a lack of sufficient clinical trials for validation. Excitingly, nanotechnology has been widely studied in the field of NB diagnosis and treatment due to its excellent performance in many aspects, thus presenting an opportunity to resolve the difficulties in the traditional diagnosis and treatment of NB. Yet, as an emerging technology, nanotechnology remains to be further optimized to accommodate current clinical needs in terms of the shortcomings in material preparation, biosafety, toxicity, analytical methods and mechanical investigations. Furthermore, nanomedicine-based chemotherapy integrated with other therapeutic modalities such as PDT and immunotherapy have shown synergistically enhanced anti-cancer effects. In addition to traditional therapeutic approaches, novel approaches focusing on the suppression of NB cell growth and malignant phenotype based on programmed cell death are ongoing directions in nanomedicine, such as ferroptosis induction (Zafar et al., 2021). Furthermore, some researchers achieved drug loading and transport by effectively utilizing the physiological conditions of the organism itself as biocompatible carriers for the purpose of certain tumor treatment, such as red blood cells (RBCs) (Li et al., 2021b; Wu et al., 2021). Most of the previous studies on the application of nanomaterials in NB diagnostics and therapeutics are mainly conducted through cellular and animal experiments, and more efforts are required to accomplish the clinical translation of these scientific findings. We believe that the advancement of nanomedicine will definitely provide an unprecedented opportunity for clinically precise treatment of NB patients in the future, such as tumor-specific targeting, favorable biocompatibility and an ease in functionalization. More importantly, a number of nanomedicines have been approved for clinical trials or launched for clinical application. It is believed that nanomedicine will bring a brighter perspective for the diagnosis and therapy of NB with a rapid and enormous advancement in the coming future.

AUTHOR CONTRIBUTIONS

HY: Conceptualization, Searching and organizing literature, Writing—Original draft preparation, Writing—Review and ; Editing. BZ: Searching and organizing literature, Project administration, Validation. QZ: Supervision, Validation. ZY: Conceptualization, Writing—Review and ; Editing, YZ: Visualization, Supervision, Project administration, Resources, Article revision, Funding acquisition. All authors have no conflict of interest.

FUNDING

We thank the Henan medical science and technology project (No. LHGJ20210629, LHGJ20190958), and the Scientific and Technological Projects of Henan province (No.222102310026).

REFERENCES

Abdal Dayem, A., Lee, S. B., Choi, H. Y., and Cho, S. G. (2018). Silver Nanoparticles: Two-Faced Neuronal Differentiation-Inducing Material in Neuroblastoma (SH-Sy5y) Cells. *Int. J. Mol. Sci.* 19 (5). doi:10.3390/ijms19051470

Aleassa, E. M., Xing, M., and Keijzer, R. (2015). Nanomedicine as an Innovative Therapeutic Strategy for Pediatric Cancer. *Pediatr. Surg. Int.* 31 (7), 611–616. doi:10.1007/s00383-015-3683-2

Alphandéry, E. (2022). Ultrasound and Nanomaterial: an Efficient Pair to Fight Cancer [J]. *J. nanobiotechnology* 20 (1), 139.doi:10.1186/s12951-022-01243-w

Amerigos Daddy J C, K., Chen, M., Raza, F., Xiao, Y., Su, Z., and Ping, Q. (2020). Co-Encapsulation of Mitoxantrone and β-Elemene in Solid Lipid Nanoparticles to Overcome Multidrug Resistance in Leukemia. *Pharmaceutics* 12 (2). doi:10.3390/pharmaceutics12020191

Amoroso, L., Castel, V., Bisogno, G., Michela, C., Marquez-Vega, C., Julia, C. C., et al. (2020). Phase II Results from a Phase I/II Study to Assess the Safety and Efficacy of Weekly Nab-Paclitaxel in Paediatric Patients with Recurrent or Refractory Solid Tumours: A Collaboration with the European Innovative Therapies for Children with Cancer Network [J]. *Eur. J. cancer* 135, 89–97. doi:10.1016/j.ejca.2020.04.031

Anderson, J., Majzner, R. G., Sondel, P. M., Francoise, F., Jeanette, L., and Regine, P-S. (2022). Immunotherapy of Neuroblastoma: Facts and Hopes [J]. *Clin. cancer Res* 28, OF1–OF11. doi:10.1158/1078-0432.CCR-21-1356

Atluri, R., Atmaramani, R., Tharaka, G., McCallister, T., Peng, J., Diercks, D., et al. (2018). Photo-Magnetic Irradiation-Mediated Multimodal Therapy of Neuroblastoma Cells Using a Cluster of Multifunctional Nanostructures. *Nanomater. (Basel)* 8 (10), 774. doi:10.3390/nano8100774

Bacanlı, M., Eşi M, Ö., Erdoğan, H., Sarper, M., Erdem, O., and Özkan, Y. (2021). Evaluation of Cytotoxic and Genotoxic Effects of Paclitaxel-Loaded PLGA Nanoparticles in Neuroblastoma Cells. *Food Chem. Toxicol.* 154, 112323. doi:10.1016/j.fct.2021.112323

Batrakova, E. V., and Kabanov, A. V. (2008). Pluronic Block Copolymers: Evolution of Drug Delivery Concept from Inert Nanocarriers to Biological Response Modifiers. *J. Control Release* 130 (2), 98–106. doi:10.1016/j.jconrel.2008.04.013

Bechet, D., Couleaud, P., Frochot, C., Viriot, M. L., Guillemin, F., and Barberi-Heyob, M. (2008). Nanoparticles as Vehicles for Delivery of Photodynamic Therapy Agents. *Trends Biotechnol.* 26 (11), 612–621. doi:10.1016/j.tibtech.2008.07.007

Berlanga, P., Cañete, A., and Castel, V. (2017). Advances in Emerging Drugs for the Treatment of Neuroblastoma. *Expert Opin. Emerg. Drugs* 22 (1), 63–75. doi:10.1080/14728214.2017.1294159

Bilynsky, C., Millot, N., and Papa, A. L. (2022). Radiation Nanosensitizers in Cancer Therapy-From Preclinical Discoveries to the Outcomes of Early Clinical Trials [J]. *Bioeng. Transl. Med.* 7 (1), e10256. doi:10.1002/btm2.10256

Boisselier, E., and Astruc, D. (2009). Gold Nanoparticles in Nanomedicine: Preparations, Imaging, Diagnostics, Therapies and Toxicity. *Chem. Soc. Rev.* 38 (6), 1759–1782. doi:10.1039/b806051g

Boloix, A., Feiner-Gracia, N., Köber, M., Javier, R., Rosa, P., Aroa, S., et al. (2022). Engineering pH-Sensitive Stable Nanovesicles for Delivery of MicroRNA Therapeutics [J]. *Small (Weinheim der Bergstrasse, Ger.* 18 (3), e2101959. doi:10.1002/smll.202101959

Braoudaki, M., Hatziagapiou, K., Zaravinos, A., and George, I. L. (2021). MYCN in Neuroblastoma: "Old Wine into New Wineskins" [J]. *Diseases* 9 (4). doi:10.3390/diseases9040078

Bukhari, S. I., Imam, S. S., Ahmad, M. Z., Vuddanda, P. R., Alshehri, S., Mahdi, W. A., et al. (2021). Recent Progress in Lipid Nanoparticles for Cancer Theranostics: Opportunity and Challenges. *Pharmaceutics* 13 (6). doi:10.3390/pharmaceutics13060840

Burgos-Panadero, R., El Moukhtari, S. H., Noguera, I., Rodríguez-Nogales, C., Martín-Vañó, S., Vicente-Munuera, P., et al. (2021). Unraveling the Extracellular Matrix-Tumor Cell Interactions to Aid Better Targeted Therapies for Neuroblastoma. *Int. J. Pharm.* 608, 121058. doi:10.1016/j.ijpharm.2021.121058

Burgos-Panadero, R., Noguera, I., Cañete, A., Navarro, S., and Noguera, R. (2019). Vitronectin as a Molecular Player of the Tumor Microenvironment in Neuroblastoma. *BMC Cancer* 19 (1), 479. doi:10.1186/s12885-019-5693-2

Busquets, M. A., and Estelrich, J. (2020). Prussian Blue Nanoparticles: Synthesis, Surface Modification, and Biomedical Applications. *Drug Discov. Today* 25 (8), 1431–1443. doi:10.1016/j.drudis.2020.05.014

Calugaru, V., Magné, N., Hérault, J., Bonvalot, S., Le Tourneau, C., and Thariat, J. (2015). Nanoparticles and Radiation Therapy. *Bull. Cancer* 102 (1), 83–91. doi:10.1016/j.bulcan.2014.10.002

Cano-Mejia, J., Burga, R. A., Sweeney, E. E., Fisher, J. P., Bollard, C. M., Sandler, A. D., et al. (2017). Prussian Blue Nanoparticle-Based Photothermal Therapy Combined with Checkpoint Inhibition for Photothermal Immunotherapy of Neuroblastoma. *Nanomedicine* 13 (2), 771–781. doi:10.1016/j.nano.2016.10.015

Cano-Mejia, J., Shukla, A., Ledezma, D. K., Palmer, E., Villagra, A., and Fernandes, R. (2020). CpG-coated Prussian Blue Nanoparticles-Based Photothermal Therapy Combined with Anti-CTLA-4 Immune Checkpoint Blockade Triggers a Robust Abscopal Effect against Neuroblastoma. *Transl. Oncol.* 13 (10), 100823. doi:10.1016/j.tranon.2020.100823

Cañón, E., Cosgaya, J. M., Scsucova, S., and Ana, A. (2004). Rapid Effects of Retinoic Acid on CREB and ERK Phosphorylation in Neuronal Cells [J]. *Mol. Biol. cell* 15 (12), 5583–5592. doi:10.1091/mbc.e04-05-0439

Cao, J., Qin, X., and Li, Z. (2022). Synthesis of Silver Nanoparticles from the Polysaccharide of Farfarae Flos and Uncovering its Anticancer Mechanism Based on the Cell Metabolomic Approach. *J. Proteome Res.* 21 (1), 172–181. doi:10.1021/acs.jproteome.1c00668

Chen, D. S., and Mellman, I. (2013). Oncology Meets Immunology: the Cancer-Immunity Cycle. *Immunity* 39 (1), 1–10. doi:10.1016/j.immuni.2013.07.012

Chen, Y., Nan, J., Lu, Y., Wang, C., Chu, F., and Gu, Z. (2015). Hybrid Fe3O4-Poly(acrylic Acid) Nanogels for Theranostic Cancer Treatment. *J. Biomed. Nanotechnol.* 11 (5), 771–779. doi:10.1166/jbn.2015.2001

Chen, Y. S., Hung, Y. C., Liau, I., and Huang, G. S. (2009). Assessment of the *In Vivo* Toxicity of Gold Nanoparticles. *Nanoscale Res. Lett.* 4 (8), 858–864. doi:10.1007/s11671-009-9334-6

Chertok, B., Moffat, B. A., David, A. E., Yu, F., Bergemann, C., Ross, B. D., et al. (2008). Iron Oxide Nanoparticles as a Drug Delivery Vehicle for MRI Monitored Magnetic Targeting of Brain Tumors. *Biomaterials* 29 (4), 487–496. doi:10.1016/j.biomaterials.2007.08.050

Choudhary, A., Singh, S., and Ravichandiran, V. (2022). Toxicity, Preparation Methods and Applications of Silver Nanoparticles: an Update. *Toxicol. Mech. Methods*, 1–12. doi:10.1080/15376516.2022.2064257

Colletti, M., Paolo, V. D., Galardi, A., Milano, G. M., Mastronuzzi, A., Locatelli, F., et al. (2017). Nano-Delivery in Pediatric Tumors: Looking Back, Moving Forward. *Anticancer Agents Med. Chem.* 17 (10), 1328–1343. doi:10.2174/1871520617666170103101141

de Thé, H. (2018). Differentiation Therapy Revisited [J]. *Nat. Rev. Cancer* 18 (2), 117–127. doi:10.1038/nrc.2017.103

Della Sala, F., Fabozzi, A., di Gennaro, M., Nuzzo, S., Makvandi, P., Solimando, N., et al. (2022). Advances in Hyaluronic-Acid-Based (Nano)Devices for Cancer Therapy. *Macromol. Biosci.* 22 (1), e2100304. doi:10.1002/mabi.202100304

Devarakonda, S. B., Myers, M. R., Lanier, M., Dumoulin, C., and Banerjee, R. K. (2017). Assessment of Gold Nanoparticle-Mediated-Enhanced Hyperthermia Using MR-Guided High-Intensity Focused Ultrasound Ablation Procedure. *Nano Lett.* 17 (4), 2532–2538. doi:10.1021/acs.nanolett.7b00272

Di Paolo, D., Brignole, C., Pastorino, F., Carosio, R., Zorzoli, A., Rossi, M., et al. (2011). Neuroblastoma-targeted Nanoparticles Entrapping siRNA Specifically Knockdown ALK. *Mol. Ther.* 19 (6), 1131–1140. doi:10.1038/mt.2011.54

Dilnawaz, F., Acharya, S., and Sahoo, S. K. (2018). Recent Trends of Nanomedicinal Approaches in Clinics. *Int. J. Pharm.* 538 (1-2), 263–278. doi:10.1016/j.ijpharm.2018.01.016

Floros, K. V., Cai, J., Jacob, S., Kurupi, R., Fairchild, C. K., Shende, M., et al. (2021). MYCN-amplified Neuroblastoma Is Addicted to Iron and Vulnerable to Inhibition of the System Xc-/Glutathione Axis. *Cancer Res.* 81 (7), 1896–1908. doi:10.1158/0008-5472.CAN-20-1641

Frentzel, J., Sorrentino, D., and Giuriato, S. (2017). Targeting Autophagy in ALK-Associated Cancers. *Cancers (Basel)* 9 (12). doi:10.3390/cancers9120161

Fu, G., Liu, W., Li, Y., Jin, Y., Jiang, L., Liang, X., et al. (2014). Magnetic Prussian Blue Nanoparticles for Targeted Photothermal Therapy under Magnetic Resonance Imaging Guidance. *Bioconjug Chem.* 25 (9), 1655–1663. doi:10.1021/bc500279w

Ganguly, K., Shah, A., Atri, P., Sanchita, R., Moorthy, P. P., Sushil, K., et al. (2022). Chemokine-Mucinome Interplay in Shaping the Heterogeneous Tumor Microenvironment in Pancreatic Cancer [J]. *Seminars cancer Biol.* doi:10.1016/j.semcancer.2022.03.022

George, R. E., Diller, L., and Bernstein, M. L. (2010). Pharmacotherapy of Neuroblastoma. *Expert Opin. Pharmacother.* 11 (9), 1467–1478. doi:10.1517/14656566.2010.482100

Ghosh, A. K., Chowdhury, M., and Kumar Das, P. (2021). Nipecotic-Acid-Tethered, Naphthalene-Diimide-Based, Orange-Emitting Organic Nanoparticles as Targeted Delivery Vehicle and Diagnostic Probe toward GABAA-Receptor-Enriched Cancer Cells. *ACS Appl. Bio Mater* 4 (10), 7563–7577. doi:10.1021/acsabm.1c00830

Gong, F., Chen, J., Han, X., Zhao, J., Wang, M., Feng, L., et al. (2018). Core-shell TaOx@MnO2 Nanoparticles as a Nano-Radiosensitizer for Effective Cancer Radiotherapy. *J. Mater Chem. B* 6 (15), 2250–2257. doi:10.1039/c8tb00070k

Gonzalez-Molina, J., Moyano-Galceran, L., Single, A., Gultekin, O., Alsalhi, S., and Lehti, K. (2022). Chemotherapy as a Regulator of Extracellular Matrix-Cell Communication: Implications in Therapy Resistance [J]. *Seminars cancer Biol.* 21, S1044-579X(22)00068-2. doi:10.1016/j.semcancer.2022.03.012

González-Ruiz, V., Cores, Á., Martín-Cámara, O., Karen, O., Cervera-Carrascón, V., Patrycja, M., et al. (2021). Enhanced Stability and Bioactivity of Natural Anticancer Topoisomerase I Inhibitors through Cyclodextrin Complexation [J]. *Pharmaceutics* 13 (10), 1609. doi:10.3390/pharmaceutics13101609

Haimov, E., Weitman, H., Polani, S., Schori, H., Zitoun, D., and Shefi, O. (2018). meso-Tetrahydroxyphenylchlorin-Conjugated Gold Nanoparticles as a Tool to Improve Photodynamic Therapy. *ACS Appl. Mater Interfaces* 10 (3), 2319–2327. doi:10.1021/acsami.7b16455

Hishiki, T., Horie, H., Higashimoto, Y., Yotsumoto, K., Komatsu, S., Okimoto, Y., et al. (2014). Histological Features of Primary Tumors after Induction or High-Dose Chemotherapy in High-Risk Neuroblastoma. *Pediatr. Surg. Int.* 30 (9), 919–926. doi:10.1007/s00383-014-3564-0

Ho, W. J., Jaffee, E. M., and Zheng, L. (2020). The Tumour Microenvironment in Pancreatic Cancer - Clinical Challenges and Opportunities. *Nat. Rev. Clin. Oncol.* 17 (9), 527–540. doi:10.1038/s41571-020-0363-5

Hu, Y., Yang, J., Wei, P., Li, J., Ding, L., Zhang, G., et al. (2015). Facile Synthesis of Hyaluronic Acid-Modified Fe3O4/Au Composite Nanoparticles for Targeted Dual Mode MR/CT Imaging of Tumors. *J. Mater Chem. B* 3 (47), 9098–9108. doi:10.1039/c5tb02040a

Huang, W., Xing, Y., Zhu, L., Zhuo, J., and Cai, M. (2021). Sorafenib Derivatives-Functionalized Gold Nanoparticles Confer Protection against Tumor Angiogenesis and Proliferation via Suppression of EGFR and VEGFR-2. *Exp. Cell Res.* 406 (1), 112633. doi:10.1016/j.yexcr.2021.112633

Hurbankova, M., Volkovova, K., Hraskova, D., Wimmerova, S., and Moricova, S. (2017). Respiratory Toxicity of Fe3O4 Nanoparticles: Experimental Study. *Rev. Environ. Health* 32 (1-2), 207–210. doi:10.1515/reveh-2016-0022

Jiang, Y., Zhang, H., Wang, J., Liu, Y., Luo, T., and Hua, H. (2022). Targeting Extracellular Matrix Stiffness and Mechanotransducers to Improve Cancer Therapy. *J. Hematol. Oncol.* 15 (1), 34. doi:10.1186/s13045-022-01252-0

Jiao, P., Otto, M., Geng, Q., Li, C., Li, F., Butch, E. R., et al.(2016). Enhancing Both CT Imaging and Natural Killer Cell-Mediated Cancer Cell Killing by a GD2-Targeting Nanoconstruct. *J. Mater Chem. B* 4 (3), 513–520. doi:10.1039/C5TB02243F

Jiao, P., Zhou, H., Otto, M., Mu, Q., Li, L., Su, G., et al. (2011). Leading neuroblastoma cells to die by multiple premeditated attacks from a multifunctionalized nanoconstruct. *J. Am. Chem. Soc.* 133 (35), 13918–13921. doi:10.1021/ja206118a

Kale, S. S., Burga, R. A., Sweeney, E. E., Zun, Z., Sze, R. W., Tuesca, A., et al. (2017). Composite Iron Oxide-Prussian Blue Nanoparticles for Magnetically Guided T1-Weighted Magnetic Resonance Imaging and Photothermal Therapy of Tumors. *Int. J. Nanomedicine* 12, 6413–6424. doi:10.2147/IJN.S144515

Kenny, G. D., Villegas-Llerena, C., Tagalakis, A. D., Campbell, F., Welser, K., Botta, M., et al. (2012). Multifunctional Receptor-Targeted Nanocomplexes for Magnetic Resonance Imaging and Transfection of Tumours. *Biomaterials* 33 (29), 7241–7250. doi:10.1016/j.biomaterials.2012.06.042

Khan, M. W., Zhao, P., Khan, A., Raza, F., Raza, S. M., Sarfraz, M., et al. (2019). Synergism of Cisplatin-Oleanolic Acid Co-loaded Calcium Carbonate Nanoparticles on Hepatocellular Carcinoma Cells for Enhanced Apoptosis and Reduced Hepatotoxicity. *Int. J. Nanomedicine* 14, 3753–3771. doi:10.2147/IJN.S196651

Kim, S. T., Chompoosor, A., Yeh, Y. C., Agasti, S. S., Solfiell, D. J., and Rotello, V. M. (2012). Dendronized Gold Nanoparticles for siRNA Delivery. *Small* 8 (21), 3253–3256. doi:10.1002/smll.201201141

Kiselyov, V. V., Li, S., Berezin, V., and Bock, E. (2009). Insight into the Structural Mechanism of the Bi-modal Action of an NCAM Mimetic, the C3 Peptide. *Neurosci. Lett.* 452 (3), 224–227. doi:10.1016/j.neulet.2009.01.080

Kovács, D., Igaz, N., and Gopisetty, M. K. (2022). Cancer Therapy by Silver Nanoparticles: Fiction or Reality? [J]. *Int. J. Mol. Sci.* 23 (2).

Krummel, M. F., and Allison, J. P. (1995). CD28 and CTLA-4 Have Opposing Effects on the Response of T Cells to Stimulation. *J. Exp. Med.* 182 (2), 459–465. doi:10.1084/jem.182.2.459

Kuai, R., Ochyl, L. J., Bahjat, K. S., Schwendeman, A., and Moon, J. J. (2017). Designer Vaccine Nanodiscs for Personalized Cancer Immunotherapy. *Nat. Mater* 16 (4), 489–496. doi:10.1038/nmat4822

Kwong, B., Liu, H., and Irvine, D. J. (2011). Induction of Potent Anti-tumor Responses while Eliminating Systemic Side Effects via Liposome-Anchored Combinatorial Immunotherapy. *Biomaterials* 32 (22), 5134–5147. doi:10.1016/j.biomaterials.2011.03.067

Lee, J., Jeong, E. J., Lee, Y. K., Kim, K., Kwon, I. C., and Lee, K. Y. (2016). Optical Imaging and Gene Therapy with Neuroblastoma-Targeting Polymeric Nanoparticles for Potential Theranostic Applications. *Small* 12 (9), 1201–1211. doi:10.1002/smll.201501913

Lee, J., Min, H. S., You, D. G., Kim, K., Kwon, I. C., Rhim, T., et al. (2016). Theranostic Gas-Generating Nanoparticles for Targeted Ultrasound Imaging and Treatment of Neuroblastoma. *J. Control Release* 223, 197–206. doi:10.1016/j.jconrel.2015.12.051

Lee, J. H., Jun, Y. W., Yeon, S. I., Shin, J. S., and Cheon, J. (2006). Dual-mode Nanoparticle Probes for High-Performance Magnetic Resonance and Fluorescence Imaging of Neuroblastoma. *Angew. Chem. Int. Ed. Engl.* 45 (48), 8160–8162. doi:10.1002/anie.200603052

Lee, J. H., Jun, Y. W., Yeon, S. I., Shin, J. S., and Cheon, J. (2006). Dual-Mode Nanoparticle Probes for High-Performance Magnetic Resonance and Fluorescence Imaging of Neuroblastoma. *Angew. Chem. Int. Ed. Engl.* 45 (48), 8160–8162. doi:10.1002/anie.200603052

Li, N., Zhao, P., and Astruc, D. (2014). Anisotropic Gold Nanoparticles: Synthesis, Properties, Applications, and Toxicity. *Angew. Chem. Int. Ed. Engl.* 53 (7), 1756–1789. doi:10.1002/anie.201300441

Li, T., Stayrook, S. E., Tsutsui, Y., Zhang, J., Wang, Y., Li, H., et al. (2021). Structural Basis for Ligand Reception by Anaplastic Lymphoma Kinase. *Nature* 600 (7887), 148–152. doi:10.1038/s41586-021-04141-7

Li, X., Zhang, Y., Liu, G., Luo, Z., Zhou, L., Xue, Y., et al. (2022). Recent Progress in the Applications of Gold-Based Nanoparticles towards Tumor-Targeted Imaging and Therapy. *RSC Adv.* 12 (13), 7635–7651. doi:10.1039/d2ra00566b

Li, Y., Raza, F., Liu, Y., Wei, Y., Rong, R., Zheng, M., et al. (2021). Clinical Progress and Advanced Research of Red Blood Cells Based Drug Delivery System. *Biomaterials* 279, 121202. doi:10.1016/j.biomaterials.2021.121202

Li, Z., Li, B., Wang, M., Xie, M., Shen, H., Shen, S., et al. (2013). The Role of Endosome Evasion Bypass in the Reversal of Multidrug Resistance by Lipid/nanoparticle Assemblies. *J. Mater Chem. B* 1 (10), 1466–1474. doi:10.1039/c3tb00386h

Lim, C. K., Heo, J., Shin, S., Jeong, K., Seo, Y. H., Jang, W. D., et al. (2013). Nanophotosensitizers toward Advanced Photodynamic Therapy of Cancer. *Cancer Lett.* 334 (2), 176–187. doi:10.1016/j.canlet.2012.09.012

Lin, Y. S., Chen, Y., Tsai, Y. H., Tseng, S. H., and Lin, K. S. (2021). *In Vivo* imaging of Neuroblastomas Using GD2-Targeting Graphene Quantum Dots. *J. Pediatr. Surg.* 56 (7), 1227–1232. doi:10.1016/j.jpedsurg.2021.03.035

Liu, R., Tang, J., Xu, Y., and Dai, Z. (2019). Bioluminescence Imaging of Inflammation *In Vivo* Based on Bioluminescence and Fluorescence Resonance Energy Transfer Using Nanobubble Ultrasound Contrast Agent. *ACS Nano* 13 (5), 5124–5132. doi:10.1021/acsnano.8b08359

Liu, W., Mirzoeva, S., Yuan, Y., Deng, J., Chen, S., Lai, B., et al. (2021). Development of Fe3O4 Core-TiO2 Shell Nanocomposites and Nanoconjugates as a Foundation for Neuroblastoma Radiosensitization. *Cancer nano.* 12 (1), 12. doi:10.1186/s12645-021-00081-z

Markovsky, E., Eldar-Boock, A., Ben-Shushan, D., Baabur-Cohen, H., Yeini, E., Pisarevsky, E., et al. (2017). Targeting NCAM-Expressing Neuroblastoma with

Polymeric Precision Nanomedicine. *J. Control Release* 249, 162–172. doi:10.1016/j.jconrel.2017.01.044

Matsumura, Y., and Maeda, H. (1986). A New Concept for Macromolecular Therapeutics in Cancer Chemotherapy: Mechanism of Tumoritropic Accumulation of Proteins and the Antitumor Agent Smancs. *Cancer Res.* 46 (12 Pt 1), 6387–6392.

Matthay, K. K. (2018). Interleukin 2 Plus Anti-GD2 Immunotherapy: Helpful or Harmful? *Lancet Oncol.* 19 (12), 1549–1551. doi:10.1016/S1470-2045(18)30627-2

Matthay, K. K., Maris, J. M., Schleiermacher, G., Nakagawara, A., Mackall, C. L., Diller, L., et al. (2016). Neuroblastoma. *Nat. Rev. Dis. Prim.* 2, 16078. doi:10.1038/nrdp.2016.78

Mohammadniaei, M., Yoon, J., Choi, H. K., Placide, V., Bharate, B. G., Lee, T., et al. (2019). Multifunctional Nanobiohybrid Material Composed of Ag@Bi2Se3/RNA Three-Way Junction/miRNA/Retinoic Acid for Neuroblastoma Differentiation. *ACS Appl. Mater Interfaces* 11 (9), 8779–8788. doi:10.1021/acsami.8b16925

Montiel Schneider, M. G., Martin, M. J., Coral, D. F., Muraca, D., Gentili, C., Fernández van Raap, M., et al. (2018). Selective Contrast Agents with Potential to the Earlier Detection of Tumors: Insights on Synthetic Pathways, Physicochemical Properties and Performance in MRI Assays. *Colloids Surf. B Biointerfaces* 170, 470–478. doi:10.1016/j.colsurfb.2018.06.044

Moreno, F., Lopez Marti, J., Palladino, M., Lobos, P., Gualtieri, A., and Cacciavillano, W. (2016). Childhood Neuroblastoma: Incidence and Survival in Argentina. Report from the National Pediatric Cancer Registry, ROHA Network 2000-2012. *Pediatr. Blood Cancer* 63 (8), 1362–1367. doi:10.1002/pbc.25987

Moreno, L., Casanova, M., Chisholm, J. C., Pablo, B., Pascal, B. C., Sylvain, B., et al. (2018). Phase I Results of a Phase I/II Study of Weekly Nab-Paclitaxel in Paediatric Patients with Recurrent/refractory Solid Tumours: A Collaboration with Innovative Therapies for Children with Cancer [J]. *Eur. J. cancer* 100, 27–34. doi:10.1016/j.ejca.2018.05.002

Mount, C. W., Majzner, R. G., Sundaresh, S., Arnold, E. P., Kadapakkam, M., Haile, S., et al. (2018). Potent Antitumor Efficacy of Anti-GD2 CAR T Cells in H3-K27m+ Diffuse Midline Gliomas. *Nat. Med.* 24 (5), 572–579. doi:10.1038/s41591-018-0006-x

Mukherjee, P., Bhattacharya, R., Wang, P., Wang, L., Basu, S., Nagy, J. A., et al. (2005). Antiangiogenic Properties of Gold Nanoparticles. *Clin. Cancer Res.* 11 (9), 3530–3534. doi:10.1158/1078-0432.CCR-04-2482

Mulik, R. S., Mönkkönen, J., Juvonen, R. O., Mahadik, K. R., and Paradkar, A. R. (2012). ApoE3 Mediated Polymeric Nanoparticles Containing Curcumin: Apoptosis Induced *In Vitro* Anticancer Activity against Neuroblastoma Cells. *Int. J. Pharm.* 437 (1-2), 29–41. doi:10.1016/j.ijpharm.2012.07.062

Murayama, C., Kawaguchi, A. T., Ishikawa, K., Kamijo, A., Kato, N., Ohizumi, Y., et al. (2012). Liposome-encapsulated Hemoglobin Ameliorates Tumor Hypoxia and Enhances Radiation Therapy to Suppress Tumor Growth in Mice. *Artif. Organs* 36 (2), 170–177. doi:10.1111/j.1525-1594.2011.01418.x

Nakagawara, A., Li, Y., Izumi, H., Muramori, K., Inada, H., and Nishi, M. (2018). Neuroblastoma. *Jpn. J. Clin. Oncol.* 48 (3), 214–241. doi:10.1093/jjco/hyx176

Nasir, A., Khan, A., Li, J., Naeem, M., Khalil, A. A. K., Khan, K., et al. (2021). Nanotechnology, A Tool for Diagnostics and Treatment of Cancer. *Curr. Top. Med. Chem.* 21 (15), 1360–1376. doi:10.2174/1568026621666210701144124

Nicholas, N. S., Apollonio, B., and Ramsay, A. G. (2016). Tumor Microenvironment (TME)-driven Immune Suppression in B Cell Malignancy. *Biochim. Biophys. Acta* 1863 (3), 471–482. doi:10.1016/j.bbamcr.2015.11.003

Norris, R. E., Shusterman, S., Gore, L., Muscal, J. A., Macy, M. E., Fox, E., et al. (2014). Phase 1 Evaluation of EZN-2208, a Polyethylene Glycol Conjugate of SN38, in Children Adolescents and Young Adults with Relapsed or Refractory Solid Tumors. *Pediatr. Blood Cancer* 61 (10), 1792–1797. doi:10.1002/pbc.25105

Ommer, J., Selfe, J. L., Wachtel, M., O'Brien, E. M., Laubscher, D., Roemmele, M., et al. (2020). Aurora A Kinase Inhibition Destabilizes PAX3-FOXO1 and MYCN and Synergizes with Navitoclax to Induce Rhabdomyosarcoma Cell Death. *Cancer Res.* 80 (4), 832–842. doi:10.1158/0008-5472.CAN-19-1479

Otto, T., Horn, S., Brockmann, M., Eilers, U., Schüttrumpf, L., Popov, N., et al. (2009). Stabilization of N-Myc Is a Critical Function of Aurora A in Human Neuroblastoma. *Cancer cell* 15 (1), 67–78. doi:10.1016/j.ccr.2008.12.005

Pan, Y., Leifert, A., Ruau, D., Neuss, S., Bornemann, J., Schmid, G., et al. (2009). Gold Nanoparticles of Diameter 1.4 Nm Trigger Necrosis by Oxidative Stress and Mitochondrial Damage. *Small* 5 (18), 2067–2076. doi:10.1002/smll.200900466

Panáček, A., Kvítek, L., Smékalová, M., Renata, V., Milan, K., Magdalena, R., et al. (2018). Bacterial Resistance to Silver Nanoparticles and How to Overcome it [J]. *Nat. Nanotechnol.* 13 (1), 65–71. doi:10.1038/s41565-017-0013-y

Pastorino, F., Brignole, C., Di Paolo, D., Perri, P., Curnis, F., Corti, A., et al. (2019). Overcoming Biological Barriers in Neuroblastoma Therapy: The Vascular Targeting Approach with Liposomal Drug Nanocarriers. *Small* 15 (10), e1804591. doi:10.1002/smll.201804591

Perkins, S. M., Shinohara, E. T., DeWees, T., and Frangoul, H. (2014). Outcome for Children with Metastatic Solid Tumors over the Last Four Decades. *PloS one* 9 (7), e100396. doi:10.1371/journal.pone.0100396

Poelaert, B. J., Romanova, S., Knoche, S. M., Olson, M. T., Sliker, B. H., Smits, K., et al. (2020). Nanoformulation of CCL21 Greatly Increases its Effectiveness as an Immunotherapy for Neuroblastoma. *J. Control Release* 327, 266–283. doi:10.1016/j.jconrel.2020.07.024

Pudela, C., Balyasny, S., and Applebaum, M. A. (2020). Nervous System: Embryonal Tumors: Neuroblastoma. *Atlas Genet. Cytogenet Oncol. Haematol.* 24 (7), 284–290. doi:10.4267/2042/70771

Putra, V., Hulme, A. J., Tee, A. E., Sun, J. Q. J., Atmadibrata, B., Ho, N., et al. (2021). The RNA-Helicase DDX21 Upregulates CEP55 Expression and Promotes Neuroblastoma. *Mol. Oncol.* 15 (4), 1162–1179. doi:10.1002/1878-0261.12906

Rajwanshi, A., Srinivas, R., and Upasana, G. (2009). Malignant Small Round Cell Tumors. *J. Cytol.* 26 (1), 1–10. doi:10.4103/0970-9371.54861

Raza, F., Siyu, L., Zafar, H., Kamal, Z., Zheng, B., Su, J., et al. (2022). Recent Advances in Gelatin-Based Nanomedicine for Targeted Delivery of Anti-cancer Drugs. *Curr. Pharm. Des.* 28 (5), 380–394. doi:10.2174/1381612827666211102100118

Raza, F., Zafar, H., You, X., Khan, A., Wu, J., and Ge, L. (2019). Cancer Nanomedicine: Focus on Recent Developments and Self-Assembled Peptide Nanocarriers. *J. Mater Chem. B* 7 (48), 7639–7655. doi:10.1039/c9tb01842e

Raza, F., Zafar, H., Zhang, S., Kamal, Z., Su, J., Yuan, W. E., et al. (2021). Recent Advances in Cell Membrane-Derived Biomimetic Nanotechnology for Cancer Immunotherapy. *Adv. Healthc. Mater* 10 (6), e2002081. doi:10.1002/adhm.202002081

Ren, B., Cai, Z. C., Zhao, X. J., Li, L. S., and Zhao, M. X. (2021). Evaluation of the Biological Activity of Folic Acid-Modified Paclitaxel-Loaded Gold Nanoparticles. *Int. J. Nanomedicine* 16, 7023–7033. doi:10.2147/IJN.S322856

Ren, G., Hao, X., Yan, S., Chen, J., Qiu, G., Ang, K. P., et al. (2022). Abies Spectabilis-Mediated Silver Nanoparticles Inhibits Cell Growth and Promotes Apoptosis in Breast Cancer MCF-7 Cells. *J. Environ. Pathol. Toxicol. Oncol.* 41 (1), 73–83. doi:10.1615/jenvironpatholtoxicoloncol.2021039805

Reynolds, C. P., Kane, D. J., Einhorn, P. A., Matthay, K. K., Crouse, V. L., Wilbur, J. R., et al. (1991). Response of Neuroblastoma to Retinoic Acid *In Vitro* and *In Vivo*. *Prog. Clin. Biol. Res.* 366, 203–211.

Rickman, D. S., Schulte, J. H., and Eilers, M. (2018). The Expanding World of N-MYC-Driven Tumors. *Cancer Discov.* 8 (2), 150–163. doi:10.1158/2159-8290.CD-17-0273

Rodríguez-Nogales, C., Noguera, R., Couvreur, P., and Blanco-Prieto, M. J. (2019). Therapeutic Opportunities in Neuroblastoma Using Nanotechnology [J]. *J. Pharmacol. Exp. Ther.* 370 (3), 625–635. doi:10.1124/jpet.118.255067

Rössler, J., Taylor, M., Geoerger, B., Francoise, F., Jeanette, L., Regine, P-S., et al. (2008). Angiogenesis as a Target in Neuroblastoma [J]. *Eur. J. cancer* 44 (12), 1645–1656. doi:10.1016/j.ejca.2008.05.015

Roy, I., Ohulchanskyy, T. Y., Bharali, D. J., Pudavar, H. E., Mistretta, R. A., Kaur, N., et al. (2005). Optical Tracking of Organically Modified Silica Nanoparticles as DNA Carriers: a Nonviral, Nanomedicine Approach for Gene Delivery. *Proc. Natl. Acad. Sci. U. S. A.* 102 (2), 279–284. doi:10.1073/pnas.0408039101

Sait, S., and Modak, S. (2017). Anti-GD2 Immunotherapy for Neuroblastoma. *Expert Rev. Anticancer Ther.* 17 (10), 889–904. doi:10.1080/14737140.2017.1364995

Sanchez-Martos, M., Martinez-Navarrete, G., Bernabeu-Zornoza, A., Lawrence, H., and Eduardo, F. (2021). Evaluation and Optimization of Poly-D-Lysine as a Non-natural Cationic Polypeptide for Gene Transfer in Neuroblastoma Cells. *J. Nanomater. (Basel, Switz.* 11 (7). doi:10.3390/nano11071756

Saw, P. E., Chen, J., and Song, E. (2022). Targeting CAFs to Overcome Anticancer Therapeutic Resistance [J]. *Trends cancer*. doi:10.1016/j.trecan.2022.03.001

Schulz, G., Cheresh, D. A., Varki, N. M., Yu, A., Staffileno, L. K., and Reisfeld, R. A. (1984). Detection of Ganglioside GD2 in Tumor Tissues and Sera of Neuroblastoma Patients. *Cancer Res.* 44 (12 Pt 1), 5914–5920.

Sekhri, P., Ledezma, D. K., Shukla, A., Sweeney, E. E., and Fernandes, R. (2022). The Thermal Dose of Photothermal Therapy Generates Differential Immunogenicity in Human Neuroblastoma Cells. *Cancers (Basel)* 14 (6), 1447. doi:10.3390/cancers14061447

Setua, S., Menon, D., Asok, A., Nair, S., and Koyakutty, M. (2010). Folate Receptor Targeted, Rare-Earth Oxide Nanocrystals for Bi-modal Fluorescence and Magnetic Imaging of Cancer Cells. *Biomaterials* 31 (4), 714–729. doi:10.1016/j.biomaterials.2009.09.090

Shokouhimehr, M., Soehnlen, E. S., Hao, J., Griswold, M., Flask, C., Fan, X., et al. (2010). Dual Purpose Prussian Blue Nanoparticles for Cellular Imaging and Drug Delivery: a New Generation of T1-Weighted MRI Contrast and Small Molecule Delivery Agents. *J. Mat. Chem.* 20 (25), 5251–5259. doi:10.1039/b923184f

Shukla, A., Cano-Mejia, J., Andricovich, J., Burga, R. A., Sweeney, E. E., and Fernandes, R. (2021). An Engineered Prussian Blue Nanoparticles-Based Nanoimmunotherapy Elicits Robust and Persistent Immunological Memory in a TH-MYCN Neuroblastoma Model. *Adv. Nanobiomed Res.* 1 (8). doi:10.1002/anbr.202100021

Skóra, B., Piechowiak, T., and Szychowski, K. A. (2022). Epidermal Growth Factor-Labeled Liposomes as a Way to Target the Toxicity of Silver Nanoparticles into EGFR-Overexpressing Cancer Cells *In Vitro* [J]. *Toxicol. Appl. Pharmacol.* 443, 116009.

Soenen, S. J., Parak, W. J., Rejman, J., and Manshian, B. (2015). (Intra)cellular Stability of Inorganic Nanoparticles: Effects on Cytotoxicity, Particle Functionality, and Biomedical Applications. *Chem. Rev.* 115 (5), 2109–2135. doi:10.1021/cr400714j

Song, X., Feng, L., Liang, C., Yang, K., and Liu, Z. (2016). Ultrasound Triggered Tumor Oxygenation with Oxygen-Shuttle Nanoperfluorocarbon to Overcome Hypoxia-Associated Resistance in Cancer Therapies. *Nano Lett.* 16 (10), 6145–6153. doi:10.1021/acs.nanolett.6b02365

Sosnik, A., and Carcaboso, A. M. (2014). Nanomedicines in the Future of Pediatric Therapy. *Adv. Drug Deliv. Rev.* 73, 140–161. doi:10.1016/j.addr.2014.05.004

Swift, C. C., Eklund, M. J., Kraveka, J. M., and Alazraki, A. L. (2018). Updates in Diagnosis, Management, and Treatment of Neuroblastoma. *Radiographics* 38 (2), 566–580. doi:10.1148/rg.2018170132

Swift, C. C., Eklund, M. J., Kraveka, J. M., and Alazraki, A. L. (2018). Updates in Diagnosis, Management, and Treatment of Neuroblastoma. *RadioGraphics* 38 (2), 566–580. doi:10.1148/rg.2018170132

Tian, C., Ding, P., Yuan, Z., Li, H., Zhao, Y., Sun, L., et al. (2015). A Novel Dual EGFR/HER2 Inhibitor KU004 Induces Cell Cycle Arrest and Apoptosis in HER2-Overexpressing Cancer Cells. *Apoptosis* 20 (12), 1599–1612. doi:10.1007/s10495-015-1164-7

Tian, C., Yuan, Z., Xu, D., Ding, P., Wang, T., Zhang, L., et al. (2017). Inhibition of Glycolysis by a Novel EGFR/HER2 Inhibitor KU004 Suppresses the Growth of HER2+ Cancer. *Exp. Cell Res.* 357 (2), 211–221. doi:10.1016/j.yexcr.2017.05.019

Tian, Y., Guo, R., Wang, Y., and Yang, W. (2016). Coordination-Induced Assembly of Intelligent Polysaccharide-Based Phototherapeutic Nanoparticles for Cancer Treatment. *Adv. Healthc. Mater* 5 (24), 3099–3104. doi:10.1002/adhm.201600877

Ullah, A., Chen, G., Hussain, A., Khan, H., Abbas, A., Zhou, Z., et al. (2021). Cyclam-Modified Polyethyleneimine for Simultaneous TGFβ siRNA Delivery and CXCR4 Inhibition for the Treatment of CCl4-Induced Liver Fibrosis. *Int. J. Nanomedicine* 16, 4451–4470. doi:10.2147/IJN.S314367

van der Burg, S. H., Arens, R., Ossendorp, F., van Hall, T., and Melief, C. J. (2016). Vaccines for Established Cancer: Overcoming the Challenges Posed by Immune Evasion. *Nat. Rev. Cancer* 16 (4), 219–233. doi:10.1038/nrc.2016.16

Varon, E., Blumrosen, G., Sinvani, M., Haimov, E., Polani, S., Natan, M., et al. (2022). An Engineered Nanocomplex with Photodynamic and Photothermal Synergistic Properties for Cancer Treatment. *Int. J. Mol. Sci.* 23 (4). doi:10.3390/ijms23042286

Vignaroli, G., Calandro, P., Zamperini, C., Coniglio, F., Iovenitti, G., Tavanti, M., et al. (2016). Improvement of Pyrazolo[3,4-D]pyrimidines Pharmacokinetic Properties: Nanosystem Approaches for Drug Delivery. *Sci. Rep.* 6, 21509. doi:10.1038/srep21509

Vossen, L. I., Markovsky, E., Eldar-Boock, A., Tschiche, H. R., Wedepohl, S., Pisarevsky, E., et al. (2018). PEGylated Dendritic Polyglycerol Conjugate Targeting NCAM-Expressing Neuroblastoma: Limitations and Challenges. *Nanomedicine* 14 (4), 1169–1179. doi:10.1016/j.nano.2018.02.009

Wachowiak, R., Rawnaq, T., Metzger, R., Quaas, A., Fiegel, H., Kähler, N., et al. (2008). Universal Expression of Cell Adhesion Molecule NCAM in Neuroblastoma in Contrast to L1: Implications for Different Roles in Tumor Biology of Neuroblastoma? *Pediatr. Surg. Int.* 24 (12), 1361–1364. doi:10.1007/s00383-008-2264-z

Wang, L., Chen, C., Song, Z., Wang, H., Ye, M., Wang, D., et al. (2022). EZH2 Depletion Potentiates MYC Degradation Inhibiting Neuroblastoma and Small Cell Carcinoma Tumor Formation. *Nat. Commun.* 13 (1), 12. doi:10.1038/s41467-021-27609-6

Wang, X., Zheng, M., Raza, F., Liu, Y., Wei, Y., Qiu, M., et al. (2022). Recent Developments in Mesoporous Silica Nanoparticles for Tumor Theranostic Applications. *Curr. Pharm. Des.* 28 (2), 151–164. doi:10.2174/1381612827666211111152839

Wang, Y., Luo, S., Wu, Y., Peng, T., Jiajun, L., Zeying, L., et al. (2020). Highly Penetrable and On-Demand Oxygen Release with Tumor Activity Composite Nanosystem for Photothermal/Photodynamic Synergetic Therapy [J]. *ACS Nano* 14, 17046–17062. doi:10.1021/acsnano.0c06415

Weinstein, J. L., Katzenstein, H. M., and Cohn, S. L. (2003). Advances in the Diagnosis and Treatment of Neuroblastoma. *Oncologist* 8 (3), 278–292. doi:10.1634/theoncologist.8-3-278

Wen, H., Dong, C., Dong, H., Shen, A., Xia, W., Cai, X., et al. (2012). Engineered Redox-Responsive PEG Detachment Mechanism in PEGylated Nano-Graphene Oxide for Intracellular Drug Delivery. *Small* 8 (5), 760–769. doi:10.1002/smll.201101613

Whittle, S. B., Smith, V., Doherty, E., Zhao, S., McCarty, S., and Zage, P. E. (2017). Overview and Recent Advances in the Treatment of Neuroblastoma. *Expert Rev. Anticancer Ther.* 17 (4), 369–386. doi:10.1080/14737140.2017.1285230

Wohlrab, J., Wohlrab, D., Wohlrab, L., Wohlrab, C., and Wohlrab, A. (2014). Use of Hyaluronidase for Pharmacokinetic Increase in Bioavailability of Intracutaneously Applied Substances. *Skin. Pharmacol. Physiol.* 27 (5), 276–282. doi:10.1159/000360545

Wu, W., Pu, Y., and Shi, J. (2022). Nanomedicine-enabled Chemotherapy-Based Synergetic Cancer Treatments. *J. Nanobiotechnology* 20 (1), 4. doi:10.1186/s12951-021-01181-z

Wu, X., Li, Y., Raza, F., Wang, X., Zhang, S., Rong, R., et al. (2021). Red Blood Cell Membrane-Camouflaged Tedizolid Phosphate-Loaded PLGA Nanoparticles for Bacterial-Infection Therapy. *Pharmaceutics* 13 (1). doi:10.3390/pharmaceutics13010099

Yan, M., and Liu, Q. (2016). Differentiation Therapy: a Promising Strategy for Cancer Treatment. *Chin. J. Cancer* 35, 3. doi:10.1186/s40880-015-0059-x

Yeasmin, S., Datta, H. K., Chaudhuri, S., Malik, D., and Bandyopadhyay, A. (2017). *In-vitro* Anti-cancer Activity of Shape Controlled Silver Nanoparticles (AgNPs) in Various Organ Specific Cell Lines. *J. Mol. Liq.* 242, 757–766. doi:10.1016/j.molliq.2017.06.047

Yoshida, S., Duong, C., Oestergaard, M., Fazio, M., Chen, C., Peralta, R., et al. (2020). MXD3 Antisense Oligonucleotide with Superparamagnetic Iron Oxide Nanoparticles: A New Targeted Approach for Neuroblastoma. *Nanomedicine* 24, 102127. doi:10.1016/j.nano.2019.102127

Yu, J., Hung, J. T., Wang, S. H., Cheng, J. Y., and Yu, A. L. (2020). Targeting Glycosphingolipids for Cancer Immunotherapy. *FEBS Lett.* 594 (22), 3602–3618. doi:10.1002/1873-3468.13917

Zafar, H., Raza, F., Ma, S., Wei, Y., Zhang, J., and Shen, Q. (2021). Recent Progress on Nanomedicine-Induced Ferroptosis for Cancer Therapy. *Biomater. Sci.* 9 (15), 5092–5115. doi:10.1039/d1bm00721a

Zakaria, H., Abdelaziz, W. S., and Youssef, T. (2016). Effect of Size, Concentration, and Type of Spherical Gold Nanoparticles on Heat Evolution Following Laser Irradiation Using Tissue-Simulating Phantoms. *Lasers Med. Sci.* 31 (4), 625–634. doi:10.1007/s10103-016-1886-y

Zhan, Y., Ling, S., Huang, H., Zhang, Y., Chen, G., Huang, S., et al. (2021). Rapid Unperturbed-Tissue Analysis for Intraoperative Cancer Diagnosis Using an Enzyme-Activated NIR-II Nanoprobe. *Angew. Chem. Int. Ed. Engl.* 60 (5), 2637–2642. doi:10.1002/anie.202011903

Zhan, Y., Shi, S., Ehlerding, E. B., Graves, S. A., Goel, S., Engle, J. W., et al. (2017). Radiolabeled, Antibody-Conjugated Manganese Oxide Nanoparticles for Tumor Vasculature Targeted Positron Emission Tomography and Magnetic Resonance Imaging. *ACS Appl. Mater Interfaces* 9 (44), 38304–38312. doi:10.1021/acsami.7b12216

Zhang, L., Marrano, P., Kumar, S., Leadley, M., Elias, E., Thorner, P., et al. (2013). Nab-paclitaxel Is an Active Drug in Preclinical Model of Pediatric Solid Tumors. *Clin. Cancer Res.* 19 (21), 5972–5983. doi:10.1158/1078-0432.CCR-13-1485

Zhang, L., Wang, M., Zhu, Z., Chen, S., Wu, H., Yang, Y., et al. (2021). A GD2-Aptamer-Mediated, Self-Assembling Nanomedicine for Targeted Multiple Treatments in Neuroblastoma Theranostics. *Mol. Ther. Nucleic Acids* 26, 732–748. doi:10.1016/j.omtn.2021.08.021

Zhang, L., Wang, M., Zhu, Z., Ding, C., Chen, S., Wu, H., et al. (2021). A Novel pH-Sensitive Multifunctional DNA Nanomedicine: An Enhanced and Harmless GD2 Aptamer-Mediated Strategy for Guiding Neuroblastoma Antitumor Therapy. *Int. J. Nanomedicine* 16, 3217–3240. doi:10.2147/IJN.S302450

Zhao, J., Cai, X., Gao, W., Zhang, L., Zou, D., Zheng, Y., et al. (2018). Prussian Blue Nanozyme with Multienzyme Activity Reduces Colitis in Mice. *ACS Appl. Mater Interfaces* 10 (31), 26108–26117. doi:10.1021/acsami.8b10345

Zhao, R., Xiang, J., Wang, B., Chen, L., and Tan, S. (2022). Recent Advances in the Development of Noble Metal NPs for Cancer Therapy. *Bioinorg. Chem. Appl.* 2022, 2444516. doi:10.1155/2022/2444516

Zhou, Y., Yan, H., Zhou, Q., Feng, R., Wang, P., Yang, F., et al. (2021). Beta-Lapachone Attenuates BMSC-Mediated Neuroblastoma Malignant Transformation by Inhibiting Gal-3/Gal-3BP/IL6 Axis. *Front. Pharmacol.* 12, 766909. doi:10.3389/fphar.2021.766909

Zhu, Q., Feng, C., Liao, W., Zhang, Y., and Tang, S. (2013). Target Delivery of MYCN siRNA by Folate-Nanoliposomes Delivery System in a Metastatic Neuroblastoma Model. *Cancer Cell Int.* 13 (1), 65. doi:10.1186/1475-2867-13-65

Zhu, R., Wang, Z., Liang, P., He, X., Zhuang, X., Huang, R., et al. (2017). Efficient VEGF Targeting Delivery of DOX Using Bevacizumab Conjugated SiO2@LDH for Anti-neuroblastoma Therapy. *Acta Biomater.* 63, 163–180. doi:10.1016/j.actbio.2017.09.009

Conflict of Interest: The authors declare that the research was conducted in the absence of any commercial or financial relationships that could be construed as a potential conflict of interest.

Publisher's Note: All claims expressed in this article are solely those of the authors and do not necessarily represent those of their affiliated organizations, or those of the publisher, the editors and the reviewers. Any product that may be evaluated in this article, or claim that may be made by its manufacturer, is not guaranteed or endorsed by the publisher.

frontiers | Frontiers in Pharmacology

ORIGINAL RESEARCH
published: 30 June 2022
doi: 10.3389/fphar.2022.911771

Formulation Development and Characterization of pH Responsive Polymeric Nano-Pharmaceuticals for Targeted Delivery of Anti-Cancer Drug (Methotrexate)

Farhad Ullah[1], Zafar Iqbal[1], Amjad Khan[2], Saeed Ahmad Khan[2], Lateef Ahmad[3], Amal Alotaibi[4], Riaz Ullah[5] and Muhammad Shafique[6]**

[1]Department of Pharmacy, University of Peshawar, Peshawar, Pakistan, [2]Department of Pharmacy, Kohat University of Science and Technology (KUST), Kohat, Pakistan, [3]Department of Pharmacy, University of Swabi, Swabi, Pakistan, [4]Department of Basic Science, College of Medicine, Princess Nourah Bint Abdulrahman University, Riyadh, Saudi Arabia, [5]Medicinal, Aromatic, and Poisonous Plants Research Center, Department of Pharmacognosy, College of Pharmacy, King Saud University, Riyadh, Saudi Arabia, [6]Department of Pharmaceutical Sciences, College of Pharmacy-Boys, Al-Dawadmi Campus, Shaqra University, Shaqra, Saudi Arabia

OPEN ACCESS

Edited by:
Donato Cosco, University of Catanzaro "Magna Graecia", Italy

Reviewed by:
Jennifer Martins Noro, University of Minho, Portugal
Raj Kumar, University of Nebraska Medical Center, United States

***Correspondence:**
Amjad Khan
dr.amjad@kust.edu.pk
Muhammad Shafique
shafiqueph@yahoo.com

Specialty section:
This article was submitted to Experimental Pharmacology and Drug Discovery, a section of the journal Frontiers in Pharmacology

Received: *03 April 2022*
Accepted: *11 May 2022*
Published: *30 June 2022*

Citation:
Ullah F, Iqbal Z, Khan A, Khan SA, Ahmad L, Alotaibi A, Ullah R and Shafique M (2022) Formulation Development and Characterization of pH Responsive Polymeric Nano-Pharmaceuticals for Targeted Delivery of Anti-Cancer Drug (Methotrexate). Front. Pharmacol. 13:911771. doi: 10.3389/fphar.2022.911771

Oral administration of pH sensitive/stimuli responsive nanoparticles are gaining importance because of the limited side effects, minimum dose and controlled drug release. The objective of this study was to develop and evaluate pH sensitive polymeric nanoparticles for methotrexate with the aim to maximize the drug release at target site. In the presented study, pH sensitive polymeric nanoparticles of methotrexate were developed through modified solvent evaporation technique using polymer Eudragit S100. Different process parameters like drug to polymer ratio, speed of sonication, concentration of surfactant and time of sonication were optimized by evaluating their effects on particle size, PDI, zeta potential, entrapment/encapsulation efficiency. The developed formulations were evaluated for their size, polydispersity (PDI), zeta potential, encapsulation efficiency, XRD, scanning electron microscopy, *in-vitro* drug release and stability studies. Best results were obtained with poloxamer-407 and PVA and were selected as surfactants. Physicochemical characterization of the developed formulations showed that the particle size lies in the range 165.7 ± 1.85–330.4 ± 4.19, PDI 0.119 ± 0.02–0.235 ± 0.008, zeta potential –0.163 ± 0.11––5.64 ± 0.36 mV, and encapsulation efficiency more than 61%. The results of scanning electron microscopy revealed that nanoparticles have regular geometry with spherical shape. Initially the drug release occur through diffusion followed by erosion. The present studies showed that MTX-ES100 nanoparticles prepared during this study have the desired physicochemical properties, surface morphology and release characteristics used to target the desired organs.

Keywords: Eudragit, methotrexate, targeted drug delivery, polymeric nanoparticles, solvent evaporation method

1 INTRODUCTION

Drug administration by oral route is the most ideal owing to its simplicity, convenience, minimal pain and suitability, especially for chronic therapy (Sarmad et al., 2021). It is expected to solve the noncompliance-related problems associated with injections and other aggressive dosage forms (Benish et al., 2021). In addition, oral formulations have unique advantages for both physicians and industry, such as flexible dosing schedules, less demands on staff, reduced costs through less hospital or clinic visits, and less expensive production costs (Sharma et al., 2016; Amjad, 2019). However, orally delivered drugs are exposed to extreme conditions and variable pH throughout the GIT which can adversely affect drug absorption. Some drugs like peptides and protein, may be degraded by digestive enzymes (Late et al., 2009) and by variation in pH of the gastrointestinal (GI) tract. In GIT the pH varies from highly acidic in the stomach (pH 1–3) to neutral or slightly alkaline in the duodenum (pH 6) and along the jejunum and ileum (pH 6–7.5) (Hadi et al., 2012; Amjad et al., 2016) and can result in hydrolysis, oxidation or de-amidation of protein. The intestinal epithelium is also a barrier to the absorption of hydrophilic macromolecules such as peptide, proteins, nucleic acids, and polysaccharides due to their hydrophilicity and high molecular weight, which makes it difficult to across the cell membranes (Hazal et al., 2021). Due to possibility of low bioavailability after oral administration of many drugs, such as proteins, it has become a challenge to achieve consistent and adequate bioavailability for their oral administration (Dilpreet, 2021). Of varied methods for overcoming the barriers, pH triggered release mechanisms are extensively used in oral administration. The pH-responsive carriers for oral drug delivery have been proven to enhance the stability of drug delivery in stomach and achieve controlled release in intestines. A pH-responsive and colon-specific capsule which is potential to be used as a reliable carrier for colon-specific drug delivery has been reported (Bohrey et al., 2016).

Polymeric nanoparticles (NPs) have been extensively studied for oral delivery as it can protect encapsulated drugs from the low pH environment, drug efflux pumps, and enzymatic degradation. Recently, through cellular targeting with surface-functionalized ligands, transepithelial transport, and greater gastric retention, pH-responsive mechanisms have been included in novel nanomedicines to improve systemic exposure. One widespread approach to realize organ-specific drug release is to prepare NPs that exhibit pH-responsive swelling. For instance, when using acrylic-based polymers (e.g., PMAA), NPs retain a hydrophobic, collapsed state in the stomach because of carboxyl protonation. After moving though gastric passage, increasing pH results in NPs swelling due to the ionization of carboxyl groups and hydrogen bond breakage (Madani et al., 2018).

Eudragits, is poly(methacrylic acid-co-methyl acrylate) copolymers, and is widely used in formulation of pH-responsive NPs. Depending upon their solubility, Eudragit are classified as;

- Eudragit E100: Eudragit E100 is a cationic copolymer which dissolves in stomach,
- Eudragit S100: Eudragit S100 is an anionic copolymers and dissolves at pH4.5
- Eudragit L100: Eudragit L100 is an anionic copolymers which dissolves at pH7

Due to variability in their solubility at different pH eudragit can be used in formulation of pH responsive drug delivery system for oral administration (Yoo et al., 2011). Objective of the study was to develop pH responsive, colon targeted drug delivery system for oral administration of anti-cancer drug (methotrexate). In the present study, Eudragit S100 based nanoparticles were prepared by solvent evaporation technique and evaluated for various quality control parameters and pH dependent drug release.

2 MATERIALS AND METHODS

2.1 Materials and Solvents

Methotrexate (purity ≥99.9%) (Huzhou Zhanwang Pharma Co., Ltd., China), Eudragit® S100 (Evonik, Germany), Poloxamer-407 (Sigma-Aldrich), Poloxamer-407 (POL) (Merck, Germany), Cetyl Trimethyl Ammonium Bromide (CTAB) (Merck, Germany), Poy vinyl alcohol (PVA)Sigma-Aldrich, Sodium Bicarbonate (Fluka) (purity 99.95%), Sodium dodecyl sulphate (SDS) (Sigma-Aldrich), Sodium Chloride (NaCl), Dialysis Tubing (Size 6 Inf, Dia "27/32," 21.5 mm; 30 M) (Sigma-Aldrich) (MWCO: 12–14 kDa), Potassium Chloride (KCl) (Scharlau Chemie Spain), (Na_2HPO_4) Disodium Hydrogen Phosphate (Scharlau Chemie Spain), (KH_2PO_4) Potassium Di-hydrogen Phosphate (Sigma-Aldrich).

2.2 Preparation of Drug Loaded Polymeric Nanoparticles

Polymeric nanoparticles of methotrexate were formulated by modified emulsion solvent evaporation technique (Nasef et al., 2015). Different stabilizers like POL, cetyl trimethyl ammonium bromide, polyvinyl alcohol and sodium dodecyl sulphate (SDS) were used in different concentrations (0.5%, 0.25%, and 0.125%). The solutions of surfactant were formed by solubilizing in distilled water and used constant volume (10 ml) of solutions of different concentrations. Both the drug and polymer (Eudragit) were dissolved in methanol (5 ml) and an aliquot (5 ml) was added dropwise to aqueous solution of surfactant (10 ml) under continuous magnetic stirring. After complete addition of organic phase, the resulting mixture was subjected to sonication at 99% amplitude for 3 min with the help of probe sonicator (Soniprep, 150 instruments; Sanyo, United Kingdom) fitted with exponential microprobe, having an end diameter of 3 mm. The resultant emulsion was then stirred at low speed with magnetic stirrer in order to remove organic solvents completely and centrifuged at 15,000 rpm for 30 min at 4°C to collect the drug loaded nanoparticles. The obtained nanoparticles were washed three times with double distilled water and lyophilized. **Figure 1** shows schematic presentation of the process of preparation of methotrexate loaded polymeric nanoparticles while detailed composition of different formulations is presented in **Table 1**.

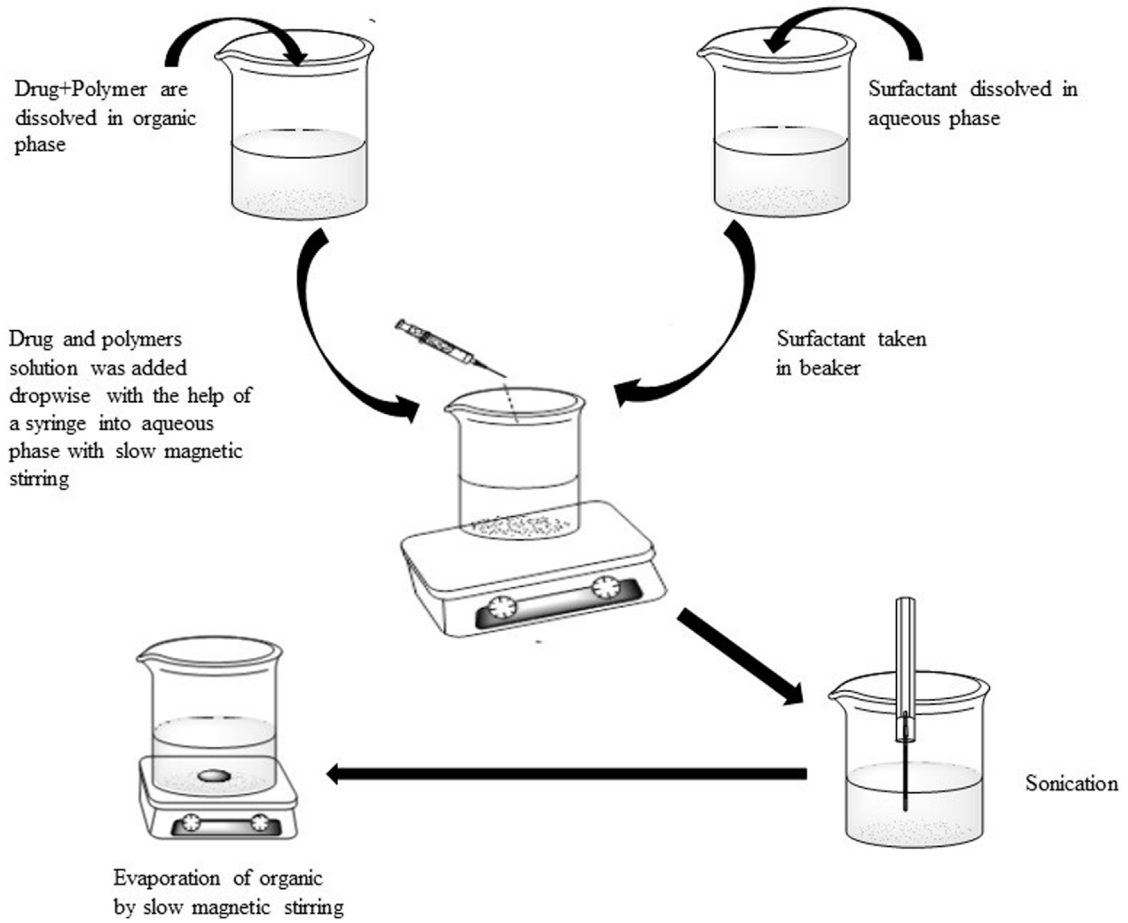

FIGURE 1 | Schematic presentation of the process of preparation of methotrexate loaded polymeric nanoparticles.

2.3 Optimization of Process Variables

Different formulation and process variables like polymer concentration, surfactant concentration, type of surfactant, time of sonication, amplitude of sonication and drug concentration were then optimized for nanoparticles.

For optimization of polymer quantity, different drug to polymer ratios (10, 20, and 30 mg) were studied and their effect on results was evaluated. Different surfactant (POL, PVA, SDS, and CTAB) were tested for emulsification and the selected surfactant was studied at different concentrations (0.125%, 0.25%, and 0.5% w/v) to get the optimal results.

Emulsification was performed at different homogenization speeds (60%, 80%, and 99%) and effect on characteristics of the droplets were evaluated. Similarly, sonication time was varied between 1–6 min and its effect was evaluated.

To optimize the effect of amount of drug in the nanoparticles, variable amount of drug (2–6 mg) was added to the organic phase and its effect on encapsulation efficiency and other characteristics was evaluated. Details of optimization parameters are mentioned in **Table 2**.

2.4 Characterization of Polymeric Nanoparticles of Methotrexate

2.4.1 Measurement of Particle Size and Polydispersibility Index

The nanoparticles size and PDI was evaluated through dynamic light scattering technique by means of Zeta Sizer (Zeta sizer Nano, ZS-90; Malvern Instruments Ltd., United Kingdom). The distilled water was added to the dispersion of nanoparticles when required. The nanoparticles were analyzed at scattering angle of 90° at room temperature (Nasef et al., 2015). The size of particles and PDI was determined through Malvern software. All the values were calculated three times and their mean and standard deviation were calculated.

2.4.2 Measurement of Zeta Potential

Laser Doppler Micro-electrophoresis method was utilized for determining the zeta potential of nanoparticles utilizing Zeta Sizer Nano. Readings were taken three times and their mean and SD determined.

TABLE 1 | Composition of methotrexate nanoparticles prepared by using Eudragit S100.

Code	Drug (mg)	Eudragit S100 (mg)	Polaxamer 407 (%) (10ml)	PVA (%) (10ml)
MSX1	2	10	0.50	—
MSX2	2	10	0.25	—
MSX3	2	10	0.125	—
MSX4	2	20	0.50	—
MSX5	2	20	0.25	—
MSX6	2	20	0.125	—
MSX7	2	30	0.50	—
MSX8	2	30	0.25	—
MSX9	2	30	0.125	—
MSP1	2	10	—	0.50
MSP2	2	10	—	0.25
MSP3	2	10	—	0.125
MSP4	2	20	—	0.50
MSP5	2	20	—	0.25
MSP6	2	20	—	0.125
MSP7	2	30	—	0.50
MSP8	2	30	—	0.25
MSP9	2	30	—	0.125

All formulations are prepared at 25°C and 99% sonication speed.

TABLE 2 | Effect of process variables on particle size and encapsulation efficiency of methotrexate nanoparticles with Eudragit S100.

Code	Drug (mg)	Eudragit S100 (mg)	Polaxamer 407 (%) (10 ml)	Temp (°C)	Sonication speed (%)	Sonication time (min)	CTAB (%) (10 ml)	SDS (%) (10 ml)	PVA (%) (10 ml)
FMVs1	2	20	0.25	25	60	3	—	—	—
FMVs2	2	20	0.25	25	80	3	—	—	—
FMVs3	2	20	0.25	25	99	3	—	—	—
FMVt4	2	20	0.25	25	99	1	—	—	—
FMVt5	2	20	0.25	25	99	3	—	—	—
FMVt6	2	20	0.25	25	99	6	—	—	—
FMVr7	2	20	—	25	99	3	—	0.25	—
FMVr8	2	20	—	25	99	3	0.25	—	—
FMVr9	2	20	—	25	99	3	—	—	0.25
FMVr10	2	20	0.25	25	99	3	—	—	—
FMVd11	2	30	0.25	25	99	3	—	—	—
FMVd12	4	30	0.25	25	99	3	—	—	—
FMVd13	6	30	0.25	25	99	3	—	—	—

2.4.3 Determination of Percent Encapsulation Efficiency

The percent drug entrapment efficiency of methotrexate (MTX) was calculated by centrifuging the nanoparticle suspension so as to separate nanoparticle from aqueous medium at 15,000 rpm for 30 min 25°C. The free drug present in supernatant collected after centrifugation was calculated at 295 nm using UV spectroscopy. The % EE was obtained as per **Eq. 1**.

$$\%EE = \frac{\text{Mass of Drug in Nanoprticles}}{\text{Mass of Drug used in Formulation}} \times 100 \qquad (1)$$

2.4.4 Scanning Electron Microscopy

The surface morphology of prepared nanoparticles was determined through scanning electron microscopy, using Brass stub for sample preparation. The sample was placed on a double tape made of carbon that was attached to the stub. The excess quantity of sample was removed from the tape by blade. Then gold was coated on the surface of nanoparticles by a sputter coater ("Argon Sputtering," "SPI Module" Control) for 90 s under vacuum produced by argon gas. The surface morphology of the sample was then confirmed by electron microscope (JSM-5910, Jeol Japan).

2.4.5 X-Ray Diffraction

The X-ray diffraction patterns of different samples were measured by X-ray diffractometer so as to determine the nature of sample whether amorphous or crystalline. The x-ray diffraction pattern of the samples determined included; MTX, Poloxamer-407, PVA, Eudragit S100, and MTX-NPs. The instrument was run at 3° (2θ)–80° (2θ) angular range.

TABLE 3 | Effect of sonication speed and sonication time on particle size and encapsulation efficiency.

Parameters	Code	Sonication speed (%)[a]	Drug: polymer	Particle size (nm)	Zeta potential (mV)	PDI	% Encapsulation efficiency
Sonication speed	FMVs1	60	1:10	259 ± 1.15	–0.344 ± 0.10	0.185 ± 0.015	39.95 ± 0.7
	FMVs2	80	1:10	165.7 ± 1.85	–0.163 ± 0.11	0.215 ± 0.010	61.42 ± 2.1
	FMVs3	99	1:10	188.6 ± 3.1	–1.85 ± 0.15	0.233 ± 0.008	65.04 ± 0.8
Sonication time	FMVt4	1	1:10	270 ± 2	0.171 ± 0.14	0.207 ± 0.022	37.92 ± 2.7
	FMVt5	3	1:10	188.6 ± 3.1	–1.85 ± 0.15	0.233 ± 0.008	47.04 ± 1.9
	FMVt6	6	1:10	192.5 ± 2.83	–2.48 ± 0.20	0.237 ± 0.006	49.3 ± 1.5
Effect of surfactant	FMVr7	Poloxamer-407	1:10	165.7 ± 1.85	–0.163 ± 0.11	0.215 ± 0.010	61.42 ± 2.1
	FMVr8	SDS	1:10	1,108 ± 969.22	–53.1 ± 3.5	1 ± 0	2.55 ± 1.1
	FMVr9	CTAB	1:10	133.4 ± 8.51	51.4 ± 0.34	0.782 ± 0.07	33.19 ± 2.5
	FMVr10	PVA	1:10	187.7 ± 1.09	–0.59 ± 0.36	0.437 ± 0.020	59.01 ± 3.6

[a]*Speed of the instrument can be measured in terms of percentage.*

TABLE 4 | Effect Drug concentration on particle size and encapsulation efficiency.

Code	Drug (mg)	Eudragit S100 (mg)	Particle size (nm)	Zeta potential (mV)	PDI	% Encapsulation efficiency
FMVd11	2	30	174.6 ± 3.00	–5.64 ± 0.36	0.227 ± 0.017	70 ± 3.4
FMVd12	4	30	175.5 ± 0.43	1.58 ± 0.38	0.182 ± 0.02	30.19 ± 1.3
FMVd13	6	30	207.5 ± 13.09	1.11 ± 0.26	0.415 ± 0.06	56.96 ± 2.9

2.4.6 *In Vitro* Drug Release

The *in-vitro* drug release profile of MTX from polymeric nanoparticles was determined using dialysis bag diffusion method. Dissolution media consisted of simulated gastric fluid (0.1 N HCl pH 1.2), simulated intestinal fluid (PB pH 6.5) and simulated colonic fluid (PB pH 7.4). Dissolution media (100 ml) was taken in a flask, de aerated and equilibrated to 37°C ± 2°C on a shaking water bath. Dialysis membrane containing nano suspension (1 ml) of MTX was dipped in dissolution media. The flask containing dissolution media was agitated at 60 ± 2 rpm. Samples (1 ml) were withdrawn at specific interval of time (0.25, 0.5, 1, 1.5, 2, 3, 4, 6, 8, 10, 12, 18, 24, 36, and 48) and quantity of drug release was determined through UV spectrophotometer at 295 nm. Volume of dissolution media was adjusted by same volume after each procedure of sampling held at same temperature. All samples were analyzed three time and their average and SD were calculated (n = 3). The dissolution medias were replaced depending on the time intervals assuming that the drug keep on passing the GIT. *In vitro* drug release was initiated in simulated gastric fluid (SGF) for first 2 h and then dissolution media was replaced with simulated intestinal fluid (SIF) for next 4 h. The dissolution medium was then interchanged with simulated colonic fluid (SCF) and drug release studies were continued for 42 h.

2.5 Freeze Drying and Selection of Cryoprotectant

The developed formulations were lyophilized using freeze drier (Telstar Cryodos 50, United States) to get dried methotrexate loaded nanoparticles for reconstitution and evaluation of stability. In order to optimize and select a suitable cryoprotectant, mannitol and sucrose were tested in different concentrations (2%, 4%, and 5%) and their effect on size, PDI and encapsulation efficiency was evaluated. The process of freeze drying was carried out at −45°C and 0.250 mBar pressure for 12 h. The same procedure was applied for freeze drying of control samples without cryoprotectant. Freeze dried sample was reconstituted in distilled water (2 ml) for further studies.

2.6 Stability Study

The stability studies of methotrexate loaded Eudragit S100 nano-suspension was evaluated through storing nano-suspension at different conditions, i.e., 25°C and 4°C for 6 months. The samples were placed in closed glass vials throughout the storage phase. Analysis of the nano-formulations was performed to assess PDI, size of particle and % EE of freshly prepared nano suspensions and samples kept at stability conditions. Samples were evaluated in triplicate for each storage condition after 1, 3, and 6 months of storage.

2.7 Statistical Analysis

Different statistical parameters like mean (X), standard deviation (SD) and relative standard deviation (% RSD) were used for quantifying methotrexate in mice. The data was evaluated by student's t-test for assessing significance of difference ($p \leq 0.05$) among means of treatments.

3 RESULTS AND DISCUSSION

Objective of the research was to prepare pH sensitive nanoparticles formulations of methotrexate for oral targeted drug delivery. Eudragit® S100 was used along with different

TABLE 5 | Characterization of methotrexate nanoparticles using Eudragit S100.

Code	Drug:polymer	Particle size (nm)	Zeta potential (mV)	PDI	Amount encapsulated (mg/ml)	% Encapsulation efficiency
MSX1	1:5	114.6 ± 11.2	−2.92 ± 0.27	0.389 ± 0.22	0.78	39.26 ± 4.5
MSX2	1:5	109.7 ± 2.50	−2.36 ± 1.15	0.385 ± 0.006	0.73	36.81 ± 2.1
MSX3	1:5	135.1 ± 1.89	−1.59 ± 0.27	0.245 ± 0.016	0.65	32.68 ± 3.2
MSX4	1:10	171 ± 5.15	−0.10 ± 0.18	0.373 ± 0.045	1.14	63.02 ± 1.5
MSX5	1:10	165.7 ± 1.85	−0.163 ± 0.11	0.215 ± 0.010	1.228	61.42 ± 2.1
MSX6	1:10	185.9 ± 2.96	−3.54 ± 0.30	0.264 ± 0.014	1.01	50.7 ± 1.9
MSX7	1:15	231.9 ± 0.51	−5.06 ± 0.64	0.372 ± 0.018	1.31	65.89 ± 2.4
MSX8	1:15	174.6 ± 3.00	−5.64 ± 0.36	0.227 ± 0.017	1.4	70 ± 1.2
MSX9	1:15	202.6 ± 1.20	−2.28 ± 0.15	0.235 ± 0.008	1.38	69.19 ± 1.8
MSP1	1:5	776 ± 56	−0.23 ± 0.09	0.065 ± 0.08	1.40	70.18 ± 3.6
MSP2	1:5	492 ± 9.6	−11.5 ± 0.47	0.362 ± 0.04	1.20	60.01 ± 1.5
MSP3	1:5	1,190 ± 49	−0.161 ± 0.21	0.114 ± 0.13	0.98	49.36 ± 2.9
MSP4	1:10	981 ± 41.27	−1.97 ± 0.88	0.301 ± 0.45	1.62	81.45 ± 2.4
MSP5	1:10	872 ± 21.70	−0.841 ± 0.05	0.235 ± 0.08	1.39	69.51 ± 1.7
MSP6	1:10	1,336 ± 35.65	−1.05 ± 0.28	0.189 ± 0.46	1.08	54.47 ± 1.9
MSP7	1:15	1,241 ± 28.27	−0.67 ± 0.34	0.22 ± 0.11	1.82	91.31 ± 2.2
MSP8	1:15	1,118 ± 21.83	−0.355 ± 0.47	0.384 ± 0.35	1.51	75.82 ± 2.8
MSP9	1:15	1,528 ± 10.71	−0.796 ± 0.27	0.565 ± 0.33	1.20	60.08 ± 3.1

M, methotrexate; S, Eudragit S100; P, poly vinyl alcohol; X, Poloxamer-407.

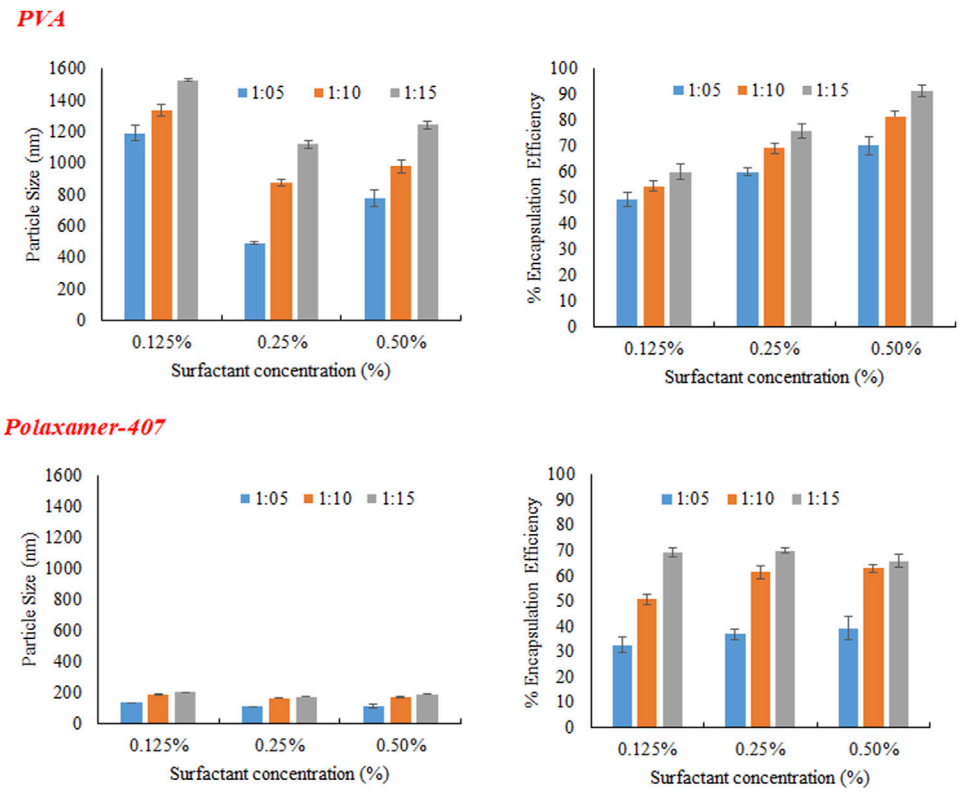

FIGURE 2 | Effect of Eudragit S100 conc. on **(A)** particles size **(B)** % Encapsulation efficiency of MTX nanoparticles using different emulsifiers (PVA and Poloxamer-407).

emulsifier (POL, PVA, SDS, and CTAB in different concentrations as 0.125%, 0.25%, and 0.5%). Over seventy formulations were prepared and were thoroughly assessed for size of their particle size, shape, zeta potential, encapsulation efficiency, poly dispersibility index and *in vitro* drug release and freeze drying.

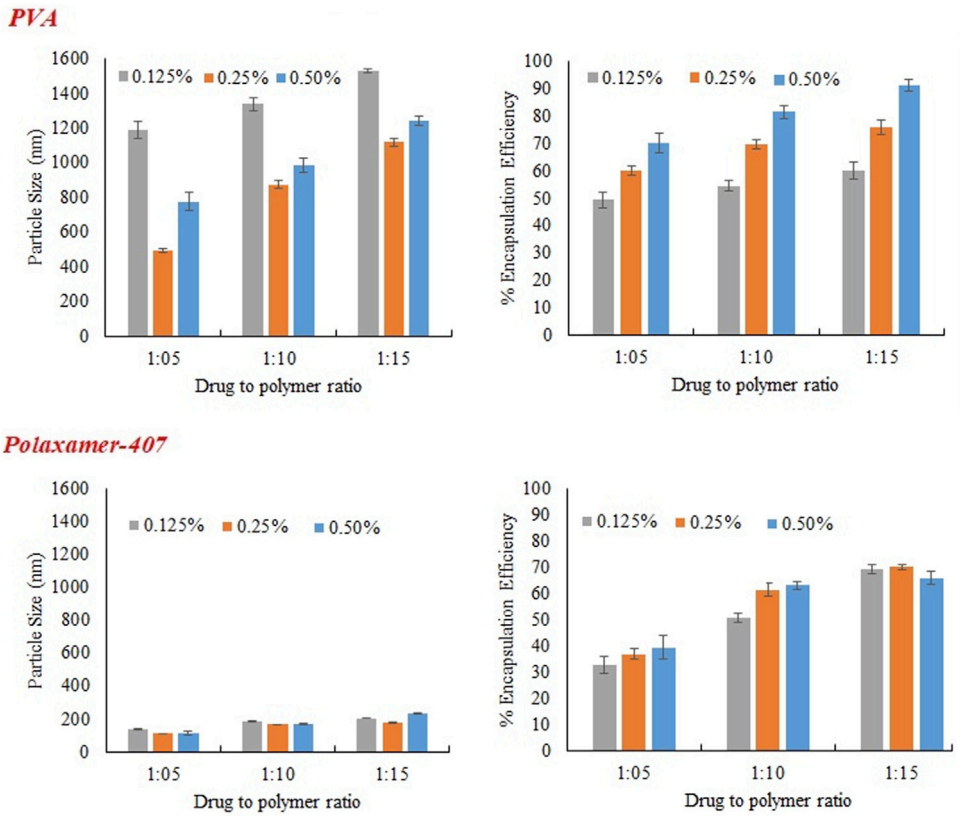

FIGURE 3 | Effect of concentration of emulsifier (PVA and Poloxamer-407) on particles size, and encapsulation efficiency of MTX nanoparticles using Eudragit S100.

3.1 Optimization of Process Variables

Nanoparticles were prepared through modified emulsion/solvent evaporation technique. This method includes the following steps;

- Solubilization of polymer and drug in organic medium
- Addition of drug polymer mixture into surfactant solution (aqueous phase)
- Sonication through probe sonicator
- Evaporation of organic solvent resulting drug encapsulation by polymer

Surfactant has a significant role in formulation development by emulsion-solvent evaporation method. Different surfactants (POL, PVA, SDS, and CTAB) were evaluated and optimal results were obtained with POL and PVA. Different formulations of nanoparticles were prepared with these two surfactants, i.e., POL and PVA in different concentration (0.5%, 0.25%, and 0.125%). Different parameters were investigated in order to get optimum size and encapsulation efficiency of nanoparticles.

3.1.1 Optimization of Sonication Speed

The effect of homogenization speed on characteristics of nanoparticle was studied by varying sonication amplitude and other parameters (drug concentration, polymer conc., and surfactant concentration) were kept constant. Nanoparticles prepared at lower sonication amplitude (60%) resulted in larger particle as compared with the higher sonication amplitude (99%) that results in smaller particles (Khatik et al., 2013) as shown in **Table 3**. High amplitude emulsification results in smaller emulsion globules leading to formation of nanoparticles of smaller size. More energy is released with increasing the homogenization amplitude, resulting in fast dispersion of organic phase, resulting in smaller sized nanoparticles (Madani et al., 2018). The encapsulation efficiency increased when emulsification speed was increased which might be due to less turbulent and unidirectional flow at lower sonication speed. Higher encapsulation efficiency at higher sonication speed can be attributed to greater surface area because of smaller size globules of the organic phase. At higher surface area drug polymer interface is larger, resulting in higher encapsulation efficiency and vice versa at lower amplitude.

3.1.2 Optimization of Sonication Time

Increase in sonication time increases energy input during emulsification (Khatik et al., 2013). The sonication time was varied from 1 to 6 min while other experimental conditions (drug concentration, polymer concentration, and surfactant concentration) were kept constant, to describe the effect of sonication time on size of nanoparticle. It was noticed that as with increasing sonication time (from 1 to 3 min) resulted in a

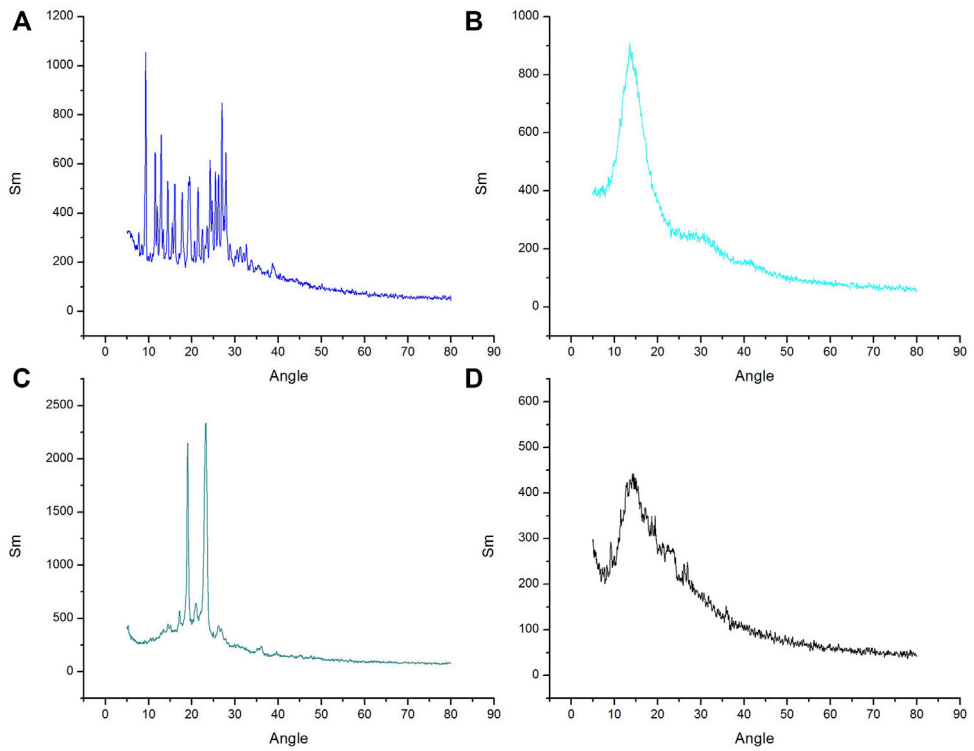

FIGURE 4 | XRD curve of **(A)** MTX, **(B)** Eudragit S100 **(C)** Poloxamer-407 and **(D)** MTX- Eudragit S100 nanoparticles (MSX8).

decrease in the size of nanoparticles, as summarized in **Table 3**. Furthermore, with the increase in time of sonication from 3 to 6 min, the size of particle increases. It may be due to agglomeration or de-emulsification process.

3.1.3 Optimization of Surfactant

Type and concentration of surfactant play an important role during emulsification and controls particle size through decreasing surface tension. Different types of surfactants having different HLB values were assessed for their possible effect on size of nanoparticle and process yield. Cetyl trimethylammonium bromide (CTAB) gave lowest particle size as compared with POL and sodium dodecyl sulfate (SDS). However the encapsulation efficiency was lower as compared with POL. Nanoparticles formulation was assessed by employing four different surfactants, that is, POL, PVA, SDS, and CTAB (**Table 3**). The innate characteristic of surfactants especially that adsorb at the interface reduces the surface tension and results in smaller size nanoparticles. This can be further described by the increased viscosity of surfactant solution which stabilizes the system and preventing coalescence of the particles (Nasef et al., 2017).

3.1.4 Optimization of Drug to Polymer Ratio

The mean particle size of nanoparticles increased with increasing the quantity of drug (**Table 4**). It was observed that increased quantity of drug led to more viscous disperse phase, resulting in larger particle size (Madani et al., 2018). The encapsulation efficiency showed a slight downward tendency with increase in drug quantity in the formulation. The encapsulation efficiency of nanoparticles is influenced by drug miscibility in polymer and polymer-drug interactions.

3.2 Characterization of Methotrexate Loaded Nanoparticles

3.2.1 Particle Size

Three different concentrations of Eudragit S100 (10, 20, and 30 mg) were used, keeping the drug concentration constant (2 mg), the size of particle, encapsulation efficiency and zeta potential were evaluated, results are presented in **Table 5**. Formulations were prepared with Eudragit S100, through emulsion solvent evaporation method, using emulsifier POL, and PVA in different concentrations (0.5%, 0.25%, and 0.125%). As ratio of drug to polymer was raised from 1:5 to 1:15 (by weight), increase in particle size and the reason was increased in viscosity of the polymer solution, leading to decreased dispersion of polymer solution into the aqueous phase (Qindeel et al., 2019).

As evident from **Figure 2** that irrespective of type and concentration of the surfactant increase in polymer concentration increases size of the nanoparticles. It was noticed that as concentration of POL was increased from 0.125% to 0.25%, the size of NPs was decreased as shown in **Figure 3**. This may be because of the reason that increase in surfactant concentration causes reduction in surface tension and facilitating particles partition. The reduction in the particle size is

TABLE 6 | Characteristics of optimized formulations of methotrexate.

Code	Particle size (nm)	Zeta potential (mV)	PDI	Amount encapsulated (mg/ml)	% Encapsulation efficiency
MSX5	165.7 ± 1.85	−0.163 ± 0.11	0.215 ± 0.010	1.228	61.42 ± 2.1
MSX8	174.6 ± 3.00	−5.64 ± 0.36	0.227 ± 0.017	1.4	70 ± 1.2
MSX9	202.6 ± 1.20	−2.28 ± 0.15	0.235 ± 0.008	1.42	71.19 ± 1.8

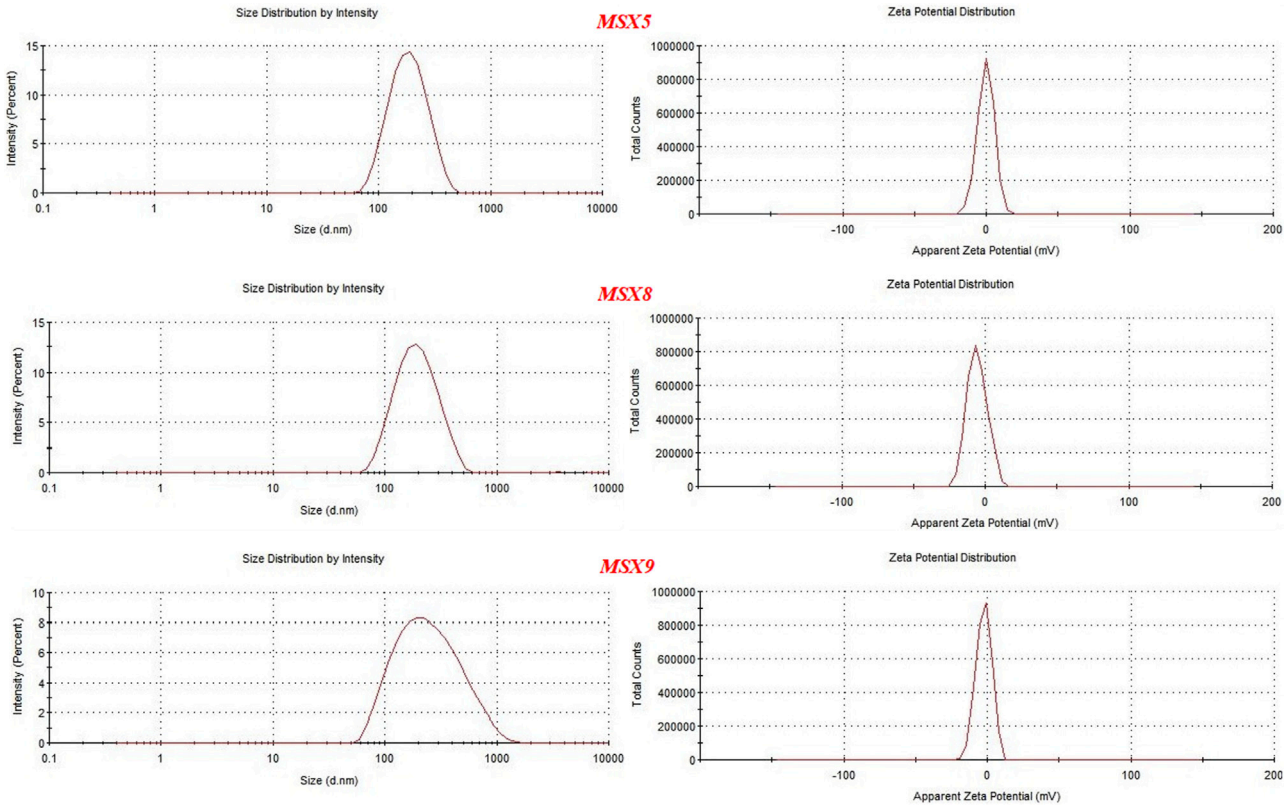

FIGURE 5 | Graphs showing particle size and zeta potential of optimal formulation of methotrexate loaded nanopatricles.

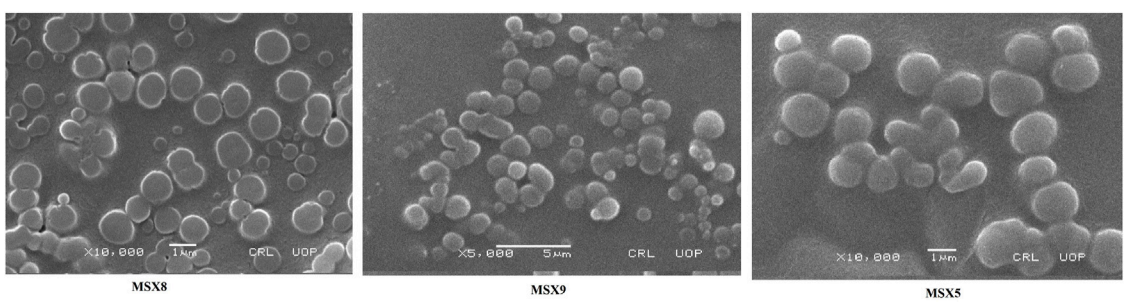

FIGURE 6 | SEM images of methotrexate loaded nanoparticles prepared using Eudragit S100.

usually supplemented by a quick increase in the surface area (Madani et al., 2018). Further increasing the POL concentration to 0.5%; the size of particle increases which may be due to increased interaction between the molecules of stabilizers, leading to increased adsorption of surfactant on surface of nanoparticle forming multiple layer (Sharma et al., 2016).

TABLE 7 | The impact of Freeze drying on methotrexate nano-formulations with different cryoprotectant (Mannitol and sucrose).

Status	Parameter	MSX5	MSX8	MSX9
Initial	Size (nm)	165.7 ± 1.85	174.6 ± 3.00	202.6 ± 1.20
	PDI	0.215 ± 0.010	0.227 ± 0.017	0.235 ± 0.008
Without cryoprotectant	Size (nm)	218.5 ± 16.74	242.7 ± 9.78	258.5 ± 13.85
	PDI	0.271 ± 0.024	0.291 ± 0.013	0.243 ± 0.004
2% Sucrose	Size (nm)	249.5 ± 10.7	265.3 ± 15.31	293.4 ± 16.25
	PDI	0.251 ± 0.02	0.316 ± 0.05	0.28 ± 0.02
4% Sucrose	Size (nm)	258.6 ± 18.04	289.5 ± 16.08	306.8 ± 14.38
	PDI	0.423 ± 0.02	0.321 ± 0.04	0.338 ± 0.02
8% Sucrose	Size (nm)	318.3 ± 12.73	322.1 ± 15.69	340.9 ± 19.95
	PDI	0.301 ± 0.02	0.268 ± 0.05	0.297 ± 0.04
2% Mannitol	Size (nm)	184.2 ± 10.30	188.9 ± 9.37	209.3 ± 11.64
	PDI	0.248 ± 0.03	0.173 ± 0.04	0.341 ± 0.01
4% Mannitol	Size (nm)	199.2 ± 9.17	200.3 ± 14.81	226.1 ± 13.70
	PDI	0.339 ± 0.04	0.159 ± 0.07	0.303 ± 0.02
8% Mannitol	Size (nm)	231.1 ± 15.74	239.3 ± 11.95	269.4 ± 18.95
	PDI	0.225 ± 0.05	0.283 ± 0.05	0.199 ± 0.07

TABLE 8 | Results of stability studies of methotrexate nanoparticles.

Time	Code	Stored at 4°C			Stored at 25°C		
		Size (nm)	PDI	% EE	Size (nm)	PDI	% EE
Day 01	MSX5	165.7	0.215	61.42	167.6	0.202	61.42
	MSX8	174.6	0.227	70	175.1	0.223	70
	MSX9	202.6	0.235	71.19	203.5	0.252	71.19
1 Week	MSX5	167.7	0.218	61.42	169.6	0.252	61.42
	MSX8	175.2	0.237	70	179.1	0.224	70
	MSX9	204.4	0.222	71.19	204.5	0.301	71.19
1 Month	MSX5	166.4	0.236	60.52	171.9	0.302	58.35
	MSX8	177.2	0.247	69.5	180.3	0.281	68.51
	MSX9	204.6	0.322	70.01	207.7	0.311	68.19
3 Month	MSX5	169.9	0.253	59.65	176.8	0.322	56.43
	MSX8	176.6	0.221	68.91	185.5	0.301	67.01
	MSX9	206.4	0.266	70.01	213.3	0.334	67.29
6 Month	MSX5	170.8	0.299	58.89	175.2	0.311	57.35
	MSX8	179.5	0.244	68.02	187.6	0.312	67.01
	MSX9	207.1	0.282	69.54	214.5	0.339	67.17

PVA was used in three different concentration (0.125%, 0.25%, and 0.5%) as a stabilizer. At low concentration (0.125%) particles of larger size were obtained initially because of non-uniform and poor PVA coating onto freshly prepared emulsion droplets. Increasing the concentration of PVA from 0.125% to 0.25%, there was a sharp decrease in size of particle as obvious from **Figure 3**. The sharp reduction in size of particles may be due to decrease interfacial tension and prevention of droplet agglomeration. Increasing the concentration of PVA further up to 0.5% leads to increase in particle size. The size of particle decreases as concentration of surfactant increases in aqueous phase up to certain limit may be because of the lining up of surfactant molecule at the interface leading to a decrease in interfacial tension. Further increasing the concentration of surfactant in external phase above certain limits causes an increase in size of particle and this might be because of the increased viscosity and a reduction in net shear stress resulting in the larger particles formation.

3.2.2 Zeta Potential

Zeta potential was evaluated through electrophoretic mobility of the particles. It is a key parameter to assess the *in-vivo* properties as well stability of nanoparticles. Generally negative zeta potential was obtained for MTX with Eudragit S100 because of the free acrylic acid groups available on Eudragit S100 (Jang et al., 2019). The zeta potential varied between −0.10 ± 0.018 and −11.50 ± 0.47 for MTX nanoparticles but there was no specific decrease or increase pattern with increasing or decreasing Eudragit S100 as shown in **Table 5**. There was no specific pattern for decrease or increase is followed by enhancing poloxamer 407 concentration.

3.2.3 Encapsulation Efficiency

The concentration of polymer in organic medium effects encapsulation efficiency, significantly. The % EE improved by increasing the concentration of polymer from 1:05 to 1:15 with respect to drug. Highest encapsulation efficiency was obtained when ratio of drug to polymer was 1:15. The viscosity of organic phase increased with higher concentration of polymer, resulting in more resistance to drug diffusion from organic to aqueous phase, which led to higher encapsulation efficiency (Madani et al., 2018). At higher polymer concentration, polymer precipitation time decreases, which reduces drug diffusion out of nanoparticles. Concentration of PVA has directly proportional effect on % EE as shown in the **Figure 3**. It may be due to augmented viscosity of external medium as a result of thick layer of stabilizer and minimum diffusion of drug to external aqueous medium.

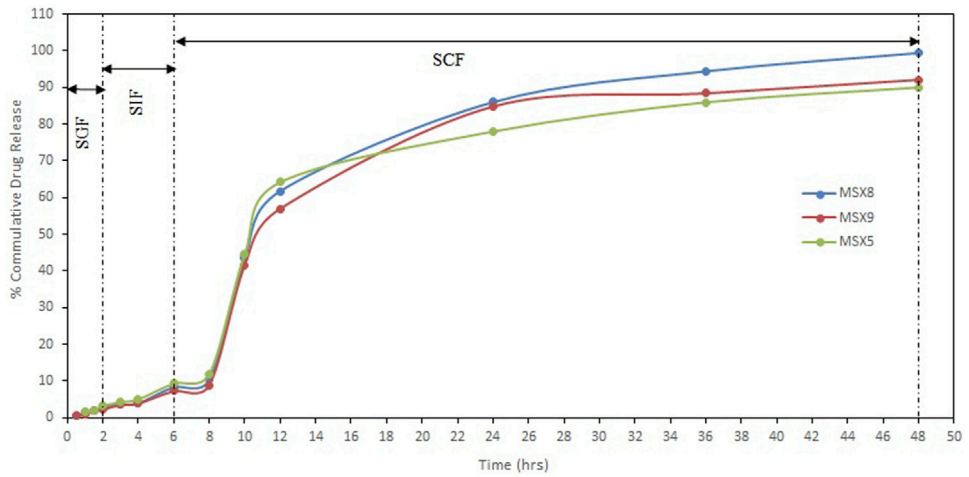

FIGURE 7 | *In-vitro* release profile of methotrexate from eudragit S100 nanoparticles in different simulated GI tract fluids (SGF, simulated gastric fluid; SIF, simulated intestinal fluid; SCF, simulated colonic fluid).

Similarly, higher encapsulation efficiency was obtained with increasing the concentration of surfactant (POL) which might be due to stronger binding contacts between drug and polymer.

3.2.4 X-Ray Diffraction

X-ray diffraction was applied to study the crystalline nature of drug. The X-Ray diffractometer, was utilized to study the XRD patterns of excipients, drugs and drug-loaded nanoparticles. All the XRD patterns were recorded at ambient temperature at diffraction angle of 2θ in a range of 3°–80°. The diffractogram of pure MTX comprised of numerous characteristic sharp peaks. The most promising peaks of MTX were present at 7.90, 10.6, 11.8, 13.1, 14.5, 19.3, 21.6, and 28, confirming crystalline nature of pure MTX. The XRD characteristic peak for POL was determined at 18° and 23.2° (2 Theta) and there was no peak for Eudragit S100 as shown in **Figure 4**. In case of MTX-Eudragit S100 nanoparticles with POL no peaks were observed indicating that the drug is in amorphous state.

3.3 Selection of Optimal Formulations

Different formulations of nanoparticles were developed using Eudragit S100 as polymer and POL and polyvinyl alcohol. For the selection of optimized formulations three main parameters were considered, i.e., particle size, encapsulation efficiency, and zeta potential and on this basis three formulations were selected, including MSX5, MSX8, and MSX9 (In nomenclature of the formulations, M denotes methotrexate, S denotes Eudragit S100 and X denotes Poloxamer-407), as shown in **Table 6**. Size distribution and zeta potential curves of the optimal formulations are presented in **Figure 5**.

The morphology of nanoparticles is important in biodistribution, targeting drug to various organs and circulation time. Results of SEM images of the optimized formulation showed that nanoparticles obtained were spherical with smooth surfaces (**Figure 6**).

3.4 Freeze Drying of the Developed Nanoparticles

The smaller particle size, increase surface area and colloidal nature of nanoparticles may lead to the physical instability, including aggregation and fusion of particle. Chemical instability includes hydrolysis of polymer and drug leakage from nanoparticles. So as to minimize problem of instability freeze drying or lyophilization process is used to remove water from the developed formulation and get dry nanoparticles. In this study, the optimized formulations were freeze dried with or without the addition cryoprotectants. Two different cryoprotectants; mannitol and sucrose were evaluated in three different concentrations, i.e., 2%, 4%, and 8%. The samples which were freeze dried were reconstituted with purified water (2 ml). The impact of the cryoprotectants on the various properties of the nanoparticles is shown in **Table 7**. The mannitol (2%) showed very slight variations in size of particle and PDI and hence selected as a cryoprotectant.

3.5 Stability Study

For evaluation of stability, the developed optimal formulation was stored at 4°C and 25°C and their encapsulation efficiency, particle size and PDI were evaluated. The results are shown in **Table 8** indicating slight differences on size, PDI and EE of nanoparticle when stored at 4°C for 6 months. The kinetic energy at low temperature is reduced and therefore particles contact is prevented leading to decreased particles aggregation (Chacon et al., 1999). When the formulations were stored at 25°C, prominent changes were observed in PDI, % EE and particle size. Thus the formulations may be kept at 4°C to avoid variation in particle size, PDI and % EE.

3.6 *In Vitro* Drug Release

In vitro release of MTX from polymeric nanoparticles was studied by dialysis bag diffusion method in a shaking water bath.

Dissolution media consisted of simulated gastric fluid (SGF) (0.1 N HCl pH 1.2), simulated intestinal fluid (SIF) (phosphate buffer pH 6.5), and simulated colonic fluid (SCF) (phosphate buffer pH 7.4). The results of "*in-vitro*" release are presented in **Figure 7**.

The pH-dependent drug release from NPs was evaluated between the pH of the medium in the range of 1.2, 6.5, and 7.4, which resemble the stomach, small intestine, and colon pH, respectively. Release of methotrexate during the first 2 h in SGF (resembling stomach pH 1.2) from Eudragit S100 nanoparticles was 2.22%–3.26%. The release of drug in simulated intestinal fluid (resembling intestinal pH 6.5) for further 4 h is about 7.27%–9.34% from Eudragit S100 nanoparticles. The release of methotrexate from Eudragit S100 nanoparticles during the next 42 h in simulated colonic fluid (resembling colonic pH 7.4) is about 90.01%–99.41%. The pH dependent release profile of Eudragit S100 shows a slow drug release at acidic pH that ascended to a quick release upon changing the pH. The Eudragit S100 prevents the drug release at gastric pH and drug is released as in neutral and alkaline medium which may be due to the carboxyl group of Eudragit that ionize in neutral to alkaline media (Matlhola et al., 2015).

4 CONCLUSION

The present study was carried out to develop pH sensitive, targeted polymeric nanoparticles of methotrexate using Eudragit S100 in combination with different surfactants by modified emulsion solvent evaporation technique. The prepared nanoparticles showed good physicochemical properties in terms of size, zeta potential, PDI, and encapsulation efficiency. The prepared nanoparticles were suitable for colon drug targeting. Stability studies showed that optimized nanoparticles were quite stable when stored at 4°C for 6 months. The *in-vitro* release study showed that initially the drug released through diffusion and followed by the erosion of polymeric chains. It is concluded that the desired properties of nanoparticles (particle size and surface charge) can be achieved by utilizing proper type and concentration of surfactant. Furthermore, emulsion solvent evaporation technique was proven to be highly effective for preparation of nanoparticles of hydrophobic drugs.

DATA AVAILABILITY STATEMENT

The original contributions presented in the study are included in the article/supplementary material, further inquiries can be directed to the corresponding authors.

AUTHOR CONTRIBUTIONS

FU: Experimental work and manuscript writing; AK: Experimental work and manuscript writing; ZI: Supervision of the whole study; LA, SAK, and RU: Data evaluation and critical revision of the manuscript. AA and MS: Manuscript revision and funding. All authors approved the final version of the manuscript.

FUNDING

This research was funded by Princes Nourah Bint Abdulrahman University researchers Supporting Project (No. PNURSP 2022R33), Princess Nourah Bint Abdulrahman University, Riyadh, Saudi Arabia.

ACKNOWLEDGMENTS

Authors wish to thank Princes Nourah bint Abdulrahman University researchers Supporting Project (No. PNURSP 2022R33), Princess Nourah bint Abdulrahman University, Riyadh, Saudi Arabia for financial support.

REFERENCES

Amjad, K. (2019). Optimization of the Process Variables of Roller Compaction, on the Basis of Granules Characteristics (Flow, Mechanical Strength and Disintegration Behavior): An Application of SeDeMODT Expert System. *Drug Dev. indust. Pharm.* 45 (9), 1537–1546. doi:10.1080/03639045.2019.1634094

Amjad, K., Zafar, I., Muhammad, A. M., Abad, K., Zia, U., and Ismail, K. (2016). Modulation of pH Independent Release of Class-Iı Drug (Domperidone) from Polymeric Matrix Using Acidic Excipients. *Dissolution Technol.* 23 (1), 32–40. doi:10.14227/DT230116P32

Benish, A., Amjad, K., Hamad, S. A., MajeedullahAbdul, W., Munair, B., and Attiqa, N. (2021). Evaluation of the Effect of Carrier Material on Modification of Release Characteristics of Poor Water Soluble Drug from Liquisolid Compacts. *PLOSONE* 16 (8), 1–18. doi:10.1371/journal.pone.0249075

Bohrey, S., Chourasiya, V., and Pandey, A. (2016). Polymeric Nanoparticles Containing Diazepam: Preparation, Optimization, Characterization, *Iin-Vvitro* Drug Release and Release Kinetic Study. *Nano Converg.* 3, 3. doi:10.1186/s40580-016-0061-2

Chacón, M., Molpeceres, J., Berges, L., Guzmán, M., and Aberturas, M. R. (1999). Stability and Freeze-Drying of Cyclosporine Loaded Poly(D,L lactide-glycolide) Carriers. *Eur. J. Pharm. Sci.* 8, 99–107. doi:10.1016/s0928-0987(98)00066-9

Dilpreet, S. (2021). Self-nano Emulsifying Drug Delivery System: A Versatile Carrier for Lipophilic Drugs. *Pharm. Nanotechnol.* 09 (3), 166–176. doi:10.2174/2211738509666210422124023

Hadi, M. A., Babu, V. L., and Pal, N. (2012). Formulation and Evaluation of Sustained Release Matrix Tablets of Glimepiride Based on Combination of Hydrophilic and Hydrophobic Polymers. *J. Appl. Pharmac. Scie.* 02, 101–107. doi:10.7324/japs.2012.2613

Hazal, E. G., Serdar, T., Fatmanur, T. D., and Füsun, A. (2021). 3D Printed Extended Release Tablets for once Daily Use: An *In Vitro* and *In Vivo* Evaluation Study for a Personalized Solid Dosage Form. *Int. J. Pharm.* 596, 120222. doi:10.1016/j.ijpharm.2021.120222

Jang, J. H., Jeong, S. H., and Lee, Y. B. (2019). Preparation and *In Vitro*/*In Vivo* Characterization of Polymeric Nanoparticles Containing Methotrexate to Improve Lymphatic Delivery. *Int. J. Mol. Sci.* 20, 3312. doi:10.3390/ijms20133312

Khatik, R., Mishra, R., Verma, A., Dwivedi, P., Kumar, V., Gupta, V., et al. (2013). Colon-specific Delivery of Curcumin by Exploiting Eudragit-Decorated Chitosan Nanoparticles *In Vitro* and *In Vivo*. *J. Nanopart Res.* 15, 1893. doi:10.1007/s11051-013-1893-x

Late, S. M., Yu, Y. Y., and Banga, A. K. (2009). Effects of Disintegration Promoting Agent, Lubricants and Moisture Treatment on Optimized Fast Disintegrating Tablets. *Intern. J. Pharm.* 365 (1-2), 4–11. doi:10.1016/j.ijpharm.2008.08.010

Madani, F., Esnaashari, S. S., Mujokoro, B., Dorkoosh, F., Khosravani, M., and Adabi, M. (2018). Investigation of Effective Parameters on Size of Paclitaxel Loaded PLGA Nanoparticles. *Adv. Pharm. Bull.* 8, 77–84. doi:10.15171/apb.2018.010

Matlhola, K., Katata-Seru, L., Tshweu, L., Bahadur, I., Makgatho, G., and Balogun, M. (2015). Formulation and Optimization of Eudragit RS PO-Tenofovir Nanocarriers Using Box-Behnken Experimental Design. *J. Nanomater.* 6, 630690. doi:10.1155/2015/630690

Nasef, A. M., Gardouh, A., and Ghorab, M. (2015). Polymeric Nanoparticles: Influence of Polymer, Surfactant and Composition of Manufacturing Vehicle on Particle Size. *World J. Pharm. Sci.* 3, 2308–2322.

Nasef, A. M., Gardouh, A. R., and Ghorab, M. M. (2017). Formulation and Iin-Vvitro Evaluation of Pantoprazole Loaded pH-Sensitive Polymeric Nanoparticles. *Future J. Pharm. Sci.* 3, 103–117. doi:10.1016/j.fjps.2017.04.004

Qindeel, M., Ahmed, N., Sabir, F., Khan, S., and Ur-Rehman, A. (2019). Development of Novel pH-Sensitive Nanoparticles Loaded Hydrogel for Transdermal Drug Delivery. *Drug Dev. Ind. Pharm.* 45, 629–641. doi:10.1080/03639045.2019.1569031

Sarmad, A., Mehrin, S., Amjad, K., Zia-Ur-Rahman, Q., MajeedullahHamad, S. A., Muhammad, L., et al. (2021). Investigation of Plantago Ovata Husk as Pharmaceutical Excipient for Solid Dosage Form (Orodispersible Tablets). *Biomed. Res. Intern* 2021, 1–10. doi:10.1155/2021/5538075

Sharma, N., Madan, P., and Lin, S. (2016). Effect of Process and Formulation Variables on the Preparation of Parenteral Paclitaxel-Loaded Biodegradable Polymeric Nanoparticles: A Co-surfactant Study. *Asian J. Pharm. Sci.* 11, 404–416. doi:10.1016/j.ajps.2015.09.004

Yoo, J. W., Giri, N., and Lee, C. H. (2011). pH-Sensitive Eudragit Nanoparticles for Mucosal Drug Delivery. *Int. J. Pharm.* 403, 262–267. doi:10.1016/j.ijpharm.2010.10.032

Conflict of Interest: The authors declare that the research was conducted in the absence of any commercial or financial relationships that could be construed as a potential conflict of interest.

Publisher's Note: All claims expressed in this article are solely those of the authors and do not necessarily represent those of their affiliated organizations, or those of the publisher, the editors and the reviewers. Any product that may be evaluated in this article, or claim that may be made by its manufacturer, is not guaranteed or endorsed by the publisher.

frontiers | Frontiers in Pharmacology

REVIEW
published: 01 July 2022
doi: 10.3389/fphar.2022.909526

Application Perspectives of Nanomedicine in Cancer Treatment

Shanshan Hou[1†], Muhammad Hasnat[3†], Ziwei Chen[1], Yinong Liu[4], Mirza Muhammad Faran Ashraf Baig[5], Fuhe Liu[1] and Zelong Chen[2*]*

[1]Department of Pharmacy, Zhejiang Pharmaceutical College, Ningbo, China, [2]The Affiliated Cancer Hospital of Zhengzhou University & Henan Cancer Hospital, Henan Province Engineering Research Center of Artificial Intelligence and Internet of Things Wise Medical, Zhengzhou, China, [3]Institute of Pharmaceutical Sciences, University of Veterinary and Animal Sciences, Lahore, Pakistan, [4]Hospital Laboratory of Nangjing Lishui People's Hospital, Nangjing, China, [5]Laboratory of Biomedical Engineering for Novel Bio-functional, and Pharmaceutical Nanomaterials, Prince Philip Dental Hospital, Faculty of Dentistry, The University of Hong Kong, Hong Kong, Hong Kong SAR, China

Cancer is a disease that seriously threatens human health. Based on the improvement of traditional treatment methods and the development of new treatment modes, the pattern of cancer treatment is constantly being optimized. Nanomedicine plays an important role in these evolving tumor treatment modalities. In this article, we outline the applications of nanomedicine in three important tumor-related fields: chemotherapy, gene therapy, and immunotherapy. According to the current common problems, such as poor targeting of first-line chemotherapy drugs, easy destruction of nucleic acid drugs, and common immune-related adverse events in immunotherapy, we discuss how nanomedicine can be combined with these treatment modalities, provide typical examples, and summarize the advantages brought by the application of nanomedicine.

Keywords: nanomedicine, chemotherapy, gene therapy, immunotherapy, cancer

OPEN ACCESS

Edited by:
Faisal Raza,
Shanghai Jiao Tong University, China

Reviewed by:
Ruoning Wang,
Nanjing University of Chinese Medicine, China
Chunming Tang,
Nanjing Medical University, China

***Correspondence:**
Zelong Chen
zlyyczl4266@zzu.edu.cn
Fuhe Liu
89994226@qq.com

[†]These authors have contributed equally to this work

Specialty section:
This article was submitted to Experimental Pharmacology and Drug Discovery, a section of the journal Frontiers in Pharmacology

Received: *31 March 2022*
Accepted: *16 May 2022*
Published: *01 July 2022*

Citation:
Hou S, Hasnat M, Chen Z, Liu Y, Faran Ashraf Baig MM, Liu F and Chen Z (2022) Application Perspectives of Nanomedicine in Cancer Treatment. Front. Pharmacol. 13:909526. doi: 10.3389/fphar.2022.909526

INTRODUCTION

In recent years, the incidence and mortality of cancer have been increasing year by year under the influence of many factors such as population aging, work pressure, and environmental changes, etc. According to the 2020 Global Cancer Statistics Report, there were approximately 19.3 million new cancer cases and 10 million deaths that year (Sung et al., 2021). The treatment of cancer has now become an important issue to be solved urgently in the medical field. For the treatment of cancers, chemotherapy is a commonly used and effective drug therapy. However, its shortcomings and limitations in clinical application have also been shown, such as application limitations due to poor water solubility, serious adverse events caused by non-specific distribution, etc. In recent years, with the development of technology and the innovation of treatment concepts, new treatment methods such as gene therapy and immunotherapy are changing the pattern of tumor treatment (Libutti, 2019; Tan et al., 2020). However, the *in vivo* delivery of anti-tumor gene therapy and immunotherapy drugs still faces challenges, such as low tumor cell uptake rate and poor tumor permeability, which seriously affect the therapeutic effect. Nanoparticulate delivery systems (NDSs)is an important way to optimize drug delivery, which can effectively improve the accumulation, penetration and target cell uptake of drugs in tumor tissue and achieve controllable drug release. Replacing traditional drug delivery with NDSs can enhance the efficacy of treatment and reduce the incidence of adverse events, and has shown significant clinical benefits (Collins and Thrasher, 2015; Raza et al., 2019; Riley et al., 2019; Yahya and Alqadhi, 2021; Raza et al., 2022). In this review, we will review the progress of NDSs

and the application of nanomedicine in cancer therapy, focusing on the new progress in the application of nanomedicine in chemotherapy, gene therapy and immunotherapy.

NANOPARTICULATE DELIVERY SYSTEMS

Relying on the vigorous development of nanotechnology, NDSs have attracted more and more attention of scientists, and also showed great application value and broad development prospects. Nanomaterials refer to particles with a size of less than 100 nm, or with a size of less than 1 μm that can exhibit nanoparticle properties, and whose structural units are generally smaller than the cell volume. Compared with traditional drug delivery systems, NDSs can effectively improve pharmacokinetics and pharmacodynamics due to their specificity in size, material, and shape (Kinnear et al., 2017). Due to the heterogeneity and complexity of tumors, nanomaterials used in cancer therapy are often designed as multifunctional nanoplatforms, which are usually composed of loaded drugs, structural frameworks and functional units. Compared with traditional drugs, NDSs has obvious advantages in tumor treatment: 1) NDSs can effectively deliver drugs with different physicochemical properties, such as: solving the difficult problem of hydrophobic drug delivery, effectively delivering charged nucleic acid drugs and protecting them from nuclease degradation. 2) NDSs can deliver multiple types of drugs simultaneously. 3) NDSs can simultaneously realize tumor diagnosis and treatment. 4) NDSs can improve the targeting of drugs, and both passive targeting based on enhanced permeability and retention effects and active targeting under functional element modification have demonstrated distinct advantages. 5) NDSs can achieve controlled release of drugs. Namely engineered stimuli-responsive nanomaterials enable precise drug delivery and controlled release under the influence of endogenous or exogenous stimuli (Zhu G. et al., 2017; Bhushan et al., 2017; Liu et al., 2017; Cao et al., 2020; Zhu et al., 2020; Gote et al., 2021; Li et al., 2021; Yang et al., 2021; Liu et al., 2022).

CHEMOTHERAPY NANOMEDICINE

Chemotherapy is currently one of the most widely used and mature tumor treatment methods in clinical practice. However, there are many problems in the clinical application, such as the lacking target and the large side effects of conventional chemotherapeutic drugs and the poor water solubility of many first-line chemotherapeutic drugs (doxorubicin, paclitaxel, etc.), aggravating the difficulty of clinical treatment. The development and application of nanomaterials optimize the delivery of the above-mentioned chemotherapeutic drugs, and effectively improve the safety and efficacy of chemotherapy (Wei et al., 2021). Nanomaterials currently used for chemotherapeutic drug delivery include organic nanomaterials (Zhang D. Y. et al., 2020), inorganic nanomaterials (Wang C.-S. et al., 2021), composite nanomaterials (Akgöl et al., 2021), and biological nanomaterials (Wang J. et al., 2021). Among them, biological nanomaterials have very high application value in drug delivery because of their high safety, good biocompatibility, easy degradation, and certain targeting properties. Biological nanomaterials include endogenous natural nanomaterials and biomimetic nanomaterials (Navya et al., 2019). Here we take the classic DNA and protein nanomaterials as examples to introduce their application in chemotherapy (**Figure 1A**).

DNA-Based Nanoparticles (NPs)

DNA is the carrier of the genetic information of the organism, plays an important regulatory role in the physiological and pathological processes of the organism, and is an ideal natural drug carrier material. As an emerging drug delivery carrier in recent years, DNA-based nanoparticles (NPs) have significant advantages, with excellent degradability, biocompatibility, and sequence programmability (Xu et al., 2021). DNA-based NPs can effectively load a variety of drugs, and achieve targeted drug delivery to tumor tissues with the assistance of specific functional elements, while improving cellular drug uptake and stimuli-responsive drug release. It is an effective tool to solve common problems of chemotherapy (low efficacy of drugs, large toxic and side effects, etc) and many progress have been made in recent years (Lv et al., 2021). In 1982, Seeman's group proposed that DNA molecules can construct precise and ordered nanostructures based on the A-T, G-C Watson-Crick base pairing principle, which opened the prelude to DNA nanotechnology. Through rational design, DNA molecules can self-assemble into various kinds of 2D or 3D NPs. The existing DNA self-assembly techniques include DNA Tile self-assembly, rolling circle amplification (RCA), DNA origami, and DNA single-stranded tile self-assembly (Lau and Sleiman, 2016; Mohsen and Kool, 2016; Evans and Winfree, 2017; Ji et al., 2021). In physiological environment, self-assembled DNA NPs can resist degradation to a certain extent and show stronger stability than natural single-stranded or double-stranded DNA, which has high clinical application value (Ahn et al., 2020; Ramezani and Dietz, 2020).

At present, DNA-based NPs have successfully achieved effective delivery of chemotherapeutic drugs such as doxorubicin, daunorubicin, platinum, etc (Halley et al., 2016; Zhang L. et al., 2019; Wu et al., 2019). Doxorubicin, used alone or in combination with other drugs, is one of the most effective chemotherapeutic drugs commonly used clinically, which can treat a variety of tumors including solid tumors and hematological tumors by inhibiting DNA synthesis (Carvalho et al., 2009). We take doxorubicin as an example to illustrate how DNA-based NPs deliver chemotherapeutic drugs. At present, DNA-based NPs of various shapes have been reported for the delivery of doxorubicin by virtue of the drug-embedding properties, covering RCA-based nanostructures (Zhao et al., 2018), DNA tetrahedra (Zhang J. et al., 2021), dendritic DNA nanostructures (Li et al., 2020), and nanostructures based on DNA origami technology (Liu J. et al., 2018), in which tubular and triangular DNA nanocarriers based on DNA origami technology have the characteristics of high drug loading (Guan et al., 2021). Interestingly, DNA-based NPs with specific

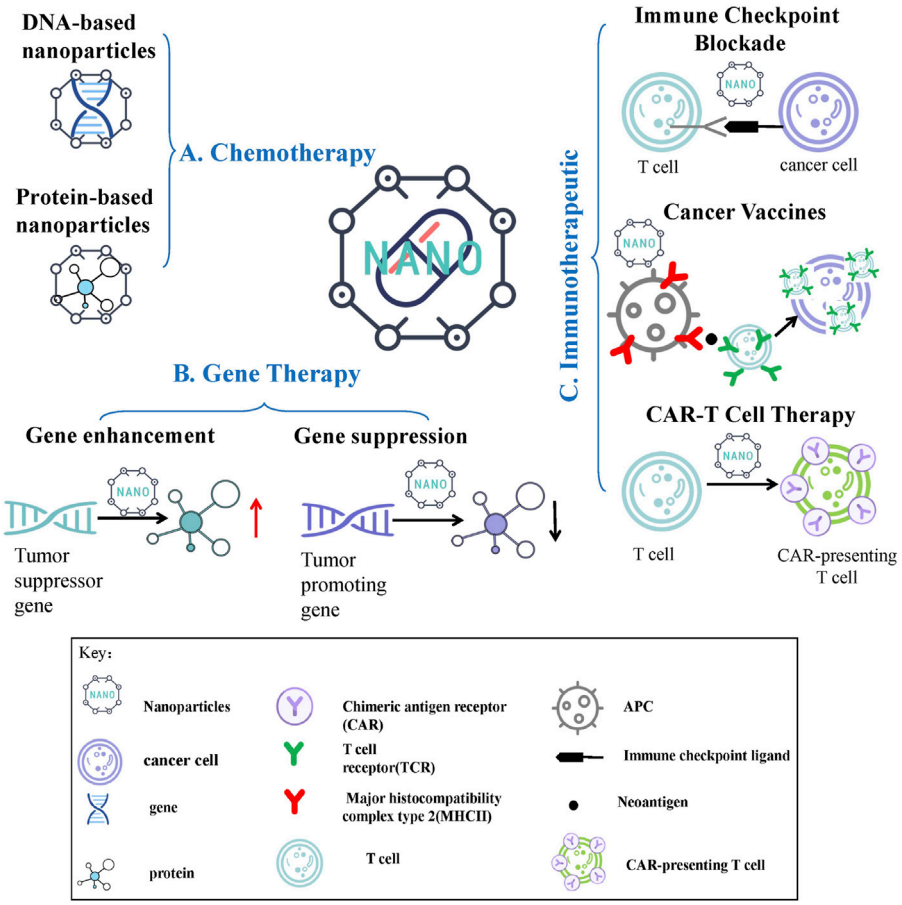

FIGURE 1 | Nanomedicine Delivery Strategies for Chemotherapy, Cancer Gene Therapy and Immunotherapy. **(A)** Chemotherapy nanomedicine: DNA-based nanoparticles and protein-based nanoparticles are shown in this article. **(B)** Gene therapy nanomedicine: gene enhancement therapy and gene suppression therapy are shown in this article. **(C)** Immunotherapeutic nanomedicine: immune checkpoint blockade therapy, cancer vaccines and chimeric antigen receptor T cell therapy are shown in this article.

hydrodynamic dimensions and geometries (triangular DNA origami nanostructures) can passively accumulate in tumor tissues, showing excellent targeting (Zhang et al., 2014; Jiang B. et al., 2019). In order to further improve the targeting of chemotherapeutic drugs and reduce the occurrence of adverse reactions, the latest research pays more attention to the progress of modification. With the help of functional elements such as aptamers, DNA-based NPs can improve the efficacy of chemotherapeutic drugs and reduce adverse reactions through active targeting. For example, Zhang et al. demonstrated that Sgc8 aptamer-modified DNA nanoflowers (NFs) can selectively recognize the cell membrane protein tyrosine kinase 7, and Sgc8-NFs-Ferrocene/Doxorubicin can be selectively protein tyrosine kinase 7 positive cancer cells, significantly improving the tumor-targeting ability of the drug (Zhang Q. et al., 2019). In addition, the significantly different physiological characteristics of tumor tissue and normal tissue have inspired scientists to design many tumor microenvironment-responsive NDSs. Compared with normal tissue, tumor tissue has the following different physiological characteristics, including: 1) high concentration of reducing substances in tumor cells; 2) high concentration of ATP in tumor cells; 3) abnormally expressed enzymes in tumor cells, such as telomerase, matrix metalloproteinase, etc; 4) pH imbalance inside and outside tumor cells (Dai et al., 2017; Jin and Jin, 2020). Given this, the designed DNA-based NPs trigger structural reorganization, exposing the coated drug under the influence of external stimuli such as pH (Zhao et al., 2018), reducing environment (Liu X. et al., 2018), enzymes (Zhang G. et al., 2017), ATP (Lu et al., 2018), etc., which better achieves the precise delivery and release of the drug, thereby effectively increasing the anti-tumor effect of the chemotherapeutic drugs and reducing the damage to normal tissues. For example, Zhao et al. (2018) developed a doxorubicin-loaded DNA NPs with a cancer cell targeting Sgc8 aptamer and a hairpin structure showing pH-responsive doxorubicin loading-releasing capability, which exhibited good biological stability, comparable to doxorubicin loading capacity, specific tumor targeting capacity, and sustained release of pH responsive doxorubicin. The delivery of doxorubicin with the designed DNA-based NPs realized the targeted, controllable and precise

TABLE1 | DNA nanoparticles in chemotherapy.

Chemotherapeutic Drugs	DNA Nanostructures	Modification	Effect	Ref
Doxorubicin	DNA tetrahedron	Folate receptor	Apoptosis promoting	Zhang et al. (2017b)
		KLA peptide	Drug delivery and apoptosis promoting	Yan et al. (2020)
		AS1411 + MUC1 aptamer	Breast cancer cell imaging and drug delivery	Liu et al. (2018a)
		Affibody	Selectivity and inhibition of breast cancer cells	Zhang et al. (2017c)
	DNA octahedron	Folate	Selective targeting	Raniolo et al. (2018)
	DNA icosahedron	MUC1 aptamer	Efficient and specific internalization for killing epithelial cancer cells	Chang et al. (2011)
	DNA NFs	Sgc8	Nuclease resistance and binding of different functional moieties	Lv et al. (2015)
	DNA triangle and tube	-	Increased doxorubicin cellular internalization and elevated susceptibility to drug-resistant adenocarcinoma cells	Bertrand et al. (2014)
	RCA-based nanostructures	Imotif sequence, Sgc8	pH-Responsive Drug Delivery	Zhao et al. (2018)
Daunorubicin	DNA nanorod	-	Circumvent drug-resistance mechanisms in a leukemia model	Halley et al. (2016)
Platinum	DNA tetrahedron	-	Targeted platinum drug delivery	Wu et al. (2019)
	DNA icosahedron	Telomerase-Responsive	Precise delivery of platinum nanodrugs to cisplatin-resistant cancer	Ma et al. (2018)

release of chemotherapeutic drugs, which enhanced the efficacy of the drug and reduced the occurrence of adverse events. The applications of other DNA nanoparticles in chemotherapy are shown in **Table 1**.

Protein-Based Nanoparticles (NPs)

Also as a very important natural biological macromolecules, proteins have been widely constructed as nanocarriers for chemotherapeutic drugs in recent years. Similar to DNA-based NPs, protein-based NPs also have many outstanding advantages, such as: 1) good biocompatibility and degradability; 2) natural biological sources, high availability and low toxicity; 3) unique three-dimensional structure; 4) amphiphilic of hydrophilic and hydrophobic molecules or solvents; 5) amino, carboxyl and hydroxyl groups for chemical bonding (Martínez-López et al., 2020). Proteins often designed as nanocarriers mainly include albumin, transferrin, ferritin, low-density lipoprotein, high-density lipoprotein, etc (Iqbal et al., 2021). The application of protein-based NPs to deliver chemotherapeutic drugs has been widely studied, and has shown good clinical application prospects.

When it comes to protein-based NDSs, the most classic one belongs to albumin-bound paclitaxel. Paclitaxel, a hydrophobic anticancer drug, needs to be dissolved in polyoxyethylene castor oil for clinical use, which may cause severe allergic reactions in some patients. Paclitaxel was loaded into albumin via hydrophobic interaction and then constructed into albumin-bound paclitaxel NPs with a diameter of 130 nm, which is traded as Abraxane (Celgene) (Zhang Y. et al., 2020). As the most abundant serum protein in the human body, albumin does not have the immune response caused by castor oil, which not only solves the problem of allergies, but also improves the efficacy and reduces the toxicity to normal tissues and organs. Currently, Abraxane has become one of the best-selling anticancer drugs and is a milestone in protein-based NPs (Yardley, 2013). In addition to non-covalent interactions such as hydrophobic interactions and electrostatic interactions, albumin has abundant binding sites (amine, thiol and carboxyl groups) and also can be used in combination with chemotherapeutic drugs, showing the huge application prospects of albumin (Hoogenboezem and Duvall, 2018; An and Zhang, 2017). Multiple clinical trials of Albumin NPs are currently being pursued, which we list in **Table 2**. Such as NCT01673438, NCT01580397, NCT02014844, NCT02049905, NCT00477529, NCT00635284, NCT02009332, NCT02494570 (https://clinicaltrials.gov/). Moreover, with the deepening of the research on protein-based NPs, stimuli-responsive NDSs have emerged to further improve the targeting efficiency, which can specifically respond to stimuli in the tumor microenvironment and precisely deliver the drug to the tumor area, enabling targeted therapy (Mi, 2020). As an example, Yang et al. (2020) designed and developed a doxorubicin-loaded NPs containing pH-sensitive Schiff bovine serum albumin, which not only has a high loading capacity but can also trigger the release of doxorubicin by pH.

Another class of proteins commonly constructed as NDSs are iron homeostasis-related proteins, including transferrin and ferritin, both of which have excellent performance in receptor-mediated active targeted delivery. Transferrin, mainly produced by hepatocytes in the human body, is the main iron-containing hydrophilic transporter in plasma, and is mainly responsible for transporting iron in hepatocytes to cells in other tissues. Transferrin is composed of a single-chain glycoprotein and is

TABLE 2 | Albumin nanoparticles approved or in clinical trials for chemotherapy.

Chemotherapeutic Drugs	Name	Indication(s)	Clinicaltrials Gov Identifier
Paclitaxel	Nab-paclitaxel (Abraxane)	non-small-cell lung cancer; Breast cancer; pancreatic cancer	Approved
Doxorubicin	Al-doxorubicin (DOXO-EMCH	Advanced solid tumour	NCT01673438
	INNO-206)	Pancreatic ductal adenocarcinoma	NCT01580397
		Glioblastoma	NCT02014844
		Metastatic, locally advanced or unresectable soft tissue sarcoma	NCT02049905
Docetaxel	Nab-docetaxel (ABI-008)	Hormone-refractory prostate cance	NCT00477529
Rapamycin	Nab-rapamycin (ABI-009)	Solid tumours	NCT00635284
		Non-muscle-invasive bladder cancer	NCT02009332
		PEComa	NCT02494570

divided into two evolutionary lobes, namely C-lobe (343 amino acids) and Nlobe (336 amino acids), which are connected to each other by a short spacer (Elsayed et al., 2016; Gou et al., 2018; Zhang et al., 2018). Transferrin mediates iron uptake by binding to the transferrin receptor (TfR). TfR, a transmembrane glycoprotein including TfR1 and TfR2, is the major protein receptor for iron metabolism *in vivo* (Fernandes et al., 2021). TfR is expressed in both normal and cancer tissues. However, studies have confirmed that the expression rate of TfR in cancer cells is nearly 100 times higher than that in normal cells. Cancer cells grow rapidly and their demand for iron is greatly increased during DNA synthesis, differentiation and regeneration. Therefore, TfR expression is increased in cancer cells in order to adapt to the increased iron requirement and maintain rapid cell division (Candelaria et al., 2021; Guo et al., 2021).

Based on this active transport capability, transferrin NPs can be used for tumor diagnosis and targeted delivery of therapeutic drugs. Goswami et al. designed Transferrin -templated copper nanoclusters-doxorubicin NPs for bioimaging and targeted drug delivery (Goswami et al., 2018). In addition, transferrin can also be used alone as a ligand to provide active tumor targeting capabilities of drug delivery systems. Research by Wei et al.showed that doxorubicin -loaded Transferrin-binding peptide CGGGHKYLRW significantly enhanced the antitumor efficacy in mice bearing HCT-116 tumors compared to polymersomes without transferrin binding (Wei et al., 2020).

Ferritin, found in most living cells, is the major iron storage protein in organisms. At present, various sources of ferritin have been used in biological nanocarriers, including human ferritin (HFt), horse spleen ferritin (HoSF), *Archaeoglobus fulgidus* ferritin (AfFtn), *Pyrococcus furiosus* ferritin (PfFt), and rat heavy-chain ferritin (Zhang P. et al., 2021; Zafar et al., 2021). HFt is a naturally formed spherical hollow nanocages with an outer diameter of 12 nm and an inner diameter of 8 nm, which is composed of 24 subunits of two types: heavy chain ferritin (HFn) and light chain ferritin (LFn). The inner cavity of each ferritin can store up to 4,500 Fe^{3+} atoms (Chakraborti and Chakrabarti, 2019). At the junction of these subunits, there are 8 hydrophilic channels and 6 hydrophobic channels, wherein the hydrophobic channel has three-fold symmetry and the hydrophilic channel has four-fold symmetry. In particular, hydrophilic channels are flexible enough to allow larger-sized molecules to penetrate into the ferritin cavity (Zhao et al., 2016; Tesarova et al., 2020). More importantly, HFn can selectively bind to tumor cells *via* TfR1 mediated specific targeting followed by rapid internalization *in vitro* and *in vivo*. Therefore, HFn can selectively deliver therapeutic drugs into tumors (Zang et al., 2017; Cheng et al., 2020). The unique nanocage structure and inherent tumor-targeting properties of ferritin make it a highly valuable biological nanocarrier. However, despite the above advantages, the low purification efficiency of natural protein brings difficulties to its practical application, and the recombinant ferritin constructed in various ways makes up for the above shortcomings (Veroniaina et al., 2021). According to the characteristics of ferritin nanocages, metal-based chemotherapeutic drugs such as carboplatin and cisplatin are the first to achieve effective precipitation in the cavity of iron nanocages. Subsequently, ferritin nanocages have also been used to load other non-metallic chemotherapeutic drugs such as doxorubicin (Song et al., 2021). Here we list the applications of ferritin in the delivery of chemotherapeutic drugs in **Table 3**.

Lipoproteins are mainly responsible for the transport of cholesterol and various lipids in human blood vessels. According to their different densities, human plasma lipoproteins can be divided into chylomicrons, very low density lipoproteins (VLDL), and low density lipoproteins (LDL). and high-density lipoprotein (HDL) (Salter and Brindley, 1988). Lipoproteins are spherical biological macromolecules. Each lipoprotein molecule consists of a non-polar or hydrophobic core composed of cholesterol or triglycerides, and an outer shell of phospholipids and apoproteins, whose structure is a natural NPs (Orlova et al., 1999). Based on structural features and size advantages (less than 25 nm), LDL and HDL are commonly used to deliver chemotherapeutic drug.

LDL is a kind of spherical particles with a diameter of 19–25 nm. Its core is 1,500 cholesteryl esters wrapped by an outer layer of 800 phospholipids and 500 unesterified cholesterol molecules. The hydrophilic head of the phospholipid molecules is exposed outside, making the LDL is soluble in the blood (Hevonoja et al., 2000; Sherman et al., 2003). LDL is a very potential delivery vehicle, which has good biocompatibility as a biological macromolecule. Another very important reason is that there is apolipoprotein B-100 (ApoB-100) with a relative

TABLE 3 | Ferritin nanoparticles in chemotherapy.

Chemotherapeutic Drugs	Ferriatin Types	Indication(s)	Ref
Doxorubicin	human HFn	Targeting drug delivery	(Liang et al., 2014; Gu et al., 2020; Inoue et al., 2021)
	Recombinant human HFn	Targeting drug delivery	Zhen et al. (2013)
	Recombinant HFt	Targeting drug delivery	Falvo et al. (2018)
	HoSF	Targeting drug delivery	(Kilic et al., 2012; Zhang et al., 2019a)
	PfFt	Hepatocellular carcinoma	Jiang et al. (2019b)
		Targeting drug delivery	
Cisplatin	Recombinant human HFn	Targeting drug delivery	(Falvo et al., 2013; Monti et al., 2019)
	HoSF	Targeting drug delivery	Xing et al. (2009)
Oxaliplatin	Recombinant human HFn	Targeting drug delivery and photodynamic therapy	Liu et al. (2020b)
	HoSF	Targeting drug delivery	Xing et al. (2009)
Paclitaxel	Recombinant human HFn	Targeting drug delivery glioma	Liu et al. (2020c)
Epirubicin	HoSF	Targeting drug delivery	Tan et al. (2018)
	Recombinant human HFn	Targeting drug delivery	Wang et al. (2022)
Mitoxantrone	Recombinant human HFn	Targeting drug delivery	Falvo et al. (2018)
		Tumor therapy (colon, breast, sarcoma and pancreas)	

molecular weight of 514 kDa in the outermost layer of LDL, which can be recognized by and bind to LDL receptors with high specificity. Moreover, studies have confirmed that LDL receptors are highly expressed on the surface of tumor cells, which provide the necessary lipid matrix for the synthesis of membrane systems for fast growing tumor cells (Ng et al., 2011; Harisa and Alanazi, 2014). As a delivery carrier, LDL can encapsulate various hydrophobic loads such as photosensitizers, radiolabels, and various chemotherapeutic drugs (Thaxton et al., 2016; Li et al., 2019; Di and Maiseyeu, 2021). Lo et al. (2002) conjugated doxorubicin to the ApoB protein of LDL, and the results showed that it significantly reduced the occurrence of adverse reactions. Meanwhile, LDL can also take advantage of the inherent targeting ability of LDL through the strategy of combining with independent nanocarriers. Such as Zhu et al. reported a new "binary polymer" low-density lipoprotein-N-succinyl chitosan-cystamine-urocanic acid with dual pH/redox sensitivity and targeting effect, which was synthesized for the co-delivery of breast cancer resistance protein small interfering RNA and paclitaxel, showing significant tumor targeting and effectively inhibited tumor growth (Zhu WJ. et al., 2017). In addition, natural LDL is derived from plasma separation, which is difficult to produce on a large scale, and there are more and more studies on recombinant/synthetic LDL (Zhu G. et al., 2017). For example, Li et al. (2019) constructed a pH-sensitive ApoB-100/oleic acid-doxorubicin/nanostructured lipid carrier NPs, similar to LDL, which showed a increased accumulation at tumor site, pH-dependent release of doxorubicin, and potent breast cancer inhibition.

HDL is an endogenous nanocarrier with a structure similar to LDL and a diameter of 8–13 nm (Mulder et al., 2018). Similarly, blood HDL cholesterol levels in cancer patients are also lower than in normal healthy people (Ganjali et al., 2021). Unlike LDL, which recognizes receptors and mediates endocytosis, HDL specifically recognizes scavenger receptor class B type 1 (SR-B1) and the main protein of HDL stays on the surface of the cell membrane, while its core lipophilic cholesteryl ester directly enters the cell cytoplasm (Krieger, 1999). Furthermore, the major apolipoproteins of HDL contain fewer amino acids than those of LDL, effectively avoiding the formation of large irreversible aggregates (Mulder et al., 2018). The above-mentioned points all provide a good basis and favorable conditions for HDL as a delivery vehicle. It is rare to use natural HDL as a delivery vehicle in existing reports, and recombinant HDL (rHDL) NPs can be used to deliver chemotherapeutic drugs. For example, Wang et al. constructed a doxorubicin -loaded rHDL NPs with high affinity for SR-B1 to treat liver cancer. The results confirm that doxorubicin can be efficiently delivered into cells. After SR-B1 was blocked with antibodies, the delivery efficiency was significantly reduced, which well confirmed that the drug delivery efficiency was dependent on the active targeting of SR-B1 expressed in tumors by apolipoprotein A-1 contained in rHDL NPs (Wang et al., 2014). In addition, rHDL can also be used as a co-delivery carrier for the combination therapy of multiple chemotherapeutic drugs, or the combination therapy of chemotherapy and immunotherapy (Iqbal et al., 2021; Mei et al., 2021). Such as Rui et al. (2017) developed a developed a rHDL NPs for paclitaxel and doxorubicin, which were remarkably effective in increasing the ratiometric accumulation of drugs in cancer cells and enhancing antitumor response at synergistic drug ratios. In particular, they exhibited more efficacious anticancer effects in an *in vitro* cytotoxicity evaluation and in a xenograft tumor model of hepatoma compared with free drug cocktail solutions. Scheetz et al. (2020) co-loaded docetaxel and cholesterol-modified Toll-like receptor 9 agonist CpG oligonucleotides in synthetic HDL to prepare a nanoplatform for combined chemotherapy and immunotherapy. Compared with chemotherapy alone, it can be used for significant Improve survival outcomes.

GENE THERAPY NANOMEDICINE

In recent years, with the increasing maturity of gene manipulation technologies such as gene silencing and gene editing, scientists have begun to treat various diseases by site-

specific up-regulation or down-regulation of target genes, and have achieved certain progress and widespread attention, especially in cancer therapy. The drugs used in gene therapy are nucleic acid therapeutics with lower cytotoxicity, which show significantly fewer adverse reactions and better therapeutic effects compared with conventional treatments such as chemotherapy (Gutierrez et al., 1992). However, gene therapy also faces certain difficulties. For example, commonly used gene therapy agents are not easily taken up by cells and have poor stability during circulation *in vivo*; traditional viral vectors (lentivirus, adenovirus, adeno-associated virus, etc.) are limited in application due to safety concerns such as insertional mutagenesis and immunogenicity. NDSs solve the above problems well, showing low toxicity and immunogenicity, high payload capacity, sustained and controlled release characteristics. Commonly used gene therapy strategies include gene enhancement therapy and gene suppression therapy, in which the application value of nanomedicine will be described here (**Figure 1B**) (Rui et al., 2019).

Gene Enhancement Therapy

Gene enhancement therapy generally refers to "expressing a certain gene" or "expressing a certain protein" by introducing a plasmid or mRNA. Tumor suppressor genes can inhibit cell proliferation when activated or overexpressed. Overexpression of one or more tumor suppressor genes can effectively inhibit the growth and progression of tumors, among which protein 53 (*p53*) gene and phosphatase and tensin homolog (*PTEN*)gene are the most classical and the most deeply studied (Lee and Muller, 2010; Álvarez-Garcia et al., 2019; Lacroix et al., 2020). Both mRNA and plasmid can achieve protein expression, but the way via mRNA quickly and without mutation, integration or other adverse events, which is safer and more efficient (Akeno et al., 2015; Que et al., 2018; Sobhani et al., 2021). However, RNA molecules are unstable and impermeable to membranes, requiring rational design of delivery systems. Kong et al. designed a redox-responsive NPs platform for efficient delivery of mRNA encoding *p53*, which delayed the growth of hepatoma and non-small cell lung cancer cells by inducing cell cycle arrest and apoptosis (Kong et al., 2019). Islam et al. reintroduced *PTEN* mRNA into *PTEN*-null prostate cancer cells through polymer-lipid hybrid NPs coated with polyethylene glycol shell, which significantly inhibited tumor growth (Islam et al., 2018). In addition, the suicide gene therapy systems are also commonly used for gene enhancement, such as herpes simplex virus thymidine kinase (HSV-TK), of which TK gene is a drug-susceptibility gene. After tumor cells were transfected with this gene, they were sensitized and killed by the nontoxic prodrugs glycoxyguanosine or acyclovir (Zhao et al., 2014). A study reported that *in vivo* delivery of the TK-p53- nitroreductase triple therapeutic gene by poly (D,L-lactic-co-glycolic acid)-poly (ethylene glycol)-Polyethylenimine NPs functionalized with SP94 peptide (a peptide that targets hepatocytes) restored *p53* function and enhanced cancer cells' response to the prodrug ganximation glycoxyguanosine and CB 1954 (Sukumar et al., 2020). Due to the negative charge of mRNA, most of the NPs currently used to deliver mRNA drugs contain a cationic gradient, which can form stable complexes with mRNA to achieve high loading rates, such as ionizable lipid NPs (Ding et al., 2021), polymer-lipid hybrids NPs (Islam et al., 2018), and biological nanostructures with higher biocompatibility (Li et al., 2017; Forterre et al., 2020), etc.

Gene Suppression Therapy

Gene suppression can also treat cancer by silencing specific genes that produce abnormal or harmful proteins, such as small interfering RNA (siRNA) therapy. Several *in vitro* and *in vivo* studies have confirmed that siRNA-mediated silencing can significantly inhibit abnormal cancer cell proliferation (Shi et al., 2019; Han et al., 2021; Krishn et al., 2022). In addition, siRNA can sensitize drug-resistant cancer cells, showing great promise in enhancing chemotherapy (Shen et al., 2020). An ideal delivery system should protect siRNA from degradation by nucleases, as well as deliver and release it into the cytoplasm of targeted tumor cells without adverse effects. At present, the research on nanocarriers for siRNA delivery has been relatively mature, including lipid nanocarriers, polymer NPs, dendrimers, inorganic NPs, etc (Babu et al., 2017; Subhan and Torchilin, 2019). In addition, the aforementioned biological NPs can also deliver siRNA with high loading and high biocompatibility. Wang et al. constructed a DNA nanodevice using DNA origami technology to co-deliver siRNA and the doxorubicin (Nanodevice-siBcl2-si P-glycoprotein- doxorubicin), which induced potent cytotoxicity and tumor growth inhibition with no observable systemic toxicity (Wang X. et al., 2021).

CRISPR/Cas9 gene editing technology, another cancer gene-suppression therapy, has the potential to permanently destroy tumor survival genes, which overcomes the repeated dosing limitations of traditional cancer therapy and improves the therapeutic effect (Rafii et al., 2022). CRISPR/Cas9 consists of two parts: Cas9, a nuclease that cuts DNA at a target site, and a single guide RNA (sgRNA) that directs Cas9 to cut at a specific or desired site in DNA. Since the CRISPR/Cas9 complex requires manipulation of the nuclear genome, its components need to be translocated into the nucleus (Zhan et al., 2019; Zhang S. et al., 2021). Therefore, it is necessary to overcome the barriers of tissue and cell membranes to effectively deliver CRISPR/Cas9 to the target site, facing considerable challenges. In recent years, nanomaterials have gradually shown unique advantages in gene delivery. Currently developed CRISPR/Cas9 NDSs include cationic liposomes (Yin et al., 2020), lipid NPs (Rosenblum et al., 2020), cationic polymers (Zhang Y. et al., 2019), vesicles (Horodecka and Düchler, 2021), and gold NPs (Tao et al., 2021). In order to better reduce the off-target effects, researchers have developed a stimulus-based intelligent NDSs. Intelligent NPs can be based on endogenous signals (including pH, redox and ATP) and exogenous signals (including radiation, magnetic ultrasound), to control or regulate the delivery of CRISPR/Cas9 to specific cells. For example, Wang et al. designed a multifunctional NPs modified with pH-sensitive epidermal growth factor receptor targeting and nuclear guide peptides to efficiently deliver CRISPR/Cas9 and epirubicin to the human tongue squamous cell carcinoma SAS cells and SAS tumor mice, providing a pH-responsive co-delivery platform for

chemotherapy and CRISPR/Cas (Wang Z. et al., 2021). Another study reported near-infrared light-responsive nanocarriers of CRISPR-Cas9 to inhibit tumor cell proliferation *in vitro* and *in vivo* through near-infrared light-activated gene editing (Pan et al., 2019). DNA-based NPs can load Cas9/sgRNA complexes by sequence hybridization. Shi et al. designed a miR-21 (overexpressed in tumor cell)-responsive Cas9/sgRNA ribonucleoprotein delivery system based on DNA NFs, which could significantly improve genome editing efficiency and make it possible to control the expression of endogenous genes in a cell-type-specific manner through specific endogenous or exogenous miRNAs (Shi et al., 2020).

IMMUNOTHERAPEUTIC NANOMEDICINE

In recent years, immunotherapy has developed rapidly and gradually matured, and its emergence has revolutionized the treatment standard and treatment concept of cancer (Abdelbaky et al., 2021; Aktar et al., 2022). Radiotherapy and chemotherapy of traditional treatment methods generally use toxic drugs or radiation to directly ablate cancer cells. However, the target of tumor immunotherapy is mainly immune cells, which can activate the body's anti-tumor immune response to kill tumor cells by inhibiting negative immune regulators and enhancing the ability of immune cells to recognize tumor cell surface antigens (van den Bulk et al., 2018; Zhong et al., 2020). In the early stage of tumor immunotherapy, the main method is to directly attack tumor cells with cytokines produced by immune cells. With the gradual deepening of cancer immunotherapy research, immune checkpoint inhibitors, tumor vaccine immunization and chimeric antigen receptor T (CAR-T) cell therapy have emerged, and they have become the main force in immunotherapy (Sahin and Türeci, 2018; Ma et al., 2019; Galluzzi et al., 2020; Holstein and Lunning, 2020; Raza et al., 2021) With the deepening of research, the value of nanomedicine in tumor immunotherapy is constantly emerging (**Figure 1C**).

Immune Checkpoint Blockade Therapy

Inhibitory immune checkpoints can suppress the body's immune response and prevent the occurrence of autoimmunity. Tumor cells can suppress the body's immune response, thereby evading clearance by the body's immune system via expressing inhibitory immune checkpoint molecules that interact with T cells (Jhunjhunwala et al., 2021). Currently widely studied immune checkpoints are cytotoxic-T-lymphocyte-associated protein 4 (CTLA-4), program death 1 (PD-1) and program death-ligand 1 (PD-L1), according to which monoclonal antibodies (mAbs) drugs are designed such as ipilimumab (CTLA-4 inhibitor), pembrolizumab (PD-1 inhibitor), atezolizumab (PD-L1 inhibitors) have been approved by the FDA for marketing (Vaddepally et al., 2020). Nanomedicine is being adapted in various ways to improve immune checkpoint inhibitors (ICIs), increasing the effectiveness and surpassing the limitations. MAbs are difficult to penetrate the blood-brain barrier, and NPs -mediated ICIs mAbs are an effective way to solve this problem (Diesendruck and Benhar, 2017). Galstyan et al. covalently attached ICIs (anti-CTLA-4 and/or anti-PD-1) to poly-β-L-malic acid biopolymer scaffolds, and such nanoscale immunoconjugates allow ICIs mAbs to cross the blood-brain barrier to the tumor environment and modulate immune responses. In particular, the use of nanoscale immunoconjugates has shown promising antitumor activity in the treatment of glioblastoma (Galstyan et al., 2019). Moreover, NDSs have also shown their advantages in reducing the dosage of ICIs or controlling immune-related adverse events (irAIEs) Meir et al., reported that αPDL1-conjugated gold NPs effectively prevented tumor growth at a dose reduced to 1/5 the clinical standard of care dose (Meir et al., 2017). Shen et al. coated PD-L1-overexpressing mesenchymal stem cells plasma membranes on polylactic-co-glycolic acid NPs to design immunosuppressive NPs, managing and reducing irAIEs (Shen et al., 2021). Furthermore, nanocarriers can also be designed as smart platforms for controlled drug release in response to different stimuli present in the tumor microenvironment, which is expected to further enhance the therapeutic efficacy of nanoformulations. For example, researchers have developed a class of liposomes that are dual-responsive to pH and matrix metalloproteinases in combination with PD-L1 inhibitor conjugates and low-dose chemotherapy doxorubicin. In an *in vivo* mouse B16F10 melanoma model, the synergistic effect of chemotherapeutic agents and ICIs enabled dual-responsive liposomes to achieve an optimal tumor suppression efficiency of 78.7% (Liu et al., 2019). Besides, ICIs do not elicit adequate responses in the vast majority of patients with poorly immunogenic tumors due to targeting only major inhibitory axes. Therefore, combining ICIs with nanotechnology-driven immunostimulatory treatments (e.g., nanochemicals, light, and thermal therapy) may help to locally break immune tolerance and enhance systemic antitumor immunity, thereby expanding the availability of proportion of cancer patients benefiting from treatment. Based on the above, the role of nanomaterials in immunotherapy has gone beyond the concept of adjuvant or carrier, which is an effective means to improve the efficacy of ICIs and reduce their toxicity through rational design. At the same time, the dosing cycle and interval time, possible off-target potential and other aspects should be improved to obtain the best solution (Cremolini et al., 2021).

Cancer Vaccines

Cancer vaccines kill tumor cells without damaging healthy cells by activating the body's immune system, and they can trigger immune memory to provide long-term protection against tumor recurrence. As a potential drug development concept, cancer vaccines are extremely valuable whether they are used alone or in combination with other immunotherapies (Igarashi and Sasada, 2020; Saxena et al., 2021). With the deepening of research, the advantages of applying nanomedicine in cancer vaccines have gradually emerged (Liu J. et al., 2020). Cancer vaccines are typically combinations of immunogenic components (eg, neoantigens and adjuvants) that are delivered to antigen-presenting cells in peripheral lymphoid tissue. First, encapsulating immunogenic components in nanocarriers can prevent antigen degradation and effectively improve antigen

stability (Zhang Z. et al., 2019). Second, nanovaccines co-encapsulate and co-deliver antigens and adjuvants, which can effectively enhance the immunogenicity and therapeutic efficacy of vaccines (Zhu WJ. et al., 2017). Heo and Lim et al. developed a poly (lactic-co-glycolic acid) NPs loaded with ovalbumin for the activation of DCs through the toll-like receptor 7, which proved that the nanovaccine loaded with multivalent antigens and adjuvants can effectively reduce tumor volume (Heo and Lim, 2014). Further, nanovaccine can achieve efficient delivery to immune organs (lymph nodes, spleen). Through rational design of physical properties (such as size, colloidal stability, electrostatic interactions, deformability) or chemical properties (such as light, pH, and enzyme responsiveness), nanovaccines are able to deliver more antigens from injection sites or tumors to lymph nodes, or delivered from the blood to the spleen (Evans et al., 2018; Musetti and Huang, 2018; Chen et al., 2020; Gupta et al., 2021). In particular, nanovaccines further modified by targeting ligands can also be actively targeted and delivered to specific subregions of immune cells (Cai et al., 2021). For example, a click chemistry-based active lymphatic accumulation system was developed to enhance the delivery of antigens and adjuvants to the lymphatic subcapsular sinus (Qin et al., 2021). Ultimately, NPs can enhance immune responses through sustained or controlled release capabilities. For example, Chen et al. (2018) showed that a single injection of clay NPs sustained the release of immunogenic agents, which significantly enhanced the immune response in regional lymph nodes for up to 35 days.

CAR-T Cell Therapy

One of the strategies for immune evasion of tumor cells is to reduce the expression of their surface antigens, so that T cells cannot be activated in a human leukocyte antigen-dependent manner, thereby evading the attack of the immune system (Pham et al., 2018). CAR-T works by modifying a patient's own T cells to more effectively recognize and kill tumor cells (Huang et al., 2020). Initially, the application of nanomedicine to CAR-T therapy was mainly to replace viral vectors for *in vitro* genetic modification of T cells to reduce costs and improve safety (Olden et al., 2018; Billingsley et al., 2020). However, *in vitro* CAR-T cell programming is complicated and expensive, and one solution is to program T cells *in vivo*. Nanomedicines were shown to directly construct chimeric antigen receptors *in situ* on circulating T cells without *ex vivo* manipulation in mouse models. Smith et al. designed a polymer NPs carrying a chimeric antigen receptor (CAR)-encoding plasmid and injected leukemia-targeting CAR genes can be efficiently introduced into T cell nuclei, followed by efficient leukemia regression in mice, which is comparable to *ex vivo* programmed CAR-T cells (Smith et al., 2017). Subsequently, this team reported an injectable nanocarrier that deliverd *in vitro* transcribed CAR or T cell receptors mRNA for transient reprogramming of circulating T cells to recognize disease-associated antigens (Parayath et al., 2020). Another important advantage of nanomedicine in this field is the safe and effective enhancement of T cell therapy. Tang et al. (2018) designed a T cell receptors signaling-responsive protein nanogel to co-deposit immunostimulatory cytokines, such as interleukin-15 agonists, onto the surface of CAR-T cells, which significantly extended the therapeutic window and improved tumor clearance in CAR-T cell therapy against solid tumors.

PERSPECTIVES AND FUTURE DIRECTIONS

In recent years, the concept, method and pattern of tumor treatment are constantly changing, which provides a broad space and prospect for the application of nanomedicine. It is the application of intelligent NDSs for tumor chemotherapy, gene therapy and immunotherapy to solve the problem of drug (chemotherapy, biological drug) delivery, optimize its delivery efficiency, and achieve targeted, precise and controllable delivery to a certain degree. However, how to translate preclinically studied antitumor nanomedicines into clinically feasible therapeutics still faces several key challenges. For example: 1) how to optimize patient population stratification in clinical trials; 2) how to optimize the dosing regimen of nanomedicines in combination therapy; 3) how to ensure high quality and reproducibility for industrialized production of nanomedicines, etc. Expectantly, with the deepening of nanotechnology research, the combination of molecular-level scientific design and precise control of process engineering is expected to overcome the core technology of NDSs research and development, thereby opening a new situation for NDSs.

AUTHOR CONTRIBUTIONS

SH, ZC, and YL reviewed the literature and drafted the article. MH, ZWC, and FL finalized the paper and provided suggestions to improve it. SH, MMFAB and ZC drew the figure. MMFAB provided suggestions to improve the article. All authors participated in designing the concept of this manuscript. All authors contributed to the article and approved the submitted version.

FUNDING

This work was supported by the Ningbo Natural Science Foundation (2019A610311); by Scientific Research Fund of Zhejiang Provincial Education Department (Y202045025); by the Zhejiang Province Public Welfare Technology Application Research Project of China (No. LGF18H090015).

REFERENCES

Abdelbaky, S. B., Ibrahim, M. T., Samy, H., Mohamed, M., Mohamed, H., Mustafa, M., et al. (2021). Cancer Immunotherapy from Biology to Nanomedicine. *J. Control. Release* 336, 410–432. doi:10.1016/j.jconrel.2021.06.025

Ahn, S. Y., Liu, J., Vellampatti, S., Wu, Y., and Um, S. H. (2020). DNA Transformations for Diagnosis and Therapy. *Adv. Funct. Mat.* 31, 2008279. doi:10.1002/adfm.202008279

Akeno, N., Miller, A. L., Ma, X., and Wikenheiser-Brokamp, K. A. (2015). p53 Suppresses Carcinoma Progression by Inhibiting mTOR Pathway Activation. *Oncogene* 34, 589–599. doi:10.1038/onc.2013.589

Akgöl, S., Ulucan-Karnak, F., Kuru, C. İ., and Kuşat, K. (2021). The Usage of Composite Nanomaterials in Biomedical Engineering Applications. *Biotech. Bioeng.* 118, 2906–2922. doi:10.1002/bit.27843

Aktar, N., Yueting, C., Abbas, M., Zafar, H., Paiva-Santos, A. C., Zhang, Q., et al. (2022). Understanding of Immune Escape Mechanisms and Advances in Cancer Immunotherapy. *J. Oncol.* 2022, 8901326. doi:10.1155/2022/8901326

Álvarez-Garcia, V., Tawil, Y., Wise, H. M., and Leslie, N. R. (2019). Mechanisms of PTEN Loss in Cancer: It's All about Diversity. *Seminars Cancer Biol.* 59, 66–79. doi:10.1016/j.semcancer.2019.02.001

An, F.-F., and Zhang, X.-H. (2017). Strategies for Preparing Albumin-Based Nanoparticles for Multifunctional Bioimaging and Drug Delivery. *Theranostics* 7, 3667–3689. doi:10.7150/thno.19365

Babu, A., Munshi, A., and Ramesh, R. (2017). Combinatorial Therapeutic Approaches with RNAi and Anticancer Drugs Using Nanodrug Delivery Systems. *Drug Dev. Industrial Pharm.* 43, 1391–1401. doi:10.1080/03639045.2017.1313861

Bertrand, N., Wu, J., Xu, X., Kamaly, N., and Farokhzad, O. C. (2014). Cancer Nanotechnology: the Impact of Passive and Active Targeting in the Era of Modern Cancer Biology. *Adv. Drug Deliv. Rev.* 66, 2–25. doi:10.1016/j.addr.2013.11.009

Bhushan, B., Khanadeev, V., Khlebtsov, B., Khlebtsov, N., and Gopinath, P. (2017). Impact of Albumin Based Approaches in Nanomedicine: Imaging, Targeting and Drug Delivery. *Adv. Colloid Interface Sci.* 246, 13–39. doi:10.1016/j.cis.2017.06.012

Billingsley, M. M., Singh, N., Ravikumar, P., Zhang, R., June, C. H., and Mitchell, M. J. (2020). Ionizable Lipid Nanoparticle-Mediated mRNA Delivery for Human CAR T Cell Engineering. *Nano Lett.* 20, 1578–1589. doi:10.1021/acs.nanolett.9b04246

Cai, T., Liu, H., Zhang, S., Hu, J., and Zhang, L. (2021). Delivery of Nanovaccine Towards Lymphoid Organs: Recent Strategies in Enhancing Cancer Immunotherapy. *J. Nanobiotechnol.* 19, 389. doi:10.1186/s12951-021-01146-2

Candelaria, P. V., Leoh, L. S., Penichet, M. L., and Daniels-Wells, T. R. (2021). Antibodies Targeting the Transferrin Receptor 1 (TfR1) as Direct Anti-cancer Agents. *Front. Immunol.* 12, 607692. doi:10.3389/fimmu.2021.607692

Cao, J., Huang, D., and Peppas, N. A. (2020). Advanced Engineered Nanoparticulate Platforms to Address Key Biological Barriers for Delivering Chemotherapeutic Agents to Target Sites. *Adv. Drug Deliv. Rev.* 167, 170–188. doi:10.1016/j.addr.2020.06.030

Carvalho, C., Santos, R., Cardoso, S., Correia, S., Oliveira, P., Santos, M., et al. (2009). Doxorubicin: The Good, the Bad and the Ugly Effect. *Cmc* 16, 3267–3285. doi:10.2174/092986709788803312

Chakraborti, S., and Chakrabarti, P. (2019). Self-Assembly of Ferritin: Structure, Biological Function and Potential Applications in Nanotechnology. 313–329. doi:10.1007/978-981-13-9791-2_10

Chang, M., Yang, C.-S., and Huang, D.-M. (2011). Aptamer-Conjugated DNA Icosahedral Nanoparticles as a Carrier of Doxorubicin for Cancer Therapy. *ACS Nano* 5, 6156–6163. doi:10.1021/nn200693a

Chen, W., Zuo, H., Li, B., Duan, C., Rolfe, B., Zhang, B., et al. (2018). Clay Nanoparticles Elicit Long-Term Immune Responses by Forming Biodegradable Depots for Sustained Antigen Stimulation. *Small* 14, e1704465. doi:10.1002/smll.201704465

Chen, Y., De Koker, S., and De Geest, B. G. (2020). Engineering Strategies for Lymph Node Targeted Immune Activation. *Acc. Chem. Res.* 53, 2055–2067. doi:10.1021/acs.accounts.0c00260

Cheng, X., Fan, K., Wang, L., Ying, X., Sanders, A. J., Guo, T., et al. (2020). TfR1 Binding with H-Ferritin Nanocarrier Achieves Prognostic Diagnosis and Enhances the Therapeutic Efficacy in Clinical Gastric Cancer. *Cell Death Dis.* 11, 92. doi:10.1038/s41419-020-2272-z

Collins, M., and Thrasher, A. (2015). Gene Therapy: Progress and Predictions. *Proc. R. Soc. B* 282, 20143003. doi:10.1098/rspb.2014.3003

Cremolini, C., Vitale, E., Rastaldo, R., and Giachino, C. (2021). Advanced Nanotechnology for Enhancing Immune Checkpoint Blockade Therapy. *Nanomater. (Basel)* 11 (3), 661. doi:10.3390/nano11030661

Dai, Z., Leung, H. M., and Lo, P. K. (2017). Stimuli-Responsive Self-Assembled DNA Nanomaterials for Biomedical Applications. *Small* 13 (7). doi:10.1002/smll.201602881

Di, L., and Maiseyeu, A. (2021). Low-Density Lipoprotein Nanomedicines: Mechanisms of Targeting, Biology, and Theranostic Potential. *Drug Deliv.* 28, 408–421. doi:10.1080/10717544.2021.1886199

Diesendruck, Y., and Benhar, I. (2017). Novel Immune Check Point Inhibiting Antibodies in Cancer Therapy-Opportunities and Challenges. *Drug Resist. Updat.* 30, 39–47. doi:10.1016/j.drup.2017.02.001

Ding, F., Zhang, H., Cui, J., Li, Q., and Yang, C. (2021). Boosting Ionizable Lipid Nanoparticle-Mediated *In Vivo* mRNA Delivery Through Optimization of Lipid Amine-Head Groups. *Biomater. Sci.* 9, 7534–7546. doi:10.1039/d1bm00866h

Elsayed, M. E., Sharif, M. U., and Stack, A. G. (2016). Transferrin Saturation: A Body Iron Biomarker. *Adv. Clin. Chem.* 75, 71–97. doi:10.1016/bs.acc.2016.03.002

Evans, C. G., and Winfree, E. (2017). Physical Principles for DNA Tile Self-Assembly. *Chem. Soc. Rev.* 46, 3808–3829. doi:10.1039/c6cs00745g

Evans, E. R., Bugga, P., Asthana, V., and Drezek, R. (2018). Metallic Nanoparticles for Cancer Immunotherapy. *Mater. Today* 21, 673–685. doi:10.1016/j.mattod.2017.11.022

Falvo, E., Malagrinò, F., Arcovito, A., Fazi, F., Colotti, G., Tremante, E., et al. (2018). The Presence of Glutamate Residues on the PAS Sequence of the Stimuli-Sensitive Nano-Ferritin Improves *In Vivo* Biodistribution and Mitoxantrone Encapsulation Homogeneity. *J. Control. Release* 275, 177–185. doi:10.1016/j.jconrel.2018.02.025

Falvo, E., Tremante, E., Fraioli, R., Leonetti, C., Zamparelli, C., Boffi, A., et al. (2013). Antibody-Drug Conjugates: Targeting Melanoma with Cisplatin Encapsulated in Protein-Cage Nanoparticles Based on Human Ferritin. *Nanoscale* 5, 12278–12285. doi:10.1039/c3nr04268e

Fernandes, M. A., Hanck-Silva, G., Baveloni, F. G., Oshiro Junior, J. A., de Lima, F. T., Eloy, J. O., et al. (2021). A Review of Properties, Delivery Systems and Analytical Methods for the Characterization of Monomeric Glycoprotein Transferrin. *Crit. Rev. Anal. Chem.* 51, 399–410.doi:10.1080/10408347.2020.1743639

Forterre, A. V., Wang, J.-H., Delcayre, A., Kim, K., Green, C., Pegram, M. D., et al. (2020). Extracellular Vesicle-Mediated *In Vitro* Transcribed mRNA Delivery for Treatment of HER2+ Breast Cancer Xenografts in Mice by Prodrug CB1954 Without General Toxicity. *Mol. Cancer Ther.* 19, 858–867. doi:10.1158/1535-7163.mct-19-0928

Galluzzi, L., Humeau, J., Buqué, A., Zitvogel, L., and Kroemer, G. (2020). Immunostimulation with Chemotherapy in the Era of Immune Checkpoint Inhibitors. *Nat. Rev. Clin. Oncol.* 17, 725–741. doi:10.1038/s41571-020-0413-z

Galstyan, A., Markman, J. L., Shatalova, E. S., Chiechi, A., Korman, A. J., Patil, R., et al. (2019). Blood-Brain Barrier Permeable Nano Immunoconjugates Induce Local Immune Responses for Glioma Therapy. *Nat. Commun.* 10, 3850. doi:10.1038/s41467-019-11719-3

Ganjali, S., Banach, M., Pirro, M., Fras, Z., and Sahebkar, A. (2021). HDL and Cancer - Causality Still Needs to Be Confirmed? Update 2020. *Seminars Cancer Biol.* 73, 169–177. doi:10.1016/j.semcancer.2020.10.007

Goswami, U., Dutta, A., Raza, A., Kandimalla, R., Kalita, S., Ghosh, S. S., et al. (2018). Transferrin-Copper Nanocluster-Doxorubicin Nanoparticles as Targeted Theranostic Cancer Nanodrug. *ACS Appl. Mat. Interfaces* 10, 3282–3294. doi:10.1021/acsami.7b15165

Gote, V., Nookala, A. R., Bolla, P. K., and Pal, D. (2021). Drug Resistance in Metastatic Breast Cancer: Tumor Targeted Nanomedicine to the Rescue. *Int. J. Mol. Sci.* 22 (9), 4673. doi:10.3390/ijms22094673

Gou, Y., Miao, D., Zhou, M., Wang, L., Zhou, H., and Su, G. (2018). Bio-Inspired Protein-Based Nanoformulations for Cancer Theranostics. *Front. Pharmacol.* 9, 421. doi:10.3389/fphar.2018.00421

Gu, C., Zhang, T., Lv, C., Liu, Y., Wang, Y., and Zhao, G. (2020). His-Mediated Reversible Self-Assembly of Ferritin Nanocages Through Two Different

Switches for Encapsulation of Cargo Molecules. *ACS Nano* 12, 17080–17090. doi:10.1021/acsnano.0c06670

Guan, C., Zhu, X., and Feng, C. (2021). DNA Nanodevice-Based Drug Delivery Systems. *Biomolecules* 11 (12), 1855. doi:10.3390/biom11121855

Guo, Z., Zhang, Y., Fu, M., Zhao, L., Wang, Z., Xu, Z., et al. (2021). The Transferrin Receptor-Directed CAR for the Therapy of Hematologic Malignancies. *Front. Immunol.* 12, 652924. doi:10.3389/fimmu.2021.652924

Gupta, J., Safdari, H. A., and Hoque, M. (2021). Nanoparticle Mediated Cancer Immunotherapy. *Seminars Cancer Biol.* 69, 307–324. doi:10.1016/j.semcancer.2020.03.015

Gutierrez, A. A., Lemoine, N. R., and Sikora, K. (1992). Gene Therapy for Cancer. *Lancet* 339, 715–721. doi:10.1016/0140-6736(92)90606-4

Halley, P. D., Lucas, C. R., Mcwilliams, E. M., Webber, M. J., Patton, R. A., Kural, C., et al. (2016). Daunorubicin-Loaded DNA Origami Nanostructures Circumvent Drug-Resistance Mechanisms in a Leukemia Model. *Small* 12, 308–320. doi:10.1002/smll.201502118

Han, Q., Xie, Q. R., Li, F., Cheng, Y., Wu, T., Zhang, Y., et al. (2021). Targeted Inhibition of SIRT6 via Engineered Exosomes Impairs Tumorigenesis and Metastasis in Prostate Cancer. *Theranostics* 11, 6526–6541. doi:10.7150/thno.53886

Harisa, G. I., and Alanazi, F. K. (2014). Low Density Lipoprotein Bionanoparticles: From Cholesterol Transport to Delivery of Anti-Cancer Drugs. *Saudi Pharm. J.* 22, 504–515. doi:10.1016/j.jsps.2013.12.015

Heo, M. B., and Lim, Y. T. (2014). Programmed Nanoparticles for Combined Immunomodulation, Antigen Presentation and Tracking of Immunotherapeutic Cells. *Biomaterials* 35 (1), 590–600. doi:10.1016/j.biomaterials.2013.10.009

Hevonoja, T., Pentikäinen, M. O., Hyvönen, M. T., Kovanen, P. T., and Ala-Korpela, M. (2000). Structure of Low Density Lipoprotein (LDL) Particles: Basis for Understanding Molecular Changes in Modified LDL. *Biochim. Biophys. Acta* 1488, 189–210. doi:10.1016/s1388-1981(00)00123-2

Holstein, S. A., and Lunning, M. A. (2020). CAR T-Cell Therapy in Hematologic Malignancies: A Voyage in Progress. *Clin. Pharmacol. Ther.* 107, 112–122. doi:10.1002/cpt.1674

Hoogenboezem, E. N., and Duvall, C. L. (2018). Harnessing Albumin as a Carrier for Cancer Therapies. *Adv. Drug Deliv. Rev.* 130, 73–89. doi:10.1016/j.addr.2018.07.011

Horodecka, K., and Düchler, M. (2021). CRISPR/Cas9: Principle, Applications, and Delivery Through Extracellular Vesicles. *Int. J. Mol. Sci.* 22 (11), 6072. doi:10.3390/ijms22116072

Huang, R., Li, X., He, Y., Zhu, W., Gao, L., Liu, Y., et al. (2020). Recent Advances in CAR-T Cell Engineering. *J. Hematol. Oncol.* 13, 86. doi:10.1186/s13045-020-00910-5

Igarashi, Y., and Sasada, T. (2020). Cancer Vaccines: Toward the Next Breakthrough in Cancer Immunotherapy. *J. Immunol. Res.* 2020, 5825401. doi:10.1155/2020/5825401

Inoue, I., Chiba, M., Ito, K., Okamatsu, Y., Suga, Y., Kitahara, Y., et al. (2021). One-Step Construction of Ferritin Encapsulation Drugs for Cancer Chemotherapy. *Nanoscale* 13, 1875–1883. doi:10.1039/d0nr04019c

Iqbal, H., Yang, T., Li, T., Zhang, M., Ke, H., Ding, D., et al. (2021). Serum Protein-Based Nanoparticles for Cancer Diagnosis and Treatment. *J. Control. Release* 329, 997–1022. doi:10.1016/j.jconrel.2020.10.030

Islam, M. A., Xu, Y., Tao, W., Ubellacker, J. M., Lim, M., Aum, D., et al. (2018). Restoration of Tumour-Growth Suppression *In Vivo* via Systemic Nanoparticle-Mediated Delivery of PTEN mRNA. *Nat. Biomed. Eng.* 2, 850–864. doi:10.1038/s41551-018-0284-0

Jhunjhunwala, S., Hammer, C., and Delamarre, L. (2021). Antigen Presentation in Cancer: Insights into Tumour Immunogenicity and Immune Evasion. *Nat. Rev. Cancer* 21, 298–312. doi:10.1038/s41568-021-00339-z

Ji, J., Karna, D., and Mao, H. (2021). DNA Origami Nano-Mechanics. *Chem. Soc. Rev.* 50, 11966–11978. doi:10.1039/d1cs00250c

Jiang, B., Zhang, R., Zhang, J., Hou, Y., Chen, X., Zhou, M., et al. (2019a). GRP78-Targeted Ferritin Nanocaged Ultra-High Dose of Doxorubicin for Hepatocellular Carcinoma Therapy. *Theranostics* 9, 2167–2182. doi:10.7150/thno.30867

Jiang, Q., Zhao, S., Liu, J., Song, L., Wang, Z., and Ding, B. (2019b). Rationally Designed DNA-Based Nanocarriers. *Adv. Drug Deliv. Rev.* 147, 2–21. doi:10.1016/j.addr.2019.02.003

Jin, M.-Z., and Jin, W.-L. (2020). The Updated Landscape of Tumor Microenvironment and Drug Repurposing. *Sig. Transduct. Target Ther.* 5, 166. doi:10.1038/s41392-020-00280-x

Kilic, M. A., Ozlu, E., and Calis, S. (2012). A Novel Protein-Based Anticancer Drug Encapsulating Nanosphere: Apoferritin-Doxorubicin Complex. *J. Biomed. Nanotechnol.* 8, 508–514. doi:10.1166/jbn.2012.1406

Kinnear, C., Moore, T. L., Rodriguez-Lorenzo, L., Rothen-Rutishauser, B., and Petri-Fink, A. (2017). Form Follows Function: Nanoparticle Shape and its Implications for Nanomedicine. *Chem. Rev.* 117, 11476–11521. doi:10.1021/acs.chemrev.7b00194

Kong, N., Tao, W., Ling, X., Wang, J., Xiao, Y., Shi, S., et al. (2019). Synthetic mRNA Nanoparticle-Mediated Restoration of P53 Tumor Suppressor Sensitizes -deficient Cancers to mTOR Inhibition.

Krieger, M. (1999). Charting the Fate of the "Good Cholesterol": Identification and Characterization of the High-Density Lipoprotein Receptor SR-BI. *Annu. Rev. Biochem.* 68, 523–558. doi:10.1146/annurev.biochem.68.1.523

Krishn, S. R., Garcia, V., Naranjo, N. M., Quaglia, F., Shields, C. D., Harris, M. A., et al. (2022). Small Extracellular Vesicle-Mediated ITGB6 siRNA Delivery Downregulates the αVβ6 Integrin and Inhibits Adhesion and Migration of Recipient Prostate Cancer Cells. *Cancer Biol. Ther.* 23, 173–185. doi:10.1080/15384047.2022.2030622

Lacroix, M., Riscal, R., Arena, G., Linares, L. K., and Le Cam, L. (2020). Metabolic Functions of the Tumor Suppressor P53: Implications in Normal Physiology, Metabolic Disorders, and Cancer. *Mol. Metab.* 33, 2–22. doi:10.1016/j.molmet.2019.10.002

Lau, K. L., and Sleiman, H. F. (2016). Minimalist Approach to Complexity: Templating the Assembly of DNA Tile Structures with Sequentially Grown Input Strands. *ACS Nano* 10, 6542–6551. doi:10.1021/acsnano.6b00134

Lee, E. Y. H. P., and Muller, W. J. (2010). Oncogenes and Tumor Suppressor Genes. *Cold Spring Harb. Perspect. Biol.* 2, a003236. doi:10.1101/cshperspect.a003236

Li, C., Li, H., and Jie, G. (2020). Click Chemistry Reaction-Triggered DNA Walker Amplification Coupled with Hyperbranched DNA Nanostructure for Versatile Fluorescence Detection and Drug Delivery to Cancer Cells. *Microchim. Acta* 187, 625. doi:10.1007/s00604-020-04580-5

Li, J., Wang, W., He, Y., Li, Y., Yan, E. Z., Zhang, K., et al. (2017). Structurally Programmed Assembly of Translation Initiation Nanoplex for Superior mRNA Delivery. *ACS Nano* 11, 2531–2544. doi:10.1021/acsnano.6b08447

Li, W., Fu, J., Ding, Y., Liu, D., Jia, N., Chen, D., et al. (2019). Low Density Lipoprotein-Inspired Nanostructured Lipid Nanoparticles Containing Pro-Doxorubicin to Enhance Tumor-Targeted Therapeutic Efficiency. *Acta Biomater.* 96, 456–467. doi:10.1016/j.actbio.2019.06.051

Li, Y., Raza, F., Liu, Y., Wei, Y., Rong, R., Zheng, M., et al. (2021). Clinical Progress and Advanced Research of Red Blood Cells Based Drug Delivery System. *Biomaterials* 279, 121202. doi:10.1016/j.biomaterials.2021.121202

Liang, M., Fan, K., Zhou, M., Duan, D., Zheng, J., Yang, D., et al. (2014). H-Ferritin-Nanocaged Doxorubicin Nanoparticles Specifically Target and Kill Tumors with a Single-Dose Injection. *Proc. Natl. Acad. Sci. U.S.A.* 111, 14900–14905. doi:10.1073/pnas.1407808111

Libutti, S. K. (2019). Recording 25 Years of Progress in Cancer Gene Therapy. *Cancer Gene Ther.* 26, 345–346. doi:10.1038/s41417-019-0121-y

Liu, J.-p., Wang, T.-t., Wang, D.-g., Dong, A.-j., Li, Y.-p., and Yu, H.-j. (2017). Smart Nanoparticles Improve Therapy for Drug-Resistant Tumors by Overcoming Pathophysiological Barriers. *Acta Pharmacol. Sin.* 38, 1–8. doi:10.1038/aps.2016.84

Liu, J., Miao, L., Sui, J., Hao, Y., and Huang, G. (2020a). Nanoparticle Cancer Vaccines: Design Considerations and Recent Advances. *Asian J. Pharm. Sci.* 15, 576–590. doi:10.1016/j.ajps.2019.10.006

Liu, J., Song, L., Liu, S., Zhao, S., Jiang, Q., and Ding, B. (2018a). A Tailored DNA Nanoplatform for Synergistic RNAi-/Chemotherapy of Multidrug-Resistant Tumors. *Angew. Chem. Int. Ed.* 57, 15486–15490. doi:10.1002/anie.201809452

Liu, M., Zhu, Y., Wu, T., Cheng, J., and Liu, Y. (2020b). Nanobody-Ferritin Conjugate for Targeted Photodynamic Therapy. *Chem. Eur. J.* 26, 7442–7450. doi:10.1002/chem.202000075

Liu, W., Lin, Q., Fu, Y., Huang, S., Guo, C., Li, L., et al. (2020c). Target Delivering Paclitaxel by Ferritin Heavy Chain Nanocages for Glioma Treatment. *J. Control. Release* 323, 191–202. doi:10.1016/j.jconrel.2019.12.010

Liu, X., Wu, L., Wang, L., and Jiang, W. (2018b). A Dual-Targeting DNA Tetrahedron Nanocarrier for Breast Cancer Cell Imaging and Drug Delivery. *Talanta* 179, 356–363. doi:10.1016/j.talanta.2017.11.034

Liu, Y., Chen, X.-G., Yang, P.-P., Qiao, Z.-Y., and Wang, H. (2019). Tumor Microenvironmental pH and Enzyme Dual Responsive Polymer-Liposomes for Synergistic Treatment of Cancer Immuno-Chemotherapy. *Biomacromolecules* 20, 882–892. doi:10.1021/acs.biomac.8b01510

Liu, Y., Ran, Y., Ge, Y., Raza, F., Li, S., Zafar, H., et al. (2022). pH-Sensitive Peptide Hydrogels as a Combination Drug Delivery System for Cancer Treatment. *Pharmaceutics* 14, 652. doi:10.3390/pharmaceutics14030652

Lo, E. H. K., Ooi, V. E. L., and Fung, K. P. (2002). Circumvention of Multidrug Resistance and Reduction of Cardiotoxicity of Doxorubicin *In Vivo* by Coupling it with Low Density Lipoprotein. *Life Sci.* 72, 677–687. doi:10.1016/s0024-3205(02)02180-x

Lu, S., Zhao, F., Zhang, Q., and Chen, P. (2018). Therapeutic Peptide Amphiphile as a Drug Carrier with ATP-Triggered Release for Synergistic Effect, Improved Therapeutic Index, and Penetration of 3D Cancer Cell Spheroids. *Int. J. Mol. Sci.* 19, 2773. doi:10.3390/ijms19092773

Lv, Y., Hu, R., Zhu, G., Zhang, X., Mei, L., Liu, Q., et al. (2015). Preparation and Biomedical Applications of Programmable and Multifunctional DNA Nanoflowers. *Nat. Protoc.* 10, 1508–1524. doi:10.1038/nprot.2015.078

Lv, Z., Zhu, Y., and Li, F. (2021). DNA Functional Nanomaterials for Controlled Delivery of Nucleic Acid-Based Drugs. *Front. Bioeng. Biotechnol.* 9, 720291. doi:10.3389/fbioe.2021.720291

Ma, S., Li, X., Wang, X., Cheng, L., Li, Z., Zhang, C., et al. (2019). Current Progress in CAR-T Cell Therapy for Solid Tumors. *Int. J. Biol. Sci.* 15, 2548–2560. doi:10.7150/ijbs.34213

Ma, Y., Wang, Z., Ma, Y., Han, Z., Zhang, M., Chen, H., et al. (2018). A Telomerase-Responsive DNA Icosahedron for Precise Delivery of Platinum Nanodrugs to Cisplatin-Resistant Cancer. *Angew. Chem. Int. Ed.* 57, 5389–5393. doi:10.1002/anie.201801195

Martínez-López, A. L., Pangua, C., Reboredo, C., Campión, R., Morales-Gracia, J., and Irache, J. M. (2020). Protein-Based Nanoparticles for Drug Delivery Purposes. *Int. J. Pharm.* 581, 119289. doi:10.1016/j.ijpharm.2020.119289

Mei, Y., Tang, L., Xiao, Q., Zhang, Z., Zhang, Z., Zang, J., et al. (2021). Reconstituted High Density Lipoprotein (rHDL), a Versatile Drug Delivery Nanoplatform for Tumor Targeted Therapy. *J. Mat. Chem. B* 9, 612–633. doi:10.1039/d0tb02139c

Meir, R., Shamalov, K., Sadan, T., Motiei, M., Yaari, G., Cohen, C. J., et al. (2017). Fast Image-Guided Stratification Using Anti-Programmed Death Ligand 1 Gold Nanoparticles for Cancer Immunotherapy. *ACS Nano* 11, 11127–11134. doi:10.1021/acsnano.7b05299

Mi, P. (2020). Stimuli-Responsive Nanocarriers for Drug Delivery, Tumor Imaging, Therapy and Theranostics. *Theranostics* 10, 4557–4588. doi:10.7150/thno.38069

Mohsen, M. G., and Kool, E. T. (2016). The Discovery of Rolling Circle Amplification and Rolling Circle Transcription. *Acc. Chem. Res.* 49, 2540–2550. doi:10.1021/acs.accounts.6b00417

Monti, D. M., Ferraro, G., and Merlino, A. (2019). Ferritin-Based Anticancer Metallodrug Delivery: Crystallographic, Analytical and Cytotoxicity Studies. *Nanomedicine* 20. 101997. doi:10.1016/j.nano.2019.04.001

Mulder, W. J. M., van Leent, M. M. T., Lameijer, M., Fisher, E. A., Fayad, Z. A., and Pérez-Medina, C. (2018). High-Density Lipoprotein Nanobiologics for Precision Medicine. *Acc. Chem. Res.* 51, 127–137. doi:10.1021/acs.accounts.7b00339

Musetti, S., and Huang, L. (2018). Nanoparticle-Mediated Remodeling of the Tumor Microenvironment to Enhance Immunotherapy. *ACS Nano* 12, 11740–11755. doi:10.1021/acsnano.8b05893

Navya, P. N., Kaphle, A., Srinivas, S. P., Bhargava, S. K., Rotello, V. M., and Daima, H. K. (2019). Current Trends and Challenges in Cancer Management and Therapy Using Designer Nanomaterials. *Nano Converg.* 6, 23. doi:10.1186/s40580-019-0193-2

Ng, K. K., Lovell, J. F., and Zheng, G. (2011). Lipoprotein-Inspired Nanoparticles for Cancer Theranostics. *Acc. Chem. Res.* 44, 1105–1113. doi:10.1021/ar200017e

Olden, B. R., Cheng, Y., Yu, J. L., and Pun, S. H. (2018). Cationic Polymers for Non-viral Gene Delivery to Human T Cells. *J. Control. Release* 282, 140–147. doi:10.1016/j.jconrel.2018.02.043

Orlova, E. V., Sherman, M. B., Chiu, W., Mowri, H., Smith, L. C., and Gotto, A. M. (1999). Three-Dimensional Structure of Low Density Lipoproteins by Electron Cryomicroscopy. *Proc. Natl. Acad. Sci. U.S.A.* 96, 8420–8425. doi:10.1073/pnas.96.15.8420

Pan, Y., Yang, J., Luan, X., Liu, X., Li, X., Yang, J., et al. (2019). Near-Infrared Upconversion-Activated CRISPR-Cas9 System: A Remote-Controlled Gene Editing Platform. *Sci. Adv.* 5, eaav7199. doi:10.1126/sciadv.aav7199

Parayath, N. N., Stephan, S. B., Koehne, A. L., Nelson, P. S., and Stephan, M. T. (2020). In Vitro-Transcribed Antigen Receptor mRNA Nanocarriers for Transient Expression in Circulating T Cells *In Vivo*. *Nat. Commun.* 11, 6080. doi:10.1038/s41467-020-19486-2

Pham, T., Roth, S., Kong, J., Guerra, G., Narasimhan, V., Pereira, L., et al. (2018). An Update on Immunotherapy for Solid Tumors: A Review. *Ann. Surg. Oncol.* 25, 3404–3412. doi:10.1245/s10434-018-6658-4

Qin, H., Zhao, R., Qin, Y., Zhu, J., Chen, L., Di, C., et al. (2021). Development of a Cancer Vaccine Using *In Vivo* Click-Chemistry-Mediated Active Lymph Node Accumulation for Improved Immunotherapy. *Adv. Mater.* 33. e2006007. doi:10.1002/adma.202006007

Que, W.-c., Qiu, H.-q., Cheng, Y., Liu, M.-b., and Wu, C.-y. (2018). PTEN in Kidney Cancer: A Review and Meta-Analysis. *Clin. Chim. Acta* 480, 92–98. doi:10.1016/j.cca.2018.01.031

Rafii, S., Tashkandi, E., Bukhari, N., and Al-Shamsi, H. O. (2022). Current Status of CRISPR/Cas9 Application in Clinical Cancer Research: Opportunities and Challenges. *Cancers (Basel)* 14, 947. doi:10.3390/cancers14040947

Ramezani, H., and Dietz, H. (2020). Building Machines with DNA Molecules. *Nat. Rev. Genet.* 21, 5–26. doi:10.1038/s41576-019-0175-6

Raniolo, S., Vindigni, G., Ottaviani, A., Unida, V., Iacovelli, F., Manetto, A., et al. (2018). Selective Targeting and Degradation of Doxorubicin-Loaded Folate-Functionalized DNA Nanocages. *Nanomedicine Nanotechnol. Biol. Med.* 14, 1181–1190. doi:10.1016/j.nano.2018.02.002

Raza, F., Siyu, L., Zafar, H., Kamal, Z., Zheng, B., Su, J., et al. (2022). Recent Advances in Gelatin-Based Nanomedicine for Targeted Delivery of Anti-Cancer Drugs. *Cpd* 28, 380–394. doi:10.2174/1381612827666211102100118

Raza, F., Zafar, H., You, X., Khan, A., Wu, J., and Ge, L. (2019). Cancer Nanomedicine: Focus on Recent Developments and Self-Assembled Peptide Nanocarriers. *J. Mat. Chem. B* 7, 7639–7655. doi:10.1039/c9tb01842e

Raza, F., Zafar, H., Zhang, S., Kamal, Z., Su, J., Yuan, W., et al. (2021). Recent Advances in Cell Membrane-Derived Biomimetic Nanotechnology for Cancer Immunotherapy. *Adv. Healthc. Mater.* 10, e2002081. doi:10.1002/adhm.202002081

Riley, R. S., June, C. H., Langer, R., and Mitchell, M. J. (2019). Delivery Technologies for Cancer Immunotherapy. *Nat. Rev. Drug Discov.* 18, 175–196. doi:10.1038/s41573-018-0006-z

Rosenblum, D., Gutkin, A., Kedmi, R., Ramishetti, S., Veiga, N., Jacobi, A. M., et al. (2020). CRISPR-Cas9 Genome Editing Using Targeted Lipid Nanoparticles for Cancer Therapy. *Sci. Adv.* 6, eabc9450. doi:10.1126/sciadv.abc9450

Rui, M., Xin, Y., Li, R., Ge, Y., Feng, C., and Xu, X. (2017). Targeted Biomimetic Nanoparticles for Synergistic Combination Chemotherapy of Paclitaxel and Doxorubicin. *Mol. Pharm.* 14, 107–123. doi:10.1021/acs.molpharmaceut.6b00732

Rui, Y., Wilson, D. R., and Green, J. J. (2019). Non-Viral Delivery to Enable Genome Editing. *Trends Biotechnol.* 37, 281–293. doi:10.1016/j.tibtech.2018.08.010

Sahin, U., and Türeci, Ö. (2018). Personalized Vaccines for Cancer Immunotherapy. *Science* 359, 1355–1360. doi:10.1126/science.aar7112

Salter, A. M., and Brindley, D. N. (1988). The Biochemistry of Lipoproteins. *J. Inherit. Metab. Dis.* 11, 4–17. doi:10.1007/BF01800566

Saxena, M., van der Burg, S. H., Melief, C. J. M., and Bhardwaj, N. (2021). Therapeutic Cancer Vaccines. *Nat. Rev. Cancer* 21, 360–378. doi:10.1038/s41568-021-00346-0

Scheetz, L. M., Yu, M., Li, D., Castro, M. G., Moon, J. J., and Schwendeman, A. (2020). Synthetic HDL Nanoparticles Delivering Docetaxel and CpG for Chemoimmunotherapy of Colon Adenocarcinoma. *Int. J. Mol. Sci.* 21, 1777. doi:10.3390/ijms21051777

Shen, S., Dai, H., Fei, Z., Chai, Y., Hao, Y., Fan, Q., et al. (2021). Immunosuppressive Nanoparticles for Management of Immune-Related Adverse Events in Liver. *ACS Nano* 15, 9111–9125. doi:10.1021/acsnano.1c02391

Shen, Z., Zhou, L., Zhang, C., and Xu, J. (2020). Reduction of Circular RNA Foxo3 Promotes Prostate Cancer Progression and Chemoresistance to Docetaxel. *Cancer Lett.* 468, 88–101. doi:10.1016/j.canlet.2019.10.006

Sherman, M. B., Orlova, E. V., Decker, G. L., Chiu, W., and Pownall, H. J. (2003). Structure of Triglyceride-Rich Human Low-Density Lipoproteins According to Cryoelectron Microscopy. *Biochemistry* 42, 14988–14993. doi:10.1021/bi0354738

Shi, J., Yang, X., Li, Y., Wang, D., Liu, W., Zhang, Z., et al. (2020). MicroRNA-Responsive Release of Cas9/sgRNA from DNA Nanoflower for Cytosolic Protein Delivery and Enhanced Genome Editing. *Biomaterials* 256, 120221. doi:10.1016/j.biomaterials.2020.120221

Shi, S.-J., Wang, L.-J., Han, D.-H., Wu, J.-H., Jiao, D., Zhang, K.-L., et al. (2019). Therapeutic Effects of Human Monoclonal PSMA Antibody-Mediated TRIM24 siRNA Delivery in PSMA-Positive Castration-Resistant Prostate Cancer. *Theranostics* 9, 1247–1263. doi:10.7150/thno.29884

Smith, T. T., Stephan, S. B., Moffett, H. F., Mcknight, L. E., Ji, W., Reiman, D., et al. (2017). *In Situ* Programming of Leukaemia-Specific T Cells Using Synthetic DNA Nanocarriers. *Nat. Nanotech.* 12, 813–820. doi:10.1038/nnano.2017.57

Sobhani, N., Roviello, G., D'Angelo, A., Roudi, R., Neeli, P. K., and Generali, D. (2021). p53 Antibodies as a Diagnostic Marker for Cancer: A Meta-Analysis. *Molecules* 26, 6215. doi:10.3390/molecules26206215

Song, N., Zhang, J., Zhai, J., Hong, J., Yuan, C., and Liang, M. (2021). Ferritin: A Multifunctional Nanoplatform for Biological Detection, Imaging Diagnosis, and Drug Delivery. *Acc. Chem. Res.* 54, 3313–3325. doi:10.1021/acs.accounts.1c00267

Subhan, M. A., and Torchilin, V. P. (2019). Efficient Nanocarriers of siRNA Therapeutics for Cancer Treatment. *Transl. Res.* 214, 62–91. doi:10.1016/j.trsl.2019.07.006

Sukumar, U. K., Rajendran, J. C. B., Gambhir, S. S., Massoud, T. F., and Paulmurugan, R. (2020). SP94-Targeted Triblock Copolymer Nanoparticle Delivers Thymidine Kinase-P53-Nitroreductase Triple Therapeutic Gene and Restores Anticancer Function Against Hepatocellular Carcinoma *In Vivo*. *ACS Appl. Mat. Interfaces* 12, 11307–11319. doi:10.1021/acsami.9b20071

Sung, H., Ferlay, J., Siegel, R. L., Laversanne, M., Soerjomataram, I., Jemal, A., et al. (2021). Global Cancer Statistics 2020: GLOBOCAN Estimates of Incidence and Mortality Worldwide for 36 Cancers in 185 Countries. *CA A Cancer J. Clin.* 71, 209–249. doi:10.3322/caac.21660

Tan, S., Li, D., and Zhu, X. (2020). Cancer Immunotherapy: Pros, Cons and Beyond. *Biomed. Pharmacother.* 124, 109821. doi:10.1016/j.biopha.2020.109821

Tan, T., Wang, H., Cao, H., Zeng, L., Wang, Y., Wang, Z., et al. (2018). Deep Tumor-Penetrated Nanocages Improve Accessibility to Cancer Stem Cells for Photothermal-Chemotherapy of Breast Cancer Metastasis. *Adv. Sci.* 5, 1801012. doi:10.1002/advs.201801012

Tang, L., Zheng, Y., Melo, M. B., Mabardi, L., Castaño, A. P., Xie, Y.-Q., et al. (2018). Enhancing T Cell Therapy Through TCR-Signaling-Responsive Nanoparticle Drug Delivery. *Nat. Biotechnol.* 36, 707–716. doi:10.1038/nbt.4181

Tao, Y., Yi, K., Hu, H., Shao, D., and Li, M. (2021). Coassembly of Nucleus-Targeting Gold Nanoclusters with CRISPR/Cas9 for Simultaneous Bioimaging and Therapeutic Genome Editing. *J. Mater Chem. B* 9, 94–100. doi:10.1039/d0tb01925a

Tesarova, B., Musilek, K., Rex, S., and Heger, Z. (2020). Taking Advantage of Cellular Uptake of Ferritin Nanocages for Targeted Drug Delivery. *J. Control. Release* 325, 176–190. doi:10.1016/j.jconrel.2020.06.026

Thaxton, C. S., Rink, J. S., Naha, P. C., and Cormode, D. P. (2016). Lipoproteins and Lipoprotein Mimetics for Imaging and Drug Delivery. *Adv. Drug Deliv. Rev.* 106, 116–131. doi:10.1016/j.addr.2016.04.020

Vaddepally, R. K., Kharel, P., Pandey, R., Garje, R., and Chandra, A. B. (2020). Review of Indications of FDA-Approved Immune Checkpoint Inhibitors Per NCCN Guidelines with the Level of Evidence. *Cancers (Basel)* 12, 738. doi:10.3390/cancers12030738

van den Bulk, J., Verdegaal, E. M., and de Miranda, N. F. (2018). Cancer Immunotherapy: Broadening the Scope of Targetable Tumours. *Open Biol.* 8, 180037. doi:10.1098/rsob.180037

Veroniaina, H., Wu, Z., and Qi, X. (2021). Innate Tumor-Targeted Nanozyme Overcoming Tumor Hypoxia for Cancer Theranostic Use. *J. Adv. Res.* 33, 201–213. doi:10.1016/j.jare.2021.02.004

Wang, B., Yuan, Y., Han, L., Ye, L., Shi, X., and Feng, M. (2014). Recombinant Lipoproteins Reinforce Cytotoxicity of Doxorubicin to Hepatocellular Carcinoma. *J. Drug Target.* 22, 76–85. doi:10.3109/1061186x.2013.839687

Wang, C.-S., Chang, C.-H., Tzeng, T.-Y., Lin, A. M.-Y., and Lo, Y.-L. (2021a). Gene-Editing by CRISPR-Cas9 in Combination with Anthracycline Therapy via Tumor Microenvironment-Switchable, EGFR-Targeted, and Nucleus-Directed Nanoparticles for Head and Neck Cancer Suppression. *Nanoscale Horiz.* 6, 729–743. doi:10.1039/d1nh00254f

Wang, J., Li, Y., and Nie, G. (2021b). Multifunctional Biomolecule Nanostructures for Cancer Therapy. *Nat. Rev. Mater.* 6, 766–783. doi:10.1038/s41578-021-00315-x

Wang, X., Zhong, X., Li, J., Liu, Z., and Cheng, L. (2021c). Inorganic Nanomaterials with Rapid Clearance for Biomedical Applications. *Chem. Soc. Rev.* 50, 8669–8742. doi:10.1039/d0cs00461h

Wang, Z., Song, L., Liu, Q., Tian, R., Shang, Y., Liu, F., et al. (2021d). A Tubular DNA Nanodevice as a siRNA/Chemo-Drug Co-Delivery Vehicle for Combined Cancer Therapy. *Angew. Chem. Int. Ed.* 60, 2594–2598. doi:10.1002/anie.202009842

Wang, Z., Zhao, Y., Zhang, S., Chen, X., Sun, G., Zhang, B., et al. (2022). Re-Engineering the Inner Surface of Ferritin Nanocage Enables Dual Drug Payloads for Synergistic Tumor Therapy. *Theranostics* 12, 1800–1815. doi:10.7150/thno.68459

Wei, G., Wang, Y., Yang, G., Wang, Y., and Ju, R. (2021). Recent Progress in Nanomedicine for Enhanced Cancer Chemotherapy. *Theranostics* 11, 6370–6392. doi:10.7150/thno.57828

Wei, Y., Gu, X., Sun, Y., Meng, F., Storm, G., and Zhong, Z. (2020). Transferrin-Binding Peptide Functionalized Polymersomes Mediate Targeted Doxorubicin Delivery to Colorectal Cancer *In Vivo*. *J. Control. Release* 319, 407–415. doi:10.1016/j.jconrel.2020.01.012

Wu, T., Liu, J., Liu, M., Liu, S., Zhao, S., Tian, R., et al. (2019). A Nanobody-Conjugated DNA Nanoplatform for Targeted Platinum-Drug Delivery. *Angew. Chem. Int. Ed.* 58, 14224–14228. doi:10.1002/anie.201909345

Xing, R., Wang, X., Zhang, C., Zhang, Y., Wang, Q., Yang, Z., et al. (2009). Characterization and Cellular Uptake of Platinum Anticancer Drugs Encapsulated in Apoferritin. *J. Inorg. Biochem.* 103, 1039–1044. doi:10.1016/j.jinorgbio.2009.05.001

Xu, W., He, W., Du, Z., Zhu, L., Huang, K., Lu, Y., et al. (2021). Functional Nucleic Acid Nanomaterials: Development, Properties, and Applications. *Angew. Chem. Int. Ed.* 60, 6890–6918. doi:10.1002/anie.201909927

Yahya, E. B., and Alqadhi, A. M. (2021). Recent Trends in Cancer Therapy: A Review on the Current State of Gene Delivery. *Life Sci.* 269, 119087. doi:10.1016/j.lfs.2021.119087

Yan, J., Chen, J., Zhang, N., Yang, Y., Zhu, W., Li, L., et al. (2020). Mitochondria-Targeted Tetrahedral DNA Nanostructures for Doxorubicin Delivery and Enhancement of Apoptosis. *J. Mater. Chem. B* 8, 492–503. doi:10.1039/c9tb02266j

Yang, M., Li, J., Gu, P., and Fan, X. (2021). The Application of Nanoparticles in Cancer Immunotherapy: Targeting Tumor Microenvironment. *Bioact. Mater.* 6, 1973–1987. doi:10.1016/j.bioactmat.2020.12.010

Yang, Z., Zhang, N., Ma, T., Liu, L., Zhao, L., and Xie, H. (2020). Engineered Bovine Serum Albumin-Based Nanoparticles with pH-Sensitivity for Doxorubicin Delivery and Controlled Release. *Drug Deliv.* 27, 1156–1164. doi:10.1080/10717544.2020.1797243

Yardley, D. A. (2013). Nab-Paclitaxel Mechanisms of Action and Delivery. *J. Control. Release* 170, 365–372. doi:10.1016/j.jconrel.2013.05.041

Yin, H., Yuan, X., Luo, L., Lu, Y., Qin, B., Zhang, J., et al. (2020). Appropriate Delivery of the CRISPR/Cas9 System Through the Nonlysosomal Route: Application for Therapeutic Gene Editing. *Adv. Sci.* 7, 1903381. doi:10.1002/advs.201903381

Zafar, H., Raza, F., Ma, S., Wei, Y., Zhang, J., and Shen, Q. (2021). Recent Progress on Nanomedicine-Induced Ferroptosis for Cancer Therapy. *Biomater. Sci.* 9, 5092–5115. doi:10.1039/d1bm00721a

Zang, J., Chen, H., Zhao, G., Wang, F., and Ren, F. (2017). Ferritin Cage for Encapsulation and Delivery of Bioactive Nutrients: From Structure, Property to Applications. *Crit. Rev. Food Sci. Nutr.* 57, 3673–3683. doi:10.1080/10408398.2016.1149690

Zhan, T., Rindtorff, N., Betge, J., Ebert, M. P., and Boutros, M. (2019). CRISPR/Cas9 for Cancer Research and Therapy. *Seminars Cancer Biol.* 55, 106–119. doi:10.1016/j.semcancer.2018.04.001

Zhang, D. Y., Dmello, C., Chen, L., Arrieta, V. A., Gonzalez-Buendia, E., Kane, J. R., et al. (2020a). Ultrasound-Mediated Delivery of Paclitaxel for Glioma: A

Comparative Study of Distribution, Toxicity, and Efficacy of Albumin-Bound versus Cremophor Formulations. *Clin. Cancer Res.* 26, 477–486. doi:10.1158/1078-0432.ccr-19-2182

Zhang, G., Zhang, Z., and Yang, J. (2017a). DNA Tetrahedron Delivery Enhances Doxorubicin-Induced Apoptosis of HT-29 Colon Cancer Cells. *Nanoscale Res. Lett.* 12, 495. doi:10.1186/s11671-017-2272-9

Zhang, J., Cheng, D., He, J., Hong, J., Yuan, C., and Liang, M. (2021a). Cargo Loading within Ferritin Nanocages in Preparation for Tumor-Targeted Delivery. *Nat. Protoc.* 16, 4878–4896. doi:10.1038/s41596-021-00602-5

Zhang, L., Abdullah, R., Hu, X., Bai, H., Fan, H., He, L., et al. (2019a). Engineering of Bioinspired, Size-Controllable, Self-Degradable Cancer-Targeting DNA Nanoflowers via the Incorporation of an Artificial Sandwich Base. *J. Am. Chem. Soc.* 141, 4282–4290. doi:10.1021/jacs.8b10795

Zhang, P., Ouyang, Y., Sohn, Y. S., Nechushtai, R., Pikarsky, E., Fan, C., et al. (2021b). pH- and miRNA-Responsive DNA-Tetrahedra/Metal-Organic Framework Conjugates: Functional Sense-And-Treat Carriers. *ACS Nano* 15, 6645–6657. doi:10.1021/acsnano.0c09996

Zhang, Q., Chen, J., Shen, J., Chen, S., Liang, K., Wang, H., et al. (2019b). Inlaying Radiosensitizer onto the Polypeptide Shell of Drug-Loaded Ferritin for Imaging and Combinational Chemo-Radiotherapy. *Theranostics* 9, 2779–2790. doi:10.7150/thno.33472

Zhang, Q., Jiang, Q., Li, N., Dai, L., Liu, Q., Song, L., et al. (2014). DNA Origami as an *In Vivo* Drug Delivery Vehicle for Cancer Therapy. *ACS Nano* 8, 6633–6643. doi:10.1021/nn502058j

Zhang, S., Shen, J., Li, D., and Cheng, Y. (2021c). Strategies in the Delivery of Cas9 Ribonucleoprotein for CRISPR/Cas9 Genome Editing. *Theranostics* 11, 614–648. doi:10.7150/thno.47007

Zhang, Y., Fang, F., Li, L., and Zhang, J. (2020b). Self-Assembled Organic Nanomaterials for Drug Delivery, Bioimaging, and Cancer Therapy. *ACS Biomater. Sci. Eng.* 6, 4816–4833. doi:10.1021/acsbiomaterials.0c00883

Zhang, Y., Jiang, S., Zhang, D., Bai, X., Hecht, S. M., and Chen, S. (2017b). DNA-Affibody Nanoparticles for Inhibiting Breast Cancer Cells Overexpressing HER2. *Chem. Commun.* 53, 573–576. doi:10.1039/c6cc08495h

Zhang, Y., Lin, S., Wang, X., and Zhu, G. (2019c). Nanovaccines for Cancer Immunotherapy. *Wiley Interdiscip. Rev. Nanomed. Nanobiotechnol.* 11. e1559. doi:10.1002/wnan.1559

Zhang, Y., Sun, T., and Jiang, C. (2018). Biomacromolecules as Carriers in Drug Delivery and Tissue Engineering. *Acta Pharm. Sin. B* 8, 34–50. doi:10.1016/j.apsb.2017.11.005

Zhang, Z., Jiao, Y., Zhu, M., and Zhang, S. (2017c). Nuclear-Shell Biopolymers Initiated by Telomere Elongation for Individual Cancer Cell Imaging and Drug Delivery. *Anal. Chem.* 89, 4320–4327. doi:10.1021/acs.analchem.7b00591

Zhang, Z., Wan, T., Chen, Y., Chen, Y., Sun, H., Cao, T., et al. (2019d). Cationic Polymer-Mediated CRISPR/Cas9 Plasmid Delivery for Genome Editing. *Macromol. Rapid Commun.* 40, e1800068. doi:10.1002/marc.201800068

Zhao, F., Tian, J., An, L., and Yang, K. (2014). Prognostic Utility of Gene Therapy with Herpes Simplex Virus Thymidine Kinase for Patients with High-Grade Malignant Gliomas: A Systematic Review and Meta Analysis. *J. Neurooncol.* 118, 239–246. doi:10.1007/s11060-014-1444-z

Zhao, H., Yuan, X., Yu, J., Huang, Y., Shao, C., Xiao, F., et al. (2018). Magnesium-Stabilized Multifunctional DNA Nanoparticles for Tumor-Targeted and pH-Responsive Drug Delivery. *ACS Appl. Mat. Interfaces* 10, 15418–15427. doi:10.1021/acsami.8b01932

Zhao, Y., Liang, M., Li, X., Fan, K., Xiao, J., Li, Y., et al. (2016). Bioengineered Magnetoferritin Nanoprobes for Single-Dose Nuclear-Magnetic Resonance Tumor Imaging. *ACS Nano* 10, 4184–4191. doi:10.1021/acsnano.5b07408

Zhen, Z., Tang, W., Chen, H., Lin, X., Todd, T., Wang, G., et al. (2013). RGD-Modified Apoferritin Nanoparticles for Efficient Drug Delivery to Tumors. *ACS Nano* 7, 4830–4837. doi:10.1021/nn305791q

Zhong, X., Zhang, H., Zhu, Y., Liang, Y., Yuan, Z., Li, J., et al. (2020). Circulating Tumor Cells in Cancer Patients: Developments and Clinical Applications for Immunotherapy. *Mol. Cancer* 19, 15. doi:10.1186/s12943-020-1141-9

Zhu, G., Zhang, F., Ni, Q., Niu, G., and Chen, X. (2017a). Efficient Nanovaccine Delivery in Cancer Immunotherapy. *ACS Nano* 11, 2387–2392. doi:10.1021/acsnano.7b00978

Zhu, W. J., Yang, S. D., Qu, C. X., Zhu, Q. L., Chen, W. L., Li, F., et al. (2017b). Low-Density Lipoprotein-Coupled Micelles with Reduction and pH Dual Sensitivity for Intelligent Co-Delivery of Paclitaxel and siRNA to Breast Tumor. *Int. J. Nanomedicine* 12, 3375–3393. doi:10.2147/IJN.S126310

Zhu, Y., Wang, L., Li, Y., Huang, Z., Luo, S., He, Y., et al. (2020). Injectable pH and Redox Dual Responsive Hydrogels Based on Self-Assembled Peptides for Anti-Tumor Drug Delivery. *Biomater. Sci.* 8, 5415–5426. doi:10.1039/d0bm01004a

Conflict of Interest: The authors declare that the research was conducted in the absence of any commercial or financial relationships that could be construed as a potential conflict of interest.

Publisher's Note: All claims expressed in this article are solely those of the authors and do not necessarily represent those of their affiliated organizations, or those of the publisher, the editors and the reviewers. Any product that may be evaluated in this article, or claim that may be made by its manufacturer, is not guaranteed or endorsed by the publisher.

GLOSSARY

NDSs, nanoparticulate delivery systems
NPs, nanoparticles
NFs, nanoflowers
RCA, rolling circle amplification
TfR, transferrin receptor
HFt, human ferritin
HoSF, horse spleen ferritin
AfFtn, Archaeoglobus fulgidus ferritin
PfFt, Pyrococcus furiosus ferritin
HFn, heavy chain ferritin
LFn, light chain ferritin
VLDL, very low density lipoproteins
LDL, low density lipoproteins
HDL, high-density lipoprotein
rHDL, recombinant HDL apolipoprotein B-100
SR-B1, scavenger receptor class B type 1
p53, protein 53
PTEN, phosphatase and tensin homolog
HSV-TK, herpes simplex virus thymidine kinase
mRNA, messenger RNA
siRNA, small interfering RNA
sgRNA, single guide RNA
CAR-T, chimeric antigen receptor T
CTLA-4, cytotoxic-T-lymphocyte-associated protein 4
PD-1, program death 1
PD-L1, program death-ligand 1
CRISPR, clustered regularly interspaced short palindromic repeat
mAbs, monoclonal antibodies
ICIs, immune checkpoint inhibitors
irAIEs, immune-related adverse events

frontiers | Frontiers in Pharmacology

ORIGINAL RESEARCH
published: 08 July 2022
doi: 10.3389/fphar.2022.909851

In Vitro, *Ex Vivo*, and *In Vivo* Evaluation of Nanoparticle-Based Topical Formulation Against *Candida albicans* Infection

Sajid Khan Sadozai[1], *Saeed Ahmad Khan*[1]*, *Abdul Baseer*[2], *Rooh Ullah*[2], *Alam Zeb*[3] and *Marc Schneider*[4]*

[1]Department of Pharmacy, Kohat University of Science and Technology, Kohat, Pakistan, [2]Department of Pharmacy, Abasyn University, Peshawar, Pakistan, [3]Riphah Institute of Pharmaceutical Sciences, Riphah International University, Islamabad, Pakistan, [4]Department of Pharmacy, Biopharmaceutics and Pharmaceutical Technology, Saarland University, Saarbrücken, Germany

OPEN ACCESS

Edited by:
Syed Nasir Abbas Bukhari,
Al Jouf University, Saudi Arabia

Reviewed by:
Bhupinder Singh,
Lovely Professional University, India
Pedro Fonte,
University of Algarve, Portugal
Sobia Noreen,
University of Innsbruck, Austria

***Correspondence:**
Saeed Ahmad Khan
saeedkhanphd@gmail.com
Marc Schneider
marc.schneider@uni-saarland.de

Specialty section:
This article was submitted to Experimental Pharmacology and Drug Discovery, a section of the journal Frontiers in Pharmacology

Received: 31 March 2022
Accepted: 16 May 2022
Published: 08 July 2022

Citation:
Sadozai SK, Khan SA, Baseer A, Ullah R, Zeb A and Schneider M (2022) In Vitro, Ex Vivo, and In Vivo Evaluation of Nanoparticle-Based Topical Formulation Against Candida albicans Infection. Front. Pharmacol. 13:909851. doi: 10.3389/fphar.2022.909851

Ketoconazole is commonly used in the treatment of topical fungal infections. The therapy requires frequent application for several weeks. Systemic side effects, allergic reactions, and prolonged treatment are often associated with non-compliance and therapy failure. Hence, we developed an optimized topical antifungal gel that can prolong the release of drug, reduce systemic absorption, enhance its therapeutic effect, and improve patient compliance. Ketoconazole-loaded PLGA nanoparticles were prepared by the emulsion/solvent evaporation method and were characterized with respect to colloidal properties, surface morphology, and drug entrapment efficiency. The optimized ketoconazole-loaded PLGA nanoparticles and commercially available silver nanoparticles were incorporated into a Carbopol 934P-NF gel base. This arrangement was characterized and compared with commercially available 2% ketoconazole cream to assess physical characteristics of the gel, *in vitro* drug release, *ex vivo* skin permeation and retention, and *in vivo* studies on Wister male albino rats. The results showed that polymeric PLGA nanoparticles were very effective in extending the release of ketoconazole in our optimized formulation. Nanoparticles were smooth, spherical in shape, and below 200 nm in size which is consistent with the data obtained from light scattering and SEM images. The *ex vivo* data showed that our gel formulation could strongly reduce drug permeation through the skin, and more than 60% of the drug was retained on the upper surface of the skin in contrast to 38.42% of the commercial cream. The *in vivo* studies showed that gel formulation could effectively treat the infection. This study demonstrates that our topical gel could be effective in sustaining the release of drug and suggests its potential use as a possible strategy to combat antifungal-resistant *Candida albicans*.

Keywords: Ketoconazole, PLGA, topical gel, sustained release, *Candida albicans*

1 INTRODUCTION

Superficial fungal infections are very common throughout the world, and incidences are increasing day by day. The prevalence of fungal skin infections comprises 20–25% of the world population (Buil et al., 2020). Superficial fungal infections are keratinophilic in nature. They increase in the keratinized layers of the skin, hair, and nails (Borgers et al., 2005). They are predominately caused by the dermatophyte members of three common genera: *Microsporum*, *Trichophyton*, and *Epidermophyton*. *C. albicans* and other non-albicans species mostly cause superficial fungal infections. The severity of the infection depends upon the site and the involvement of fungal species (Sharifzadeh et al., 2013; Cleveland et al., 2015; Klingspor et al., 2015). In various studies, it was reported that candidiasis was treated by several compounds of different classes, either belonging to polyenes, azoles, echinocandins, nucleoside analogs, or allylamines. Their efficacy depends on the type, site of infection, and susceptibility of the *Candida* species (Pfaller et al., 2013; Pappas et al., 2016). Geographical and environmental conditions play a vital role in the causative agent and spread of fungal skin infections. Superficial fungal infections are more common in tropical regions where the temperature is warm and humid. Similarly, the chance of spread is more in low socioeconomic conditions and densely populated areas where opportunities for skin-to-skin contact are more, with poor hygienic conditions (Coates et al., 2020).

A topical drug delivery system is administered on the skin's outer surface to treat local dermatological conditions (Ashara et al., 2014). They are used when local action is desired rather than a systemic effect. The drug remains on the skin or may penetrate the dermis through the epidermal layers, but is not absorbed in the systemic circulation (Choi and Maibach, 2005). The topical dosage form is formulated to achieve maximum therapeutic effect locally by incorporating active agents, protective agents, adsorbents, cleansing agents, emollients, viscosity builders, and stabilizers (Choudhury et al., 2017). A topical drug delivery system has numerous advantages over oral and injectable systems. Therefore, researchers are focusing on developing such drug delivery systems to avoid the problems associated with other routes of administration (Borgheti-Cardoso et al., 2016). The topical dosage form is applied to the affected area only, and it by-passes the first-pass metabolism and releases the drug directly to the site where it is needed (Mayba and Gooderham, 2018). It can be easily administered, with no need for any special skills or help of another person for administration (Eastman et al., 2014). The topical dosage form is applied on the skin to deliver the drug directly to the area to be treated, thus proving prolonged localized action without frequent administration (Waghule et al., 2019).

Various antifungal agents are commercially available in conventional topical dosage forms like creams, lotions, and sprays. The problem with these conventional topical dosage forms is that they require frequent applications for several weeks until infection signs and symptoms completely disappear. Systemic side effects, as well as local side effects, are associated with it. Thus, conventional topical dosage forms are often inappropriate and might be considered inconvenient by the patient, resulting in therapy failure (Firooz et al., 2015).

Topical ketoconazole is one of the most often used azole drugs, commercially available as 2% cream and ointment (Andriole, 2000). Based on its hydrophobic nature, it belongs to Biopharmaceutics Classification System (BCS) class II drug. Ketoconazole has limited bioavailability and poor aqueous solubility (Sodeifian et al., 2021). Therefore, a higher amount of drug is required to achieve the desired antifungal activity. The mechanism of action of the azole group is to inhibit the 14α-sterol enzyme encoded by the ERG11 gene, involved in the biosynthesis of fungal cell membrane sterol ergosterol. Some species of non-candida albicans are naturally resistant to azoles, causing therapy failure when used against these species. It was reported that *Candida* had the ability to develop high-level resistance against azoles (Oxman et al., 2010; Fothergill et al., 2014). Additionally, it can cause side effects such as allergic and severe skin reactions. Similarly, prolonged therapy is required to achieve the desired results. To overcome these problems, a combination of available drugs with the blend of modern technology is required to overcome the aforementioned problems.

In nanomedicines, silver nanoparticles (AgNPs) have gained incredible popularity in recent years. AgNPs are used in different fields for different purposes (Monteiro et al., 2012). Silver's biological efficacy has been known for centuries, but their assessment as AgNPs on a scientific basis has received tremendous attention in recent years (Rasheed et al., 2017). AgNPs and specifically the released silver ions can inhibit the replication of microbial agents, including bacteria and fungi, by disrupting cellular membranes and other organelles (Tang and Zheng, 2018). AgNPs attributed synergistic effects against various resistant species when combined with antibiotics (Zhang et al., 2014; Liao et al., 2019; Sadozai et al., 2020).

Improving the efficacy of available antimicrobials against resistant strains is a key concern for future treatments. Recently in various studies, AgNPs showed promising results effectively killing antibiotic-resistant microorganisms (Scandorieiro et al., 2016; Patra and Baek, 2017; Wang et al., 2020). AgNPs could be used in combination with existing antimicrobials to enhance their effectiveness and reverse antimicrobial resistance (Pfalzgraff et al., 2018; McNeilly et al., 2021). In a recent study, biogenic silver nanoparticles in combination with fluconazole or metronidazole showed synergistic effects and reduced the effects of anticandidal agents (Aabed and Mohammed, 2021). Similarly, in another study, AgNPs in combination with antibiotics showed strong synergistic effects against *E. coli*, *P. aeruginosa*, and *S. aureus* (Deng et al., 2016). It was also reported that minimum inhibitory concentration (MIC) of β-lactam antibiotics against *E. coli* was reduced several folds when used in combination with AgNPs (Patra and Baek, 2017). It was also reported that AgNPs enhanced the activity of ampicillin, tetracycline, streptomycin, and rifampicin (Markowska et al., 2014).

The current study is being designed to overcome the bioavailability issues of ketoconazole. The emulsion/solvent evaporation method was used for the preparation of ketoconazole-loaded poly(lactide-co-glycolide) (PLGA)

TABLE 1 | Various formulations of ketoconazole-loaded PLGA nanoparticles.

Formulation	Ketoconazole (mg)	PLGA (mg)	DCM (ml)	2% PVA (ml)	Sonication	
					AMP (%)	Time (sec)
100% keto, 0% PLGA	100	0	2	10	40	90
75% keto, 25% PLGA	75	25	2	10	40	90
50% keto, 50% PLGA	50	50	2	10	40	90
25% keto, 75% PLGA	25	75	2	10	40	90
15% keto, 85% PLGA	15	85	2	10	40	90
12.5% keto, 87.5% PLGA	12.5	87.5	2	10	40	90
0% keto, 100% PLGA	0	100	2	10	40	90

Keto, ketoconazole; PLGA, poly(lactide-co-glycolide); DCM, dichloromethane; PVA, polyvinyl alcohol; AMP, amplitude.

nanoparticles (<300 nm) that could potentially assemble in wrinkles (Stracke et al., 2006; Schneider et al., 2009) and hair follicles (Lademann et al., 2008) to provide a prolonged release to the skin tissues. The optimized ketoconazole-loaded PLGA nanoparticles and commercially available silver nanoparticles (AgNPs) were incorporated into a Carbopol 934P-NF base gel for topical application. The objective of this study was to sustain the release of ketoconazole at the site of action and reduce its permeation into systemic circulation. Moreover, the optimized gel formulation was evaluated and compared with commercially available cream to effectively treat skin infection induced by the resistant strain of *Candida albicans* in Wister male albino rats.

2 MATERIALS AND METHODS

2.1 Materials

Ketoconazole was a kind gift from Bryon Pharmaceuticals Pvt. Ltd., Peshawar, Pakistan. Poly(lactide-co-glycolide) (PLGA) was purchased from Evonik Industries, Darmstadt, Germany. Silver nanoparticles (≤ 20 nm) were purchased from PHORNANO Holding GmbH, Austria. Polyvinyl alcohol (PVA) soluble in cold water was used (Mowiol 4–88, Kuraray Europe, Hattersheim, Germany); Fisher Scientific Chemicals Ltd., United Kingdom, provided dichloromethane. Methanol was purchased from VWR International GmbH (Darmstadt, Germany). Potassium dihydrogen phosphate and di-potassium hydrogen phosphate were purchased from Merck, Germany. Tween® 20 was purchased from Sigma life science. Carbopol 934P-NF and triethanolamine were purchased from Sigma-Aldrich (Steinheim, Germany). Ultra-pure distilled and deionized water was produced with Millipore ultra-pure water system (Milli-Q® Synthesis).

2.2 Preparation of Ketoconazole-Loaded PLGA Nanoparticles

As reported previously, ketoconazole-loaded PLGA nanoparticles were prepared by the emulsion/solvent evaporation method (Sadozai et al., 2020). Various formulations were designed, as shown in **Table 1**. Different drug/polymer ratios were studied to investigate their impact on the physicochemical properties of nanoparticles.

2.3 Characterization of Nanoparticles

2.3.1 Dynamic Light Scattering

The mean particle size and polydispersity index (PDI) of nanoparticles were determined by dynamic light scattering (DLS) with a Zetasizer Nano ZS (Malvern Instruments, Malvern, UK) at 25°C with a backscattering angle of 172° as discussed in our previous study (Ashjari et al., 2020; Sadozai et al., 2020).

2.3.2 Scanning Electron Microscopy

Scanning electron microscopy (SEM) was used to determine the morphology, particle size, and size distribution of nanoparticles (EVO HD 15, Carl Zeiss Microscopy GmbH. Jena, Germany). Samples were coated with a thin layer of gold to provide sufficient conductivity (Q150RES, Quorum Technologies Ltd, East Grinstead, United Kingdom). Micrographs were taken with an acceleration voltage of 5 kV (Sa-Barreto et al., 2017).

2.3.3 % Entrapment Efficiency (%EE)

The ketoconazole entrapped in nanoparticles was determined using high-performance liquid chromatography (HPLC) according to an established method with some modifications (Kanaujia et al., 2011; Sadozai et al., 2020). The entrapment efficiency (%EE) was determined indirectly according to a previously reported method (Shafique et al., 2017). Briefly, the supernatant obtained after centrifugation of nanoparticles was collected. The amount of free ketoconazole present in the supernatant was determined analytically and the encapsulation was calculated using the following equation:

$$EE\% = \frac{Total\ drug\ added\ (mg) - Free\ drug\ in\ supernatant\ (mg)}{\text{Total drug added (mg)}} \mathbf{X\ 100} \quad (1)$$

The drug loading was calculated using the entrapped drug amount (total drug–free drug) with respect to the formulation weight:

$$\text{Drug loading} = \frac{\text{Drug entrapped (mg)}}{\text{Weight of dried powder (mg)}} \text{X } 100 \quad (2)$$

2.3.4 Drug Release Studies

The drug release from nanoparticles was studied in phosphate buffered saline (PBS) pH 7.4 at 37°C. Tween-20 2.0% w/v was

TABLE 2 | Various formulations of Carbopol 934P-NF gel base.

Serial No.	Formulation	Carbopol 934P-NF (mg)	Water (ml)	pH
1	1% Carbopol gel	1	100	6.5
2	1.5% Carbopol gel	1.5	100	6.5
3	2% Carbopol gel	2	100	6.5
4	2.5% Carbopol gel	2.5	100	6.5

TABLE 3 | Various formulations of Carbopol 934P-NF containing ketoconazole and silver nanoparticles.

Ingredient	Formulations						
	Blank gel	PLGA NP gel	Keto NP gel	Keto PLGA NP gel	Keto-drug gel	AgNP gel	Keto PLGA NP + AgNP gel
Carbopol gel 934P-NF	2%	2%	2%	2%	2%	2%	2%
Blank PLGA NPs	—	16.5%	---	—	—	—	—
Ketoconazole NPs	—		2%	—	—	—	—
Ketoconazole PLGA NPs	—	—	—	*16.5%	—	—	*16.5%
Ketoconazole pure Drug	—	—	—	—	2%	—	—
Silver NPs	—	—	—	—	—	1%	1%

*PLGA NPs (100% PLGA NPs), ketoconazole NPs (100% ketoconazole NPs), ketoconazole PLGA NPs (12.5% ketoconazole + 87.5% PLGA NPs) *(16.5% w/v particles correspond to 2% ketoconazole pure drug based on entrapment efficiency).*

added to the dissolution medium to obtain sink conditions since ketoconazole is insoluble in PBS pH 7.4; briefly, 10 mg of drug-loaded nanoparticles were dispersed in 50 ml dissolution medium and stirred continuously at 37°C. 1.0 ml aliquots were withdrawn at predetermined intervals and centrifuged at 24,000 RCF. The supernatant was collected, and the pellets were redispersed in a 1.0-ml dissolution medium and then returned to the main tube (Kataoka et al., 2019). The amount of ketoconazole in the samples was analyzed using the established HPLC method.

2.4 Gel Preparation

2.4.1 Preparation of Carbopol 934P-NF Gel Base

Carbopol 934P-NF was selected as a hydrophilic polymer due to its high purity and pharmaceutical grade. Formulations were prepared based on the concentration of Carbopol 934P-NF, as shown in **Table 2**. Each formulation was prepared by taking a specific amount of Carbopol 934P-NF and adding deionized water in a beaker to make the final volume up to 100 ml. The beaker was placed on a magnetic stirrer for 3 hours to make a slurry. The polymer solution was kept in a dark place overnight for complete swelling. The pH was adjusted to 6.5 by the addition of triethanolamine (Jana et al., 2014). After adjusting the pH, physical characteristics and spreadability studies were carried out to choose the suitable Carbopol gel base.

2.4.2 Incorporation of NPs in Gel

After the selection of a suitable Carbopol 934P-NF gel base, different formulations were prepared w/w by incorporating the optimized formulation of ketoconazole-loaded PLGA nanoparticles, pure ketoconazole nanoparticles without PLGA, silver nanoparticles, optimized ketoconazole-loaded PLGA nanoparticles and silver nanoparticles in combination and pure drug (ketoconazole), as shown in **Table 3**. All formulations were mixed properly with the help of mortar and pestle to ensure uniform distribution.

2.5 Evaluation of the Gels

2.5.1 Appearance

All gel formulations' appearance was inspected visually for color, clarity, and presence of any particulate. This test is important for esthetic point of view as well as patient compliance (Parashar et al., 2013).

2.5.2 pH

pH plays an important role in the preparation of Carbopol gel 934P-NF as it is highly pH-sensitive. The pH of all the gel formulations was measured using Mettler Toledo Seven Compact S230 (Germany) pH meter. About 1 mg sample from all formulations was taken and stirred with distilled water to form a uniform suspension. The volume came up to 50 ml and pH of the suspension was measured (Parashar et al., 2013).

2.5.3 Spreadability

Spreadability is an important parameter to determine the quality of a topical preparation. The therapeutic efficacy depends on the gel's ability to spread uniformly and easily. Spreadability studies were performed using a stainless-steel apparatus having a lower plate and upper plate. In between these two plates was a sample compartment in which gel was loaded. After loading the gel in this compartment, a transparent plastic scale was set above the steel plate holding the sample in the center. Two glass plates weighing 2 kg were placed above the transparent scale. As the glass plate is placed above it, the gel spreads on the scale. The diameter was measured after 5 minutes. Each sample was measured three times to get the mean value.

TABLE 4 | Clinical parameters and therapeutic efficacy.

Serial no.	Clinical parameter	Score
1	No sign of infection	0
2	Slight erythematous skin	1
3	Redness on a well-defined area with swelling, bald patches, and scaly area	2
4	Large areas with redness and ulceration	3
5	Loss of hair and partial damage to the skin	4
6	Excessive damage to the skin with complete hair loss	5

2.5.4 Drug Content Determination

For the uniform distribution of the drug in a gel formulation, drug content was determined. The gel's drug content was determined by accurately weighing 1.0 mg of gel and dissolving it in 40 ml PBS solution containing 2% Tween-20 in a beaker under continuous stirring to make a suspension. This suspension was filtered (0.45-micron filter paper), and the drug content was analyzed by the described HPLC method.

2.6 *In Vitro* Drug Release Studies

In vitro drug release studies were carried out by using Franz diffusion cells with a spherical diameter of 25 mm and a diffusion area of 3.56 cm^2. The diffusion was investigated across a cellulose membrane with a thickness of 4.44 mm and pore size of 12–14,000 Da was placed between the lower cell reservoir and glass cell top containing the sample. The receiving compartment was filled with a solution of PBS and 2% Tween-20 with a pH adjusted to 7.4 and temperature maintained at 32.0 ± 0.5°C with a magnetic stirrer. 0.1 mg of each sample was applied evenly on the Teflon sheet, having a diameter of 14 mm which was placed above the cellulose membrane in the donor compartment. After predetermined intervals (1, 2, 4, 8, 12, and 24 h), 400 μL receptor fluid was withdrawn from the receiving compartment and was replaced with the same volume of fresh solution (Bhaskar et al., 2009). Samples were analyzed on RP-HPLC to determine the *in vitro* drug release from the Carbopol gel.

2.7 *Ex Vivo* Studies

2.7.1 Skin Permeation Studies

Excised human skin as the gold standard for *ex vivo* studies was used. The human abdominal skin from Caucasian female patients was obtained from Caritas Klinik, Lebach, Germany. The procedure was approved by the Ethical Committee of the Aerztekammer des Saarlandes, Saarbrücken, Germany (Code 204/08, 22 December 2008). The fatty tissue attached to the epidermis was removed, carefully washed with water, and stored in the refrigerator. From the stored skin, circular samples with a diameter of 25 mm were punched out with the help of a plunger and hammer. The epidermis was thoroughly washed with water and allowed to hydrate for 1 h before being mounted on the Franz diffusion cells with the stratum corneum (S.C.) facing the donor compartment (Luengo et al., 2006; Luengo et al., 2021). Drug delivery from the topical dosage form is an important parameter in developing a formulation, to determine how much drug is released or permeated through the skin to reach the dermis and potentially the systemic circulation.

2.7.2 Tape Stripping Method

The tape stripping method was employed to determine the amount of drug present in the uppermost layer of the skin stratum corneum (Luengo et al., 2021) to treat the superficial infection of the skin. After 24 h, the skin was removed from the Franz diffusion cell. The skin surface was washed 10 times with a cotton swab to remove the extra amount of gel present on the skin's surface. The skin was then placed on a flat surface and fixed with the help of pins at the corners of the skin so that the stratum corneum faced upward. Modified Scotch Magic Tape was used to remove the stratum corneum from the skin completely. A tape strip was applied on the skin, and after application, a roller was rolled with a uniform force above it in two opposite directions, and the tape strip was removed with the help of forceps. The same procedure was repeated 12 times to ensure complete removal of stratum corneum, which was also checked with the help of Squame scan, which is used to scan the stratum carenum protein content on the tape strips (Hahn et al., 2010). The first two strips were discarded, and the remaining ten were mixed with mono isopropyl amine methanol (2:500) and shaken to dissolve adhered ketoconazole in the solvent mixture. Then, the solvent mixture was allowed to evaporate the organic mixture on a magnetic stirrer. The release medium was added to dissolve the drug and filtered through a 0.45-μm membrane filter. The filtrate was analyzed for drug concentration by RP-HPLC as discussed earlier (Escobar-Chávez et al., 2008; Clausen et al., 2016).

2.7.3 Drug Retention Studies

In addition to determining the amount of drug present on SC, the percentage of drug penetrated was also analyzed by washing the skin 10 times with a cotton swab and cutting the skin into small pieces, and the skin was homogenized in the solvent mixture for 2 h to extract the drug. The resulting solution was centrifuged for 10 min at 2795 RCF, and the supernatant was analyzed on RP-HPLC with the same procedure described earlier (Minghetti et al., 2006).

2.8 *In Vivo* Studies

The *in vivo* studies were carried out according to the guidelines approved by the ethical committee of the Department of Pharmacy, KUST vide notification number "Ref NO./KUST/Ethical Committee/2286".

2.8.1 Experimental Design

Wistar albino male rats (230–250 mg) were obtained from PCSIR laboratories in Peshawar. All the animals were acclimatized under standard animal house conditions for 7 days before starting the *in*

vivo studies. The animals were randomly divided into four groups, each group containing six Wistar albino healthy male rats. Group-I was treated with keto-drug gel, 2% Carbopol gel, and 2% pure ketoconazole drug as a positive control. Group-II was considered negative control and treated with a blank gel containing 2% Carbopol gel without any drug. Group-III was treated with test gel keto PLGA NPs and AgNPs containing 2% Carbopol and 2% optimized Keto PLGA nanoparticles combined with AgNPs. Group-IV was treated with commercially available 2% ketoconazole cream considered as the reference group. After inoculation with a fungal infection, all the animals were treated once a day for 7 days, respectively.

2.8.2 Preparation of *Candida albicans* Strain

The *C. albicans* strain was obtained from Shifa International Hospital Pathology Department (ATCC-10231) and was allowed to grow for 48 h at 30°C on sabouraud dextrose agar media. The cells were collected, washed, and suspended in sterile saline to get 10^7 CFU/ml (Barros et al., 2007).

2.8.3 Induction of Fungal Infection

All rats were prepared by removing the hair on the dorsal area approximately 2 cm^2 with the help of a razor or electrical hair trimming machine. Each rat was intradermally injected with 100 µl of *C. albicans* strain having a concentration of 10^7 CFU/ml. The injected area was rubbed with cotton to avoid edema. The fungal infection was observed after 3 days of inoculation in the affected area (Araújo et al., 2009).

2.8.4 Clinical Investigations

All the animals were clinically examined periodically at days 0, 4, and 7 in a week to check the symptoms such as rashes, red or purple patches, white patches over the affected area, scaling, cracking, pimples filled with puss, hair loss, and the treatment efficacy will be scored from 0 to 5 according to a modification of the reported clinical parameters as shown in **Table 4** (Aggarwal et al., 2013).

2.9 Statistical Analysis

The results were expressed as mean ± standard deviation using different statistical tests. The results were compared by one-way analysis of variance (ANOVA). The data were considered significantly different at p-value < 0.05 by using Graph Pad Prism software (Version 5).

3 RESULTS AND DISCUSSION

To overcome the challenges faced in conventional drug delivery systems, a topical nanocarrier drug delivery system emerged as a suitable alternative (Díaz and Vivas-Mejia, 2013). The advantages of nanocarrier as a drug delivery system are high surface-to-volume ratio, nanoscale size, and easy fabrication with controlled physicochemical properties. Topical nanocarrier as a drug delivery system enhances the aqueous solubility of hydrophobic drugs. They can extend shelf life, prolong and control the release of drug (Lavan et al., 2003), improve the stability against moisture (Lockman et al., 2002), modify the pharmacodynamics and pharmacokinetics of the drug, and reduces the side effects by targeting the specific site at the cellular level (Allen and Cullis, 2004). The objective of this study was to design and fabricate a topical gel preparation that can prolong the release of ketoconazole, reduce its systemic absorption, and improve its therapeutic potential against resistant *C. albicans* strain when combined with AgNPs.

3.1 Characterization of Nanoparticles

3.1.1 Physicochemical Properties of Nanoparticles

The physicochemical properties of ketoconazole-loaded PLGA nanoparticles are reported in our previous article (Sadozai et al., 2020); briefly, a drug-to-polymer ratio was optimized in terms of particle size, PDI, and entrapment efficiency. It was observed that as the concentration of the drug increases, the particle size and PDI values increase. The maximum size was observed for formulation in which nanoparticles were prepared without PLGA polymer. The nanoparticles formulation containing 12.5% ketoconazole and 87.5% PLGA was chosen to prepare nanoparticle-laden gels since this formulation provides a sustained release of ketoconazole, shown in **Figure 1**. These nanoparticles are in the range of 150–200 nm, having discrete and homogeneous boundaries and no sign of agglomerations, as evident from SEM images (**Figure 2**), consistent with the data obtained from dynamic light scattering. However, the particles prepared with 100% drug are slightly larger.

3.1.2 Scanning Electron Microscopy

The morphology, including the shape and surface of all the formulations, were studied by SEM. The images revealed uniformity and spherically shaped particles.

3.2 Optimization of Polymer Concentration for Preparation of Gel

Before the incorporation of nanoparticles, the gel formulation was optimized based on polymer concentration. Carbopol 934P-NF–grade polymer was used for the preparation of gels. The prepared gel formulations were examined visually for appearance and homogeneity. As shown in **Table 5**, all the formulations were clear and transparent with no particles. The clarity of gel plays an important role in acceptance and compliance. So, from an esthetic point of view, patients' acceptability is important to achieve the desired results. The formulation containing 2% Carbopol 934P-NF showed excellent homogeneity without any lumps, as shown in **Table 5**, compared with other formulations. Formulation containing 2% Carbopol 934P NF showed acceptable physicochemical results at pH 6.5 compared with other formulations depicted in **Table 5**.

3.3 Incorporation of Nanoparticles in the Gel

Six different topical gel formulations were prepared, as shown in **Table 6**. Optimized ketoconazole-loaded PLGA nanoparticles (12.5% keto and 87.5% PLGA) were selected to incorporate w/w in the topical gel. This formulation was selected based on our previous studies, which showed extended release of drug for more than 24 h and the amorphous nature of the drug, which can enhance bioavailability at

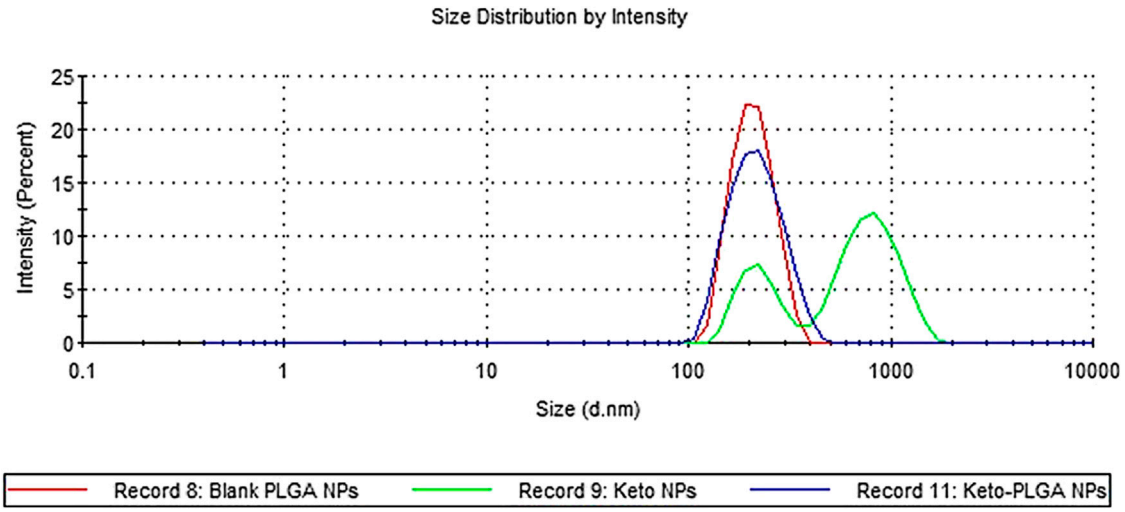

FIGURE 1 | Particle size distribution by intensity. Blank PLGA NPs contain no drug, keto PLGA NPs contain 12.5% ketoconazole and 87.5% PLGA, and keto NPs contain 100% ketoconazole.

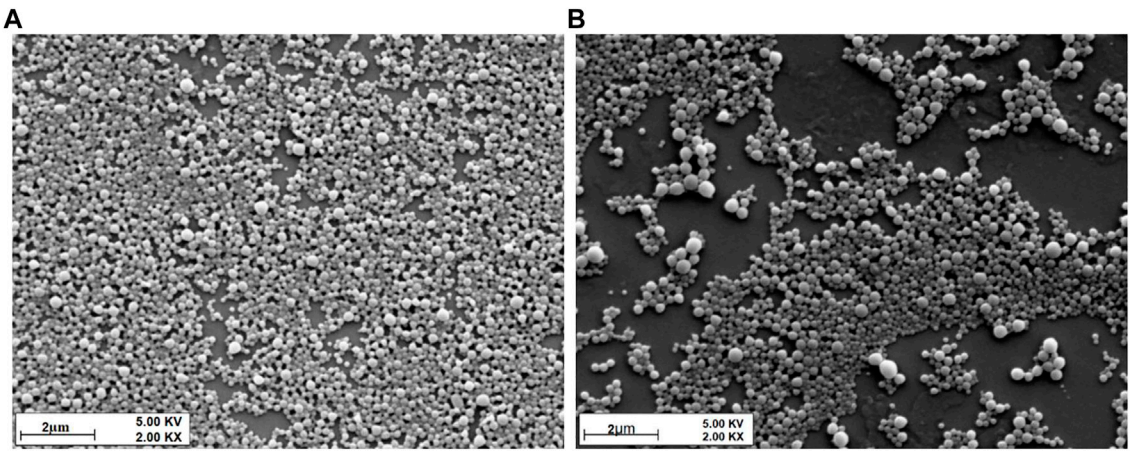

FIGURE 2 | SEM micrographs of **(A)** 12.5% keto and 87.5% PLGA NP formulation and **(B)** 100% keto and 0% PLGA formulation.

TABLE 5 | Physicochemical characteristics of Carbopol 934P-NF gel base.

S. no.	Formulation	Appearance	*Homogeneity	Spreadability (mm)
1	1% Carbopol gel	Clear	***	Out of scale
2	1.5% Carbopol gel	Clear	***	Out of scale
3	2% Carbopol gel	Clear	***	28.33 ± 0.47
4	2.5% Carbopol gel	Clear	**	20.66 ± 0.47

Homogeneity: * = Fair, ** = Good, * = Excellent.*

the site of infection. Similarly, silver nanoparticles were incorporated along with ketoconazole-loaded PLGA nanoparticles due to their synergistic effect. It was shown that silver nanoparticles could improve the efficacy of ketoconazole-loaded PLGA nanoparticles several folds when used together (Sadozai et al., 2020).

3.4 Physicochemical Properties of the Nanoparticle-Laden Gel

3.4.1 Spreadability

The spreadability of gels prepared with different concentrations of Carbopol 934P-NF was also evaluated. At the lower composition of

TABLE 6 | Physicochemical characteristics of optimized gel formulations.

	Formulation	Appearance	*Homogeneity	Spreadability (mm)	**Drug content in gel (%)
1	Blank gel	Clear, opaque	***	28.33 ± 0.47	Nil
2	PLGA NP gel	Clear, opaque	***	26.01 ± 0.80	Nil
3	Keto NP gel	Clear, opaque	***	29.66 ± 1.24	2
4	Keto PLGA NP gel	Clear, opaque	***	26.33 ± 0.47	2
5	Keto-drug gel	Clear, opaque	***	33.33 ± 0.47	2
6	AgNP gel	Clear, half-white	***	34.66 ± 1.24	Nil
7	Keto PLGA NP + AgNP gel	Clear, half-white	***	32.00 ± 0.50	2
8	Commercial cream***	Clear, white	***	26.33 ± 0.47	2

*Homogeneity: * = Fair, ** = Good, *** = Excellent.*

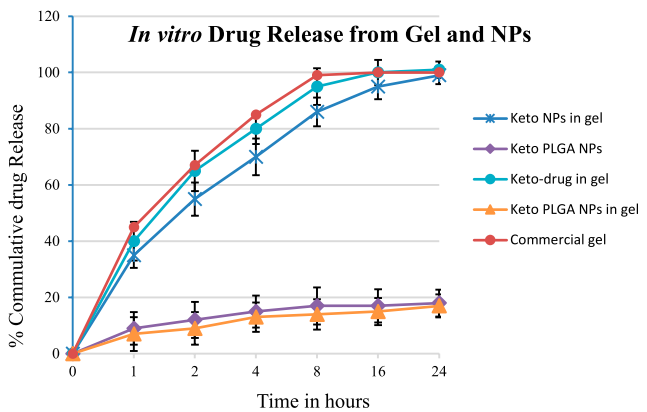

FIGURE 3 | *In vitro* drug release of optimized gel formulations using Franz diffusion cell and optimized NPs formulation (12.5% keto + 87.5% PLGA NPs). Mean ± standard deviation (n = 3).

the polymer, the formulations failed the spreadability test due to low viscosity, whereas at higher composition, the spreadability of gel decreases. 2% Carbopol 934P NF was chosen as the optimum formulation for the preparation of nanoparticle-laden gels since it showed excellent spreadability properties, that is, 28.33 ± 0.47 mm. The spreadability of the gel was not markedly affected by the incorporation of nanoparticles (**Table 6**). The spreadability values were very close to the commercially available product that was found to have 26.33 ± 0.5 mm (**Table 6**).

3.5 *In Vitro* Drug Release Studies

In vitro drug release studies were carried out using modified Franz diffusion cells together with cellulose membranes, as discussed in **Section 2.6**. The released drug amount obtained was plotted against time (**Figure 3**). The % cumulative drug released data which revealed that formulations keto-drug gel and keto NP gel release 35–40% of the drug in the first hour. In contrast, the optimized keto PLGA NP gel formulation releases 7% drug in the first hour. In comparison, the commercially available cream releases more than 45% of the drug. In 2 h, the optimized formulation releases 9% of the drug.

In contrast, keto-drug gel and keto NP gel released 55% and 65% of the drug, respectively, and commercially available cream releases up to 67% in the first 2 hours. The same pattern was observed, and 99% drug was released in the first 8 h from commercial cream, 95% from the keto-drug gel, 86% from keto NP gel, and 14% from keto PLGA NP gel. In the first 24 h, the optimized keto PLGA NP gel formulation released 17%, whereas all other formulations released more than 99% of the drug, as shown in **Figure 4**. These data suggested that not only Carbopol gel prolonged the drug release as compared to commercially available products, but the PLGA incorporating ketoconazole in the optimized formulation played an important role in delaying the drug release from the gel for several days (Chavan et al., 2021), which can be beneficial in reducing the frequency of gel application and availability of the drug for a longer period at the site of application. Similarly, keto PLGA NP gel provides an environment around the infectious skin where the drug is available for a longer period and extends the drug's release (Waghule et al., 2020). The Carbopol gel acts as a reservoir in which the drug permeates and treats the targeted infectious area (Silva et al., 2015).

3.6 *Ex Vivo* Drug Penetration Studies

Ex vivo studies were carried out using human abdominal skin obtained from Caritas Klinik, Lebach, Germany. To determine the amount of drug that permeated from the gel through the skin, was retained on the skin, and deported in the skin layers, skin permeation studies, tape stripping method, and drug as discussed in detail in **Section 2.7** were performed.

3.6.1 Skin Permeation Studies

The data obtained from skin permeation studies, as shown in **Figure 5**, revealed that the maximum amount of drug permeated from commercially available cream through the skin compared with other gel preparations. Permeation profile indicated that 154 μg/cm^2 (14.47%) of drug permeated through the skin from commercial ketoconazole cream, 135 μg/cm^2 (11.96%) from keto-drug gel, and 191 μg/cm^2 (15.98%) from keto NP gel, whereas it was 20 μg/cm^2 (1.67%) from keto PLGA NP gel. The results obtained from skin permeation studies showed that our optimized keto PLGA NP gel formulation was

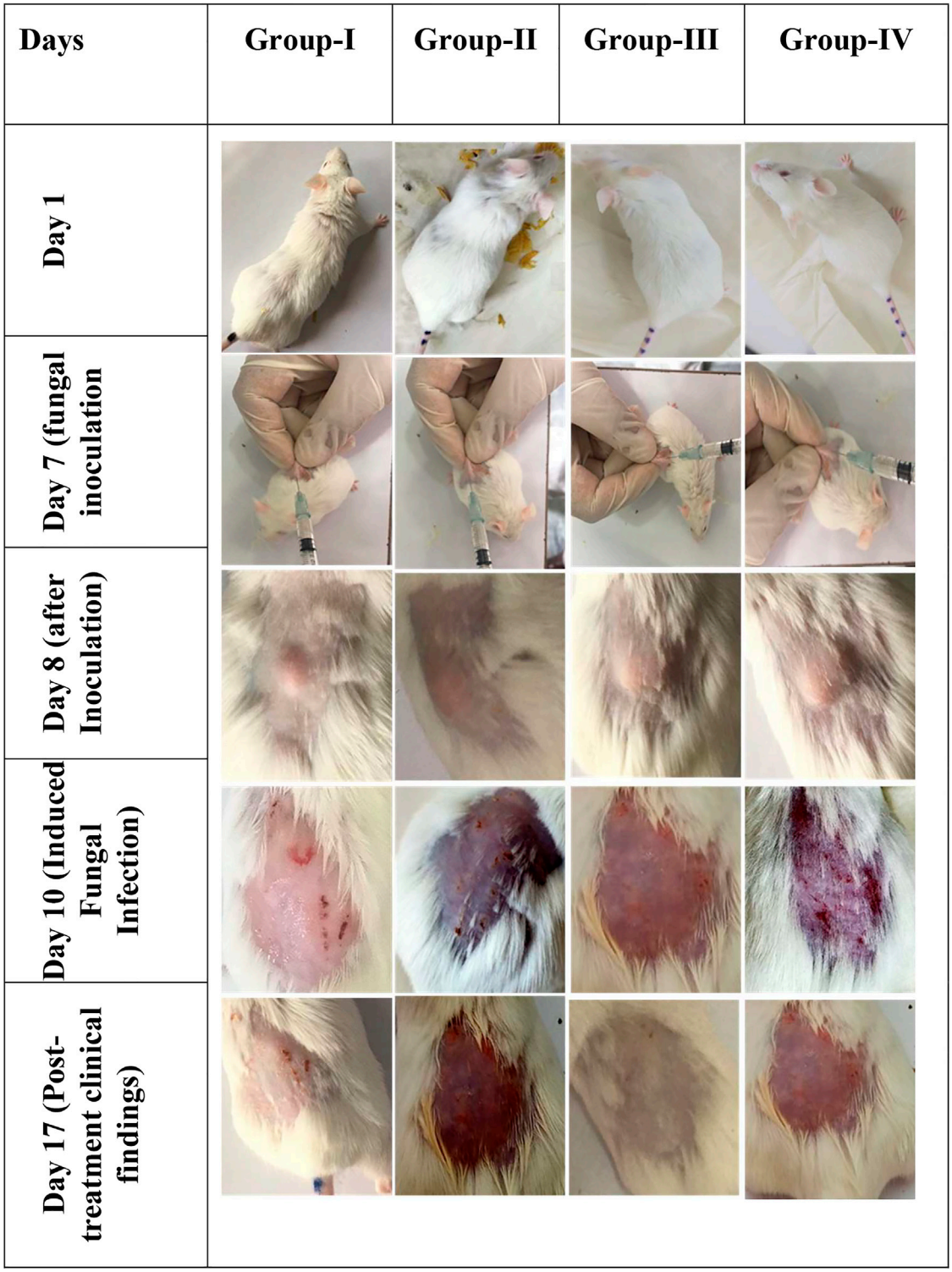

FIGURE 4 | *In vivo* images of male Wister albino rats. Gel preparations were applied on the dorsal skin surface and observed for clinical findings (n = 6).

successful in stopping the drug from permeation through the skin and only a negligible amount of drug permeated, which was less than 2% compared with the commercial cream from which more than 14% of drug permeated through the skin. Similarly, keto NP gel also showed higher permeation (15.98%) than Keto PLGA NP gel. The improved permeation of ketoconazole nanoparticles may

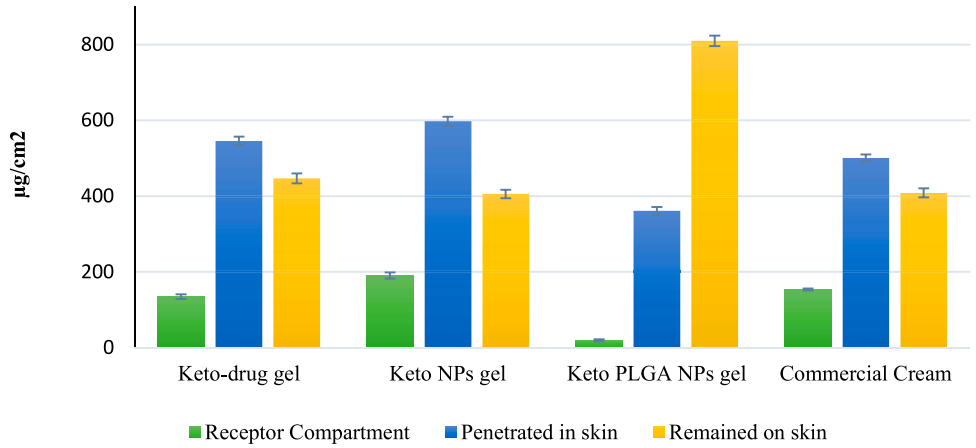

FIGURE 5 | *Ex vivo* studies on the human abdominal skin. Comparison of drug concentration at different levels of human skin. Mean ± standard deviation (n = 3).

TABLE 7 | Wister albino male rats' group for *in vivo* studies.

Group-I	Positive control	Keto-drug gel
Group-II	Negative control	Blank gel
Group-III	Test drug	Keto PLGA NPs + AgNPs gel
Group-IV	Reference drug	Commercial cream

be due to the particulate nature of ketoconazole. PLGA really retains the drug inside, thus not much material can permeate in case of ketoconazole-loaded PLGA nanoparticles. This might be due to the smaller size and larger surface area of the nanoparticles. It was also observed that PLGA polymer plays an important role in this nano-drug delivery system by providing a network-like structure in which the drug was uniformly distributed and difficult to permeate through the skin (Dinarvand et al., 2011). It was clear from these results that the optimized keto PLGA NP gel formulation is an ideal topical nano-drug delivery system that can hinder the permeation of the drug through the skin for a longer period and make it difficult to reach the systemic circulation. By controlling the skin permeation, our topical nano-drug delivery system could be used to minimize the systemic side effects co-related with these antifungal agents. Similarly, they can provide a better therapeutic reservoir on the skin to treat superficial infections effectively (Wu and Guy, 2009).

3.6.2 Tape Stripping Method

The tape stripping method was performed to evaluate the amount of drug present on the surface of the stratum corneum using modified Scotch Magic Tape. The results obtained from HPLC data, as shown in **Figure 5**, demonstrated that the least amount of drug 406 µg/cm^2 (33.97%) was present on the skin surface after applying the keto NP gel formulation. Similarly, keto-drug gel showed 447 µg/cm^2 (39.62%) of the drug on the skin surface, and commercially available cream showed 409 µg/cm^2 (38.42%) of the drug on the skin surface. Our optimized gel formulation showed excellent results as compared with the other gel formulations and commercial cream. Keto PLGA NP gel showed 810 µg/cm^2 (67.97%) of the drug on the surface of the skin's stratum corneum. For an ideal topical formulation to treat superficial infections, the drug should be on the skin's surface for a longer period and in a larger amount. The results showed that optimized gel formulation could be used as a nano-drug delivery carrier because it showed less permeation and more drug retention on the skin's surface.

3.6.3 Drug Retention Studies

A drug retention study was performed to estimate the amount of drug retained inside the skin after 24 h. The results obtained from HPLC shown in **Figure 5** demonstrated that for keto-drug gel, keto NP gel, and commercial cream, 48.40, 50.04, and 47.08% of the drug penetrated, respectively, which was far more than that from our optimized gel keto PLGA NP gel formulation (only 30.36% of the drug). The reason could be sustained release of drug from PLGA polymer within 24 h. Most of the drug remained on the surface (wrinkles and hair follicles) in the upper layer of the skin, unlike other gel preparations in which the drug release was not controlled and the drug permeated through various skin layers. These results also favored our optimized gel formulation for controlled and targeted drug release for a longer period. The PLGA played a dominant role in sustaining and retaining the drug on the skin and preventing permeation into the systemic circulation. We aimed to achieve maximum sustaining effect to avoid frequent application of the gel and minimize the drug dose. The problem of drug therapy failure could be easily addressed by applying our topical gel preparation.

3.7 *In Vivo* Evaluation of the Gel Against Fungal Infection

In vivo studies were carried out using male Wister albino rats approximately 230–250 mg in weight. All the animals were kept with care, and we strictly followed the ethical protocols. They

TABLE 8 | *In vivo* investigation of gel preparations and clinical findings.

S. no.	Group	Clinical finding	Score
1	Group-I	Slight erythematous skin, infection does not get cured completely	1
2	Group-II	Redness, loss of hair, and partial damage to the skin	4
3	Group-III	No sign of infection, hair regrowth started	0
4	Group-IV	Slight erythematous on the skin, infection does not get cured completely	1

were divided randomly into four groups, as shown in **Table 7**, and each group contained six male rats.

The infected area was treated with 1 mg of gel according to the group for 3 days, and we keenly observed the clinical parameters and effectiveness of applied gel on days 3, 5, and 7 as described in **Table 4** and scored accordingly in **Table 8**.

It was observed that Group-II showed no sign of improvement, and clinical findings showed redness of the skin, loss of hair, and partial damage to the skin at the site of infection as it was treated with blank gel without any drug. Group-I and group-IV showed a little improvement compared to Group-II, and slight erythema was present, but the infection was not completely cured at the end of treatment of the infected area. Whereas Group-III showed maximum effectiveness from the gel preparation and no sign of infection was observed, our optimized keto PLGA NP + AgNP gel successfully cured the fungal infection as compared with the commercially available cream and keto-drug gel shown in **Figure 4**. The combination of ketoconazole-loaded PLGA NPs and AgNP-laden gel could be used as an ideal topical formulation to treat superficial skin infection caused by resistant strains of *C. albicans* and as a reference for those drugs having bioavailability and resistance issues.

4 CONCLUSION

This study supported the rational selection of polymer concentration to control the particle size and prolong the drug release for more than 24 h. Carbopol 934P-NF was used as a gel base; various formulations were prepared and their physicochemical properties were studied. Physicochemical characteristics of all the gel formulations were acceptable as compared with the commercial product. *In vitro* studies showed that keto PLGA NP gel formulation sustained the drug release for more than 24 h, whereas commercial cream and keto-drug gel released 99% drug in less than 24 h. *Ex vivo* studies supported our objective by limiting the permeation of drugs through the human abdominal skin compared to the commercial product and pure ketoconazole drug and maintaining a reasonable amount of drug at the skin's surface to combat superficial fungal infection for a longer period. *In vivo* studies revealed that a combination of ketoconazole-loaded PLGA nanoparticles and AgNPs can effectively treat the fungal infection induced by a resistant strain of *C. albicans*. The combination of ketoconazole-loaded PLGA nanoparticles and AgNPs as a topical gel formulation could provide an opportunity to develop a cost-effective approach to achieve optimal therapeutic performance against resistant fungal infections at a much lower dose than is currently used. Additionally, it will enhance patient compliance by reducing the frequent application.

DATA AVAILABILITY STATEMENT

The raw data supporting the conclusion of this article will be made available by the authors, without undue reservation.

ETHICS STATEMENT

The animal study was reviewed and approved by Ethical Committee, Kohat University of Science and Technology.

AUTHOR CONTRIBUTIONS

SK: Formal analysis, and project administration. SS: Conceptualization, methodology, and drafting. AB: Interpretation. RU: Investigation. MS: Supervision and manuscript review.

FUNDING

Higher Education Commission of Pakistan–funded Project, number: 7783/KPK/NRPU/R&D/HEC/2017. KUST ORIC, Research and Development Fund Program, Ref.No. KUST/ORIC/1050.

REFERENCES

Aabed, K., and Mohammed, A. E. (2021). Synergistic and Antagonistic Effects of Biogenic Silver Nanoparticles in Combination With Antibiotics Against Some Pathogenic Microbes. *Front. Bioeng. Biotechnol.* 9, 652362. doi:10.3389/fbioe.2021.652362

Aggarwal, N., Goindi, S., and Khurana, R. (2013). Formulation, Characterization and Evaluation of an Optimized Microemulsion Formulation of Griseofulvin for Topical Application. *Colloids Surf. B Biointerfaces* 105, 158–166. doi:10.1016/j.colsurfb.2013.01.004

Allen, T. M., and Cullis, P. R. (2004). Drug Delivery Systems: Entering the Mainstream. *Science* 303 (5665), 1818–1822. doi:10.1126/science.1095833

Andriole, V. T. (2000). Current and Future Antifungal Therapy: New Targets for Antifungal Therapy. *Int. J. Antimicrob. Agents* 16 (3), 317–321. doi:10.1016/s0924-8579(00)00258-2

Araújo, C. R., Miranda, K. C., Fernandes, O. F., Soares, A. J., and Silva, M. R. (2009). *In Vitro* susceptibility Testing of Dermatophytes Isolated in Goiania, Brazil, against Five Antifungal Agents by Broth Microdilution Method. *Rev. Inst. Med. Trop. Sao Paulo* 51 (1), 9–12. doi:10.1590/s0036-46652009000100002

Ashara, K. C., Paun, J. S., Soniwala, M. M., Chavada, J. R., and Mori, N. M. (2014). Micro-emulsion Based Emulgel: a Novel Topical Drug Delivery System. *Asian Pac. J. Trop. Dis.* 4, S27–S32. doi:10.1016/s2222-1808(14)60411-4

Ashjari, M., Panahandeh, F., Niazi, Z., and Abolhasani, M. M. (2020). Synthesis of PLGA-mPEG Star-like Block Copolymer to Form Micelle Loaded Magnetite as a Nanocarrier for Hydrophobic Anticancer Drug. *J. Drug Deliv. Sci. Technol.* 56, 101563. doi:10.1016/j.jddst.2020.101563

Barros, M. E. D. S., Santos, D. A., and Hamdan, J. S. (2007). Evaluation of Susceptibility of Trichophyton Mentagrophytes and Trichophyton Rubrum Clinical Isolates to Antifungal Drugs Using a Modified CLSI Microdilution Method (M38-A). *J. Med. Microbiol.* 56 (4), 514–518. doi:10.1099/jmm.0.46542-0

Bhaskar, K., Anbu, J., Ravichandiran, V., Venkateswarlu, V., and Rao, Y. M. (2009). Lipid Nanoparticles for Transdermal Delivery of Flurbiprofen: Formulation, *In Vitro*, *Ex Vivo* and *In Vivo* Studies. *Lipids Health Dis.* 8 (1), 6. doi:10.1186/1476-511X-8-6

Borgers, M., Degreef, H., and Cauwenbergh, G. (2005). Fungal Infections of the Skin: Infection Process and Antimycotic Therapy. *Curr. Drug Targets* 6 (8), 849–862. doi:10.2174/138945005774912726

Borgheti-Cardoso, L. N., Ângelo, T. G., Gelfuso, G. M., Lopez, R. F., and Gratieri, T. (2016). Topical and Transdermal Delivery of Drug-Loaded Nano/Microsystems with Application of Physical Enhancement Techniques. *Curr. Drug Targets* 17 (13), 1545–1559. doi:10.2174/1389450116666151019095121

Buil, J. B., Meijer, E. F. J., Denning, D. W., Verweij, P. E., and Meis, J. F. (2020). Burden of Serious Fungal Infections in the Netherlands. *Mycoses* 63 (6), 625–631. doi:10.1111/myc.13089

Chavan, Y. R., Tambe, S. M., Jain, D. D., Khairnar, S. V., and Amin, P. D. (2021). Redefining the Importance of Polylactide-Co-Glycolide Acid (PLGA) in Drug Delivery. *Ann. Pharm. Françaises* S0003-4509, 00180–00182. doi:10.1016/j.pharma.2021.11.009

Choi, M. J., and Maibach, H. I. (2005). Liposomes and Niosomes as Topical Drug Delivery Systems. *Skin. Pharmacol. Physiol.* 18 (5), 209–219. doi:10.1159/000086666

Choudhury, H., Gorain, B., Pandey, M., Chatterjee, L. A., Sengupta, P., Das, A., et al. (2017). Recent Update on Nanoemulgel as Topical Drug Delivery System. *J. Pharm. Sci.* 106 (7), 1736–1751. doi:10.1016/j.xphs.2017.03.042

Clausen, M. L., Slotved, H. C., Krogfelt, K. A., and Agner, T. (2016). Tape Stripping Technique for Stratum Corneum Protein Analysis. *Sci. Rep.* 6, 19918. doi:10.1038/srep19918

Cleveland, A. A., Harrison, L. H., Farley, M. M., Hollick, R., Stein, B., Chiller, T. M., et al. (2015). Declining Incidence of Candidemia and the Shifting Epidemiology of Candida Resistance in Two US Metropolitan Areas, 2008-2013: Results from Population-Based Surveillance. *PloS one* 10 (3), e0120452. doi:10.1371/journal.pone.0120452

Coates, S. J., Enbiale, W., Davis, M. D. P., and Andersen, L. K. (2020). The Effects of Climate Change on Human Health in Africa, a Dermatologic Perspective: a Report from the International Society of Dermatology Climate Change Committee. *Int. J. Dermatol* 59 (3), 265–278. doi:10.1111/ijd.14759

Deng, H., McShan, D., Zhang, Y., Sinha, S. S., Arslan, Z., Ray, P. C., et al. (2016). Mechanistic Study of the Synergistic Antibacterial Activity of Combined Silver Nanoparticles and Common Antibiotics. *Environ. Sci. Technol.* 50 (16), 8840–8848. doi:10.1021/acs.est.6b00998

Díaz, M. R., and Vivas-Mejia, P. E. (2013). Nanoparticles as Drug Delivery Systems in Cancer Medicine: Emphasis on RNAi-Containing Nanoliposomes. *Pharmaceuticals* 6 (11), 1361–1380. doi:10.3390/ph6111361

Dinarvand, R., Sepehri, N., Manoochehri, S., Rouhani, H., and Atyabi, F. (2011). Polylactide-co-glycolide Nanoparticles for Controlled Delivery of Anticancer Agents. *Int. J. Nanomedicine* 6, 877–895. doi:10.2147/IJN.S18905

Eastman, W. J., Malahias, S., Delconte, J., and DiBenedetti, D. (2014). Assessing Attributes of Topical Vehicles for the Treatment of Acne, Atopic Dermatitis, and Plaque Psoriasis. *Cutis* 94 (1), 46–53.

Escobar-Chávez, J. J., Merino-Sanjuán, V., López-Cervantes, M., Urban-Morlan, Z., Piñón-Segundo, E., Quintanar-Guerrero, D., et al. (2008). The Tape-Stripping Technique as a Method for Drug Quantification in Skin. *J. Pharm. Pharm. Sci.* 11 (1), 104–130. doi:10.18433/j3201z

Firooz, A., Nafisi, S., and Maibach, H. I. (2015). Novel Drug Delivery Strategies for Improving Econazole Antifungal Action. *Int. J. Pharm.* 495 (1), 599–607. doi:10.1016/j.ijpharm.2015.09.015

Fothergill, A. W., Sutton, D. A., McCarthy, D. I., and Wiederhold, N. P. (2014). Impact of New Antifungal Breakpoints on Antifungal Resistance in Candida Species. *J. Clin. Microbiol.* 52 (3), 994–997. doi:10.1128/JCM.03044-13

Hahn, T., Hansen, S., Neumann, D., Kostka, K. H., Lehr, C. M., Muys, L., et al. (2010). Infrared Densitometry: a Fast and Non-destructive Method for Exact Stratum Corneum Depth Calculation for *In Vitro* Tape-Stripping. *Skin. Pharmacol. Physiol.* 23 (4), 183–192. doi:10.1159/000288165

Jana, S., Manna, S., Nayak, A. K., Sen, K. K., and Basu, S. K. (2014). Carbopol Gel Containing Chitosan-Egg Albumin Nanoparticles for Transdermal Aceclofenac Delivery. *Colloids Surf. B Biointerfaces* 114, 36–44. doi:10.1016/j.colsurfb.2013.09.045

Kanaujia, P., Lau, G., Ng, W. K., Widjaja, E., Hanefeld, A., Fischbach, M., et al. (2011). Nanoparticle Formation and Growth during *In Vitro* Dissolution of Ketoconazole Solid Dispersion. *J. Pharm. Sci.* 100 (7), 2876–2885. doi:10.1002/jps.22491

Kataoka, M., Takeyama, S., Minami, K., Higashino, H., Kakimi, K., Fujii, Y., et al. (2019). *In Vitro* Assessment of Supersaturation/Precipitation and Biological Membrane Permeation of Poorly Water-Soluble Drugs: A Case Study With Albendazole and Ketoconazole. *J. Pharm. Sci.* 108 (8), 2580–2587. doi:10.1016/j.xphs.2019.03.007

Klingspor, L., Tortorano, A. M., Peman, J., Willinger, B., Hamal, P., Sendid, B., et al. (2015). Invasive Candida Infections in Surgical Patients in Intensive Care Units: a Prospective, Multicentre Survey Initiated by the European Confederation of Medical Mycology (ECMM) (2006-2008). *Clin. Microbiol. Infect.* 21 (1), 87.e1–87.e10. doi:10.1016/j.cmi.2014.08.011

Lademann, J., Knorr, F., Richter, H., Blume-Peytavi, U., Vogt, A., Antoniou, C., et al. (2008). Hair Follicles-Aan Efficient Storage and Penetration Pathway for Topically Applied Substances. Summary of Recent Results Obtained at the Center of Experimental and Applied Cutaneous Physiology, Charité -Universitätsmedizin Berlin, Germany. *Skin. Pharmacol. Physiol.* 21 (3), 150–155. doi:10.1159/000131079

Lavan, D. A., McGuire, T., and Langer, R. (2003). Small-scale Systems for *In Vivo* Drug Delivery. *Nat. Biotechnol.* 21 (10), 1184–1191. doi:10.1038/nbt876

Liao, C., Li, Y., and Tjong, S. C. (2019). Bactericidal and Cytotoxic Properties of Silver Nanoparticles. *Int. J. Mol. Sci.* 20 (2), 449. doi:10.3390/ijms20020449

Lockman, P. R., Mumper, R. J., Khan, M. A., and Allen, D. D. (2002). Nanoparticle Technology for Drug Delivery across the Blood-Brain Barrier. *Drug Dev. Ind. Pharm.* 28 (1), 1–13. doi:10.1081/ddc-120001481

Luengo, J., Schneider, M., Schneider, A. M., Lehr, C. M., and Schaefer, U. F. (2021). Human Skin Permeation Enhancement Using PLGA Nanoparticles Is Mediated by Local pH Changes. *Pharmaceutics* 13 (10), 1608. doi:10.3390/pharmaceutics13101608

Luengo, J., Weiss, B., Schneider, M., Ehlers, A., Stracke, F., König, K., et al. (2006). Influence of Nanoencapsulation on Human Skin Transport of Flufenamic Acid. *Skin. Pharmacol. Physiol.* 19 (4), 190–197. doi:10.1159/000093114

Markowska, K., Grudniak, A. M., Krawczyk, K., Wróbel, I., and Wolska, K. I. (2014). Modulation of Antibiotic Resistance and Induction of a Stress Response in Pseudomonas aeruginosa by Silver Nanoparticles. *J. Med. Microbiol.* 63 (6), 849–854. doi:10.1099/jmm.0.068833-0

Mayba, J. N., and Gooderham, M. J. (2018). A Guide to Topical Vehicle Formulations. *J. Cutan. Med. Surg.* 22 (2), 207–212. doi:10.1177/1203475417743234

McNeilly, O., Mann, R., Hamidian, M., and Gunawan, C. (2021). Emerging Concern for Silver Nanoparticle Resistance in Acinetobacter Baumannii and Other Bacteria. *Front. Microbiol.* 12, 652863. doi:10.3389/fmicb.2021.652863

Minghetti, P., Cilurzo, F., Casiraghi, A., and Montanari, L. (2006). Evaluation of *Ex Vivo* Human Skin Permeation of Genistein and Daidzein. *Drug Deliv.* 13 (6), 411–415. doi:10.1080/10717540500466089

Monteiro, D. R., Silva, S., Negri, M., Gorup, L. F., De Camargo, E. R., Oliveira, R., et al. (2012). Silver Nanoparticles: Influence of Stabilizing Agent and Diameter on Antifungal Activity against Candida Albicans and Candida Glabrata Biofilms. *Lett. Appl. Microbiol.* 54 (5), 383–391. doi:10.1111/j.1472-765X.2012.03219.x

Oxman, D. A., Chow, J. K., Frendl, G., Hadley, S., Hershkovitz, S., Ireland, P., et al. (2010). Candidaemia Associated with Decreased *In Vitro* Fluconazole Susceptibility: Is Candida Speciation Predictive of the Susceptibility Pattern? *J. Antimicrob. Chemother.* 65 (7), 1460–1465. doi:10.1093/jac/dkq136

Pappas, P. G., Kauffman, C. A., Andes, D. R., Clancy, C. J., Marr, K. A., Ostrosky-Zeichner, L., et al. (2016). Clinical Practice Guideline for the Management of Candidiasis: 2016 Update by the Infectious Diseases Society of America. *Clin. Infect. Dis.* 62 (4), e1–50. doi:10.1093/cid/civ933

Parashar, B., Kabra, A., and Chandel, A. (2013). Formulation and Evaluation of Gel Containing Miconazole Nitrate an Antifungal Agent. *Int. J. Pharm. Res. Rev.* 2 (6), 18–28.

Patra, J. K., and Baek, K. H. (2017). Antibacterial Activity and Synergistic Antibacterial Potential of Biosynthesized Silver Nanoparticles against Foodborne Pathogenic Bacteria along with its Anticandidal and Antioxidant Effects. *Front. Microbiol.* 8, 167. doi:10.3389/fmicb.2017.00167

Pfaller, M. A., Messer, S. A., Woosley, L. N., Jones, R. N., and Castanheira, M. (2013). Echinocandin and Triazole Antifungal Susceptibility Profiles for Clinical Opportunistic Yeast and Mold Isolates Collected from 2010 to 2011: Application of New CLSI Clinical Breakpoints and Epidemiological Cutoff Values for Characterization of Geographic and Temporal Trends of Antifungal Resistance. *J. Clin. Microbiol.* 51 (8), 2571–2581. doi:10.1128/JCM.00308-13

Pfalzgraff, A., Brandenburg, K., and Weindl, G. (2018). Antimicrobial Peptides and Their Therapeutic Potential for Bacterial Skin Infections and Wounds. *Front. Pharmacol.* 9, 281. doi:10.3389/fphar.2018.00281

Rasheed, T., Bilal, M., Iqbal, H. M. N., and Li, C. (2017). Green Biosynthesis of Silver Nanoparticles Using Leaves Extract of Artemisia Vulgaris and Their Potential Biomedical Applications. *Colloids Surf. B Biointerfaces* 158, 408–415. doi:10.1016/j.colsurfb.2017.07.020

Sa-Barreto, L. C., Alvarez-Lorenzo, C., Concheiro, A., Martinez-Pacheco, R., and Gomez-Amoza, J. L. (2017). SEM-image Textural Features and Drug Release Behavior of Eudragit-Based Matrix Pellets. *J. Drug Deliv. Sci. Technol.* 42, 292–298. doi:10.1016/j.jddst.2017.04.027

Sadozai, S. K., Khan, S. A., Karim, N., Becker, D., Steinbrück, N., Gier, S., et al. (2020). Ketoconazole-loaded PLGA Nanoparticles and Their Synergism against Candida Albicans when Combined with Silver Nanoparticles. *J. Drug Deliv. Sci. Technol.* 56, 101574. doi:10.1016/j.jddst.2020.101574

Scandorieiro, S., De Camargo, L. C., Lancheros, C. A., Yamada-Ogatta, S. F., Nakamura, C. V., De Oliveira, A. G., et al. (2016). Synergistic and Additive Effect of Oregano Essential Oil and Biological Silver Nanoparticles against Multidrug-Resistant Bacterial Strains. *Front. Microbiol.* 7, 760. doi:10.3389/fmicb.2016.00760

Schneider, M., Stracke, F., Hansen, S., and Schaefer, U. F. (2009). Nanoparticles and Their Interactions with the Dermal Barrier. *Dermatoendocrinol* 1 (4), 197–206. doi:10.4161/derm.1.4.9501

Shafique, M., Khan, M. A., Khan, W. S., Ahmad, W., and Khan, S. (2017). Fabrication, Characterization, and *In Vivo* Evaluation of Famotidine Loaded Solid Lipid Nanoparticles for Boosting Oral Bioavailability. *J. Nanomater.* 2017, 1–10. doi:10.1155/2017/7357150

Sharifzadeh, A., Khosravi, A. R., Shokri, H., Asadi Jamnani, F., Hajiabdolbaghi, M., and Ashrafi Tamami, I. (2013). Oral Microflora and Their Relation to Risk Factors in HIV+ Patients with Oropharyngeal Candidiasis. *J. Mycol. Med.* 23 (2), 105–112. doi:10.1016/j.mycmed.2013.02.001

Silva, J. P., Dhall, S., Garcia, M., Chan, A., Costa, C., Gama, M., et al. (2015). Improved Burn Wound Healing by the Antimicrobial Peptide LLKKK18 Released from Conjugates with Dextrin Embedded in a Carbopol Gel. *Acta Biomater.* 26, 249–262. doi:10.1016/j.actbio.2015.07.043

Sodeifian, G., Sajadian, S. A., Razmimanesh, F., and Hazaveie, S. M. (2021). Solubility of Ketoconazole (Antifungal Drug) in SC-CO2 for Binary and Ternary Systems: Measurements and Empirical Correlations. *Sci. Rep.* 11 (1), 7546. doi:10.1038/s41598-021-87243-6

Stracke, F., Weiss, B., Lehr, C. M., König, K., Schaefer, U. F., and Schneider, M. (2006). Multiphoton Microscopy for the Investigation of Dermal Penetration of Nanoparticle-Borne Drugs. *J. Invest Dermatol* 126 (10), 2224–2233. doi:10.1038/sj.jid.5700374

Tang, S., and Zheng, J. (2018). Antibacterial Activity of Silver Nanoparticles: Structural Effects. *Adv. Healthc. Mater* 7 (13), e1701503. doi:10.1002/adhm.201701503

Waghule, T., Sankar, S., Rapalli, V. K., Gorantla, S., Dubey, S. K., Chellappan, D. K., et al. (2020). Emerging Role of Nanocarriers Based Topical Delivery of Antifungal Agents in Combating Growing Fungal Infections. *Dermatol Ther.* 33 (6), e13905. doi:10.1111/dth.13905

Waghule, T., Rapalli, V. K., Singhvi, G., Manchanda, P., Hans, N., Dubey, S. K., et al. (2019). Voriconazole Loaded Nanostructured Lipid Carriers Based Topical Delivery System: QbD Based Designing, Characterization, *In-Vitro* and *Ex-Vivo* Evaluation. *J. Drug Deliv. Sci. Technol.* 52, 303–315. doi:10.1016/j.jddst.2019.04.026

Wang, J., Zhan, L., Zhang, X., Wu, R., Liao, L., and Wei, J. (2020). Silver Nanoparticles Coated Poly(L-Lactide) Electrospun Membrane for Implant Associated Infections Prevention. *Front. Pharmacol.* 11, 431. doi:10.3389/fphar.2020.00431

Wu, X., and Guy, R. H. (2009). Applications of Nanoparticles in Topical Drug Delivery and in Cosmetics. *J. Drug Deliv. Sci. Technol.* 19 (6), 371–384. doi:10.1016/s1773-2247(09)50080-9

Zhang, T., Wang, L., Chen, Q., and Chen, C. (2014). Cytotoxic Potential of Silver Nanoparticles. *Yonsei Med. J.* 55 (2), 283–291. doi:10.3349/ymj.2014.55.2.283

Conflict of Interest: The authors declare that the research was conducted in the absence of any commercial or financial relationships that could be construed as a potential conflict of interest.

Publisher's Note: All claims expressed in this article are solely those of the authors and do not necessarily represent those of their affiliated organizations, or those of the publisher, the editors, and the reviewers. Any product that may be evaluated in this article, or claim that may be made by its manufacturer, is not guaranteed or endorsed by the publisher.

frontiers | Frontiers in Pharmacology

ORIGINAL RESEARCH
published: 12 July 2022
doi: 10.3389/fphar.2022.934156

Nanostructured Lipid Carrier-Based Delivery of Pioglitazone for Treatment of Type 2 Diabetes

Umair Ilyas[1†], Muhammad Asif[1†], Minglian Wang[2], Reem Altaf[3]*†, Hajra Zafar[4], Mirza Muhammad Faran Ashraf Baig[5], Ana Cláudia Paiva-Santos[6,7] and Muhammad Abbas[1]**

[1]Riphah Institute of Pharmaceutical Sciences, Riphah International University, Islamabad, Pakistan, [2]Faculty of Environment and Life Science, Beijing University of Technology, Bejing, China, [3]Department of Pharmacy, Iqra University Islamabad Campus, Islamabad, Pakistan, [4]School of Pharmacy, Shanghai Jiao Tong University, Shanghai, China, [5]Laboratory of Biomedical Engineering for Novel Bio-Functional, and Pharmaceutical Nano-Materials, Prince Philip Dental Hospital, Faculty of Dentistry, The University of Hong Kong, Hong Kong, China, [6]Department of Pharmaceutical Technology, Faculty of Pharmacy, University of Coimbra, Coimbra, Portugal, [7]REQUIMTE/LAQV, Group of Pharmaceutical Technology, Faculty of Pharmacy, University of Coimbra, Coimbra, Portugal

OPEN ACCESS

Edited by:
Saeed Ahmad Khan,
Kohat University of Science and Technology, Pakistan

Reviewed by:
Afzal Ahmed Dar,
Shaanxi University of Science and Technology, China
Dr. Hafiz Muhammad Zubair,
Nanjing Medical University, China

***Correspondence:**
Minglian Wang
mlw@bjut.edu.cn
Reem Altaf
reem.altaf@iqraisb.edu.pk
Muhammad Abbas
muhammad.abbas@riphah.edu.pk

[†]These authors have contributed equally to this work

Specialty section:
This article was submitted to Experimental Pharmacology and Drug Discovery, a section of the journal Frontiers in Pharmacology

Received: 02 May 2022
Accepted: 10 June 2022
Published: 12 July 2022

Citation:
Ilyas U, Asif M, Wang M, Altaf R, Zafar H, Faran Ashraf Baig MM, Paiva-Santos AC and Abbas M (2022) Nanostructured Lipid Carrier-Based Delivery of Pioglitazone for Treatment of Type 2 Diabetes. Front. Pharmacol. 13:934156. doi: 10.3389/fphar.2022.934156

Pioglitazone (PGZ) is utilized as a therapeutic agent in the management of (type 2) diabetes to control blood glucose levels. The existing research work was intended to make and optimize PGZ-containing NLCs (nanostructured lipid carriers). The fabricated nanostructured lipid carrier preparation was optimized by using different concentrations of the surfactants (Tween 80 and Span 80) and solid lipid (Compritol® 888 ATO) and liquid lipid (Labrasol®) while keeping the concentration of drug (PGZ), and co-surfactants (poloxamer 188) the same. The optimized NLC formulation (PGZ-NLCs) was further assessed for physical and chemical characterization, *in vitro* PGZ release, and stability studies. The optimized PGZ-NLCs have shown an average diameter of 150.4 nm, EE of 92.53%, PDI value of 0.076, and zeta-potential of −29.1 mV, correspondingly. The DSC thermal analysis and XRD diffractograms had not presented the spectrum of PGZ, confirming the comprehensive encapsulation of PGZ in the lipid core. PGZ-NLCs showed significantly extended release (51% in 24 h) compared to the unformulated PGZ. Our study findings confirmed that PGZ-NLCs can be a promising drug delivery system for the treatment of type 2 diabetes.

Keywords: pioglitazone, poor aqueous solubility, NLCs, nanoparticles, diabetes

1 INTRODUCTION

Pioglitazone (PGZ) is an oral therapeutic agent used in therapy of diabetes mellitus (DM). It is a thiazolidinedione derivative. The structural formula of PGZ is 5-[4-[2-(5-ethyl-2-pyridinyl) ethoxy] benzyl] thiazolidine- 2,4-dione (Waugh et al., 2006; Souri et al., 2008). In diabetic patients, insulin resistance is improved by the use of PGZ. It also reduces the macrovascular risks associated with diabetes (Mosure et al., 2019). PGZ significantly decreases the blood glucose levels in fasting and postprandial state and also reduces the glycosylated hemoglobin, while the beta-cell function is improved by its use (Shaveta et al., 2020). PGZ mainly performs its action by binding to peroxisome proliferator-activated gamma receptors (PPARs) (Smith, 2001). Stimulation of PPARs regulates the transcription of genes which controls the release of insulin responsible for the balancing of the production of glucose, glucose uptake, transport, and consumption in the organs. PGZ improves the

sensitivity of the tissue to insulin and reduces gluconeogenesis which leads to improved glycemic control and decreases insulin resistance. PGZ being a member of the Biopharmaceutics Classification System (BCS) Class II exhibits low water solubility (0.00442 mg/ml) and high permeability. The half-life of PGZ is also very short (3–6 h). The low aqueous solubility of the PGZ corresponds to low dissolution. Poor solubility and decreased dissolution rate reduce the drug absorption and impart a negative effect on blood levels of the drug leading to decrease pharmacological activity (Elbary et al., 2008). Therefore, to achieve minimum therapeutic level concentration an increased dose of PGZ is required which can cause severe adverse effects (Shaveta et al., 2020). Furthermore, PGZ also undergoes metabolism, and many metabolites are produced in the liver to activate and inactivate metabolites by the process of oxidation and hydroxylation (Eckland and Danhof, 2000). The absorption of PGZ from GIT is further delayed in the presence of food (Pandey and Kohli, 2017). Keeping in view all these shortcomings associated with PGZ there is a necessity to develop effectual delivery systems of PGZ (Bhosale et al., 2016).

A number of approaches have been employed to deal with low water solubility constraints. Physicochemical modifications in the drug molecules are the major strategies among other approaches to improve solubility and enhance the surface area and drug release rate of drug particles. Lipidic drug delivery systems and solid dispersions are also among the solubility enhancement techniques through physical modifications of the system (Sinha et al., 2013; Malamatari et al., 2018). The bioavailability of the drugs given orally with poor solubility can also be enhanced through the latest developments in particle size modification techniques. The bioavailability of these drugs mainly depends upon the dissolution rate. It has been observed that the solubility is increased when the particle size is reduced. Improved solubility results in a higher dissolution rate. As a result, the drug's bioavailability increases (Williams et al., 2013; Koradia et al., 2018). The equation of Noyes–Whitney explains the association between the dissolution velocity and the real surface area of the particles of the drug. The reduction of larger particles into smaller ones can cause a surge in the surface area and increased rate of dissolution (Pawar et al., 2014).

NLCs are taken to be the analogs of oil-in-water (o/w) emulsion as they are similarly formed as the o/w emulsion. The difference only takes place in the replacement of the oily phase of the emulsion for solid lipids in the presence of liquid lipids. Accordingly, NLCs may be comprised of a lipid blend of solid and liquid lipid distributed in a water phase at elevated temperatures. Sometimes, a surfactant or mixture of surfactants and co-surfactant is used to stabilize the formulation. NLCs have a particle size in the range of 50–1,000 nm having a spherical shape (Junghanns and Müller, 2008). NLCs have been utilized as an alternate drug carrier system to other colloidal systems of drug delivery. NLCs are comprised of solid lipids, liquid lipids, surfactants and/or cosurfactants, and water. A distinctive solid type lipid that is employed in these kinds of carrier systems should have the ability to melt above the body temperature of 37°C.

NLCs have exhibited many advantages over other colloidal drug delivery systems and simultaneously minimized the problems related with other colloidal carrier systems (Mehnert and Mäder, 2012). Generally, a solid core in NLCs offers various advantages in the presence of a liquid core. Usually, liposomes and emulsions also fail to protect the encapsulated drug. and a burst release of drug can happen from emulsions or uncontrolled release of drug from the liposomal formulation. NLCs exhibit controlled release effect, at the same time also protects the drug from degradations. NLCs have better stability and high capability to load the drug. NLCs also need lower quantities of organic solvents in production, which declines the chances of toxicity. In conclusion, by comparison with other colloidal nanoparticles, NLC production procedures are cost-effective and are easily scalable (Junghanns and Müller, 2008).

The aim of this research work was to develop and assess pioglitazone-loaded NLCs for better drug delivery and enhanced solubility that can be used to improve the antidiabetic potential of pioglitazone.

2 MATERIALS AND METHODS

2.1 Materials

Pioglitazone hydrochloride (PGZ) drug was received as a gift sample from Xellia Pharmaceuticals. Methanol, Tween 80, poloxamer 188, Span 80, Compritol® 888 ATO, and Labrasol® were procured from Sigma-Aldrich (St. Louis, MO, United States). Analytical-grade quality was assured for all chemicals.

2.2 Preparation of Pioglitazone–Nanostructured Lipid Carriers

PGZ-NLCs were formulated by nano-emulsion template technique with minor changes. In brief, the blend of PGZ, Tween 80, Span 80, Compritol® 888 ATO, Labrasol®, and poloxamer 188 were put in a water bath and melted at 65°C. Deionized water was filtered and then heated up to 65°C. A volume of 5 ml of warmed deionized water was added to the melted blend of lipids and surfactants with constant stirring at a rotation speed of 750 rpm for 30 min. A transparent nano-emulsion was obtained. The temperature of the system was sustained at 70°C throughout the making of nano-emulsion. Afterward, the warm nano-emulsion was quickly cooled down at a temperature below 4°C in the ice container along with constant stirring at 750 rpm to solidify the lipids to produce PGZ-NLCs. Free PGZ and large aggregates from the PGZ-NLC formulation were withdrawn by filtering it through a 0.45-pm syringe filter. For further study, PGZ-NLCs were held in reserve at 4°C (Rizvi et al., 2019).

2.3 Optimization of Pioglitazone–Nanostructured Lipid Carriers

PGZ-NLC formulations were optimized for different Tween 80 and Span 80 concentrations in the surfactant blend, and

TABLE 1 | Composition of all formulations.

Formulation code	PGZ	Compritol 888 ATO	Labrasol	Tween 80	Span 80	Poloxamer 188
F1	5	5	5	77	23	20
F2	5	4	6	78	22	20
F3	5	7	3	79	21	20
F4	5	8	2	85	15	20
F5	5	9	1	92	9	20

their influence on mean diameter of the particle, EE, PDI, and zeta potential was determined. The amount of PGZ and surfactant component poloxamer 188 was kept constant, while the concentration of solid lipid Compritol® 888 ATO and liquid lipid Labrasol was varied. **Table 1** contains the concentration of all the formulation components used.

2.4 Characterization of Pioglitazone–Nanostructured Lipid Carriers

2.4.1 Particle Size, Size Distribution, and Zeta Potential Analysis

Mean particle size, PDI (polydispersity index) value, and zeta potential of optimized PGZ-NLCs were determined using a Zetasizer ZS 90 (Malvern Instruments, Malvern, Worcestershire, United Kingdom). For analysis, PGZ-NLCs were suitably diluted with deionized water.

2.4.2 Encapsulation Efficiency

The amount of PGZ encapsulated in PGZ-NLCs was determined by using a UV-visible spectrophotometer. Before carrying out analysis, PGZ in free form and aggregates of larger size were removed by passing the NLC formulation through a syringe filter of 0.45 p.m. The filtered PGZ-NLCs were dissolved in methanol. Analysis for PGZ contents was carried out by using UV-visible spectrophotometer at 220 nm (V-530; JASCO Corporation, Tokyo, Japan) (Shaveta et al., 2020). The encapsulation efficiency and drug loading (%) of PGZ-NLCs are assessed by using the equations given as follows:

$$\text{Encapsulation efficiency (\%)} = \text{PGZ amount in PGZ} - \text{NLCs/PGZ total amount added} \times 100,$$

$$\text{Drug Loading (\%)} = \text{PGZ amount in PGZ} - \text{NLCs/total weight of PGZ} - \text{NLCs} \times 100.$$

2.4.3 Morphology Analysis

The morphology of PGZ-NLCs was examined using scanning electron microscopy (SEM) (Hitachi S-4100, Hitachi Ltd., Tokyo, Japan). A minute quantity of lyophilized PGZ-NLCs was spread on a carbon-coated tape and dried at room temperature. A thin layer of gold was used to sputter the sample under vacuum (Rizvi et al., 2019).

2.4.4 FTIR Analysis

To inspect the PGZ compatibility with excipients, FTIR spectra of unformulated PGZ, Compritol® 888 ATO, poloxamer 188, and lyophilized PGZ-NLCs were attained by means of an FTIR spectrophotometer (Eco Alpha II- Bruker, Billerica, MA, United States). The infra-red spectrum was gained in the range of 4,000–400 cm^{-1}. Lyophilization of PGZ-NLCs was executed using a freeze-dryer (TFD5503, IlShin BioBase Co., Ltd. Gyeonggido, Republic of Korea) (Pireddu et al., 2016; Casula et al., 2021).

2.4.5 Powdered X-Ray Diffractometry

The powder x-ray diffraction examination of lyophilized PGZ-NLCs and their specific solid constituents (unformulated PGZ, Compritol® 888 ATO, and poloxamer 188) was carried out using a powder X-ray diffractometer (D8 Advance-Bruker, Billerica, MA, United States). All the samples were scanned at an angle of 2θ in the range of 3–70°, and at 0.02°/s rotation with a current of 40 mA and 40 kV voltage (Rizvi et al., 2019).

2.4.6 Differential Scanning Calorimetry

The thermal features of lyophilized PGZ-NLCs and their different solid ingredients (unformulated PGZ, Compritol® 888 ATO, and poloxamer 188) were inspected using a differential scanning calorimeter (DSC Q20; TA Instrument, New Castle, DE, United States). For the DSC study, the sample was positioned in an aluminum pan and heated over a temperature range of 0–200°C at 10°C/min rate (Rizvi et al., 2019).

2.4.7 *In Vitro* Release of Pioglitazone–Nanostructured Lipid Carriers

The *in vitro* release profile of PGZ-loaded NLCs was estimated via the dialysis bag method with simulated gastric fluid (SGF) of pH 1.2 and simulated intestinal fluid (SIF) of pH 6.8 as dissolution medium at 37 ± 0.5°C temperature and 100 rpm rotation. PGZ-NLC formulation equal to 5 mg of PGZ was put in a dialysis membrane of 3,500 Da molecular cut-off weight (Spectrum Laboratories, Inc., Rancho Dominguez, CA, United States). Before carrying out the release study, the dialysis membrane was submerged in SGF or SIF. 0.5%, w/v Tween 80 and 5%, v/v ethanol were put into the release media for maintaining the sink conditions. Samples of 2 ml were drawn out from release media at determined time intervals for 24 h. To sustain a persistent volume after sample removal, the

TABLE 2 | Experimental results of various PGZ-NLC formulations.

Formulation code	Particle size (nm)	PDI	EE %	Zeta potential (mV)
F1	319	0.28	95.03	17
F2	187.7	0.097	91.14	20.9
F3	150.4	0.076	92.53	–29.1
F4	124.6	0.36	93.21	21.5
F5	251.7	0.441	86.63	27.1

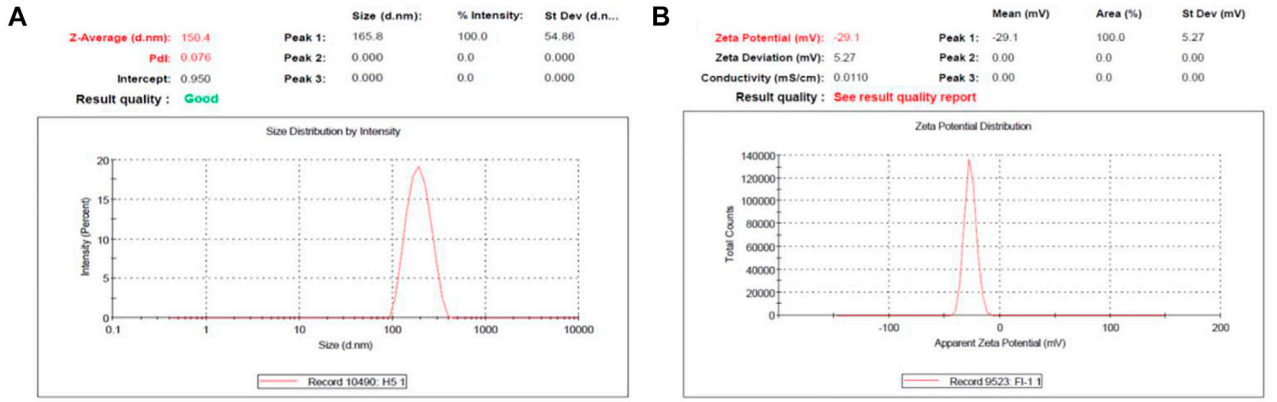

FIGURE 1 | Optimized PGZ-NLCs. **(A)** Particle size distribution; **(B)** zeta potential.

release medium was instantly substituted with an equivalent volume of fresh fluid. The samples were analyzed for PGZ at 220 nm by using a UV-visible spectrophotometer (Rizvi et al., 2019).

2.4.8 Statistical Analysis

All the experimentations were carried out in triplicate, and data were exhibited as mean ± S.D. SPSS software (SPSS Inc., Chicago, IL, United States) was utilized to analyze statistical significance amongst groups by employing Student's t-test at the $p < 0.05$ significance level.

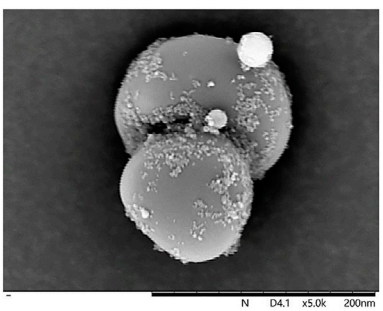

image of optimized PGZ-

FIGURE 2 | SEM image of optimized PGZ-NLCs.

3 RESULTS

3.1 Preparation of Pioglitazone–Nanostructured Lipid Carriers

PGZ-loaded NLCs were efficaciously fabricated by the nano-emulsion-based method with decent uniformity and reproducibility. Compritol® 888 ATO was utilized as lipid solid for the formation of the outer solid lipid core of PGZ-NLCs, while Labrasol was utilized as liquid lipid to fill the imperfections in the solid core, and the prepared NLC formulation was made stable by using a mixture of Tween 80 as a surfactant and Span 80 and poloxamer as co-surfactant.

3.2 Optimization of Pioglitazone–Nanostructured Lipid Carrier Formulations

Table 2 exhibits the obtained results of various formulations of PGZ-NLCs optimized for different amounts of Tween 80 and Span 80 in the surfactant blend and their effect on particle diameter, EE, PDI, and zeta potential was determined. Based upon the features of particle size, PDI, EE, and zeta potential values, formulation 3 was carefully chosen as optimized and was further characterized for various physicochemical constraints.

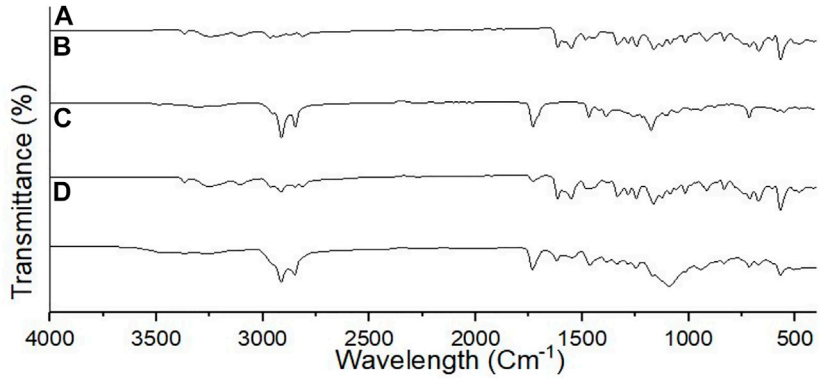

FIGURE 3 | FTIR spectra of **(A)** PGZ, **(B)** Compritol 888 ATO, **(C)** poloxamer 188, and **(D)** optimized PGZ-NLCs.

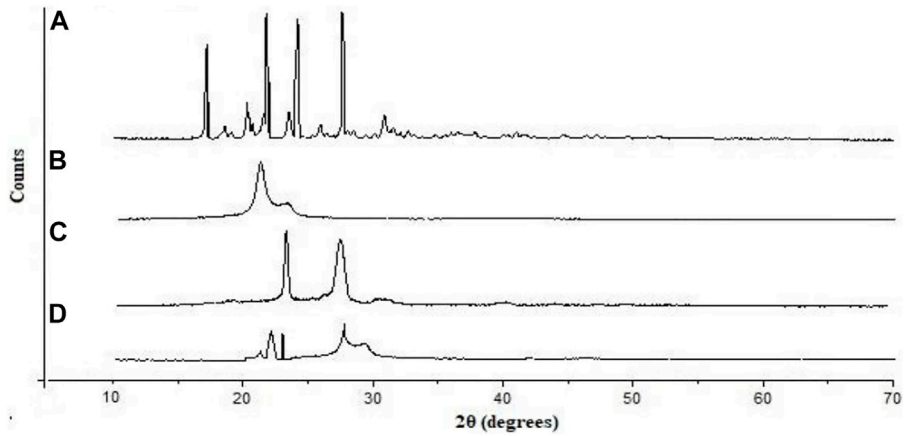

FIGURE 4 | Powder X-ray diffraction pattern of **(A)** PGZ, **(B)** Compritol 888 ATO, **(C)** poloxamer 188, and **(D)** optimized PGZ-NLCs.

3.3 Characterization of EPL-NCs

3.3.1 Particle Size and Size Distribution and Zeta Potential Analysis

PGZ-NLCs presented an average diameter of particles of 150.4 nm, a PDI value of 0.076 articulating thin size distribution, and a zeta potential value of −29.1 mV positively. **Figure 1** displays the particle size distribution (A) and zeta potential (B) of the optimized PGZ-NLCs.

3.3.2 Incorporation Efficiency

PGZ-NLCs showed a high drug encapsulation efficiency of 92.53%, and drug loading was found to be 6%.

3.3.3 Morphology Analysis

The morphology and shape analysis of PGZ-NLCs was completed over SEM, and the SEM image in **Figure 2** exposed that the shape of the PGZ-NLCs was spherical and the surfaces were smooth without any aggregation.

3.3.4 FTIR Analysis

The FTIR spectrum of unformulated PGZ, poloxamer 188, Compritol® 888 ATO, and lyophilized PGZ-NLCs was carried out to assess the compatibility of the drug with the excipients. In **Figure 3**, the FTIR spectra of PGZ showed distinctive N–H stretch at 3,069 cm^{-1}, a peak of C–H stretch at 2,985 cm^{-1}, a peak of C= O stretching at 1732 cm^{-1}, the C–C aromatic stretch at 1,601 cm^{-1}, and the peak of C–S bond at 1,220 cm^{-1}.

3.3.5 Powdered X-Ray Diffraction Studies

XRD spectra of unformulated PGZ, poloxamer 188, Compritol® 888 ATO, and PGZ-NLCs were determined, and are displayed in **Figure 4**. The unformulated PGZ diffractogram presented intense distinguishing peaks of crystalline nature at 20 angles of 11.2, 15.8, 18.2, and 21.6. Compritol® 888 ATO exhibited distinguishing diffraction peaks at 20 angles of 21.3 and 23.7. No characteristic peak of PGZ in the XRD spectrum of PGZ-NLCs was found, and the diffraction pattern of Compritol® 888 ATO was merely observed at angles of 21.1 and 23.3 of 20 diffractions.

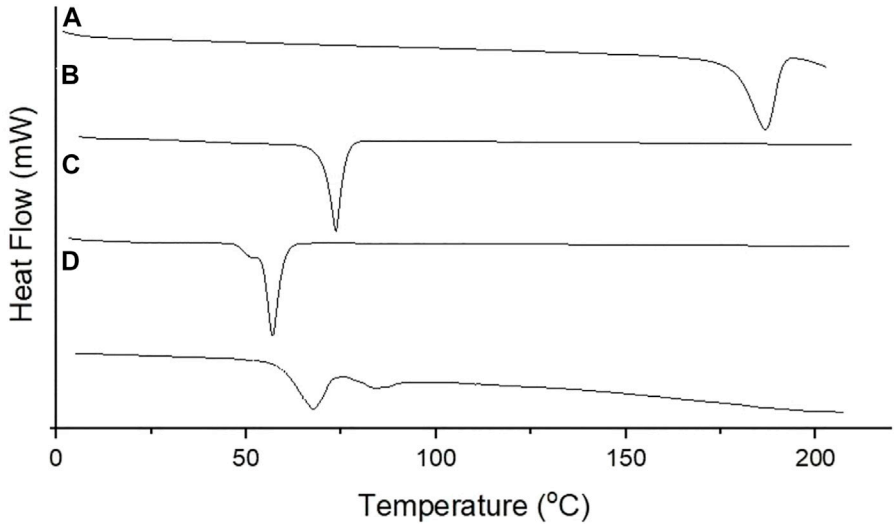

FIGURE 5 | DSC thermogram of **(A)** PGZ, **(B)** Compritol 888 ATO, **(C)** poloxamer 188, and **(D)** optimized PGZ-NLCs.

3.3.6 Differential Scanning Calorimetry

Thermal analysis of PGZ, Compritol® 888 ATO, poloxamer 188, and PGZ-NLCs was performed by DSC, and the obtained results are displayed in **Figure 5**. The thermal spectrum of PGZ showed a sharp endothermic peak at 184°C while Compritol® 888 ATO at 74.6°C, which corresponded to the melting point of drug and lipid. The thermal spectrum of PGZ-NLCs did not show any endothermic melting peak of PGZ, and the thermal spectrum presented a Compritol® 888 ATO melting peak at 66.2°C with a slight peak shifting to the lower temperature.

3.3.7 *In Vitro* Release of Pioglitazone–Nanostructured Lipid Carriers

The *in vitro* drug release of PGZ-NLCs was compared with the release profile of unformulated PGZ. The assessment of drug release was made in simulated gastric fluid at pH 1.2 and simulated intestinal fluid having pH 6.8 at 37°C. Owing to the less aqueous solubility of PGZ, Tween 80 0.5%, w/v and ethanol 5%, v/v were incorporated into the release media to sustain sink conditions by dissolving the released PGZ. **Figure 6** exhibits the results of *in vitro* release of PGZ-NLCs and unformulated PGZ in both media. PGZ-NLCs exhibited 19% of PGZ release in the early 2 h in simulated gastric fluid shadowed by slow and continual release form with a collective release of 51% within 24 h (**Figure 6A**). In differing to PGZ-NLCs, PGZ suspension displayed quicker release with 33% and 92% of PGZ released after a time of 2 and 24 h, correspondingly.

In simulated intestinal fluid, the % release of PGZ from PGZ-NLCs was ~14% at 2 h equated to 25% from PGZ dispersal. Within 24 h, PGZ-NLCs and PGZ suspension presented 54% and 93% release of PGZ, respectively.

3.3.8 Stability Study

The result of the stability study of PGZ-NLCs at room temperature and accelerated state according to the ICH guiding principle are described in **Figures 7A,B**. Subsequently, storing the samples for 6 months, the samples were examined at specified intervals. A rise in particle size and drop in EE was found on storage at room temperature and accelerated state. The particle size and entrapment efficiency noted at the start of the study were 150.4 ± 4.33 nm and 92.53% ± 4.11%, and, later a period of 180 days, the particle size at 25°C and 60% RH was increased to 231.32 ± 2.13 nm and encapsulation efficiency was decreased to 76.73% ± 3.27%, correspondingly. The particle size and entrapment efficiency outcome for PGZ-NLCs kept at 40°C were found to be significantly changed compared to the PGZ-NLCs maintained under storage conditions of 25°C. The primary particle size and entrapment efficiency were found to be 150.4 ± 4.33 nm and 92.53% ± 4.78%, and after the period of 180 days, it exposed a significant rise in particle size (254.66 ± 5.32) and drop in entrapment efficiency (71.87% ± 3.41%).

4 DISCUSSION

PGZ-loaded NLCs were efficaciously fabricated by the nano-template engineering method with decent uniformity and reproducibility. Compritol® 888 ATO was utilized as solid lipids while Labrasol as liquid lipid for the preparation of the outer solid lipid core of PGZ-NLCs, and the prepared NLCs were stabilized by using a surfactant mixture of Tween 80, Span 80, and poloxamer. Compritol® 888 ATO is a pharmaceutically suitable lipid having the characteristics of biocompatibility and biodegradability. The types of solid lipids which have a melting temperature higher than the temperature of the body own solid aquaphobic connections with lipotropic drugs which is

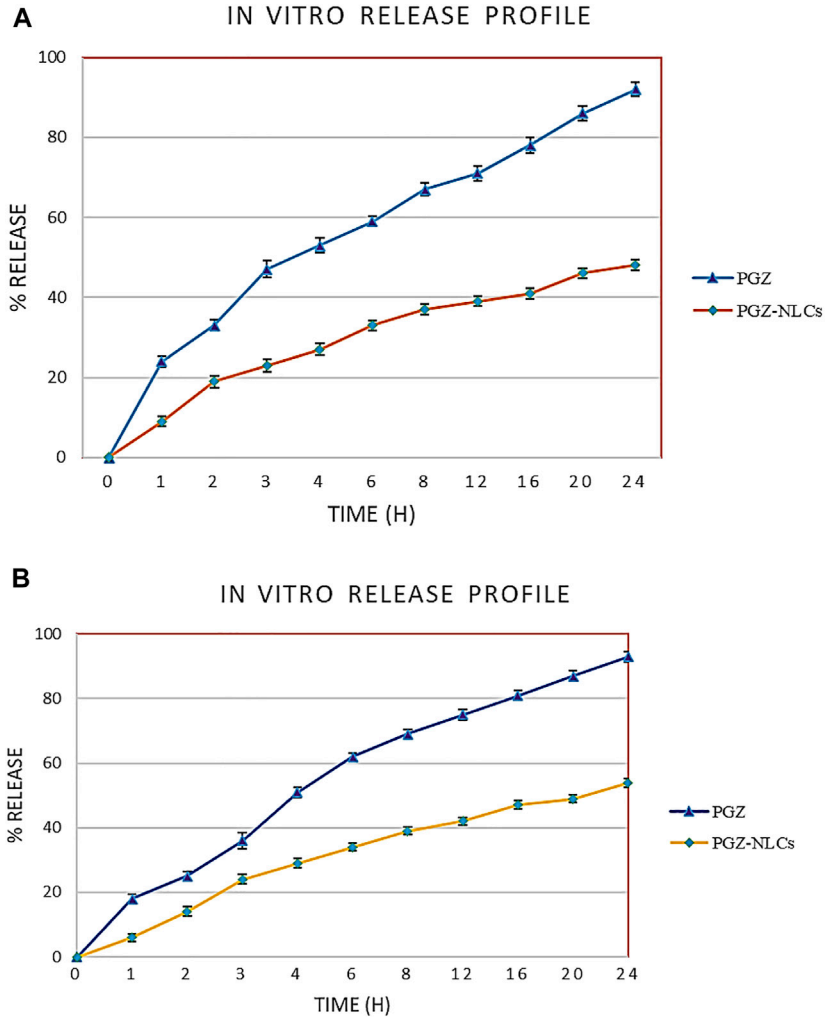

FIGURE 6 | (A) Comparative profiles of *in vitro* release of unformulated PGZ and PGZ-NLCs in simulated gastric fluid. **(B)** Comparative profiles of *in vitro* release of unformulated PGZ and PGZ-NLCs in simulated intestinal fluid.

the cause of high encapsulation efficiency of the drug and the sustained release of the drug due to stable outer core of the lipid. Tween 80 and Span 80, non-ionic surfactants, along with poloxamer 188, were utilized to form a surfactant mixture miscible with the lipid core. The selection of surfactants for the stabilization of the nano-emulsions also rests the HLB value (hydrophilic and lipophilic balance) of the surfactant-containing system. To get an optimal stability, the HLB value of the mixture of surfactants should be close to that essential for a specific lipid. The cumulative HLB of Tween 80, Span 80, and polaxamer 188 was 15.5, which is required to stabilize the Compritol® 888 ATO lipid core. PGZ-NLCs were optimized for particle size, PDI value, and encapsulation efficiency (Rizvi et al., 2019).

The NLC particle size has a significant effect on the physical stability of the NLC formulation, drug release rate, and *in vivo* performance. Various parameters affect the particle size such as the type of the lipid, surfactant, and their properties, the technique used for the production, and conditions set for the processing (such as temperature, time, and number of cycles pressure). The mean particle size of the drug-loaded NLCs rises with the surge in the melting point of lipids. It has been proposed that larger particle sizes are due to an increase in the viscosity of the dispersion medium and a rise in the lipids' melting point. Furthermore, constraints such as lipid structure, crystallization rate, and size will differ individually with the type of lipid. The composition of the lipids also considerably affects the quality of the NLCs. A lipid content higher than 5%–10% causes an increase in particle size and PDI value due to augmented viscosity of the NLC dispersions which enhances the particle agglomeration rate (Mehnert and Mäder, 2001). In addition, properties of the surfactants and their concentration used in the formulation also affect the particle size and the effectiveness of the NLCs as a system of drug delivery. Small size particles increase the surface area of NLCs. According to the Ostwald ripening

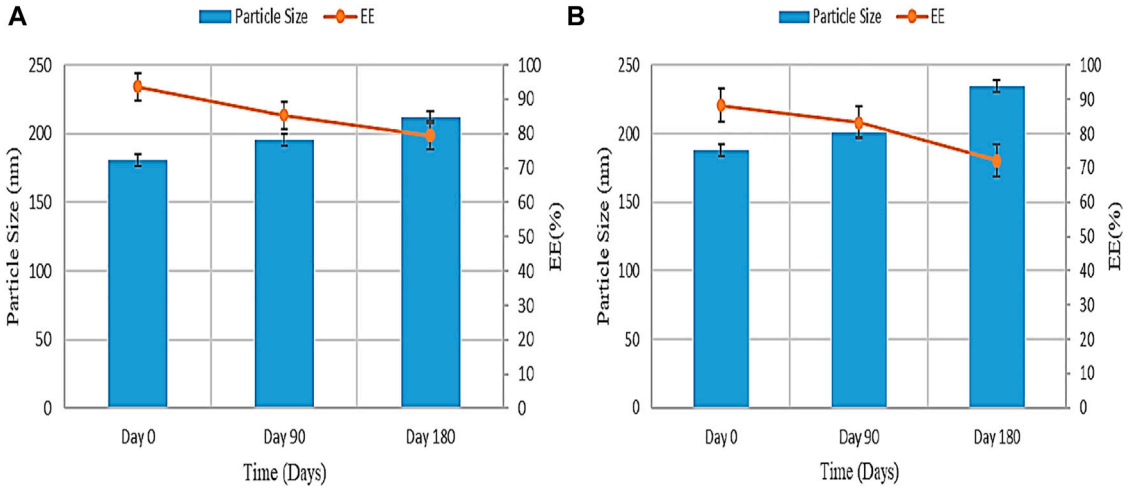

FIGURE 7 | Stability study of PGZ-NLCs **(A)** at 25°C and **(B)** 40°C.

phenomenon, the enhanced surface area causes thermodynamical variability and can result in phase separation (Mehnert and Mäder, 2001). For this reason, the amount of the surfactant used should be adequate to cover all the afresh molded surfaces in NLC fabrication. Surfactants prevent the incidence of phase separation by dropping the interfacial tension among the lipid phase and the aqueous phases. Excess surfactant might be present in the formulation in various forms such as monomers, micelles, or liposomes. It has been observed that an NLC formulation stabilized by a mixture of surfactant and co-surfactant has a small particle size and improved stability as compared to the NLCs formed with a single surfactant. Siekmann and Westesen, (1996) described that 10% w/v tyloxapol was mandatory to stabilize a dispersion of 10% w/v tripalmitin. Established that an NLC formulation stabilized by an ionic surfactant exhibited smaller particle size as equated to an NLC suspension stabilized by a surfactant of nonionic nature.

The PGZ-loaded NLC particle size and PDI value were somewhat enlarged related to blank NLCs (133.2 nm and 0.201). The reason for this effect was the entrapment of PGZ in the lipid core (Qureshi et al., 2017). The particle size of NLCs also plays a vital part in the uptake of NLCs in GIT after oral administration. For an effective drug transport into the intestinal lymphatic system, a particle size below 300 nm is favorable (Estella-Hermoso de Mendoza et al., 2009). Obtained PGZ-NLCs had a uniform size distribution as demonstrated by a smaller PDI value (0.08) and a size distribution curve of unimodal nature. PDI value < 0.2 is normally recognized as the optimal value to specify consistent nanoparticle distribution (Zhang et al., 2020). Another vital constraint that influences the physical stability of the colloidal system is zeta potential which is the degree of net surface charge. High values for zeta potential produce stability to the dispersion systems of the colloids by avoiding particle aggregation owing to electrostatic repulsion among likewise charged nanoparticles. PGZ-NLCs presented a zeta potential value of −29.1 mV, which was not dissimilar to the blank NLCs significantly (24.9 mV). A zeta potential value between −20 and −30 mV or +20 and +30 mV is considered appropriate to guarantee electrostatic steadiness.

PGZ-NLCs revealed high drug encapsulation efficiency of 92.53% and drug loading was found to be 8% which is significant for dropping the net weightiness or size of the ultimate dosage form (Zeb et al., 2020). The surface morphology and shape analysis of PGZ-NLCs was completed over SEM, and the SEM image in exposed that the shape of the PGZ-NLCs was spherical and the surfaces were smooth without any aggregation.

The FTIR spectral analysis of unformulated PGZ, Compritol® 888 ATO, poloxamer 188, and lyophilized PGZ-NLCs was carried out to assess the compatibility of the drug with the excipients. In the FTIR spectra exhibited that characteristic peaks of PGZ and Compritol 888 ATO were intact and also present in the PGZ-NLCs spectra. This result determined that no interaction took place between PGZ and formulation excipients and PGZ was compatible with all the components (Shaveta et al., 2020).

XRD spectra of pure PGZ, Compritol® 888 ATO, poloxamer 188, and PGZ-NLCs were determined and are displayed. No characteristic peak of PGZ in the XRD spectrum of PGZ-NLCs was found, and only the diffraction peaks of Compritol® 888 ATO were observed This result can be detected due to the nanosized range of NLCs and solubilization and encapsulation of PGZ in the lipid core as well as the change of crystalline PGZ to amorphic form in PGZ-NLCs (AmeeduzzafarEl-Bagory et al., 2019).

The DSC analysis of PGZ, Compritol® 888 ATO, poloxamer 188, and PGZ-NLCs was performed, and the obtained results are shown. The thermal spectrum of PGZ showed a sharp endothermic peak at 184°C while Compritol® 888 ATO at 74.6°C, which corresponded to the melting point of drug and lipid. The thermal spectrum of PGZ-NLCs did not show any endothermic melting peak of PGZ, and the thermal spectrum presented a Compritol® 888 ATO melting peak at 66.2°C with a little peak shifting to the lower temperature. This shifting of the Compritol® 888 ATO melting peak to the lower temperature in

PGZ-NLCs thermal analysis is due to the drop in the particle size. For melting big crystals, long time and more energy are required, and a decline in size enhances the particle surface area which leads to a drop in the melt temperature in comparison to Compritol® 888 ATO. This behavior can also be owing to the Compritol® 888 ATO dispersed state and surfactants presence (Span 80, Tween 80, and poloxamer 188). The nonappearance of PGZ peaks in the PGZ-loaded NLC spectrum specifies the complete encapsulation of PGZ in the lipid matrix of Compritol® 888 ATO because of the amorphization. The obtained findings were in agreement with the earlier publication (Trevaskis et al., 2015; Rizvi et al., 2019). It is notable to indicate that the alteration of crystalline PGZ to amorphous form in PGZ-NLCs may be the reason behind the enhanced solubility and improved bioavailability.

Exhibits the *in vitro* profile of PGZ-NLCs and unformulated PGZ in both media. PGZ-NLCs exhibited 19% release of PGZ in the early 2 h in simulated gastric fluid shadowed by slow and continual release form in a collective release of ~51% within 24 h (**Figure 6A**). In contrast to PGZ-NLCs, PGZ suspension displayed quicker release with 33% and 92% of PGZ released after a time of 2 and 24 h, respectively. In simulated intestinal fluid, the % release of PGZ from PGZ-NLCs was ~14% at 2 h equated to 25% from PGZ dispersal (**Figure 6B**). Within 24 h, PGZ-NLCs and PGZ suspension presented 54% and 93% release of PGZ, respectively. To some extent, the quicker release of PGZ from PGZ-NLCs in the early 2 h may be due to the fast release of a minor portion of PGZ stuck at the surface of NLCs. The preliminary increased release rates are due to this drug present on the outer surface which releases rapidly in release media. Afterward, PGZ-NLCs showed a sluggish, sustained, and partial drug liberation. The effect could be described by the slow diffusion of PGZ which was encapsulated in the lipid core of PGZ-NLCs owing to sturdy drug–lipid interactions and the steady attrition of the lipid matrix. The PGZ-NLC profile showing sustained release effect recommends a drug-enriched core model for the encapsulation of PGZ in NLCs. Though PGZ-NLCs presented somewhat quicker release first, a significant burst release effect was not detected which is an indication of drug-enriched core shell model (Rizvi et al., 2019).

The result of the stability study of PGZ-NLCs at room temperature and accelerated state according to the ICH guiding principle are described. Subsequently, storing the samples for 6 months, the samples were examined at specific time intervals. A rise in particle size and drop in EE was found on storage at room temperature and accelerated state. The particle size and entrapment efficiency noted at the start of the study were 180.6 ± 4.33 nm and 92.53% ± 4.11%, and, later a period of 180 days, the particle size at 25°C and 60% RH was increased to 211.56 ± 3.53 nm and encapsulation efficiency was decreased to 79.51% ± 4.87%, correspondingly. The particle size and entrapment efficiency outcome for PGZ-NLCs kept at 40°C were found to be significantly changed compared to the PGZ-NLCs maintained under storage conditions of 25°C. The primary particle size and entrapment efficiency were found to be 187.86 ± 3.21 nm and 88.31% ± 4.78%, and, after the period of 180 days, it exposed a significant rise in particle size (234.78 ± 7.14) and drop in entrapment efficiency (72.19% ± 4.14%). These differences in the outcomes were found due to the particle agglomeration and drug leakage from NLCs at an increased temperature and similarly may be because of the instability at the high temperature upon longer augmented storage conditions.

5 CONCLUSION

In this study, the successful development of nanostructured lipid carriers was achieved by the nano-template engineering technique. Pioglitazone was successfully incorporated into the fabricated NLCs by the temperature-controlled solidification procedure. The developed method was very simple. It was reproducible, and the NLCs were prepared without the use of any organic solvent. No sophisticated apparatuses and instruments were required, and the developed method has the potential to scale up easily for any larger-scale manufacture. The optimized PGZ-NLCs have shown a mean particle size of 150.4 nm, EE of 92.53%, PDI value of 0.076, and zeta potential of −29.1 mV, correspondingly. The DSC thermal analysis and XRD diffractograms did not present any peak of PGZ confirming the comprehensive entrapment of PGZ in the lipid core. PGZ-NLCs showed significantly extended release (51% in 24 h) compared to the unformulated PGZ. Our study findings revealed that PGZ-NLCs could be a potential drug delivery method for the treatment and management of type-2 diabetes.

Future work of this study comprises examining the consequence of pH on the *in vitro* drug release of PGZ from PGZ-NLCs and *in vitro* cell toxicity studies and *in vivo* antidiabetic studies.

DATA AVAILABILITY STATEMENT

The original contributions presented in the study are included in the article/Supplementary Material; further inquiries can be directed to the corresponding authors.

AUTHOR CONTRIBUTIONS

Conceptualization, UI, RA, and MA; writing—original draft preparation, UI, RA, and MA; writing—review and editing, MF, HZ, AP-S, MW, and MA; supervision, RA, MW, and MA. All authors have read and agreed to the published version of the manuscript.

FUNDING

This work was supported by the Beijing Natural Science Foundation (Grant No. M22032) and Riphah International University (Riphah-ORIC-21-22/FPS-51 and Riphah-ORIC-21-22/FPS-56).

REFERENCES

AmeeduzzafarEl-Bagory, I., El-Bagory, I., Alruwaili, N. K., Elkomy, M. H., Ahmad, J., Afzal, M., et al. (2019). Development of Novel Dapagliflozin Loaded Solid Self-Nanoemulsifying Oral Delivery System: Physiochemical Characterization and *In Vivo* Antidiabetic Activity. *J. Drug Deliv. Sci. Technol.* 54, 101279. doi:10.1016/j.jddst.2019.101279

Bhosale, U., Galgatte, U., and Chaudhari, P. (2016). Development of Pioglitazone Hydrochloride Lipospheres by Melt Dispersion Technique: Optimization and Evaluation. *J. App Pharm. Sci.* 6 (01), 107–117. doi:10.7324/japs.2016.600118

Casula, L., Sinico, C., Valenti, D., Pini, E., Pireddu, R., Schlich, M., et al. (2021). Delivery of Beclomethasone Dipropionate Nanosuspensions with an Electronic Cigarette. *Int. J. Pharm.* 596, 120293. doi:10.1016/j.ijpharm.2021.120293

Eckland, D., and Danhof, M. (2000). Clinical Pharmacokinetics of Pioglitazone. *Exp. Clin. Endocrinol. diabetes* 108 (Suppl. 2), 234–242. doi:10.1055/s-2000-8525

Elbary, A. A., Kassem, M. A., Abou Samra, M. M., and Khalil, R. M. (2008). Formulation and Hypoglycemic Activity of Pioglitazone-Cyclodextrin Inclusion Complexes. *Drug Discov. Ther.* 2 (2), 94–107.

Estella-Hermoso de Mendoza, A., Campanero, M. A., Mollinedo, F., and Blanco-Prieto, M. J. (2009). Lipid Nanomedicines for Anticancer Drug Therapy. *J. Biomed. Nanotechnol.* 5 (4), 323–343. doi:10.1166/jbn.2009.1042

Junghanns, J. U., and Müller, R. H. (2008). Nanocrystal Technology, Drug Delivery and Clinical Applications. *Int. J. Nanomedicine* 3 (3), 295–309. doi:10.2147/ijn.s595

Koradia, K. D., Parikh, R. H., and Koradia, H. D. (2018). Albendazole Nanocrystals: Optimization, Spectroscopic, Thermal and Anthelmintic Studies. *J. drug Deliv. Sci. Technol.* 43, 369–378. doi:10.1016/j.jddst.2017.11.003

Malamatari, M., Taylor, K. M. G., Malamataris, S., Douroumis, D., and Kachrimanis, K. (2018). Pharmaceutical Nanocrystals: Production by Wet Milling and Applications. *Drug Discov. Today* 23 (3), 534–547. doi:10.1016/j.drudis.2018.01.016

Mehnert, W., and Mäder, K. (2001). Solid Lipid Nanoparticles: Production, Characterization and Applications. *Adv. Drug Deliv. Rev.* 47 (2), 165–196. doi:10.1016/s0169-409x(01)00105-3

Mehnert, W., and Mäder, K. (2012). Solid Lipid Nanoparticles: Production, Characterization and Applications. *Adv. drug Deliv. Rev.* 64, 83–101. doi:10.1016/j.addr.2012.09.021

Mosure, S. A., Shang, J., Eberhardt, J., Brust, R., Zheng, J., Griffin, P. R., et al. (2019). Structural Basis of Altered Potency and Efficacy Displayed by a Major *In Vivo* Metabolite of the Antidiabetic PPARγ Drug Pioglitazone. *J. Med. Chem.* 62 (4), 2008–2023. doi:10.1021/acs.jmedchem.8b01573

Pandey, V., and Kohli, S. (2017). SMEDDS of Pioglitazone: Formulation, *In-Vitro* Evaluation and Stability Studies. *Future J. Pharm. Sci.* 3, 53–59. doi:10.1016/j.fjps.2017.02.003

Pawar, V. K., Singh, Y., Meher, J. G., Gupta, S., and Chourasia, M. K. (2014). Engineered Nanocrystal Technology: *In-Vivo* Fate, Targeting and Applications in Drug Delivery. *J. Control Release* 183, 51–66. doi:10.1016/j.jconrel.2014.03.030

Pireddu, R., Caddeo, C., Valenti, D., Marongiu, F., Scano, A., Ennas, G., et al. (2016). Diclofenac Acid Nanocrystals as an Effective Strategy to Reduce *In Vivo* Skin Inflammation by Improving Dermal Drug Bioavailability. *Colloids Surf. B Biointerfaces* 143, 64–70. doi:10.1016/j.colsurfb.2016.03.026

Qureshi, O. S., Kim, H. S., Zeb, A., Choi, J. S., Kim, H. S., Kwon, J. E., et al. (2017). Sustained Release Docetaxel-Incorporated Lipid Nanoparticles with Improved Pharmacokinetics for Oral and Parenteral Administration. *J. Microencapsul.* 34 (3), 250–261. doi:10.1080/02652048.2017.1337247

Rizvi, S. Z. H., Shah, F. A., Khan, N., Muhammad, I., Ali, K. H., Ansari, M. M., et al. (2019). Simvastatin-loaded Solid Lipid Nanoparticles for Enhanced Anti-hyperlipidemic Activity in Hyperlipidemia Animal Model. *Int. J. Pharm.* 560, 136–143. doi:10.1016/j.ijpharm.2019.02.002

Shaveta, S., Singh, J., Afzal, M., Kaur, R., Imam, S. S., Alruwaili, N. K., et al. (2020). Development of Solid Lipid Nanoparticle as Carrier of Pioglitazone for Amplification of Oral Efficacy: Formulation Design Optimization, *In-Vitro* Characterization and *In-Vivo* Biological Evaluation. *J. Drug Deliv. Sci. Technol.* 57, 101674. doi:10.1016/j.jddst.2020.101674

Siekmann, B., and Westesen, K. (1996). Investigations on Solid Lipid Nanoparticles Prepared by Precipitation in O/w Emulsions. *Eur. J. Pharm. Biopharm.* 42 (2), 104–109.

Sinha, B., Müller, R. H., and Möschwitzer, J. P. (2013). Bottom-up Approaches for Preparing Drug Nanocrystals: Formulations and Factors Affecting Particle Size. *Int. J. Pharm.* 453 (1), 126–141. doi:10.1016/j.ijpharm.2013.01.019

Smith, U. (2001). Pioglitazone: Mechanism of Action. *Int. J. Clin. Pract. Suppl.* (121), 13–18.

Souri, E., Jalalizadeh, H., and Saremi, S. (2008). Development and Validation of a Simple and Rapid HPLC Method for Determination of Pioglitazone in Human Plasma and its Application to a Pharmacokinetic Study. *J. Chromatogr. Sci.* 46 (9), 809–812. doi:10.1093/chromsci/46.9.809

Trevaskis, N. L., Kaminskas, L. M., and Porter, C. J. (2015). From Sewer to Saviour - Targeting the Lymphatic System to Promote Drug Exposure and Activity. *Nat. Rev. Drug Discov.* 14 (11), 781–803. doi:10.1038/nrd4608

Waugh, J., Keating, G. M., Plosker, G. L., Easthope, S., and Robinson, D. M. (2006). Pioglitazone. *Drugs* 66 (1), 85–109. doi:10.2165/00003495-200666010-00005

Williams, H. D., Trevaskis, N. L., Charman, S. A., Shanker, R. M., Charman, W. N., Pouton, C. W., et al. (2013). Strategies to Address Low Drug Solubility in Discovery and Development. *Pharmacol. Rev.* 65 (1), 315–499. doi:10.1124/pr.112.005660

Zeb, A., Cha, J.-H., Noh, A. R., Qureshi, O. S., Kim, K.-W., Choe, Y.-H., et al. (2020). Neuroprotective Effects of Carnosine-Loaded Elastic Liposomes in Cerebral Ischemia Rat Model. *J. Pharm. Investig.* 50 (4), 373–381. doi:10.1007/s40005-019-00462-y

Zhang, Q., Yang, H., Sahito, B., Li, X., Peng, L., Gao, X., et al. (2020). Nanostructured Lipid Carriers with Exceptional Gastrointestinal Stability and Inhibition of P-Gp Efflux for Improved Oral Delivery of Tilmicosin. *Colloids Surf. B Biointerfaces* 187, 110649. doi:10.1016/j.colsurfb.2019.110649

Conflict of Interest: The authors declare that the research was conducted in the absence of any commercial or financial relationships that could be construed as a potential conflict of interest.

Publisher's Note: All claims expressed in this article are solely those of the authors and do not necessarily represent those of their affiliated organizations, or those of the publisher, the editors, and the reviewers. Any product that may be evaluated in this article, or claim that may be made by its manufacturer, is not guaranteed or endorsed by the publisher.

frontiers | Frontiers in Pharmacology

TYPE Review
PUBLISHED 24 August 2022
DOI 10.3389/fphar.2022.933457

OPEN ACCESS

EDITED BY
Saeed Ahmad Khan,
Kohat University of Science and Technology, Pakistan

REVIEWED BY
Riya Biswas,
Auckland University of Technology, New Zealand
Abimanyu Sugumaran,
SRM Institute of Science and Technology, India
Shibing Wang,
Zhejiang Provincial People's Hospital, China

*CORRESPONDENCE
Aws Alshamsan,
aalshamsan@ksu.edu.sa,

†These authors have contributed equally to this work

SPECIALTY SECTION
This article was submitted to Experimental Pharmacology and Drug Discovery, a section of the journal Frontiers in Pharmacology

RECEIVED 30 April 2022
ACCEPTED 29 July 2022
PUBLISHED 24 August 2022

CITATION
Alshememry AK, Alsaleh NB, Alkhudair N, Alzhrani R and Alshamsan A (2022), Recent nanotechnology advancements to treat multidrug-resistance pancreatic cancer: Pre-clinical and clinical overview. *Front. Pharmacol.* 13:933457. doi: 10.3389/fphar.2022.933457

Recent nanotechnology advancements to treat multidrug-resistance pancreatic cancer: Pre-clinical and clinical overview

Abdullah K. Alshememry[1,2†], Nasser B. Alsaleh[2,3†], Nora Alkhudair[4], Rami Alzhrani[5] and Aws Alshamsan[1,2*]

[1]Department of Pharmaceutics, College of Pharmacy, King Saud University, Riyadh, Saudi Arabia, [2]Nanobiotechnology Unit, College of Pharmacy, King Saud University, Riyadh, Saudi Arabia, [3]Department of Pharmacology and Toxicology, College of Pharmacy, King Saud University, Riyadh, Saudi Arabia, [4]Department of Clinical Pharmacy, College of Pharmacy, King Saud University, Riyadh, Saudi Arabia, [5]Department of Pharmaceutics and Pharmaceutical Technology, College of Pharmacy, Taif University, Taif, Saudi Arabia

Pancreatic cancer (PC) remains one of the most lethal and incurable forms of cancer and has a poor prognosis. One of the significant therapeutic challenges in PC is multidrug resistance (MDR), a phenomenon in which cancer cells develop resistance toward administered therapy. Development of novel therapeutic platforms that could overcome MDR in PC is crucial for improving therapeutic outcomes. Nanotechnology is emerging as a promising tool to enhance drug efficacy and minimize off-target responses via passive and/or active targeting mechanisms. Over the past decade, tremendous efforts have been made to utilize nanocarriers capable of targeting PC cells while minimizing off-target effects. In this review article, we first give an overview of PC and the major molecular mechanisms of MDR, and then we discuss recent advancements in the development of nanocarriers used to overcome PC drug resistance. In doing so, we explore the developmental stages of this research in both pre-clinical and clinical settings. Lastly, we discuss current challenges and gaps in the literature as well as potential future directions in the field.

KEYWORDS

multidrug resistance, drug delivery, paclitaxel, tumor microenvironment, pancreatic cancer, non-clinical studies, clinical studies

Introduction

Pancreatic cancer (PC) accounts for 2.5% of all cancer cases worldwide, making it the fourth leading cause of cancer mortality (Siegel et al., 2019). An estimated 495,773 patients were diagnosed with PC in 2021 (Cancer.Net, 2022), with approximately 50% of the cases were diagnosed with metastatic disease (Bray et al., 2018). The location of the tumor

TABLE 1 Pancreatic cancer pathological types. Pancreatic cancer pathologically originates from exocrine or endocrine cells. The prevalence and common mutations are different depending on the tumor type and cell origin. Invasive ductal adenocarcinoma is a common type of PC in cells with an exocrine origin.

Type	Category	Prevalence	Mutations
Invasive ductal adenocarcinoma	Exocrine	95%	KRAS, P16/CDKN2A, TP53, SMAD4
Acinar cell carcinoma	Exocrine	1–2%	APC/β-catenin
Serous Cystadenocarcinoma	Exocrine	3%	VHL
Neuroendocrine (PENT)	Endocrine	5%	MEN1

KRAS: Kirsten rat sarcoma viral oncogene homolog; CDKN2A: Cyclin-dependent kinase inhibitor 2A; TP53: Tumor protein p53; SMAD: an acronym from the fusion of *Caenorhabditis elegans Sma* genes and the *Drosophila Mad*; APC: Adenomatous polyposis coli; VHL: Von Hippel-Lindau; MEN1: Multiple endocrine neoplasia type 1.

within the pancreas can influence the symptoms and clinical presentation (Ryan et al., 2014; Ducreux et al., 2015; Tempero et al., 2019). Almost 65% of PC tumors develop in the head and the neck of the pancreas, and patients commonly present with jaundice and abdominal pain due to bile obstruction (Ducreux et al., 2015; Tempero et al., 2019). In some cases, PC can either be located in the pancreas body (15%), and the tail (10%), or can be a multifocal tumor (2%). Furthermore, patients can present with other non-specific symptoms, including late-onset type II diabetes, abdominal pain, weight loss, and steatorrhea (Gheorghe et al., 2020).

Pathologically, PC originates from two types of cells: exocrine or endocrine cells (Bardeesy and DePinho, 2002; Ghaneh et al., 2007; Corbo et al., 2012; Aguirre and Collisson, 2017). Over 95% of all PC types are of exocrine origin, where the majority of these cases are pancreatic adenocarcinomas (PDAC) (Cowgill and Muscarella, 2003; Li and Jiao, 2003). Less common cells are those of acinar and cystadenocarcinoma origin (Table 1). The endocrine tumors include neuroendocrine tumors (PNET), which account for 5% of all PC cases (Hackeng et al., 2016). PNETs grow slowly and are less aggressive than the PDAC (Bardeesy and DePinho, 2002; Ghaneh et al., 2007). PDAC is a complex disease with poorly differentiated histological features. The high intertumoral heterogeneity, genomic instability, and stromal desmoplasia formation cause significant challenges in the early diagnosis and treatment of PDAC (Ghaneh et al., 2007; Corbo et al., 2012; Aguirre and Collisson, 2017). Pancreatic intraepithelial neoplasia (PanIN) is the most common early non-invasive precursor lesion of PDAC, in addition to mucinous cystic neoplasm and intraductal papillary mucinous neoplasm. The precursor's progression from low-grade to high-grade is due to genetic and epigenetic alterations that lead to the formation of invasive PDAC. When PDAC lesions form, the genetic mutations will continue to progress beyond primary mutations (Ghaneh et al., 2007; Rishi et al., 2015; Hackeng et al., 2016; Dreyer et al., 2017).

Drug resistance, both intrinsic (innate) and acquired (in response to drug therapy), is a key contributing factor to the poor prognosis of PC (Binenbaum et al., 2015). The survival rate of PC has remained almost unchanged for several decades, and it is considered among the lowest, with a 5-year survival rate for a maximum of 9% of cases for all stages combined (Rawla et al., 2019; Siegel et al., 2019). Such a low rate of survival is attributed to two major factors: 1) late diagnosis of typically advanced/metastasized and unresectable PC due to a lack of early diagnostic biomarkers; and 2) lack of effective therapeutic intervention (Siegel et al., 2019). There are fundamental reasons why pancreatic tumors are difficult to treat in PC. Firstly, pancreatic tumors, such as PDAC, are solid tumors comprised of a dense stromal environment of cancerous cells, non-cancerous cells such as fibroblasts, and a dense extracellular matrix. The density of these arrangements impedes drug permeation. Additionally, if a drug can permeate the cancerous stroma, the drug molecules are typically unable to differentiate between cancerous and non-cancerous cells due to the dense tumor stroma (Heidemann and Kirschner, 1978; Sofuni et al., 2005). An important determinant of peritoneal metastasis is the anatomical position of the primary tumor (Baretti et al., 2019). In some cases, cells directly attach to and invade organs and tissues in the peritoneal cavity (Avula et al., 2020) or result in intraperitoneal metastases via blood vessels or lymphatic absorption through the hematogenous route (Ge et al., 2017). In most cases of PC, metastasis has already occurred by the time of diagnosis. Furthermore, even when surgical intervention is applicable, following chemoradiotherapy, rapid relapse is often seen due to the presence of pancreatic satellite cells that promote carcinogenesis (Hosoki, 1983; Sofuni et al., 2005; Zhi et al., 2014; Binenbaum et al., 2015).

The stromal desmoplastic reactions induced by the pancreatic stellate cells (PSC), when activated by growth factors, lead to the secretion of collagen, hyaluronic acid, and other components of the extracellular matrix. Thus, PSCs induce stromal fibrosis, reduce cellular vascularity, and induce hypoxia. The stromal barrier created by PSC elevates the interstitial fluid pressure and compresses the blood vessels, preventing passive transportation of chemotherapeutic agents and eventually leading to treatment failure (Erkan et al., 2012; Hackeng et al., 2016). Efficacy of Trans-arterial chemoembolization (TACE) with TACE + radiofrequency ablation (RFA) and/or ^{125}I radioactive seed implantation for unresectable pancreatic

cancer are other approaches that have been studied retrospectively and TACE combined with either ^{125}I seed implantation and/or RFA, was shown to have improved treatment response and overall survival rate compared with TACE alone (Das et al., 2019). However, in the same study, the overall survival rates were better in the case of RFA. To summarize, based on these previous data, the sequence of use and the best combination therapy in the case of PC remains to be investigated.

While there are numerous drugs available for the treatment of PC, two nanoparticle formulations, Abraxane® and Onivyde® (irinotecan liposome injection) have been approved as of July 2022 by the US FDA for the treatment of metastasized cancers, in combination with gemcitabine. Abraxane® is a Paclitaxel Albumin-stabilized Nanoparticle Formulation, approved for the treatment of metastasized PC in combination with gemcitabine hydrochloride as a first-line treatment. More recently, the use of nanotechnology for delivering drugs to targeted sites in the body is an inexpensive and effective system for treating diseases and other conditions. Indeed, the use of nanotechnology can revolutionize the treatment of cancer, by enabling diagnostic tools for early detection of the disease (Hu et al., 2021) as well as improving drug delivery. In PC, the delivery and distribution of drugs to the tumor are compromised due to intrinsic physical and biochemical barriers, which result in increased interstitial fluid pressure, vascular compression, and hypoxia. Moreover, therapies based on targeting immune responses including therapeutic vaccines, immune checkpoint inhibition, and CAR-T cell therapy often do not show expected responses due to a highly immunosuppressive tumor microenvironment. These two factors present as a major challenge for developing effective therapies against PC. Nanoparticles have been extensively studied as delivery platforms and adjuvants for cancer and other disease therapies. Knowledge gained through using nanocarrier-based systems in other cancer types, combined with the ability to modulate nanocarriers toward targeting multiple MDR mechanisms simultaneously provides an opportunity to enable improvement in drug delivery and enhancing therapeutic outcomes for PC.

Mechanisms of resistance in pancreatic cancer

Numerous alterations at the genetic, epigenetic, and protein levels are implicated in PC drug resistance (Binenbaum et al., 2015). Although different therapy regimens exist, the current standard of care regimen therapy for PC remains largely dependent on gemcitabine (GEM), which is considered a gold standard in chemotherapy. GEM is a nucleoside analog, which provides only a modest clinical benefit (Burris et al., 1997). Multiple combination regimens of chemotherapeutics such as GEM with 5-fluorouracil (5-FU), cisplatin or paclitaxel (PTX), or FOLFIRINOX (i.e., fluorouracil, leucovorin, irinotecan, and oxaliplatin alone or alongside targeted therapies [e.g., cetuximab and bevacizumab]) have failed to demonstrate significant clinical benefits (Berlin et al., 2002; Cascinu et al., 2006; Heinemann et al., 2006). Despite the initial response to chemotherapy in the different forms of PC, the rapid development of drug resistance remains a major challenge in the treatment of PC (Binenbaum et al., 2015).

It is now well established that a variety of cancers mediate their aggressiveness and resistance to chemoradiotherapy via modulating key cellular regulatory pathways that control cell proliferation and differentiation, inflammation, and programmed cell death pathways, including apoptosis and autophagy (Xia et al., 2014). PC shows a significant up-regulation of ATP binding cassette (ABC) transporters ABCB4, ABCB11, ABCC1, ABCC3, ABCC5, ABCC10, and ABCG2 at the RNA level in tumors relative to the normal pancreas (Mohelnikova-Duchonova et al., 2013). Additionally, drug efflux pump MDR1/P-gp is highly expressed in PC cells (O'Driscoll et al., 2007), which may play a critical role in the development of resistance to chemotherapeutic agents. Therefore, it is equally important to understand the underlying molecular mechanisms of PC drug resistance for unraveling novel therapeutic interventions with improved efficacy. In addition, somatic mutations in key genes such as many proto-oncogenes (e.g., Ras, Myc, Cdk4) are critical in the initiation and progression of malignant tumors. However, cancer treatment is even more challenging because tumor exposure to therapy, including chemoradiotherapy and targeted therapy, is often associated with further mutations and the development of compensatory mechanisms that render cancer refractoriness to therapy and increased aggressiveness and metastasis (Binenbaum et al., 2015). Therefore, understanding the molecular mechanisms of drug resistance is crucial in order to intervene and eventually win the battle against cancer.

The main mutations of PDAC include KRAS, CDKN2A, TP53, and SMAD4 (Hackeng et al., 2016). Over 90% of PC is associated with KRAS mutations, most commonly KRAS^{G12D}, during both the initial stage (i.e., precursor lesions that develop into invasive pancreatic ductal adenocarcinoma, also known as pancreatic intraepithelial neoplasia) and progression stage (di Magliano and Logsdon, 2013). There have been efforts to discover new PDAC targeting agents. A phase 1 clinical trial (NCT04117087) used a long peptide vaccine combined with Nivolumab and Ipilimumab for resected MMR-p colorectal and pancreatic cancer patients. Interestingly, Govindan *et al.* discovered that AMG 510 is a novel small molecule that can bind specifically and irreversibly in KRAS^{G12C} (Govindan et al., 2019; Alzhrani et al., 2021). KRAS^{G12C} is a mutation that is predominantly found in non-small lung cancer. However, the use of AMG 510 is limited in PDAC because KRAS^{G12C} mutation only accounts for 2%. These findings will motivate the scientific

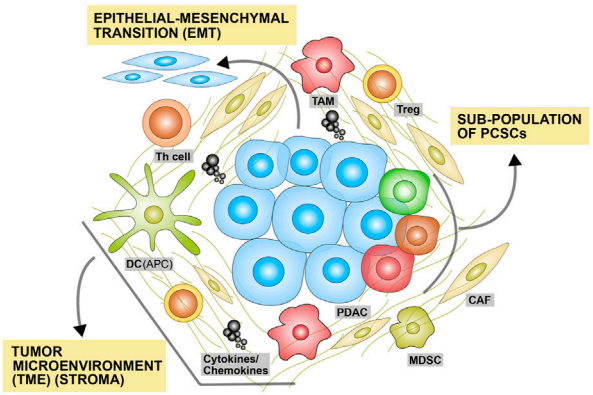

FIGURE 1
Major molecular contexts underlying drug resistance in pancreatic cancer. This figure illustrates the three major molecular contexts underlying drug resistance in pancreatic cancer. These include: 1) the process of epithelial-mesenchymal transition (EMT) in which cancer cells lose their epithelial phenotype (such as cell-to-cell contact) to gain more aggressive and metastatic mesenchymal phenotypes; 2) expansion of subpopulation of pancreatic cancer stem cells (PCSCs); and 3) dynamic tumor microenvironment (TME). The tumor stroma surrounding cancer cells and PCSCs consist non-cellular components including extracellular matrix (ECM) and multiple cell types including CAF, MDSC, Th-cells, Treg, TAM and DC. Cytokines released from the different cell types help maintaining the TME in dynamic state that supports tumor growth and metastasis. Th-cells exist in TME but are suppressed. DCs, which are key in the processing and presentation of cancer neoantigens, exist in TME but they are suppressed as well. EMT: epithelial-mesenchymal transition; PCSC: pancreatic cancer stem cell; TME: tumor microenvironment; CAF: Cancer-associated fibroblast; MDSC: myeloid-derived suppressor cell; Th-cells: Helper T cells; Treg: Regulatory T-cell; TAM: tumor-associated macrophage; DC: Dendritic cell.

community to develop new drugs that can target inactive $KRAS^{G12D}$ and $KRAS^{G12V}$, which account for 80% of PDAC (Govindan et al., 2019; Alzhrani et al., 2021).

It is worth noting that tremendous efforts over the past years have revealed numerous molecular components and intricate signaling networks that are deregulated in PC, contributing to chemoresistance. These include, but are not limited, drug transporters (e.g., hENT and hCNT), intracellular enzymes (e.g., deoxycytidine kinase), dCK, which is critical for GEM bioactivation, DNA repair mechanisms (e.g., excision repair cross-complementation 1), ERCC1, antioxidant response (e.g., Nrf and HSPs), signaling pathways that regulate cell-cycle and programmed cell death (e.g., Nuclear Factor κB [NFκB], MAPK, PI3K/Akt and p53), epigenetic components (e.g., histone deacetylase), HDAC and more recently, noncoding RNAs (ncRNAs) [e.g., microRNAs (miRNAs), long noncoding RNAs (lncRNAs) and circular RNAs (circRNAs)] (Binenbaum et al., 2015; Xie et al., 2020a; Lin et al., 2020; Pandya et al., 2020). More recently, differential upregulation and functional role of the transmembrane mucin MUC4 in PC is an attractive target for immunotherapy and MUC4β encapsulation in polyanhydride nanoparticles has been shown to provide long-term protection against rapid phagocytic and proteolytic clearance in circulation. Stable MUC4β release from these nanoparticles and its immunogenic capacity has recently been demonstrated by Liu and colleagues in mice models (Liu et al., 2021). Discussing the specific molecular mechanism is beyond the scope of this review and is discussed in detail elsewhere, but here we give an overall overview and describe three key themes involved in PC drug resistance. These are epithelial-mesenchymal transition (EMT), expansion of pancreatic cancer stem cells (PCSCs), and dynamic state of the tumor microenvironment (TME), as illustrated in (Figure 1) (Binenbaum et al., 2015; Zeng et al., 2019).

Epithelial-mesenchymal transition (EMT) is a dynamic process that involves the transitioning of differentiated epithelial cells into the mesenchymal cell phenotype. During this transformation, cells lose key features of epithelial cells such as intercellular junctions while simultaneously undergoing cytoskeletal rearrangement of the mesenchymal cell phenotype (Nieto et al., 2016). EMT is particularly critical during cancer progression and the generation of stem-like cells with a high capacity for metastasis (Nieto et al., 2016). Notably, previous literature has demonstrated the key role of EMT in conferring drug resistance against chemoradiotherapy and targeted therapy in a variety of solid tumors, including PC (Shah et al., 2007; Wang et al., 2009; Singh and Settleman, 2010; Nieto et al., 2016). For instance, chemoresistance to GEM in PC cells has been associated with increased expression of mesenchymal markers such as vimentin and ZEB1, in contrast to GEM-sensitive cells with a high E-cadherin expression: a common epithelial phenotype maker (Li et al., 2009). Similar findings have been found with other chemotherapeutics, such as 5-FU and cisplatin (Arumugam et al., 2009). Although the underlying molecular mechanisms of EMT-induced chemoresistance are not fully understood, accumulating evidence suggests the involvement of multiple signaling pathways, including NFκB, TGFβ, and Notch pathways (Ellenrieder et al., 2001; Min et al., 2008; Wang et al., 2009). Another key molecular regulator of EMT in PC cells is miRNAs: small non-coding RNAs that regulate gene expression (Yonemori et al., 2017). A multitude of miRNAs has been shown to be implicated in regulating major cellular signaling pathways involved in the development of PC (Yonemori et al., 2017). For instance, a low expression of miR-200 was found in the GEM-resistant but not in the GEM-sensitive PC cell lines (Li et al., 2009). Together, these findings indicate the critical role of EMT in the development of PC drug resistance in transformed cells.

Previous evidence has demonstrated that cancers are heterogenous in nature, with subpopulations of cells of varying phenotypes. Cancer stem cells (CSCs) represent a small subpopulation of tumor cells with a high capacity for self-renewing, differentiation, and tumor progression (Yu et al., 2012). Indeed, CSCs display a high capacity for

tumorigenesis when transplanted into a host compared to other tumor subpopulations (Yu et al., 2012). Several cellular surface markers have been identified to be expressed by CSCs in various cancers, including CD44, CD24, CD133, aldehyde dehydrogenase1 (ALDH1), and epithelial-specific antigen (ESA) (Yu et al., 2012). In PC, previous work has demonstrated that CD44, CD24, and ESA-expressing PCSCs, represented only by a small percentage of the cancer cell population (~1%), were associated with high tumorigenic potential, and it is likely that PCSCs at least partially mediate chemoradiotherapy-induced drug resistance, as evident in PCSC enrichment in response to chemoradiotherapy treatment (Du et al., 2011). Similar findings were also found in another report, demonstrating that within a pancreatic tumor, a subset of undifferentiated, stem-like cells expressing the surface marker CD133, was associated with high tumorigenic potential and chemoresistance (Hermann et al., 2007). Although there is an overlap between the two subpopulations of PCSCs in the two reports (CD44/CD24/ESA-vs. CD133-expressing PCSCs), they were not identical (Hermann et al., 2007). Additionally, another subset of cells with exclusive migratory properties expressing CD133 and CXCR4 were identified at the invasive front of pancreatic tumors. It was found that without these $CD133^{+}$/$CXCR4^{+}$ cells, metastasis was almost completely abrogated (Hermann et al., 2007). Together, these findings indicate the existence of different subsets of PCSCs within pancreatic tumors with a high capacity for tumorigenesis and drug resistance. Such findings demonstrate the heterogenic nature of cancers which has been long disregarded in cancer research. It is worth noting that EMT transformed cells can share cellular and molecular features of CSCs, which could explain an increased tumorigenic profile of EMT transformed cells as well as drug resistance. Nonetheless, these cells, unlike PCSCs, were sensitive to conventional chemotherapy. Furthermore, it is now widely accepted that subpopulations of CSCs exist in a dynamic state (quiescent vs. slow-vs. rapid-cycling CSCs), which is constantly influenced by signals and cues from their surroundings (the tumor microenvironment (TME). With their large plasticity and ability to switch to a quiescent state, CSCs can resist chemoradiotherapy (Batlle and Clevers, 2017).

The tumor microenvironment (TME) consists of cellular and non-cellular components (extracellular matrix (ECM)) and plays a crucial role in drug resistance. Indeed, one major obstacle in the treatment of PC is the dense fibrotic stroma, also known as desmoplastic stroma, surrounding tumor cells that act as a physical barrier. As such, they prevent drugs from infiltrating tumor core cells (Dauer et al., 2017). Thus, the dense fibrotic stroma is considered a histopathological hallmark of PC. It is worth noting that TME is composed of several types of cells, including fibroblasts, pancreatic stellate cells (myofibroblast-like cells), and a variety of immune cells and despite the considerable efforts made to target a multitude of cellular and noncellular components within TME, yet it was associated with limited clinical success (Ho et al., 2020). For instance, within the stromal cells, cancer-associated fibroblasts (CAFs), which are the major source of ECM, are associated with immunosuppressive properties (Kraman et al., 2010). Depletion of CAFs was associated with enhanced efficacy of immune checkpoint inhibitors (ICIs) (Feig et al., 2013). In addition to CAFs, other cell types within the TME including regulatory T-cells (Treg), myeloid-derived suppressor cell (MDSC), and tumor-associated macrophage (TAM) also possess immunosuppressive properties (Ho et al., 2020). Cancer immunotherapy has revolutionized the field over the past couple of decades. Notable success has been made against multiple solid cancers, particularly those with high tumor mutational burden (TMB) within the tumor genome, such as melanoma and lung cancer (Goodman et al., 2017; Yousefi et al., 2017). This success has not been evident in PC (Schizas et al., 2020), which has largely been attributed to the non-immunogenic nature of most types of PC. In other words, most PC types are not readily recognized by the immune cells due to low TMB and thus a low number of neoantigens, a tumor-associated antigen, and subsequent presences of TILs (Bailey et al., 2016; Danilova et al., 2019). Additionally, as mentioned earlier, PC is typically contained in a highly dense fibrotic stroma consisting of multiple cell types with immunosuppressive properties (Ho et al., 2020; Schizas et al., 2020). Unsurprisingly, together, these two factors make cancer immunotherapy less effective in PC. Utilizing the properties of TME for controlling local therapeutic delivery is an area of active research (Alshememry et al., 2017).

Nanotechnology for the treatment of pancreatic cancer

Nanomaterials and nanoparticles (NPs) are extremely small (1–100 nm) in size and hence can directly interact with biological molecules (Hosein et al., 2013). Engineered NPs are an excellent tool for drug delivery due to their unique structural properties which include a large surface-to-mass ratio, capacity to be modulated to bind different cellular targets, and ability to carry different cargo including proteins, nucleotides, and drugs. Advances in the field of nanotechnology have created tremendous prospects for improving therapeutic drug delivery (Schroeder et al., 2011; Melancon et al., 2012; Prabhu and Patravale, 2012). Currently, the use of nanotechnology in drug delivery typically involves a combination of nanomaterials and a drug of interest, and a significant number of nanoplatforms are being employed and are under testing in the different phases of clinical trials (Ogawa and Miura, 2014; Rebelo et al., 2017). These combinations utilize different types of nanomaterials such as polymeric NPs, liposomes, amphiphilic polymer NPs, small interfering RNA (siRNA), graft polymers, dendrimers, thermo-responsive polymers, mixed micelles, ultrasound-

responsive nano-emulsions, carbon nanotubes, quantum dots and inorganic NPs (magnetic-hybrid NPs, and gold NPs) (Manzur et al., 2017; Rebelo et al., 2017; Sielaff and Mousa, 2018).

Nanotechnology has been largely utilized in cancer research to improve the delivery of drugs to the tumor site exploiting the leaky vasculature of the tumor via passive or enhanced permeability and retention (EPR) effect. However, a major challenge in PC is its hypovascularization, and hence, other strategies must be utilized, such as using targeted (active) delivery (Xie et al., 2020b). As a result of this insufficient vascularization, ineffective distribution of drugs may account for much of the chemotherapy resistance seen in PC treatment. The use of nanotherapy may bypass the inefficient vascularization issues by delivering chemotherapeutic drugs directly to the pancreatic tissue, for example, by targeting stromal hedgehog receptors rather than relying on blood flow, a methodology that provides a tunable distribution of chemotherapeutic agents throughout pancreatic tumor tissue, thereby increasing drug solubility, half-life, and stability (Jiang et al., 2020). Moreover, NPs delivering chemotherapeutic drugs can bypass multidrug-resistant (MDR) efflux pumps present on the surface of most tumor cells (Lobato-Mendizabal and Ruiz-Arguelles, 1990; Blanco et al., 2011; McCarroll et al., 2014). This, among other reasons that will be discussed in later sections, supports the use of nanotechnology in PC treatment.

Nano-based intervention to overcome MDR-PC in pre-clinical and clinical settings: Key examples

The use of NPs has several advantages, including minimizing MDR and drug-related toxicities. Nanoparticles can target a wide range of physiological and metabolic characteristics of the targeted tissues, thereby increasing biodistribution and bioavailability of drugs and enhancing their plasma half-life and EPR (Parhi et al., 2012; Poon et al., 2015; Gad et al., 2016; Liu et al., 2022). Recently, the potency of the chemotherapeutic agents for the treatment of PC has been improved through the use of RNA interference (RNAi) technologies, including miRNA and siRNA, which selectively suppress the expression of target genes leading to increased drug efficacy and enhancing anti-cancer activity (Tang et al., 2021). Integrating RNAi with NPs can therefore be extremely effective at treating PC (Hiss et al., 2007; Gurunathan et al., 2018). Studies have recently shown that nano-sized exosomes are an efficient RNAi carrier, making them an attractive delivery cargo to cancerous cells (Farran and Nagaraju, 2020) Exosomes have intrinsic advantages over liposomes, as they are less toxic and can be dosed at higher concentrations in the blood to work as molecular cargos which could be used to inhibit oncogenes, activate tumor suppressor genes and modulate immune responses to control tumor cell growth (Oliveira et al., 2021) (Zhao et al., 2021b). As researchers continue to uncover the cellular and molecular basis of PC drug resistance, nanotechnology used for the delivery of drugs can be further engineered to provide effective solutions for mitigating MDR in the treatment of PC (Zhang et al., 2017). Table 2 summarizes key nano-based systems used for the delivery of antitumor drugs to mitigate MDR.

Albumin-based nanoparticles in PC

Albumin-based nanoparticles can be utilized as theranostics (i.e., to deliver therapeutic agents and simultaneously used for diagnosis). Albumin is the most abundant plasma protein and known ligand to be associated with a caveolae-mediated endocytosis mechanism. Albumin-based nanoparticles when internalized by the cell *via* caveolae-mediated endocytosis, can overcome the issue of MDR by bypassing and evading ATP-binding cassette (ABC) transporters, which are responsible for the efflux of anticancer drugs and subsequent MDR once released into the cytoplasm (Yuan et al., 2016). Nanoparticle albumin (Nab) is made by mixing human albumin in an aqueous medium under high pressure to form 100–200 nm albumin NPs. These NPs are mixed with chemotherapeutic alkaloids such as PTX (Macarulla et al., 2019). As shown in Table 3, Nab-based delivery systems are the most extensively studied nanocarrier system in the treatment of PC in human clinical trials (Von Hoff et al., 2011; Hosein et al., 2013; Von Hoff et al., 2013; Goldstein et al., 2015; Vogel et al., 2016; Macarulla et al., 2019). A common example of albumin-based nanoparticles is Nab-PTX, an albumin-binding PTX and a microtubule-stabilizing agent known to enhance microtubule polymerization during mitosis leading to cell cycle arrest in the G2/M phases. Based on these properties, Nab-PTX can stop rapid and uncontrollable cell division and help overcome MDR receptor-mediated endocytosis (Demidenko et al., 2008; Guo et al., 2018). Importantly, Nab-PTX has been shown to mitigate MDR in PC (Guo et al., 2018). In 2018, Guo et al. created GEM-resistant pancreatic cells by inducing lower rates of hENT1 expression. These cells were then exposed to free GEM or GEM delivered using human-serum albumin nanoparticles (HSA-NPs). Their results showed that GEM-HSA-NPs was more effective at slowing pancreatic cell proliferation and triggering apoptosis in comparison to free GEM alone, without any increase in toxicity, as shown *in vivo* studies. In phase III clinical trial (MPACT) on previously untreated patients with metastatic PC, a combination of Nab-PTX and GEM increased the median OS of patients receiving nab-PTX and gemcitabine to 8.7 vs. 6.6 months in patients treated with gemcitabine alone ($p < 0.0001$) (van Horssen et al., 2006; Libutti et al., 2010). Furthermore, the combination showed an increase in the cumulative delivery of gemcitabine by 2.8-fold compared to gemcitabine alone (Von Hoff et al., 2011; Von Hoff et al.,

TABLE 2 Selected examples of nano-based formulations used to overcome MDR in tumor cells.

Type of nanocarrier	Objective	Cargo	Cell/Animal model	Effects on MDR	Outcomes/results
M1Exo-GEM-DFX (Zhao et al., 2021a)	M1Exo was engineered as a drug carrier to co-delivery DFX and GEM to overcome the chemoresistance of GEM and improve its therapeutic potential	DFX and GEM	PANC-1 cells	Inhibit cell P-glycoprotein expression	M1Exo-GEM-DFX was able to overcome GEM resistance induced by P-glycoprotein expression *in vitro*
s $(DGL)_n$@Apt NPs(Chen et al., 2022)	Modulation of PDAC stromal structure and send chemotherapy drugs to the deep tumor vis the use of Aptamer-decorated hypoxia-responsive nanoparticle s $(DGL)_n$@Apt	GEM + STAT3 inhibitor (HJC0152)	Pan02 multicellular spheroids (MCSs) cells / Pan02 xenograft mice	Inhibition of the STAT3 pathway	Triggered by hypoxia, the ultra-small dual-loaded DGL NPs exhibited excellent deep-tumor penetration, promoted drugs endocytosis, and autophagy induction
PEG-Gem-cisPt-MSNs (Tarannum et al., 2022)	Development of two versions of mesoporous silica nanoparticles (MSNs), a dual loaded PEG-functionalized NPs, and MSNs containing Sonic Hedgehog (SHh) inhibitor for stroma modulation and improved delivery	GEM + CisPt	HPAF II and Miapaca-2 cells / HPAF II xenograft mice	Inhibition of sonic hedgehog (SHh) signaling pathway	The sequential combination of CyP-MSNs followed by PEG-Gem-cisPt- MSNs led to (i) effective stromal modulation (ii) increased access to secondary PEG-Gem-cisPt-MSNs at the tumor site (iii) enhanced therapeutic performance in HPAF II xenograft mice
TPMILs (Obaid et al., 2022)	Development of cetuximab (anti-EGFR mAb) targeted photoactivable multi-inhibitor liposomes (TPMILs) co-loaded with lapidated benzoporphyrin derivative (BPD-PC) photosensitizer and irinotecan to remediate desmoplasia, a major contributor to chemoresistance	(BPD-PC) + irinotecan	MIA PaCa-2 + PCAF tumor model	Reduction in stromal collagen density and collagen fiber alignment	Synchronized chemotherapeutic and a photodynamic insult to PDAC tissue was achieved with doubled overall survival
HSA NPs(Guo et al., 2018)	Enhancing the antitumor effect of GEM by the encapsulation into HSA-NPs to overcome GEM resistance in GEM-resistant PC induced by low hENT1 gene expression	GEM	BxPC-3 and SW1990 cells/ patient-derived xenograft BALB/c-nu/nu mice model	Inhibit cell proliferation, arrest cell cycle, and trigger apoptosis	GEM-loaded HSA-NPs was able to overcome GEM-resistance induced by low hENT1 expression *in vitro* and *in vivo*
HSA NPs(Han et al., 2017)	Development of tumor microenvironment targeting HSA-GEM/ IR780 complex with the redox-responsive release of GEM using GFLG cleavable peptide	GEM + IR780 (NIR dye)	BxPC-3 cells	Induction of apoptosis and Inhibition of cells proliferation	The developed theranostic nanoplatform showed high tissue accumulation and retention with: (i) targeted intracellular drug release, (ii) enhanced tumor inhibition activity (iii) insignificant side effects
Pheophorbide-a conjugated albumin NPs(Yu et al., 2017)	Inhibit PC with lymphatic metastases by the combination of chemotherapy with photodynamic therapy (PDT)	GEM	(BxPC-3-LN7) cells	Increase in drug accumulation in primary tumors as well as metastatic lymph nodes	Developed triple functional system efficiently controlled the release of GEM from the modified NPs and possessed imaging-guided theranostic properties
Nanovector- albumin-bound PTX (MSV/nAb-	Enhancing drug transport by increasing caveolin-1	PTX + GEM		Increase cellular uptake as a result of GEM-induced	GEM enhanced the transport of MSV/nAb-

(Continued on following page)

TABLE 2 (*Continued*) Selected examples of nano-based formulations used to overcome MDR in tumor cells.

Type of nanocarrier	Objective	Cargo	Cell/Animal model	Effects on MDR	Outcomes/results
PTX) (Borsoi et al., 2017)	expression (albumin transporter) via combination therapy of MSV/nAb-PTX with GEM		L3.6 pl human cells/ L3.6 pl—bearing nu/nu nude mice	high cav-1 expression, which leads to increased transport of nAb-PTX into tumor tissue	PTX in GEM-resistant pancreatic ductal adenocarcinoma
Chitosan coated solid-lipid NPs (c-SLN) (Thakkar et al., 2018)	To use nano-encapsulated c-SLNs combinations to determine the efficacy of the ACS therapeutic regimen	Aspirin (ASP)+ curcumin (CUR)+free sulforaphane (SFN); ACS	Panc-1 and MIA PaCa-2 cells/LSL-$Kras^{G12D/+}$; Pdx-$1^{Cre/+}$ transgenic mouse model	Increase in drug efficacy	Due to enhanced bioavailability of the combined ACS chemopreventive agents, the dosage for this therapeutic regimen can substantially be reduced, which by virtue reduces any potential serious side effects
SN38 (irinotecan active metabolite) polymeric prodrug-based NPs(Wang et al., 2017)	Development of a nano-based system for effective synergistic therapy to overcome fibroblast-induced drug resistance	GDC-0449 (hedgehog pathway inhibitor)	BxPC-3 cells and MIA PaCa-2 cells/PSCs and BxPC-3—bearing BALB/c nude mice	Increase in drug efficacy by modulating the fibroblast-enriched tumor microenvironment	size-tunable nanoparticles were obtained and controllable loading efficiency, which was directly correlated to the length of the hydrophobic SN38 block
(PLGA-ORM NPs) (Khan et al., 2015)	Providing effective endosomal release to the cytosol	Ormeloxifene	(HPAF-II, AsPC-1, BxPC-3, Panc-1, and MiaPaca)/a BxPC-3 xenograft mice model	Increase in drug efficacy	PLGA-ORM NPs showed substantial antitumor efficacy and effective endosomal release resulted in PC tumor suppression
PLGA-PEG NPs(Elgogary et al., 2016)	Targeting the glutamine metabolism	BPTES	P8, A6L, A32, P198, E3, P215, P10, and JD13D human PC cells/Foxn1nu athymic tumor-bearing nude mice	Increase in drug accumulation	Combination therapy of BPTES-loaded NPs and metformin were shown to be effective in blocking the metabolism of glutamine and glucose
Redox-responsive Apt/CPP-CPTD NPs(He et al., 2018)	Development of sequentially responsive NPs with redox-responsive on-demand drug release and ECM-responsive tumor penetration	Camptothecin prodrug, CPTD	MIA PaCa-2 cells/MIA PaCa-2 orthotopic human PC xenograft bearing nude mice	Enhance cytotoxicity and cellular accumulation	Formulated NPs showed selective accumulation at the tumor site with mild *in vitro* cytotoxicity and good *in vivo* antitumor efficacy
PLGA NPs(Lucero-Acuna et al., 2014)	Enhanced PH-427 delivery to the PC harboring K-ras mutation to overcome the protective stromal layer surrounding the pancreatic tumor	PH-427 (AKT/PDK1 inhibitor)	MiaPaCa-2 harboring K-ras mutation/Orthotopic MiaPaCa-2—bearing mice	Increase in cellular uptake and drug efficacy	PH-427- loaded PLGA NPs resulted in the enhanced therapeutic effect of PH-427 *in vitro* and *in vivo*
PEGylated colloidal gold NPs(Libutti et al., 2018)	Targeting components of the tumor microenvironment responsible for creating high interstitial fluid pressure to improve the delivery of anticancer drugs	TNF and a PTX prodrug	Genetically engineered mice with pancreatic ductal adenocarcinoma	Increase in drug efficacy by tumor IFP reduction	The combination of TNF (targeting tumor vasculature) with PTX (either loaded on the NPs or administered separately) increased the efficacy of the cytotoxic agent
Superparamagnetic iron oxide nanoparticle (SPION) (Khan et al., 2019)	Development of (SPION) loaded with curcumin (SP-CUR), which is known for its anti-inflammatory and antitumor activity, to overcome GEM resistance and enhance its therapeutic potential *in vitro* and *in vivo*	Curcumin + GEM	Panc-1, HPAF, CPSC, and HPSC cells / HPAF-II human PSCs—bearing athymic Nu/Nu mice	Suppression of sonic hedgehog (SHH) signaling pathway and oncogenic CXCR4/CXCL12 signaling axis	Efficient delivery of curcumin was achieved, which also played a role in sensitizing cells to standard GEM therapy
		Cisplatin			

(Continued on following page)

TABLE 2 (*Continued*) Selected examples of nano-based formulations used to overcome MDR in tumor cells.

Type of nanocarrier	Objective	Cargo	Cell/Animal model	Effects on MDR	Outcomes/results
Nanogels (NGs) (Soni et al., 2019)	Development of Cisplatin-loaded mAb-coated NGs for targeted delivery to PCs and the evaluation of antitumor activity in combination with GEM		T3M4/Luc cells/ T3M4/Luc—bearing Nu-Nu nude mice	Increase in drug efficacy by targeted therapy using an anti-STn antibody (TKH2 mAb)	Enhanced drug delivery, as well as synergistic cytotoxic effect, was observed after sequential exposure of PC cells to GEM followed by CDDP
Fucose-bound liposomes (Yoshida et al., 2012)	Development of liposomal formulation functionalized with L-fucose to target the fucosylated antigens highly expressed on the surface of cancer cells to enhance cisplatin delivery	Cisplatin	BxPC-3, AsPC-1, PK59, and HuCCT1 cell lines/ Subcutaneous model:AsPC-1-bearing mice; Liver metastasis and orthotopic models: BxPC-3-Luc-bearing mice	Increase in cellular uptake and cytotoxicity	Cisplatin-loaded Fucose-bound liposomes were effectively delivered to PC cells and resulted in effective inhibition of tumor growth as well as extending survival in the mouse xenograft models
Au-GO@ZC-DOX stealth nanovesicles (Thapa et al., 2018)	development of pH-triggered stealth nanovesicles for chemophototherapy	DOX	Panc-1 cells and Mia PaCa-2 cells/PANC-1- bearing BALB/c nude mice	Increase in cellular uptake and cytotoxicity	The multi-componential nanovesicle showed effective Macrophage opsonization inhibition, resulting in anti-cancer and anti-migration effects
HA-SMA Micelles (Kesharwani et al., 2015)	Development of functionalized micelles with HA to target the PC overexpressed CD44 receptors to overcome MDR	3, 4-difluorobenzylidene curcumin (CDF)	MiaPaCa-2 and AsPC-1 cells	Inhibition of NF-κB in $CD44^+$ cells	The developed nanosystem showed remarkable colloidal stability and sustained drug release and potent anticancer activity
Polymeric Micelles (Xu et al., 2015)	Development (TPGS–GEM) prodrug micelles to protect the drug from enzymatic metabolism	TPGS–GEM (prodrug)	BxPC-3 cells	Enhanced drug efficacy as the micellar formulation protected the drug from enzymatic metabolism	Long circulation half-life of GEM was obtained in addition to enhanced anticancer activity
Ultra-pH-sensitive micelles (UPSM) (Kong et al., 2019)	Development of UPSM improved pH buffer capacity for simultaneous inhibition of lysosomal acidification and enhancement of therapeutic delivery	Triptolide prodrug-	KRAS mutant PANC-1 and MIA PaCa-2/MIA PaCa-2-luc—bearing BALB/C nude mice	Disruption of lysosomal catabolism and growth inhibition of KRAS mutant	The newly developed nanosystem revealed more efficient lysosomal catabolism when compared with conventional lysosomotropic agents. In addition, pH-sensitive UPSM showed significant cytotoxicity when compared to non-pH-sensitive micelles

2013; Goldstein et al., 2015). Based on the findings of the trial, GEM plus nab-PTX became the first therapy recommended by the National Institute for Health and Care Excellence in the United Kingdom for the management of previously untreated metastatic PC (Von Hoff et al., 2011).

Metal-based nanoparticles in PC

Metal-based NPs such as gold, silver, iron, platinum, and titanium are commonly used for imaging, as drug delivery carriers, and as radiosensitizers in radiation, proton, or photodynamic therapy (Klebowski et al., 2018). Due to their inherent physicochemical properties, metal NPs could overcome MDR via different mechanisms (Sharma et al., 2018), as shown in Figure 2. The endosomal-based cellular uptake mechanism can be considered one of the main advantages of metal-based NPs in overcoming MDR. This is achieved by selectively releasing intracellular drugs after evading the membrane-embedded multidrug efflux pumps (Ayers and Nasti, 2012). Khan *et al.* developed a nanoformulation of superparamagnetic iron oxide nanoparticles (SPION) loaded with curcumin (SP-CUR), an anti-inflammatory and anti-tumorigenic compound. They tested the activity of this nanoformulation in combination with GEM on GEM-resistant pancreatic cells. Efficient delivery of curcumin was achieved using their formulation, and they found that SP-

TABLE 3 Selected examples of clinical trials applying nano-based formulations in PC treatment.

Study	Testing	Study type	Dosing regimen	Median survival	Main outcomes
Von Hoff et al., 2011 (Von Hoff et al., 2011)	GEM + Nab-PTX	Phase I/II	67 patients 100, 125, and 150 mg/m^2 nab-paclitaxel plus 1,000 mg/m^2 gemcitabine on days 1, 8, and 15 every 28 days	12.2 months	Response rate 48%, Overall Survival (OS) 12.2, and 1-year survival rate 48%
NCT00844649					
Hosein et al., 2013 (Hosein et al., 2013)	nab-PTX	Phase II	19 patients were treated with nab-paclitaxel 100 mg/m^2 on days 1, 8, and 15 of a 28-day cycle	7.3 months	6 months OS 58%, median OS 7.3 months
Von Hoff et al., 2013 (Von Hoff et al., 2013)	GEM + Nab-PTX vs. GEM	Phase III	Group 1: 431 patients given nab-PTX (125 mg/m^2) followed by GEM (1,000 mg/m^2) on days 1, 8, and 15 every 4 weeks	Median survival was 8.5 months in GEM + Nab-PTX vs. 6.7 months in the GEM group	Group 1 vs. Group 2: Median survival 8.5 vs. 6.7 months; 1-year survival rate 35vs. 22%; 2-year survival rate 9 vs. 4%; higher risks of peripheral neuropathy and myelosuppression with group 1 compared to group 2
NCT00844649			Group 2: 430 patients given GEM monotherapy (1,000 mg/m^2) weekly for 7 of 8 weeks (cycle 1) and then on days 1, 8, and 15 every 4 weeks (cycle 2)		
Goldstein et al., 2015 (Goldstein et al., 2015)	GEM + Nab-PTX vs. GEM	Phase III	Patients (n = 861) randomly assigned to receive GEM + Nab-PTX vs. GEM	Median survival was 8.7 months in GEM + Nab-PTX vs. 6.6 months in the GEM group	OS and long-term survival (>3 years) were higher amongst GEM + Nab-PTX compared to the GEM monotherapy group
Update on OS of NCT00844649					
Vogel et al., 2016 (Vogel et al., 2016)	GEM + Nab-PTX vs. GEM	Phase III	Patients randomly assigned to receive GEM + Nab-PTX vs. GEM alone	Median survival was 9.8 months in GEM + Nab-PTX vs. 7.5 months in the GEM group	OS 8% with GEM + Nab-PTX vs. 4% from GEM alone; Overall Response Rate 27 vs. 9% with GEM + Nab-PTX vs. GEM alone respectively
Sub-analysis of NCT00844649					
Macarulla et al., 2019 (Macarulla et al., 2019)	GEM + Nab-PTX vs. GEM	Phase I/II	6 groups inducted in phase I and 2 groups in phase II both using GEM + Nab-PTX at different doses (100 g/m^2 or 125 mg/m^2 Nab-PTX + 1,000 mg/m^2 GEM)	NA	Improvement in overall survival irrespective of the dose of Nab-PTX used
NCT02382263					
Libutti et al., 2010 (Libutti et al., 2010)	CYT-6091 (colloidal gold)	Phase I	3 participants were given 50 mg/m^2 to 600 mg/m^2 of rhTNF via the CYT-6091 delivery system	NA	CYT-6091 delivery system led to great tumor tissue concentration of rhTNF compared to normal tissues
NCT00356980					
Stathopoulos et al., 2005 (Stathopoulos et al., 2005)	Lipoplatin	Phase I	Dose starting at 25 mg/m^2 and was increased by 25–125 mg/m^2	NA	No significant nephrotoxicity or systemic toxicity noted with this preparation
Greek trial					
Stathopoulos et al., 2005 (Stathopoulos et al., 2005)	Lipoplatin	Phase II	GEM dose 1,000 mg/m^2 and the lipoplatin dose was escalated from 25 mg/m^2 to 125 mg/m^2	3 months	Partial response (>50% tumor reduction) was seen in 2 patients. Stable disease (<25–50% reduction in the tumor) was seen in 14 patients
Greek trial					
Syrigos et al., 2002 (Syrigos et al., 2002)	Docetaxel and liposomal doxorubicin	Phase II	21 patients given docetaxel (80 mg/m^2), and liposomal doxorubicin (30 mg/m^2) was administered on day 1, every 3 weeks	10 months	Median survival 10, 1-year survival 33.3%
Greek trial					
Hamaguchi et al., 2007 (Hamaguchi et al., 2007)	NK105 (PTX-polymeric micelles)	Phase I	Initially given 10 mg/m^2 and successively increased the dose	NA	The size of liver mets reduced by 90% in patients receiving a dose of 150 mg/m^2 or higher dose

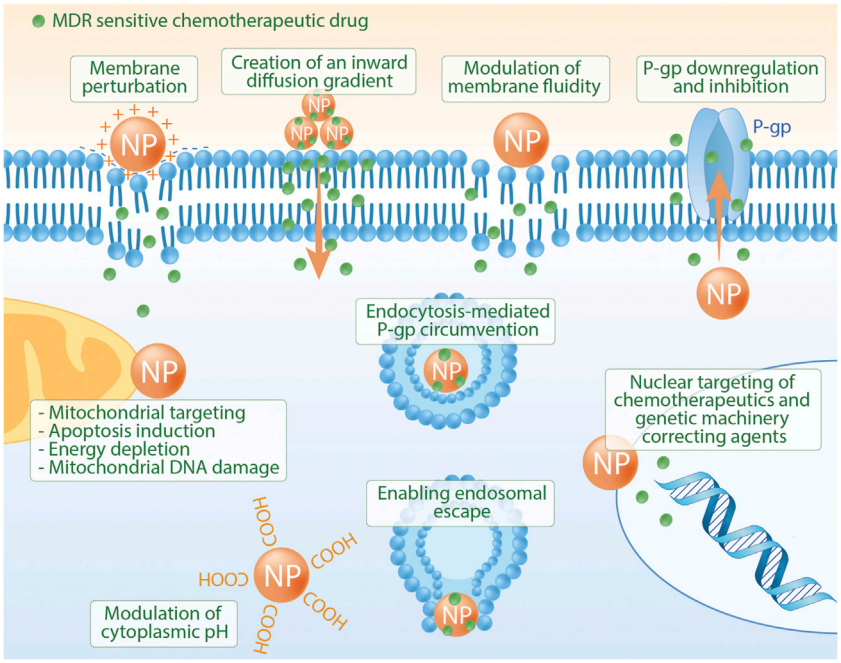

FIGURE 2
Common nanomedicine strategies to overcome multidrug-resistant tumors. Reprinted from Pharmacological Research, 126, Manu S. Singh, Salma N. Tammam, Maryam A. Shetab Boushehri, Alf Lamprecht, MDR in cancer: Addressing the underlying cellular alterations with the use of nanocarriers, 2-30, Copyright (2017), with permission from Elsevier.

CUR increased the effectiveness of GEM therapy through suppressing two signal transduction pathways that are implemented in MDR: 1) sonic hedgehog (SHH) and 2) oncogenic CXCR4/CXCL12. Following their endosomal escape, SPION particles showed increased cellular internalization where they were observed to be more closely associated with cytosol/mitochondria to prevent lysosomal degradation (Khan et al., 2019). In 2010, Libutti *et al.* used a novel drug delivery system, CYT-6091, surface-modified colloidal gold nanoparticles, to increase tumor levels of rhTNF and reduce its systemic metabolism and toxicity (Libutti et al., 2010). CYT-6091 is constructed by combining rhTNF and thiolyated glycol to the surface of 27 nm gold colloidal particles. CYT9061 was studied at doses between 50 mg/m2 to 600 mg/m2 in a phase I clinical trial conducted with three patients with pancreatic adenocarcinoma. Using the gold colloidal nanoparticles, researchers were able to administer extremely high concentrations of rhTNF compared to when given in isolation: the highest isolated tolerated concentration of pure rhTNF is 1 mg per cycle. After treatment, examination by electron microscope of normal and tumor tissues was carried out and found gold particles isolated within tumor tissues or at anticipated clearance sites (Ladd et al., 2017). These findings suggest that gold-based, colloidal nano-delivery systems can be used to deliver chemotherapy drugs to target tissues. However, subsequent clinical trials remain to be conducted to prove their efficacy and safety.

Polymeric micelles in PC

Polymeric micelles, including both hydrophobic and hydrophilic moieties (Manzur et al., 2017), are the largest class of nanomaterials being investigated for PC treatment in pre-clinical settings. These nanoparticles contain linear or highly branched and symmetrical polymers, with hydrophilic dendritic extensions and a hydrophobic core. The terminal groups at the dendritic extensions can be adjusted to allow for better solubility depending upon the carrier medium and allow for superior anchorage and permeability into target tissues (Chiba and Twyman, 2017; Ladd et al., 2017). Polymeric micelles are NPs formed by the self-assembly of amphiphilic block copolymers when present in certain solvents with a surfactant concentration above a critical micelle concentration (c.m.c). They are efficient drug delivery systems for cancer treatment with the ability to inhibit P-gp action, alter drug internalization, enable selective drug targeting, and enable subcellular localization. Polymeric micelles can circumvent MDR through a combination of mechanisms, including the EPR effect, endosomal-triggered active internalization, and drug escape (Kapse-Mistry et al., 2014).

In our literature review, we found at least seven published studies using polymeric micelles for the delivery of anti-tumor drugs in clinical trials, including Genexol®-PM, NK105, NC-4016, NK012, NC-6004, NK911, and SP1049C (Gong et al., 2012). NK105 is a nanoparticle formulation that incorporates PTX into a "core-shell-type" polymeric micelle. In a phase I trial conducted by Hamaguchi et al. (2007), the pharmacokinetics of NK105, a micelle carrier for PTX, was studied. The study included 19 patients with advanced PC who were given an initial dose of 10 mg/m^2 of NK105; this dose increased successively. The size of metastatic liver tumors was reduced by 90% in patients given a 150 mg/m^2 dose of the drug (Hamaguchi et al., 2007).

Lipid-based nanoformulations in PC

Lipid-based nanoformulations have been extensively studied for the delivery of antitumor agents, including natural products (Kashyap et al., 2019). Liposomes are lipid bilayer systems that can cross the lipid bilayer to selectively target cancer cells based on biomarkers, overly expressed on PC cells (Urey et al., 2017). There are several strategies whereby liposomes can enhance drug bioavailability and efficacy in drug-resistant cancer. These include 1) liposomes modified for controlled and on-demand release; and 2) ligand-targeted liposomes such as immunoliposomes, which facilitate intracellular drug delivery into tumor cells. Liposomes can also directly inhibit P-gp through endocytosis and consequently enhance intracellular drug accumulation (Kapse-Mistry et al., 2014). In 2012, the use of liposomes in PC treatment was explored by Yoshida *et al.* They targeted fucosylated antigens that are highly expressed on the surface of PC cells. They engineered L-fucose-bound liposomes that encapsulated Cy5.5 or cisplatin. *In vitro* studies on CA19-9 expressing PC cells showed that L-fucose-bound liposomes encapsulating either Cy5.5 or cisplatin were effectively delivered and in mouse xenograft models, cisplatin-loaded liposomes were successfully delivered to PC cells and inhibited tumor growth (Yoshida et al., 2012). Furthermore, in the second-line setting of metastatic PDAC following administration of GEM-based regimens, nanoliposomes irinotecan (nal-IRI) was approved by the FDA in combination with 5-FU and leucovorin (5-FU/LV) in 2015. In phase III, the NAPOLI-1 trial, the median progression-free survival (PFS) was 3.1 and 1.5 months ($p < 0.001$) in patients who received nal-IRI + 5-FU/LV and patient's 5-FU/LV alone, respectively (Wang-Gillam et al., 2016). In the final OS analysis of the NAPOLI-1 trial, the median OS was increased by 2 months ($p = 0.042$) in the nal-IRI + 5-FU/LV group (Wang-Gillam et al., 2016).

Nanogels in PC

Nanogels can utilize the unique characteristics of tumor microenvironments such as pH and temperature, to release drugs within the cell, resulting in efficient drug delivery (Damaghi et al., 2013). In a study by Damaghi et al., a nanogel-based platform for PC therapy was reported (Soni et al., 2019). They developed a cisplatin-loaded, mAb-coated nanogel for targeted delivery and used it in combination with GEM. *In vitro* results revealed an increase in drug efficacy. Additionally, enhanced drug delivery and synergistic cytotoxic effect were observed after sequential exposure of PC cells to GEM. Together, these studies have all demonstrated the advantage and improved therapeutic outcomes with the use of nanomaterials and nano-drug platforms, particularly and most importantly against MDR in experimental models and clinical trials (Kesharwani et al., 2015; Borsoi et al., 2017; Guo et al., 2018; Kong et al., 2019). Such advantage to the use of nanomaterials is mediated through a wide range of mechanisms, including enhanced cellular uptake, evading endosomal-lysosomal drug breakdown, inhibition of drug efflux, and increasing plasma half-life.

Key limitations on the clinical translation of nanomedicine in PC

There has been a tremendous effort to understand the structural and functional properties of nanoparticles directed against cancer but their translation to clinical practice has been largely limited. This can primarily be attributed to a poor understanding of the biological barriers and nanomaterial behavior inside the body and cells, as well as the overemphasis and relying on animal models during pre-clinical evaluation, which does not necessarily represent the same disease phenotype in humans (Gonzalez-Valdivieso et al., 2021).

There are several major challenges in the treatment of PC, which need to be overcome to make the use of nanotherapies a success against PCs. These include off-target toxicity, low bioavailability of chemotherapeutic drugs, and undesirable pharmacokinetics. One way to address these obstacles is through the use of nanotechnology as an effective vehicle for chemotherapeutic drugs. Currently, only 16 nano-based cancer drugs are approved by FDA and around 75 nanoformulations are being investigated in clinical trials (He et al., 2019). It is extremely important to narrow the gap between preclinical toxicity studies and toxicity studies in patients, as nanomedicines have been shown to exert additional unintended and often toxic effects on normal cellular function. Moreover, there has been a lack of convincing data on the process of excretion of nanomedicines from the human system, as most data is available from animal disease models. Nanomedicines can pose safety issues at different levels (apart from the intrinsic toxicity of the API itself). Furthermore, the biodistribution of nanoparticles changes unpredictably resulting in uptake and accumulation in certain organs, which may result in target off-target effects and local

overexposure. Indeed, some nanoparticles have a known tendency to accumulate in lymphoid organs and kidneys (for some polymer-bound drugs) (Metselaar and Lammers, 2020).

Furthermore, there remains a general lack of understanding on the cost-effectiveness, manufacturing, and scaling up, as well as regulation with regard to using nanomedicines for cancer (van der Meel et al., 2017). As the science behind the structural-functional relationship provides clarity on the interaction of nanomedicines *in vivo*, the regulatory challenges must be addressed simultaneously to bring these potentially game-changing therapeutics to the frontline against fighting pancreatic cancer.

Conclusion and future directions

Numerous noncarriers have been developed and investigated for the treatment of PC to overcome the problem of MDR seen with chemotherapy and other therapeutic options, however, with limited success Even though nano-based carriers show great promise in treating various cancers, they have several limitations, including potential toxicity, difficult scalability, and low loading efficiency that could be responsible for their low success rate reaching clinical settings. Notably, the albumin-based nanocarrier was the most successful in clinical studies for PC. This is mainly because albumin nanoparticles were successful in encapsulating widely used chemotherapeutics that are less soluble/insoluble in water. Additionally, albumin is highly biocompatibility and biodegradability, making it an attractive material for drug delivery applications. The development of future therapies for cancer and nano-based therapeutics should not be limited by designing nanocarriers only for passive targeting of cancerous cells. Internalization of chemotherapeutic agents into tumor cells can be further improved via the utilization of an active targeting approach to enhance drug delivery efficacy. Additionally, research into novel biomarkers to enable active targeting will empower delivery strategies of nanocarriers to combat cancer resistance.

While we have certainly made huge progress in understanding the drug resistance mechanisms in PC and the signaling pathways responsible for PC cell metastases, investigations on the use of nanomedicine in this field lag behind. Currently, the majority of work in the field of nanomedicine is largely focused on increasing drug stability, accumulation, and targeting, which is yet of critical importance, particularly in nucleoside transporter (e.g., ENT1 and CNT1)-mediated drug resistance against GEM (Hung et al., 2015; Poon et al., 2015). Future studies utilizing nanotechnology against MDR pancreatic cancers should integrate multiple modalities and exploit the rapidly accumulating mechanistic knowledge in this cancer model (e.g., targeting PCSCs, dual delivery of potential drug modalities, etc.). In addition, utilizing the endogenous properties of the TME to trigger the release of cancer therapeutics from nanocarriers should be considered during the delivery system design. Such a design will add another dimension of controlled release that can impact clinical efficacy, where adverse effects can be minimized while retaining therapeutic benefits.

The main goal of PC treatment is to enhance the efficiency of drug delivery and minimize drug resistance. Despite the tremendous effort in making novel nanocarriers in pre-clinical settings, the development of clinical translation to the bedside remains laborious. Extrapolation of scientific findings from animals to humans is extremely challenging, mainly due to differences in physiology and anatomy between species, making direct extrapolation unreliable. Furthermore, unlike the experimental settings in clinical studies, animals are designed with syngeneic backgrounds, and disease models are designed to produce as homogenous a population as possible. On the other hand, heterogeneity is the basis of ineffectiveness in clinical trials. Moreover, individual variability in lifestyle and disease progression plays key roles in the overall efficacy, unlike the well-controlled animal experiments.

The promise of nanomedicine will be realized by moving away from designing a targeting strategy against a single target to including targeting approaches that address multiple signaling mechanisms and molecular targets, considering the complexity of both the human physiology and the tumor microenvironment, including the development of MDR mechanisms.

Author contributions

Conception of the work, draft, and revision of the work: AKA, NBA, NA, RA, and AA.

Acknowledgments

The authors are thankful to the Research Center, College of Pharmacy, and the Deanship of Scientific Research, King Saud University for their support to conduct this work.

Conflict of interest

The authors declare that the research was conducted in the absence of any commercial or financial relationships that could be construed as a potential conflict of interest.

Publisher's note

References

Aguirre, A. J., and Collisson, E. A. (2017). Advances in the genetics and biology of pancreatic cancer. *Cancer J.* 23 (6), 315–320. doi:10.1097/PPO.0000000000000286

Alshememry, A. K., El-Tokhy, S. S., and Unsworth, L. D. (2017). Using properties of tumor microenvironments for controlling local, on-demand delivery from biopolymer-based nanocarriers. *Curr. Pharm. Des.* 23 (35), 5358–5391. doi:10.2174/1381612823666170522100545

Alzhrani, R., Alsaab, H. O., Vanamala, K., Bhise, K., Tatiparti, K., Barari, A., et al. (2021). Overcoming the tumor microenvironmental barriers of pancreatic ductal adenocarcinomas for achieving better treatment outcomes. *Adv. Ther.* 4 (6), 2000262. doi:10.1002/adtp.202000262

Arumugam, T., Ramachandran, V., Fournier, K. F., Wang, H., Marquis, L., Abbruzzese, J. L., et al. (2009). Epithelial to mesenchymal transition contributes to drug resistance in pancreatic cancer. *Cancer Res.* 69 (14), 5820–5828. doi:10.1158/0008-5472.CAN-08-2819

Avula, L. R., Hagerty, B., and Alewine, C. (2020). Molecular mediators of peritoneal metastasis in pancreatic cancer. *Cancer Metastasis Rev.* 39 (4), 1223–1243. doi:10.1007/s10555-020-09924-4

Ayers, D., and Nasti, A. (2012). Utilisation of nanoparticle technology in cancer chemoresistance. *J. Drug Deliv.* 2012, 265691. doi:10.1155/2012/265691

Bailey, P., Chang, D. K., Nones, K., Johns, A. L., Patch, A. M., Gingras, M. C., et al. (2016). Genomic analyses identify molecular subtypes of pancreatic cancer. *Nature* 531 (7592), 47–52. doi:10.1038/nature16965

Bardeesy, N., and DePinho, R. A. (2002). Pancreatic cancer biology and genetics. *Nat. Rev. Cancer* 2 (12), 897–909. doi:10.1038/nrc949

Baretti, M., Pulluri, B., Tsai, H. L., Blackford, A. L., Wolfgang, C. L., Laheru, D., et al. (2019). The significance of ascites in patients with pancreatic ductal adenocarcinoma: A case-control study. *Pancreas* 48 (4), 585–589. doi:10.1097/mpa.0000000000001262

Batlle, E., and Clevers, H. (2017). Cancer stem cells revisited. *Nat. Med.* 23 (10), 1124–1134. doi:10.1038/nm.4409

Berlin, J. D., Catalano, P., Thomas, J. P., Kugler, J. W., Haller, D. G., and Benson, A. B., 3rd (2002). Phase III study of gemcitabine in combination with fluorouracil versus gemcitabine alone in patients with advanced pancreatic carcinoma: Eastern Cooperative Oncology Group Trial E2297. *J. Clin. Oncol.* 20 (15), 3270–3275. doi:10.1200/JCO.2002.11.149

Binenbaum, Y., Na'ara, S., and Gil, Z. (2015). Gemcitabine resistance in pancreatic ductal adenocarcinoma. *Drug resist. updat.* 23, 55–68. doi:10.1016/j.drup.2015.10.002

Blanco, E., Hsiao, A., Mann, A. P., Landry, M. G., Meric-Bernstam, F., and Ferrari, M. (2011). Nanomedicine in cancer therapy: Innovative trends and prospects. *Cancer Sci.* 102 (7), 1247–1252. doi:10.1111/j.1349-7006.2011.01941.x

Borsoi, C., Leonard, F., Lee, Y., Zaid, M., Elganainy, D., Alexander, J. F., et al. (2017). Gemcitabine enhances the transport of nanovector-albumin-bound paclitaxel in gemcitabine-resistant pancreatic ductal adenocarcinoma. *Cancer Lett.* 403, 296–304. doi:10.1016/j.canlet.2017.06.026

Bray, F., Ferlay, J., Soerjomataram, I., Siegel, R. L., Torre, L. A., and Jemal, A. (2018). Global cancer statistics 2018: GLOBOCAN estimates of incidence and mortality worldwide for 36 cancers in 185 countries. *Ca. Cancer J. Clin.* 68 (6), 394–424. doi:10.3322/caac.21492

Burris, H. A., 3rd, Moore, M. J., Andersen, J., Green, M. R., Rothenberg, M. L., Modiano, M. R., et al. (1997). Improvements in survival and clinical benefit with gemcitabine as first-line therapy for patients with advanced pancreas cancer: A randomized trial. *J. Clin. Oncol.* 15 (6), 2403–2413. doi:10.1200/JCO.1997.15.6.2403

Cancer.Net (2022). *Pancreatic Cancer: Statistics* [Online]. Available: https://www.cancer.net/cancer-types/pancreatic-cancer/statistics (Accessed July 15, 2022).

Cascinu, S., Verdecchia, L., Valeri, N., Berardi, R., and Scartozzi, M. (2006). New target therapies in advanced pancreatic cancer. *Ann. Oncol.* 17 (5), v148–152. doi:10.1093/annonc/mdj971

Chen, H., Guo, Q., Chu, Y., Li, C., Zhang, Y., Liu, P., et al. (2022). Smart hypoxia-responsive transformable and charge-reversible nanoparticles for the deep penetration and tumor microenvironment modulation of pancreatic cancer. *Biomaterials* 287, 121599. doi:10.1016/j.biomaterials.2022.121599

Chiba, F., and Twyman, L. J. (2017). Effect of terminal-group functionality on the ability of dendrimers to bind proteins. *Bioconjug. Chem.* 28 (8), 2046–2050. doi:10.1021/acs.bioconjchem.7b00350

Corbo, V., Tortora, G., and Scarpa, A. (2012). Molecular pathology of pancreatic cancer: From bench-to-bedside translation. *Curr. Drug Targets* 13 (6), 744–752. doi:10.2174/138945012800564103

Cowgill, S. M., and Muscarella, P. (2003). The genetics of pancreatic cancer. *Am. J. Surg.* 186 (3), 279–286. doi:10.1016/s0002-9610(03)00226-5

Damaghi, M., Wojtkowiak, J. W., and Gillies, R. J. (2013). pH sensing and regulation in cancer. *Front. Physiol.* 4, 370. doi:10.3389/fphys.2013.00370

Danilova, L., Ho, W. J., Zhu, Q., Vithayathil, T., De Jesus-Acosta, A., Azad, N. S., et al. (2019). Programmed cell death ligand-1 (PD-L1) and CD8 expression profiling identify an immunologic subtype of pancreatic ductal adenocarcinomas with favorable survival. *Cancer Immunol. Res.* 7 (6), 886–895. doi:10.1158/2326-6066.CIR-18-0822

Das, S. K., Wang, J. L., Li, B., Zhang, C., and Yang, H. F. (2019). Clinical effectiveness of combined interventional therapy as a salvage modality for unresectable pancreatic carcinoma. *Oncol. Lett.* 18 (1), 375–385. doi:10.3892/ol.2019.10323

Dauer, P., Nomura, A., Saluja, A., and Banerjee, S. (2017). Microenvironment in determining chemo-resistance in pancreatic cancer: Neighborhood matters. *Pancreatology* 17 (1), 7–12. doi:10.1016/j.pan.2016.12.010

Demidenko, Z. N., Kalurupalle, S., Hanko, C., Lim, C. U., Broude, E., and Blagosklonny, M. V. (2008). Mechanism of G1-like arrest by low concentrations of paclitaxel: Next cell cycle p53-dependent arrest with sub G1 DNA content mediated by prolonged mitosis. *Oncogene* 27 (32), 4402–4410. doi:10.1038/onc.2008.82

di Magliano, M. P., and Logsdon, C. D. (2013). Roles for KRAS in pancreatic tumor development and progression. *Gastroenterology* 144 (6), 1220–1229. doi:10.1053/j.gastro.2013.01.071

Dreyer, S. B., Chang, D. K., Bailey, P., and Biankin, A. V. (2017). Pancreatic cancer genomes: Implications for clinical management and therapeutic development. *Clin. Cancer Res.* 23 (7), 1638–1646. doi:10.1158/1078-0432.CCR-16-2411

Du, Z., Qin, R., Wei, C., Wang, M., Shi, C., Tian, R., et al. (2011). Pancreatic cancer cells resistant to chemoradiotherapy rich in "stem-cell-like" tumor cells. *Dig. Dis. Sci.* 56 (3), 741–750. doi:10.1007/s10620-010-1340-0

Ducreux, M., Cuhna, A. S., Caramella, C., Hollebecque, A., Burtin, P., Goere, D., et al. (2015). Cancer of the pancreas: ESMO clinical practice guidelines for diagnosis, treatment and follow-up. *Ann. Oncol.* 26 (5), v56–68. doi:10.1093/annonc/mdv295

Elgogary, A., Xu, Q., Poore, B., Alt, J., Zimmermann, S. C., Zhao, L., et al. (2016). Combination therapy with BPTES nanoparticles and metformin targets the metabolic heterogeneity of pancreatic cancer. *Proc. Natl. Acad. Sci. U. S. A.* 113 (36), E5328–E5336. doi:10.1073/pnas.1611406113

Ellenrieder, V., Hendler, S. F., Boeck, W., Seufferlein, T., Menke, A., Ruhland, C., et al. (2001). Transforming growth factor beta1 treatment leads to an epithelial-mesenchymal transdifferentiation of pancreatic cancer cells requiring extracellular signal-regulated kinase 2 activation. *Cancer Res.* 61 (10), 4222–4228.

Erkan, M., Hausmann, S., Michalski, C. W., Fingerle, A. A., Dobritz, M., Kleeff, J., et al. (2012). The role of stroma in pancreatic cancer: Diagnostic and therapeutic implications. *Nat. Rev. Gastroenterol. Hepatol.* 9 (8), 454–467. doi:10.1038/nrgastro.2012.115

Farran, B., and Nagaraju, G. P. (2020). Exosomes as therapeutic solutions for pancreatic cancer. *Drug Discov. Today* 25 (12), 2245–2256. doi:10.1016/j.drudis.2020.09.037

Feig, C., Jones, J. O., Kraman, M., Wells, R. J., Deonarine, A., Chan, D. S., et al. (2013). Targeting CXCL12 from FAP-expressing carcinoma-associated fibroblasts synergizes with anti-PD-L1 immunotherapy in pancreatic cancer. *Proc. Natl. Acad. Sci. U. S. A.* 110 (50), 20212–20217. doi:10.1073/pnas.1320318110

Gad, A., Kydd, J., Piel, B., and Rai, P. (2016). Targeting cancer using polymeric nanoparticle mediated combination chemotherapy. *Int. J. Nanomed. Nanosurg.* 2 (3), 10.16966/2470-3206.116. doi:10.16966/2470-3206.116

Ge, W., Chen, G., and Fan, X. S. (2017). Pathway of peritoneal carcinomatosis maybe hematogenous metastasis rather than peritoneal seeding. *Oncotarget* 8 (25), 41549–41554. doi:10.18632/oncotarget.14607

Ghaneh, P., Costello, E., and Neoptolemos, J. P. (2007). Biology and management of pancreatic cancer. *Postgrad. Med. J.* 56 (8), 478–497. doi:10.1136/gut.2006.103333

Gheorghe, G., Bungau, S., Ilie, M., Behl, T., Vesa, C. M., Brisc, C., et al. (2020). Early diagnosis of pancreatic cancer: The key for survival. *Diagn. (Basel)* 10 (11), E869. doi:10.3390/diagnostics10110869

Goldstein, D., El-Maraghi, R. H., Hammel, P., Heinemann, V., Kunzmann, V., Sastre, J., et al. (2015). nab-Paclitaxel plus gemcitabine for metastatic pancreatic cancer: long-term survival from a phase III trial. *J. Natl. Cancer Inst.* 107 (2), dju413. doi:10.1093/jnci/dju413

Gong, J., Chen, M., Zheng, Y., Wang, S., and Wang, Y. (2012). Polymeric micelles drug delivery system in oncology. *J. Control. Release* 159 (3), 312–323. doi:10.1016/j.jconrel.2011.12.012

Gonzalez-Valdivieso, J., Girotti, A., Schneider, J., and Arias, F. J. (2021). Advanced nanomedicine and cancer: Challenges and opportunities in clinical translation. *Int. J. Pharm.* 599, 120438. doi:10.1016/j.ijpharm.2021.120438

Goodman, A. M., Kato, S., Bazhenova, L., Patel, S. P., Frampton, G. M., Miller, V., et al. (2017). Tumor mutational burden as an independent predictor of response to immunotherapy in diverse cancers. *Mol. Cancer Ther.* 16 (11), 2598–2608. doi:10.1158/1535-7163.MCT-17-0386

Govindan, R., Fakih, M., Price, T., Falchook, G., Desai, J., Kuo, J., et al. (2019). OA02. 02 Phase 1 study of safety, tolerability, PK and efficacy of AMG 510, a novel KRASG12C inhibitor, evaluated in NSCLC. *J. Thorac. Oncol.* 14 (10), S208. doi:10.1016/j.jtho.2019.08.412

Guo, Z., Wang, F., Di, Y., Yao, L., Yu, X., Fu, D., et al. (2018). Antitumor effect of gemcitabine-loaded albumin nanoparticle on gemcitabine-resistant pancreatic cancer induced by low hENT1 expression. *Int. J. Nanomedicine* 13, 4869–4880. doi:10.2147/IJN.S166769

Gurunathan, S., Kang, M. H., Qasim, M., and Kim, J. H. (2018). Nanoparticle-mediated combination therapy: Two-in-One approach for cancer. *Int. J. Mol. Sci.* 19 (10), E3264. doi:10.3390/ijms19103264

Hackeng, W. M., Hruban, R. H., Offerhaus, G. J., and Brosens, L. A. (2016). Surgical and molecular pathology of pancreatic neoplasms. *Diagn. Pathol.* 11 (1), 47. doi:10.1186/s13000-016-0497-z

Hamaguchi, T., Kato, K., Yasui, H., Morizane, C., Ikeda, M., Ueno, H., et al. (2007). A phase I and pharmacokinetic study of NK105, a paclitaxel-incorporating micellar nanoparticle formulation. *Br. J. Cancer* 97 (2), 170–176. doi:10.1038/sj.bjc.6603855

Han, H., Wang, J., Chen, T., Yin, L., Jin, Q., and Ji, J. (2017). Enzyme-sensitive gemcitabine conjugated albumin nanoparticles as a versatile theranostic nanoplatform for pancreatic cancer treatment. *J. Colloid Interface Sci.* 507, 217–224. doi:10.1016/j.jcis.2017.07.047

He, H., Liu, L., Morin, E. E., Liu, M., and Schwendeman, A. (2019). Survey of clinical translation of cancer nanomedicines-lessons learned from successes and failures. *Acc. Chem. Res.* 52 (9), 2445–2461. doi:10.1021/acs.accounts.9b00228

He, X., Chen, X., Liu, L., Zhang, Y., Lu, Y., Zhang, Y., et al. (2018). Sequentially triggered nanoparticles with tumor penetration and intelligent drug release for pancreatic cancer therapy. *Adv. Sci.* 5 (5), 1701070. doi:10.1002/advs.201701070

Heidemann, S. R., and Kirschner, M. W. (1978). Induced formation of asters and cleavage furrows in oocytes of *Xenopus laevis* during *in vitro* maturation. *J. Exp. Zool.* 204 (3), 431–444. doi:10.1002/jez.1402040314

Heinemann, V., Quietzsch, D., Gieseler, F., Gonnermann, M., Schonekas, H., Rost, A., et al. (2006). Randomized phase III trial of gemcitabine plus cisplatin compared with gemcitabine alone in advanced pancreatic cancer. *J. Clin. Oncol.* 24 (24), 3946–3952. doi:10.1200/JCO.2005.05.1490

Hermann, P. C., Huber, S. L., Herrler, T., Aicher, A., Ellwart, J. W., Guba, M., et al. (2007). Distinct populations of cancer stem cells determine tumor growth and metastatic activity in human pancreatic cancer. *Cell Stem Cell* 1 (3), 313–323. doi:10.1016/j.stem.2007.06.002

Hiss, D. C., Gabriels, G. A., and Folb, P. I. (2007). Combination of tunicamycin with anticancer drugs synergistically enhances their toxicity in multidrug-resistant human ovarian cystadenocarcinoma cells. *Cancer Cell Int.* 7, 5. doi:10.1186/1475-2867-7-5

Ho, W. J., Jaffee, E. M., and Zheng, L. (2020). The tumour microenvironment in pancreatic cancer - clinical challenges and opportunities. *Nat. Rev. Clin. Oncol.* 17 (9), 527–540. doi:10.1038/s41571-020-0363-5

Hosein, P. J., de Lima Lopes, G., Jr., Pastorini, V. H., Gomez, C., Macintyre, J., Zayas, G., et al. (2013). A phase II trial of nab-Paclitaxel as second-line therapy in patients with advanced pancreatic cancer. *Am. J. Clin. Oncol.* 36 (2), 151–156. doi:10.1097/COC.0b013e3182436e8c

Hosoki, T. (1983). Dynamic CT of pancreatic tumors. *AJR. Am. J. Roentgenol.* 140 (5), 959–965. doi:10.2214/ajr.140.5.959

Hu, X., Xia, F., Lee, J., Li, F., Lu, X., Zhuo, X., et al. (2021). Tailor-made nanomaterials for diagnosis and therapy of pancreatic ductal adenocarcinoma. *Adv. Sci.* 8 (7), 2002545. doi:10.1002/advs.202002545

Hung, S. W., Marrache, S., Cummins, S., Bhutia, Y. D., Mody, H., Hooks, S. B., et al. (2015). Defective hCNT1 transport contributes to gemcitabine chemoresistance in ovarian cancer subtypes: Overcoming transport defects using a nanoparticle approach. *Cancer Lett.* 359 (2), 233–240. doi:10.1016/j.canlet.2015.01.017

Jiang, B., Zhou, L., Lu, J., Wang, Y., Liu, C., You, L., et al. (2020). Stroma-targeting therapy in pancreatic cancer: One coin with two sides? *Front. Oncol.* 10, 576399. doi:10.3389/fonc.2020.576399

Kapse-Mistry, S., Govender, T., Srivastava, R., and Yergeri, M. (2014). Nanodrug delivery in reversing multidrug resistance in cancer cells. *Front. Pharmacol.* 5, 159. doi:10.3389/fphar.2014.00159

Kashyap, D., Tuli, H. S., Yerer, M. B., Sharma, A., Sak, K., Srivastava, S., et al. (2019). Natural product-based nanoformulations for cancer therapy: Opportunities and challenges. *Semin. Cancer Biol.* 69, 5–23. doi:10.1016/j.semcancer.2019.08.014

Kesharwani, P., Banerjee, S., Padhye, S., Sarkar, F. H., and Iyer, A. K. (2015). Hyaluronic acid engineered nanomicelles loaded with 3, 4-difluorobenzylidene curcumin for targeted killing of CD44+ stem-like pancreatic cancer cells. *Biomacromolecules* 16 (9), 3042–3053. doi:10.1021/acs.biomac.5b00941

Khan, S., Chauhan, N., Yallapu, M. M., Ebeling, M. C., Balakrishna, S., Ellis, R. T., et al. (2015). Nanoparticle formulation of ormeloxifene for pancreatic cancer. *Biomaterials* 53, 731–743. doi:10.1016/j.biomaterials.2015.02.082

Khan, S., Setua, S., Kumari, S., Dan, N., Massey, A., Hafeez, B. B., et al. (2019). Superparamagnetic iron oxide nanoparticles of curcumin enhance gemcitabine therapeutic response in pancreatic cancer. *Biomaterials* 208, 83–97. doi:10.1016/j.biomaterials.2019.04.005

Klebowski, B., Depciuch, J., Parlinska-Wojtan, M., and Baran, J. (2018). Applications of noble metal-based nanoparticles in medicine. *Int. J. Mol. Sci.* 19 (12), E4031. doi:10.3390/ijms19124031

Kong, C., Li, Y., Liu, Z., Ye, J., Wang, Z., Zhang, L., et al. (2019). Targeting the oncogene KRAS mutant pancreatic cancer by synergistic blocking of lysosomal acidification and rapid drug release. *ACS Nano* 13 (4), 4049–4063. doi:10.1021/acsnano.8b08246

Kraman, M., Bambrough, P. J., Arnold, J. N., Roberts, E. W., Magiera, L., Jones, J. O., et al. (2010). Suppression of antitumor immunity by stromal cells expressing fibroblast activation protein-alpha. *Science* 330 (6005), 827–830. doi:10.1126/science.1195300

Ladd, E., Sheikhi, A., Li, N., van de Ven, T. G. M., and Kakkar, A. (2017). Design and synthesis of dendrimers with facile surface group functionalization, and an evaluation of their bactericidal efficacy. *Molecules* 22 (6), E868. doi:10.3390/molecules22060868

Li, D., and Jiao, L. (2003). Molecular epidemiology of pancreatic cancer. *Int. J. Gastrointest. Cancer* 33 (1), 3–14. doi:10.1385/IJGC:33:1:3

Li, Y., VandenBoom, T. G., 2nd, Kong, D., Wang, Z., Ali, S., Philip, P. A., et al. (2009). Up-regulation of miR-200 and let-7 by natural agents leads to the reversal of epithelial-to-mesenchymal transition in gemcitabine-resistant pancreatic cancer cells. *Cancer Res.* 69 (16), 6704–6712. doi:10.1158/0008-5472.CAN-09-1298

Libutti, S. K., Paciotti, G. F., Byrnes, A. A., Alexander, H. R., Jr., Gannon, W. E., Walker, M., et al. (2010). Phase I and pharmacokinetic studies of CYT-6091, a novel PEGylated colloidal gold-rhTNF nanomedicine. *Clin. Cancer Res.* 16 (24), 6139–6149. doi:10.1158/1078-0432.CCR-10-0978

Libutti, S. K., Tamarkin, L., and Nilubol, N. (2018). Targeting the invincible barrier for drug delivery in solid cancers: Interstitial fluid pressure. *Oncotarget* 9 (87), 35723–35725. doi:10.18632/oncotarget.26267

Lin, Z., Lu, S., Xie, X., Yi, X., and Huang, H. (2020). Noncoding RNAs in drug-resistant pancreatic cancer: A review. *Biomed. Pharmacother.* 131, 110768. doi:10.1016/j.biopha.2020.110768

Liu, L., Kshirsagar, P., Christiansen, J., Gautam, S. K., Aithal, A., Gulati, M., et al. (2021). Polyanhydride nanoparticles stabilize pancreatic cancer antigen MUC4β. *J. Biomed. Mat. Res. A* 109 (6), 893–902. doi:10.1002/jbm.a.37080

Liu, L., Kshirsagar, P. G., Gautam, S. K., Gulati, M., Wafa, E. I., Christiansen, J. C., et al. (2022). Nanocarriers for pancreatic cancer imaging, treatments, and immunotherapies. *Theranostics* 12 (3), 1030–1060. doi:10.7150/thno.64805

Lobato-Mendizabal, E., and Ruiz-Arguelles, G. J. (1990). Leukemia and malnutrition. II. The magnitude of maintenance chemotherapy as a prognostic factor in the survival of patients with standard-risk acute lymphoblastic leukemia. *Rev. Invest. Clin.* 42 (2), 81–87.

Lucero-Acuna, A., Jeffery, J. J., Abril, E. R., Nagle, R. B., Guzman, R., Pagel, M. D., et al. (2014). Nanoparticle delivery of an AKT/PDK1 inhibitor improves the therapeutic effect in pancreatic cancer. *Int. J. Nanomedicine* 9, 5653–5665. doi:10.2147/IJN.S68511

Macarulla, T., Pazo-Cid, R., Guillen-Ponce, C., Lopez, R., Vera, R., Reboredo, M., et al. (2019). Phase I/II trial to evaluate the efficacy and safety of nanoparticle albumin-bound paclitaxel in combination with gemcitabine in patients with pancreatic cancer and an ECOG performance status of 2. *J. Clin. Oncol.* 37 (3), 230–238. doi:10.1200/JCO.18.00089

Manzur, A., Oluwasanmi, A., Moss, D., Curtis, A., and Hoskins, C. (2017). Nanotechnologies in pancreatic cancer therapy. *Pharmaceutics* 9 (4), E39. doi:10.3390/pharmaceutics9040039

McCarroll, J., Teo, J., Boyer, C., Goldstein, D., Kavallaris, M., and Phillips, P. A. (2014). Potential applications of nanotechnology for the diagnosis and treatment of pancreatic cancer. *Front. Physiol.* 5, 2. doi:10.3389/fphys.2014.00002

Melancon, M. P., Stafford, R. J., and Li, C. (2012). Challenges to effective cancer nanotheranostics. *J. Control. Release* 164 (2), 177–182. doi:10.1016/j.jconrel.2012.07.045

Metselaar, J. M., and Lammers, T. (2020). Challenges in nanomedicine clinical translation. *Drug Deliv. Transl. Res.* 10 (3), 721–725. doi:10.1007/s13346-020-00740-5

Min, C., Eddy, S. F., Sherr, D. H., and Sonenshein, G. E. (2008). NF-kappaB and epithelial to mesenchymal transition of cancer. *J. Cell. Biochem.* 104 (3), 733–744. doi:10.1002/jcb.21695

Mohelnikova-Duchonova, B., Brynychova, V., Oliverius, M., Honsova, E., Kala, Z., Muckova, K., et al. (2013). Differences in transcript levels of ABC transporters between pancreatic adenocarcinoma and nonneoplastic tissues. *Pancreas* 42 (4), 707–716. doi:10.1097/MPA.0b013e318279b861

Nieto, M. A., Huang, R. Y., Jackson, R. A., and Thiery, J. P. (2016). Emt: 2016. *Cell* 166 (1), 21–45. doi:10.1016/j.cell.2016.06.028

O'Driscoll, L., Walsh, N., Larkin, A., Ballot, J., Ooi, W. S., Gullo, G., et al. (2007). MDR1/P-glycoprotein and MRP-1 drug efflux pumps in pancreatic carcinoma. *Anticancer Res.* 27 (4B), 2115–2120.

Obaid, G., Bano, S., Thomsen, H., Callaghan, S., Shah, N., Swain, J. W. R., et al. (2022). Remediating desmoplasia with EGFR-targeted photoactivable multi-inhibitor liposomes doubles overall survival in pancreatic cancer. *Adv. Sci. (Weinh).*, 24, e2104594. doi:10.1002/advs.202104594

Ogawa, K., and Miura, T. (2014). Aphid polyphenisms: trans-generational developmental regulation through viviparity. *Front. Physiol.* 5, 1. doi:10.3389/fphys.2014.00001

Oliveira, C., Calmeiro, J., Carrascal, M. A., Falcão, A., Gomes, C., Miguel Neves, B., et al. (2021). Exosomes as new therapeutic vectors for pancreatic cancer treatment. *Eur. J. Pharm. Biopharm.* 161, 4–14. doi:10.1016/j.ejpb.2021.02.002

Pandya, G., Kirtonia, A., Sethi, G., Pandey, A. K., and Garg, M. (2020). The implication of long non-coding RNAs in the diagnosis, pathogenesis and drug resistance of pancreatic ductal adenocarcinoma and their possible therapeutic potential. *Biochim. Biophys. Acta. Rev. Cancer* 1874 (2), 188423. doi:10.1016/j.bbcan.2020.188423

Parhi, P., Mohanty, C., and Sahoo, S. K. (2012). Nanotechnology-based combinational drug delivery: An emerging approach for cancer therapy. *Drug Discov. Today* 17 (17-18), 1044–1052. doi:10.1016/j.drudis.2012.05.010

Poon, C., He, C., Liu, D., Lu, K., and Lin, W. (2015). Self-assembled nanoscale coordination polymers carrying oxaliplatin and gemcitabine for synergistic combination therapy of pancreatic cancer. *J. Control. Release* 201, 90–99. doi:10.1016/j.jconrel.2015.01.026

Prabhu, P., and Patravale, V. (2012). The upcoming field of theranostic nanomedicine: An overview. *J. Biomed. Nanotechnol.* 8 (6), 859–882. doi:10.1166/jbn.2012.1459

Rawla, P., Sunkara, T., and Gaduputi, V. (2019). Epidemiology of pancreatic cancer: Global trends, etiology and risk factors. *World J. Oncol.* 10 (1), 10–27. doi:10.14740/wjon1166

Rebelo, A., Molpeceres, J., Rijo, P., and Reis, C. P. (2017). Pancreatic cancer therapy review: From classic therapeutic agents to modern nanotechnologies. *Curr. Drug Metab.* 18 (4), 346–359. doi:10.2174/1389200218666170201151135

Rishi, A., Goggins, M., Wood, L. D., and Hruban, R. H. (2015). Pathological and molecular evaluation of pancreatic neoplasms. *Semin. Oncol.* 42 (1), 28–39. doi:10.1053/j.seminoncol.2014.12.004

Ryan, D. P., Hong, T. S., and Bardeesy, N. (2014). Pancreatic adenocarcinoma. *N. Engl. J. Med.* 371 (11), 1039–1049. doi:10.1056/NEJMra1404198

Schizas, D., Charalampakis, N., Kole, C., Economopoulou, P., Koustas, E., Gkotsis, E., et al. (2020). Immunotherapy for pancreatic cancer: A 2020 update. *Cancer Treat. Rev.* 86, 102016. doi:10.1016/j.ctrv.2020.102016

Schroeder, A., Heller, D. A., Winslow, M. M., Dahlman, J. E., Pratt, G. W., Langer, R., et al. (2011). Treating metastatic cancer with nanotechnology. *Nat. Rev. Cancer* 12 (1), 39–50. doi:10.1038/nrc3180

Shah, A. N., Summy, J. M., Zhang, J., Park, S. I., Parikh, N. U., and Gallick, G. E. (2007). Development and characterization of gemcitabine-resistant pancreatic tumor cells. *Ann. Surg. Oncol.* 14 (12), 3629–3637. doi:10.1245/s10434-007-9583-5

Sharma, A., Goyal, A. K., and Rath, G. (2018). Recent advances in metal nanoparticles in cancer therapy. *J. Drug Target.* 26 (8), 617–632. doi:10.1080/1061186X.2017.1400553

Siegel, R. L., Miller, K. D., and Jemal, A. (2019). Cancer statistics, 2019. *Ca. Cancer J. Clin.* 69 (1), 7–34. doi:10.3322/caac.21551

Sielaff, C. M., and Mousa, S. A. (2018). Status and future directions in the management of pancreatic cancer: Potential impact of nanotechnology. *J. Cancer Res. Clin. Oncol.* 144 (7), 1205–1217. doi:10.1007/s00432-018-2651-3

Singh, A., and Settleman, J. (2010). EMT, cancer stem cells and drug resistance: An emerging axis of evil in the war on cancer. *Oncogene* 29 (34), 4741–4751. doi:10.1038/onc.2010.215

Sofuni, A., Iijima, H., Moriyasu, F., Nakayama, D., Shimizu, M., Nakamura, K., et al. (2005). Differential diagnosis of pancreatic tumors using ultrasound contrast imaging. *J. Gastroenterol.* 40 (5), 518–525. doi:10.1007/s00535-005-1578-z

Soni, K. S., Thomas, D., Caffrey, T., Mehla, K., Lei, F., O'Connell, K. A., et al. (2019). A polymeric nanogel-based treatment regimen for enhanced efficacy and sequential administration of synergistic drug combination in pancreatic cancer. *J. Pharmacol. Exp. Ther.* 370 (3), 894–901. doi:10.1124/jpet.118.255372

Stathopoulos, G. P., Boulikas, T., Vougiouka, M., Deliconstantinos, G., Rigatos, S., Darli, E., et al. (2005). Pharmacokinetics and adverse reactions of a new liposomal cisplatin (Lipoplatin): phase I study. *Oncol. Rep.* 13 (4), 589–595. doi:10.3892/or.13.4.589

Syrigos, K. N., Michalaki, B., Alevyzaki, F., Machairas, A., Mandrekas, D., Kindilidis, K., et al. (2002). A phase-II study of liposomal doxorubicin and docetaxel in patients with advanced pancreatic cancer. *Anticancer Res.* 22 (6B), 3583–3588.

Tang, S., Hang, Y., Ding, L., Tang, W., Yu, A., Zhang, C., et al. (2021). Intraperitoneal siRNA nanoparticles for augmentation of gemcitabine efficacy in the treatment of pancreatic cancer. *Mol. Pharm.* 18 (12), 4448–4458. doi:10.1021/acs.molpharmaceut.1c00653

Tarannum, M., Holtzman, K., Dreau, D., Mukherjee, P., and Vivero-Escoto, J. L. (2022). Nanoparticle combination for precise stroma modulation and improved delivery for pancreatic cancer. *J. Control. Release* 347, 425–434. doi:10.1016/j.jconrel.2022.05.019

Tempero, M. A., Malafa, M. P., Chiorean, E. G., Czito, B., Scaife, C., Narang, A. K., et al. (2019). Pancreatic adenocarcinoma, version 1.2019. *J. Natl. Compr. Canc. Netw.* 17 (3), 202–210. doi:10.6004/jnccn.2019.0014

Thakkar, A., Desai, P., Chenreddy, S., Modi, J., Thio, A., Khamas, W., et al. (2018). Novel nano-drug combination therapeutic regimen demonstrates significant efficacy in the transgenic mouse model of pancreatic ductal adenocarcinoma. *Am. J. Cancer Res.* 8 (10), 2005–2019.

Thapa, R. K., Ku, S. K., Choi, H. G., Yong, C. S., Byeon, J. H., and Kim, J. O. (2018). Vibrating droplet generation to assemble zwitterion-coated gold-graphene oxide stealth nanovesicles for effective pancreatic cancer chemo-phototherapy. *Nanoscale* 10 (4), 1742–1749. doi:10.1039/c7nr07603g

Urey, C., Hilmersson, K. S., Andersson, B., Ansari, D., and Andersson, R. (2017). Development and *in vitro* characterization of a gemcitabine-loaded MUC4-targeted immunoliposome against pancreatic ductal adenocarcinoma. *Anticancer Res.* 37 (11), 6031–6039. doi:10.21873/anticanres.12050

van der Meel, R., Lammers, T., and Hennink, W. E. (2017). Cancer nanomedicines: Oversold or underappreciated? *Expert Opin. Drug Deliv.* 14 (1), 1–5. doi:10.1080/17425247.2017.1262346

van Horssen, R., Ten Hagen, T. L., and Eggermont, A. M. (2006). TNF-Alpha in cancer treatment: Molecular insights, antitumor effects, and clinical utility. *Oncologist* 11 (4), 397–408. doi:10.1634/theoncologist.11-4-397

Vogel, A., Rommler-Zehrer, J., Li, J. S., McGovern, D., Romano, A., and Stahl, M. (2016). Efficacy and safety profile of nab-paclitaxel plus gemcitabine in patients with metastatic pancreatic cancer treated to disease progression: A subanalysis from a phase 3 trial (MPACT). *BMC Cancer* 16 (1), 817. doi:10.1186/s12885-016-2798-8

Von Hoff, D. D., Ervin, T., Arena, F. P., Chiorean, E. G., Infante, J., Moore, M., et al. (2013). Increased survival in pancreatic cancer with nab-paclitaxel plus gemcitabine. *N. Engl. J. Med.* 369 (18), 1691–1703. doi:10.1056/NEJMoa1304369

Von Hoff, D. D., Ramanathan, R. K., Borad, M. J., Laheru, D. A., Smith, L. S., Wood, T. E., et al. (2011). Gemcitabine plus nab-paclitaxel is an active regimen in patients with advanced pancreatic cancer: A phase I/II trial. *J. Clin. Oncol.* 29 (34), 4548–4554. doi:10.1200/JCO.2011.36.5742

Wang, L., Liu, X., Zhou, Q., Sui, M., Lu, Z., Zhou, Z., et al. (2017). Terminating the criminal collaboration in pancreatic cancer: Nanoparticle-based synergistic therapy for overcoming fibroblast-induced drug resistance. *Biomaterials* 144, 105–118. doi:10.1016/j.biomaterials.2017.08.002

Wang, Z., Li, Y., Kong, D., Banerjee, S., Ahmad, A., Azmi, A. S., et al. (2009). Acquisition of epithelial-mesenchymal transition phenotype of gemcitabine-resistant pancreatic cancer cells is linked with activation of the notch signaling pathway. *Cancer Res.* 69 (6), 2400–2407. doi:10.1158/0008-5472.CAN-08-4312

Wang-Gillam, A., Li, C. P., Bodoky, G., Dean, A., Shan, Y. S., Jameson, G., et al. (2016). Nanoliposomal irinotecan with fluorouracil and folinic acid in metastatic pancreatic cancer after previous gemcitabine-based therapy (NAPOLI-1): A global, randomised, open-label, phase 3 trial. *Lancet* 387 (10018), 545–557. doi:10.1016/S0140-6736(15)00986-1

Xia, Y., Shen, S., and Verma, I. M. (2014). NF-κB, an active player in human cancers. *Cancer Immunol. Res.* 2 (9), 823–830. doi:10.1158/2326-6066.CIR-14-0112

Xie, V. K., He, J., and Xie, K. (2020a). Protein arginine methylation promotes therapeutic resistance in human pancreatic cancer. *Cytokine Growth Factor Rev.* 55, 58–69. doi:10.1016/j.cytogfr.2020.07.011

Xie, Y., Hang, Y., Wang, Y., Sleightholm, R., Prajapati, D. R., Bader, J., et al. (2020b). Stromal modulation and treatment of metastatic pancreatic cancer with local intraperitoneal triple miRNA/siRNA nanotherapy. *ACS Nano* 14 (1), 255–271. doi:10.1021/acsnano.9b03978

Xu, Y., Meng, H., Du, F., Lu, W., Liu, S., Huang, J., et al. (2015). Preparation of intravenous injection nanoformulation of VESylated gemcitabine by co-assembly with TPGS and its anti-tumor activity in pancreatic tumor-bearing mice. *Int. J. Pharm.* 495 (2), 792–797. doi:10.1016/j.ijpharm.2015.09.030

Yonemori, K., Kurahara, H., Maemura, K., and Natsugoe, S. (2017). MicroRNA in pancreatic cancer. *J. Hum. Genet.* 62 (1), 33–40. doi:10.1038/jhg.2016.59

Yoshida, M., Takimoto, R., Murase, K., Sato, Y., Hirakawa, M., Tamura, F., et al. (2012). Targeting anticancer drug delivery to pancreatic cancer cells using a fucose-bound nanoparticle approach. *PLoS One* 7 (7), e39545. doi:10.1371/journal.pone.0039545

Yousefi, H., Yuan, J., Keshavarz-Fathi, M., Murphy, J. F., and Rezaei, N. (2017). Immunotherapy of cancers comes of age. *Expert Rev. Clin. Immunol.* 13 (10), 1001–1015. doi:10.1080/1744666X.2017.1366315

Yu, X., Zhu, W., Di, Y., Gu, J., Guo, Z., Li, H., et al. (2017). Triple-functional albumin-based nanoparticles for combined chemotherapy and photodynamic therapy of pancreatic cancer with lymphatic metastases. *Int. J. Nanomedicine* 12, 6771–6785. doi:10.2147/IJN.S131295

Yu, Z., Pestell, T. G., Lisanti, M. P., and Pestell, R. G. (2012). Cancer stem cells. *Int. J. Biochem. Cell Biol.* 44 (12), 2144–2151. doi:10.1016/j.biocel.2012.08.022

Yuan, Y., Cai, T., Xia, X., Zhang, R., Chiba, P., and Cai, Y. (2016). Nanoparticle delivery of anticancer drugs overcomes multidrug resistance in breast cancer. *Drug Deliv.* 23 (9), 3350–3357. doi:10.1080/10717544.2016.1178825

Zeng, S., Pottler, M., Lan, B., Grutzmann, R., Pilarsky, C., and Yang, H. (2019). Chemoresistance in pancreatic cancer. *Int. J. Mol. Sci.* 20 (18), E4504. doi:10.3390/ijms20184504

Zhang, M., Liu, E., Cui, Y., and Huang, Y. (2017). Nanotechnology-based combination therapy for overcoming multidrug-resistant cancer. *Cancer Biol. Med.* 14 (3), 212–227. doi:10.20892/j.issn.2095-3941.2017.0054

Zhao, Y., Zheng, Y., Zhu, Y., Zhang, Y., Zhu, H., and Liu, T. (2021a). M1 macrophage-derived exosomes loaded with Gemcitabine and deferasirox against chemoresistant pancreatic cancer. *Pharmaceutics* 13 (9), 1493. doi:10.3390/pharmaceutics13091493

Zhao, Y., Zheng, Y., Zhu, Y., Zhang, Y., Zhu, H., and Liu, T. (2021b). M1 macrophage-derived exosomes loaded with gemcitabine and deferasirox against chemoresistant pancreatic cancer. *Pharmaceutics* 13 (9), 1493. doi:10.3390/pharmaceutics13091493

Zhi, X., Tao, J., Xie, K., Zhu, Y., Li, Z., Tang, J., et al. (2014). MUC4-induced nuclear translocation of beta-catenin: A novel mechanism for growth, metastasis and angiogenesis in pancreatic cancer. *Cancer Lett.* 346 (1), 104–113. doi:10.1016/j.canlet.2013.12.021

frontiers | Frontiers in Pharmacology

TYPE Original Research
PUBLISHED 12 September 2022
DOI 10.3389/fphar.2022.922388

OPEN ACCESS

EDITED BY
Faisal Raza,
Shanghai Jiao Tong University, China

REVIEWED BY
Majid Sharifi-Rad,
Zabol University, Iran
Sonia Malik,
Université d'Orléans, France

*CORRESPONDENCE
Muhammad Irfan,
mirfan310@yahoo.com

SPECIALTY SECTION
This article was submitted to Experimental Pharmacology and Drug Discovery, a section of the journal Frontiers in Pharmacology

RECEIVED 17 April 2022
ACCEPTED 25 July 2022
PUBLISHED 12 September 2022

CITATION
Musa M, Jan G, Jan FG, Hamayun M, Irfan M, Rauf A, Alsahammari A, Alharbi M, Suleria HAR and Ali N (2022), Pharmacological activities and gas chromatography–mass spectrometry analysis for the identification of bioactive compounds from Justicia adhatoda L.
Front. Pharmacol. 13:922388.
doi: 10.3389/fphar.2022.922388

Pharmacological activities and gas chromatography–mass spectrometry analysis for the identification of bioactive compounds from *Justicia adhatoda* L.

Muhammad Musa[1], Gul Jan[1], Farzana Gul Jan[1], Muhammad Hamayun[1], Muhammad Irfan[1,2,3]*, Abdur Rauf[4], Abdulrahman Alsahammari[5], Metab Alharbi[5], Hafiz A. R. Suleria[6] and Niaz Ali[7]

[1]Department of Botany, Abdul Wali Khan University, Mardan, Pakistan, [2]Department of Botany, University of Swabi, Swabi, Pakistan, [3]Missouri Botanical Garden, St. Louis, MO, United States, [4]Department of Chemistry, University of Swabi, Swabi, Pakistan, [5]Department of Pharmacology and Toxicology, College of Pharmacy, King Saud University, Riyadh, Saudi Arabia, [6]Faculty of Veterinary and Agricultural Sciences, School of Agriculture and Food, The University of Melbourne, Parkville, VIC, Australia, [7]Department of Botany, Hazara University, Mansehra, Pakistan

The current study aimed to assess the pharmacological potential of *Justicia adhatoda* by evaluating the presence of biologically active compounds using the gas chromatography–mass spectrometry approach and to undertake biological activities for the effectiveness of the present compounds using standard tests. A total of 21 compounds were identified in the gas chromatography–mass spectrometry analysis of the ethyl acetate fraction in which 14 of the identified compounds are recognized for their pharmacological potential in the literature. In total, four fractions (ethyl acetate, chloroform, n-hexane, and aqueous) were evaluated for pharmacological activities. In carrageenan-induced inflammation, the chloroform fraction exhibited high anti-inflammatory activity (46.51%). Similarly, the analgesic potential of ethyl acetate fraction was the most effective (300 mg/kg) in the acetic acid-induced test. Similarly, in the formalin test, ethyl acetate fraction exhibited maximum inhibition in both early (74.35%) and late phases (88.38). Maximum inhibition of pyrexia (77.98%) was recorded for the ethyl acetate fraction (300 mg/kg). In DPPH assay, the ethyl acetate fraction revealed the highest scavenging potential among other fractions (50 µg/ml resulted in 50.40% and 100 µg/ml resulted in 66.74% scavenging).

KEYWORDS

antioxidant, analgesic, antispasmodic, anti-inflammatory, antibacterial, medicinal plants

Introduction

Plants have been used by humans for the treatment of various diseases, and this practice date back to ancient civilizations. Furthermore, plants and/or their products have played an immensely important role in the development of pharmaceutical industries due to the presence of unique bioactive compounds (Sundur et al., 2014). Over the last few decades, a number of pharmacologically important compounds have been isolated from plants, and even today the use of medicinal plants in pharmaceutical industries is extensive. It is widely acknowledged that some 80% of the world population of the developing countries of Africa, Asia, and elsewhere still rely on plants as sources of their medications (Khan et al., 2021). New plant taxa have been added to the Flora of Pakistan having great medicinal importance (Ali et al., 2017). Worldwide interest in traditional medicines is rising; this is evident from the increasing number of plant-based commercial companies as well as the international legislation and treaties that allow judicious and sustainable utilization of medicinal plants or their products (Bashir et al., 2011; Khan et al., 2017).

Nonetheless, in folklore, plants have been used in the form of powder, decoctions, infusions, or tablets to treat a variety of human illnesses with little or no information on the safe dosages. Furthermore, the mode of administration and dosage taken varies with culture and traditional beliefs (Khan et al., 2017). Thus, with no known intrinsic standards, low or higher dosages of medicinal plants (also referred to as ethnomedicines) are often associated with complications (Irfan et al., 2022; Ullah et al., 2022). To overcome these limitations, one of the leading and reliable approaches in pharmacology is the use of a model organism to check the efficacy of a specific plant extract and/or dosage applied against disorder/s (Jan and Khan, 2016; Ullah et al., 2019).

There are worldwide growing interests in the identification of new as well as unique plant-based formulations that could be applied for treating inflammations, as antioxidants, and relieving pain and pyrexia, etc. (Simmons, 2006; Bhowmick et al., 2014: Ji et al., 2016; Jan and Khan, 2016; Shah et al., 2017; Ullah et al., 2019).

Justicia adhatoda L. belongs to the Acanthaceae family, and it is locally referred to as Vasaka and Malabar nut. The plant is a perennial, green shrub scattered over wide ranges of Southeast Asian tropical regions (Kaur et al., 2013). Its leaves are used for the treatment of diarrhea (Ahmad et al., 2016); leaves and roots are used in treating diabetes and vomiting (Irfan et al., 2017); leaves and flowers are used against cough, wound healing, and dysentery (Irfan et al., 2018a); leaves are used in treating bronchitis and cough and prevent loose motion (Irfan et al., 2018b); leaf extract is used for the treatment of rheumatism and asthma (Irfan et al., 2018c); decoction of leaves is used against dysentery and for the treatment of scabies (Irfan et al., 2018d; Irfan et al., 2018e); the extract of leaves is used as expectorant and antispasmodic and as antipyretic agent (Irfan et al., 2018f). A literature survey revealed reports of *Justicia adhatoda* being used for biological activities, i.e., anti-tubercular, bronchodilator, antibacterial, and anti-asthmatic potential (Latha et al., 2018). However, to the best of our knowledge, no report was found regarding the anti-inflammatory potential of *Justicia adhatoda*. Therefore, the current study was designed to integrate the folklore use of *Justicia adhatoda* with a gas chromatography–mass spectrometry approach to identify biologically active compounds and then investigate the potency of different fractions of *Justicia adhatoda* in pharmacological bioassays using animal models.

Materials and methods

Plant collection

Justicia adhatoda L. was collected from Charsadda District, Khyber Pakhtunkhwa, Pakistan, in May 2021. The plant was identified with the help of the relevant literature (Malik and Ghafoor, 1988), and a voucher specimen (AWK0518) was deposited in the Herbarium, Department of Botany, Abdul Wali Khan University Mardan, Pakistan.

Extraction

Leaves were manually separated from branches and washed with tap water for 10 min before leaves were shade-dried for 20 days. These dried leaves were ground to a coarse powder using a grinder. For extraction, 6 kg of leaf powder was soaked in 23 L methanol (80%) for 18 days. The filtrate was mixed and condensed through a rotary evaporator, and finally 400 g of crude methanol extract was obtained (Sharifi-Rad et al., 2020a).

Fractionation

The crude methanolic extract of *Justicia adhatoda* L. was shifted into a separating funnel and diluted with 500 ml distilled water followed by the addition of 500 ml. The mixture was kept until it formed the upper and lower layers. The n-hexane layer was isolated, and this procedure was repeated three times, adding 500 ml n-hexane each time. For the final fraction, all of the n-hexane layers were combined in a rotary evaporator to the final concentrated n-hexane fraction of 20 g. The same process was performed to obtain chloroform and ethyl acetate fractions weighing 27 and 80 g, respectively. Finally, a dry water fraction (120 g) was also obtained (Zeb et al., 2017; Sharifi-Rad and Pohl, 2020).

Experimental animals

The whole set of experiments was monitored in albino mice of mixed sexes that were obtained from the Veterinary Research Institute, Peshawar, Khyber Pakhtunkhwa, Pakistan. All experimentation followed stringent biosafety protocols and

bioethical procedures as approved by the Biosafety and Bioethics Committee of the Department of Botany, AWKUM.

Acute toxicity bioassay

Two major groups consisting of control and test (treatments) were made, each comprised four test models. The fractions were orally administered using different dosages, i.e., 150–1800 mg/kg. Tween-80 was used as a solvent in preparation for the dosages. Mice were examined for the next 72 h for decreased allergic symptoms and any abnormal behavior after receiving the dose/s (Zeb et al., 2016).

Anti-inflammatory activity

Carrageen-induced inflammatory test

The carrageenan-induced paw edema test was carried out following Winter et al. (1962). Albino mice were grouped, and initial paw volume was measured, and then carrageenan solution was injected in the hind paw of mice, i.e., subcutaneously injected at 0.05 ml (1%). A standard drug (diclofenac) was injected, and different fractions such as ethyl acetate, n-hexane, chloroform, and aqueous were injected at doses of 150 and 300 mg/kg to the respective groups. The procedure of the plethysmometer (Ugo Basil 7150) method was followed after the first, second, third, and fourth hour of injections of standard drug and fraction (Sharifi-Rad et al., 2021).

Analgesic activity

Acetic acid-induced writhing test

For analgesic potential, the acetic acid writhing test was carried out on *Justicia adhatoda* L. The mice were divided into different groups, while oral dosages at 150 mg/kg and 300 mg/kg of ethyl acetate, n-hexane, chloroform, and aqueous fractions were administered, consequently, after 30 min, and 10 ml/kg of acetic acid (0.6%) was injected intraperitoneally to the model mice. Group I control 0.5% was administered with Tween-80 (3 ml/kg), and Group II was considered standard and administered with the standard drug (10 mg/kg). The number of writhes (contraction of the abdomen extension of body and limbs, twisting of the mice trunk, and elongation) was counted from 5, 15, 30, and 60 min after the injection of acetic acid (Franzotti et al., 2000).

Analgesic activity

Formalin-induced licking paw test

The formalin-induced licking paw test was carried out for the assessment of analgesic ability of *Justicia adhatoda* (Santos and Calixto, 1997). Mice were categorized into groups, where group I received 0.5 percent Tween-80 (3 ml/kg) of negative regulation and group II received standard drug morphine (5 mg/kg), while other groups received ethyl acetate, n-hexane, and chloroform fractions of *Justicia adhatoda* with doses of 150 mg/kg and 300 mg/kg divided into respective groups, while 2.5% formalin (20 µl) was subcutaneously injected into the plantar surface of the mice's hind paw after 30 min. Formalin-induced paw licking was recorded as an important signal for understanding the harmful sexual behavior. The behavioral responses to the sensation of nociception were properly noted like, the leakage and bite of the injected paw, respectively. Total time taken was 30 min, where the first 15 min were considered the early stage of the nociceptive reaction and the later 15 min were considered the late stage of the nociceptive reaction (Sharifi-Rad et al., 2020b).

Analgesic activity

Tail immersion test

Tail immersion potential was evaluated by the method of Imam and Sumi, (2014). Ethyl acetate, n-hexane, chloroform, and aqueous fractions were administered using doses of 150 mg/kg and 300 mg/kg and morphine (10 mg/kg), respectively, before 30 min of the experiment. Then, 15 min ahead of the trial, 1 cm to 2 cm of mice tail was submerged in warm water and held at 52 ± 1°C stable. The response time was the time the mice needed to bounce the tail. The latency time of tail removal response was taken as the ant nociception index (Sharifi-Rad et al., 2022).

Antipyretic activity

Brewer's yeast-induced pyrexia method

The antipyretic activity was evaluated for *Justicia adhatoda* L. using the method of Muhammad et al. (2012). The albino mice of both sexes were used, and each test contained four mice. At the beginning of the experiment, normal mice's body temperature was taken *via* a digital thermometer, and pyrexia was then induced in all mice by injecting 20% brewer's yeast. Mice were fasted overnight but permitted free access to drinking water, and the rectal temperature of each mouse was recorded after 24 h. Group I was injected with normal saline (10 ml/kg) as a negative regulation and Group II received paracetamol (10 mg/kg), while ethyl-acetate, n-hexane, chloroform, and aqueous fractions of *Justicia adhatoda* at the concentration of 150 mg/kg and 300 mg/kg were administrated to other groups.

Antioxidant activity

DPPH method

The scavenging effect of *Justicia adhatoda* was evaluated following Feghhi-Najafabadi et al. (2019). Fractions with the

concentration of 50 and 100 μL/ml were tested. DPPH methanol solution was applied to various plant extracts at concentration levels of 50 and 100 μg/ml. DPPH solution was prepared, and the mixture of fraction and solution (2 ml of DPPH methanol solution and 50 and 100 μg/ml) was gently mixed, and the absorbance was measured at 517 nm using a spectrophotometer after 60 min of incubation in dark. For the calculation of % inhibition, the following formula was followed:

$$\text{Inhibition}\,(\%) = [(A^{\circ} - A1)/A^{\circ}]\times 100\,,$$

where A° represents the absorbance of the control and A1 represents the absorbance of the sample.

Antispasmodic activity by normal intestinal transit

Albino mice were divided into groups of four animals each. The first group was considered control and saline solution was administrated (10 ml/kg). Other groups were treated with aqueous, ethyl acetate, chloroform, and n-hexane fractions of *Justicia adhatoda* at different doses, while one group in each was considered the standard group. After thirty minutes, a regular charcoal meal (0.2 ml/mouse of 10% charcoal suspension in 5% gum acacia) was given to the mice orally (Hsu, 1982). On charcoal administration in mice meal, the tested animals were slaughtered in 30 min, and the small intestine was immediately removed. Similarly, the peristaltic index of each mouse was monitored by subtracting the distance traveled by the charcoal meal in the intestine from the total length of the small intestine (Than et al., 1989).

Gas chromatography–mass spectrometry analysis of the extract and identification of the phytocompounds

For the identification of bioactive phytochemicals in the ethyl acetate fraction of *Justicia adhatoda*, gas chromatography–mass spectrometry (Thermo Scientific Co.) was used. Identification of active phytochemicals was as per the 'National Institute of Standards and Technology 2008' (NIST-2008) database that contained over 62,000 patterns used for interpreting gas chromatography–mass spectrometry mass spectra. A comparison of the spectrum of an unknown component with the spectrum of the known component in the NIST library was performed (Sher et al., 2022).

Statistical analysis

Data were recorded in the form of triplicate and expressed as mean ± standard error of the mean (SEM). The data were then quantified for normality and homogeneity, and the statistical investigations were carried out by means of one-way analysis of variance (ANOVA), followed by multiple Duncan's range test using statistical software SPSS, V 20.0 (SPSS, Chicago, IL, United States). As compared to control/standard, significant stimulatory/inhibitory effects were monitored using the following formula, and significant differences were considered by means of various statistical bars at $p < 0.05$.

(1) Reduction in pyrexia was evaluated by the following formula used by Muhammad et al. (2012):

$$\text{Percent reduction} = \text{B} - \text{Cn/B} - \text{A}\times 100,$$

where B represents the temperature after pyrexia induction, Cn represents the temperature after 1, 2, 3, 4, and 5 h, and A represents the normal body temperature.

(2) The % inhibition of inflammatory effect of different fractions was calculated using the formula of Hossain et al. (2016):

$$\text{Percentage inhibition of inflammation} = [(\text{Vc} - \text{Vt})/\text{Vc}]\times 100,$$

where Vc is the average inflammation of the control group and Vt is the average degree of inflammation by the test group.

(3)The percent inhibition of inflammation was calculated at different time intervals using the following formula (Shah and Shah 2015):

$$\text{Percent inhibition} = \text{A} - \text{T}/\text{A}\times 100,$$

where A is the average inflammation of control and T is the paw volume of the test group.

(4) The following standard formula (Than et al., 1989) was used to calculate the initial transit percentage (percent) of antispasmodic action:

$$\text{Intestinal Transit}\,(\%) = \text{D/L}\times 100,$$

where D = charcoal meal length (cm) and L = total intestinal length (cm).

Results

Anti-inflammatory activity

The effect of *Justicia adhatoda* on carrageenan-induced hind paw edema is shown in Figure 1. The mice paw becomes edematous after injection of carrageenan. It was noted that the reference drug (diclofenac) inhibited paw edema up to 47.67%, while the administration of chloroform fraction at a higher concentration (300 mg/kg) showed significant anti-inflammatory activity at fourth hour with a paw edema inhibition rate of 46.51%. Moreover, the

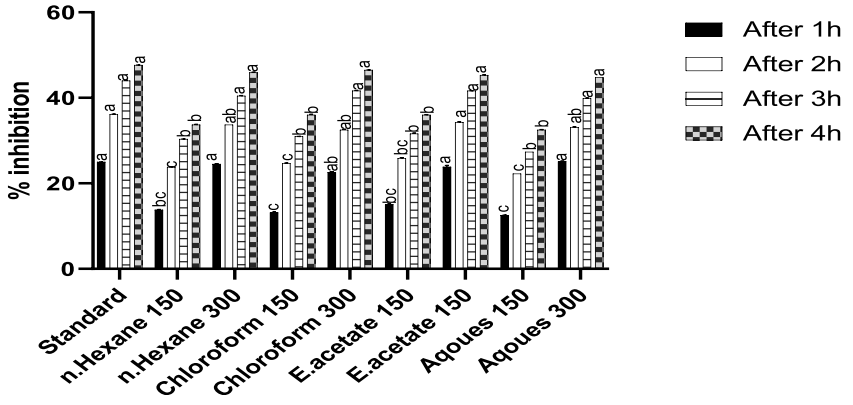

FIGURE 1
Anti-inflammatory activity of different fractions of *Justicia adhatoda* at doses of 150 and 300 mg/kg in carrageenan-induced paw edema in Swiss albino mice after 1, 2, 3, and 4 h. Various bars represent statistical difference at $p < 0.05$.

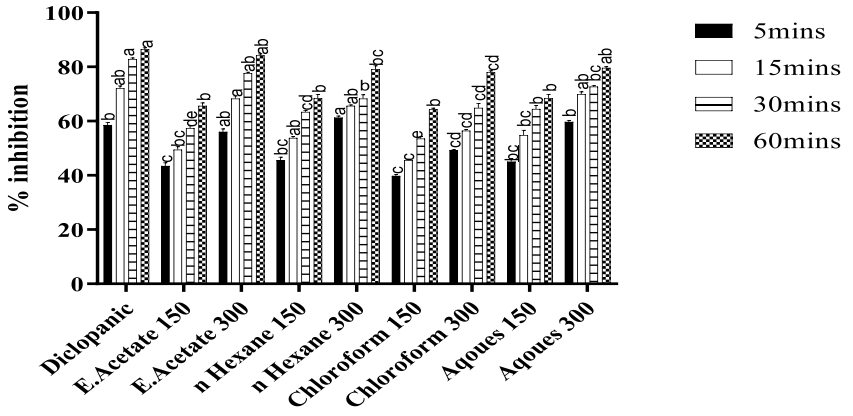

FIGURE 2
Analgesic activity of *Justicia adhatoda*'s different fractions was monitored at the dose of 150 and 300 mg/kg in acetic acid-induced Swiss albino mice. Different statistical bars represent statistical differences at $p < 0.05$.

other fractions, namely, n-hexane, ethyl acetate, and aqueous at higher extract dose also showed inhibition on fourth hour, i.e., 45.93%, 45.34%, and 44.76%, respectively.

Writhing test

The isolated fractions of *Justicia adhatoda* were checked for analgesic activity using the writhing test (Figure 2). As compared to the standard diclofenac sodium (10 mg/kg) that significantly inhibited the writhing (86.44%), the ethyl-acetate fraction also caused significant inhibition (84.18%). Similarly, the other fractions, i.e., chloroform, n-hexane, and aqueous at a higher dose of 300 mg/kg also inhibited writhing after 6 min by 77.96, 79.09, and 79.66%, respectively.

Formalin test

Two concentrations of each fraction (150 and 300 mg/kg) obtained from *Justicia adhatoda* were orally administered and that significantly inhibited the formalin-induced paw licking at early and late phases of the test (Table 1; Figure 3). As compared to the standard, i.e., morphine (86.06% in the late phase), the ethyl acetate fraction was found effective at a higher dose of 300 mg/kg that significantly reduced the paw licking up to 74.35 and 88.38% in the early and late phases, respectively. Moreover, the chloroform, aqueous, and n-hexane fractions were also effective at higher concentrations (300 mg/kg) and inhibited the induced paw licking in the early phase by 61.71, 71.58, and 69.23% as well as in the late phase by 87.55, 85.06, and 87.55%, respectively.

TABLE 1 Effect of *Justicia adhatoda* in different fractions on formalin-induced pain in mice.

Treatment	Dose	Early phase	% Inhibition at the early phase	Late phase	% Inhibition at the late phase
Negative control (tween-80)	3 ml/kg (0.50%)	48.75 ± 2.2^{e}	. . .	60.25 ± 0.70^{d}	. . .
Morphine	5 mg/kg	8.25 ± 0.62^{a}	83.07	4.25.47^{a}	92.94
Ethyl acetate	150 mg/kg	25 ± 0.91^{c}	48.71	16.75 ± 2.3^{c}	72.19
	300 mg/kg	12.5 ±1^{b}	74.35	7 ± 0.91^{ab}	88.38
n-Hexane	150 mg/kg	27.75 ± 1.3^{cd}	44.1	17.5 ± 1^{c}	70.4
	300 mg/kg	15 ± 1.2^{b}	69.23	10.5 ± 0.95^{b}	82.57
Chloroform	150 mg/kg	30.75 ± 0.85^{d}	36.92	18 ± 0.4^{c}	70.12
	300 mg/kg	11.5 ± 0.64^{ab}	61.71	7.5 ± 0.28^{b}	87.55
Aqueous	150 mg/kg	30.5 ± 1.3^{d}	37.43	17.5 ± 0.64^{c}	70.95
	300 mg/kg	13.25 ± 0.85^{b}	71.58	9 ± 0.7^{b}	85.06

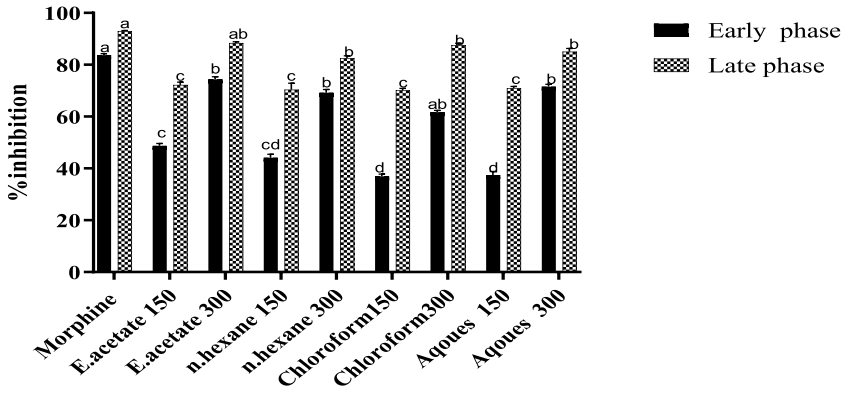

FIGURE 3
Effect of various fractions of *Justicia adhatoda* at doses of 150 and 300 mg/kg in the formalin-induced licking paw test in Swiss albino mice.

Tail immersion test in mice

The reflex time for tail withdrawal after administration of different fractions increased in a dose-dependent manner (Figure 4). Chloroform and aqueous fractions showed preferred results as compared to the reference drug (morphine).

Antipyretic test

The effect of different fractions of *Justicia adhatoda* on pyrexia induced by brewery yeast is shown in Figure 5. The pyrexia inhibition was dose-dependent and significantly related to a higher dose (300 mg/kg). As compared to the standard (85.71%), maximum inhibition (77.98%) was shown at 300 mg/kg of ethyl acetate fraction, while the other fractions, viz., aqueous (77.03%), followed by n-hexane (75.82%) and chloroform (75.70%) also showed considerable inhibition rates.

2, 2′-Diphenyl-1-picrylhydrazyl free radical-scavenging activity

The antioxidant activity was assessed by DPPH free radical-scavenging activity (Figure 6). As compared to the standard, ascorbic acid showed 76.49% and 82.33% inhibition at concentrations of 50 and 100 µg/ml, while the ethyl acetate fraction showed a scavenging effect of 50.40% at 50 µg/ml and 66.74% at 100 µg/ml. Similarly, the aqueous fractions were followed by n-hexane and

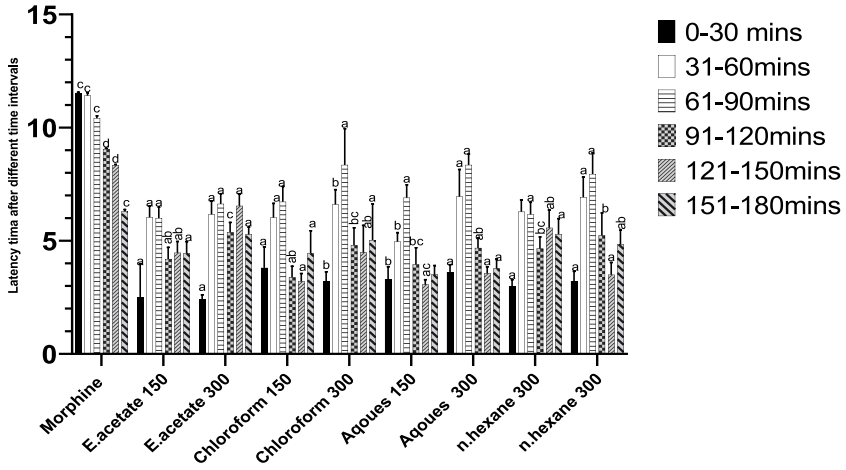

FIGURE 4
Effect of *Justicia adhatoda*'s fractions at different time intervals in the tail immersion test in Swiss albino mice.

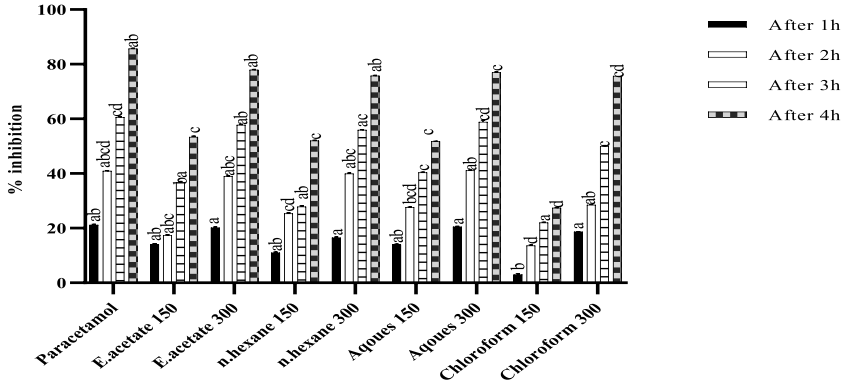

FIGURE 5
Antipyretic activity of various fractions of *Justicia adhatoda* at doses of 150 and 300 mg/kg by brewer's yeast-induced pyrexia in Swiss albino mice after 1, 2, 3, and 4 h.

chloroform with inhibition rates of 77.03, 75.82, and 75.70, respectively.

Antispasmodic activity

The antispasmodic activity of *Justicia adhatoda* fractions was assessed using charcoal-induced intestinal spam in mice, i.e., 150 and 300 mg/kg (Table 2). As compared to the standard drug, i.e., atropine sulfate, the intestinal transit was 94.57%, and significant % inhibition of the n-hexane fraction at 300 mg/kg was 72.75%. The other fractions also revealed inhibition at a higher concentration of dose (300 mg/kg), i.e., chloroform (71.55%), followed by ethyl acetate (71.47%) and aqueous (67.94%), respectively.

Gas chromatography–mass spectrometry analysis of the ethyl acetate fraction

The gas chromatography–mass spectrometry analysis of *Justicia adhatoda* ethyl acetate fraction was carried out using the NIST (National Institute Standard and Technology) library of known compounds of approximately 62,000 patterns. Our gas chromatography–mass spectrometry analysis revealed the presence of 21 compounds (secondary metabolites) that could

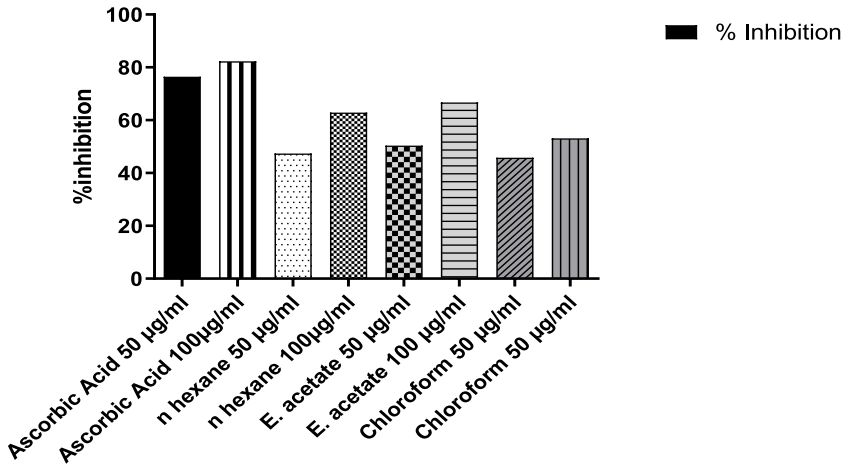

FIGURE 6
Percent inhibition of DPPH free radical-scavenging activity of *Justicia adhatoda* at different concentrations.

TABLE 2 Effect of different fractions of *Justicia adhatoda* on intestinal transit in mice.

Treatment	Dose	Total intestine length	Charcoal meal length	% Inhibition
Atropin sulfate	10 mg/kg	51.675 ± 1.4^{a}	48.85 ± 1.83^{d}	94.54
Chloroform	150 mg/kg	50.775 ± 2.2^{a}	26.4750 ± 2.09^{a}	52.13
	300 mg/kg	50.1 ± 3.5^{a}	35.85 ± 3.8^{b}	71.55
Ethyl acetate	150 mg/kg	49.275 ± 2.5^{a}	26.2750 ± 3.39^{a}	53.31
	300 mg/kg	47.575 ± 1.6^{a}	34 ± 1.3^{ab}	71.47
n-Hexane	150 mg/kg	51.25 ± 2.5^{a}	30.2250 ± 3.89^{ab}	58.96
	300 mg/kg	50.1 ± 0.70^{a}	36.45± 0.5^{b}	72.75
Aqueous	150 mg/kg	48.72 ± 2.4^{a}	22.3250 ± 1.36^{a}	45.81
	300 mg/kg	50 ± 2.8^{a}	33.975 ± 3.0^{ab}	67.94

possibly contribute to the medicinal properties of the plant. The identifications of these phytochemicals were confirmed based on peak area, molecular weight, and retention time (Table 3; Figure 7).

Discussion

Plants have been recognized as rich sources of medicines, colors, flavors, food, cosmetics, and fuel since the dawn of human civilization. However, compared to the other uses, medicinal plants have been widely used for the treatment of different disorders due to the presence of active phytochemicals (Jan and Khan, 2016; Ullah et al., 2018; Iftikhar et al., 2019; Irfan et al., 2019). With the tremendous technological advancements over the years, isolation and identification of novel phytochemicals from plants has gained more interest and attention, particularly *via* various pharmacological bioassays (Ibrahim et al., 2018; Khan et al., 2021). *Justicia adhatoda* is a well-known medicinal plant and has been widely used for treating a variety of infectious diseases, including asthma, tuberculosis, bronchitis, antibacterial, bronchodilator, anti-asthmatic, anti-tubercular, and anti-inflammatory potential. For scientific validation as well as search for novel compound isolation and identification, different pharmacological activities were undertaken to evaluate the anti-inflammatory activities of *Justicia adhatoda*.

Inflammation and its secondary forms like fever and pain are recognized because of the high level of interleukins, TNF- α, and prostaglandins (Muhammad, et al., 2012). For the assessment of anti-inflammatory effect of *J. adhatoda*'s different fractions, carrageenan-induced paw edema was considered (Linardi et al., 2000). In the carrageenan-induced paw edema test, the fractions exhibited significant anti-inflammatory effects in a dose-dependent manner. Among other fractions, the

TABLE 3 List of phytochemicals identified in the ethyl acetate fraction of *Justicia adhatoda* through the gas chromatography–mass spectrometry approach.

S. no.	Compound	Area (%)	Rt	Probability	Chemical formula
1	Phenol, 2-methyl-5-(1-methylethyl)-	0.06	10.51	53.88	$C_{12}H_{18}O$
2	Cyclotetradecane	0.01	11.80	5.60	$C_{14}H_{28}$
3	Cyclohexene, 1-methyl-4-hexenyl)-, (S)-	0.01	13.63	11.52	$C_{10}H_{16}$
4	1-Hexadecene	0.01	15.03	12.03	$C_{16}H_{32}$
5	10-Heneicosene (c,t)	0.01	4.70	18.01	$C_{21}H_{42}$
6	3,7,11,15-Tetramethyl-2-hexadecen-1-ol	0.16	18.48	37.42	$C_{20}H_{40}O$
7	10-Heneicosene (c,t)	0.01	18.01	4.70	$C_{21}H_{42}$
8	Z-(13,14-Epoxy)tetradec-11-enol acetate	0.01	8.24	8.24	$C_{16}H_{28}O_3$
9	Isophytol	0.00	19.41	43.63	$C_{20}H_{40}O$
10	Hexadecanoic acid, ethyl ester	0.06	19.76	72.13	$C_{18}H_{36}O_2$
11	Phytol	0.29	20.62	78.03	$C_{20}H_{40}O$
12	9,12,15-Octadecatrienoic acid, ethyl ester, (Z,Z,Z)-	0.05	20.96	18.79	$C_{19}H_{32}O_2$
13	3,7,11,15-Tetramethyl-2-hexadecen-1-ol	0.01	21.25	6.92	$C_{20}H_{40}O$
14	Thiophene, 3-methyl-2-pentadecyl-	0.00	22.04	22.45	$C_{20}H_{36}S$
15	Pentacosane	0.00	22.80	13.86	$C_{25}H52$
16	1,2-Benzenedicarboxylic acid, diisooctyl ester	2.14	23.14	34.29	$C_{24}H_{38}O_4$
17	1-Monolinoleoylglycerol trimethylsilyl ether	0.01	23.77	36.37	$C_{27}H56\ O_4\ Si_2$
18	Tetratetracontane	0.01	24.71	7.64	$C_{44}H_{90}$
19	Oleanolic acid	0.00	25.40	18.41	$C_{30}H48\ O_3$
20	Stigmasta-5,22-dien-3-ol, acetate, (3á)-	0.01	25.67	13.06	$C_{31}H_{50}\ O_2$
21	á-Sitosterol	0.01	27.09	45.96	$C_{29}H_{50}\ O$

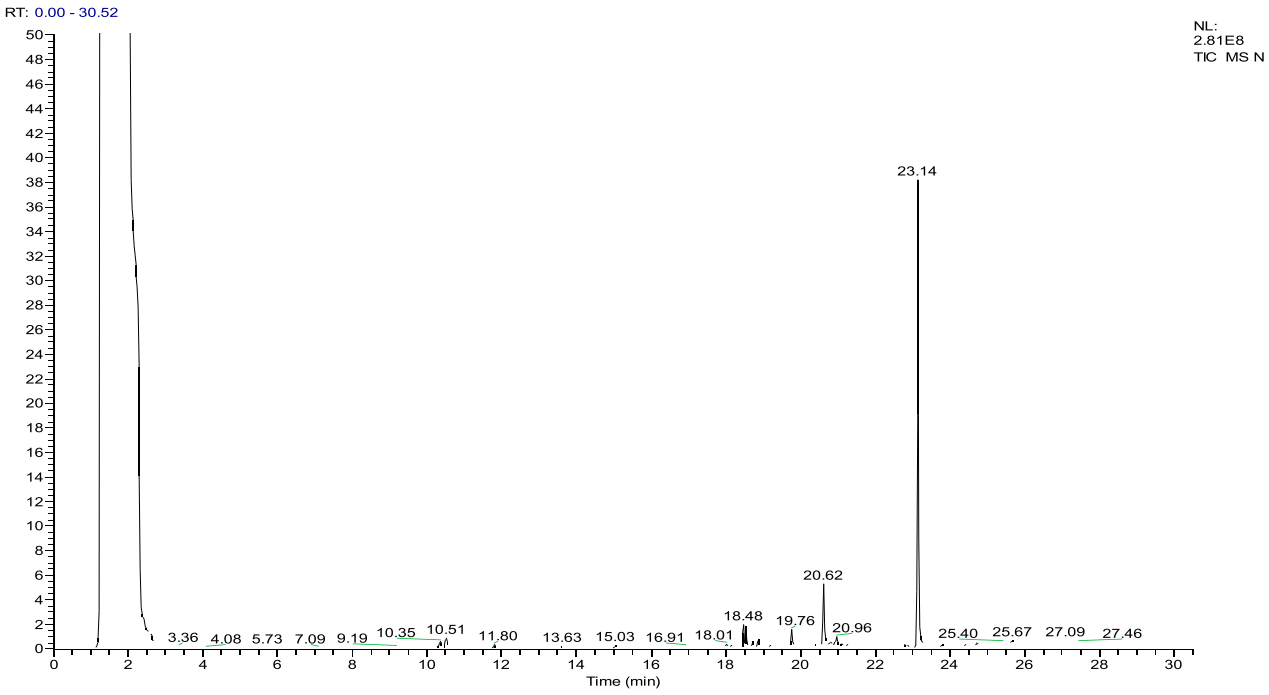

FIGURE 7
Chromatogram of the ethyl acetate fraction. Identification of phytochemical is based on peak area, molecular weight, and retention time.

chloroform fraction of 300 mg/kg was found more effective (Yam et al., 2010; Pournamdari et al., 2018) in 1–4 h, which caused 46.51% inhibition. Our results also showed a number of compounds *via* gas chromatography–mass spectrometry analysis as shown in Table 3.

Anti-nociceptive activities of different fractions of *Justicia adhatoda* were tested. Three different models were chosen to investigate the peripheral-mediated influence of *Justicia adhatoda*'s fractions. In the current study, four fractions of *Justicia adhatoda* in two concentrations, i.e, 150 and 300 mg/kg decreased the writhing, and specifically, the ethyl acetate fraction resulted in the highest reduction of writhing (84.18%). Our results are in alignment with previous findings (Abdul-Wahab et al., 2012). Similarly, the current result revealed that a higher dose of the ethyl acetate fraction is much effective against acetic acid-induced peripheral pain (Figure 2). The writhing (induced by acetic acid) model in mice is a useful test for the evaluation of the analgesic effects of therapeutic drugs (Gou et al., 2017). However, writhing caused by acetic acid affects the peripheral nervous system. The abdominal writhing procedure caused by acetic acid is a type of acute chronic nociception and a common model for intense pain in which acetic acid is used as a congenic agent (Feng et al., 2003). When injected intraperitoneally, acetic acid causes acute pain in animals by activating primary afferent sensory Aɗ and C nerve fibers 16, and the procedure is typically common in peripheral analgesic agent identification (Azi et al., 2014).

The formalin test is a reliable predictor for acute tonic pain, which has the advantage of detecting pain in central and peripheral mechanisms. Currently, both phases of the formalin paw licking test of *Justicia adhatoda* showed a significant anti-nociceptive effect in a dose-dependent manner. Ethyl acetate fractions at doses of 150 and 300 mg/kg significantly reduced the formalin-induced paw licking (88.38 and 77.24%, respectively) in the late and early phases. Furthermore, the result revealed that ethyl acetate fractions of *Justicia adhatoda* are effective in both phases, while other fractions showed minimum potential as compared to ethyl acetate. Previously, it was concluded that formalin-induced persistent nociception in mice paws provided a marked response to biphasic licking (Hunskaar and Hole., 1987; Bukhari et al., 2010).

The tail immersion model was used for the evaluation of acute pain. In our study, mice increase in latency time was noted, and the thermal pain threshold was inhibited. The dose of 300 mg/kg of *Justicia adhatoda* had a potent anti-nociceptive effect. *Justicia adhatoda's* chloroform and aqueous fractions have shown significant analgesic effects in acetic acid-induced pain, as well as in the late phase of formalin and tail immersion tests. Similar results have been reported earlier (Saha et al., 2013). The tail withdrawal response of mice is mainly considered to be selective for centrally acting analgesics, while the peripherally acting drugs are known to be inactive on such heat-induced pain responses (Imam and Sumi 2014). This approach is established on the finding that morphine-like medications extend the tail withdrawal time from hot water in mice (Moniruzzaman and Imam, 2014).

Antipyretic effectiveness of the *Justicia adhatoda* fractions was assessed by subcutaneous injection of brewer's yeast-induced pyrexia in animal models. Prostaglandin synthesis was elevated during this process, and the inhibition capability of plant-based medicine on prostaglandin synthesis was used as a test for antipyretic capacity (Shah et al., 2017). Here, the injection of ethyl acetate, n-hexane, chloroform, and aqueous fractions of *Justicia adhatoda* significantly decreased the rectal temperature of yeast-induced febrile mice (Figure 4). Among these fractions, the ethyl acetate fraction at 300 mg/kg had the most efficient antipyretic effect in yeast-produced temperature by mitigation of rectal temperature as well as normal body temperature in mice. Ullah et al. (2016) used the hydro-ethanolic extract from *Monotheca boxfolia* and concluded the presence of an active antipyretic compound oleanolic acid as well as phytol (Islam et al., 2020). Notably, phytol and oleanolic acid were identified in the current gas chromatography–mass spectrometry analysis (Table 3). The strong antipyretic potential of ethyl acetate could be the possible effect of oleanolic acid and phytol (Kashyap et al., 2016). Oleanolic acid is a pentacyclic triterpenoid compound that is known to have the properties of downregulation of many intracellular and extracellular molecular targets that are linked directly or indirectly with the disease progression (Castellano et al., 2013; Xu et al., 2021). However, the major anti-inflammatory properties of oleanolic acid and phytol have been reported to be involved in the inactivation of STATE3/6, NF, and Akt/mTOR pathways (Kashyap et al., 2016).

The ability of plant-based products to donate electrons can be evaluated by bleaching 2, 2′-diphenyl-1-picrylhydrazyl radical (DPPH) assay. The process is based on DPPH scavenging by adding a free radical-donating species or any sort of antioxidants in order to decolorize the DPPH solution. The degree of change in the color is directly linked with the antioxidant potential (Saeed et al., 2012). The ethyl acetate fraction was found to have a potent scavenging activity at 50 µg/ml with 50.40%, while at 100 µg/ml it showed 66.74%. The reason for the ethyl acetate fraction performing better might be due to its high polarity that solubilizes chemical components better than aqueous, ethanolic, and methanolic fractions (Zhang et al., 2011). However, most of the diseases due to free radicals are neurodegenerative diseases. Similarly, plant-derived antioxidants are much better for the treatment of serious diseases like cancer because of their scavenging potential (Veeru et al., 2009). The search for potent natural

TABLE 4 List of biological activities of compounds of *Justicia adhatoda* identified through gas chromatography–mass spectrometry.

S. no.	Compound	Biological activities	References
1	Phenol, 2-methyl-5-(1-methylethyl)-	Antioxidant, anti-inflammatory, and analgesic	Majid et al. (2015)
2	1-Hexadecene	Antimicrobial and antioxidant, analgesic, and anti-inflammatory	Mou et al. (2013)
3	3,7,11,15-Tetramethyl-2-hexadecen-1-ol	Anti-inflammatory and antioxidant and analgesic	Chansiw et al. (2019), Majid et al. (2015)
4	Z-(13,14-Epoxy)tetradec-11-en-1-ol acetate	Antioxidant, antipyretic anti-inflammatory, and analgesic	Chetia and Phukan, (2014), Shaaganti and Amareshwari, (2019)
5	Hexadecanoic acid, ethyl ester	Antioxidant activities and anti-inflammatory	Kim et al. (2020), Guerrero et al. (2017)
6	Phytol	Anti-nociceptive, antioxidant, anti-inflammatory, and antipyretic	Santos et al. (2013), Islam et al. (2020)
8	Isophytol	Anti-inflammatory and antioxidant	Keawsa-Ard et al. (2012), Elsharkawy et al. (2013), Sanseera et al. (2012)
9	9,12,15-Octadecatrienoic acid ethyl ester, (Z,Z,Z)-	Anti-inflammatory and antioxidant	Guerrero et al. (2017), Tian et al. (2018)
10	Pentacosane	Antioxidant	Marrufo et al. (2013)
11	1,2-Benzenedicarboxylic acid, diisooctyl ester	Antioxidant	Sivasubramanian and Brindha, (2013)
12	1-Monolinoleoylglycerol trimethylsilyl ether	Antioxidant and anti-inflammatory	Majumder et al. (2019), Mary and Giri, (2016)
13	Tetratetracontane	Antioxidant	Rhetso et al. (2020)
14	Oleanolic acid	Anti-inflammatory, anti-nociceptive, and antipyretic	Singh et al. (1992), Ullah et al. (2016)

antioxidants is a high priority because of the adverse effects associated with synthetic antioxidants (Kumar et al., 2012).

Diarrhea is the release of excessive liquids through the gastrointestinal tract, and it may lead to motility (Kumpf, 2014). Based on ethnomedicinal uses of *Justicia adhatoda* in folklore, the antispasmodic potential was also evaluated by charcoal meal intestinal transit (Table 2). High inhibition (72.75%) was observed at 300 mg/kg of n-hexane fraction, which might be due to the presence of a variety of alkaloids in the form of deoxyvasicine, vasicine, and vasicinine, and these are previously reported to be excellent antispasmodic agents (Rashmi et al., 2012).

Gas chromatography–mass spectrometry analysis of the current study revealed the presence of different anti-inflammatory compounds in *Justicia adhatoda* which are active against inflammation. The gas chromatography–mass spectrometry approach of *Justicia adhatoda* revealed various biologically active compounds that possess a number of pharmacological activities. Of the 21 compounds identified by GCMS analysis, 14 are bioactive compounds and are known for their excellent anti-inflammatory, anti-nociceptive, antipyretic, antioxidant, and other pharmacological activities (Tables 3, 4; Figure 7), while no activity has been reported for some compounds, i.e., cyclotetradecane, cxyclohexene, 1-methyl-4-hexenyl)-, (S)-, 10-heneicosene (c,t), thiophene, 3-methyl-2-pentadecyl-, stigmasta-5,22-dien-3-ol, acetate, and (3á)-, á-sitosterol.

Conclusion

The potential of *Justicia adhatoda* fractions was confirmed in different pharmacological activities. Furthermore, the gas chromatography–mass spectrometry analysis also confirmed a number of biological compounds that are already acknowledged for their anti-nociceptive, analgesic, anti-inflammatory, antipyretic, antispasmodic, and antioxidant potential. Taken as a whole, *Justicia adhatoda* plant has immense potential to be used for such bioassays in clinical trials. These fractions identified here could offer better sources for the isolation and identification of different biologically active compounds that may lead to novel plant-based drugs. However, additional studies are required for purification, characterization, and structural elucidation of these bioactive compounds.

Data availability statement

The raw data supporting the conclusion of this article will be made available by the authors, without undue reservation.

Ethics statement

The animal study was reviewed and approved by the Biosafety and Bioethics Committee of the Department of Botany, Abdul Wali Khan University Mardan, Pakistan.

Author contributions

MM and GJ designed the project and performed the experiments; FJ, MH, and MI collected the data and wrote the very first draft of the manuscript, and NA helped in reviewing the manuscript; and AR, AA, MA, and HS helped in funding acquisition.

Acknowledgments

The authors are thankful to the researchers supporting project number (RSP2022R462), King Saud University, Riyadh, Saudi Arabia.

Conflict of interest

The authors declare that the research was conducted in the absence of any commercial or financial relationships that could be construed as a potential conflict of interest.

Publisher's note

All claims expressed in this article are solely those of the authors and do not necessarily represent those of their affiliated organizations, or those of the publisher, the editors, and the reviewers. Any product that may be evaluated in this article, or claim that may be made by its manufacturer, is not guaranteed or endorsed by the publisher.

References

Abdul-Wahab, I. R., Guilhon, C. C., Fernandes, P. D., and Boylan, F. (2012). Anti-nociceptive activity of *Pereskia bleo* Kunth. (Cactaceae) leaves extracts. *J. Ethnopharmacol.* 144 (3), 741–746. doi:10.1016/j.jep.2012.10.029

Ahmad, I., Irfan, M., Ali, I., Khan, J., Saeed, S. H., and Gulfaraz, A. (2016). Checklist of some medicinal plants of district Lower Dir, Pakistan. *J. Agri. Bio-Chem. Sci.* 1 (1), 15–22.

Ali, A., Rashid, M., Sultan, A., and Irfan, M. (2017). *Anisochilus carnosus* (L. f.) Wall. ex Benth. (Lamiaceae) A new generic record for Pakistan. *Plant Sci. Today* 4 (3), 102–105. doi:10.14719/pst.2017.4.3.316

Azi, I. H., Eric, B. G., Donatus, A. W., Agyei, A. F., and Eric, W. (2014). Antinociceptive activity of various solvent extracts of *Maerua angolensis* DC stem bark in rodents. *J. Phytopharm.* 3 (1), 1–8. doi:10.31254/phyto.2014.3108

Bashir, S., Memon, R., and Gilani, A. H. (2011). Antispasmodic and antidiarrheal activities of *Valeriana hardwickii* Wall. rhizome are putatively mediated through calcium channel blockade. *Evid. Based. Complement. Altern. Med.* 2011, 304960–304966. doi:10.1155/2011/304960

Bhowmick, R., Sarwar, M. S., RahmanDewan, S. M., Das, A., Das, B., Nasiruddin, M. M., et al. (2014). *In vivo* analgesic, antipyretic, and anti-inflammatory potential in Swiss albino mice and *in vitro* thrombolytic activity of hydroalcoholic extract from *Litsea glutinosa* leaves. *Biol. Res.* 47 (1), 56–58. doi:10.1186/0717-6287-47-56

Bukhari, I. A., Khan, R. A., Gilani, A. H., Ahmed, S., and Saeed, S. A. (2010). Analgesic, anti-inflammatory and anti-platelet activities of the methanolic extract of *Acacia modesta* leaves. *Inflammopharmacology* 18 (4), 187–196. doi:10.1007/s10787-010-0038-4

Castellano, J. M., Guinda, A., Delgado, T., Rada, M., and Cayuela, J. A. (2013). Biochemical basis of the antidiabetic activity of oleanolic acid and related pentacyclic triterpenes. *Diabetes* 62 (6), 1791–1799. doi:10.2337/db12-1215

Chansiw, N., Chotinantakul, K., and Srichairatanakool, S. (2019). Anti-inflammatory and antioxidant activities of the extracts from leaves and stems of *Polygonum odoratum* Lour. *Antiinflamm. Antiallergy. Agents Med. Chem.* 18 (1), 45–54. doi:10.2174/1871523017666181109144548

Chetia, B., and Phukan, A. (2014). Chemical composition and antioxidant activities of the essential oil of *Olax acuminata*. *J. Essent. Oil Bear. Plants* 17 (4), 696–701. doi:10.1080/0972060x.2014.956807

Elsharkawy, E., Elshathely, M., Jaleel, G. A., and Al-Johar, H. I. (2013). Anti-inflammatory effects of medicinal plants mixture used by Bedouin people in Saudi Arabia. *Herba Pol.* 59 (3), 76–87. doi:10.2478/hepo-2013-0018

Feghhi-Najafabadi, S., Safaeian, L., and Zolfaghari, B. (2019). *In vitro* antioxidant effects of different extracts obtained from the leaves and seeds of *Allium ampeloprasum* subsp. *persicum*. *J. Herbmed Pharmacol.* 8 (3), 256–260. doi:10.15171/jhp.2019.37

Feng, Y., Cui, M., and Willis, W. D. (2003). Gabapentin markedly reduces acetic acid induced visceral nociception. *Anesthesiology* 98 (3), 729–733. doi:10.1097/00000542-200303000-00023

Franzotti, E. M., Santos, C. V. F., Rodrigues, H. M. S. L., Mourao, R. H. V., Andrade, M. R., and Antoniolli, A. R. (2000). Anti-inflammatory, analgesic activity and acute toxicity of *Sida cordifolia* L. (*Malva-branca*). *J. Ethnopharmacol.* 72 (1-2), 273–277. doi:10.1016/S0378-8741(00)00205-1

Gou, K. J., Zeng, R., Dong, Y., Hu, Q. Q., Hu, H. W. Y., Maffucci, K. G., et al. (2017). Anti-inflammatory and analgesic effects of *Polygonum orientale* L. extracts. *Front. Pharmacol.* 8, 562. doi:10.3389/fphar.2017.00562

Guerrero, R. V., Vargas, R. A., and Petricevich, V. L. (2017). Chemical compounds and biological activity of an extract from *bougainvillea* x *buttiana* (var. rose) holttum and standl. *Int. J. Pharm. Pharm. Sci.* 9 (3), 42–46. doi:10.22159/ijpps.2017v9i3.16190

Hossain, H., Rahman, S. E., Akbar, P. N., Khan, T. A., Rahman, M., and Jahan, I. A. (2016). HPLC profiling, antioxidant and *in vivo* anti-inflammatory activity of the ethanol extract of *Syzygium jambos* available in Bangladesh. *BMC Res. Notes* 9 (1), 191–198. doi:10.1186/s13104-016-2000-z

Hsu, W. H. (1982). Xylazine-induced delay of small intestinal transit in mice. *Eur. J. Pharmacol.* 83 (1-2), 55–60. doi:10.1016/0014-2999(82)90285-0

Hunskaar, S., and Hole, K. (1987). The formalin test in mice: dissociation between inflammatory and non-inflammatory pain. *Pain* 30 (1), 103–114. doi:10.1016/0304-3959(87)90088-1

Ibrahim, M., Amin, M. N., Akhter, S., Ahammed, M. S., Boby, F. Y., Rahman, M. M., et al. (2018). *In-vivo* analgesic and anti-inflammatory activities in Swiss albino mice and *in-vitro* thrombolytic activity of methanol extract of ten days mature whole plant of *Triticum aestivum*. *Disc. Phytomed.* 5 (4), 43–47. doi:10.15562/phytomedicine.2018.68

Iftikhar, S., Ali, W., Ullah, S., Khan, W., and Irfan, M. (2019). Comparative antibacterial potential of methanolic extract of the leaves of wild and cultivated *Ficus carica* L. *Int. J. Bot. Stud.* 4 (4), 139–143.

Imam, M. Z., and Sumi, C. D. (2014). Evaluation of antinociceptive activity of hydromethanol extract of *Cyperus rotundus* in mice. *BMC Complement. Altern. Med.* 14 (1), 83–85. doi:10.1186/1472-6882-14-83

Irfan, M., Ahmad, I., and Saeed, S. H. (2017). Traditional medicinal plant knowledge of some spermatophytes of Samar Bagh Valley, Lower Dir district, Pakistan. *Plant Sci. Today* 4 (4), 151–153. doi:10.14719/pst.2017.4.4.334

Irfan, M., Ali, D., Jan, G., and Murad, W. (2018a). Ethnobotanical survey of the flora of tehsil balakot, district mansehra, khyber Pakhtunkhwa, Pakistan. *Spec. J. Biol. Sci.* 4 (3), 7–14.

Irfan, M., Ali, I., and Kashif, R. A. (2018b). Ethnobotanical survey of the flora of maidan valley, lower dir district, khyber Pakhtunkhwa province, Pakistan. *Plant Sci. Today* 5 (2), 68–71. doi:10.14719/pst.2018.5.2.379

Irfan, M., Khan, I., Ali, A., Khan, R., Ali, A., and Jan, G. (2018c). Ethnomedicinal uses of the plants of tehsil laalqilla, district lower dir, khyber Pakhtunkhwa, Pakistan. *J. Appl. Environ. Biol. Sci.* 8 (6), 61–66.

Irfan, M., Nabeela, Kamil, M., Khan, N. A., Ali, A., Ullah, Z., Ilyas, M., et al. (2018d). Ethnomedicinal applications of plant taxa by the local communities of tehsil adenzai, district lower dir, khyber Pakhtunkhwa, Pakistan. *Int. J. Biosc.* 13 (5), 40–49. doi:10.12692/ijb/13.5.40-49

Irfan, M., Nabeela, Kamil, M., Khan, N. A., Ilyas, M., Ali, A., Ullah, S., et al. (2018e). Ethomedicinal and traditional knowledge of phanerogames of tehsil munda, district lower dir, khyber Pakhtunkhwa, Pakistan. *Int. J. Biosc.* 13 (4), 208–218. doi:10.12692/ijb/13.4.208-218

Irfan, M., Nabeela, Kamil, M., Khan, N. A., Khan, H., Khalil, S., Ullah, S., et al. (2018f). Ethnomedicinal plants uses of tehsil khall, district lower dir, khyber Pakhtunkhwa, Pakistan. *Int. J. Biosc.* 13 (4), 219–229. doi:10.12692/ijb/13.4.219-229

Irfan, M., Jan, G., Murad, W., Jan, F. G., Rauf, A., Alsayari, A., et al. (2022). Ethnomedicinal and traditional uses of the Ferns of Khyber Pakhtunkhwa, Pakistan. *Braz. J. Biol.* 84, 1–10. doi:10.1590/1519-6984.250256

Irfan, M., Nabeela, Khan, H., and Khan, S. (2019). A review of different phytochemicals and pharmacological activities evaluations of *Morus alba L. Special. J. Chem.* 4 (2), 1–9.

Islam, M. T., Ayatollahi, S. A., Zihad, S. N. K., Sifat, N., Khan, M. R., Paul, A., et al. (2020). Phytol anti-inflammatory activity: pre-clinical assessment and possible mechanism of action elucidation. *Cell. Mol. Biol.* 66 (4), 264–269. doi:10.14715/cmb/2020.66.4.31

Jan, S., and Khan, M. R. (2016). Antipyretic, analgesic and anti-inflammatory effects of *Kickxia ramosissima*. *J. Ethnopharmacol.* 182, 90–100. doi:10.1016/j.jep.2016.02.020

Ji, R. R., Chamessian, A., and Zhang, Y. Q. (2016). Pain regulation by non-neuronal cells and inflammation. *Science* 354 (6312), 572–577. doi:10.1126/science.aaf8924

Kashyap, D., Sharma, A., S Tuli, H., Punia, S., and K Sharma, A. (2016). Ursolic acid and oleanolic acid: pentacyclic terpenoids with promising anti-inflammatory activities. *Recent Pat. Inflamm. Allergy Drug Discov.* 10 (1), 21–33. doi:10.2174/1872213x10666160711143904

Kaur, R., Ruhil, S., Balhara, M., Dhankhar, S., and Chhillar, A. K. (2013). A review on *Justicia adhatoda*: A potential source of natural medicine. *Afr. J. Plant Sci.* 5 (11), 620–627. doi:10.5897/AJPS.9000004

Keawsa-Ard, S., Liawruangrath, B., Liawruangrath, S., Teerawutgulrag, A., and Pyne, S. G. (2012). Chemical constituents and antioxidant and biological activities of the essential oil from leaves of *Solanum spirale*. *Nat. Prod. Commun.* 7 (7), 1934578X1200700–958. doi:10.1177/1934578X1200700740

Khan, A., Ali, S., Murad, W., Hayat, K., Siraj, S., Jawad, M., et al. (2021). Phytochemical and pharmacological uses of medicinal plants to treat cancer: A case study from khyber Pakhtunkhwa, north Pakistan. *J. Ethnopharmacol.* 281, 114437. doi:10.1016/j.jep.2021.114437

Khan, I., Rahman, H., Abd El-Salam, N. M., Tawab, A., Hussain, A., Khan, T. A., et al. (2017). *Punica granatum* peel extracts: HPLC fractionation and LC MS analysis to quest compounds having activity against multidrug resistant bacteria. *BMC Complement. Altern. Med.* 17 (1), 247–256. doi:10.1186/s12906-017-1766-4

Kim, B. R., Kim, H. M., Jin, C. H., Kang, S. Y., Kim, J. B., Jeon, Y. G., et al. (2020). Composition and antioxidant activities of volatile organic compounds in radiation-bred *Coreopsis* cultivars. *Plants* 9 (6), 717. doi:10.3390/plants9060717

Kumar, U., Mishra, M., and Prakash, V. (2012). Assessment of antioxidant enzymes and free radical scavenging activity of selected medicinal plants. *Free Radicals Antioxidants* 2 (3), 58–63. doi:10.5530/ax.2012.3.8

Kumpf, V. J. (2014). Pharmacologic management of diarrhea in patients with short bowel syndrome. *JPEN. J. Parenter. Enter. Nutr.* 38, 38S–44S. doi:10.1177/0148607113520618

Latha, D., Prabu, P., Arulvasu, C., Manikandan, R., Sampurnam, S., and Narayanan, V. (2018). Enhanced cytotoxic effect on human lung carcinoma cell line (A549) by gold nanoparticles synthesized from *Justicia adhatoda* leaf extract. *Asian pac. J. Trop. Biomed.* 8 (11), 540. doi:10.4103/2221-1691.245969

Linardi, A., Costa, S. K., da Silva, G. R., and Antunes, E. (2000). Involvement of kinins, mast cells and sensory neurons in the plasma exudation and paw oedema induced by staphylococcal enterotoxin B in the mouse. *Eur. J. Pharmacol.* 399 (2-3), 235–242. doi:10.1016/S0014-2999(00)00375-7

Majid, M., Khan, M. R., Shah, N. A., Haq, I. U., Farooq, M. A., Ullah, S., et al. (2015). Studies on phytochemical, antioxidant, anti-inflammatory and analgesic activities of *Euphorbia dracunculoides*. *BMC Complement. Altern. Med.* 15 (1), 349–415. doi:10.1186/s12906-015-0868-0

Majumder, R., Dhara, M., Adhikari, L., Ghosh, G., and Pattnaik, S. (2019). Evaluation of *in vitro* antibacterial and antioxidant activity of aqueous extracts of *Olax psittacorum*. *Indian J. Pharm. Sci.* 81 (1), 99–109. doi:10.4172/pharmaceutical-sciences.1000484

Malik, K. A., and Ghafoor, A. (1988). "Acanthaceae," in *Flora of Pakistan*. Editors E. Nasir and S. I. Ali Karachi, 188, 1–62.

Marrufo, T., Nazzaro, F., Mancini, E., Fratianni, F., Coppola, R., De-Martino, L., et al. (2013). Chemical composition and biological activity of the essential oil from leaves of *Moringa oleifera* Lam. cultivated in Mozambique. *Molecules* 18 (9), 10989–11000. doi:10.3390/molecules180910989

Mary, A. P. F., and Giri, D. R. S. (2016). Phytochemical screening and GC-MS analysis in ethanolic leaf extracts of *ageratum conyzoides* L. *World J. Pharm. Res.* 5 (7), 1019–1029. doi:10.20959/wjpr20167-6505

Moniruzzaman, M., and Imam, M. Z. (2014). Evaluation of antinociceptive effect of methanolic extract of leaves of *Crataeva nurvala* Buch.-Ham. . *BMC Complement. Altern. Med.* 14 (1), 354–357. doi:10.1186/1472-6882-14-354

Mou, Y., Meng, J., Fu, X., Wang, X., Tian, J., Wang, M., et al. (2013). Antimicrobial and antioxidant activities and effect of 1-hexadecene addition on palmarumycin C2 and C3 yields in liquid culture of endophytic fungus *Berkleasmium* sp. Dzf12. *Molecules* 18 (12), 15587–15599. doi:10.3390/molecules181215587

Muhammad, N., Saeed, M., and Khan, H. (2012). Antipyretic, analgesic and anti-inflammatory activity of *Viola betonicifolia* whole plant. *BMC Complement. Altern. Med.* 12 (1), 59–68. doi:10.1186/1472-6882-12-59

Pournamdari, M., Mandegary, A., Sharififar, F., Zarei, G., Zareshahi, R., Asadi, A., et al. (2018). Anti-inflammatory subfractions separated from acidified chloroform fraction of fenugreek seeds (*Trigonella foenum-graecum* L.). *J. Diet. Suppl.* 15 (1), 98–107. doi:10.1080/19390211.2017.1326431

Rashmi, P. A., John, R., and Mathew, L. (2012). Isolation and characterization of vasicine from *in vitro* cultures of *Justicia adhatoda*. *Int. J. Pharm. Bio. Sci.* 3, 58–64.

Rhetso, T., Shubharani, R., Roopa, M. S., and Sivaram, V. (2020). Chemical constituents, antioxidant, and antimicrobial activity of *Allium chinense* G. Don. *Futur. J. Pharm. Sci.* 6 (1), 102–109. doi:10.1186/s43094-020-00100-7

Saeed, N., Khan, M. R., and Shabbir, M. (2012). Antioxidant activity, total phenolic and total flavonoid contents of whole plant extracts *Torilis leptophylla* L. *BMC Complement. Altern. Med.* 12 (1), 221–312. doi:10.1186/1472-6882-12-221

Saha, S., Guria, T., Singha, T., and Maity, T. K. (2013). Evaluation of analgesic and anti-inflammatory activity of chloroform and methanol extracts of *Centella asiatica* L. *ISRN Pharmacol.* 2013, 789613. doi:10.1155/2013/789613

Sanseera, D., Niwatananun, W., Liawruangrath, B., Liawruangrath, S., Baramee, A., and Pyne, S. G. (2012). Chemical composition and biological activities of the essential oil from leaves of *Cleidion javanicum* Bl. *J. Essent. Oil Bear. Plants* 15 (2), 186–194. doi:10.1080/0972060X.2012.10644035

Santos, A. R., and Calixto, J. B. (1997). Ruthenium red and capsazepine antinociceptive effect in formalin and capsaicin models of pain in mice. *Neurosci. Lett.* 235 (1-2), 73–76. doi:10.1016/S0304-3940(97)00722-2

Santos, C. C. D. M. P., Salvadori, M. S., Mota, V. G., Costa, L. M., de Almeida, A. A. C., de Oliveira, G. A. L., et al. (2013). Antinociceptive and antioxidant activities of phytol *in vivo* and *in vitro* models. *Neurosci. J.* 2013, 949452. doi:10.1155/2013/949452

Shaaganti, M., and Amareshwari, P. (2019). Phytochemistry, micropropagation and pharmacology of near threatened plant *Pseudarthria viscida* (L.) wight & arn. *J. Pharmacog. Phytochem.* 8 (1), 2102–2108.

Shah, M., Parveen, Z., and Khan, M. R. (2017). Evaluation of antioxidant, anti-inflammatory, analgesic and antipyretic activities of the stem bark of *Sapindus mukorossi*. *BMC Complement. Altern. Med.* 17 (1), 526–616. doi:10.1186/s12906-017-2042-3

Shah, S. M. M., and Shah, S. M. H. (2015). Phytochemicals, antioxidant, antinociceptive and anti-inflammatory potential of the aqueous extract of *Teucrium stocksianum* bioss. *BMC Complement. Altern. Med.* 15 (1), 351–357. doi:10.1186/s12906-015-0872-4

Sharifi-Rad, M., Epifano, F., Fiorito, S., and Álvarez-Suarez, J. M. (2020a). Phytochemical analysis and biological investigation of *Nepeta juncea* benth. *Differ. Extr. Plants* 9, 646. doi:10.3390/plants9050646

Sharifi-Rad, M., Pohl, P., Epifano, F., and Álvarez-Suarez, J. M. (2020b). Green synthesis of silver nanoparticles using *Astragalus tribuloides* delile. Root extract: Characterization, antioxidant, antibacterial, and anti-inflammatory activities. *Nanomaterials* 10, 2383. doi:10.3390/nano10122383

Sharifi-Rad, M., Pohl, P., and Epifano, F. (2021). Phytofabrication of silver nanoparticles (AgNPs) with pharmaceutical capabilities using *Otostegia persica* (burm.) boiss. *Leaf Extr. Nanomater.* 11, 1045. doi:10.3390/nano11041045

Sharifi-Rad, M., Pohl, P., Epifano, F., Zengin, G., Jaradat, N., and Messaoudi, M. (2022). *Teucrium polium* (L.): Phytochemical screening and biological activities at different phenological stages. *Molecules* 27, 1561. doi:10.3390/molecules27051561

Sharifi-Rad, M., and Pohl, P. (2020). Synthesis of biogenic silver nanoparticles (AgCl-NPs) using a *Pulicaria vulgaris* gaertn. Aerial Part Extract and their application as antibacterial, antifungal and antioxidant agents. *Nanomaterials* 10, 638. doi:10.3390/nano10040638

Sher, A. A., Iqbal, A., Adil, M., Ullah, S., Bawazeer, S., Binmahri, M. K., et al. (2022). GC-MS analysis of organic fractions of *Chrozophora tinctoria* (L.) A.Juss. and their prokinetic propensity in animal models. *Braz. J. Biol.* 84, e260566. doi:10.1590/1519-6984.260566

Simmons, D. L. (2006). What makes a good anti-inflammatory drug target? *Drug Discov. Today* 11 (5-6), 210–219. doi:10.1016/S1359-6446(05)03721-9

Singh, G. B., Singh, S., Bani, S., Gupta, B. D., and Banerjee, S. K. (1992). Anti-inflammatory activity of oleanolic acid in rats and mice. *J. Pharm. Pharmacol.* 44 (5), 456–458. doi:10.1111/j.2042-7158.1992.tb03646.x

Sivasubramanian, R., and Brindha, P. (2013). *In-vitro* cytotoxic, antioxidant and GC-MS studies on *Centratherum punctatum* Cass. *Int. J. Pharm. Pharm. Sci.* 5 (3), 364–367.

Sundur, S., Shrivastava, B., Sharma, P., Raj, S. S., and Jayasekhar, V. L. (2014). A review article of pharmacological activities and biological importance of. *Calophyllum Inophyllum. Int. J. Advan. Res.* 2 (12), 599–603.

Than, A., Kulkarni, H. J., Hmone, W., and Tha, S. J. (1989). Anti-diarrhoeal efficacy of some Burmese indigenous drug formulations in experimental diarrhoeal test models. *Int. J. crude drug Res.* 27 (4), 195–200. doi:10.3109/13880208909116903

Tian, C., Gao, X., Yang, J., Guo, Y., Wang, H., and Liu, M. (2018). Chemical compositions, extraction technology, and antioxidant activity of petroleum ether extract from *Abutilon theophrasti* Medic. leaves. *Int. J. Food Prop.* 21 (1), 1789–1799. doi:10.1080/10942912.2018.1494198

Ullah, I., Khan, J. A., Shahid, M., Khan, A., Adhikari, A., Hannan, P. A., et al. (2016). Pharmacological screening of *Monotheca buxifolia* (Falc.) A. DC. for antinociceptive, anti-inflammatory and antipyretic activities. *BMC Complement. Altern. Med.* 16 (1), 273–278. doi:10.1186/s12906-016-1257-z

Ullah, R., Khan, M., Shah, S. A., Saeed, K., and Kim, M. O. (2019). Natural antioxidant anthocyanins, Ahidden therapeutic candidate in metabolic disorders with major focus in neurodegeneration. *Nutrients* 11 (6), 1195. doi:10.3390/nu11061195

Ullah, K., Shah, G. M., Alam, J., Gul, A., and Irfan, M. (2022). Ethnomedicinal uses of the Ferns of Shishikoh Valley, District Chitral, Pakistan. *Plant Sci. Today* 9 (3), 687–692. doi:10.14719/pst.1690

Ullah, S., Khan, W., Ali, W., Khan, M. S., Sajad, M. A., Nabeela, et al. (2018). Antibacterial and antifungal potentials of the various solvents extracts of Quercus incana fruits. *Int. J. Biosci.* 13 (5), 438–447. doi:10.12692/ijb/13.5.438-447

Veeru, P., Kishor, M. P., and Meenakshi, M. (2009). Screening of medicinal plant extracts for antioxidant activity. *J. Med. Plants Res.* 3 (8), 608–612. doi:10.5897/JMPR.9001114

Winter, C. A., Risley, E. A., and Nuss, G. W. (1962). Carrageenin-induced edema in hind paw of the rat as an assay for antiiflammatory drugs. *Proc. Soc. Exp. Biol. Med.* 111 (3), 544–547. doi:10.3181/00379727-111-27849

Xu, Q. F., Peng, H. P., Lu, X. R., Hu, Y., Xu, Z. H., and Xu, J. K. (2021). Oleanolic acid regulates the Treg/Th17 imbalance in gastric cancer by targeting IL-6 with miR-98-5p. *Cytokine* 148, 155656. doi:10.1016/j.cyto.2021.155656

Yam, M. F., Lim, V., Salman, I. M., Ameer, O. Z., Ang, L. F., Rosidah, N., et al. (2010). HPLC and anti-inflammatory studies of the flavonoid rich chloroform extract fraction of *Orthosiphon stamineus* leaves. *Molecules* 15 (6), 4452–4466. doi:10.3390/molecules15064452

Zeb, A., Ahmad, S., Ullah, F., Ayaz, M., and Sadiq, A. (2016). Anti-nociceptive activity of ethnomedicinally important analgesic plant *Isodon rugosus* Wall. ex Benth: Mechanistic study and identifications of bioactive compounds. *Front. Pharmacol.* 7 (200), 200–210. doi:10.3389/fphar.2016.00200

Zeb, A., Ullah, F., Ayaz, M., Ahmad, S., and Sadiq, A. (2017). Demonstration of biological activities of extracts from *Isodon rugosus* Wall. Ex Benth: Separation and identification of bioactive phytoconstituents by GC-MS analysis in the ethyl acetate extract. *BMC Complement. Altern. Med.* 17 (284), 284–316. doi:10.1186/s12906-017-1798-9

Zhang, Y., Shi, S., Wang, Y., and Huang, K. (2011). Target-guided isolation and purification of antioxidants from *Selaginella sinensis* by offline coupling of DPPH-HPLC and HSCCC experiments. *J. Chromatogr. B Anal. Technol. Biomed. Life Sci.* 879 (2), 191–196. doi:10.1016/j.jchromb.2010.12.004

Advantages of publishing in Frontiers

OPEN ACCESS
Articles are free to read for greatest visibility and readership

FAST PUBLICATION
Around 90 days from submission to decision

HIGH QUALITY PEER-REVIEW
Rigorous, collaborative, and constructive peer-review

TRANSPARENT PEER-REVIEW
Editors and reviewers acknowledged by name on published articles

Frontiers
Avenue du Tribunal-Fédéral 34
1005 Lausanne | Switzerland

Visit us: www.frontiersin.org
Contact us: frontiersin.org/about/contact

REPRODUCIBILITY OF RESEARCH
Support open data and methods to enhance research reproducibility

DIGITAL PUBLISHING
Articles designed for optimal readership across devices

FOLLOW US
@frontiersin

IMPACT METRICS
Advanced article metrics track visibility across digital media

EXTENSIVE PROMOTION
Marketing and promotion of impactful research

LOOP RESEARCH NETWORK
Our network increases your article's readership